EVALUATION AND SELECTION OF GROUND MOTION INTENSITY
MEASURES FOR NONLINEAR SEISMIC DEMAND AND FRAGILITY
ANALYSIS OF MDOF SYSTEMS

A THESIS SUBMITTED TO
THE GRADUATE SCHOOL OF NATURAL AND APPLIED SCIENCES
OF
MIDDLE EAST TECHNICAL UNIVERSITY

BY

KORAY KADAŞ

IN PARTIAL FULFILLMENT OF THE REQUIREMENTS
FOR
THE DEGREE OF DOCTOR OF PHILOSOPHY
IN
CIVIL ENGINEERING

MAY 2021

Approval of the thesis:

EVALUATION AND SELECTION OF GROUND MOTION INTENSITY MEASURES FOR NONLINEAR SEISMIC DEMAND AND FRAGILITY ANALYSIS OF MDOF SYSTEMS

submitted by **KORAY KADAŞ** in partial fulfillment of the requirements for the degree of **Doctor of Philosophy in Civil Engineering, Middle East Technical University** by,

Prof. Dr. Halil Kalıpçılar
Dean, Graduate School of **Natural and Applied Sciences**   _____

Prof. Dr. Ahmet Türer
Head of the Department, **Civil Engineering**   _____

Prof. Dr. Ahmet Yakut
Supervisor, **Civil Engineering, METU**   _____

Examining Committee Members:

Prof. Dr. Murat Altuğ Erberik
Civil Engineering, METU   _____

Prof. Dr. Ahmet Yakut
Civil Engineering, METU   _____

Assoc. Prof. Dr. Mustafa Tolga Yılmaz
Engineering Sciences, METU   _____

Prof. Dr. İlker Kazaz
Civil Engineering, Erzurum Technical University   _____

Prof. Dr. Özgür Avşar
Civil Engineering, Eskişehir Technical University   _____

Date: 21.05.2021

I hereby declare that all information in this document has been obtained and presented in accordance with academic rules and ethical conduct. I also declare that, as required by these rules and conduct, I have fully cited and referenced all material and results that are not original to this work.

Name, Last name : Koray Kadaş

Signature :

ABSTRACT

EVALUATION AND SELECTION OF GROUND MOTION INTENSITY MEASURES FOR NONLINEAR SEISMIC DEMAND AND FRAGILITY ANALYSIS OF MDOF SYSTEMS

Kadaş, Koray
Doctor of Philosophy, Civil Engineering
Supervisor: Prof. Dr. Ahmet Yakut

May 2021, 426 pages

In performance-based seismic design methodology, intensity measures are thought to be key parameters of ground motion records that relate the seismic hazard levels with the structural response or damage. Therefore, it is important to identify efficient intensity measures that are capable of reducing the variability in seismic demand predictions. There exist several simple-to-advanced scalar and vector ground motion intensity measures; however, the literature is limited in the number of comparative studies investigating the efficiency of these parameters, especially in the entire response range of structures. In order to compensate for such shortcoming, a comprehensive research study has been undertaken to identify the most efficient intensity measures that would correlate well with key engineering demand parameters of low- to relatively high-rise reinforced concrete frames. The study elaborates on the subject utilizing both single- and multi-degree-of-freedom systems. Based on the correlation performances of a long list of simple scalar intensity parameters, a manageable list of indices has been shortlisted on which alternative ground motion record subsets were formed. The more complex multi-degree-of-

freedom systems were later analyzed under these alternative record subsets to investigate the efficiency of an expanded list of intensity measures covering more advanced scalar and vector indices as well. Besides, the sufficiency of these parameters with respect to moment magnitude and source-to-site distance were evaluated through statistical analyses. Based on the interpretations of this second stage evaluation which utilizes a regression equation-based statistical approach, the best candidates have been identified for the reinforced concrete systems examined. In the last part of the study, the effect of shortlisted intensity measures on the ground motion selection stage of fragility analyses has been examined. Eventually, recommendations on the number of bins and records in each bin have been made to obtain reliable fragility curves that would lead to sufficiently accurate loss estimations of seismic vulnerability studies.

Keywords: Intensity Measures, Seismic Demand Analysis, Efficiency, Sufficiency, Fragility Analysis

ÖZ

ÇOK SERBESTLİK DERECELİ SİSTEMLERİN DOĞRUSAL OLMAYAN SİSMİK VE KIRILGANLIK ANALİZİ İÇİN YER HAREKETİ ŞİDDET ÖLÇÜLERİNİN DEĞERLENDİRİLMESİ VE SEÇİMİ

Kadaş, Koray
Doktora, İnşaat Mühendisliği
Tez Yöneticisi: Prof. Dr. Ahmet Yakut

Mayıs 2021, 426 sayfa

Performansa dayalı sismik tasarım yönteminde, şiddet ölçüleri, sismik tehlike seviyesi ile yapıların davranışını veya hasarını ilişkilendiren önemli yer hareketi parametreleridir. Bu nedenle, sismik talep tahminlerindeki değişkenliği azaltabilen etkin şiddet ölçülerinin belirlenmesi önem arz etmektedir. Literatürde basitten gelişmişe bir çok skalar ve vektör şiddet ölçüsü mevcut olmasına rağmen bu parametrelerin özellikle yapıların tüm davranış seviyelerindeki etkinliğini inceleyen karşılaştırmalı çalışmaların sayısı sınırlıdır. Bu eksikliği gidermek amacıyla, az ve nispeten yüksek katlı betonarme çerçevelerin kritik mühendislik talep parametreleri ile yüksek korelasyon gösteren etkin şiddet ölçülerinin saptanması amacıyla kapsamlı bir çalışma üstlenilmiştir. Çalışma, konuyu tek ve çok serbestlik dereceli sistemlerden yararlanarak detaylandırmaktadır. Basit skalar şiddet parametrelerinden oluşan uzun bir listenin korelasyon performanslarına göre daha yönetilebilir bir şiddet ölçüsü listesi teşkil edilmiş ve bu parametrelere göre alternatif yer hareketi kayıt altkümeleri oluşturulmuştur. Bu alternatif kayıt setleri kullanılarak daha karmaşık çok serbestlik dereceli sistemler analiz edilmiş, ve daha gelişmiş skalar ve vektör ölçülerinden oluşturulmuş genişletilmiş bir listenin etkinlikleri

incelenmiştir. Ayrıca, bu parametrelerin moment magnitüdü ve sahaya olan uzaklığa dayalı yeterlilikleri istatistiki analizler aracılığı ile değerlendirilmiştir. Bağlanım denklemine dayalı istatistiki yaklaşım kullanılarak yapılan ikinci aşama değerlendirmenin yorumlarına göre incelenen betonarme sistemler için en uygun adaylar belirlenmiştir. Çalışmanın son kısmında, kısa listeye giren şiddet ölçülerinin, kırılganlık analizlerinde yer hareketi kayıtlarının seçimi aşamasına olan etkileri incelenmiştir. Sonuç olarak, sismik kırılganlık çalışmalarında yeterince doğru kayıp tahminlerinin hesaplanmasında kullanılacak güvenilir kırılganlık eğrilerinin elde edilebilmesi için gerekli şiddet seviyesi sayısı ve bu seviyelerde seçilmesi gereken kayıt sayılarına yönelik tavsiyelerde bulunulmuştur.

Anahtar Kelimeler: Şiddet Ölçüleri, Sismik Talep Analizi, Etkinlik, Yeterlilik, Kırılganlık Analizi

To my family

ACKNOWLEDGMENTS

TABLE OF CONTENTS

LIST OF TABLES

LIST OF FIGURES

FIGURES

xviii

xx

xxxiv

LIST OF ABBREVIATIONS

ABBREVIATIONS

A_{95}	Energy-based Acceleration-related Parameter
AI	Arias Intensity (generally shown as I_a in the literature)
ASI	Acceleration Spectrum Intensity
ASI*	Modified Acceleration Spectrum Intensity (0.1-2.5s period range)
BS	Base Shear (interchangeably shown as V)
CAV	Cumulative Absolute Velocity
CD	Closest Distance
CP	Collapse Prevention
EDP	Engineering Demand Parameter
ESDOF	Equivalent Single Degree-of-Freedom
FC	Fragility Curve
HI	Housner Intensity
I_a	Riddell-Garcia - Acceleration-based Index
I_c	Characteristic Intensity
I_d	Riddell-Garcia - Displacement-based Index
I_F	Fajfar Intensity
I_v	Riddell-Garcia - Velocity-based Index
IM	Intensity Measure
IO	Immediate Occupancy

GM	Ground Motion
GMI	Ground Motion Intensity Measure
LS	Life Safety
MDOF	Multi Degree-of-Freedom
MIDR	Maximum Interstory Drift Ratio
M_w	Moment Magnitude
NLTHA	Nonlinear Time History Analysis
NTH	Nonlinear Time History
PBEE	Performance-Based Earthquake Engineering
PEER	Pacific Earthquake Engineering Research Center
PGA	Peak Ground Acceleration
PGD	Peak Ground Displacement
PGV	Peak Ground Velocity
PoE	Probability of Exceedance
R_{JB}	Joyner-Boore Distance
$S_a(T_1)$	Spectral Acceleration at the Fundamental Period of the Structure
$S_d(T_1)$	Spectral Displacement at the Fundamental Period of the Structure
$S_v(T_1)$	Spectral Velocity at the Fundamental Period of the Structure
SDOF	Single Degree-of-Freedom
SED	Specific Energy Density
SMA	Sustained Maximum Acceleration

SMV	Sustained Maximum Velocity
t_{5-95}	Significant Duration (t_r could be used interchangeably)
t_d	Ground Motion Duration
t_r	Significant Duration (t_{5-95} could be used interchangeably)
T_1	Fundamental Period
TD	Top Displacement
VSI	Velocity Spectrum Intensity

CHAPTER 1

INTRODUCTION

The primary responsibility of a structural engineer is to design and create structures that satisfy adequate safety and serviceability requirements generally dictated by the design codes. The fundamental philosophy defining this adequacy level is to ensure the life safety of humankind especially after sudden hazardous events such as earthquakes, and secondarily, to minimize the damage in the structural and non-structural components due to the loads imposed on these elements. To accomplish these imperative objectives, the structural engineers were simply proportioning the structural elements for strength, and then checking for drift with the utilization of a wide range of analytical tools, ranging from linear static analyses to advanced nonlinear inelastic analyses, during the course of his/her profession. However, recent years have exhibited the paradigm shift –as genuinely expressed by Prof. Mete Sözen- from force-based approach towards displacement-based design approach, where displacement-based approach dictates proportioning on the basis of drift, and then checking for strength (Gülkan, 2020). In both approaches, the acceptability criteria for a satisfactory design depend on various "performance objectives" defined either at the structural element level or at the global level. Regarding these objectives, last 40 years of structural engineering community have witnessed the development of performance based engineering, which has originated from vital challenges and critical observations of earthquake engineering field. Performance based engineering, (more specifically, performance-based earthquake engineering, PBEE) has enabled to define alternate performance levels for various loading conditions, and has focused on the analytical identification of these "performance levels" (Priestley, 2000).

Having a closer look at the design approach of this engineering trend; in performance-based seismic design methodology, a decision maker generally makes choices between alternate performance levels. To achieve this, the decision maker must consider the appropriate level of seismic hazard to which the structure should be designed as well as the acceptable risk that would guide structural performance expectations. Implicit in this process is an evaluation of costs and benefits. Figure 1.1 depicts the Pacific Earthquake Engineering Research Center's approach where there are four stages: hazard analysis, structural analysis, damage analysis, and loss analysis (Porter, 2003).
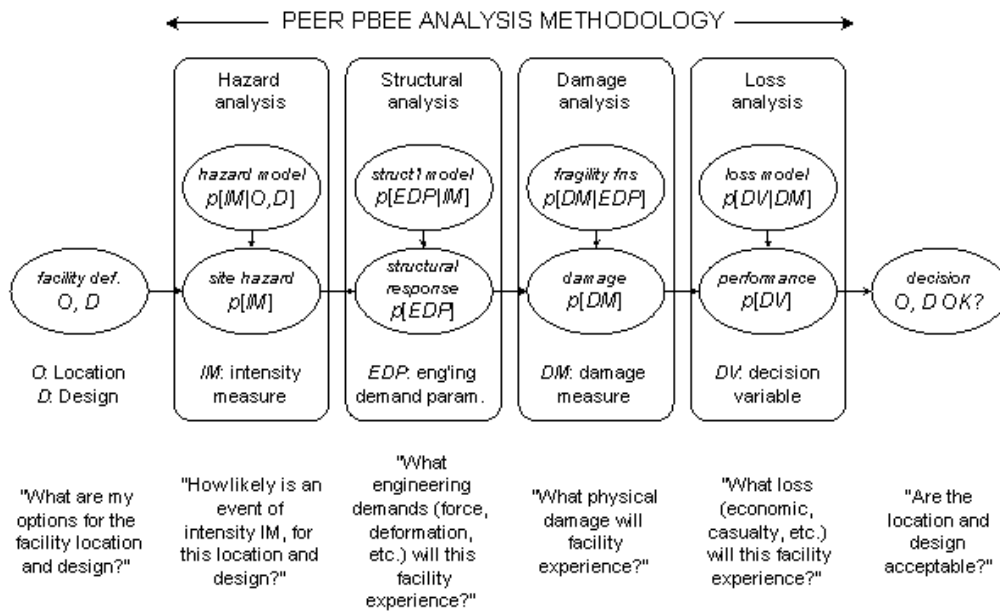
Figure 1.1. PEER methodology (Porter, 2003)

In the hazard analysis, one evaluates the seismic hazard at the facility site, producing sample ground-motion time histories whose intensity measure (IM) is appropriate to varying hazard levels. In the structural-analysis phase, a nonlinear time-history structural analysis is performed to calculate the response of the facility to a ground motion (GM) of given IM in terms of drifts, accelerations, or other engineering

demand parameters (EDP). In the damage-analysis phase, these EDPs are used with component fragility functions to determine measures of damage (DM) to the facility components. Finally, given DM, one evaluates repair efforts to determine repair costs, operability, and repair duration, and the potential for casualties. These measures of performance are referred to as decision variables (DV), since they can be used to inform stakeholder decisions about future performance. Each relationship, from location and design to IM, IM to EDP, EDP to DM, and DM to DV, involves uncertainty and is treated probabilistically.

An important step in this process is the identification of certain properties of a recorded ground motion that are most strongly related to the response or damage caused in the structure. A value that quantifies the effect of a record on a structure is often called an intensity measure (IM).

1.1   Overview

The strong ground motion records; either naturally recorded, artificially generated or simulated, exhibit distinctive amplitude, frequency content and duration characteristics, and contain valuable information that could be utilized to differentiate individual records from others. These information, defining the uniqueness of each record, can be demonstrated in simple numerical forms or can be revealed with some further computations yielding to more advanced IMs. At this point, a list of major IMs from the literature will be briefly presented herein to exemplify such variations that would also assist in forming a basis for the elaboration of the research subject. Even though short descriptions will be provided in this section, interested readers are referred essentially to original references listed and alternatively to general references such as Kramer (1996) and companion manuscripts; Yılmaz (2007), Hancılar (2009), Ye et al. (2013) and Seismosoft (2016) manual.

Peak Ground Acceleration (PGA) is the largest absolute acceleration value obtained from the accelerogram of any strong ground motion. It is one of the simplest amplitude-based parameters in the time domain, having a direct relationship with inertial forces developed within the structures during seismic events. PGA is suited to characterize the GM amplitude at short frequencies. However, it lacks information regarding the duration and frequency content of the strong ground motion.

Peak Ground Velocity (PGV) is the largest absolute velocity obtained from the velocity time history of a record, and is more suitable to characterize the GM amplitude at intermediate frequencies.

Peak Ground Displacement (PGD) is a displacement-based amplitude parameter obtained from the displacement history of a record, and is generally related to low-frequency components of the GM record.

PGV/PGA is simply the ratio of PGV to PGA, and regarded as a significant IM which reveals information about the frequency content (i.e., seismological characteristics) of the GM (Zhu et al., 1988; Tso et al., 1992; Sucuoğlu and Nurtuğ, 1995; Sucuoğlu et al., 1998).

Root-Mean-Square of Acceleration (a_{rms}) is a single parameter combining the effects of frequency content and amplitude of the GM record, thus eliminating the dominancy of large and high-frequency accelerations. However, it is influenced by the duration definition used in the calculation. Correspondingly, the term inside the square root is termed as *average acceleration intensity* or *mean-squared acceleration*.

$$a_{rms} = \sqrt{\frac{1}{t_d} \int_0^{t_d} [a(t)]^2 \, dt} = \sqrt{P_a} \qquad (1.1)$$

There also exist velocity and displacement counterparts of a_{rms}, namely *Root-Mean-Square of Velocity (v_{rms})* and *Root-Mean-Square of Displacement (d_{rms})* as well.

$$v_{rms} = \sqrt{\frac{1}{t_d} \int_0^{t_d} [v(t)]^2 \, dt} = \sqrt{P_v} \tag{1.2}$$

$$d_{rms} = \sqrt{\frac{1}{t_d} \int_0^{t_d} [d(t)]^2 \, dt} = \sqrt{P_d} \tag{1.3}$$

Arias Intensity (AI), an IM proposed by Arias (1970), is based on the energy content of the GM and reflects all three characteristics (i.e., amplitude, frequency content and duration). *(It is generally abbreviated as I_a in the literature, but to differentiate it from Riddell-Garcia's Acceleration-related index, AI will be used throughout the text).*

$$I_a \equiv AI = \frac{\pi}{2g} \int_0^{t_d} [a(t)]^2 \, dt \tag{1.4}$$

Nau and Hall (1982) presented a similar index archetype as *AI* for acceleration, velocity and displacement traces of a GM yielding to *Nau and Hall indices* and their root forms, a_{rs}, v_{rs}, and d_{rs}, respectively.

$$E_a = \int_0^{t_d} [a(t)]^2 \, dt \quad \rightarrow \quad a_{rs} = \sqrt{E_a} \tag{1.5}$$

$$E_v = \int_0^{t_d} [v(t)]^2 \, dt \quad \rightarrow \quad v_{rs} = \sqrt{E_v} \tag{1.6}$$

$$E_d = \int_0^{t_d} [d(t)]^2 \, dt \quad \rightarrow \quad d_{rs} = \sqrt{E_d} \tag{1.7}$$

Araya and Saragoni (1984) modified the intensity index proposed by Arias (1970), with a term v_0, that is the number of zero-crossings per unit time on the acceleration-based trace, to improve the reflection of frequency characteristics of GMs.

$$AI_{modified} \equiv P_D = \frac{AI}{v_0^2} \tag{1.8}$$

Characteristic Intensity (I$_C$), alternatively termed as Park-Ang intensity, was proposed as an indicator of structural damage due to destructiveness of the earthquakes and is the combination of root-mean-square-of-acceleration, a_{rms}, and duration definition, t_d (Park et al., 1985; Ang, 1990).

$$I_C = a_{rms}^{1.5} t_d^{0.5} \tag{1.9}$$

Specific Energy Density (SED) is an IM representing the overall energy of the GM record and based on squared-velocity over the entire duration.

$$SED = \int_0^{t_d} [v(t)]^2 \, dt \tag{1.10}$$

Cumulative Absolute Velocity (CAV), an intensity index proposed by Electrical Power Research Institute (EPRI, 1998), is the absolute area under the GM accelerogram and reflects all three characteristics (i.e., amplitude, frequency content and duration) as well.

$$CAV = \int_0^{t_d} |a(t)| \, dt \tag{1.11}$$

Spectral Acceleration (S$_a$(T$_1$)) is generally considered as the *elastic spectral acceleration* at the fundamental period of the structure, and its velocity and displacement counterparts are *Spectral Velocity (S$_v$(T$_1$))* and *Spectral Displacement (S$_d$(T$_1$)),* respectively. These spectral IMs are fundamentally based on the response spectrum concept where the maximum responses (in terms of displacement, velocity and acceleration) of elastic single-degree-of-freedom (SDOF) systems with different periods and with specific damping ratios constitute the elastic response spectra of the specific GM record, correspondingly. This group of IMs are eventually structure-specific; thus, indirectly reflects considerable information about the GM characteristics which are filtered by the SDOF response (Kramer, 1996).

Acceleration Spectrum Intensity (ASI), a parameter proposed by Von Thun et al. (1988) for characterization of GMs for concrete dams with fundamental periods less

than 0.5 sec, considers the area under the elastic acceleration response spectrum for the period range defined below.

$$ASI = \int_{0.1}^{0.5} S_a(\xi = 0.05, T)\, dT \tag{1.12}$$

A modified version of *ASI*, *Modified Acceleration Spectrum Intensity (ASI*)*, has been recently recommended by Yakut and Yılmaz (2008) after their observation that the expanded period range of 0.1-2.5 sec for consideration of the area under the elastic acceleration response spectrum correlates better with the seismic demands of moment-resisting frames.

$$ASI^* = \int_{0.1}^{2.5} S_a(\xi = 0.05, T)\, dT \tag{1.13}$$

Velocity Spectrum Intensity (VSI), an intensity index proposed by Von Thun et al. (1988) for characterization of GMs for rockfill and earthfill dams with fundamental periods between 0.6 and 2.0 sec, considers the area under the elastic velocity response spectrum for the period range defined below.

$$VSI = \int_{0.1}^{2.5} S_v(\xi = 0.05, T)\, dT \tag{1.14}$$

Housner Intensity (HI), an IM proposed by Housner (1952), considers pseudo velocity spectrum with a period range considering the fundamental periods of most of the structures, and was considered to be a relation between the earthquake intensity and the forces imposed on the structures.

$$HI = \int_{0.1}^{2.5} PSV(\xi = 0.05, T)\, dT \tag{1.15}$$

Sustained Maximum Acceleration (SMA), an IM defined by Nuttli (1979), is taken as the 3rd highest absolute acceleration value of accelerogram, whereas its velocity counterpart, *Sustained Maximum Velocity (SMV)*, is defined similarly using the velocity time history.

Effective Design Acceleration (EDA), is an intensity parameter corresponding to the peak acceleration value obtained after application of low-pass filter (with cut-off frequency of 9 Hz) on the accelerogram (Benjamin and Associates, 1988).

A_{95} parameter, an index proposed by Sarma and Yang (1987), is closely related with AI of the GM record and determined as the limit acceleration level where the total AI is computed as 95% of the original AI value.

Predominant Period (T_P) is simply the period of SDOF system yielding the highest spectral acceleration in an elastic acceleration response spectrum for a damping ratio of 5%. Alternatively, it can be defined as the period corresponding to the highest value of the Fourier Amplitude Spectrum. It is considered as an indicator crudely related to the frequency content of the GM record.

Mean Period (T_m) is an IM after Rathje et al. (1998), characterizing the frequency content of a GM record by utilizing the Fourier amplitudes between frequencies of 0.25 and 20 Hz.

Significant Duration (t_r or t_{5-95} interchangeably) as defined by Trifunac and Brady (1975), is a key duration-related parameter aimed at characterizing the duration of the strong motion portion of an accelerogram from engineering point of view. It is defined as the time interval where the portion of total AI (i.e., thresholds between 5% and 95% of total AI) is accumulated. There are other duration definitions (such as bracketed duration, uniform duration and effective duration) (Bommer and Martinez-Pereira, 1999) that could be utilized as an IM (or at least part of a compound IM) as well; however, this study neglects other alternative definitions for the sake of simplicity and focuses on this widely-preferred form based on the conclusions of aforementioned study.

Effective Peak Acceleration (EPA), an index introduced by Applied Technology Council (1978), is generally used in the definition of smoothed design spectra presented in building codes. Along with its velocity counterpart, *Effective Peak Velocity (EPV),* they are considered to be normalization factors for the standard

8

spectra. *EPA* is defined as the arithmetic average of 5%-damped spectral acceleration values within the period range 0.1-0.5 sec divided by standard amplification factor 2.5, whereas *EPV* is defined as the 5%-damped spectral velocity value at 1 sec divided by 2.5. Kurama and Farrow (2003) elaborated further on the definition of *EPV* and recommended that the average of spectral velocity values within the period range 0.8-1.2 sec to be considered. The consideration of specific period ranges in the calculation of *EPA* and *EPV* eventually prevents the domination of local high values in the response spectra, making them better alternatives with respect to PGA especially (Yılmaz, 2007).

$$EPA = \frac{S_a(0.1s, 0.5s)}{2.5} \tag{1.16}$$

$$EPV = \frac{S_v(0.8s, 1.2s)}{2.5} \tag{1.17}$$

Yang et al. (2009) recommended improved versions of EPA and EPV, *IEPA* and *IEPV*, respectivly, with consideration of pulse effects in near-fault ground motions and proposed the use of average values obtained within a period band around T_{PA} and T_{PV} where these two anchor points refer to the periods at which spectral acceleration and spectral velocity reach maxima, respectively.

$$IEPA = \frac{S_a(T_{PA} - 0.2s, T_{PA} + 0.2s)}{2.5} \tag{1.18}$$

$$IEPV = \frac{S_v(T_{PV} - 0.2s, T_{PV} + 0.2s)}{2.5} \tag{1.19}$$

Fajfar Index (I_F), a compound index introduced by Fajfar et al. (1990), is used as an indicator of GM capacity to damage structures which have fundamental periods in the intermediate range and is a combination of PGV and significant duration.

$$I_F = v_{max} t_d^{0.25} \tag{1.20}$$

Demonstrating the poor correlation performance of miscellaneous IMs with input and dissipated energy, Riddell and Garcia (2001) similarly proposed 3 alternative

compound indices, I_a, I_v, and I_d, to normalize GMs to estimate energy dissipation corresponding to *acceleration-*, *velocity-* and *displacement-*sensitive regions of the hysteretic energy spectrum, respectively. They recommended utilization of significant duration definition in the duration-related parameter.

$$I_a = a_{\max} t_d^{1/3} \tag{1.21}$$

$$I_v = v_{max}^{2/3} t_d^{1/3} \tag{1.22}$$

$$I_d = d_{max} t_d^{1/3} \tag{1.23}$$

The literature is not limited to the IMs listed above indeed; on the contrary, there exist various other parameters (particularly, the unmentioned indices that can be found in Kramer (1996)) that might assist interested scholars in trying to characterize the ground motions. However, the inevitable necessity to limit the list to a manageable and traceable size, even for research purposes, has prevented those to be considered within the scope of the study. Nonetheless, a further list of relatively more essential IMs proposed in the last two decades will be presented in the remaining part of this sub-section, as the incorporation of these indices will eventually elaborate the research study.

Cordova et al. (2000) stated that spectral quantities based on linear response spectrum are inadequate to account for period softening of the structures responding in inelastic range due to damages caused by the strong motions. As the period of the structure lengthens due to reduction in the lateral stiffness of the system, the structure may attract larger seismic forces which is dependent on the spectral characteristic of the GM. This phenomenon was tried to be incorporated into a new two-parameter seismic IM through the additional term $R_{S_a}{}^{\alpha}$ where this term modifies the effect of the spectral value corresponding to the structure examined.

$$S_{aC} \equiv S_a(T_1) R_{S_a}{}^{\alpha} \quad \text{where} \quad R_{S_a} = \frac{S_a(cT_1)}{S_a(T_1)} \tag{1.24}$$

10

The two parameters, c and α, are recommended as 2.0 and 0.5, respectively, by Cordova et al. (2000) which were calibrated for a limited frame and GM record set. However, their proposal still remains as a single value, will be represented as S_{aC} from now on, and is relatively practical to calculate.

$$S_{aC} \equiv S_a(T_1) \left\{ \frac{S_a(2T_1)}{S_a(T_1)} \right\}^{0.5} \tag{1.25}$$

Baker and Cornell (2004) transformed this single parameter into a new form with two individual parameters, and brought the concept of vector IM into picture.

$$\begin{Bmatrix} S_a(T_1) \\ R_{T_1,T_2} \end{Bmatrix} \quad \text{where} \quad R_{T_1,T_2} = \frac{S_a(T_2)}{S_a(T_1)} \tag{1.26}$$

They performed a thorough investigation for the choice of T_2 (for a more reliable calculation of the second parameter R_{T_1,T_2}) and concluded that this period can be either the period corresponding to the second mode of vibration of the system responding elastically or can attain values larger than T_1 for increasing levels of ductility of the systems responding in the inelastic range.

Baker and Cornell (2005) subsequently modified their proposal by switching R_{T_1,T_2} with ε parameter, an index reflecting the spectral shape characteristic, where the epsilon is instructed to be calculated as the difference between the mean obtained from a ground motion prediction equation (GMPE) and the spectral acceleration of the GM record. Similar to R_{T_1,T_2}, this ε value has been shown to be an important predictor of structural response.

$$\begin{Bmatrix} S_a(T_1) \\ \varepsilon \end{Bmatrix} \tag{1.27}$$

Luco and Cornell (2007) introduced various scalar but complex IMs, IM_{1E}, IM_{1I}, $IM_{1E\&2E}$ and $IM_{1I,2E}$, that are specific to a structure by utilizing the concepts of modal analysis and modal combination rule square-root-of-sum-of-squares (SRSS). By a step-by-step development procedure, the writers finally attained $IM_{1I\&2E}$ which combines the effects of nonlinearity and the contribution from the second mode.

$$IM_{1E} = \left|PF_1^{[1]}\right| S_d(T_1, \zeta_1) \propto S_a(T_1) \tag{1.28}$$

$$IM_{1I} = \left|PF_1^{[1]}\right| S_d^I(T_1, \zeta_1, d_y) = \frac{S_d^I(T_1, \zeta_1, d_y)}{S_d(T_1, \zeta_1)} IM_{1E} \tag{1.29}$$

$$IM_{1E\&2E} = \sqrt{\left[PF_1^{[2]} S_d(T_1, \zeta_1)\right]^2 + \left[PF_2^{[2]} S_d(T_2, \zeta_2)\right]^2} \tag{1.30}$$

$$IM_{1E\&2E} = \sqrt{1 + R_{2E/1E}^2} \left|\frac{PF_1^{[2]}}{PF_1^{[1]}}\right| IM_{1E} \tag{1.31}$$

$$R_{2E/1E} = \frac{PF_2^{[2]} S_d(T_2, \zeta_2)}{PF_1^{[2]} S_d(T_1, \zeta_1)} \tag{1.32}$$

$$IM_{1I\&2E} = \frac{S_d^I(T_1, \zeta_1, d_y)}{S_d(T_1, \zeta_1)} IM_{1E\&2E} \tag{1.33}$$

$$IM_{1I\&2E} = \sqrt{1 + R_{2E/1E}^2} \left|\frac{PF_1^{[2]}}{PF_1^{[1]}}\right| IM_{1I} \tag{1.34}$$

As a similar approach to estimate the inelastic response of structural systems under GMs through a simple index, Bianchini (2008) proposed a scalar IM, $S_{a,avg}$, where this measure is computed as the average of spectral acceleration values over a specific period range intended to cover the elongated period and periods corresponding to higher modes of vibration of MDOF systems. More proper notation for this parameter is $S_{a,gm}$, as the index is calculated as the geometric mean of the spectral ordinates,

$$S_{a,gm}(T^{(1)}, T^{(n)}) = \left(\prod_{i=1}^{n} S_a(T^{(i)})\right)^{1/n} \tag{1.35}$$

Kadaş et al. (2011) introduced a spectrum-based IM considering both period elongation of the structural system and approximate structural capacity reflected through yield spectral acceleration. This IM was recommended to be used for pre-selection of ground motion records that would lead to various levels of nonlinear response.

12

$$I_{am} = \frac{1}{(T_f - T_i)A_y} \int_{T_i}^{T_f} S_a(T, \xi)(T - T_i) \, dT \tag{1.36}$$

$$T_f = 1.07 \times T_i \times \left[\frac{S_a(T_i, \xi)}{A_y}\right]^{0.45} \leq 2.0 T_i \tag{1.37}$$

Lin et al. (2011) proposed a general form for their new spectral-based IM, S_N, considering the spectral contributions essentially from $S_a(T_1)$ through $S_a(T_1)^\alpha$; additionally, from the second vibration mode of MDOF system through $S_a(T_2)$, and from the inelastic response through $S_a(T_f)$.

$$S_N \equiv S_a(T_1)^\alpha \times S_a(T_2)^\beta \times S_a(T_f)^\gamma \tag{1.38}$$

Since the reliable determination of the parameters α, β, γ and $T_f (\equiv CT_1)$ is not straightforward, they simplified this formulation into two different expressions, one formula for structures generally responding inelastically, and one index for structures under significant effects of the second mode.

For inelastic case;

$$S_{N1} \equiv S_a(T_1)^\alpha \times S_a(CT_1)^{1-\alpha} \tag{1.39}$$

For higher mode effects case;

$$S_{N2} \equiv S_a(T_1)^\beta \times S_a(T_2)^{1-\beta} \tag{1.40}$$

As a major alternative to $\langle S_a(T_1), R_{T_1,T_2} \rangle$, which was introduced by Baker and Cornell (2005), Bojórquez and Iervolino (2010, 2011) proposed two spectral shape-based IMs, the prime one in vector form as $\langle S_a(T_1), N_p \rangle$ and the secondary alternative simplifying the former IM as I_{N_p} to a scalar form. They also considered the geometric mean of spectral ordinates over a specified period range to define N_p, but normalized it with $S_a(T_1)$. The logic behind the use of average spectral values is the fact that a single spectral value at the fundamental period is not a good representative for the spectral shape of a GM record where the spectral ordinates at other periods might be influential on either nonlinear or higher mode behavior.

$$\begin{Bmatrix} S_a(T_1) \\ N_p \end{Bmatrix} \quad \text{where} \quad N_p = \frac{S_{a_{avg}}(T_1,\dots,T_N)}{S_a(T_1)} \tag{1.41}$$

$$I_{N_p} = S_a(T_1)N_p{}^{\alpha} \tag{1.42}$$

De Biasio et al. (2014) has introduced a scalar IM termed as *relative average spectral acceleration*, ASA_R, accounting for nonlinear structural behavior. They considered the amount of drop in the fundamental frequency of the system through the parameter, R, reflecting the elongation of the period of the system.

$$ASA_R(T_1) = \frac{T_1}{(1-X_f)} \int_{T_1}^{\frac{T_1}{X_f}} \frac{S_{pa}(T,\xi)}{T^2} dT \quad \text{where} \quad X_f = 1 - (R/100) \tag{1.43}$$

Theophilou et al. (2017) has recently recommended a more complex vector IM, $\langle S_a(T_1), S_{dN}(T_1, T_2) \rangle$, incorporating a normalized spectral displacement-based area index as the second parameter as opposed to the vector IM, $\langle S_a(T_1), \varepsilon \rangle$, which was proposed by Baker and Cornell (2005).

$$\begin{Bmatrix} S_a(T_1) \\ S_{dN}(T_1, T_2) \end{Bmatrix} \tag{1.44}$$

$$S_{dN}(T_1, T_2) = \frac{1}{S_d(T_1)T_N} \int_{T_1}^{T_2} S_d(T) \, dT, \quad T_1 < T_2 \text{ and } T_N = 1.0 \, s \tag{1.45}$$

Without questioning the individual starting points or goals of relatively outmoded as well as recently-proposed IMs exemplified in this section at this stage, overall portraying of these parameters has revealed that the literature comprises a great deal of IM definitions varying from basic scalar forms to more complex vector forms, each trying to the characterize the GM records and generally attempting to relate these characteristics to response of the structural systems subjected to seismic events.

The aforementioned intensity measures and many others can be categorized in several schemes, as illustrated in Figure 1.2, and this categorization generally supports the researchers from the earthquake engineering field to establish their discussions and arguments on IMs around comprehensible classes or groups.
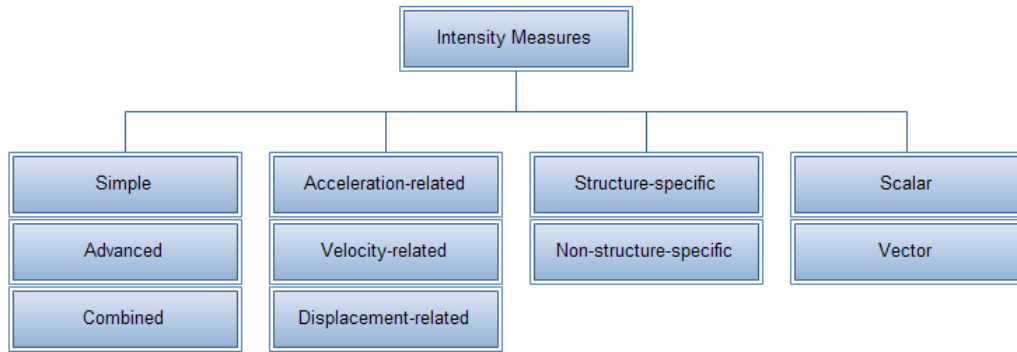
Figure 1.2. Categorization of intensity measures

The first grouping refers to the simplicity of the intensity index; whether it is formed from a single term and straightforward to determine-present, such as PGA or PGV, or requires reasonable-to-extensive computations to achieve the numerical index, as in the case of AI or $IM_{1I\&2E}$, or a combination of two or more individual parameters, such as I$_F$. The second classification approach is mainly considering the relevancy of the index with certain aspects of the ground motion record, whether the subject IM is basically acceleration-, velocity- or displacement-related parameter. The long list of IMs presented above has displayed that some parameters rely on the response spectrum concept and require spectral values specific to structures examined. This requirement brings the differentiation of IMs in two groups; structure-specific (can be exemplified as S_a–type indices) and non-structure-specific (can be demonstrated as PGA, PGV, and AI), which constitutes the third categorization approach. The reader will notice from the novel indices that the contemporary research focus has been given to structure-specific parameters. The final grouping, in contrast, looks for the case whether the subject intensity parameter is a single index (as in the cases of ASI, VSI and $S_a(T_1)$) or it is in a vectorial form with two or more individual parameters (that can be illustrated as $\langle S_a(T_1), R_{T_1,T_2} \rangle, \langle S_a(T_1), N_p \rangle$ and $\langle S_a(T_1), S_{dN}(T_1, T_2) \rangle$).

Disregarding the recently proposed advanced IMs, which are structure-specific and mostly acceleration-related, the aforementioned scalar IMs can be sorted according to the second grouping approach as presented in Table 1.1. Particular discussions throughout the text will occasionally refer to this categorization.

Table 1.1 Acceleration-, velocity- and displacement-related scalar IMs

Acceleration related	Velocity related	Displacement related
PGA	PGV	PGD
a_{rms}, E_a, a_{rs}	v_{rms}, E_v, v_{rs}	d_{rms}, E_d, d_{rs}
AI, A_{95}, CAV	SED	
$S_a(T_1)$	$S_v(T_1)$	$S_d(T_1)$
ASI, ASI^*	VSI, HI	
$EDA, EPA, IEPA$	$EPV, IEPV$	
I_a, I_C	I_v, I_F	I_d

1.2   Problem Statement

The fundamental requirement to numerically define a hazard level for a site on which the structure is built and to associate this hazard definition with various performance metrics via monitorable responses of the structure has directed the researchers and professionals of the earthquake engineering field to pick and utilize an easily quantifiable intensity measure, and to select and employ GM records that sufficiently fit the defined hazard from the IM perspective. The use of such "appropriate" records, especially in nonlinear time history analyses, significantly improves the reliability of the technical evaluations and decisions made upon the analysis results due to the reduction in the dispersion of peak monitored responses (i.e., EDPs). The choice of the "best candidate" intensity measure(s) from a list of competitors, which

is the first crucial step here, necessitated the establishment of competency criteria and has brought *efficiency, sufficiency, practicality, scaling robustness,* and *hazard computability* concepts into the picture (Luco, 2002; Buratti, 2012; Kazantzi and Vamvatsikos, 2015; Kohrangi et al., 2016a, 2016b; O'Reilly et al., 2018):

Efficiency is simply defined as the capability to reduce the variability in the EPDs obtained from the analyses, thus allowing to reduce the number of GM records to be utilized or the number of analyses to be performed for a target accuracy level.

Sufficiency is defined as the ability of a parameter to render EDP independently without requiring additional information such as seismological features; earthquake magnitude (for instance, Mw), source-to-site distance (for instance, R_{JB}), or epsilon (ε).

Practicality, which is rarely mentioned, is generally referred to as easiness in the calculation of the subject parameter.

Scaling robustness refers to the feature of an IM when scaling of GM records does not introduce bias to the EDPs as compared to unscaled GMs.

Hazard computability is the suitability of an IM for the direct use of current GMPEs in extensive hazard computations or at least allowing for the practical generation of new GMPEs.

Even though it was expressed previously by Housner and Jennings (1977) that the complex earthquake (EQ) phenomenon cannot be fully described by a single intensity index to inherently reflect complicated EQ characteristics, getting marked as "efficient" was adequate in the past for a "good candidate" IM. However, the contemporary approach has forced the pursuit of more strict evaluation criteria for candidate IMs, requiring all five aforementioned aspects for screening. Formerly, the first criterion was implicitly being investigated through correlation statistics which will be described in Chapter 2. Based on the calculation of correlations with

monitored EDPs occurring under various seismic events, the IMs having the highest coefficients were deemed to be the most essential predictors of structural damage. With the frequent utilization of probabilistic approaches utilizing theoretically advanced mathematical methods, the evaluation of the efficiency has transformed into the calculation of the dispersion of EDPs, and the parameters leading to smaller dispersions have been marked as relatively efficient. As an ongoing process of this mathematical approach, evaluation of both sufficiency (generally with respect to earthquake magnitude and source-to-site distance) and scaling robustness criteria was handled generally through the residuals from the former calculations. Determination of practicality, yet remained as an expert opinion rather than a mathematical definition, whereas determination of hazard computability remained as a specialist's conclusion based on the availability of corresponding ground motion prediction equations or constructability of the new ones.

Although with the emerge of performance-based engineering concepts, the probabilistic approaches have enforced the last three criteria to be inquired as well, "efficiency" constitutes the core criterion in the characterization of ground motions and in the reliable use as damage or engineering demand predictors. Starting from mid 1980s, the research studies have focused on this norm to identify and incorporate suitable parameters in the selection and scaling of GM records (Ay, 2012). The following section will briefly present key studies focusing from this perspective.

1.3   Literature Survey

The literature harbors a long list of studies majorly focusing on revealing the relationship of structural responses and resulting damages with intensity measures, and correspondingly, attempting to identify the most influential parameter to reflect the ground motion characteristics, especially in terms of their damage potential. Among those; relatively dated studies of Uang and Bertero (1988), Cabanas et al. (1997), Sucuoğlu (1997), Elenas (2000), Elenas and Meskouris (2001), Liao et al. (2001), Wu et al. (2004), Akkar and Özen (2005), Riddell (2007) have been referred

18

by Yılmaz (2007) and crucial observations of these studies have been marked therein. Owing to the fact that these studies were limited in the employed number of ground motion records, structural systems or intensity measures, Yılmaz (2007) carried out a more comprehensive correlation study as opposed to previous endeavors with a larger set of both ground motion records (i.e., 80 records) and structural models (16 low- to relatively-high rise moment-resisting RC frames with a fundamental period range of 0.17-1.07 sec), and evaluated 11 scalar IMs (PGA, PGV, EPA, AI, HI, I_C, CAV, ASI, VSI, I_F, S_a). Along with its companion manuscript Yakut and Yılmaz (2008), this notable research study has revealed important observations about the correlation performance of the fundamental IMs considering maximum top displacement and maximum inter-story drift ratio. Yakut and Yılmaz (2008) additionally introduced an improved version of *ASI*, *ASI**, yielding higher correlations, especially for mid-rise frames. This study is regarded as a cornerstone subsequent to the collection of relevant former studies fundamentally investigating the efficiency of scalar IMs that are relatively easy to compute. Considering the period after the publishment of this study, several studies focusing and elaborating on the subject have started to emerge. These studies will be briefly summarized in the remaining part of this section without going further into the detailed discussions and conclusions.

Hancılar (2009) similarly attempted to investigate the correlation between IMs and structural response parameters through nonlinear time history analysis of multi degree-of-freedom systems. The study utilized 12 low- to high-rise planar frames with a fundamental period range of 0.55-2.15 sec and a much larger record database with 734 accelerograms. The study principally considered 8 scalar IMs (PGA, PGV, PGD, AI, CAV, S_a, S_v, S_d) and 4 different response parameters (maximum inter-story drift ratio, maximum floor displacement, maximum floor acceleration, maximum plastic end rotation of beams) to derive conclusions on the correlation performance of selected IMs.

Buratti (2012) is one of the pioneer studies evaluating the efficiency of a long list of scalar and vector IMs, and their sufficiency with respect to M_w and R_{JB} as well. The

study employed a very large set of accelerograms with 1704 records to follow a regression analysis-based methodology to obtain dispersion statistics of maximum displacement demands of various SDOF systems (with a period range of 0.1-2.0 sec) and maximum inter-story drift ratio demands of 3 planar RC frames (with a fundamental period range of 0.46-0.84 sec). The fundamental conclusion of this advanced study is to use highly efficient I_{N_p} by Bojórquez and Iervolino (2011) for both SDOF and MDOF systems that might be improved with the use of its vectorial form as well.

Cantagallo et al. (2012) utilized 9 RC three-dimensional MDOF systems and two different GM sets (with 61 and 85 records corresponding to two distinct hazard levels) to investigate the efficiency of a limited number of IMs (PGA, PGV, HI, ASI, and three different S_a-based parameters) in estimating the maximum inter-story drift ratio demands. They recommended the use of S_a-based parameters as a general approach.

Ye et al. (2013) similarly employed a large seismic index set with 30 simple-to-compound scalar IMs to evaluate the correlation performance of the indices with response parameters obtained from nonlinear time history analyses single and multi-degree-of-freedom systems subjected to a limited set of 60 GM records. They explicitly presented the period-wise variation of correlation results for numerous IMs grouped as acceleration-, velocity- and displacement-related indices, and finally proposed the use of PGV, as opposed to PGA, in performance-based seismic analysis due to its sufficient simplicity, but raised concerns regarding the use of S_a.

Van Cao and Ronagh (2014a, 2014b) alternatively investigated the correlation performance of 23 IMs monitored under 204 near-fault (with pulse-type motions) and 1040 far-fault GM records. They considered the maximum inter-story drift ratio and a damage index calculated for a three-story planar frame with a fundamental period of 0.11 sec. Their limited interpretations from both studies have led to the recommendation of VSI as the best descriptor which is followed by HI and S_a.

Kostinakis et al. (2015) also considered 3D models (with a fundamental period range of 0.70-1.00 sec) in the evaluation of 19 widely used IMs. They utilized 64 pairs of GM records and monitored structural responses as well as the overall structural damage index. They concluded that S_a, followed by VSI, PGV and HI, are the most efficient IMs for the structures employed when the structural response parameters are considered.

Ozmen and Inel (2016) followed an SDOF system-based evaluation approach to examine the correlation of 19 common scalar IMs with seismic displacement demands. They employed 466 GM records from 28 seismic events and 1056 SDOF models (with a period range of 0.14-1.20 sec) representing low- to mid-rise RC buildings. They marked VSI and PGV as the best IMs for correlation with seismic demands of the examined building stock. Following this study, Ozmen (2017) elaborated on the analyses and attempted to develop hybrid intensity parameters, and monitored the improvements in correlation performance.

Palanci and Senel (2019) lately evaluated nine different scalar IMs (PGA, PGV, d_{rms}, I_a, CAV, ASI, VSI) utilizing both SDOF (with a period range of 0.1-5.0 sec) and MDOF (with a fundamental period range of 0.65-1.36 sec) models which were subjected to 168 accelerograms. They have comprehensively examined the effect of lateral strength ratios (i.e., the ratio of strength capacity at yielding to seismic weight, V_t/W), post-yield stiffness ratios, hysteretic models, and soil types on nonlinear displacement demands of the structural systems. They have concluded that VSI is the most suitable parameter for buildings with a dominant vibration period between 0.5-2.0 sec. Additionally, they emphasized the pronounced effect of lateral strength ratios, whereas VSI is less sensitive to post-yield stiffness ratio, hysteretic behavior, and soil type with respect to other IMs they examined.

Bhasker and Menon (2020) recently utilized the three-story plan irregular SPEAR building to assess the correlation of 21 simple-to-advanced scalar IMs with maximum inter-story drift ratio under a far-fault GM set including 50 pairs of accelerograms. They have concluded for their specific structure that the IM proposed

by Bianchini (2008) with consideration of T_1-$2T_1$ period range is the most efficient IM, and geometric averaging approach for combining the values from individual components to obtain a single scalar descriptor is the best combination method with respect to other alternatives examined.

The above-mentioned references constitute the list of studies mainly focusing on the comparative evaluation of scalar IMs generally. In addition to such holistic examinations, there also exist specific studies with the aim of proposing new IMs and comparatively evaluating the performance of their proposition with respect to the limited number of commonly used practical IMs. Riddell and Garcia (2001), Cordova et al. (2000), Baker and Cornell (2004), Baker and Cornell (2005), Luco and Cornell (2007), Bianchini (2008), Lin et al. (2011), Bojórquez and Iervolino (2010, 2011), De Biasio et al. (2014, Theophilou et al. (2017), Yakchalian et al. (2019) could be emphasized among many other studies available in the literature, which have introduced new IM candidates, as already described in Section 1.1. Neglecting Riddell and Garcia (2001), these studies, however, were limited to the presentation of efficiency and sufficiency metrics as compared to the results of spectrum-based S_a in order to display the superiority of their IM proposal over S_a. Here, the logic behind the selection of S_a as the reference point could be explained in a way that spectrum-based S_a, which is a structure-specific IM, had been once regarded as the most efficient parameter with respect to simple scalar IMs such as PGA, PGV, or similar, but has been shown later in the literature that S_a –in its original form- is not "sufficiently efficient" when the collapse capacities of the structural systems are being sought or when the higher modes of structures are apparent as in the case of high-rise buildings. Apart from this phenomenon, the utilization of different structural systems and distinct GM record datasets in the above-mentioned studies complicates the mission of any interested scholar on identifying the "most efficient" or "best candidate" IM(s) that would be suitable for his/her own seismic assessment studies. Consequently, the lack of a holistic study evaluating the comparative performance of both simple scalar parameters formerly

considered and more advanced scalar and vector IMs recently proposed has created a motivation for this research study.

1.4   Scope and Organization

The main objective of this dissertation is to primarily evaluate the efficiency of simple-to-advanced scalar as well as recently-proposed vector IMs to reveal their correlations with major seismic demands on multi-degree-of-freedom systems, reinforced concrete planar frames in particular. Eventually, this goal extends to the identification of the most efficient intensity parameter(s), that will be sufficiently practical as well, and checking of their sufficiencies with respect to earthquake magnitude and source-to-site distance. The approach of this study to identify the most efficient IM(s) is two-fold: a single-degree-of-freedom system based evaluation stage has been followed first to identify candidate IMs from a long list of basic scalar IMs, later utilized to form alternative ground motion record subsets that will be employed in the multi-degree-of-freedom system-based evaluation stage. In the second stage, the evaluation of efficiency and sufficiency of an expanded list of IMs, including more advanced scalar and vector forms, has been elaborated via a regression equation-based (i.e., Cloud Analysis oriented) approach.

The second objective of this study is to examine the effect of a shortened list of IMs on the derivation of analytical fragility curves, which are very crucial for seismic vulnerability assessments. The selection of an efficient, but also practical IM to define the GM record subset and correspondingly derive the fragility curve as a function of the selected IM or any other suitable alternative has been investigated together with the required number of records to form the GM datasets for accurate determination of the resulting curves.

This study differentiates from recent studies by employing hazard definition-independent ground motion records in the evaluation stages to reveal the resulting dispersion characteristics in the entire response range of the structures analyzed. This

approach is considered to be much more suitable for earthquake engineers dealing with accelerated regional loss assessment studies without the need for region-specific data.

This thesis includes seven chapters generally describing different stages of the evaluations and a suite of appendices supplementing these chapters:

- Chapter 1 introduces the research subject and problem, presents definitions and general classifications of major intensity measures, and provides a brief collection of literature studies evaluating the problem.

- Chapter 2 presents the main seismological features of the ground motion database utilized throughout the thesis study and evaluates some of the major IMs according to the inter-dependency among them.

- Chapter 3 presents the structural models utilized in this thesis study and briefly explains the modelling details and the analysis types performed on the mathematical models.

- Chapter 4 describes the methodology and steps to evaluate the efficiency of essential IMs from the SDOF system perspective and summarizes the key findings that will support MDOF system-based evaluation stages.

- Chapter 5 explains in detail the MDOF system-based approach for the evaluation of the efficiency and sufficiency of an expanded list of IMs. It, firstly, refers to the ground motion selection problem and directs to the supplementary Appendix section, which explains the sampling methods utilized to form suitably sized ground motion record subsets that will be employed for NTH analyses. It presents key findings obtained from ESDOF model-based analyses and correspondingly points out proper GM subsets for the utilization in MDOF-based NTH analyses. As an intermediate step, the correlation of selected engineering demand parameters of MDOF systems with shortlisted IMs is evaluated and comparatively displayed to reduce the subset alternatives to fewer cases. The chapter continues with the presentation of the prediction equation-based evaluation methodology

incorporating certain statistical metrics to validate the prediction equations. The chapter discusses the performances of individual IMs under a fewer number of alternative GM subsets via these statistical metrics and concludes with the representation of best candidate IM(s) qualified from the expanded list.

- Chapter 6 is devoted to the evaluation of the effect of candidate IMs as well as widely-used IMs such as PGA and PGV on the derivation of fragility curves. IM to be considered for the formation of GM subset, IM to be selected on which the fragility curve function will be established, and the number of bins and records to be utilized for the derivation of accurate fragility curves are the topics evaluated and discussed within this chapter.

- Chapter 7 summarizes the steps and key conclusions from individual evaluation stages and concludes the thesis with future work recommendations.

CHAPTER 2

GROUND MOTION DATABASE

2.1   Introduction

Comprehensive evaluation of intensity measures from an intensity-based perspective necessitates a large database of strong ground motion records with various seismological characteristics. Databases such as Pacific Earthquake Engineering Research Center's (PEER) Ground Motion Databases, Consortium of Organizations for Strong Motion Observation Systems's (COSMOS) Strong-Motion Virtual Data Center (VDC), K-NET and KiK-net of Japan, Turkish Accelerometric Database and Analysis System (TADAS) (formerly known as Daphne) have been continuously updated and expanded by the responsible institutions with several ground motion data, and accelerograms have been made available for researchers and engineering practitioners worldwide. This study preferred the use of ground motion records available in PEER's NGA-West Database, and this chapter will present the main seismological features of this database and some distinct characteristics from the intensity perspective.

2.2   The Main Ground Motion Database

The main dataset for this study has been formed employing the accelerograms from the former NGA-West Database, which was also known as PEER Ground Motion Database (PGMD). PGMD was an improved successor of the Design Ground Motion Library software, and the online database was established to facilitate the development of improved attenuation relations as part of the Next Generation Attenuation Models (NGA) project (Power et al., 2008; Chiou et al., 2008).

2.2.1   Major Seismological Features of the Main Set

NGA-West Database contains 3'551 three-component strong-motion records from 173 shallow crustal earthquakes that typically occur in the western part of the United States and in Turkey as well. The set, accordingly, includes several earthquakes with different fault mechanisms, as summarized in Table 2.1.

Table 2.1 Fault mechanism features of the main set

Fault Mechanism	# of record sequences
Not defined	85
Strike-Slip	1004
Normal	91
Reverse	1587
Reverse – Oblique	695
Normal - Oblique	89
Total	3'551

The Moment Magnitude (M_w) range of the seismic events in the database is between 4.27 and 7.90, where this seismological data is missing for an insignificant number of record sequences in the set, as could be observed from the flat file of the PGMD. Similarly, Joyner-Boore Distance (R_{jb}) data is missing for a considerable amount of recordings, whereas the Epicentral Distance (EpiD) data is complete for all of the record sequences. The ranges of R_{jb} and EpiD for the recordings are 0-472.56 km and 0.44-557.63 km, respectively. Figures Figure 2.1 and Figure 2.2 display EpiD-M_w and R_{jb}- M_w marginal plots with distributions, pointing out the dominance of moment magnitudes ~5.90, ~6.20, ~6.30, and ~7.60. Figure 2.3, on the other hand, shows the relation between EpiD and R_{jb} for a reduced number of events where both seismological data are available.
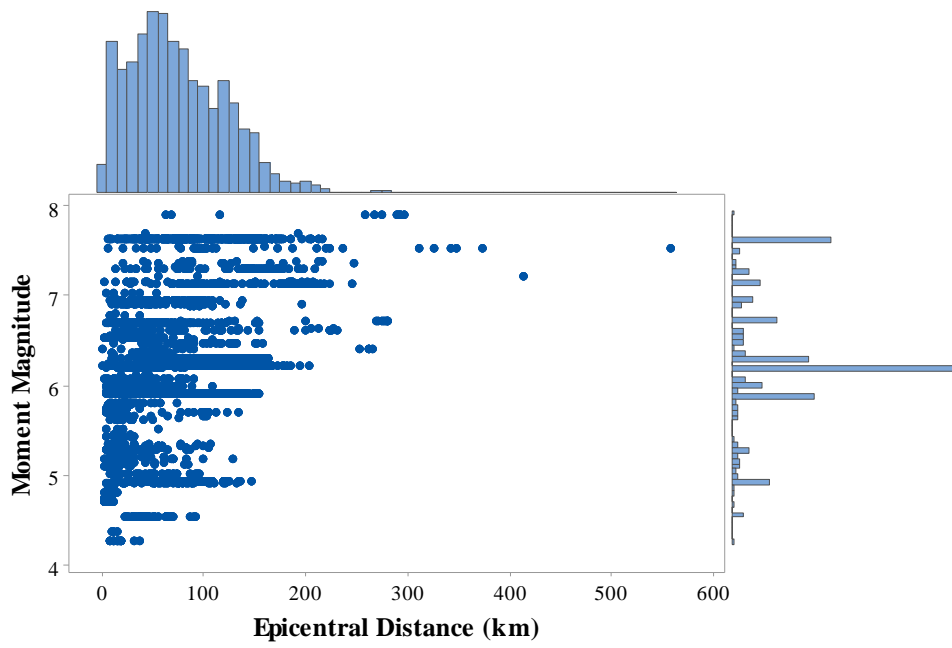
Figure 2.1. Epicentral distance vs moment magnitude distribution
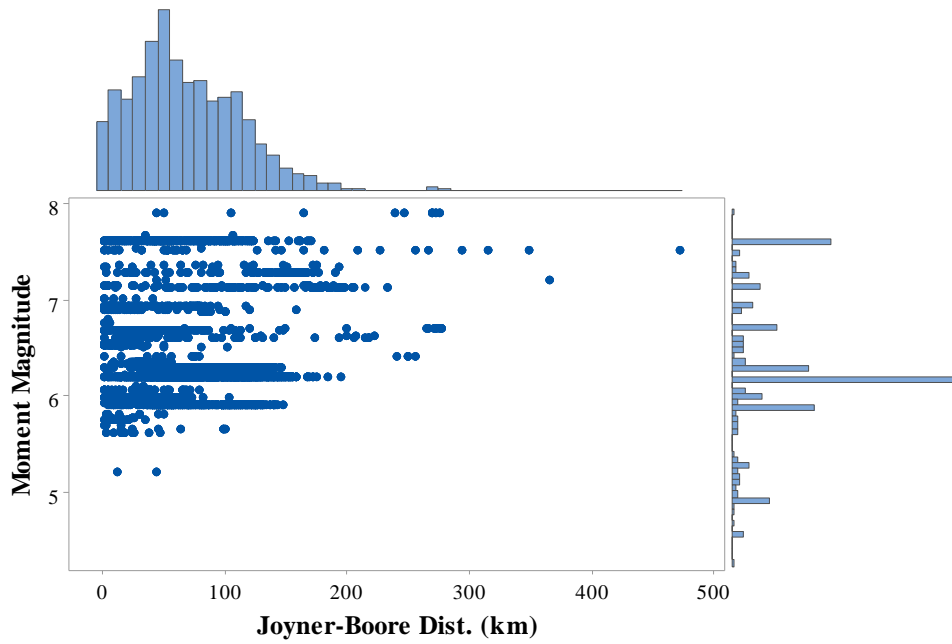
Figure 2.2. Joyner-Boore distance vs moment magnitude distribution
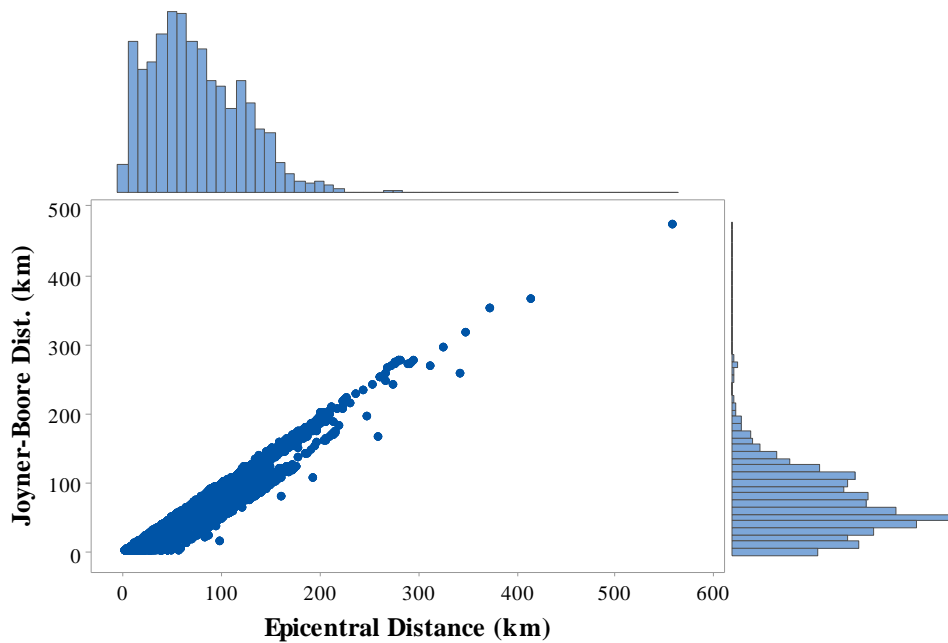
Figure 2.3. Epicentral distance vs Joyner-Boore distance distribution

2.2.2 Intensity Measure-based Features of the Main Set

6'883 horizontal records available from the NGA-West database have been processed via SeismoSignal software to compute the fundamental IMs and to derive the 5% damped elastic acceleration, velocity, and displacement spectra for a period range of 0.02-10.0 seconds. The list of the IMs calculated at this stage is as follows:

- PGA, PGV, PGD, PGV/PGA
- a_{rms}, v_{rms}, d_{rms}
- AI, SED, CAV
- I_C^* (with consideration of total duration of the GM record)
- ASI, ASI^*, VSI, HI
- SMA, SMV
- EDA, EPA, EPV
- A95

- T_p
- T_m
- t_r

In addition to the list above, the following compound IMs are calculated from the computed values:

- I_C (with consideration of significant duration of the GM record)
- I_a, I_v, I_d (with consideration of significant duration of the GM record)
- I_F

To visualize the general characteristics of the main dataset from the intensity measure perspective, histogram plots have been prepared for the above-listed IMs. Figure 2.4 shows two sample cases displaying the statistical distributions for PGA and PGV. The histogram plots for the remaining cases are presented in Figure A.1 thru Figure A.4, which can be found in Appendix.
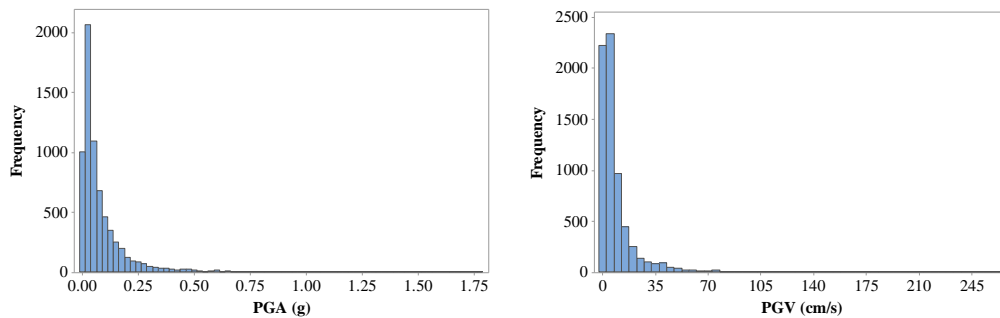
Figure 2.4. Histogram plots for PGA and PGV

The charts generally reveal that the number of records with low seismic intensities outnumber the records of moderate-to-high levels, thus causing skewed distributions. In fact, this is a general problem of the ground motion databases worldwide with the scarcity of large magnitude seismic events. Along with the histogram charts showing the distributions of the available data, scatter diagrams have been prepared to display the relation among a selected group of IMs, namely PGA, PGV, PGV/PGA, ASI, ASI*, VSI, HI, and t_r. Figure 2.5 and Figure 2.6 present the essential cases for PGA and PGV, respectively. The scatter plots show that there are indications of a relationship between the IMs examined, except for PGV/PGA and t_r cases; however, the dispersion increases with increasing levels of seismic intensity as defined with PGA or PGV in these sample figures. The graphical observations herein bring forward the possibility of correlation among the parameters examined, which will be investigated in the next section.

2.3   Correlation Statistics

Any interdependence or association between two or more variable quantities can be expressed as correlation, and the degree of this relationship between the variables can be quantified by correlation metrics. Among various alternatives from the field of Statistics; widely-used, yet simple examples are Pearson's product-moment correlation and Spearman's rank-order correlation (Chen and Popovich, 2002; Garson, 2013).

Pearson's product-moment correlation, as proposed by Karl Pearson, measures the strength of linear interdependence between two continuous variables X and Y. The numerical output for Pearson's correlation coefficient (also known as Pearson's r or ρ) is a value between +1 and −1 inclusive, and shows both the strength and direction of the relationship (Chen and Popovich, 2002). Correspondingly, the direction, expressed with the sign of the numerical value, can be positive, null, or negative, indicating whether the variables increase or decrease together.
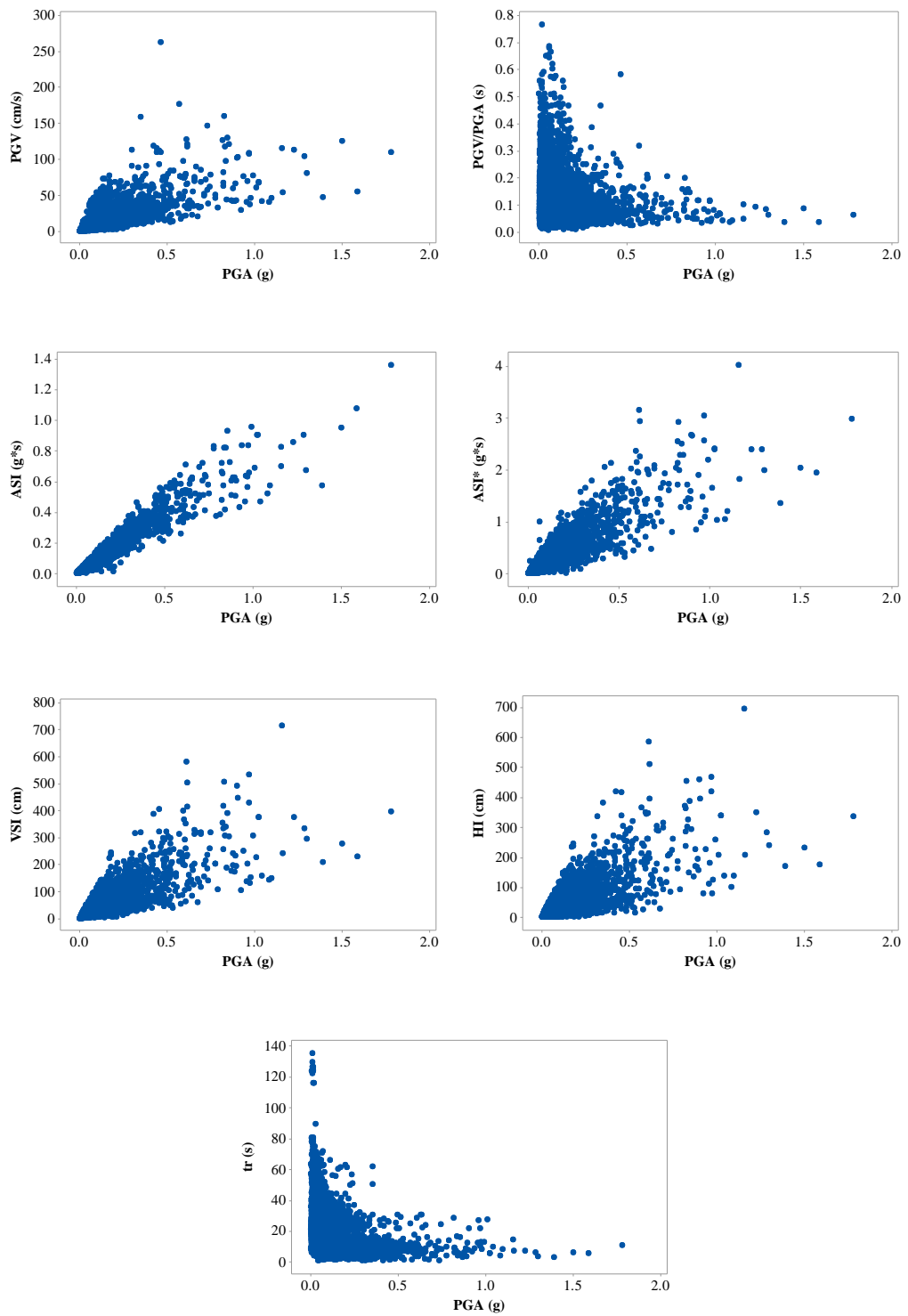
Figure 2.5. Scatter plots for selected IMs against PGA (main set)
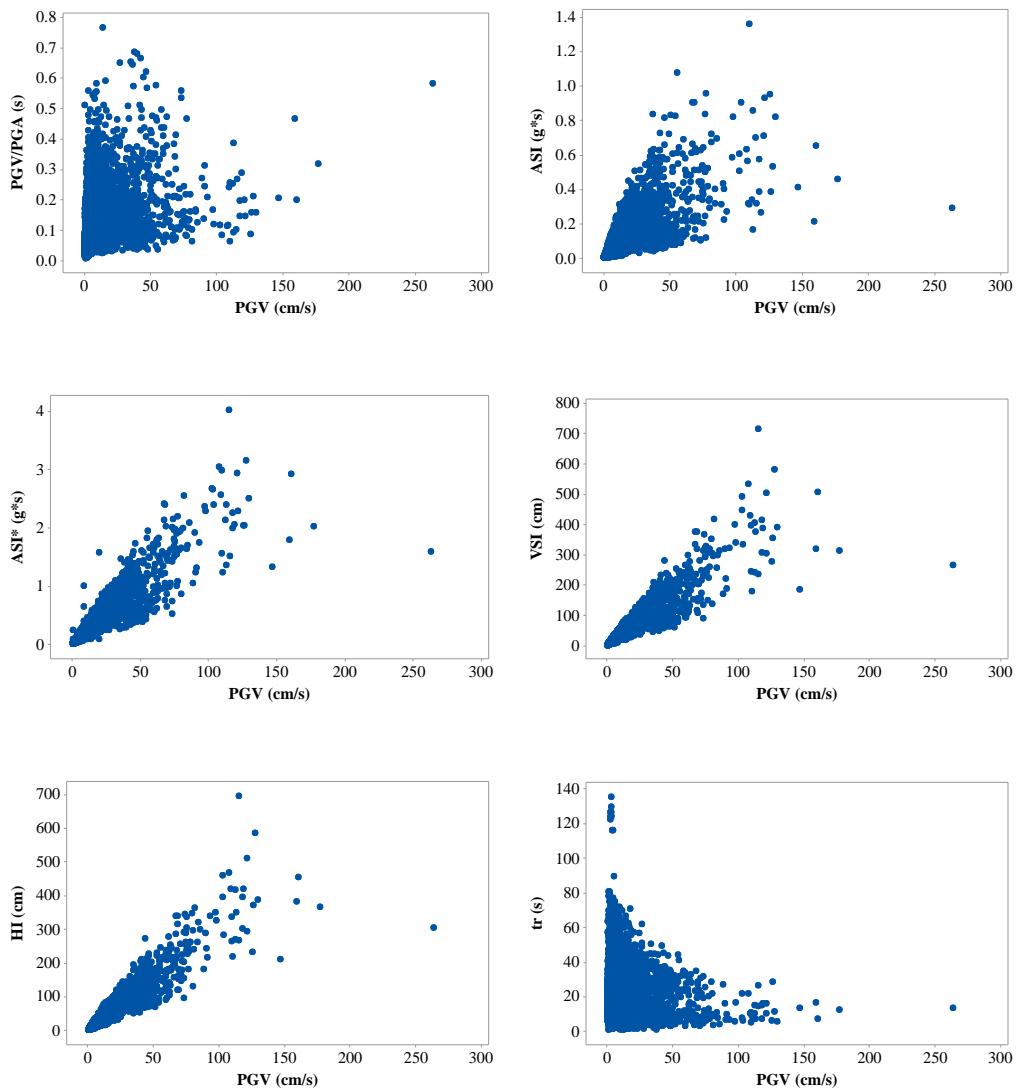
Figure 2.6. Scatter plots for selected IMs against PGV (main set)

Pearson's correlation, although the most commonly used alternative, is a parametric measure and has certain assumptions. The fundamental assumption of Pearson is the pre-acceptance of a linear relationship between the variables. Therefore, Pearson's correlation can not capture the true relationship when there is nonlinear dependence between the variables. The second important issue is the normality assumption which assumes that the continuous random variables are bivariate normal. For cases of non-

normally distributed data, the results have been reported to be quite sensitive (Kowalski, 1972). The third crucial assumption of Pearson's correlation is the constant variance assumption which is also known as homoscedasticity. In statistics, homogeneity of variance is established when all the variables have the same finite variance. On the other hand, when the random variables are heteroscedastic, the variance along the sequence of data variables will not be constant, the estimates of standard errors will be biased, and thus, it is highly possible that the Pearson coefficient will be affected. Figure 2.7 exemplifies the scatter of the data for homoscedastic and heteroscedastic cases.

(a) (b)
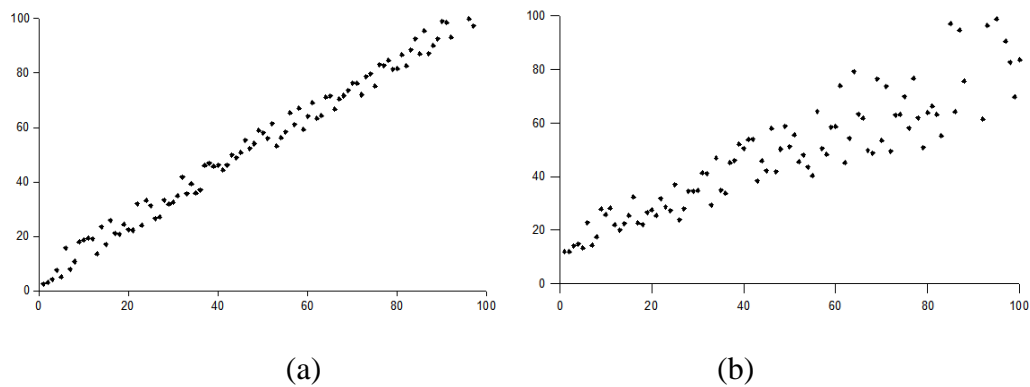
Figure 2.7. Scatter plots exemplifying (a) homoscedasticity and (b) heteroscedasticity (taken from Wikimedia Commons)

The above-mentioned assumptions also constitute the drawbacks of Pearson's correlation. One additional drawback of this correlation index is that the metric is highly sensitive to the strong outliers in the data, and therefore, should be used with care in the presence of outliers.

In contrast to Pearson's product-moment correlation, the alternative correlation index, Spearman's rank-order correlation (also known as Spearman's ρ), is a non-parametric measure and does not assume any distribution for the data in advance (Sriramula et al., 2007). It is suitable for both continuous data and discrete ordinal variables, and assesses the degree of relationship between rankings of two variables

using a monotonic function. Besides, it is much less sensitive to the nature of the data with respect to Pearson's correlation. Figure 2.8 and Figure 2.9 show sample cases with resulting correlation coefficients where two of the aforementioned drawbacks of Pearson's correlation are present.
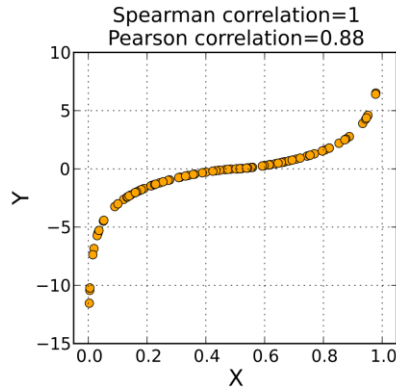
Figure 2.8. Correlations for a sample case when the relationship is nonlinear (taken from Wikimedia Commons)
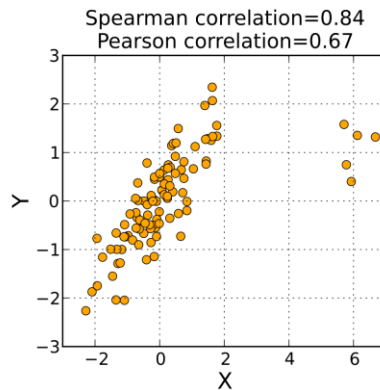
Figure 2.9. Correlations for a sample case when there are outliers in the data (taken from Wikimedia Commons)

The figures reveal that Spearman's correlation has certain advantages over its counterpart, but has gained less interest in the field of earthquake engineering. The general approach in similar research-oriented studies was to utilize Pearson's product-moment correlation, but applying an ln-transformation to the data before conducting the correlation analyses. Such modification is attributed to the fact that

the IMs (and EDPs as well) are log-normally distributed, and shall be transformed before the performance of regression analyses related to the research question (Kramer, 1996; Romao et al., 2011). After the proper application of data transformation, Pearson's correlation coefficient generally improves (i.e., the strength of the dependence increases), whereas Spearman's correlation coefficient remains unchanged, and could be utilized as a validation measure for the widely-used Pearson's metric.

2.4   Inter-correlational Evaluation

As expressed earlier in this chapter, there is a possibility of interdependence among the IMs computed at this stage. The clarification and quantification of such inter-correlations are crucial for the advancement of the study, since this attempt will facilitate the grouping of IMs so that choosing too many intensity parameters from each group for further examinations might be prevented. Consequently, calculation of Pearson and Spearman coefficients among the long list of intensity parameters have been performed, and Table 2.2 and Table 2.3 display the strength of relationship among these measures in terms of Pearson and Spearman metrics, respectively. The cells in both tables are highlighted with dark green color showing perfect correlation, with light green color for correlation values above 0.90 indicating strong correlation, with yellow color for correlation values between 0.50 and 0.90 indicating moderate correlation, with red color for correlation values less than zero implying negative correlation, and remaining cells are left as white color pointing out to weak or insignificant correlation.

Table 2.2 Pearson correlation coefficients for (ln-transformed) selected IMs

IM	PGA	PGV	PGD	PGV/PGA	a_{rms}	v_{rms}	d_{rms}	AI	I_c^*	SED	CAV	ASI	ASI*	VSI	HI	SMA	SMV	EDA	A_{95}	T_p	T_m	t_t	I_c	I_a	I_F	I_v	I_d
PGA	1.000	0.859	0.631	-0.114	0.966	0.778	0.590	0.946	0.959	0.715	0.830	0.980	0.901	0.848	0.790	0.979	0.823	0.992	1.000	-0.132	-0.140	-0.438	0.929	0.983	0.804	0.736	0.558
PGV	0.859	1.000	0.910	0.411	0.896	0.971	0.878	0.944	0.934	0.954	0.932	0.861	0.976	0.981	0.968	0.875	0.983	0.877	0.858	0.221	0.344	-0.095	0.930	0.902	0.991	0.966	0.869
PGD	0.631	0.910	1.000	0.641	0.697	0.943	0.989	0.796	0.768	0.971	0.871	0.641	0.851	0.889	0.916	0.671	0.931	0.657	0.629	0.342	0.562	0.207	0.784	0.720	0.941	0.955	0.993
PGV/PGA	-0.114	0.411	0.641	1.000	0.020	0.499	0.653	0.147	0.105	0.578	0.330	-0.074	0.289	0.393	0.472	-0.045	0.441	-0.065	-0.116	0.664	0.917	0.597	0.151	0.000	0.491	0.563	0.693
a_{rms}	0.966	0.896	0.697	0.020	1.000	0.859	0.674	0.969	0.987	0.783	0.871	0.963	0.934	0.894	0.847	0.971	0.874	0.966	0.965	-0.038	-0.031	-0.372	0.979	0.960	0.851	0.791	0.630
v_{rms}	0.778	0.971	0.943	0.499	0.859	1.000	0.936	0.905	0.895	0.981	0.922	0.789	0.947	0.965	0.971	0.809	0.979	0.801	0.776	0.275	0.453	0.020	0.915	0.838	0.977	0.967	0.915
d_{rms}	0.590	0.878	0.989	0.653	0.674	0.936	1.000	0.766	0.740	0.959	0.850	0.604	0.820	0.860	0.894	0.635	0.907	0.617	0.588	0.344	0.577	0.246	0.768	0.684	0.914	0.934	0.987
AI	0.946	0.944	0.796	0.147	0.969	0.905	0.766	1.000	0.997	0.876	0.959	0.949	0.969	0.944	0.912	0.965	0.936	0.951	0.945	0.048	0.097	-0.193	0.986	0.975	0.922	0.885	0.747
I_c^*	0.959	0.934	0.768	0.105	0.987	0.895	0.740	0.997	1.000	0.850	0.936	0.960	0.964	0.934	0.896	0.974	0.922	0.963	0.958	0.019	0.054	-0.255	0.991	0.977	0.904	0.859	0.712
SED	0.715	0.954	0.971	0.578	0.783	0.981	0.959	0.876	0.850	1.000	0.939	0.730	0.921	0.950	0.967	0.755	0.974	0.740	0.712	0.332	0.536	0.166	0.867	0.801	0.979	0.988	0.960
CAV	0.830	0.932	0.871	0.330	0.871	0.922	0.850	0.959	0.936	0.939	1.000	0.845	0.941	0.940	0.933	0.871	0.948	0.842	0.827	0.169	0.285	0.082	0.942	0.907	0.946	0.944	0.853
ASI	0.980	0.861	0.641	-0.074	0.963	0.789	0.604	0.949	0.960	0.730	0.845	1.000	0.914	0.858	0.807	0.976	0.832	0.984	0.979	-0.117	-0.112	-0.398	0.935	0.969	0.811	0.749	0.572
ASI*	0.901	0.976	0.851	0.289	0.934	0.947	0.820	0.969	0.964	0.921	0.941	0.914	1.000	0.990	0.972	0.918	0.966	0.919	0.900	0.173	0.268	-0.149	0.958	0.936	0.960	0.927	0.805
VSI	0.848	0.981	0.889	0.393	0.894	0.965	0.860	0.944	0.934	0.950	0.940	0.858	0.990	1.000	0.992	0.870	0.976	0.869	0.846	0.249	0.377	-0.067	0.933	0.896	0.975	0.954	0.852
HI	0.790	0.968	0.916	0.472	0.847	0.971	0.894	0.912	0.896	0.967	0.933	0.807	0.972	0.992	1.000	0.821	0.974	0.816	0.789	0.295	0.461	0.024	0.904	0.853	0.975	0.965	0.889
SMA	0.979	0.875	0.671	-0.045	0.971	0.809	0.635	0.965	0.974	0.755	0.871	0.976	0.918	0.870	0.821	1.000	0.859	0.974	0.978	-0.103	-0.095	-0.367	0.950	0.975	0.830	0.771	0.605
SMV	0.823	0.983	0.931	0.441	0.874	0.979	0.907	0.936	0.922	0.974	0.948	0.832	0.966	0.976	0.974	0.859	1.000	0.842	0.821	0.246	0.390	-0.014	0.924	0.880	0.984	0.970	0.899
EDA	0.992	0.877	0.657	-0.065	0.966	0.801	0.617	0.951	0.963	0.740	0.842	0.984	0.919	0.869	0.816	0.974	0.842	1.000	0.992	-0.084	-0.088	-0.413	0.934	0.980	0.826	0.761	0.585
A_{95}	1.000	0.858	0.629	-0.116	0.965	0.776	0.588	0.945	0.958	0.712	0.827	0.979	0.900	0.846	0.789	0.978	0.821	0.992	1.000	-0.133	-0.142	-0.441	0.927	0.982	0.803	0.734	0.555
T_p	-0.132	0.221	0.342	0.664	-0.038	0.275	0.344	0.048	0.019	0.332	0.169	-0.117	0.173	0.249	0.295	-0.103	0.246	-0.084	-0.133	1.000	0.710	0.380	0.042	-0.064	0.272	0.318	0.377
T_m	-0.140	0.344	0.562	0.917	-0.031	0.453	0.577	0.097	0.054	0.536	0.285	-0.112	0.268	0.377	0.461	-0.095	0.390	-0.088	-0.142	0.710	1.000	0.629	0.104	-0.021	0.429	0.505	0.620
t_t	-0.438	-0.095	0.207	0.597	-0.372	0.020	0.246	-0.193	-0.255	0.166	0.082	-0.398	-0.149	-0.067	0.024	-0.367	-0.014	-0.413	-0.441	0.380	0.629	1.000	-0.177	-0.265	0.037	0.167	0.322
I_c	0.929	0.930	0.784	0.151	0.979	0.915	0.768	0.986	0.991	0.867	0.942	0.935	0.958	0.933	0.904	0.950	0.924	0.934	0.927	0.042	0.104	-0.177	1.000	0.960	0.910	0.875	0.738
I_a	0.983	0.902	0.720	0.000	0.960	0.838	0.684	0.975	0.977	0.801	0.907	0.969	0.936	0.896	0.853	0.975	0.880	0.980	0.982	-0.064	-0.021	-0.265	0.960	1.000	0.870	0.824	0.664
I_F	0.804	0.991	0.941	0.491	0.851	0.977	0.914	0.922	0.904	0.979	0.946	0.811	0.960	0.975	0.975	0.830	0.984	0.826	0.803	0.272	0.429	0.037	0.910	0.870	1.000	0.991	0.915
I_v	0.736	0.966	0.955	0.563	0.791	0.967	0.934	0.885	0.859	0.988	0.944	0.749	0.927	0.954	0.965	0.771	0.970	0.761	0.734	0.318	0.505	0.167	0.875	0.824	0.991	1.000	0.945
I_d	0.558	0.869	0.993	0.693	0.630	0.915	0.987	0.747	0.712	0.960	0.853	0.572	0.805	0.852	0.889	0.605	0.899	0.585	0.555	0.377	0.620	0.322	0.738	0.664	0.915	0.945	1.000

Table 2.3 Spearman correlation coefficients for selected IMs

IM	PGA	PGV	PGD	PGV/PGA	a_{rms}	v_{rms}	d_{rms}	AI	I_c^*	SED	CAV	ASI	ASI*	VSI	HI	SMA	SMV	EDA	A_{95}	T_p	T_m	t_r	I_c	I_a	I_F	I_v	I_d
PGA	1.000	0.851	0.619	-0.117	0.966	0.770	0.580	0.945	0.959	0.700	0.820	0.980	0.899	0.840	0.783	0.980	0.815	0.993	1.000	-0.129	-0.145	-0.418	0.930	0.983	0.793	0.722	0.546
PGV	0.851	1.000	0.904	0.386	0.888	0.969	0.871	0.941	0.929	0.948	0.928	0.853	0.975	0.980	0.968	0.868	0.982	0.872	0.850	0.208	0.322	-0.069	0.925	0.897	0.990	0.961	0.861
PGD	0.619	0.904	1.000	0.622	0.683	0.942	0.988	0.786	0.755	0.971	0.869	0.627	0.843	0.884	0.914	0.659	0.927	0.645	0.617	0.328	0.551	0.226	0.771	0.708	0.938	0.954	0.992
PGV/PGA	-0.117	0.386	0.622	1.000	0.005	0.472	0.634	0.131	0.088	0.557	0.317	-0.090	0.265	0.376	0.453	-0.053	0.418	-0.075	-0.119	0.647	0.921	0.614	0.127	-0.008	0.469	0.543	0.675
a_{rms}	0.966	0.888	0.683	0.005	1.000	0.847	0.659	0.967	0.986	0.764	0.859	0.962	0.929	0.884	0.836	0.971	0.864	0.967	0.965	-0.043	-0.045	-0.354	0.979	0.959	0.836	0.772	0.614
v_{rms}	0.770	0.969	0.942	0.472	0.847	1.000	0.933	0.898	0.887	0.977	0.917	0.777	0.942	0.962	0.968	0.799	0.977	0.794	0.768	0.258	0.427	0.038	0.907	0.831	0.975	0.962	0.911
d_{rms}	0.580	0.871	0.988	0.634	0.659	0.933	1.000	0.755	0.726	0.958	0.847	0.590	0.810	0.853	0.890	0.623	0.901	0.606	0.577	0.329	0.566	0.260	0.754	0.672	0.910	0.932	0.987
AI	0.945	0.941	0.786	0.131	0.967	0.898	0.755	1.000	0.996	0.864	0.954	0.947	0.971	0.941	0.909	0.964	0.932	0.952	0.943	0.041	0.083	-0.185	0.985	0.975	0.915	0.873	0.734
I_c^*	0.959	0.929	0.755	0.088	0.986	0.887	0.726	0.996	1.000	0.835	0.927	0.960	0.963	0.928	0.890	0.973	0.915	0.965	0.958	0.012	0.038	-0.246	0.991	0.976	0.894	0.843	0.697
SED	0.700	0.948	0.971	0.557	0.764	0.977	0.958	0.864	0.835	1.000	0.937	0.711	0.912	0.945	0.966	0.740	0.970	0.727	0.698	0.317	0.517	0.184	0.851	0.787	0.977	0.987	0.960
CAV	0.820	0.928	0.869	0.317	0.859	0.917	0.847	0.954	0.927	0.937	1.000	0.834	0.939	0.937	0.934	0.862	0.947	0.837	0.818	0.160	0.274	0.076	0.932	0.898	0.943	0.941	0.850
ASI	0.980	0.853	0.627	-0.090	0.962	0.777	0.590	0.947	0.960	0.711	0.834	1.000	0.911	0.849	0.795	0.976	0.822	0.986	0.979	-0.112	-0.134	-0.391	0.935	0.970	0.798	0.731	0.557
ASI*	0.899	0.975	0.843	0.265	0.929	0.942	0.810	0.971	0.963	0.912	0.939	0.911	1.000	0.989	0.969	0.965	0.920	0.920	0.898	0.158	0.236	-0.139	0.956	0.936	0.956	0.920	0.795
VSI	0.840	0.980	0.884	0.376	0.884	0.962	0.853	0.941	0.928	0.945	0.937	0.849	0.989	1.000	0.992	0.975	0.864	0.839	0.839	0.235	0.353	-0.049	0.927	0.891	0.974	0.950	0.846
HI	0.783	0.968	0.914	0.453	0.836	0.968	0.890	0.909	0.890	0.966	0.934	0.795	0.969	0.992	1.000	0.814	0.975	0.810	0.781	0.279	0.433	0.032	0.896	0.848	0.976	0.965	0.886
SMA	0.980	0.868	0.659	-0.053	0.971	0.799	0.623	0.964	0.973	0.740	0.862	0.976	0.965	0.975	0.814	1.000	0.850	0.977	0.980	-0.099	-0.102	-0.363	0.950	0.976	0.818	0.756	0.592
SMV	0.815	0.982	0.927	0.418	0.864	0.977	0.901	0.932	0.915	0.970	0.947	0.822	0.920	0.864	0.975	0.850	1.000	0.837	0.813	0.233	0.368	-0.001	0.917	0.874	0.984	0.967	0.893
EDA	0.993	0.872	0.645	-0.075	0.967	0.794	0.606	0.952	0.965	0.727	0.837	0.986	0.920	0.839	0.810	0.977	0.837	1.000	0.993	-0.086	-0.103	-0.393	0.938	0.983	0.817	0.748	0.574
A_{95}	1.000	0.850	0.617	-0.119	0.965	0.768	0.577	0.943	0.958	0.698	0.818	0.979	0.898	0.839	0.781	0.980	0.813	0.993	1.000	-0.129	-0.147	-0.421	0.929	0.983	0.791	0.720	0.544
T_p	-0.129	0.208	0.328	0.647	-0.043	0.258	0.329	0.041	0.012	0.317	0.160	-0.112	0.158	0.235	0.279	-0.099	0.233	-0.086	-0.129	1.000	0.690	0.377	0.031	-0.064	0.259	0.304	0.361
T_m	-0.145	0.322	0.551	0.921	-0.045	0.427	0.566	0.083	0.038	0.517	0.274	-0.134	0.236	0.353	0.433	-0.102	0.368	-0.103	-0.147	0.690	1.000	0.646	0.081	-0.032	0.409	0.488	0.610
t_r	-0.418	-0.069	0.226	0.614	-0.354	0.038	0.260	-0.185	-0.246	0.184	0.076	-0.391	-0.139	-0.049	0.032	-0.363	-0.001	-0.393	-0.421	0.377	0.646	1.000	-0.182	-0.265	0.055	0.176	0.331
I_c	0.930	0.925	0.771	0.127	0.979	0.907	0.754	0.985	0.991	0.851	0.932	0.935	0.956	0.927	0.896	0.950	0.917	0.938	0.929	0.031	0.081	-0.182	1.000	0.959	0.900	0.859	0.721
I_a	0.983	0.897	0.708	-0.008	0.959	0.831	0.672	0.975	0.976	0.787	0.898	0.970	0.936	0.891	0.848	0.976	0.874	0.983	0.983	-0.064	-0.032	-0.265	0.959	1.000	0.861	0.810	0.651
I_F	0.793	0.990	0.938	0.469	0.836	0.975	0.910	0.915	0.894	0.977	0.943	0.798	0.956	0.974	0.976	0.818	0.984	0.817	0.791	0.259	0.409	0.055	0.900	0.861	1.000	0.990	0.911
I_v	0.722	0.961	0.954	0.543	0.772	0.962	0.932	0.873	0.843	0.987	0.941	0.731	0.920	0.950	0.965	0.756	0.967	0.748	0.720	0.304	0.488	0.176	0.859	0.810	0.990	1.000	0.943
I_d	0.546	0.861	0.992	0.675	0.614	0.911	0.987	0.734	0.697	0.960	0.850	0.557	0.795	0.846	0.886	0.592	0.893	0.574	0.544	0.361	0.610	0.331	0.721	0.651	0.911	0.943	1.000

When the acceleration-related parameters are examined, PGA, a_{rms}, AI, I_C^*, ASI, ASI*, SMA, EDA, A_{95}, I_C, I_a show a strong correlation among themselves, whereas these parameters show moderate correlation with velocity- and displacement-related intensity measures. However, the degree of correlation between acceleration- and displacement-related indices is lower with respect to acceleration- versus velocity-related parameters, as expected. As a general observation, acceleration-related, velocity-related, and displacement-related IMs correlate better among their own classes.

The PGV/PGA ratio display generally weak forms of both negative and positive correlation with acceleration- and velocity-related parameters, whereas it shows moderate correlation with the pulse period T_p, the duration related parameter, and t_r, I_v, I_d, and strong correlation with the mean period T_m.

The pulse period T_p, the mean period T_m generally show weak forms of both positive and negative correlations with the remaining IM set. In contrast, the duration-related parameter t_r mostly shows a negative correlation with the IMs other than T_p and T_m, yet the coefficient values remain below 0.5 level. Thus, it can be emphasized that significant duration or specific GM period-related parameters do not have a significant correlation with other GM intensity indices.

The numerical results displaying the inter-correlational characteristics between the IMs are aligned with the outcomes of previous studies (Elenas, 2000; Riddell, 2007; Yakut and Yılmaz, 2008). However, the values reported here are generally higher than the results of companion studies, which is attributed to the presence of a large number of GM records with low intensity levels in the main ground motion database employed.

Finally, considering Pearson and Spearman correlation coefficients calculated for each IM_i - IM_j case, it can be expressed that the results are generally compatible, supporting the ln-transformation approach before the calculation of Pearson coefficients.

CHAPTER 3

STRUCTURAL MODEL DATABASE

3.1 Introduction

This chapter presents the structural models utilized throughout the research study to primarily evaluate the correlation performance of alternative intensity measures (IMs) with selected engineering demand parameters (EDPs) essential for building structures. The following sections give general information about the building models employed, explains their mathematical modelling details, and summarizes their structural characteristics.

3.2 Description of Structural Systems Utilized

This study inherits a collection of seven reinforced concrete frames from a former study, Kadaş (2006), where the structural model set was intended to cover short-to-relatively long-period range in terms of the fundamental mode characteristic. This set contains low- to mid-rise two-dimensional (2D) moment-resisting frames (MRFs) possessing different number of stories and bays, which yields their building id's as follows:

- F2S2B is a two-story-two-bay MRF from a California-based building that complies with the requirements of Uniform Building Code-1982 (ICBO, 1982),
- F2S2B2 is another two-story-two-bay MRF obtained from an existing building located in the city of Bursa in Turkey,

- F3S2B is a three-story-two-bay MRF from an existing structure located in Bursa-Turkey,

- F5S2B is a five-story-two-bay MRF from an existing building located in Bursa-Turkey,

- F5S4B is a five-story-four-bay MRF from a California-based building complying with the requirements of Uniform Building Code-1982,

- F5S7B is a five-story-seven-bay MRF obtained from an existing structure located in Bursa-Turkey,

- F8S3B is an eight-story-three-bay MRF obtained from a Uniform Building Code-1982 compatible building located in California.

The general geometrical properties of the frames employed are displayed in Figure 3.1, and the total weight-height properties of the systems are summarized in Table 3.1, accordingly. The reader is referred to the former manuscript, Kadaş (2006), for further information regarding the structural properties of the frames utilized.

Table 3.1 Total weight and height of the selected frames (Kadaş, 2006)

Frame	Total Weight (kN)	Total Height (m)
F2S2B	2700.25	7.92
F2S2B2	1350.13	6.00
F3S2B	2221.76	9.00
F5S2B	2552.33	15.00
F5S4B	9879.85	19.81
F5S7B	7545.07	14.20
F8S3B	17815.65	31.70

3.3   Mathematical Modelling of Frames

Two-dimensional multi-degree-of-freedom (MDOF) representations of the employed MRFs were originally created in the well-known OpenSees (McKenna et al., 2000) software framework. The fundamental reason for utilizing this open-source analysis platform was to facilitate the performance of several simulation-based analyses with a reliable modelling and analysis code suite.

In the mathematical models of the structural systems, the load-carrying structural elements (i.e., beams and columns) of the selected frames were defined with force-based *nonlinearBeamColumn* elements allowing for distributed plasticity via fiber sections with nonlinear constitutive models. *Concrete01* uniaxial material type was chosen for the unconfined and confined concrete zones of the sections with parameters corresponding to individual frame cases. The reinforcing bars, on the other hand, were defined with *Steel01* uniaxial material type.

Selected uniaxial material types, as illustrated in Figure 3.2, seem to be the simplest alternatives among various constitutive definitions available in OpenSees; however, these material definitions generally lead to sufficiently reliable numerical results in simulations from the perspective of engineering practice. Eventually, they have been preferred within the scope of this study with a modification; consideration of steel rebar rupture via *MinMax* uniaxial material modifier definition, which influences sectional, elemental and global capacities, correspondingly.

The structural elements of the frames were not assigned any distributed mass, but the seismic masses due to dead and 25% of live loads were lumped to the mass center of each story, and applied accordingly. Rigid diaphragm action and second-order effects were not considered in the models. Concerning the viscous damping of the structural system under seismic excitations, the damping phenomenon was represented using Rayleigh Damping, assuming a 5% damping ratio and stiffness proportional damping. Mass proportional damping, however, was neglected due to its insignificant effect, especially in the nonlinear response range.
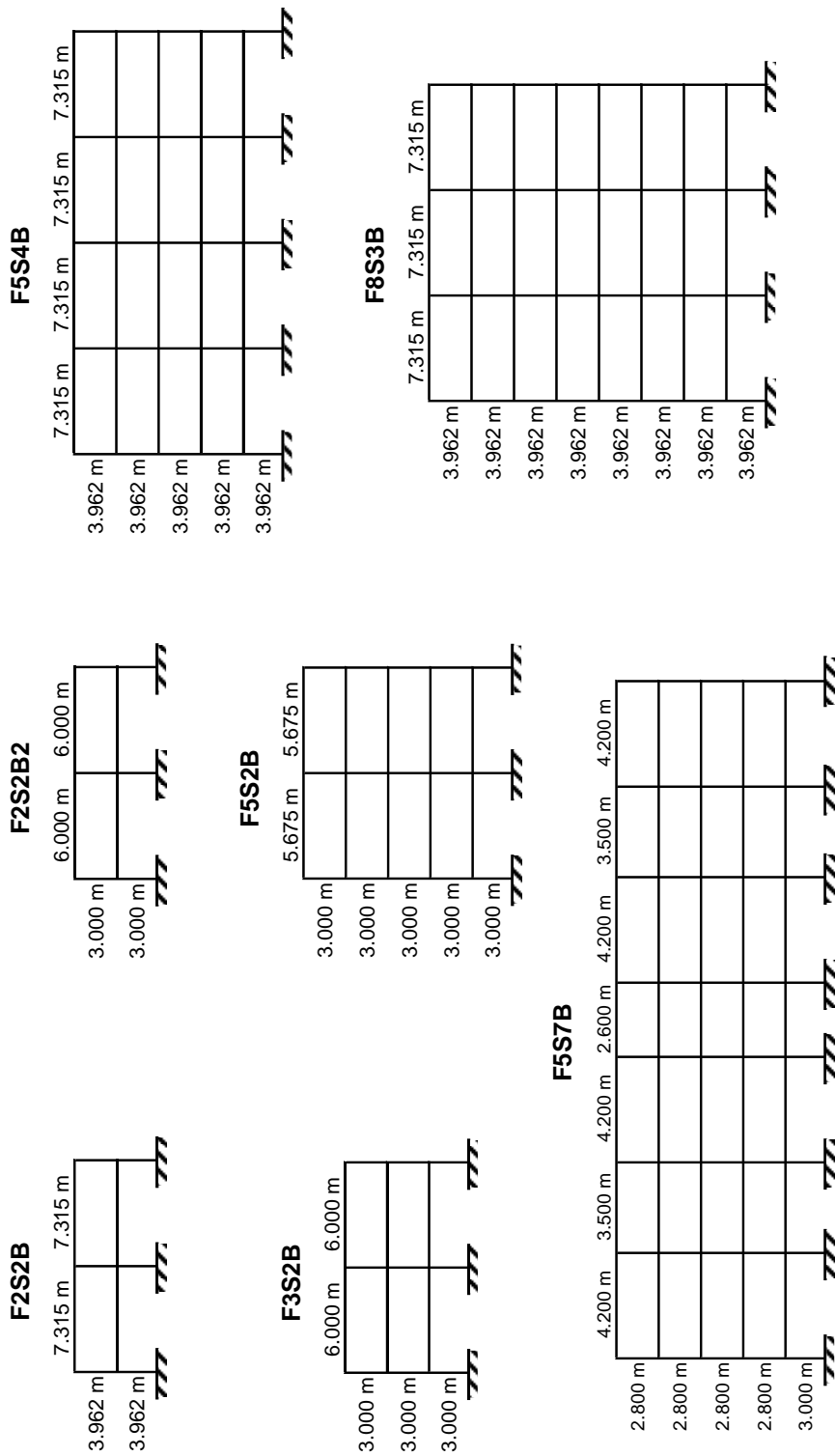
Figure 3.1. General properties of selected frames (taken from Kadaş, 2006)

Stress

Strain

ε_{cu} ε_{c0}

σ_{cu}

σ_c

$2*\varepsilon_{c0}/\sigma_c$
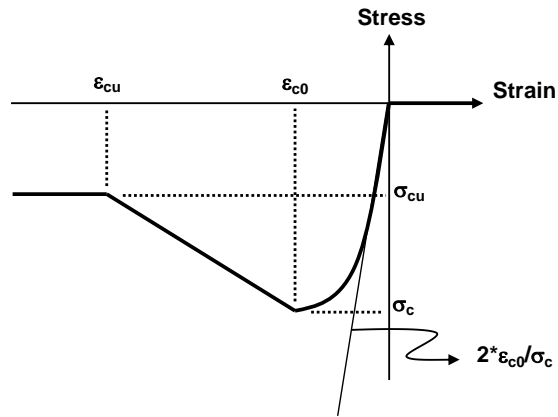
Concrete01 material

Stress

σ_y

E_0

$\$b*E_0$

Strain

$-\sigma_y$
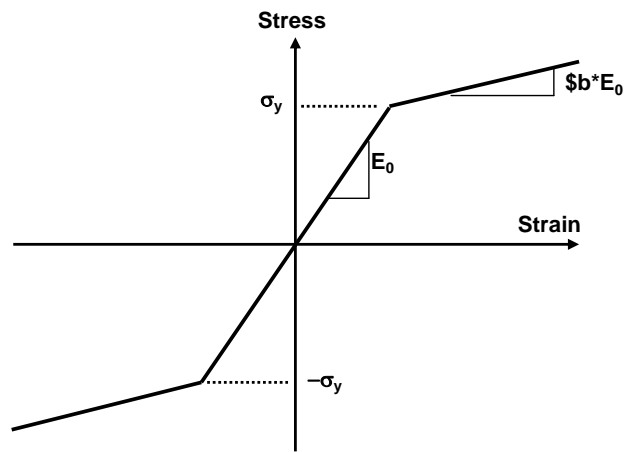
Steel01 material

Figure 3.2. Concrete01 and Steel01 material models (Kadaş, 2006)

3.4 Description of Analyses Performed on the Structural Systems

Throughout the study, three different analysis types have been performed on the mathematical models, which are briefly described in the previous section:

(i) Eigenvalue analysis

(ii) Nonlinear static analysis

(iii)   Nonlinear time history analysis

Eigenvalue analysis was used to determine the dynamic characteristics of the frames and was performed after an initial static analysis under gravity loads. Considering the modal properties, which are summarized in Table 3.2, it can be expressed that the selected MRF frames cover short-to-relatively long period range in terms of the fundamental period of the systems, and the structures generally vibrate predominantly in their first modes.

Table 3.2 Dynamic characteristics of selected frames (Kadaş, 2006)

FRAME	Total Mass (t)	Fundamental Period T_1 (s)	Modal Participation Factor (Γ_1)	Modal Mass Factor (α_1)
F2S2B	275.3	0.59	1.339	0.814
F2S2B2	137.6	0.30	1.339	0.815
F3S2B	226.5	0.45	1.416	0.768
F5S2B	260.2	0.75	1.293	0.794
F5S4B	1007.1	0.95	1.362	0.776
F5S7B	769.1	0.66	1.285	0.804
F8S3B	1816.1	1.20	1.430	0.705

The second analysis type, nonlinear static analysis, was used to reveal the global lateral behavior of the MRF frames. Generally applied in the form of a pushover analysis by the engineering profession, this simplified nonlinear analysis technique considers variant or invariant lateral load patterns, and roughly yields an estimate of the lateral strength capacity of the structural system beyond the elastic range (Oğuz, 2005; Kadaş, 2006). Among alternative invariant lateral load patterns such as Uniform, Triangular, Elastic First Mode; it was previously evaluated in Kadaş (2006) that Elastic First Mode based invariant load pattern is practical and sufficient to derive the capacity curves of the frames utilized herein. Even though there exist relevant studies criticizing the drawbacks of pushover analyses with invariant load

patterns and/or proposing relatively improved but more complex methodologies (Chopra and Goel, 2002; Antoniou and Pinho, 2004a; Antoniou and Pinho, 2004b; Hernandez-Montes et al., 2004; Goel and Chopra, 2005; Papanikolaou et al., 2005; Papanikolaou et al., 2006), these approaches are not followed within the scope of this study to preserve the practicality from professional engineers' perspective, and Elastic First Mode based lateral load pattern was considered in the nonlinear static analyses of the frames which were performed after the initial static analysis under gravity loads. This approach is thought to be suitable considering the first-mode dominant characteristics of the frame set. Subjected to increasing lateral load profile with a displacement controlled nonlinear static analysis option, the frames have been pushed laterally until the frames lose their lateral strength more than 15% of their ultimate strength, and capacity curves (i.e., top displacement vs. base shear force data) have been re-obtained due to the modelling modification made on the original frames of Kadaş (2006). The resulting capacity curves will be presented in the following section with their bi-linearized equivalents (please refer to Figure 3.5-Figure 3.7); however, the height-wise inter-story drift profiles at specific global drift levels are presented next in Figure 3.3. As stated in Kadaş (2006), the drift profiles at various global drift levels are coherent with the general expectations that low-rise frames exhibit almost a uniform drift distribution, whereas mid-rise systems yield maximum inter-story drift ratio at the second story level. Besides, relatively high-rise systems yield maximum inter-story drift ratio at middle stories. These trends in the drift profiles turned out to be preserved for high global drift levels as well.

The last analysis type applied to the selected frames is the nonlinear time history analysis (NLTHA). This analysis approach is generally appraised as the most advanced method in the engineering and research community struggling with numerical simulations of any structural system. Combined with carefully defined advanced constitutive models and structural element modelling details, the numerical analysis results obtained under specific strong-motion acceleration records are considered as 'true responses' of the structural system subjected to those specific events. However, it is apparent that the computational cost for performing

nonlinear time history (NTH) analyses on MDOF models is generally very high, and the results might be very sensitive to the ground motions complicating the evaluation-decision process for the analyst. Consequently, engineering practice eventually either favors the use of nonlinear static procedure as opposed to NTH, or tries to utilize simplified equivalent versions of the complex MDOF systems to make an estimation of the 'true response' with some accuracy trade-off. In the performance of NTH analyses, 2D MDOF systems have been subjected to gravity loads first, analyzed with a nonlinear static analysis approach, and afterwards, transient analyses have been performed for individual ground motion records using Newmark's time integration method. Throughout the analyses, element forces, nodal displacements, and story drifts have been recorded, and these outputs have been considered as 'true response' from the simulations conducted. As stated in Kadaş (2006) as well, parameters defining convergence criteria and result tolerances have been carefully defined to obtain accurate numerical results and to keep the non-converging analyses as few in the overall simulation set as possible. However, there exist peculiar cases for relatively weak frames from which reliable results could not be attained. The results from converging NTH analyses have been processed to obtain the corresponding absolute maximum values in terms of top displacement 'TD', inter-story drift ratio 'MIDR', and base shear 'BS'.

The planar frames utilized herein are relatively simple models with respect to more complex 3D MDOF models; consequently, these structural models could be preferably further simplified into equivalent single-degree-of-freedom (ESDOF) systems to accelerate NLTHA-based assessments. This study considers results from these simple models as well during evaluations, and the next section will describe the formation of these simple models from the capacity curves previously derived.
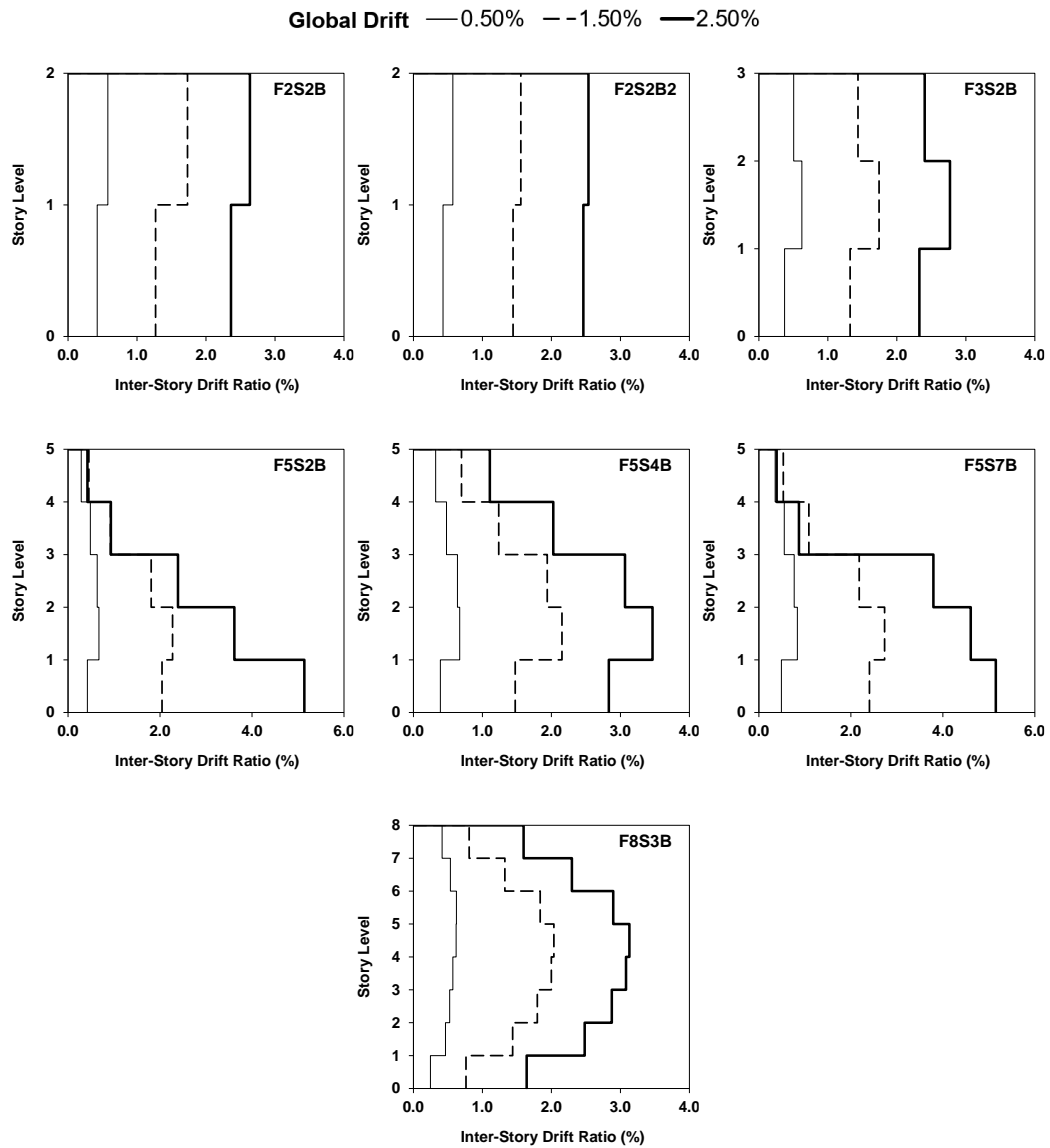
Figure 3.3. Inter-story drift profiles at various global drift levels

3.5   Equivalent SDOF Systems

Nonlinear static analysis methods, Capacity Spectrum Method (ATC-40, 1996) and Displacement Coefficient Method (FEMA-356, 2000), have been employed by the earthquake engineering community for long while to determine the seismic displacement demand of structures, and resulting element-based forces and deformations at the estimated target displacements. Both approaches basically rely

on an idealized form of the pushover curve of the structural system under consideration and have also led to the development and utilization of simplified equivalent systems in the form of SDOF systems. Although there are no strict rules on how to define an idealized version of a capacity curve, there exist several approaches in the literature, yet remained as recommendations. Kadaş (2006) investigated four alternatives of available idealization methods (i.e., MULTI-linear, ATC, FEMA, and 75%V_y), and recommended the use of the FEMA approach for conservative ESDOF-based results with small dispersion.

In this approach, the capacity curve is bi-linearized, and the elastic part of the idealized curve and the yield point (i.e., yield displacement) is defined with an iterative procedure to satisfy the following two criteria as depicted in Figure 3.4:

- The areas under the original curve and the idealized curve must be approximately equal,
- The elastic segment of the idealized curve must intersect the original pushover curve at a strength level approximately 60% of the resulting yield base shear.
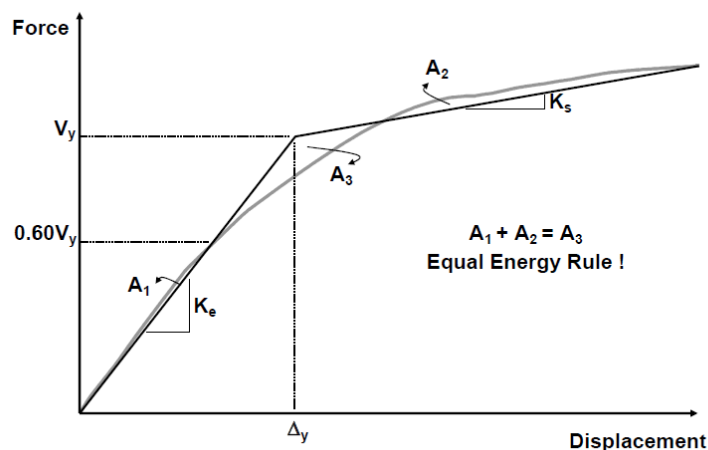
Figure 3.4. FEMA bi-linearization method (Kadaş, 2006)

50

The ultimate displacement of the idealized curve normally should be defined as the estimated/resulting target displacement under a specific seismic hazard event, thus implicitly satisfying the equal energy rule via the equal-area rule. However, this approach is not practical to follow while utilizing the idealized capacity curve for repetitive evaluations under various hazard levels. Consequently, the ultimate point is generally considered as the displacement where the lateral strength of the system reduces by 15% from the maximum base shear. Based on these concepts, the capacity curves obtained from the nonlinear static analyses described in the previous section have been idealized, and the resulting idealizations are displayed in Figure 3.5-Figure 3.7, along with the original pushover curves.

As the next step, these FEMA-based bi-linearized force-displacement relationships have been converted to the force-displacement relationships of ESDOF systems following the method presented in ATC-40. The reader can refer to Kadaş (2006) for a detailed explanation of the calculation steps. The dynamic characteristics of the ESDOF systems obtained from the simplification of the structural models with this approach are summarized in Table 3.3.

Table 3.3 Properties of the ESDOF systems

Frame	T_{eff} (s)	Sa_y (g)	Sd_y (m)	F_y (kN)	M* (t)	K* (kN/m)	α (%)
F2S2B	0.710	0.526	0.066	1155.9	224.0	17556.7	0.20
F2S2B2	0.356	1.179	0.037	1297.3	112.2	34975.6	0.06
F3S2B	0.544	0.708	0.052	1207.4	174.0	23215.4	3.28
F5S2B	0.881	0.375	0.072	759.4	206.5	10500.0	0.03
F5S4B	1.046	0.436	0.119	3342.6	781.7	28184.0	0.42
F5S7B	0.785	0.482	0.074	2926.3	618.6	39656.7	0.14
F8S3B	1.392	0.306	0.147	3844.2	1281.1	26109.3	0.49
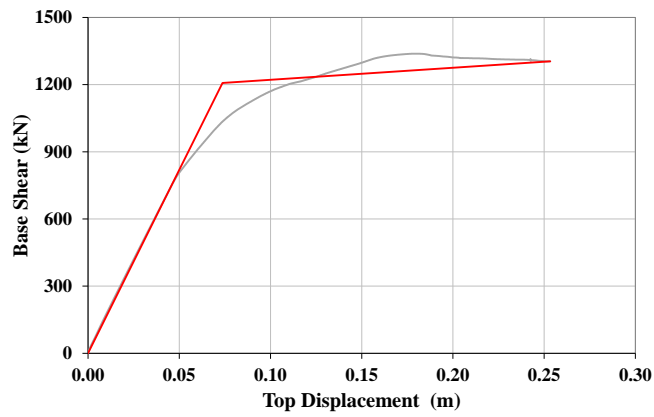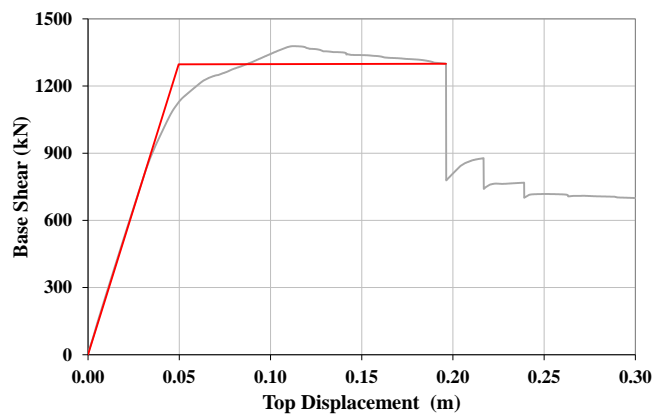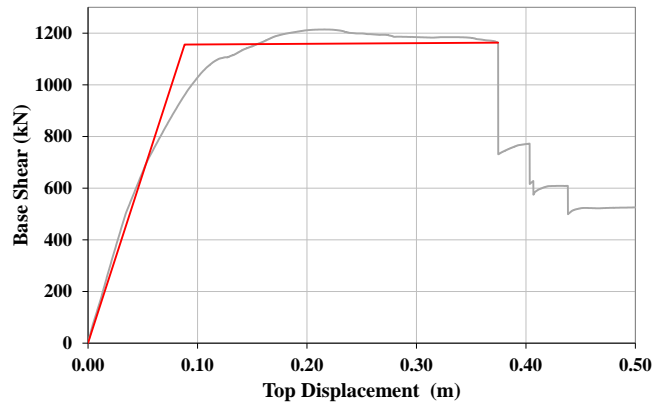
Figure 3.5. Capacity curves for F2S2B, F2S2B2, F3S2B and their bi-linear equivalents
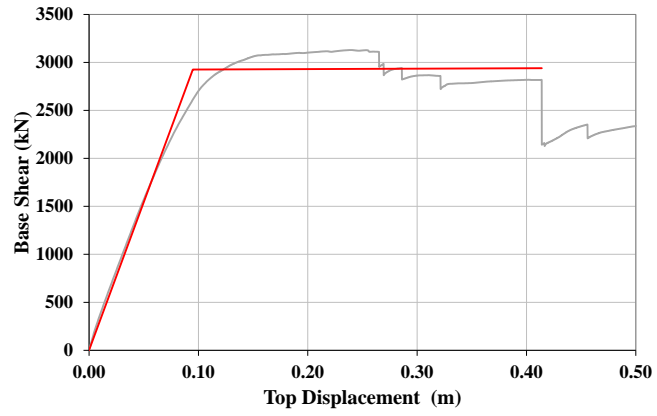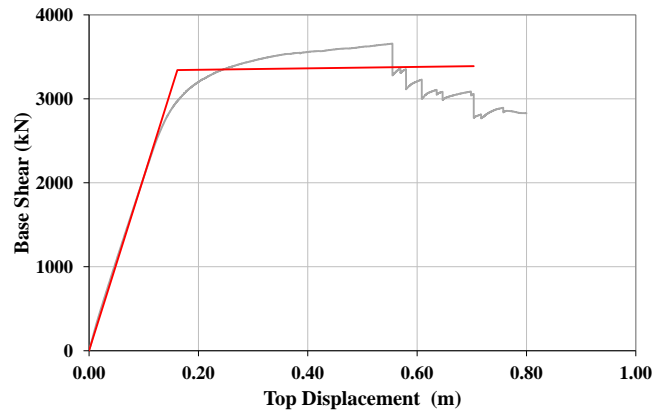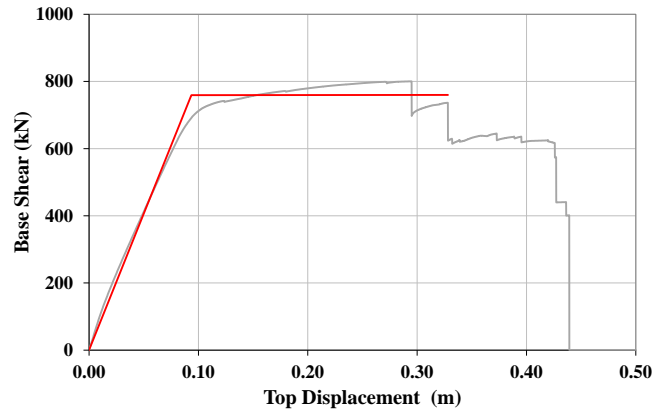
Figure 3.6. Capacity curves for F5S2B, F5S4B, F5S7B and their bi-linear equivalents

53
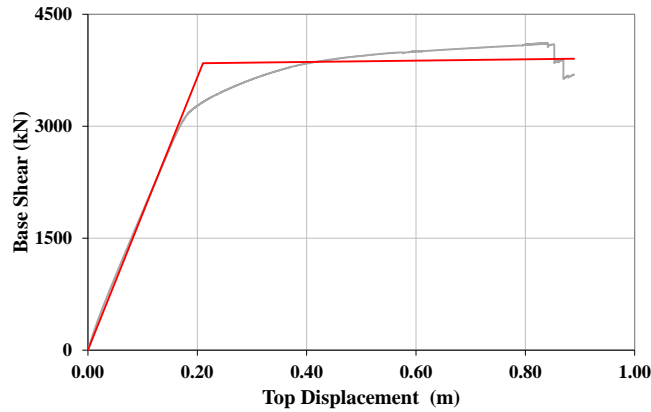
Figure 3.7. Capacity curve for F8S3B and its bi-linear equivalent

3.6   Assumed Performance Level Limits

The peak responses from NTH analyses of MDOF or ESDOF systems are generally utilized to determine the local (i.e., at the element or section level) or global damage states where the damage levels of the structures are differentiated via defined limit states (Ay, 2006; Mazılıgüney, 2020). This study considers three performance limit states; Immediate Occupancy (IO), Collapse Prevention (CP), and Life Safety (LS), as reference points to track the distribution of the EDPs in the entire response range. On the basis of bi-linearized capacity curves of the employed frames, the limit for each performance level has been determined at the global level, i.e., considering top drift as the basis, and has been considered as invariable. For each frame, the limit for Immediate Occupancy (IO) performance level has been defined at the yield displacement of the system along, while the Collapse Prevention (CP) performance limit has been defined at the (nonlinear static analysis-based) collapse displacement of the system. The limit for Life Safety (LS) performance level has been assumed as three-quarters of the collapse displacement (i.e., CP limit). The inter-story drift ratio limits for these performance levels have been taken as the average inter-story drift ratios at respective top drifts (i.e., global drift ratios). The displacements and drift

ratios corresponding to the assumed performance level limits are summarized in Table 3.4.

Table 3.4 Top drift and drift ratio values corresponding to assumed performance limits of the frames

FRAME	TD-IO (m)	TD-LS (m)	TD-CP (m)	IDR-IO	IDR-LS	IDR-CP
F2S2B	0.088	0.281	0.375	1.1%	3.5%	4.7%
F2S2B2	0.050	0.147	0.196	0.8%	2.5%	3.3%
F3S2B	0.074	0.190	0.253	0.8%	2.1%	2.8%
F5S2B	0.094	0.246	0.328	0.6%	1.6%	2.2%
F5S4B	0.162	0.528	0.704	0.8%	2.7%	3.6%
F5S7B	0.095	0.311	0.414	0.7%	2.2%	2.9%
F8S3B	0.211	0.667	0.889	0.7%	2.1%	2.8%

CHAPTER 4

EVALUATION OF EFFICIENCY OF INTENSITY MEASURES BASED ON SINGLE-DEGREE-OF-FREEDOM SYSTEMS

4.1   Introduction

This chapter presents the methodology regarding the evaluation of a preliminary list of intensity measures in terms of the "efficiency" criterion from the single-degree-of-freedom (SDOF) system-based perspective. The performance of the selected IMs for various strength, ductility, and yield base shear coefficient levels has been displayed, and key findings are discussed to pre-select a manageable group of parameters for future stages of the research study.

4.2   Description of Generic Structural Systems and Analysis Approach

The endeavor to relate certain characteristics of a GM record to resulting structural responses directs any researcher to employ a suit of strong-motion records and a couple of structural systems in their simulation-based study. Starting with a very large GM record set, it becomes quite cumbersome for the analyst to utilize advanced 3D structural models if the instant goal is to make a general inference over the subject. Giving preference to simple structural forms (i.e., single-degree-of-freedom systems indeed) brings in practicality eventually, and assists in performing simulations and drawing conclusions relatively quickly. This simple approach has been undertaken by various studies (Miranda, 2001; Chopra and Chintanapakdee, 2004; Akkar and Özen, 2005) and has been shown to yield sufficiently accurate results for ordinary systems predominantly oscillating in their fundamental mode of vibration (Kadaş, 2006; Ozmen and Inel, 2016).

This study, with the principal aim of identifying the most "efficient" IM(s), follows this simple approach initially and utilizes generic single-degree-of-freedom (SDOF) systems (Figure 4.1) to reveal the general relationship between some fundamental intensity indices and seismic demands. SA4NOR analysis engine of USDP (2008) software was used to form various single mass-spring systems demonstrating different period, strength, ductility, and yield base shear coefficient characteristics:

- A total of 44 individual periods ranging between 0.02 and 4.00 sec (i.e., T=0.02, 0.04, 0.06, 0.08, 0.1, 0.2, ..., 4.0 s) has been considered to examine the period-wise variation of the results.

- Totally, 6 strength reduction (R) factor levels (i.e., R=1, 2, 3, 4, 6, 8) and 6 ductility (μ) levels (i.e., μ=1, 2, 3, 4, 6, 8) has been considered to investigate the variation of the results with respect to strength and ductility levels. Additionally, 5 different yield base shear coefficient ($\eta = F_y/W$) levels (i.e., η=0.05, 0.10, 0.15, 0.20, 0.25) have been examined to supplement the evaluations.
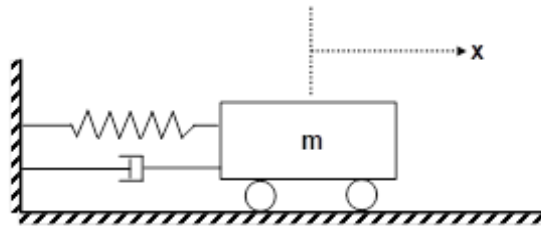
Figure 4.1. A typical representation of an SDOF system

For the force-deformation definition of generic SDOF systems, two distinct hysteresis cases, namely elastic-perfectly-plastic (i.e., α=0%) and bi-linear hardening (i.e., α=5%) hysteresis models, have been considered (Figure 4.2). Despite the availability of more advanced models incorporating stiffness/strength degradation and/or pinching behavior (such as Takeda, Clough, or Modified Clough), the

58

hysteresis definitions were limited to the most basic alternatives in order to keep the focus on general variation of the results with different period, strength and ductility cases neglecting further complexities introduced by the advanced models.

(a) Elastic-perfectly-plastic case   (b) Bi-linear hardening case
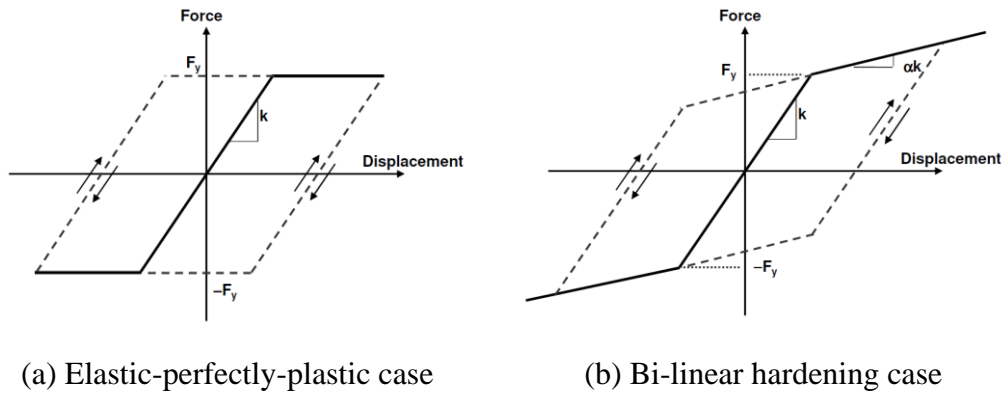
Figure 4.2. Typical representations of (a) elastic-perfectly-plastic and (b) bi-linear hardening hysteresis models

Each SDOF model (with a damping ratio of $\xi=5\%$) has been employed to conduct nonlinear time history analyses under the full set of 6'883 GM records that are available in the main dataset, and drift response of the system has been recorded to extract the peak demand from the transient motion. Engineering demand parameters (EDPs) such as residual values or energy-related outputs are not considered within the scope of the study due to the fact that the peak drift-based responses of SDOF systems are the most essential damage indicators of simple equivalents of ordinary systems.

4.3   Evaluation and Discussion of Results

Extracting peak responses from nearly 10 million SDOF-based analyses, the numerical computations continued with the calculation of Pearson and Spearman correlation coefficient for each period and for specific R, μ and η cases to reveal the

degree of relationship between the displacement demands and a selected list of intensity parameters. The long list contains PGA, PGV, PGD, PGV/PGA, a_{rms}, v_{rms}, d_{rms}, AI, I_C^*, SED, CAV, ASI, VSI, HI, SMA, SMV, EDA, A_{95}, T_p, T_m, t_r, I_C, I_a, I_F, I_v, I_d, ASI^*, EPA, EPV, S_a, S_v, S_d, and were previously computed as a part of Chapter 2. Discarding the Spearman-based approach, the Pearson coefficients were calculated upon ln-transformed values of both demands and intensity indices, where the reason for such transformation is already discussed in Chapter 2. Since both coefficients are inherently related to the dispersion in the data variables, they have been utilized to visualize the variation in the degree of dispersion with respect to the aforementioned aspects; and consequently, both assisted in screening candidate IMs according to the "efficiency" criterion for further stages of the study.

The period-wise variation of the numerical results (i.e., ρ-T relationships) have been graphically presented for subject IMs with differentiated strength reduction factor (R) and ductility (μ) levels as well as yield base shear coefficient (η) levels. Figure 4.3 and Figure 4.4 illustrate the case for PGA, whereas graphics for remaining IM alternatives are presented in Appendix B (Figure A.5-Figure A.35 for R- and μ-based charts, and Figure A.36-Figure A.66 for η-based charts). The evaluations based on these figures will be elaborated in 3 sub-sections (strength reduction factor level-, ductility level-, and yield base shear coefficient level-based evaluations) to identify the correlation levels corresponding to each IM alternative as strong (ρ>0.9), moderate (0.5<ρ<0.9), weak (0<ρ<0.5) and negative correlation (ρ<0).
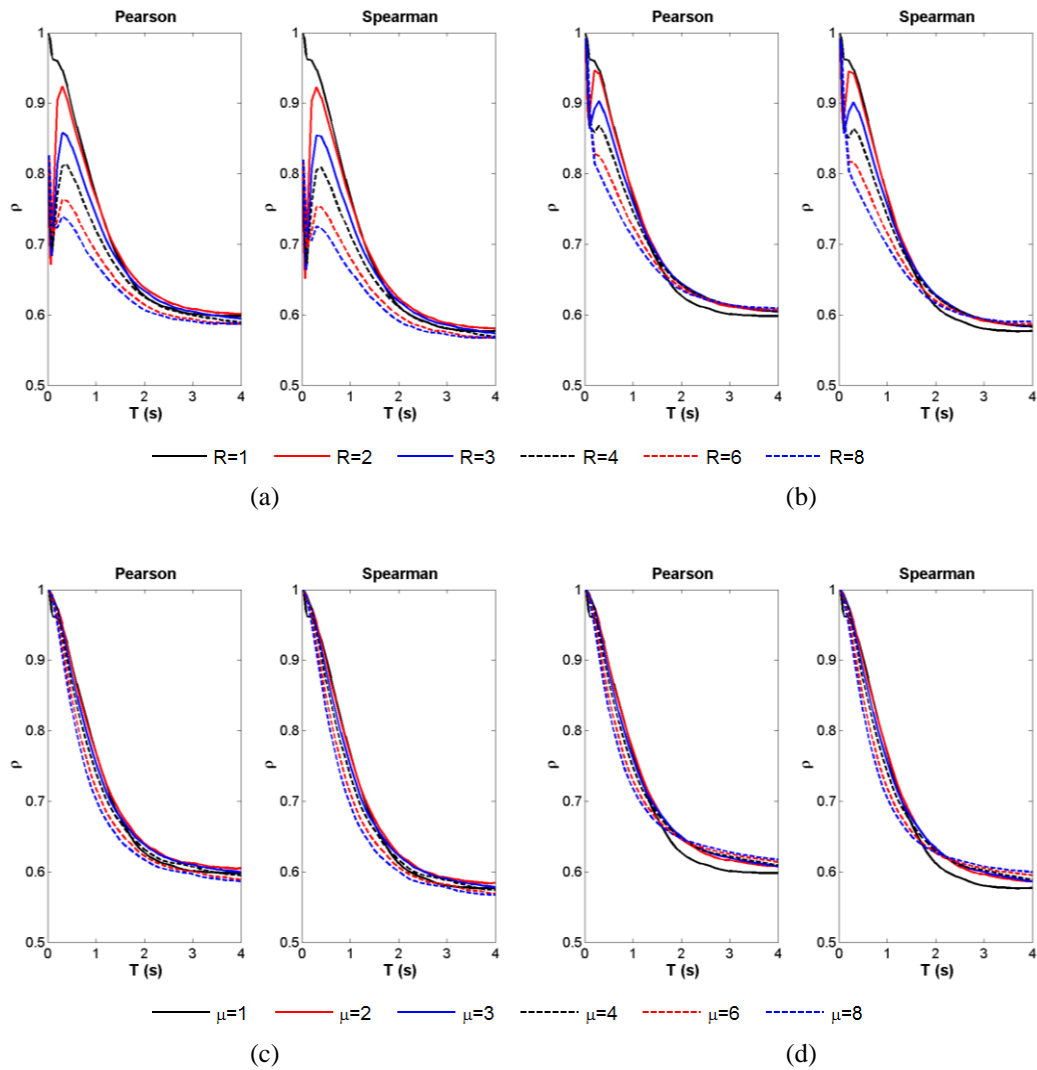
Figure 4.3. Variation of correlation coefficient values with period (correlation of IM **PGA** with EDP **SDOF top drift** for different R and μ cases (a) Elastic-Perfectly-Plastic, (b) Bilinear Hardening (α=5%), (c) Elastic-Perfectly-Plastic, (d) Bilinear Hardening (α=5%))
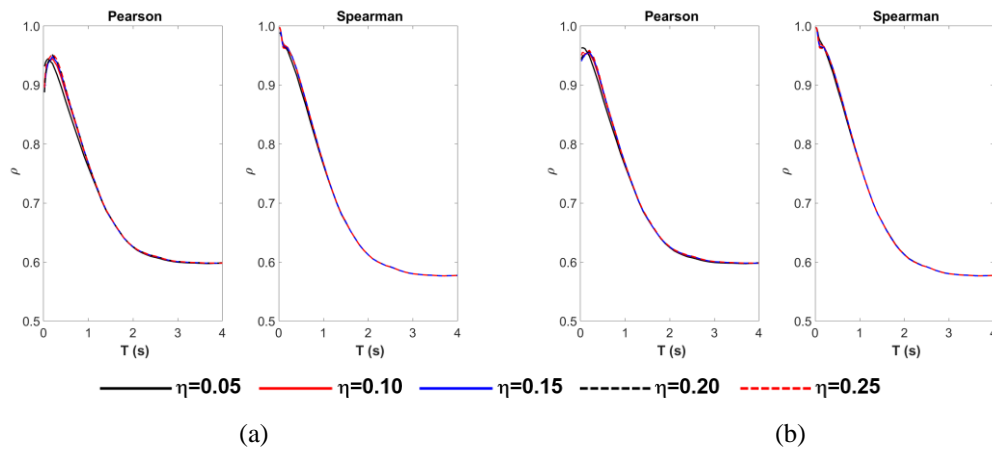
Figure 4.4. Variation of correlation coefficient values with period (correlation of IM **PGA** with EDP **SDOF top drift** for different η cases (a) Elastic-Perfectly-Plastic and (b) Bilinear Hardening (α=5%)

4.3.1 Evaluations Based on Strength Reduction Factor (R) Levels

The examinations on PGA-specific Pearson- and Spearman-based charts have revealed that PGA is correlating very well with the deformation demands when the elastic (i.e., R=1 case) very short period structural systems are considered. Systems with higher R have shown moderate correlation, especially for elastic-perfectly-plastic (EPP) systems, whereas systems showing bi-linear hardening hysteretic behavior have shown higher correlations with respect to EPP systems. However, this performance, represented with ρ values corresponding to Pearson or Spearman correlation coefficients, rapidly diminishes with increasing periods of the SDOF system (especially after T=0.5-1.0 sec). The correlation values generally saturated to a value of 0.60 after T=2 sec regardless of R level.

PGV-specific charts have shown that the correlation performance is relatively moderate for short-period systems, yet improves for SDOF systems with intermediate periods approaching 0.95 and finally accumulates to a value of 0.90. Elastic (R=1) cases eventually show lower correlations with regard to R>1 cases,

however, the variation in correlation results with respect to R is much less when considered to the cases of PGA. EPP and bi-linear hardening cases did yield similar performances.

Elastic (R=1) cases of PGD-based graphics have yielded a weak-to-moderate correlation level with a value of 0.5-0.7 for short-to-medium period (T=0.02-0.5 sec) systems, whereas R>1 cases have yielded ρ values of 0.7-0.9 for this period range. Starting with intermediate period range, the values started to increase and surpassed 0.9 level around T=1.0 sec, pointing to strong correlations for long period systems. The two hysteresis cases gave similar trends for periods above T=1.0 sec, in contrast, for short-to-intermediate period ranges, the R-wise variation of results is much more pronounced for EPP cases, yielding to slightly stronger correlations for EPP cases at short periods.

PGV/PGA ratio-based charts have shown that there is a weak correlation between this index and SDOF-based drift demands, especially for short-to-intermediate systems. Negative correlation values have been observed especially for R=1 cases. The correlation performance of this index improved to some extent after T=1.0, reaching a value of 0.6. The two hysteresis cases generally yielded similar responses, but differentiated in short period range, EPP case causing much variation to R-wise outcomes.

When a_{rms}-based figure set is examined, a moderate-to-strong correlation performance was observed for different R levels of short-period systems. After intermediate periods (T>0.5 sec), rapid decay of the ρ values are significant, whereas the values generally saturate around 0.65 after T=2.0 sec. EPP case seemed to introduce variability to the results as opposed to the bi-linear hardening case. Except for R=1 cases, the period-wise variation trend has been found to be similar to PGA-based cases, where PGA is generally superior to a_{rms} for very short period systems.

The v_{rms}-based figure set has yielded moderate correlation for short-to-intermediate period systems where this correlation performance has improved for systems around T=1.0 sec. The correlation performance stayed constant slightly above 0.9 for long

period systems. R levels caused observable variations in the results for short period systems (i.e., the case of R=1 is significantly different than other R cases), whereas hysteresis definition did not seem influential.

The observations from d_{rms}-based charts are similar to the cases of PGD-based set pointing out to poor performance (ρ=0.5-0.85) at short-to-intermediate period (T=0.02-0.5 sec) range along with significant variations for different R levels and alternate hysteresis definitions. The correlations increase after T=1.0 sec surpassing 0.9 level, and gradually approach 0.95.

When charts particular to AI are examined, it has been observed that bi-linear hardening case gave values slightly larger than 0.9 (i.e., approximately 0.95 at peak) for systems with short and medium periods, especially for low R levels, where ρ values decay approximately to 0.8 for long period systems. Results for EPP systems with higher R and T<1.0 sec tended to be smaller with respect to the outputs of bi-linear hardening models (i.e., ρ values are as low as 0.80 for very rigid systems).

Period-wise variation of I_C^*-based results have been observed to be similar to AI-specific outputs except for long period region, where the saturation level for coefficients is around 0.75. The effect of increasing R on decreasing ρ values is significant for short-to-medium period structures with EPP hysteretic behavior.

When SED-specific results are evaluated for different periods and R levels, significant variations have been observed for short and medium-period systems regardless of hysteresis models. As the fundamental periods of the structures approach to T=1.0 sec, the correlation performances improved to 0.9 levels, and stayed constant around 0.95 for longer periods.

CAV has yielded a moderate correlation performance (with a ρ range of 0.75-0.9) for systems with periods T<1.0 sec, and after this period level, the correlations stayed constant slightly below 0.90 level. The observations are generally valid for all R levels (except for the R=1 case) and for both hysteresis cases.

The correlation of ASI with deformation demands turned out to be highly variable with respect to R levels, fundamental periods, and hysteresis cases. Even the superior performance (with ρ levels of 0.90) of short-period systems with low R diminishes with increasing T, and approaches to 0.6 level after T=2.0 sec. The negative effect of increasing R level for short-to-long period systems (T=0.02-1.0 sec) was observed to be much more influential for EPP systems.

VSI has shown a strong correlation (ρ>0.90), especially for systems R>1, yielding a peak value of 0.95 approximately around T=1.0 sec, and gradually decreased to 0.90 band. Both hysteresis cases showed similar variation with the R=1 case yielding lower coefficients for T<1.0 sec.

SMA-based correlation coefficients exhibited high variation (ρ=0.7-0.95 for EPP model and ρ=0.80-0.95 for bilinear hardening model) for period range T=0.02-1.0 sec where the correlations seemed to decrease with increasing R. After T=1.5 sec, the coefficients converged to a level of 0.65 designating moderate correlation at long periods.

SMV, similar to VSI, generally showed a relatively strong correlation for systems R>1 where coefficients remained constant around 0.90 level after T=1.0 sec. The elastic systems with T<1.0 sec seemed to give lower correlation coefficients. Bilinear hardening model generally seems to show similar variation as compared to the EPP model except for the cases with high R levels and short-period systems.

Period-wise variation of ρ values based on EDA and A_{95} has shown that the general trends for these IMs are parallel with SMA for all R levels and for both hysteresis cases.

Predominant period (T_p)- and mean period (T_m)-based indices exhibited very weak correlations where the results are highly variable (i.e., dependent on R level), especially for systems T<1.0 sec. Even negative correlations have been observed for R=1 cases for T<0.5 sec period region. The hysteresis model definition also seemed to have a significant effect on the correlation performance of short-period (T<0.5

sec) systems. For structures with periods T>2.0 sec, T_m is relatively superior to T_p, as the correlation coefficients converge to 0.6 and 0.35, respectively, for long period systems.

When the charts based on significant duration (t_r) are examined, it has been observed that the duration-related index of GM records generally exhibits negative correlations for systems with T<1.0 sec invariant of R levels (except R=6, 8) and hysteresis models. After T=1.0 sec, on the other hand, low ρ values (converging around 0.25 level) pointed out significantly weak correlations for long period systems. The variation in EPP system-based results is comparable as opposed to bilinear hardening cases.

When the result set corresponding to I_C is evaluated, it has been realized that ρ values noticeably varied between 0.80-0.90 range for short-to-intermediate periods with the deteriorating effect of R level significantly pronounced for EPP systems. The relatively strong correlation performance gradually diminishes after T=1.0 sec and consolidates around 0.8 level.

It has been observed for Riddell and Garcia's acceleration-, velocity- and displacement-based compound indices, I_a, I_v, I_d, that the correlation performances turned out to be very similar to the individual cases of a_{rms}, v_{rms} and d_{rms}, respectively. The duration parameter in the compound indices did not seem to affect the overall correlation performances.

Fajfar Index, I_F, exhibited a period-wise variation similar to I_v, but yielding higher ρ values, especially for short-to-medium period systems. The trends are almost the same for both hysteresis cases and for all R levels except R=1, and where R=1 level noticeably differentiated from others.

The acceleration spectrum-based intensity parameter proposed by Yakut and Yılmaz, ASI[*], has shown much better correlation performance with respect to the original ASI definition, where ρ values remained within 0.8-0.95 band (0.8 for R=1 case as the worst) for a period range of T=0.02-1.0 sec. After T=1.0 sec, the

correlation coefficients seemed to decrease to a level of 0.8 gradually. Both hysteresis cases yielded similar variation, whereas the effect of R levels is slightly noticeable for EPP systems.

Considering a relatively wide period range of T=0.02-4.0 sec, EPA performed similarly with respect to PGA in general. The noticeable superiority of PGA or EPA over its rival has only been identified for the R=1 (elastic) case for the T=0.02-0.5 sec period range. Unlike EPA, EPV has performed slightly superior with respect to PGV and VSI in the period range of T=0.02-1.5 sec; however, this performance gradually diminished for periods T>1.5 sec, and finally saturated just below 0.85 level. The variation in the results with respect to R is noticeable for the EPP case, especially in the period range of T=0.5-1.5 sec range.

Spectral acceleration at SDOF vibration period, S_a, exhibited a perfect correlation with the deformation demands for the R=1 case, which is an expected outcome. However, considering the EPP case; the correlation performance of S_a for R>1 cases turned out to be highly variable between ρ values of 0.5-0.95 for T=0.01-1.0 sec, starting from an approximate value of 0.8 and abruptly decaying to 0.5 levels and then again rising to 0.95 levels. The results exhibited a strong correlation (ρ values gradually approaching 1.0) after T=0.5-1.0 sec for R>1 cases, while values are slightly lower for increasing R levels. For the bi-linear hardening case, in contrast, the period-wise correlation variations ranged between 0.7-1.0 levels for T=0.02-1.0 sec, emphasizing the effect of the hysteretic model definition. After T=1.0 sec, the trends are similar with EPP cases.

Spectral velocity at SDOF vibration period, S_v, showed strong correlation performance for the R=1 case, as expected. However, the ρ values showed significant variation for R>1 levels, generally changing within the range of 0.5-0.95 with higher R levels yielding slightly lower ρ values. After medium-to-long periods, the correlation coefficients converged to an approximate value of 0.95. The trends turned out to be similar for both hysteretic models except for very short periods.

Spectral displacement, S_d, exhibited a perfect correlation with the deformation demands for the R=1 case, which is also an expected outcome. However, considering the EPP case of R>1 levels; S_d has yielded highly variable ρ values in the range of 0.5-0.95 for T=0.01-1.0 sec, starting from an approximate value of 0.8 and suddenly decreasing to 0.5 levels, afterwards, again rising to 0.95 levels. The results exhibited strong correlation (ρ values gradually approaching 1.0) after T=0.5-1.0 sec for R>1 cases, while values are slightly lower for increasing levels of R. For bi-linear hardening case, in contrast, the period-wise correlation variations ranged between 0.7-1.0 levels for T=0.02-1.0 sec, emphasizing the effect of hysteretic model definition. After T=1.0 sec, the trends are alike EPP cases.

The overall comparison of Pearson-based correlation coefficients with their Spearman-based counterparts has shown that the numerical results are generally comparable.

Finally, the numerical results evaluated in this section were compared with the results of a companion study, Ye et al. (2013), and the correlation values presented herein were found to be slightly higher.

4.3.2   Evaluations Based on Ductility (μ) Levels

The observations on PGA-specific Pearson- and Spearman-based charts have revealed that PGA is correlating very well with the deformation demands of very short period structural systems irrespective of ductility (μ) levels and hysteresis cases; however, ρ values fall below 0.8 after T=1.0 sec and generally saturate around 0.6.

PGV-specific charts have shown that the correlation performance is relative moderately for short-period systems, yet improves for SDOF systems with intermediate periods approaching 0.95 and finally saturates to a value of 0.90. Elastic (μ=1) cases eventually show lower correlations with regard to inelastic (μ>1) cases, however, the variation in correlation results with respect to μ is much less when

considered to the case with different R levels. EPP and bi-linear hardening cases did yield similar performances.

The ρ values of PGD-based charts particular to different μ levels start around 0.6-0.7 band, indicating a weak-to-moderate correlation performance for short-period systems, but increase to 0.9 level around T=1.0 sec, pointing out to strong correlation especially for long-period systems. The variability in the μ-based results is limited with respect to the R-based charts. The correlation values are generally insignificant to hysteresis cases.

It has been observed for PGV/PGA ratio-based charts that there is a very weak correlation for short-to-intermediate period systems (even negative correlation for very short period systems) regardless of ductility level and hysteresis case. This poor performance slightly improves to a value of 0.6 for long period systems (T>1.0 sec). The correlation values are generally insignificant to hysteresis cases.

When a_{rms}-based figure set is examined, the strong correlation for short period systems immediately decays with increasing periods, finally saturating to a value of 0.65-0.70 after T=2.0 sec. The ductility level and hysteresis model definition did not seem to cause significant variations in the period-wise results.

The v_{rms}-based figure set has yielded moderate correlation for short-to-intermediate period systems where this correlation performance has improved for systems around T=1.0 sec. The correlation performance stayed constant slightly above 0.9 for long-period systems, regardless of μ levels and hysteresis cases.

The correlation performance of d_{rms} seemed to increase rapidly from weak correlation levels (ρ=0.5) to ρ=0.9 in the short-to-long period (T=0.02-1.0 sec) range without showing observable variation due to μ levels or hysteresis model alternatives. After T=1.0 sec, the correlation values gradually increase to 0.95.

Charts particular to AI have revealed the relatively strong correlation performance of AI in the short-to-intermediate period range regardless of μ level or hysteresis

model. However, this superiority was lost after T=1.0 sec, and the coefficients decreased to $\rho=0.80$ corresponding to moderate correlation.

The period-wise variation of ρ values for $I_C{}^*$ turned out to be similar to AI-specific results, with the exception for long-period systems, where ρ saturates around 0.75. No significant difference was observed with respect to μ levels or hysteresis model definitions.

μ-wise variation of SED-based results showed a general trend similar to R-wise variations where the only observable difference is that the effect of R level on the ρ results is much more significant for structures with T=0.01-1.0 sec. The moderate-to-strong correlation performance of SED is valid for both hysteresis cases.

CAV has yielded a moderate correlation performance (with a ρ range of 0.75-0.9) for systems with periods T<1.0 sec, and after this period level, the correlations stayed constant slightly below 0.90 level. The observations are valid for all ductility levels and for both hysteresis cases.

ASI-based charts showed that this intensity measure is effective for short-to-medium period structures with ρ values higher than 0.9, whereas this superior performance worsened rapidly after T=0.5 sec saturating at a ρ level of 0.6. The results did not show observable differences considering alternating μ levels and hysteresis cases.

VSI has shown a strong correlation ($\rho>0.90$), especially for medium-to-long period systems regardless of μ levels, approaching $\rho=0.95$ roughly around T=1.0 sec, and gradually decreased to 0.90 band. However, the coefficients remained below 0.90, pointing out to moderate correlation performance for the short-to-medium range. The observations are valid for both hysteresis models.

SMA-based correlation coefficients exhibited a strong correlation ($\rho=0.9-0.95$ for T=0.02-0.5 sec, however, decreased rapidly after this period level converging to 0.65, indicating a weak correlation performance for medium-to-long period systems. The results did not seem to vary with μ levels and alternative hysteresis models.

SMV, similar to VSI, generally showed a strong correlation for systems having a fundamental period T>0.5 sec irrespective of μ levels and hysteresis models. For short period systems with T<0.5, the correlation coefficients were lower than 0.9, indicating a moderate correlation performance.

Period-wise variation of ρ values based on EDA and A_{95} has shown that the general trends for these IMs are parallel with SMA for all μ levels and for both hysteresis cases.

Predominant period (T_P)- and mean period (T_m)-based indices exhibited very weak correlations, especially for systems T<1.0 sec, whereas the correlations increase and saturate to 0.35 and 0.60, respectively. The hysteresis model definition and μ levels did not seem to affect the trends.

When the charts based on significant duration (t_r) are examined, it has been observed that duration-related index of GM records generally exhibit negative correlations for systems with T<1.0 sec, whereas after T=1.0 sec, low ρ values (converging around 0.25 level) pointed out to significantly weak correlations for long period systems. Results are invariant of μ levels and hysteresis models.

When the result set corresponding to I_C is evaluated, it has been realized that the relatively strong correlation performance at short periods gradually disappears after T=1.0 sec and converges to a ρ level of 0.8. The observations are valid for both hysteresis cases and for all μ levels.

Riddell and Garcia's acceleration-, velocity- and displacement-based compound indices, I_a, I_v, I_d, exhibited very similar correlation performance variations with the individual cases of a_{rms}, v_{rms} and d_{rms}, respectively. The duration parameter in the compound indices did not seem to affect the overall correlation performances.

Fajfar Index, I_F, also showed a period-wise variation similar to I_v, but yielding higher ρ values, especially for short-to-medium period systems. The observations are the same for all μ levels and for both hysteresis cases.

ASI[*], has shown much better correlation performance with respect to the original ASI definition, where ρ values remained within 0.8-0.95 band regardless of μ level for a period range of T=0.02-1.0 sec. After T=1.0 sec, the correlation coefficients seemed to decrease to a level slightly above 0.8 gradually. Both hysteresis cases yielded similar trends.

Considering a relatively wide period range of T=0.02-4.0 sec, EPA performed similarly with respect to PGA in general. The noticeable superiority of PGA over its rival has only been identified for the T=0.02-0.5 sec period range. Unlike EPA, EPV has performed slightly superior with respect to PGV and VSI in the period range of T=0.02-1.5 sec; however, this performance gradually diminished for periods T>1.5 sec, and finally saturated just below 0.85 level. The trends turned out to be alike for all μ levels and for both hysteretic behavior cases.

Spectral acceleration, S_a, exhibited a perfect correlation with the deformation demands for the μ=1 case, which is an expected outcome. For other μ cases, the correlation coefficients are changing between 0.9-1.0, indicating a strong correlation, though the variation of results due to μ is noticeable for the T=0.02-1.0 sec period range. Both hysteresis cases yielded similar trends.

Spectral velocity, S_v, generally showed strong correlation performance for μ =1 case, exhibiting almost perfect correlation at medium periods (T $\approx$ 0.5 sec). However, the ρ values showed variation for other μ levels, generally changing within the range of 0.85-0.95 with higher μ levels yielding lower ρ values. After medium-to-long periods, the correlation coefficients converged to an approximate value of 0.95. The trends turned out to be alike for both hysteretic models.

Spectral displacement, S_d, displayed a perfect correlation with the deformation demands for the μ=1 case, while for other μ cases, the correlation coefficients changed between 0.9-1.0, indicating a strong correlation. The results showed variation due to changing μ levels for the T=0.02-1.0 sec period range. The trends of EPP and bilinear hardening models are similar to the case of S_a, as expected.

Finally, the overall comparison of Pearson-based correlation coefficients with their Spearman-based counterparts has shown that the numerical results are generally almost the same, in accordance with R-based observations.

4.3.3   Evaluations Based on Yield Base Shear Coefficient (η) Levels

Overall examination of the period-wise charts developed with respect to changing yield base shear coefficients (η) has revealed that the variations of the correlation values are generally alike the μ-based variations. Besides, the correlation variations are mainly insensitive to changing η except for specific observations for very rigid systems (T<0.1 sec). Despite the fact that relatively limited cases of η (i.e., five distinct η values representing structural systems with low lateral strength capacities) have been evaluated throughout the analyses, these particular cases are considered to be representative of the general trend as well.

The numerical results roughly evaluated in this section were compared with the results of two relevant companion studies, Palanci and Senel (2019), and Karimzadeh et al. (2021), respectively. The correlation trends (with different η levels) presented herein were found to be comparable in general with the result set of Karimzadeh et al. (2021), yet significantly different than the results of Palanci and Senel (2019).

4.3.4   Discussion of Correlation Performances of Intensity Measures

The SDOF-based evaluation of ρ-T variations of the selected intensity measures with changing strength reduction factor (R) and ductility (μ) levels has revealed the following interpretations in general:

- PGA, the simplest acceleration-related scalar IM, correlates well with the displacement demands of short-period systems; however, as the period of the

systems enters into medium or long period range, the correlation performance immediately diminishes (Figure 4.5).

- PGV, the simplest velocity-related scalar IM, shows lower correlation performance at short periods with respect to PGA, but it demonstrates much higher correlations at intermediate and relatively long periods, compensating for its drawback (Figure 4.5). This observation is in parallel with the conclusions of key literature (Akkar and Özen, 2005).
- The basic displacement-related scalar IM, PGD, shows a strong correlation for long-period structural systems invariant of R and μ level (Figure 4.5).
- PGV/PGA ratio, which is a measure related to the frequency content of the ground motion, shows a weak correlation for short-to-medium periods irrespective of T, R, and μ, whereas its performance slightly improves for long-period systems (Figure 4.5).
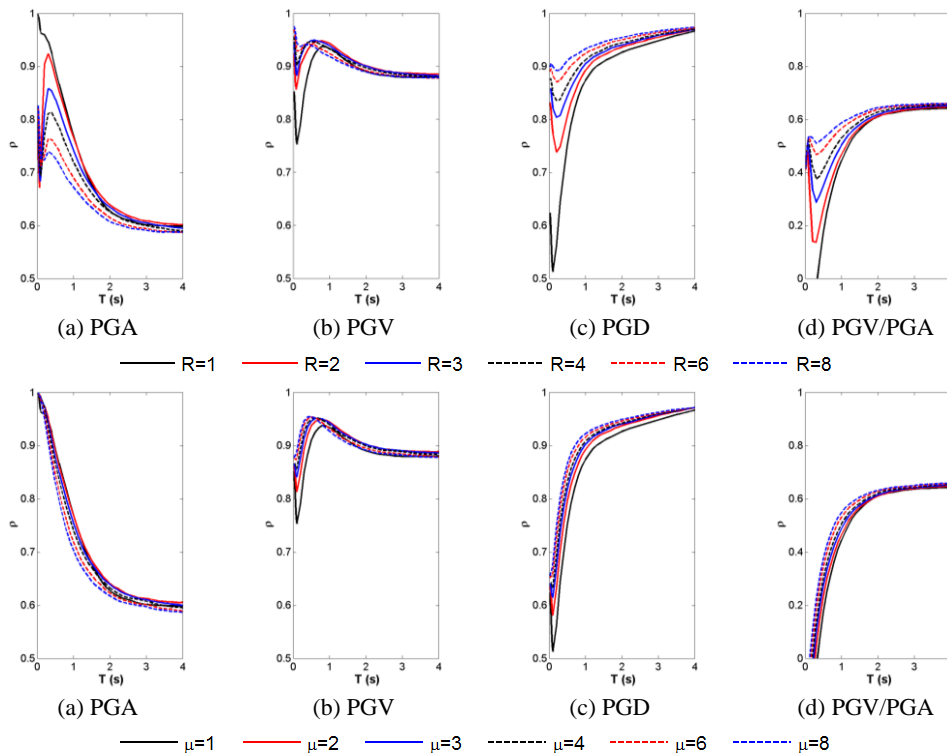
Figure 4.5. Comparison of Pearson-based results for PGA-PGV-PGD-PGV/PGA (Elastic-Perfectly-Plastic case)

- The acceleration-, velocity- and displacement-related indices a_{rms}, v_{rms} and d_{rms} show trends similar to their simpler counterparts, PGA, PGV, and PGD, while a_{rms} and v_{rms} correlate slightly better at longer periods with respect to PGA and PGV, respectively (Figure 4.6).

(a) PGA   (b) a_{rms} (c) PGV   (d) v_{rms}
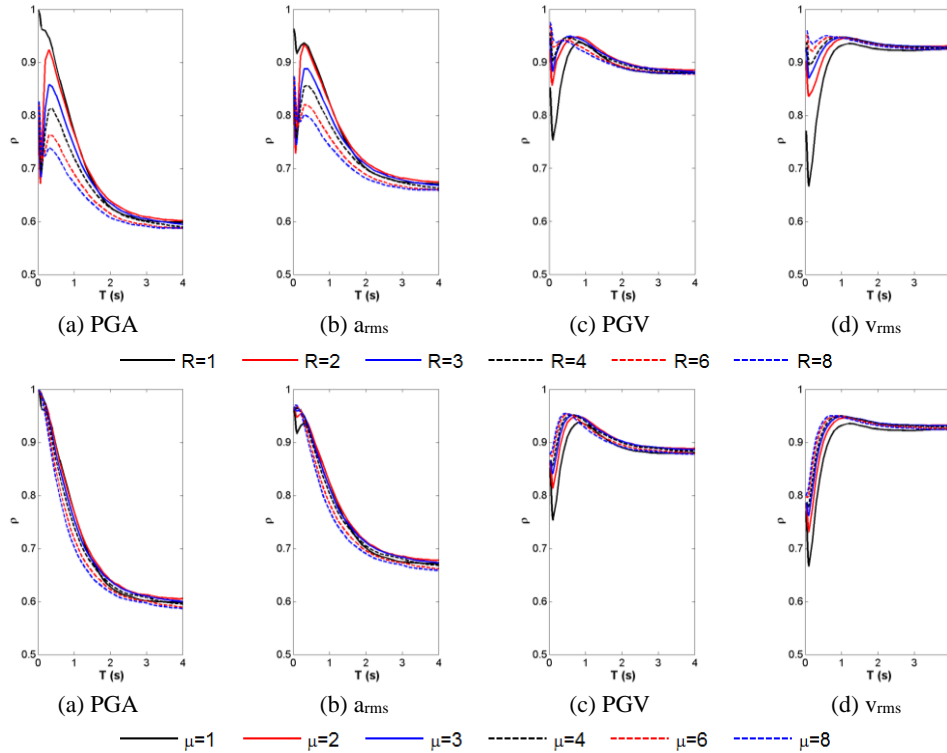
Figure 4.6. Comparison of Pearson-based results for PGA-a_{rms}-PGV-v_{rms} (Elastic-Perfectly-Plastic case)

- Arias Intensity, AI, and Characteristic Intensity, I_C, are akin to PGA, but they exhibit higher correlations at long periods. Besides, The acceleration-related parameters ASI, SMA, EDA, and A_{95} exhibit comparable variations with respect to PGA, which has been expected due to their high inter-correlations with PGA. On the other hand, the modified version of ASI, ASI*, shows a better correlation performance with respect to ASI except for very short periods, and accordingly, is more efficient with respect to ASI (Figure 4.14).
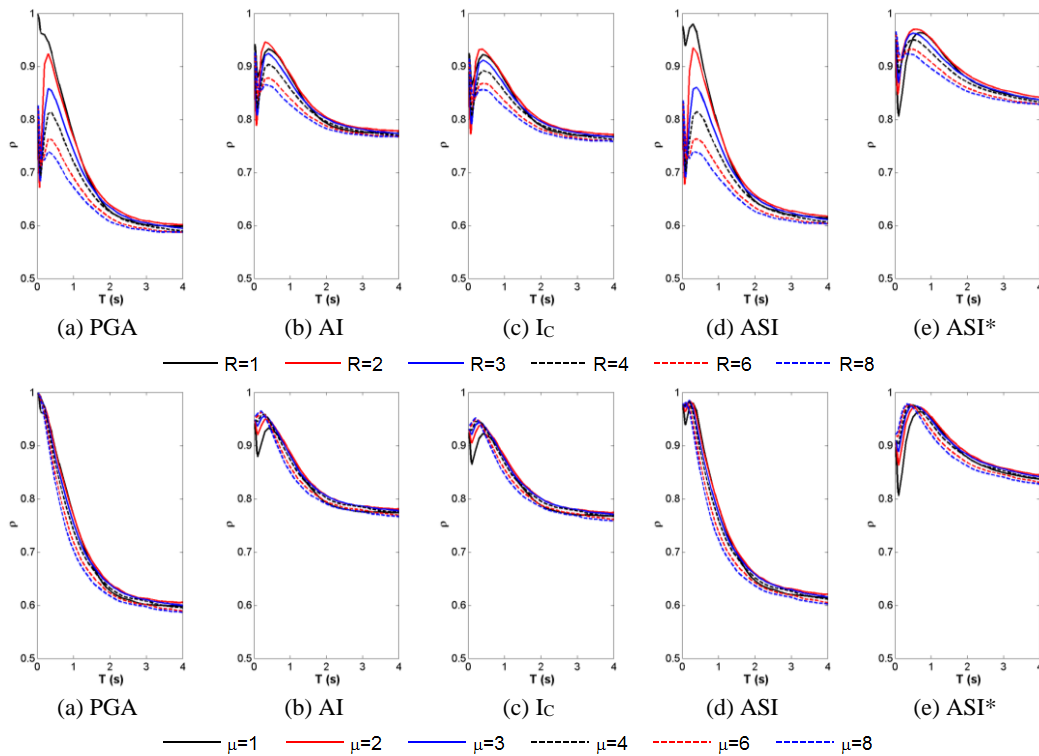
Figure 4.7. Comparison of Pearson-based results for selected PGA-AI-I_C-ASI-ASI*

(Elastic-Perfectly-Plastic case)

- SED and CAV show stable and relatively high correlation performance for long period systems, where SED is superior to CAV. However, for the short-to-intermediate period range, CAV correlates noticeably better than SED (Figure 4.8).

- The velocity-related parameters VSI and SMV, similarly, show comparable ρ-T variations with respect to PGV (Figure 4.8).
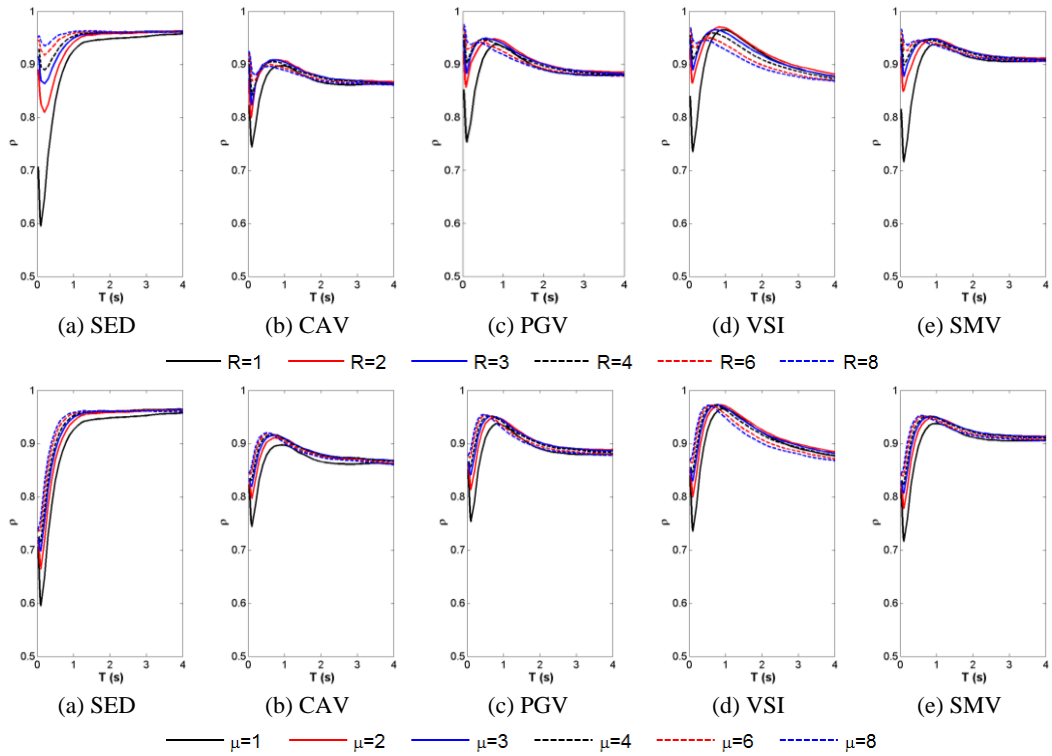
Figure 4.8. Comparison of Pearson-based results for SED-CAV-PGV-VSI-SMV
(Elastic-Perfectly-Plastic case)

- EPA and EPV generally trend similarly with respect to PGA and PGV. Although EPV correlates slightly better with respect to PGV for medium- to relatively long-period systems (up to T=1.5 sec), after this period limit, the performance of EPV is slightly worse (Figure 4.9).

- Ground motion period-related parameters T_P, T_m, and duration-related index, t_r, poorly correlate with the drift demands and could not be regarded as efficient intensity measures. On the other hand, it had been stated by Riddell (2007) and Yang et al. (2009) that incorporation of significant duration into intensity parameters to form compound IMs would improve the correlations of PGA and PGV; however, this improvement has been found minor in this study (Figure 4.10).

- Among I_a, I_F, I_v, and I_d; Fajfar Intensity, I_F and Riddell and Garcia's velocity-related index, I_v, show a stable and good correlation with the displacement demands of SDOF systems at a wide period range (Figure 4.10).

77

(a) PGA (b) EPA (c) PGV (d) EPV

—— R=1 —— R=2 —— R=3 ------ R=4 ------ R=6 ------ R=8

(a) PGA (b) EPA (c) PGV (d) EPV

—— μ=1 —— μ=2 —— μ=3 ------ μ=4 ------ μ=6 ------ μ=8
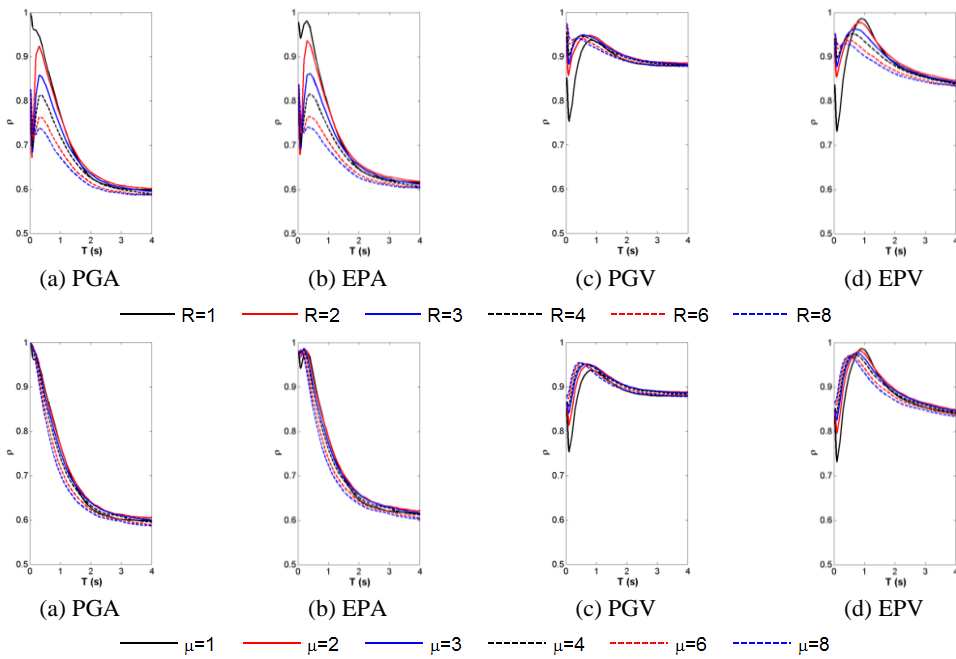
Figure 4.9. Comparison of Pearson-based results for PGA-EPA-PGV-EPV
(Elastic-Perfectly-Plastic case)

(a) PGA (b) I_a (c) PGV (d) I_F (e) I_v

—— R=1 —— R=2 —— R=3 ------ R=4 ------ R=6 ------ R=8

(a) PGA (b) I_a (c) PGV (d) I_F (e) I_v

—— μ=1 —— μ=2 —— μ=3 ------ μ=4 ------ μ=6 ------ μ=8
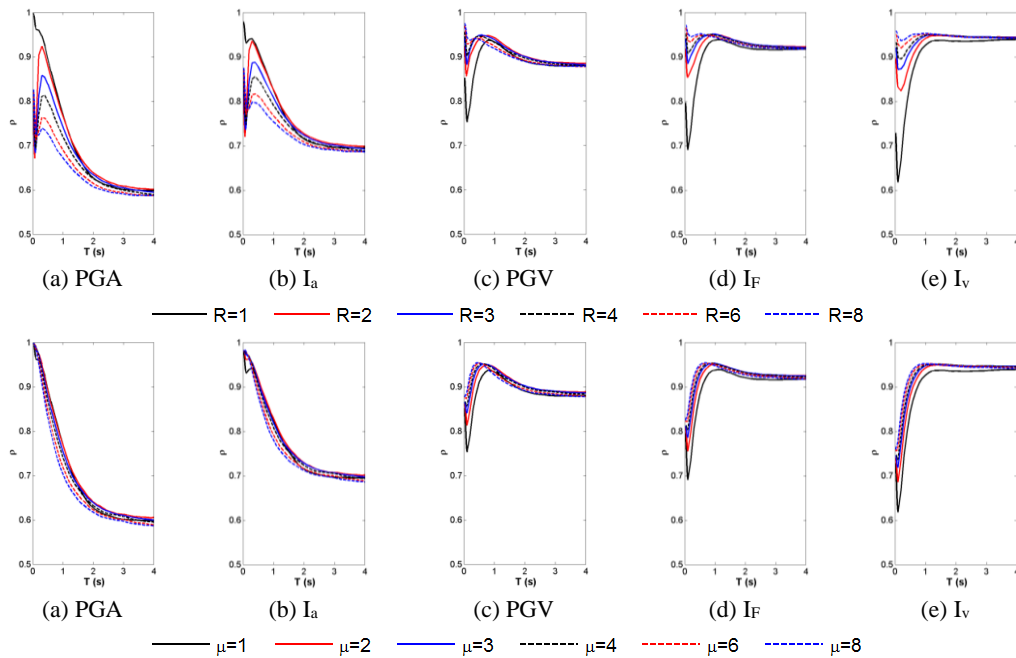
Figure 4.10. Comparison of Pearson-based results for PGA-I_a-PGV-I_F-I_v (Elastic-
Perfectly-Plastic case)

- To re-emphasize, the spectrum-based intensity measures, S_a, S_v, and S_d, are of structure-specific parameters and require SDOF response-based calculations as opposed to the indices listed above. Among these spectral parameters, S_a, and S_d show perfect correlation with drift demands of elastic systems, albeit they reveal good correlation for different μ levels. Both of them are superior to S_v. However, for different R levels, the performance of S_a and S_d couple is very low for short-to-medium periods.
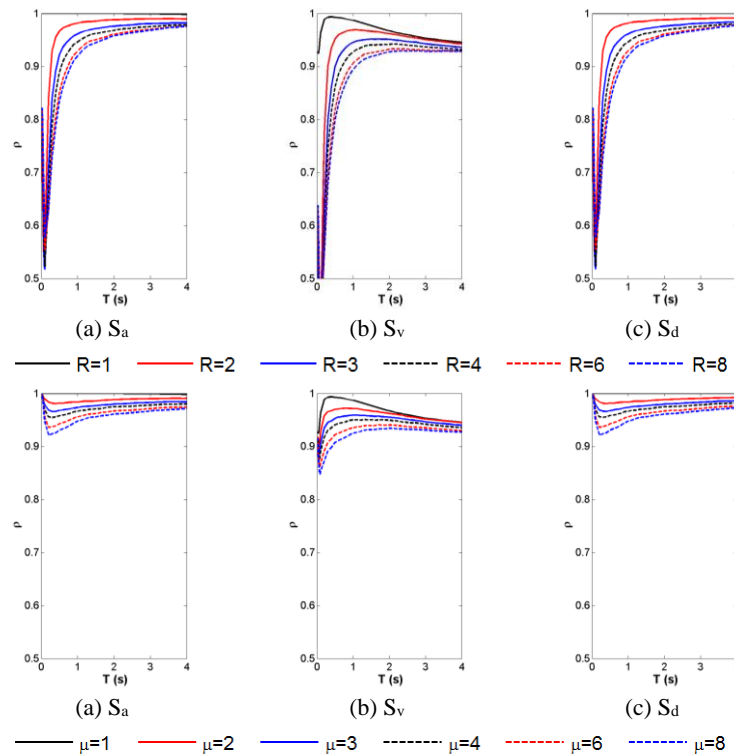
Figure 4.11. Comparison of Pearson-based results for S_a-S_v-S_d (Elastic-Perfectly-Plastic case)

- In overall, the general observation that acceleration-, velocity- and displacement-related IMs are correlating well with the seismic displacement demands of the systems in short, medium, and long period ranges, respectively, has been re-confirmed with the period-wise variations. Besides, the effect of R level on the correlation results seems to be significant up to a

period limit of T=1.5 sec; in contrast, the effect of μ or η level does not seem to affect the period-wise variations significantly. This observation is generally valid for all IMs.

- When the effect of hysteretic model behavior is considered, the correlation results are generally much more sensitive to R factors for EPP systems as opposed to SDOF systems with bi-linear hardening hysteretic behavior. This observation is valid for periods up to a limiting value of T=1.5 sec. However, the general trends do not differ significantly.

SDOF-based observations suggest that acceleration-based IMs PGA, AI, ASI, and ASI* could be considered as qualifying indices for short-period systems, whereas, for medium-to-long periods, IMs such as PGV, SED, CAV, VSI, I_F, and I_v could be considered as these parameters exhibit high and stable correlation performance at these period levels. The latter IM set is also considered to be efficient for structural systems that are expected to undergo various degrees of inelasticity.

The period-wise correlation variations of the shortlisted IMs for different R, μ and η levels are re-presented in Figure 4.12 thru Figure 4.14.
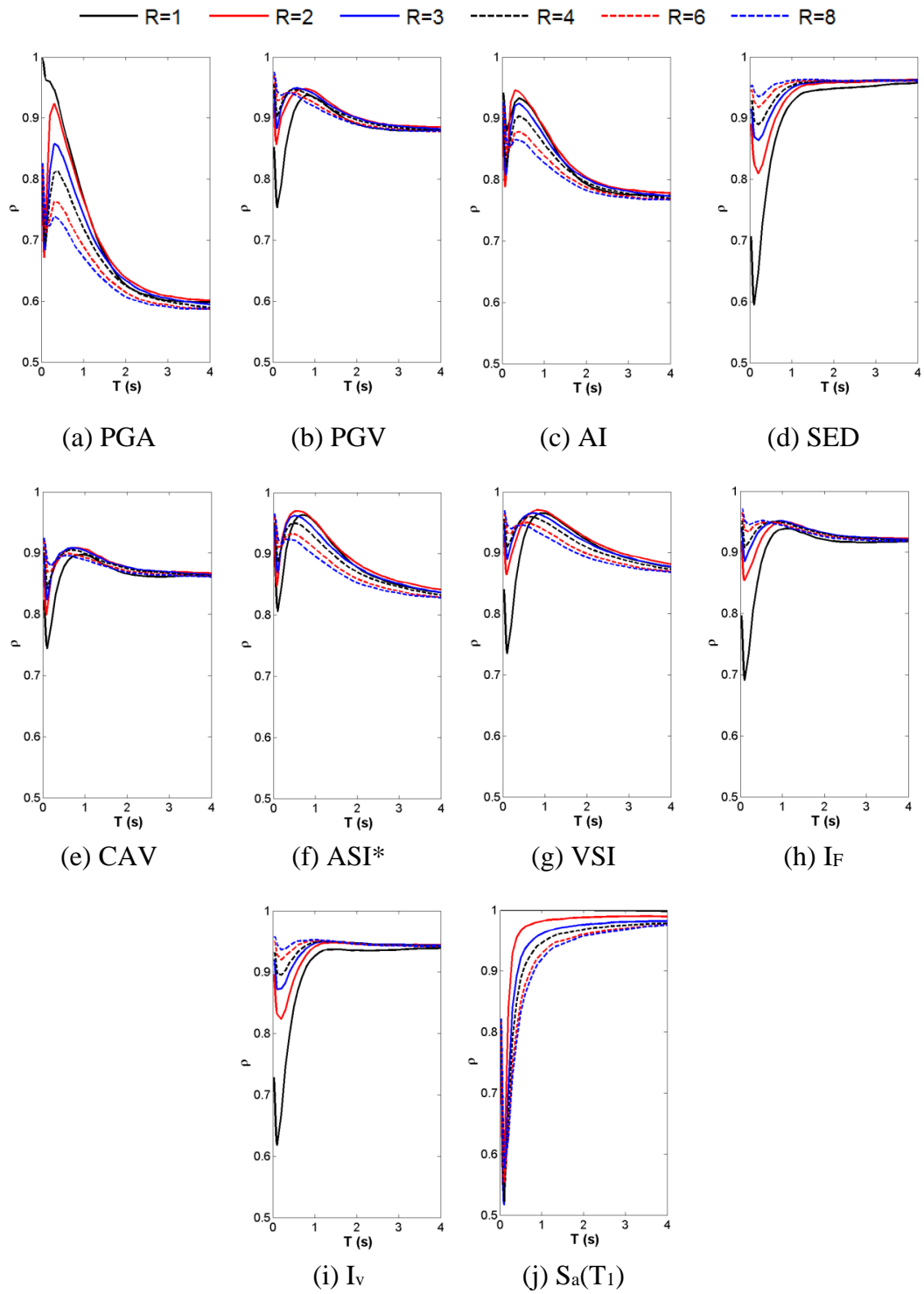
Figure 4.12. Variation of Pearson correlation coefficient values with period for different R levels
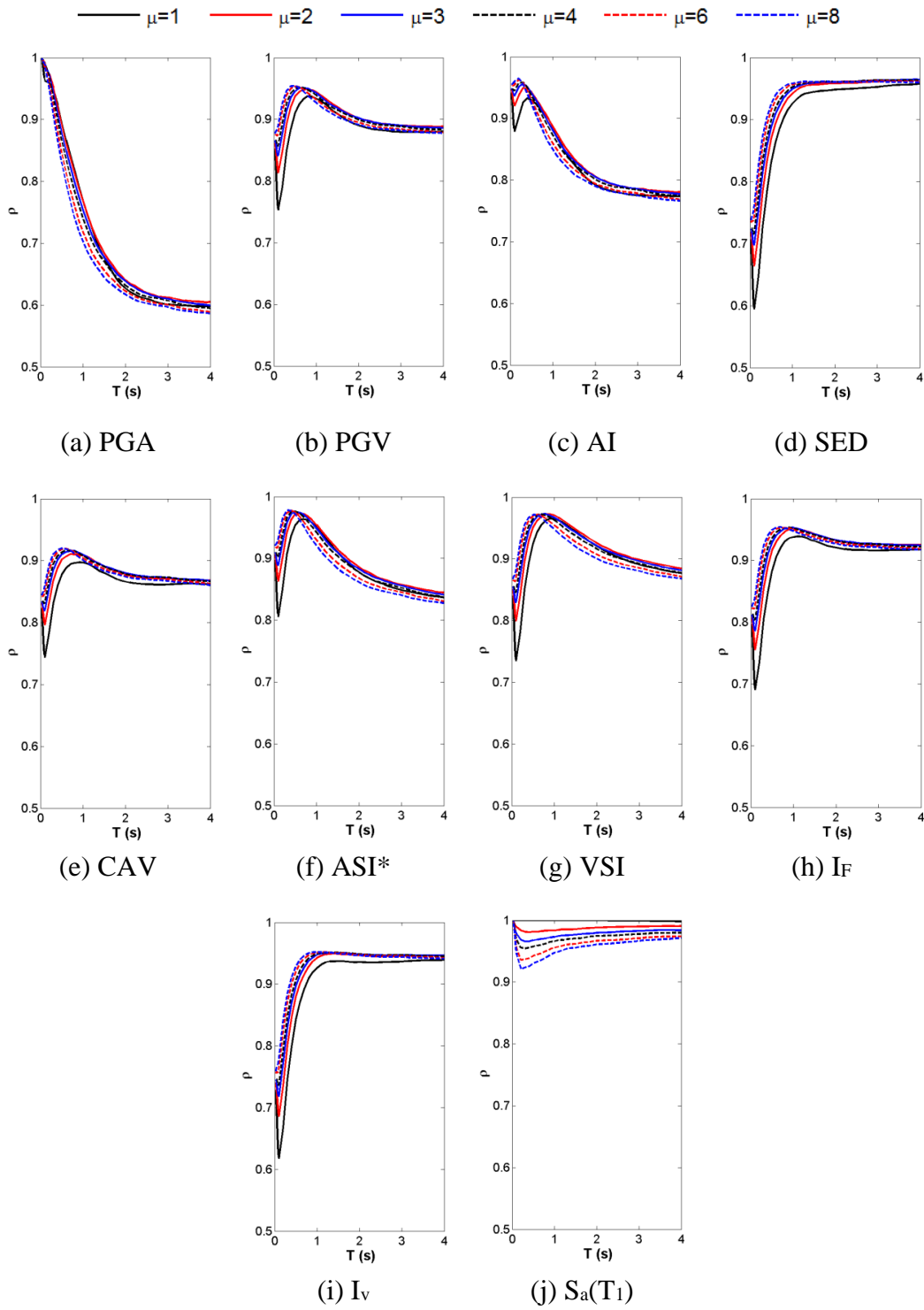
Figure 4.13. Variation of Pearson correlation coefficient values with period for different μ levels
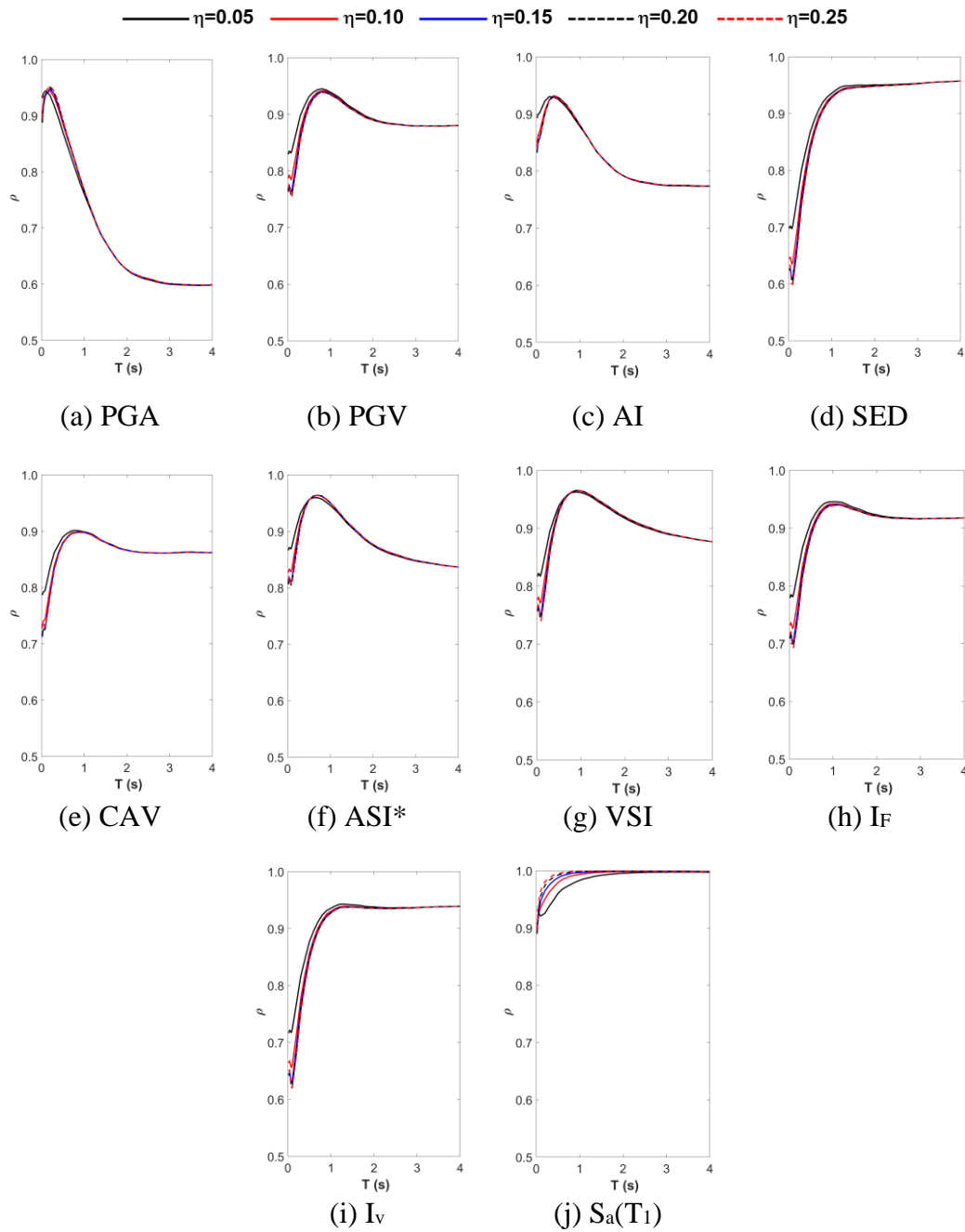
Figure 4.14. Variation of Pearson correlation coefficient values with period for different η levels

CHAPTER 5

EVALUATION OF EFFICIENCY AND SUFFICIENCY OF INTENSITY MEASURES BASED ON MULTI-DEGREE-OF-FREEDOM SYSTEMS

5.1   Introduction

This chapter explains in detail the multi-degree-of-freedom (MDOF) system-based approach for the evaluation of the efficiency and sufficiency of an expanded list of simple-to-advanced scalar and vector intensity measures (IMs). As the initial step of this endeavor, a record dataset with a sufficient number of ground motion (GM) records is needed for its utilization in nonlinear time history analyses of MDOF systems. Two sampling methods are described and applied to the main GM database accordingly to form alternative GM subsets considering the scalar IMs shortlisted in the previous chapter. The results from nonlinear time history (NTH) analyses performed on seven plane-frame MDOF models and their simplified equivalents (i.e., ESDOF models) are used to evaluate the correlation performance of the shortlisted scalar IMs and in addition, to designate proper GM subsets that will be considered for the next step. The chapter continues with the introduction of novel scalar and vector IMs, and the explanation of the prediction equation-based evaluation approach to comparatively evaluate the shortlisted scalar IMs with the novel scalar and vector counterparts. Afterwards, the resulting statistical metrics are comprehensively evaluated to mark the best candidate IM(s) outperforming in terms of efficiency and sufficiency.

5.2   Ground Motion Selection

The structural analysis stage is one of the crucial stages of the well-known PEER methodology directly linking the seismic hazard to the structural responses, generally causing structural and non-structural damages (Porter, 2003). As part of

this stage, several analytical tools could be utilized to assess the expected seismic performance of an existing structure or a new one that is under design process. Accordingly, the increasing availability of computational power after the 1990s has facilitated the use of linear and nonlinear time history analyses in such endeavor, while this advancement has also complicated the tasks of the analyst with the challenge of reliable selection of ground motion records needed for this analysis approach. A relatively recent document, NIST GCR 11-917-15 (NIST, 2011), has also focused on this challenge and urged the professionals of the earthquake engineering field to determine their goal of analysis as the first step. Referring to the companion guideline, FEMA P-58-1 (FEMA, 2012) (originally referenced as 90% draft of ATC-58-1, Seismic Performance Assessment of Buildings; ATC, 2011), the document set the focus on seismic performance assessment and defined three different types for this goal, which can be listed as intensity-based assessment, scenario-based assessment, and risk-based assessment.

In the intensity-based assessment, the response of a building structure along with its structural components is computed for a specific intensity level defined by the ground shaking. Both the best estimates and the distributions could be considered, but necessitating the consideration of different GM selection and scaling procedures. Generally, this assessment type is involved in a code-based design approach, where mathematical models of the buildings are analyzed under a set of GM records, and the mean or average of monitored responses is considered. Scenario-based assessment, in contrast, considers the average response and corresponding variability for a building subjected to a specified seismic event, usually defined with earthquake magnitude and source-to-site distance. The final type, risk-based assessment, is the most advanced assessment and requires many intensity-based assessments covering a range of ground motion intensity levels which is defined for a specific period of time (i.e., the design life of the building or one year for annual rate calculations). The outputs from individual assessments are then combined to estimate the annual rates of exceedance.

In all three assessment types listed above, the ground motion selection and scaling step takes an important place, as the average and/or distribution of monitored responses significantly rely on the size and characteristics of the GM dataset employed. Correspondingly, a long list of research studies has focused on this challenge, generally proposing new methodologies stated as superior to former methods. Along with NIST GCR 11-917-15 document (NIST, 2011), Katsanos et al. (2010), Kalkan and Chopra (2010, 2011), Ay (2012), Lin (2012), Bradley et al. (2015), Kwong and Chopra (2015), Zengin (2016) and Kohrangi et al. (2017) reviewed in detail the former methodologies, and a majority of these presented novel methods for GM selection and/or scaling to predict structural responses with sufficient accuracy and much less variability. The common point of these studies recommending a new method is that the target for the employed GM dataset to be matched is either a code-based or a user-specified target spectrum (i.e., Uniform Hazard Spectrum (UHS) or Conditional Mean Spectrum (CMS)), which considers 5% damped elastic spectral acceleration at a period, $S_a(T)$, as the conditioning IM. As an extension of the subject through the utilization of alternative intensity indices as conditioning IM, Bradley (2010) had conceptualized the "generalized conditional intensity measure (GCIM)" approach and later compared it with the results of a conventional intensity-based seismic performance assessment approach (Bradley, 2013). The author, as a conclusion, drew attention to lower seismic demand hazards due to the use of average seismic demands from intensity-based assessments and recommended a resolution for improvements, accordingly. The study is considered as a valuable contribution to the field of GM selection-related research due to the re-incorporation of alternative IMs in lieu of $S_a(T)$. Re-appraisal of IMs different than $S_a(T)$, correspondingly, requires the comparative evaluation of the efficiency and sufficiency of alternative IMs at various levels of elastic-to-inelastic response, calling for intensity-based assessments at various intensity levels. Such endeavor eventually differentiates from the code-based or hazard-consistent GM selection (and scaling) methodologies, and necessitates a set of GM records collectively representing various ground motion characteristics. The next section describes the

general approach to form such a dataset (alternative GM subsets, indeed) for their use in further elaboration of the thesis study.

5.3   Formation of GM Subsets for MDOF-based Analyses

The first stage of this research study, SDOF-based evaluation, has utilized -with a greedy approach- the full database of GM records, the main characteristics of which are presented in Chapter 2. However, it is definitely unreasonable to employ such a large dataset in the MDOF-based evaluation stage. An adequately-sized set of records exhibiting a wide range of ground motion attributes will better suit the research purpose of evaluating the efficiency of various IMs with much less computational effort. Nonetheless, as previously raised as a concern by Riddell (2007), Yılmaz (2007), and Yakut and Yılmaz (2008), the set of records formed with simple selection criteria generally does not yield uniform distributions of tracked IMs simultaneously, which may affect the IM-specific correlation metrics due to the requirement of homoscedasticity in relevant statistical calculations.

The two distinct criteria; (1) the necessity to include a wide range of ground motion characteristics (while following a hazard-independent selection approach), and (2) to satisfy the uniform distribution of intensities as much as possible, pose a sampling problem. This study has managed to overcome this problem through the application of two distinct sampling methods:

- Stratified Random Sampling
- Cluster Sampling

The reader is referred to Appendix C at this point for detailed explanations regarding these two methods, while the supplementary text also describes their applications to the subject research study. As a by-product of this stage, the above-mentioned sampling methods have yielded 11 alternative GM subsets in total, while one of these sets is a structure-specific set conditioned on $S_a(T_1)$. Combining 10 individual random sampling-based subsets, a random sampling-combined set for each frame

(resulting in ~420-450 records in total) has been obtained to be able to compare with structure-invariant cluster sampling-based collection (with 400 records in total).

5.4 Nonlinear Time History Analyses and Preliminary Evaluation of the Sampling Subsets

To check the suitability of the alternative GM subsets for further stages of the study, nonlinear time history analyses have been performed employing the simplified equivalents (i.e., ESDOF systems) of the MDOF structural models, which were already presented in Chapter 3. The maximum seismic displacement demands of the ESDOF systems have been extracted from the transient analysis results, and corresponding MDOF system top drifts (TD) have been computed. In addition to this engineering demand parameter, maximum inter-story drift ratio (MIDR) and maximum base shear (BS) values corresponding to these computed target displacements have been extracted from the pushover curves of individual frames. The reason for selecting these 3 EDPs for response monitoring is the fact that TD and MIDR are considered to be the most essential EDPs for MDOF systems, practically indicating the overall structural performance, whereas BS is considered to be representative of the seismic demand from a force-based perspective. Even though several other EDPs (such as beam/column plastic end rotations, floor acceleration demands) and/or resulting damage indices could have been monitored as well, the study is limited to the aforementioned EDPs to evaluate the correlation of IMs with the global response of the structure.

The NLTHA-based TD results corresponding to random sampling-combined and cluster sampling sets are plotted against the shortlisted IMs to comparatively display the scatters. Figure 5.1 and Figure 5.2 are the representative plots corresponding to ESDOF-based TD results of F2S2B2 frame with T_1=0.30 sec, whereas Figure 5.3 and Figure 5.4 are the sample charts corresponding to ESDOF-based MIDR results of the same frame. The set of figures for the remaining frames can be found in Appendix D (please refer to Figure A.104 thru Figure A.115 for ESDOF-based TD

results, Figure A.116 thru Figure A.127 for ESDOF-based MIDR results). It is necessary to note here that the green, orange, and red-colored horizontal lines in the figures correspond to the assumed performance level limits (green for IO, orange for LS, and red for CP) as defined in Table 3.4.
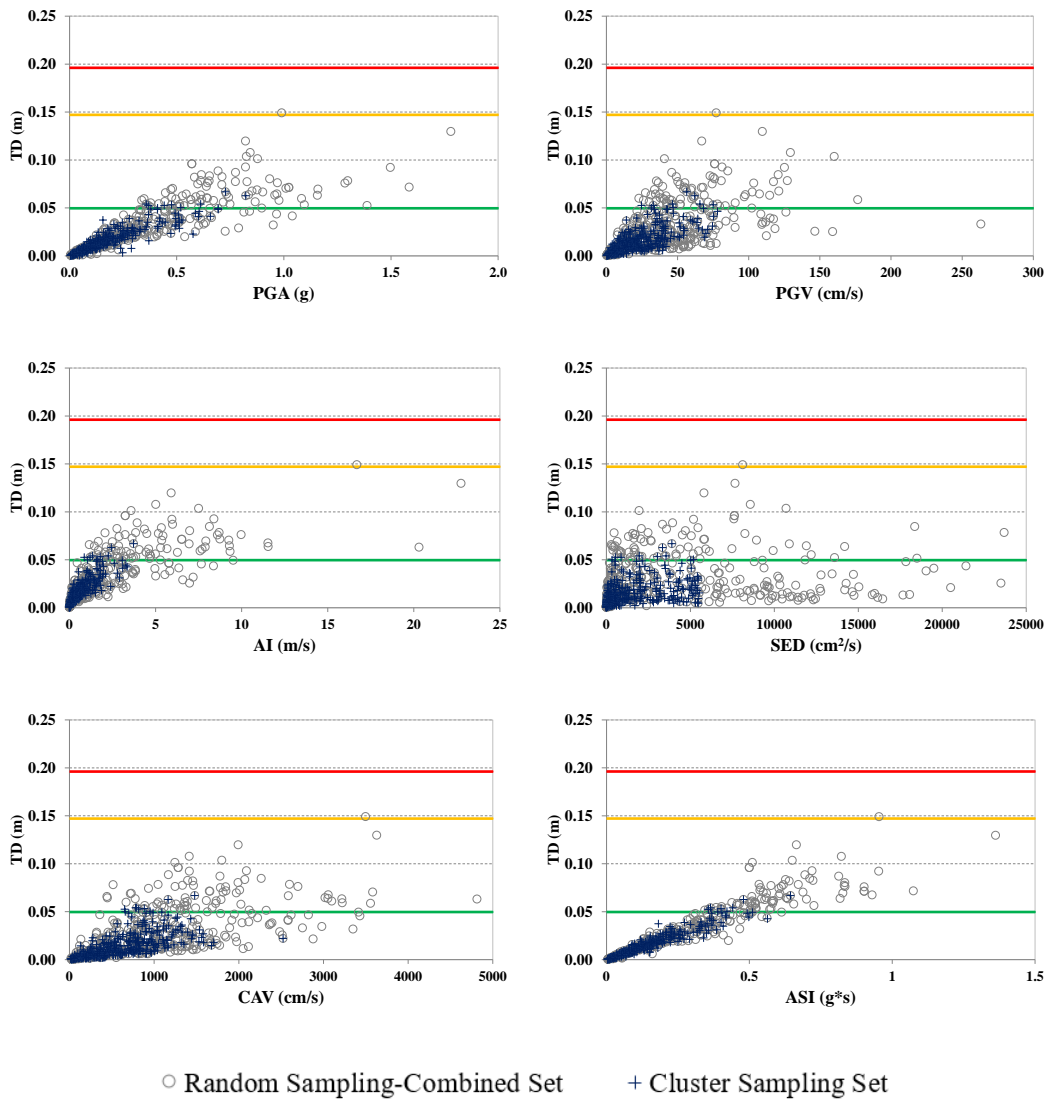
Figure 5.1. Scatter plots for selected IMs (PGA, PGV, AI, SED, CAV, ASI) versus Top Drift for F2S2B2 (T_1=0.30 s) (ESDOF)
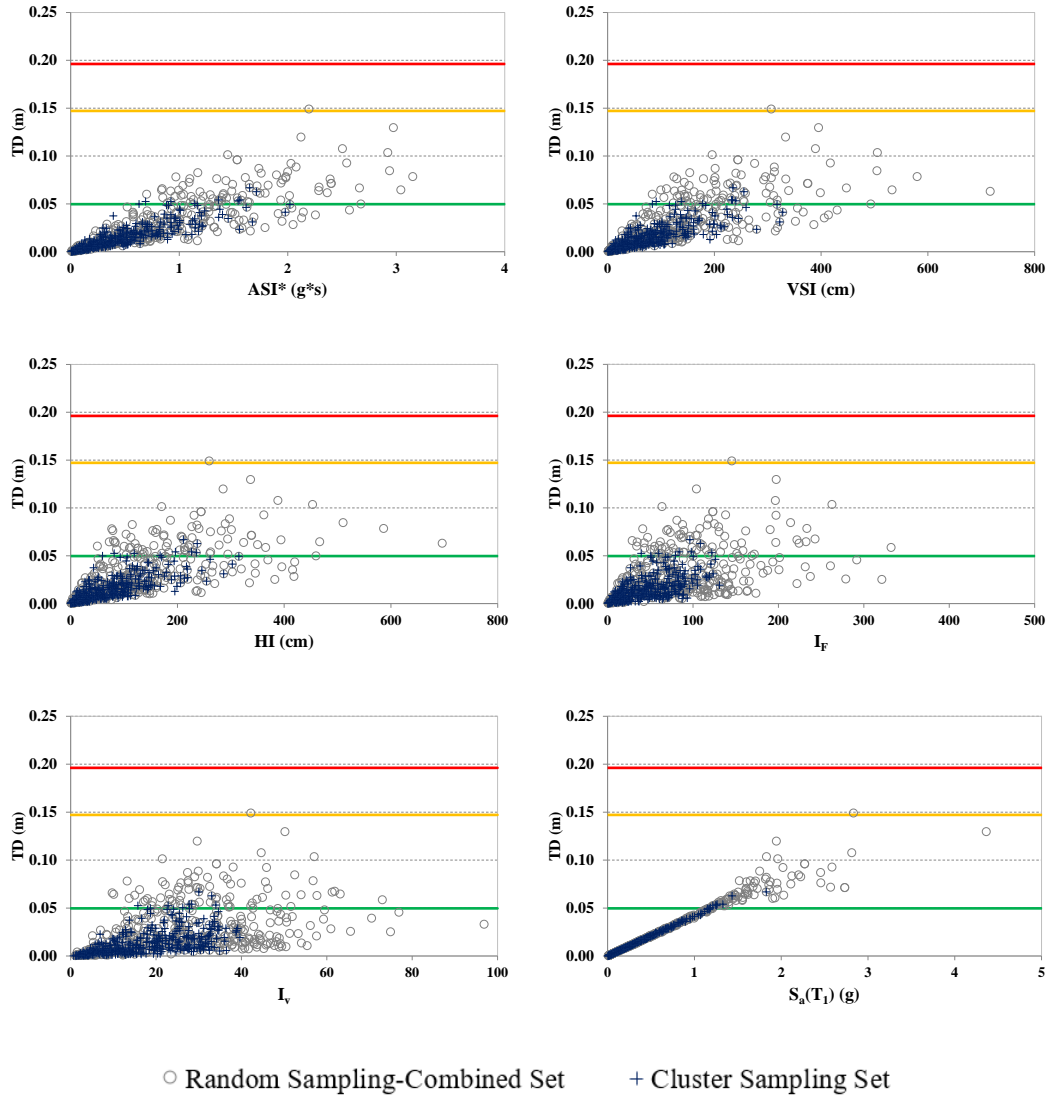
Figure 5.2. Scatter plots for selected IMs (ASI*, VSI, HI, I_F, I_V, $S_a(T_1)$) versus Top Drift for F2S2B2 (T_1=0.30 s) (ESDOF)
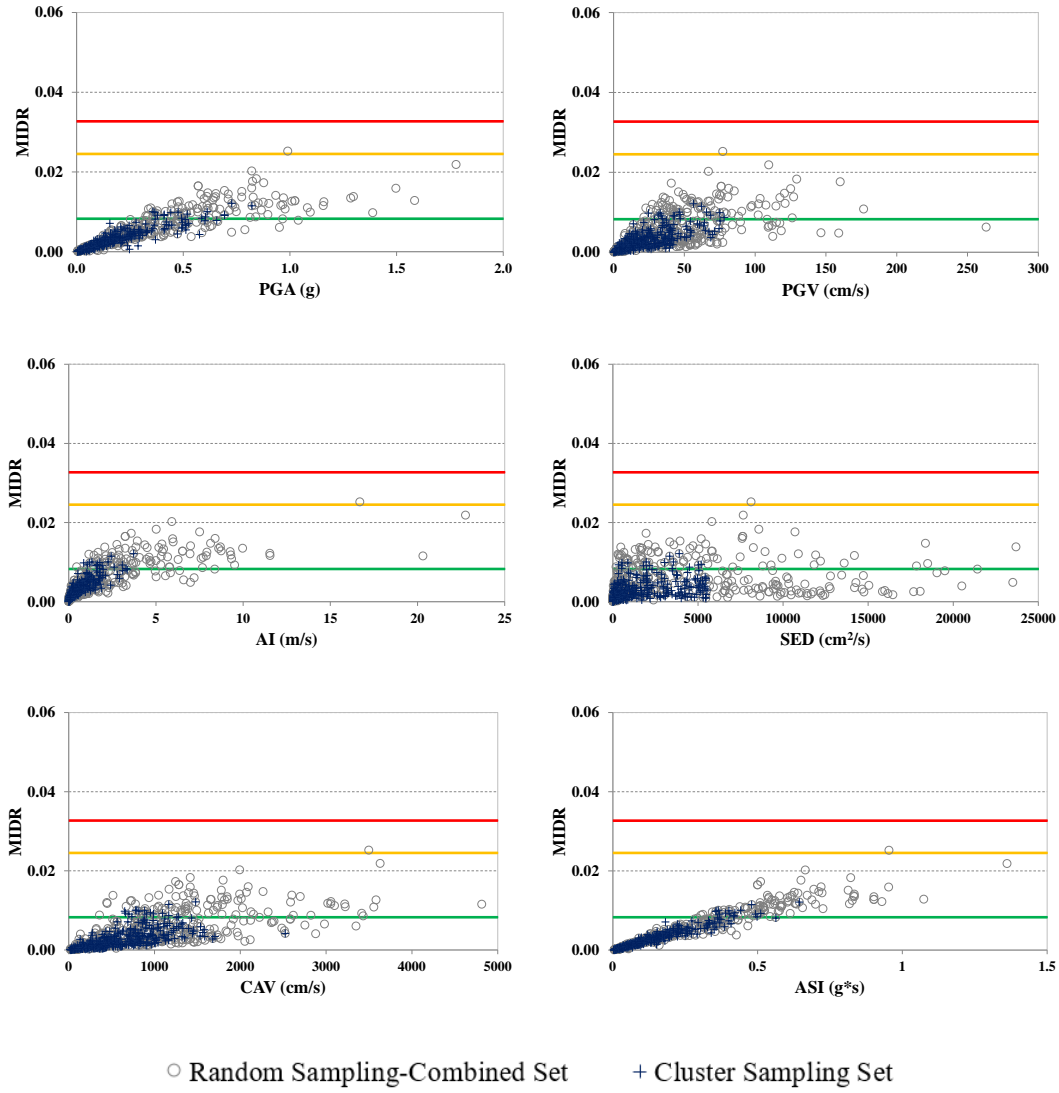
Figure 5.3. Scatter plots for selected IMs (PGA, PGV, AI, SED, CAV, ASI) versus MIDR for F2S2B2 (T_1=0.30 s) (ESDOF)
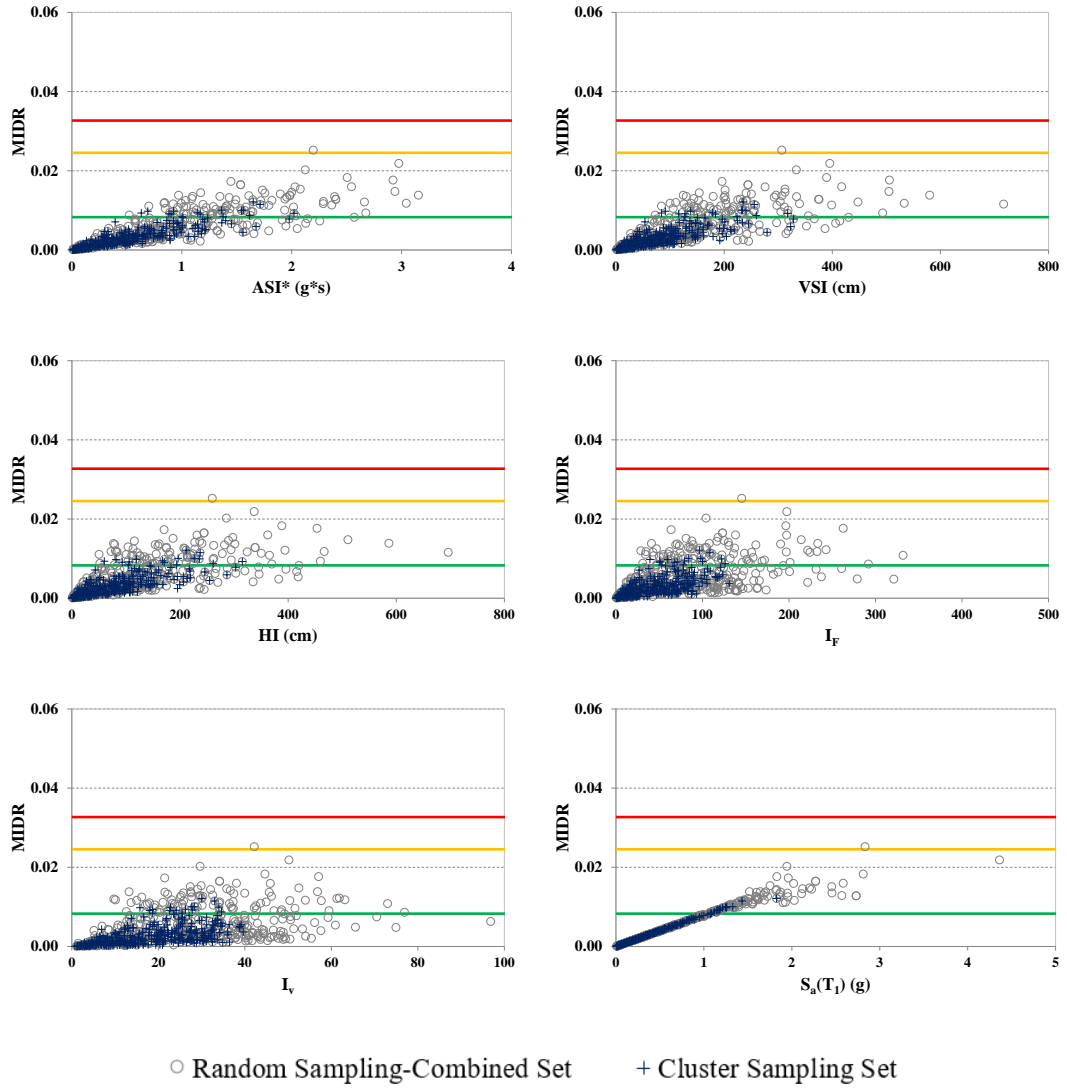
Figure 5.4. Scatter plots for selected IMs (ASI*, VSI, HI, I_F, I_V, $S_a(T_1)$) versus MIDR for F2S2B2 (T_1=0.30 s) (ESDOF)

The examination of the TD-based scatter plots for all frames have clearly revealed that the maximum response results computed under the Cluster Sampling Set generally do not cover the entire response range as expected, nevertheless, concentrate in the elastic range and beyond the IO limit state, and are very few in numbers in the moderate ductility levels (considering IO-LS range), whereas the distributions of the MIDR results are comparably better. In contrast, the Stratified Random Sampling-based Combined GM Set has obviously yielded a wider coverage with respect to the Cluster Sampling Set, leading to increased dispersion at higher intensity levels. The effect of the sampling method is much more clear in the case of S_a-based plots.

When the visual evaluations are elaborated with respect to the IMs, it can be easily expressed that S_a, in most of the cases, exhibited limited variability. PGA and ASI as a group, ranked the second-best for short-period systems, while ASI seemed to be comparably better than PGA. The variability was higher for PGV, ASI*, VSI, and HI for short-period systems, whereas ASI* was relatively better in condition with respect to PGV, VSI, and HI. For the rest of the list, the scattering of the results in SED-, CAV-, I_F, and I_v-based plots are significant. Unlike these, AI has also shown relatively less variability with respect to PGV for both frames and especially PGA for F3S2B frame having a fundamental period close to medium period systems. On the other hand, for medium-to relatively long-period systems, it has been observed that the variability in PGA- and ASI-based plots increased with increasing periods. Unlike these two, the group of PGV, ASI*, VSI, and HI has shown much smaller variability in the results, while PGV has been surpassed by the latters. It was observed in the SED-, CAV-, I_F, and I_v-based plots that the degree of variability decreased with the increasing period of the system. AI exhibited relatively limited variability as well, performing better than PGA.

5.5 ESDOF-based Evaluation of Efficiency of the Shortlisted Scalar Intensity Measures through Correlation Studies

The visual interpretations presented in the previous section have been quantified next through the calculation of Pearson correlation coefficients between the shortlisted IMs and the monitored EDPs, TD, MIDR, and BS. In accordance with the approach followed in Chapter 4, the computations have been performed over the ln-transformed data. The results from individual (Stratified Random Sampling-based) GM subsets conditioned on each scalar IM have been explicitly considered as well, to show the correlation performance of the shortlisted scalar IMs under different GM subset cases. Table 5.1-Table 5.3 summarize the numerical results corresponding to TD, MIDR, and BS, respectively, for the complete set of ESDOF models employed as simplified equivalents of the more complex MDOF frames. The results of (Stratified) Random Sampling-Combined Set and Cluster Sampling Set (presented in Table 5.1-Table 5.3) are comparatively visualized in Figure 5.5-Figure 5.7 to reveal the variation of correlation performances of the subject IMs with the fundamental period of the structural systems employed. The order of the frames in the plots has been arranged accordingly to facilitate this evaluation.

Table 5.1 Correlation of TD demands with alternative IMs under different GM record sets

IM	F2S2B2 (T₁ = 0.30 s)			F3S2B (T₁ = 0.45 s)			F2S2B (T₁ = 0.59 s)			F5S7B (T₁ = 0.66 s)			F5S2B (T₁ = 0.75 s)			F5S4B (T₁ = 0.95 s)			F8S3B (T₁ = 1.20 s)		
	Stratified Random Sampling		Cluster Sampling Set	Stratified Random Sampling		Cluster Sampling Set	Stratified Random Sampling		Cluster Sampling Set	Stratified Random Sampling		Cluster Sampling Set	Stratified Random Sampling		Cluster Sampling Set	Stratified Random Sampling		Cluster Sampling Set	Stratified Random Sampling		Cluster Sampling Set
	Individual Set	Combined Set		Individual Set	Combined Set		Individual Set	Combined Set		Individual Set	Combined Set		Individual Set	Combined Set		Individual Set	Combined Set		Individual Set	Combined Set	
PGA	0.903	0.954	0.943	0.830	0.920	0.909	0.807	0.890	0.874	0.800	0.881	0.860	0.790	0.857	0.839	0.768	0.834	0.806	0.720	0.774	0.749
PGV	0.855	0.847	0.857	0.872	0.904	0.905	0.901	0.921	0.921	0.924	0.934	0.927	0.917	0.938	0.932	0.940	0.940	0.932	0.955	0.936	0.925
AI	0.946	0.935	0.935	0.944	0.941	0.942	0.914	0.934	0.930	0.915	0.933	0.926	0.893	0.925	0.917	0.886	0.911	0.901	0.862	0.885	0.866
SED	0.527	0.712	0.747	0.677	0.805	0.824	0.708	0.840	0.853	0.755	0.865	0.867	0.786	0.883	0.884	0.801	0.902	0.900	0.826	0.923	0.919
CAV	0.884	0.829	0.840	0.912	0.867	0.878	0.925	0.880	0.885	0.929	0.890	0.890	0.921	0.896	0.892	0.906	0.896	0.898	0.892	0.892	0.884
ASI	N/A	0.982	0.977	N/A	0.936	0.930	N/A	0.894	0.887	N/A	0.882	0.874	N/A	0.862	0.848	N/A	0.833	0.812	N/A	0.781	0.756
ASI*	0.952	0.934	0.933	0.971	0.966	0.965	0.978	0.971	0.966	0.981	0.974	0.967	0.978	0.970	0.965	0.970	0.962	0.958	0.961	0.939	0.934
VSI	0.895	0.897	0.892	0.943	0.949	0.942	0.963	0.966	0.955	0.981	0.974	0.962	0.981	0.975	0.968	0.982	0.975	0.970	0.981	0.962	0.962
HI	N/A	0.857	0.861	N/A	0.922	0.924	N/A	0.951	0.942	N/A	0.965	0.953	N/A	0.972	0.964	N/A	0.977	0.973	N/A	0.976	0.976
I_F	0.829	0.793	0.815	0.861	0.865	0.877	0.868	0.894	0.900	0.890	0.913	0.910	0.880	0.923	0.920	0.909	0.932	0.929	0.939	0.939	0.932
I_v	0.757	0.722	0.758	0.802	0.805	0.832	0.859	0.846	0.863	0.869	0.873	0.877	0.876	0.889	0.891	0.895	0.904	0.910	0.915	0.922	0.923
S_a(T₁)	0.992	0.999	1.000	0.989	0.997	1.000	0.985	0.995	0.998	0.991	0.997	0.999	0.994	0.996	0.998	0.992	0.997	0.999	0.992	0.997	0.999
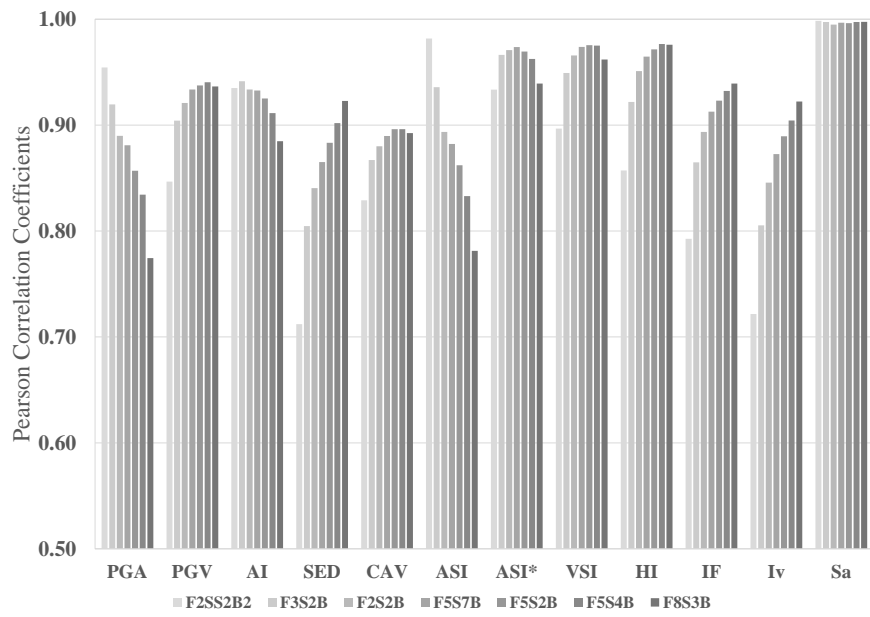
(a) Stratified Random Sampling-Combined Set
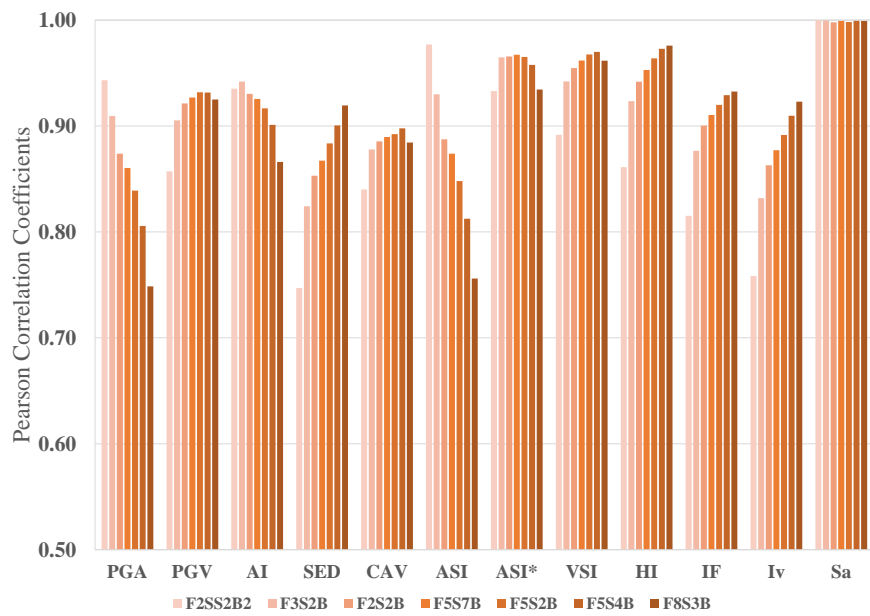
(b) Cluster Sampling Set

Figure 5.5. Comparison of ESDOF-TD-based Pearson correlation coefficients calculated for the shortlisted IMs

Table 5.2 Correlation of MIDR demands with alternative IMs under different GM record sets

IM	F2S2B2 (T₁ = 0.30 s)			F3S2B (T₁ = 0.45 s)			F2S2B (T₁ = 0.59 s)			F5S7B (T₁ = 0.66 s)			F5S2B (T₁ = 0.75 s)			F5S4B (T₁ = 0.95 s)			F8S3B (T₁ = 1.20 s)		
	Stratified Random Sampling		Cluster Sampling Set	Stratified Random Sampling		Cluster Sampling Set	Stratified Random Sampling		Cluster Sampling Set	Stratified Random Sampling		Cluster Sampling Set	Stratified Random Sampling		Cluster Sampling Set	Stratified Random Sampling		Cluster Sampling Set	Stratified Random Sampling		Cluster Sampling Set
	Individual Set	Combined Set		Individual Set	Combined Set		Individual Set	Combined Set		Individual Set	Combined Set		Individual Set	Combined Set		Individual Set	Combined Set		Individual Set	Combined Set	
PGA	0.905	0.955	0.943	0.832	0.919	0.910	0.809	0.889	0.873	0.801	0.883	0.862	0.790	0.859	0.841	0.768	0.835	0.807	0.720	0.776	0.750
PGV	0.857	0.848	0.857	0.878	0.907	0.906	0.904	0.922	0.921	0.922	0.931	0.925	0.914	0.935	0.931	0.940	0.940	0.931	0.955	0.936	0.925
AI	0.949	0.936	0.935	0.947	0.942	0.943	0.917	0.934	0.930	0.915	0.932	0.925	0.894	0.925	0.916	0.888	0.912	0.901	0.865	0.885	0.866
SED	0.529	0.713	0.746	0.687	0.809	0.826	0.714	0.842	0.853	0.740	0.860	0.863	0.772	0.879	0.880	0.797	0.901	0.900	0.816	0.920	0.917
CAV	0.887	0.830	0.839	0.918	0.869	0.880	0.929	0.882	0.886	0.925	0.887	0.886	0.918	0.894	0.889	0.906	0.896	0.897	0.891	0.891	0.882
ASI	N/A	0.982	0.977	N/A	0.935	0.930	N/A	0.894	0.887	N/A	0.883	0.874	N/A	0.864	0.849	N/A	0.834	0.813	N/A	0.782	0.757
ASI*	0.954	0.934	0.933	0.972	0.967	0.965	0.979	0.971	0.965	0.981	0.973	0.967	0.979	0.969	0.965	0.971	0.963	0.958	0.962	0.940	0.935
VSI	0.899	0.897	0.892	0.947	0.950	0.943	0.966	0.966	0.954	0.980	0.973	0.961	0.981	0.975	0.967	0.982	0.975	0.970	0.981	0.962	0.962
HI	N/A	0.858	0.861	N/A	0.924	0.924	N/A	0.952	0.942	N/A	0.963	0.951	N/A	0.970	0.963	N/A	0.976	0.973	N/A	0.976	0.976
I_F	0.833	0.794	0.815	0.866	0.868	0.878	0.873	0.895	0.900	0.888	0.909	0.908	0.878	0.920	0.918	0.909	0.932	0.929	0.940	0.938	0.931
I_v	0.759	0.723	0.758	0.807	0.809	0.833	0.862	0.848	0.863	0.864	0.868	0.874	0.871	0.886	0.888	0.894	0.903	0.909	0.914	0.920	0.921
S_a(T₁)	0.992	0.998	1.000	0.989	0.997	0.999	0.985	0.995	0.998	0.991	0.997	0.999	0.994	0.996	0.998	0.992	0.998	0.999	0.993	0.998	0.999

(a) Stratified Random Sampling-Combined Set

(b) Cluster Sampling Set

Figure 5.6. Comparison of ESDOF-MIDR-based Pearson correlation coefficients calculated for the shortlisted IMs

Table 5.3 Correlation of BS demands with alternative IMs under different GM record sets

IM	F2S2B2 (T₁ = 0.30 s) Individual Set	F2S2B2 Combined Set	F2S2B2 Cluster Sampling Set	F3S2B (T₁ = 0.45 s) Individual Set	F3S2B Combined Set	F3S2B Cluster Sampling Set	F2S2B (T₁ = 0.59 s) Individual Set	F2S2B Combined Set	F2S2B Cluster Sampling Set	F5S7B (T₁ = 0.66 s) Individual Set	F5S7B Combined Set	F5S7B Cluster Sampling Set	F5S2B (T₁ = 0.75 s) Individual Set	F5S2B Combined Set	F5S2B Cluster Sampling Set	F5S4B (T₁ = 0.95 s) Individual Set	F5S4B Combined Set	F5S4B Cluster Sampling Set	F8S3B (T₁ = 1.20 s) Individual Set	F8S3B Combined Set	F8S3B Cluster Sampling Set
PGA	0.906	0.951	0.943	0.829	0.905	0.904	0.794	0.865	0.862	0.793	0.857	0.849	0.767	0.821	0.821	0.762	0.814	0.795	0.710	0.750	0.732
PGV	0.873	0.856	0.857	0.896	0.912	0.907	0.911	0.925	0.923	0.919	0.933	0.926	0.909	0.932	0.929	0.932	0.935	0.930	0.947	0.926	0.920
AI	0.955	0.937	0.936	0.949	0.938	0.943	0.908	0.925	0.930	0.901	0.923	0.924	0.871	0.908	0.912	0.890	0.903	0.899	0.859	0.871	0.860
SED	0.556	0.727	0.747	0.732	0.824	0.831	0.805	0.861	0.865	0.834	0.878	0.876	0.879	0.897	0.896	0.873	0.908	0.908	0.905	0.926	0.925
CAV	0.904	0.837	0.841	0.937	0.875	0.884	0.941	0.888	0.896	0.945	0.895	0.898	0.924	0.898	0.903	0.922	0.899	0.905	0.908	0.892	0.890
ASI	N/A	0.977	0.977	N/A	0.922	0.927	N/A	0.873	0.882	N/A	0.863	0.868	N/A	0.831	0.837	N/A	0.818	0.807	N/A	0.763	0.745
ASI*	0.961	0.937	0.933	0.967	0.962	0.964	0.960	0.959	0.962	0.958	0.961	0.964	0.945	0.948	0.958	0.950	0.949	0.953	0.939	0.919	0.926
VSI	0.919	0.902	0.892	0.957	0.948	0.942	0.960	0.957	0.952	0.961	0.964	0.960	0.951	0.958	0.962	0.960	0.962	0.967	0.953	0.942	0.954
HI	N/A	0.864	0.861	N/A	0.925	0.925	N/A	0.947	0.942	N/A	0.958	0.953	N/A	0.958	0.961	N/A	0.967	0.972	N/A	0.959	0.971
I_F	0.853	0.805	0.816	0.883	0.879	0.881	0.890	0.905	0.907	0.896	0.919	0.914	0.878	0.927	0.925	0.903	0.932	0.932	0.926	0.935	0.932
I_v	0.768	0.736	0.759	0.826	0.824	0.839	0.876	0.865	0.875	0.884	0.885	0.886	0.888	0.902	0.903	0.905	0.910	0.916	0.920	0.924	0.928
$S_a(T_1)$	0.976	0.993	0.999	0.970	0.987	0.997	0.952	0.976	0.990	0.960	0.980	0.993	0.960	0.972	0.986	0.963	0.982	0.994	0.955	0.979	0.993

100
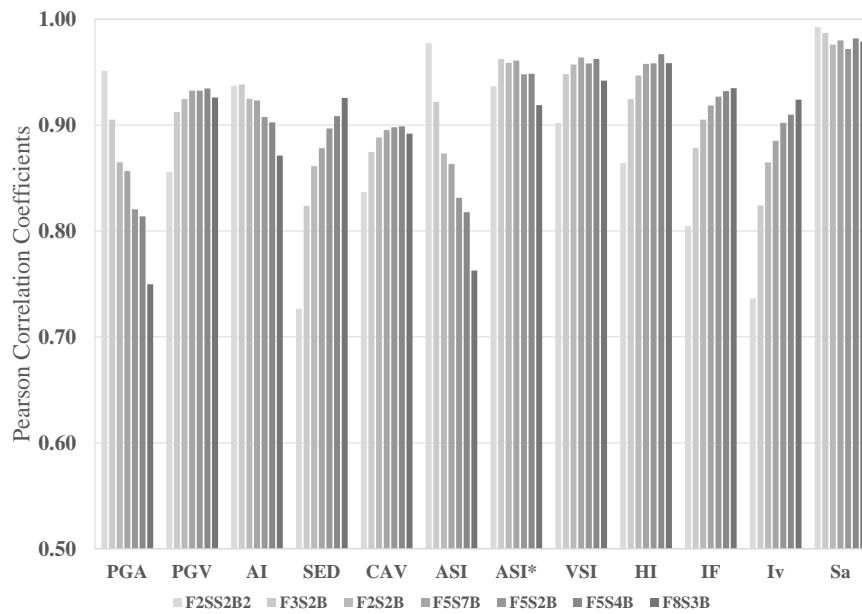
(a) Stratified Random Sampling-Combined Set
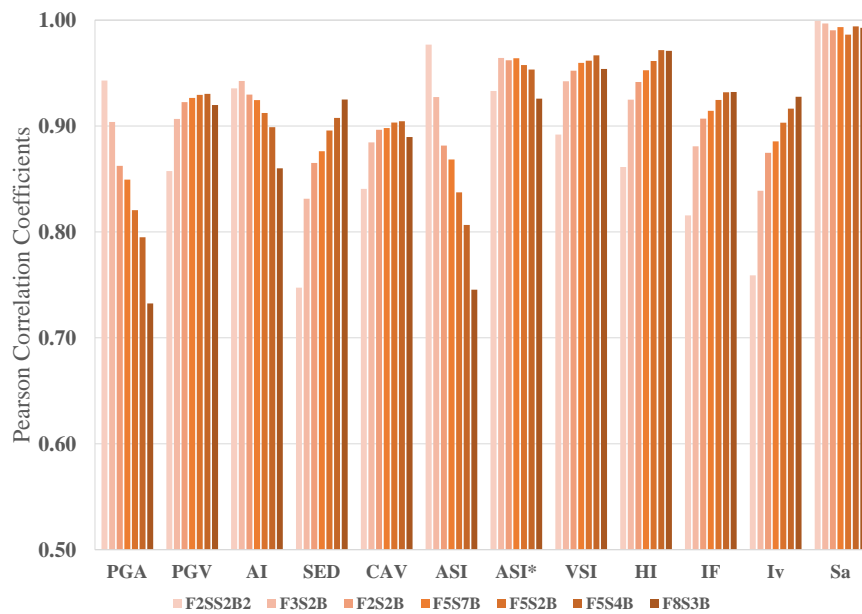
(b) Cluster Sampling Set

Figure 5.7. Comparison of ESDOF-BS-based Pearson correlation coefficients calculated for the shortlisted IMs

Figure 5.5 has revealed again that PGA is strongly correlating with TD demands of short periods, however, it is not efficient for medium- and long-period systems. With relative superiority over PGA at short periods, ASI has also exhibited similar behavior. In contrast, AI showed a much more stable performance considering the entire short-to-medium period range of the structures analyzed. PGV, with moderate correlation performance at short periods, has exhibited a better performance considering the systems with higher periods. ASI*, considering a wider period range, displayed a correlation performance similar to VSI, thus outperformed the original ASI with a steady performance over the entire period range. VSI and HI generally exhibited similar behavior, while HI was inefficient at very short periods. The trends in SED, CAV, I_F, and I_V were generally similar, SED and I_V being the worst two at very short periods. Unlike the rest, S_a turned out to be the most efficient parameter, with Pearson coefficients reaching 1.0. Finally, though the suitability of the Cluster Sampling Set has been questioned above, no significant difference in the overall results has been identified; eventually, both GM sets yielded similar patterns. The correlation trends of the intensity indices with both ESDOF-based MIDR and BS demands, as displayed in Figure 5.6 and Figure 5.7, support the findings of TD-based evaluations. As a key remark from the observations noted above; it could be stated that relatively better performance of ASI* and VSI (in terms of efficiency) over the entire period range considered (i.e., T_1=0.3-1.2 sec for this study) makes these two parameters better candidates with respect to the rest of the non-structure specific IMs. The structure-specific S_a, on the other hand, remained the best candidate among the set of shortlisted scalar IMs, as expected. Finally, the numerical results reported herein are generally complying with the results of SDOF-based evaluations (which are presented in Chapter 4), thus leading to similar trends in the period-wise variations.

5.6　MDOF-based Evaluation of Efficiency of the Shortlisted Scalar Intensity Measures through Correlation Studies

The efficiency of a downsized list of scalar IMs has been thoroughly questioned up to this section via generic SDOF systems and a set of ESDOF models corresponding to selected typical reinforced concrete frames. This section extends the analyses and numerical correlation evaluations to MDOF realizations of the employed structural models in order to check the validity of the ESDOF-based interpretations. However, the Cluster Sampling GM dataset has been considered not to be utilized after the observations from the previous sections regarding the uneven distribution of the set of results concentrated at relatively low intensity levels. Conversely, this section utilizes the individual GM subsets originally formed with the Stratified Random Sampling approach to evaluate the main problem. With this respect, PGA-, PGV-, AI-, SED-, CAV-, ASI*-, VSI-, I_F-, I_v- and structure specific-$S_a(T_1)$-based GM subsets have been employed to perform NTH analyses on the MDOF systems, and the results from these analyses have been considered as "true response".

Figure 5.8 and Figure 5.9 represent the TD-based scatter in data with respect to the shortlisted IMs for frame F2S2B2 with T_1=0.30 sec, whereas Figure 5.10 and Figure 5.11 display MIDR-based scatter with respect to the same IMs. The set of figures for the remaining frames can be found in Appendix D (please refer to Figure A.128 thru Figure A.139 for MDOF-based TD results, Figure A.140 for MDOF-based MIDR results Figure A.151). The continuous black lines in these figures are simply the lines connecting the bin-wise mean responses, thus, visualizing the change/trend in response means along the entire intensity considered, while the dashed lines refer to mean ± one standard deviation bands calculated again bin-wise. For the bins where the number of results available is less than 3, the standard deviation is not calculated; thus, the mean ± one standard deviation band lines are not plotted. The coloured horizontal lines correspond to assumed IO, LS, and CP limit states of the structure, respectively.
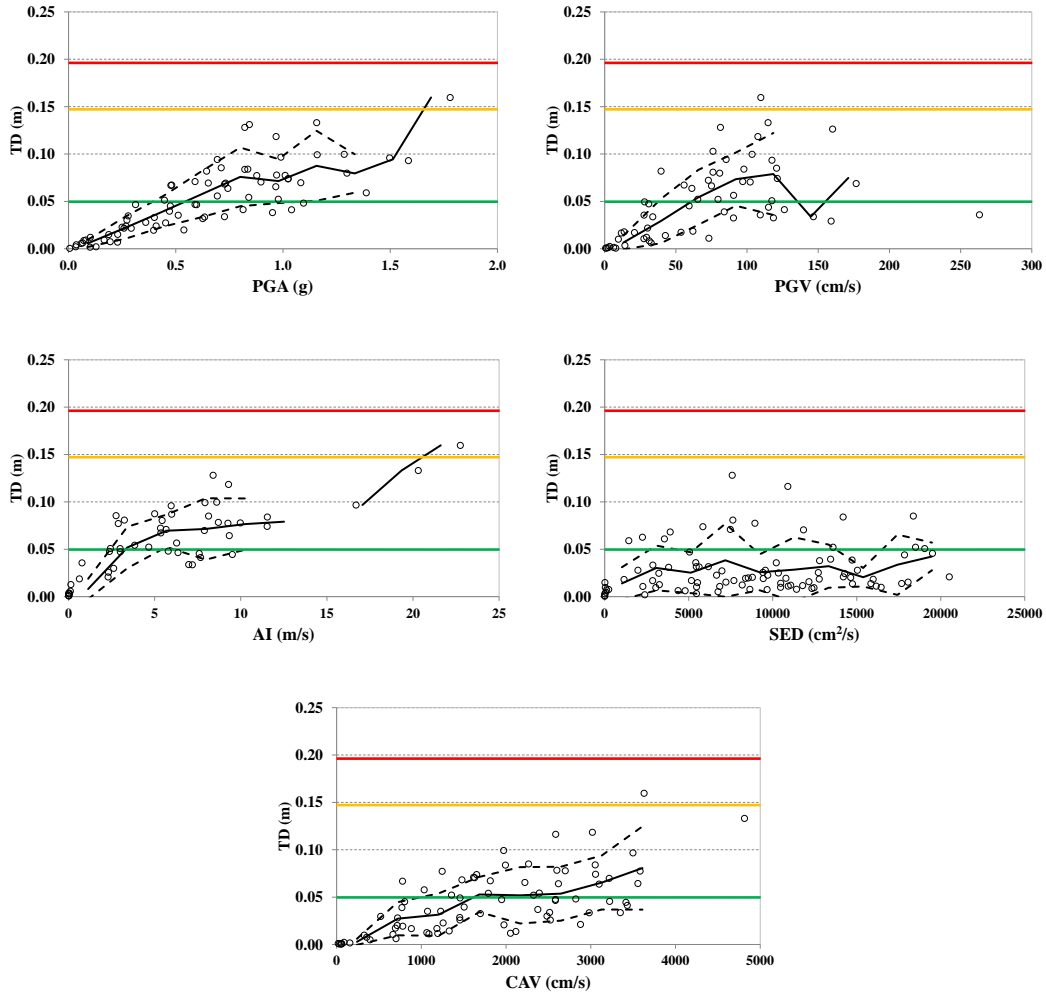
Figure 5.8. Scatter plots for selected IMs (PGA, PGV, AI, SED, CAV) versus Top Drift for F2S2B2 (T_1=0.30 s) (MDOF)
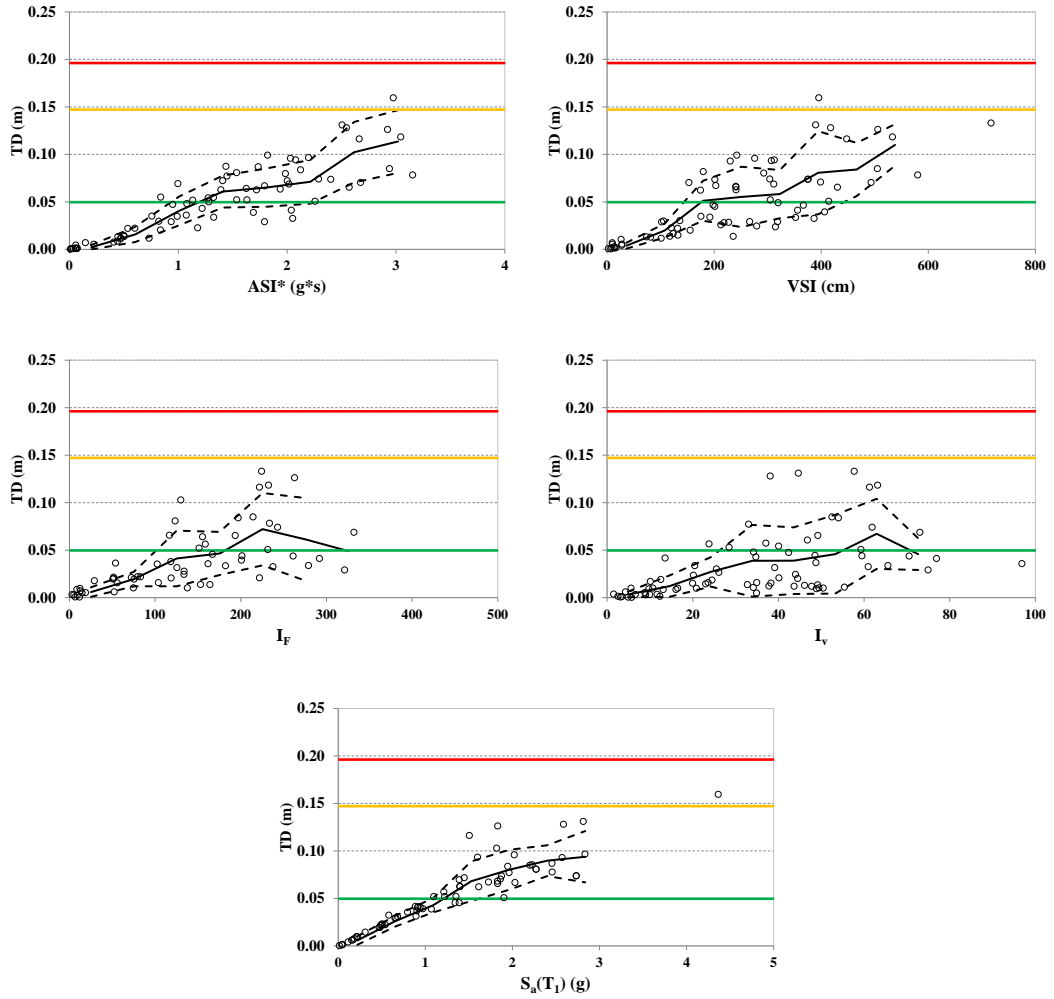
Figure 5.9. Scatter plots for selected IMs (ASI*, VSI, I_F, I_V, $S_a(T_1)$) versus Top Drift for F2S2B2 (T_1=0.30 s) (MDOF)
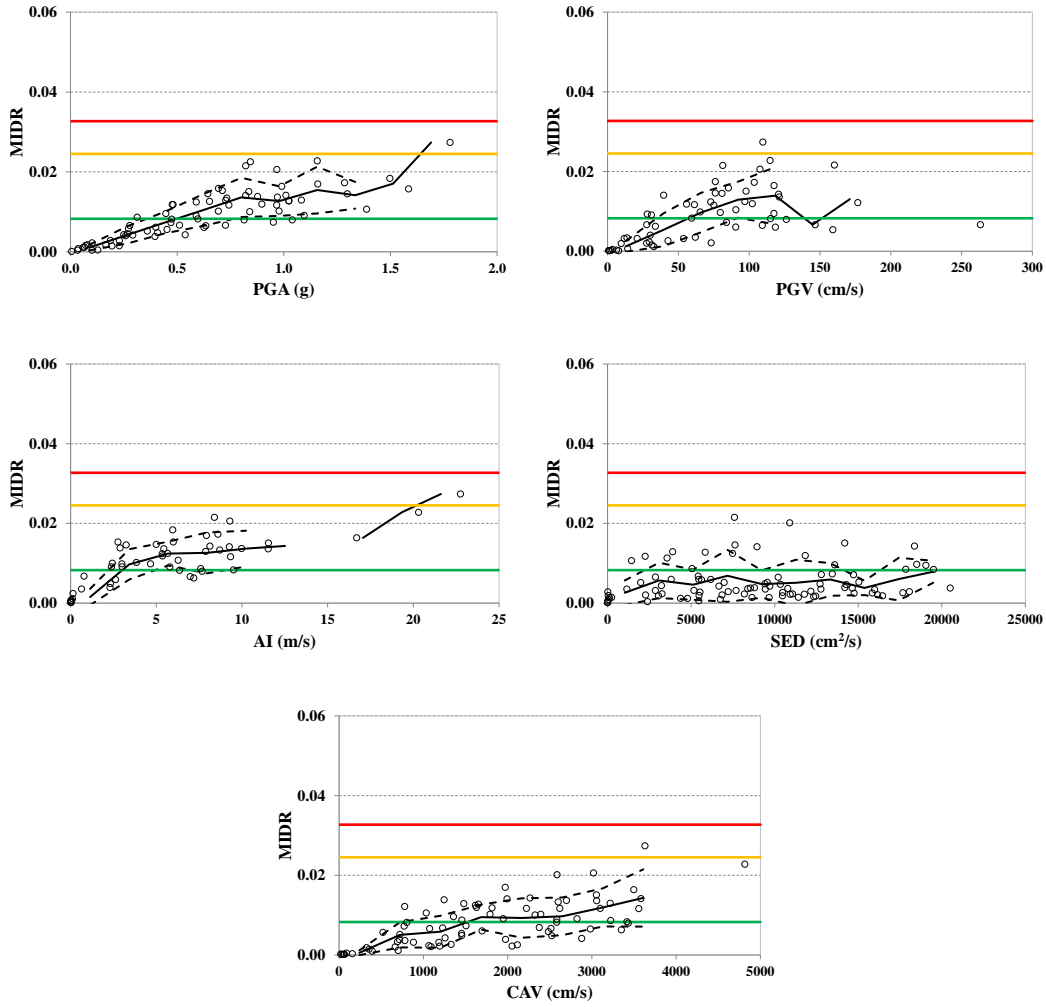
Figure 5.10.Scatter plots for selected IMs (PGA, PGV, AI, SED, CAV) versus MIDR for F2S2B2 (T_1=0.30 s) (MDOF)

106
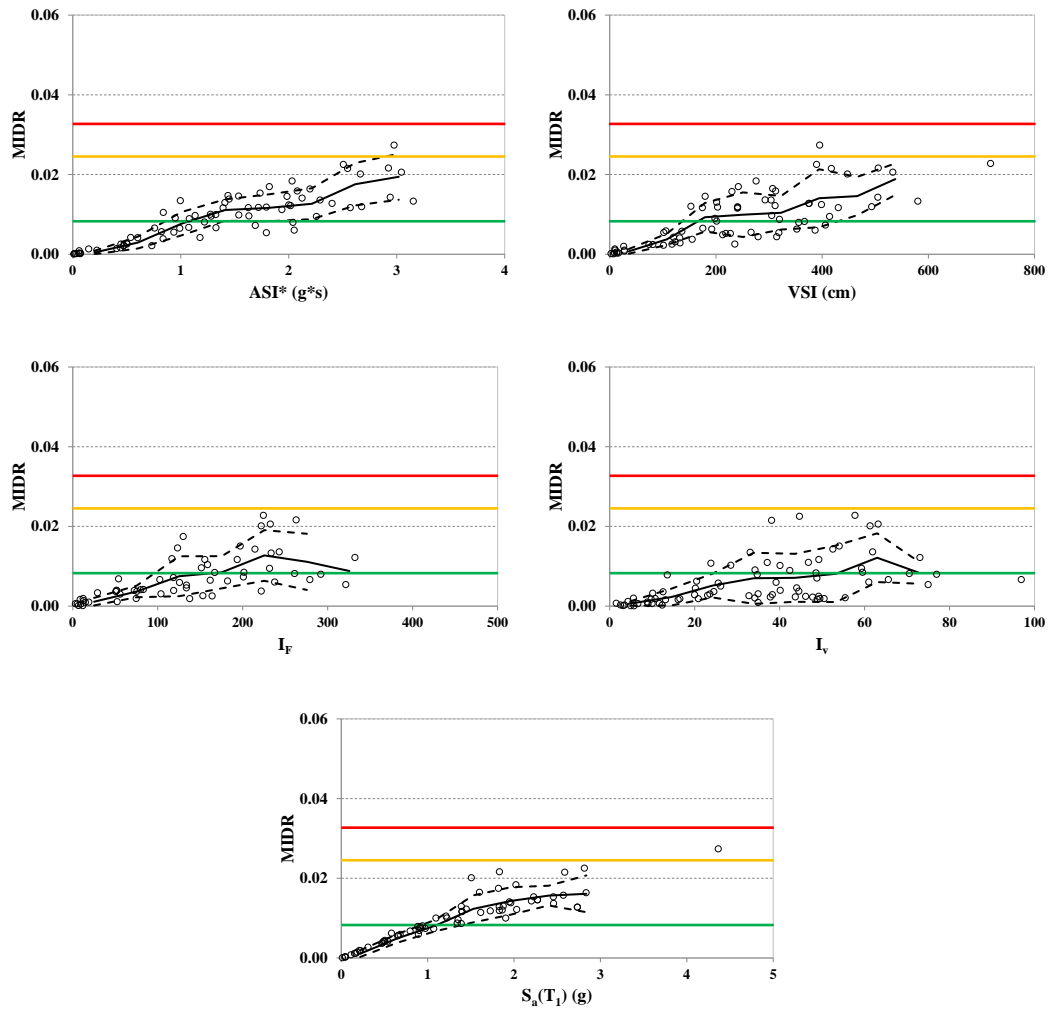
Figure 5.11. Scatter plots for selected IMs (ASI*, VSI, I_F, I_V, $S_a(T_1)$) versus MIDR for F2S2B2 (T_1=0.30 s) (MDOF)

It is crucial to note for these figures here that each IM vs. TD/MIDR plot corresponds to a different GM subset (made available by the Stratified Random Sampling approach) where the IM defines the conditioning IM as well (in other words, DB IM=IM).

Overall evaluation of these figures has revealed similar observations with the ESDOF-based charts such that structure-specific S_a and structure-independent but spectrum-based ASI*-VSI alternatives yield the least dispersion, marking their superior efficiency over AI, SED, CAV, I_F, and I_v. Besides, PGA and PGV have confirmed their expected performances as well, in terms of reducing the dispersion in the results for short- and medium-period systems, respectively. The increase in bin-wise dispersions with increasing levels of intensities has been clearly observed generally through the widening of the $\pm 1 \sigma$ bands. The degree of bin-wise dispersions has been quantified especially for MIDR case via the statistical parameter "coefficient of variation" calculated through:

$$\mu_{\ln MIDR} = \frac{1}{n} \sum_{i=1}^{n} (lnMIDR_i) \tag{5.1}$$

$$\sigma_{\ln MIDR} = \sqrt{\frac{1}{n-1} \sum_{i=1}^{n} (lnMIDR_i - \mu_{\ln MIDR})^2} \tag{5.2}$$

$$CoV = \frac{\sigma_{\ln MIDR}}{\mu_{\ln MIDR}} \tag{5.3}$$

The results have been thoroughly evaluated to identify the minimum and maximum values, later used to reveal the characteristics of the shortlisted IMs. Figure 5.12 and Figure 5.13 display the range of bin-wise CoV values corresponding to each IM and frame case, where the latter plot is prepared with an approach that the CoV values calculated from the first bins of the GM subsets are neglected due to the sensitivity of numerical results in low intensity levels. Consequently, Figure 5.13 has revealed

a much better representation of the dispersion performance of the subject IMs, $S_a(T_1)$, ASI*, and VSI generally put forward based on their low CoV_{min} levels.
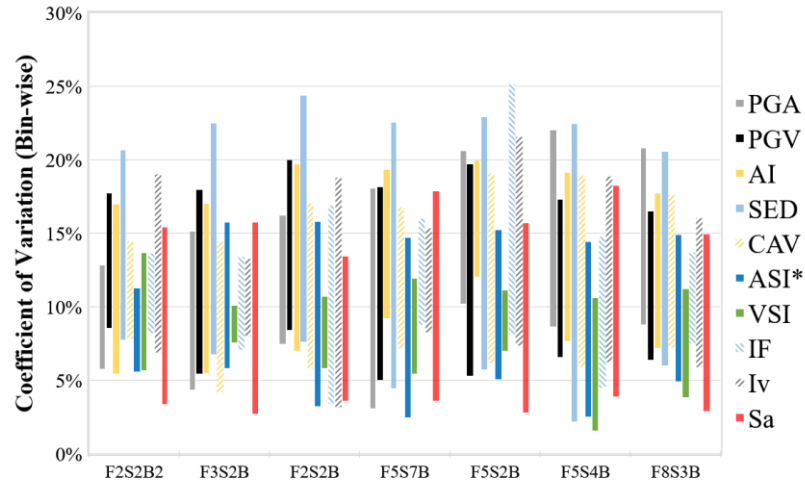
Figure 5.12. Min-max ranges of bin-wise coefficient of variation values corresponding to MIDR under different GM subsets
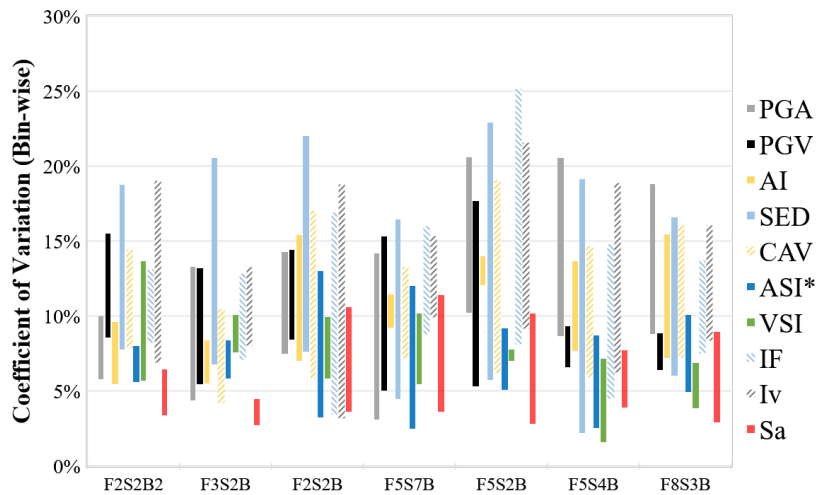
Figure 5.13. Min-max ranges of bin-wise coefficient of variation values corresponding to MIDR under different GM subsets (neglecting the initial intensity bin-based results)

As the next step, Pearson correlation coefficients between the shortlisted IMs and the monitored EDPs of MDOF systems were calculated applying ln-transformation in advance. Table 5.4 summarizes the numerical results obtained from MDOF-based analyses along with the corresponding set of results obtained from the ESDOF-based systems, whereas Figure 5.14-Figure 5.16 portray the variation of correlation performances of the subject IMs with the fundamental periods.

Figure 5.14-Figure 5.15 couple has exhibited that SED is the least efficient IM among the shortlisted IMs, while the performance is slightly better for BS-based correlations. PGA showed a strong correlation for just one case, F2S2B2 frame, while this performance has rapidly diminished with other frames having higher fundamental periods. PGV and AI relatively showed better performance in the entire period range of consideration (T=0.3-1.2 sec). I_F and I_v exhibited slightly lower correlations with respect to PGV and AI, yet improved with increasing periods. ASI* and VSI generally showed a good stable performance, while VSI yielded a lower correlation for the short period structure. CAV has also exhibited a stable correlation performance, but relatively lower with respect to ASI* and VSI. The results are generally comparable within ESDOF- and MDOF-based results sets. Figure 5.16 has revealed that SED correlated better with BS in contrast to its correlations with TD and MIDR. The rest of the shortlisted IMs generally preserved their correlation performances.

In addition to the comparative Pearson-metric-based evaluations over ESDOF- and MDOF-based result sets, the correlation between the ESDOF- and MDOF- results has also been investigated to check the validity of equivalent system-based analysis results. Table 5.5 presents Pearson-metrics as well as other statistical terms (i.e., minimum, maximum, mean, median, and coefficient of variation) computed from the ratio, $response_{equivalent}/response_{true}$. The Pearson-metric, mean, and median-based statistics confirm the suitability of the use of simple equivalent systems; nonetheless, the extreme values of min-max values eventually raise concerns for individual cases.

110

Table 5.4 Correlation results (10 distinct Random-Sampling based subsets)

Maximum Top Displacement (TD)

IM	F2S2B2 (T1 = 0.30 s) SDOF	MDOF	F3S2B (T1 = 0.45 s) SDOF	MDOF	F2S2B (T1 = 0.59 s) SDOF	MDOF	F7S7B (T1 = 0.66 s) SDOF	MDOF	F2S2B (T1 = 0.75 s) SDOF	MDOF	F4S4B (T1 = 0.95 s) SDOF	MDOF	F8S3B (T1 = 1.20 s) SDOF	MDOF
PGA	0.903	0.918	0.830	0.829	0.807	0.812	0.800	0.786	0.790	0.770	0.768	0.773	0.720	0.729
PGV	0.855	0.854	0.872	0.885	0.901	0.916	0.924	0.921	0.917	0.908	0.940	0.947	0.955	0.962
AI	0.946	0.954	0.944	0.936	0.914	0.924	0.915	0.928	0.893	0.888	0.886	0.894	0.862	0.866
SED	0.527	0.552	0.677	0.686	0.708	0.713	0.755	0.814	0.786	0.758	0.801	0.805	0.826	0.842
CAV	0.884	0.895	0.912	0.923	0.925	0.916	0.929	0.948	0.921	0.889	0.906	0.908	0.892	0.897
ASI*	0.952	0.965	0.971	0.969	0.978	0.982	0.981	0.984	0.978	0.973	0.970	0.977	0.961	0.963
VSI	0.895	0.911	0.943	0.953	0.963	0.977	0.981	0.981	0.981	0.978	0.982	0.984	0.981	0.980
I_F	0.829	0.826	0.861	0.863	0.868	0.882	0.890	0.888	0.880	0.878	0.909	0.918	0.939	0.943
I_v	0.757	0.752	0.802	0.815	0.859	0.859	0.869	0.879	0.876	0.854	0.895	0.895	0.915	0.924
$S_a(T_1)$	0.992	0.986	0.989	0.986	0.985	0.975	0.991	0.990	0.994	0.987	0.992	0.991	0.992	0.986

Maximum Inter-story Drift Ratio (MIDR)

IM	F2S2B2 (T1 = 0.30 s) SDOF	MDOF	F3S2B (T1 = 0.45 s) SDOF	MDOF	F2S2B (T1 = 0.59 s) SDOF	MDOF	F7S7B (T1 = 0.66 s) SDOF	MDOF	F2S2B (T1 = 0.75 s) SDOF	MDOF	F4S4B (T1 = 0.95 s) SDOF	MDOF	F8S3B (T1 = 1.20 s) SDOF	MDOF
PGA	0.905	0.927	0.832	0.847	0.809	0.843	0.801	0.818	0.790	0.797	0.768	0.801	0.720	0.795
PGV	0.857	0.855	0.878	0.886	0.904	0.911	0.922	0.916	0.914	0.920	0.940	0.950	0.955	0.962
AI	0.949	0.955	0.947	0.941	0.917	0.933	0.915	0.926	0.894	0.908	0.888	0.915	0.865	0.920
SED	0.529	0.548	0.687	0.693	0.714	0.703	0.740	0.797	0.772	0.763	0.797	0.791	0.816	0.784
CAV	0.887	0.897	0.918	0.926	0.929	0.925	0.925	0.946	0.918	0.907	0.906	0.912	0.891	0.909
ASI*	0.954	0.965	0.972	0.970	0.979	0.984	0.981	0.984	0.979	0.979	0.971	0.983	0.962	0.984
VSI	0.899	0.911	0.947	0.955	0.966	0.977	0.980	0.983	0.981	0.987	0.982	0.984	0.981	0.988
I_F	0.833	0.827	0.866	0.865	0.873	0.880	0.888	0.885	0.878	0.886	0.909	0.917	0.940	0.938
I_v	0.759	0.751	0.807	0.817	0.862	0.856	0.864	0.871	0.871	0.853	0.894	0.895	0.914	0.912
$S_a(T_1)$	0.992	0.986	0.989	0.985	0.985	0.979	0.991	0.988	0.994	0.989	0.992	0.991	0.993	0.986

Maximum Base Shear (V)

IM	F2S2B2 (T1 = 0.30 s) SDOF	MDOF	F3S2B (T1 = 0.45 s) SDOF	MDOF	F2S2B (T1 = 0.59 s) SDOF	MDOF	F7S7B (T1 = 0.66 s) SDOF	MDOF	F2S2B (T1 = 0.75 s) SDOF	MDOF	F4S4B (T1 = 0.95 s) SDOF	MDOF	F8S3B (T1 = 1.20 s) SDOF	MDOF
PGA	0.906	0.911	0.829	0.876	0.794	0.875	0.793	0.835	0.767	0.822	0.762	0.823	0.710	0.822
PGV	0.873	0.873	0.896	0.905	0.911	0.919	0.919	0.924	0.909	0.920	0.932	0.947	0.947	0.953
AI	0.955	0.962	0.949	0.958	0.908	0.948	0.901	0.943	0.871	0.915	0.890	0.929	0.859	0.929
SED	0.556	0.591	0.732	0.739	0.805	0.799	0.834	0.842	0.879	0.866	0.873	0.865	0.905	0.886
CAV	0.904	0.908	0.937	0.940	0.941	0.945	0.945	0.953	0.924	0.939	0.922	0.936	0.908	0.931
ASI*	0.961	0.971	0.957	0.971	0.960	0.969	0.958	0.973	0.945	0.959	0.950	0.969	0.939	0.971
VSI	0.919	0.934	0.957	0.964	0.960	0.968	0.961	0.968	0.951	0.969	0.960	0.968	0.953	0.967
I_F	0.853	0.860	0.883	0.886	0.890	0.900	0.896	0.887	0.878	0.897	0.903	0.913	0.926	0.943
I_v	0.768	0.775	0.826	0.836	0.876	0.878	0.884	0.882	0.888	0.888	0.905	0.913	0.920	0.930
$S_a(T_1)$	0.976	0.970	0.970	0.970	0.952	0.956	0.960	0.970	0.960	0.971	0.963	0.970	0.955	0.968
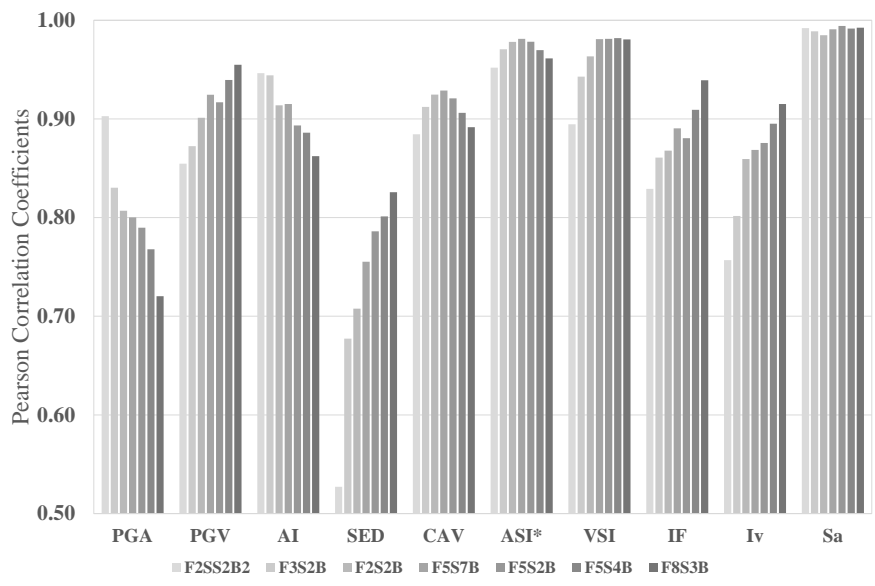
(a) ESDOF-based results
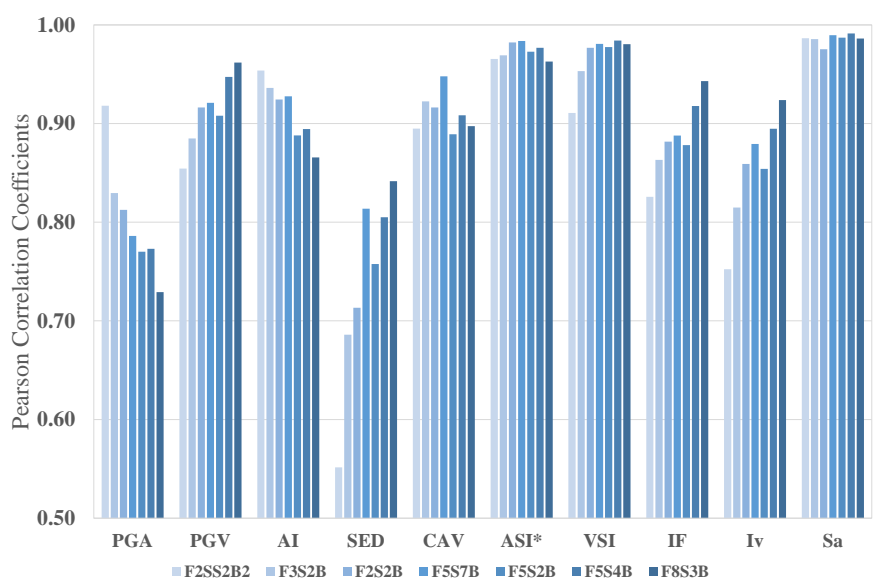
(b) MDOF-based results

Figure 5.14. Comparison of TD-based Pearson correlation coefficients calculated
for the shortlisted IMs
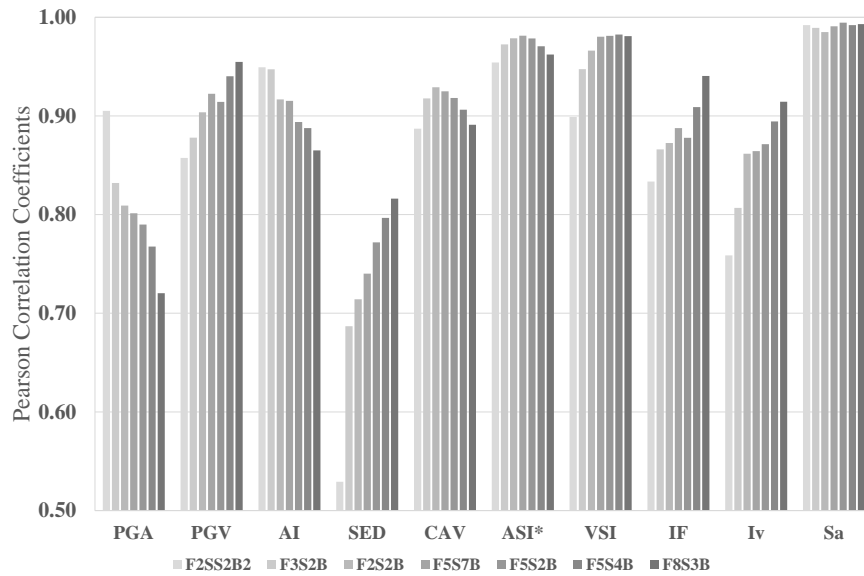
(a) ESDOF-based results
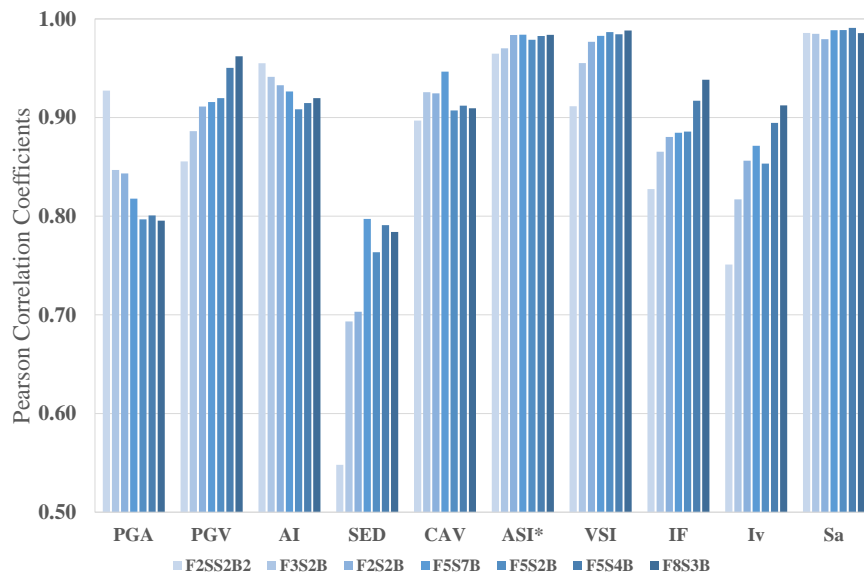
(b) MDOF-based results

Figure 5.15. Comparison of MIDR-based Pearson correlation coefficients
calculated for the shortlisted IMs
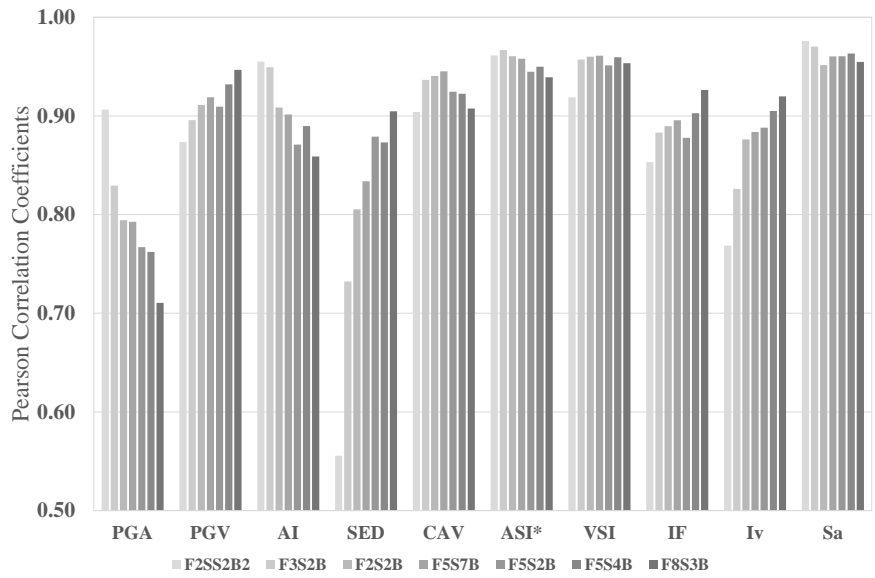
(a) ESDOF-based results
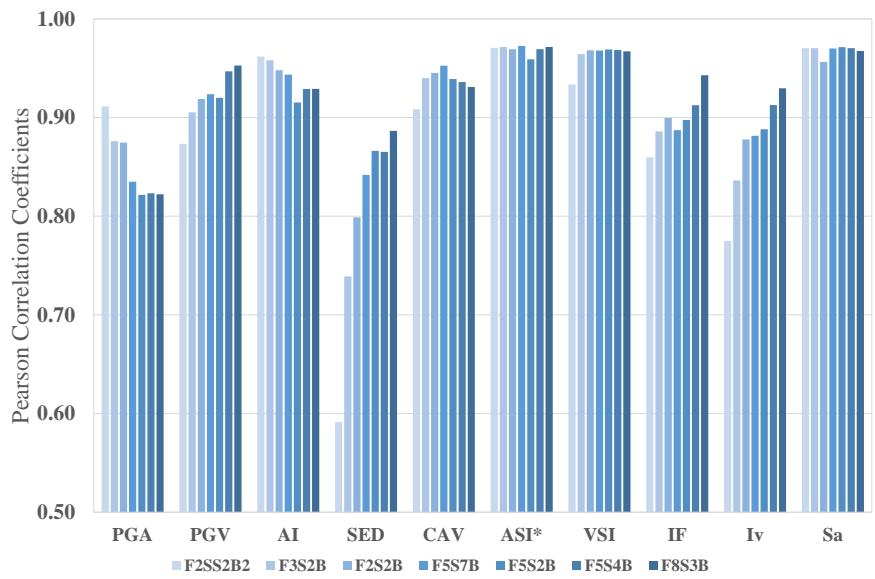
(b) MDOF-based results
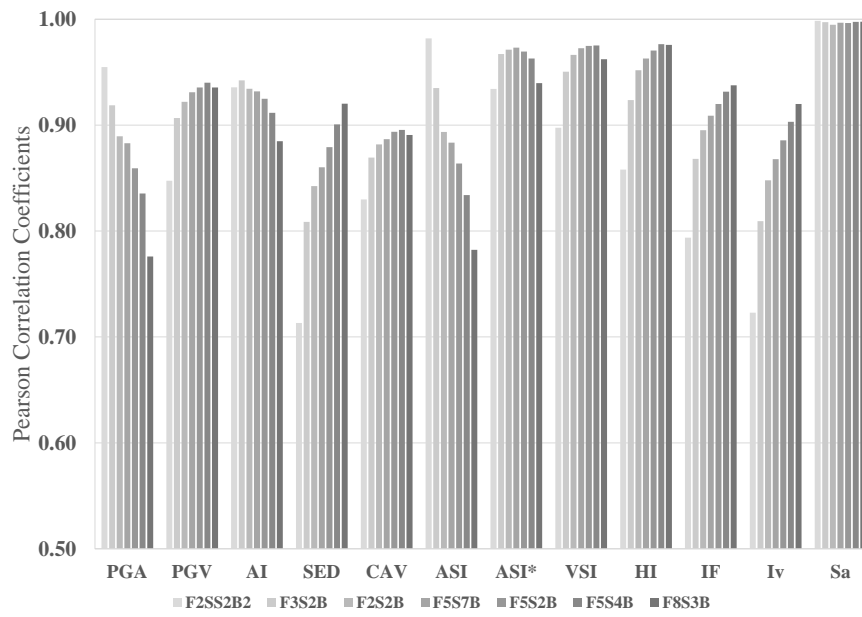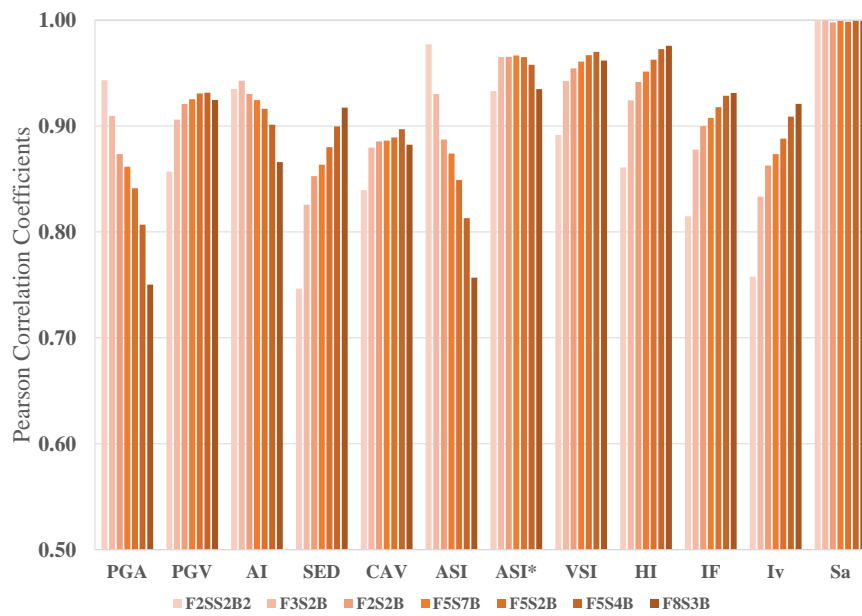
Figure 5.16. Comparison of BS-based Pearson correlation coefficients calculated for the shortlisted IMs

Table 5.5 Correlation and other statistical results among ESDOF and MDOF-based analyses

EDP	Statistical Parameter	F2S2B2 (T₁ = 0.30 s)	F3S2B (T₁ = 0.45 s)	F2S2B (T₁ = 0.59 s)	F5S7B (T₁ = 0.66 s)	F5S2B (T₁ = 0.75 s)	F5S4B (T₁ = 0.95 s)	F8S3B (T₁ = 1.20 s)
TD	PEARSON	0.994	0.991	0.991	0.988	0.983	0.996	0.995
	MIN	0.474	0.171	0.498	0.077	0.132	0.539	0.604
	MAX	1.658	1.944	1.971	2.417	1.889	1.681	1.536
	MEDIAN	0.956	0.966	1.025	0.997	0.992	0.994	0.968
	MEAN	0.985	0.993	1.053	1.030	1.015	1.005	0.995
	COV	0.164	0.182	0.178	0.182	0.220	0.126	0.137
MIDR	PEARSON	0.995	0.991	0.991	0.979	0.986	0.994	0.982
	MIN	0.508	0.195	0.465	0.024	0.180	0.394	0.191
	MAX	1.709	1.956	1.730	2.349	1.915	1.610	1.441
	MEDIAN	0.967	0.967	1.005	0.996	0.975	0.998	0.916
	MEAN	0.993	0.989	1.024	1.022	0.998	0.998	0.891
	COV	0.163	0.180	0.178	0.199	0.226	0.144	0.218
BS	PEARSON	0.996	0.991	0.989	0.992	0.990	0.990	0.977
	MIN	0.695	0.313	0.284	0.461	0.382	0.281	0.156
	MAX	1.539	1.703	1.714	1.712	1.634	1.417	1.431
	MEDIAN	0.973	0.954	1.003	0.993	0.965	0.989	0.902
	MEAN	0.993	0.970	1.008	1.013	0.988	0.982	0.887
	COV	0.122	0.144	0.142	0.139	0.158	0.140	0.195

The conclusions from ESDOF- and MDOF-based evaluations have oriented the study to primarily employ the structure-independent ASI*- and VSI-based GM subsets as well as the structure-specific S_a-based GM subsets for the next stage. The utilization of PGA- and PGV-based datasets, on the other hand, has been considered for comparison purposes only, where these two parameters generally lead to the simplest way of forming a GM record set.

5.7 Description of Additional Intensity Measures Evaluated

The evolution of the seismic intensity indices, as briefly summarized in Section 1.1, actualized in the form of advancement of the parameters from simple peak value-based scalar forms into compound and/or more advanced scalar as well as vector intensity measures with two or more parameters. The favorance of the structure-specific elastic spectral acceleration, indeed, had originated from the poor performance of the antiquated scalar IMs in characterizing the damage potential of the ground motions on the structures, yet later started to be found inefficient by itself, and has led to the development of new proposals. This study, with the principal goal of evaluating the alternatives in detail, has utilized the most basic indices so far, where even the long list of relatively simple scalar IMs has been evaluated comprehensively in the SDOF-based evaluation stage together with the ESDOF- and MDOF-based evaluations made over the shortlisted indices. Nevertheless, it is of paramount importance to continue on the evaluations with an expanded list of IMs that would rather incorporate the major proposals, especially after Cordova et al. (2000). Apparently, this suite would include more advanced scalar and vector forms that generally rely on the elastic spectral acceleration. In an effort to form such an expanded list to elaborate further on the research subject, the following IMs have been considered within the context of the research:

- The shortlisted scalar IMs as recommendations of Chapter 4 and HI

  (*PGA, PGV, AI, SED, CAV, ASI*, VSI, I_F, I_v, $S_a(T_1)$, ASI, HI*)

- Effective Peak Acceleration (*EPA*) and Effective Peak Velocity (*EPV*) (ATC, 1978)

- Improved definitions of *EPA* and *EPV* (Yang et al., 2009)
  (*IEPA, IEPV*)

- The scalar IM proposed by Cordova et al. (2000) (will be referred as S_{aC})

116

(*) The two parameters c and α have been taken as c=2.0 and α=0.5 with reference to the recommendation of the original manuscript. A calibration study for optimal values corresponding to individual frames of this research study might have been performed, but not undertaken.

$$S_{aC} \equiv S_a(T_1) \left\{ \frac{S_a(2T_1)}{S_a(T_1)} \right\}^{0.5} \tag{5.4}$$

- The vector IM by Baker and Cornell (2004)

  (*) T_2 has been considered as $2T_1$

$$\begin{Bmatrix} S_a(T_1) \\ R_{T_1,T_2} \end{Bmatrix} \quad \text{where} \qquad R_{T_1,T_2} = \frac{S_a(2T_1)}{S_a(T_1)} \tag{5.5}$$

- The vector IM by Bojórquez and Iervolino (2010, 2011) and its scalar counterpart

  (*) T_N has been considered as $2T_1$, whereas α has been taken as 0.40.

$$\begin{Bmatrix} S_a(T_1) \\ N_p \end{Bmatrix} \quad \text{where} \qquad N_p = \frac{S_{a_{avg}}(T_1,\dots,2T_1)}{S_a(T_1)} \tag{5.6}$$

$$I_{N_p} = S_a(T_1) N_p^{0.40} \tag{5.7}$$

- The scalar IM of Lin et al. (2011) proposed for the inelastic case (will be referred as S_{aCM})

(*) The two parameters C and α have been taken as C=1.5 and α=0.5 with reference to the recommendation of the original manuscript for structural systems with T<1.5 sec. A calibration study for optimal values corresponding to individual frames of this research study might have been performed, but not undertaken.

$$S_{aCM} \equiv S_a(T_1) \left\{ \frac{S_a(1.5T_1)}{S_a(T_1)} \right\}^{0.5} \tag{5.8}$$

- The scalar IM by Adam et al. (2014) (will be referred as S_{agm}) (based on the generic form proposed by Bianchini et al., 2009)

$$S_{a,gm}\left(T^{(1)}, T^{(n)}\right) = \left(\prod_{i=1}^{n} S_a\left(T^{(i)}\right)\right)^{1/n} \tag{5.9}$$

$$S_{a,gm}(0.2T_1, 1.6T_1) = \left(\prod_{i=1}^{n} S_a\left(T^{(i)}\right)\right)^{1/n} \tag{5.10}$$

(*) In the calculation of the geometric mean of the spectral accelerations over the specified period range, equally-spaced ($\Delta T=0.01$ sec) S_a data have been employed.

- The scalar IM by De Biasio et al. (2014) (will be referred as ASA_{40})

(*) R factor has been assumed as 40.

$$ASA_R(T_1) = \frac{T_1}{(1-X_f)} \int_{T_1}^{\frac{T_1}{X_f}} \frac{S_{pa}(T,\xi)}{T^2} dT \quad \text{where} \quad X_f = 1 - \left(R/100\right) \tag{5.11}$$

$$ASA_{40}(T_1) = 2.5T_1 \int_{T_1}^{1.67T_1} \frac{S_{pa}(T,\xi)}{T^2} dT \tag{5.12}$$

- The vector IM by Theophilou et al. (2017)

(*) T_2 has been calculated according to Kadas et al. (2011), as the equation therein had been developed utilizing the structural systems used herein.

$$\left\{ \begin{matrix} S_a(T_1) \\ S_{dN}(T_1, T_2) \end{matrix} \right\} \tag{5.13}$$

$$S_{dN}(T_1, T_2) = \frac{1}{S_d(T_1)T_N} \int_{T_1}^{T_2} S_d(T) \, dT, \quad T_1 < T_2 \text{ and } T_N = 1.0 \, s \tag{5.14}$$

- The vector IM by Yakhchalian et al. (2015, 2019)

(*) DSI has been considered as the area under the elastic spectral displacement between T=2.0 sec and T=5.0 sec.

$$\begin{Bmatrix} S_a(T_1) \\ S_a(T_1)/_{DSI} \end{Bmatrix} \tag{5.15}$$

- Vector IMs considering *PGV/PGA* ratio for consideration of frequency content where IM_1 has been considered as PGA, PGV, ASI, ASI*, VSI, HI, and $S_a(T_1)$, alternatively.

$$\begin{Bmatrix} IM_1 \\ PGV/_{PGA} \end{Bmatrix} \tag{5.16}$$

- Vector IMs considering significant duration *$t_{5\text{-}95}$* ratio for consideration of the ground motion duration where IM_1 has been considered as PGA, PGV, ASI, ASI*, VSI, HI, and $S_a(T_1)$, alternatively.

$$\begin{Bmatrix} IM_1 \\ t_{5-95} \end{Bmatrix} \tag{5.17}$$

It will be explanatory to state the reason for not utilizing the ε-based vector IM of Baker and Cornell (2005) in this study that this parameter requires the use of a ground motion prediction equation for the calculation of the ε parameter. Nevertheless, this study is following a hazard-independent evaluation approach, and thus, makes the IM irrelevant.

The consideration of the above-listed parameters resulted in an expanded list with 39 specific IMs in total. All these indices have been computed for the PGA-, PGV-, ASI*-, VSI- and structure-specific S_a-based GM subsets along with the structural characteristics of the employed frames, when needed.

5.8 Description of the Regression-based Evaluation Methodology

The in-depth evaluation of the statistical distribution of EDPs at specific IM levels to reveal the efficiency characteristics of the subject IM necessitates a common statistical approach that will be applicable to both scalar and vector IM cases. The probabilistic seismic demand models, which are defining the relationship between IM and structural responses (i.e., EDPs) in a probabilistic manner, utilize rigorous analysis techniques to derive the statistical characteristics. Stripe Analysis, Multiple Stripe Analysis, and Cloud Analysis mainly constitute the advanced solutions to the problem, where stripe analysis and multiple stripe analysis generally require scaling of the GM records to specific intensity levels. In contrast, the cloud analysis mostly employs a set of unscaled records to achieve a seismic demand model. Although Giovenale et al. (2004) had raised concerns about this approach, Zengin (2016) has marked the superiority of this approach in regional loss assessment studies where probabilistic seismic demand models could be established for a large suite of structures. The large number of IM alternatives together with a different set of EDP results due to distinct GM subsets pose a similar problem that the effectiveness of cloud analysis could resolve.

Established upon the fundamentals of cloud analysis approach, this study utilizes a linear seismic demand model assuming a log-normal distribution of the related random variables (Shome et al., 1998; Aslani and Miranda, 2005).

$$ln(EDP) = \beta_0 + \beta_1 ln(IM) + \varepsilon \qquad (5.18)$$

$$ln(EDP) = \beta_0 + \beta_1 ln(IM_1) + \beta_2 ln(IM_2) + \varepsilon \qquad (5.19)$$

In both equations, the uncertainty in the seismic demand due to record-to-record variability is reflected through the ε parameter, which is a log-normal random

variable with a median 1.0 and logarithmic standard deviation $\sigma_{ln\varepsilon} = \beta_{EDP|IM}$ or $\sigma_{ln\varepsilon} = \beta_{EDP|IM_1\&IM_2}$ (Celik and Ellingwood, 2010).

Either dependent on a single predictor as in the case of a scalar IM or two predictors as in the case of vector IMs, the regression equation is essentially formed assuming a constant variance, while the nature of data (for seismic demands) are generally stated to be violating this requirement, especially at high intensity levels. As a resolution, Aslani and Miranda (2005) proposed the consideration of a variance function dependent back on the IM data. In addition to the non-constant variance problem, some researchers have identified the non-linear trend in scattering of the data in the ln(EDP)-ln(IM) space and proposed the use of bi-linear demand models. (Ramamoorthy et al., 2006, 2008; Bai et al., 2011; Azari Sisi, 2016, O'Reilly and Monteiro, 2019) This study, on the other hand, has considered relying on the practicality of linear demand model with constant variance assumption (though with some trade-off), and did not consider any more advanced approaches.

MATLAB software has been utilized to perform the regression studies to derive the linear demand models, and the following statistical metrics have been computed to quantify the quality of the alternative regression models.

- **Pearson correlation coefficient:** This metric has not been computed from the regression model indeed, but calculated in between the variables ln(IM) and ln(EDP) for scalar intensity measure cases to show the correlation performance of the IM to predict the resulting EDP.

- **R^2-ordinary** (Coefficient of determination): A regression statistic to show how well terms (data points) fit a curve or line. An R^2-value close to 1.0 designates the superiority of the model.

$$R^2 = 1 - \frac{SS_{res}}{SS_{tot}} \qquad (5.20)$$

$$SS_{res} = \sum_i (y_i - \bar{y})^2 \tag{5.21}$$

where

$$\bar{y} = \frac{1}{n} \sum_{i=1}^{n} y_i \tag{5.22}$$

$$SS_{tot} = \sum_i (y_i - f_i)^2 \tag{5.23}$$

where

y_i denotes the observed data

f_i denotes the fitted data

- **R²-adjusted:** A modified version of regression statistic R^2 that accounts for the increasing nature of R^2 when there are extra explanatory variables added to the regression model. To exemplify, when the models herein with two predictors generally yield higher R^2 values, R²-adjusted considers the extra predictors and penalizes the original R^2 values. This metric is considered to be more appropriate (with respect to R^2 metric) while evaluating a model fit in comparison with alternative models, and a value close to 1.0 designates the superiority of the model.

$$R^2_{adjusted} = 1 - (1 - R^2) - \frac{n-1}{n-p-1} \tag{5.24}$$

where

n is the sample size

p is the number of predictors

- **MSE (Mean Square Error):** This metric simply quantifies the quality of the predictor by considering the sum of squared distances between the target

variable and the predicted values. Decreasing values of MSE show the relative improvement in the goodness of fit in the models.

$$MSE = \frac{1}{n} \sum_{i=1}^{n} (y_i - f_i)^2 \qquad (5.25)$$

where

n denotes the sample size

y_i denotes the observed data

f_i denotes the fitted data

- **RMSE (Root Mean Square Error):** This metric is simply the square root of MSE and corresponds to the standard deviation of the residuals (prediction errors). Decreasing values of RMSE show the relative improvement in the goodness of fit in the models.

$$RMSE = \sqrt{MSE} \qquad (5.26)$$

- **PRESS (Predicted Residual Error Sum of squares):** This statistical parameter is computed as the sums of squares of the prediction residuals from individual models re-fitted with a sample of observations that were not themselves used to construct the model. This metric is generally considered as a means of cross-validation of candidate models corresponding to the same dataset. The lowest values of PRESS eventually designate the best model structures.

$$PRESS = \sum_{i=1}^{n} \left(y_i - f_{i,-i} \right)^2 \qquad (5.27)$$

where

$f_{i,-i}$ denotes the out-of-sample predicted data with
omitted observation in each case observation is
removed

- **AIC (Akaike Information Criterion):** is an estimator relatively quantifying the quality of each model given a set of alternative models, thus provides a basic tool for model selection. Established on information theory, this criterion simply estimates the relative information loss by a regression model , but penalizes the increasing number of predictors, which in fact results in improved values of the goodness of fit among the alternative regression models. Consequently, while evaluating candidate regression models, models with smaller AIC values are preferred. For a detailed explanation of this criterion, the reader is referred to Akaike (1973, 1998) and Narisetty (2020). Another metric, Mallow's C_p, is also frequently considered to comparatively evaluate the alternative models, and is equivalent to AIC in the case of linear regression models, but this parameter has not been incorporated into the metrics utilized herein.

- **AICc (Corrected Akaike Information Criterion):** This metric is a modified version of AIC, making a correction for small sample sizes, which normally leads to the selection of models with too many parameters (Cavanaugh, 1997; Burnham and Anderson, 2002). The models with lower AICc values are preferred.

- **BIC (Bayesian Information Criterion):** This is a criterion, based on a likelihood function, used for model selection among a finite set of models. It considers a different penalty function as opposed to AIC (Schwarz, 1978). The models with lower BIC values are preferred.

- **CAIC (Consistent AIC):** This criterion is a variation of the original AIC, which has a stronger penalty for over parametrized models with respect to AIC (Bozdogan, 1987). The models with lower CAIC values are preferred.

- **F-value:** The F-test for linear regression tests via the analysis of variance (ANOVA) approach whether any of the independent variables in a multiple linear regression model are significant. In this study, this test is used to test the significance of the regression model against the intercept-only model (i.e., a model with no predictors). The larger values of resulting F-value are considered to be indicators of regression models with greater goodness of fit.

- **p-value(s):** p-value for the t-statistic of the hypothesis tests whether the examined coefficient is equal to zero (H_0: $\beta_i=0$) or not (H_1: $\beta_i\neq0$). If the p-value of the t-statistic for β_i (β_0 in the case of models with one predictor, and β_0 & β_1 individually in the case of models with two predictors) is greater than 0.05, so the term is not significant at the 5% significance level given the other terms in the model.

- **rho(1,2):** This final metric stands for the Pearson correlation coefficient calculated in between the two predictors (applicable to vector IM-based equations only), and is used to check whether there exists moderate to strong correlation between the predictors. There might be specific cases where the candidate models could be marked as highly qualifying, but involve predictors significantly correlating among each other. Such cases could be identified with the combined evaluation of R^2-adjusted values (or F-values, alternatively) and rho(1,2) metrics.

To evaluate the efficiency of the scalar intensity measures along with their vector rivals, a performance parameter (similar to Pearson correlation coefficient in the case

of Correlation studies) was needed. Among the statistical metrics quantifying the quality of alternate regression modes, the **R^2-adjusted value** corresponding to each regression model has been considered as the best simple metric to establish a common ground for comparisons. R^2-ordinary, RMSE, MSE, PRESS, and F-value have also been computed and presented, but regarded as the supporting parameters. On the other hand, the information criteria AIC, AICc, BIC, CAIC have been calculated and used to evaluate the significance of alternating IM_2 predictors in two-predictor regression models, while this set of information criteria might be used to determine the 'best second' parameter in the vector IMs. A good example to this type of problem can be illustrated as the IM set with S_a (i.e., scalar IM S_a and vector IMs $\langle S_a, PGV/PGA \rangle$, $\langle S_a, t_{5-95} \rangle$, $\langle S_a, R(T_1, T_2) \rangle$, $\langle S_a, N_p \rangle$, $\langle S_a, S_a/DSI \rangle$ and $\langle S_a, S_{dN} \rangle$). Finally, the p-values have been checked whether the parameter(s) considered in the regression model (especially the second predictors) are significant to determine the response (i.e., to predict the selected EDP) or not.

As an extension of the efficiency-based evaluation study, the sufficiency of the competing scalar and vector IMs with respect to moment magnitude, M_w, and source-to-site distance, R_{JB} has been evaluated through regression studies with predictors M_w or logarithm of R_{JB} against the residuals obtained from the previous linear regression models (Equations (5.18) and (5.19)). The p-values (for the t-statistic of the hypothesis tests whether the examined coefficients corresponding to M_w and R_{JB} are equal to zero or not) have been calculated to mark the significance of the seismological properties, separately. If the resulting p-value (p-val(M_w) or p-val(R_{JB})) is greater than 0.05, the term is not significant at the 5% significance level given the constant in the model, leading to a conclusion that the subject IM is considered as sufficient with respect to the seismological property considered (i.e., M_w or R_{JB}). On the other hand, when the p-value is less than 0.05, the IM (or the IM couple) is considered as "not sufficient" with respect to this seismological characteristic-based predictor. The two different cases, the dependency on M_w or R_{JB} (i.e., could be termed as *biased* as well), or the sufficiency with respect to those (i.e., could be alternatively termed as *unbiased*), are visually illustrated in Figure 5.17.
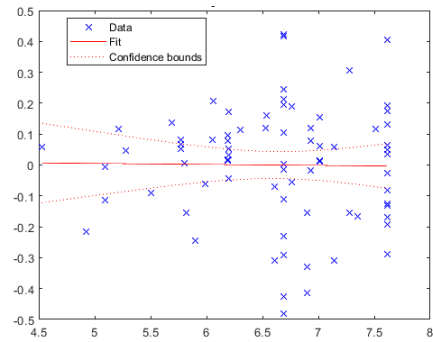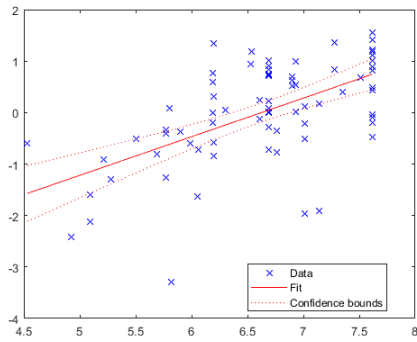
(a) Moment magnitude (M_w) check
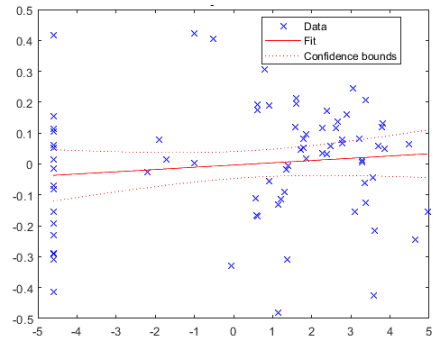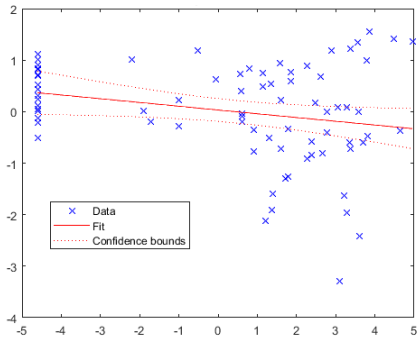
(b) Source-to-site distance (R_{JB}) check

Figure 5.17. Representative cases for sufficiency check with respect to M_w and R_{JB} (the left pane for "statistically significant bias" case, $p \leq 0.05$, and the right pane for "statistically no bias" case, $p > 0.05$)

5.9 Evaluation of Efficiency and Sufficiency of the Complete Set of Intensity Measures

This regression model study has been repeated for 39 IM cases, and each list has been sorted (i.e., ranked) according to the R^2-adjusted values of the IMs, clearly showing the top-performing IMs for the selected EDP and for the utilized GM record subset considering different DB IM (i.e., PGA, PGV, ASI*, VSI and $S_a(T_1)$ alternatively). A sample ranking table for F2S2B2 frame (DB IM: PGA – EDP: TD case) is presented in Table 5.6. The complete set of resulting tables (corresponding to 7-frame, 5-DB IM, and 3-EDP cases) is provided in Appendix E.

The evaluations will primarily focus on the efficiency of the IMs, where the following sub-sections will briefly discuss the numerical outcomes frame by frame. Afterwards, a general overview will be made in order to comparatively display the efficiencies of a down-sized list of common and novel IMs. This overview section will be followed by a section that will present and briefly discuss the set of statistical results, which further examines the efficiency of candidate IMs differentiating the linear and nonlinear response sets for two typical frames. This additional examination would assist in identifying the superiority of IMs in different response levels. The in-depth evaluations for efficiencies will be followed by the examination of the sufficiencies of IMs with respect to M_w and R_{JB}, respectively, presented as summary tables.

Table 5.6 Sample table for regression model comparison results

DB	EDP	IM	Rank	Pearson	R2-adj*	R2-ord	RMSE	MSE	PRESS	AIC	AICc	BIC	CAIC	F-value	p-value (1)	p-value (2)	rho(1,2)	p-val (Mw)	p-val (Rjb)
PGA	TD	20-ASA40	1	0.989	0.979	0.979	0.1646	0.0271	2.1532	-56.6286	-56.4643	-51.9672	-49.9672	3436.27	9.002E-64			1.390E-01	9.646E-01
PGA	TD	18-SaCM	2	0.987	0.973	0.974	0.1841	0.0339	2.6622	-39.5343	-39.3699	-34.8729	-32.8729	2729.22	3.713E-60			1.711E-01	5.963E-01
PGA	TD	36-Sa, R(T1,T2)	3		0.972	0.973	0.1877	0.0352	2.8854	-35.6771	-35.3437	-28.6849	-25.6849	2549.31	1.600E-58	6.139E-03	0.116	4.341E-01	6.804E-01
PGA	TD	38-Sa, SdN	4		0.972	0.973	0.1877	0.0352	2.8084	-35.6620	-35.3287	-28.6698	-25.6698	1470.78	4.045E-50	6.188E-03	0.703	1.414E-01	5.193E-01
PGA	TD	39-Sa, Sa/DSI	5		0.972	0.973	0.1877	0.0352	2.8213	-35.6470	-35.3137	-28.6548	-25.6548	2597.66	8.210E-59	6.238E-03	-0.046	8.237E-01	5.165E-01
PGA	TD	37-Sa, Np	6		0.972	0.972	0.1896	0.0359	2.9393	-34.1467	-33.8134	-27.1545	-24.1545	2503.83	3.031E-58	1.391E-02	0.113	3.308E-01	4.795E-01
PGA	TD	26-Sa, PGV/PGA	7		0.971	0.972	0.1920	0.0369	2.9573	-32.1883	-31.8550	-25.1961	-22.1961	2488.49	3.769E-58	4.089E-02	0.038	6.713E-01	4.010E-01
PGA	TD	10-Sa	8	0.985	0.970	0.970	0.1963	0.0385	3.0651	-29.8062	-29.6418	-25.1447	-23.1447	2392.42	4.240E-58			1.355E-01	3.767E-01
PGA	TD	33-Sa, t5-95	9		0.969	0.970	0.1970	0.0388	3.0946	-28.2877	-27.9543	-21.2955	-18.2955	2289.57	7.214E-57	4.979E-01	-0.204	3.305E-01	3.786E-01
PGA	TD	21-INp	10	0.984	0.967	0.967	0.2049	0.0420	3.2812	-23.2686	-23.1042	-18.6071	-16.6071	2189.12	1.024E-56			7.028E-02	7.232E-01
PGA	TD	27-ASI, PGV/PGA	11		0.953	0.954	0.2448	0.0599	4.8289	4.6871	5.0205	11.6793	14.6793	1503.78	1.868E-50	5.440E-08	-0.076	9.341E-01	5.755E-01
PGA	TD	17-SaC	12	0.976	0.951	0.952	0.2481	0.0615	4.8389	5.7516	5.9160	10.4131	12.4131	1470.81	1.411E-50			8.782E-01	2.523E-01
PGA	TD	19-Sagm	13	0.973	0.946	0.947	0.2611	0.0682	5.3747	13.5662	13.7306	18.2277	20.2277	1319.86	6.351E-49			3.687E-03	8.456E-01
PGA	TD	24-ASI*, PGV/PGA	14		0.935	0.937	0.2868	0.0823	6.5410	28.7767	29.1101	35.7689	38.7689	1075.45	1.994E-45	6.509E-07	0.245	3.838E-01	2.573E-02
PGA	TD	34-ASI, t5-95	15		0.933	0.935	0.2908	0.0846	6.7975	30.8770	31.2103	37.8692	40.8692	1011.66	1.609E-44	3.269E-02	-0.259	2.042E-01	9.401E-01
PGA	TD	31-ASI*, t5-95	16		0.932	0.933	0.2945	0.0867	6.8689	32.7831	33.1165	39.7753	42.7753	984.79	4.023E-44	4.759E-06	-0.040	7.976E-01	4.638E-02
PGA	TD	11-ASI	17	0.965	0.930	0.931	0.2981	0.0888	7.0284	33.6391	33.8235	38.3206	40.3206	996.04	1.134E-44			3.299E-03	9.766E-01
PGA	TD	13-EPA	18	0.965	0.930	0.930	0.2988	0.0893	7.0682	34.0599	34.2243	38.7213	40.7213	990.41	1.379E-44			3.321E-01	9.810E-01
PGA	TD	25-VSI, PGV/PGA	19		0.917	0.919	0.3252	0.1057	8.3722	47.8586	48.1920	54.8508	57.8508	820.45	1.923E-41	1.100E-09	0.322	5.479E-01	3.935E-02
PGA	TD	15-IEPA	20	0.955	0.911	0.912	0.3354	0.1125	8.8613	51.5972	51.7615	56.2586	58.2586	771.07	7.107E-41			5.965E-02	5.123E-01
PGA	TD	6-ASI*	21	0.955	0.910	0.911	0.3379	0.1142	8.8510	52.7214	52.8858	57.3829	59.3829	758.67	1.229E-40			4.799E-03	1.677E-01
PGA	TD	23-PGV, PGV/PGA	22		0.902	0.904	0.3530	0.1246	10.2862	60.3220	60.6553	67.3142	70.3142	685.32	7.707E-39	1.295E-11	0.383	9.304E-01	6.141E-01
PGA	TD	22-PGA, PGV/PGA	23		0.902	0.904	0.3530	0.1246	10.2866	60.3222	60.6555	67.3144	70.3144	685.32	7.708E-39	1.960E-09	-0.180	9.305E-01	6.143E-01
PGA	TD	32-VSI, t5-95	24		0.900	0.903	0.3552	0.1262	9.9237	61.2931	61.6264	68.2853	71.2853	653.92	3.616E-38	8.171E-07	0.010	6.144E-01	1.474E-01
PGA	TD	28-HI, PGV/PGA	25		0.895	0.898	0.3641	0.1325	10.3845	65.0372	63.3705	72.0294	75.0294	639.70	7.444E-38	9.502E-13	0.417	4.147E-01	9.351E-02
PGA	TD	35-HI, t5-95	26		0.868	0.871	0.4095	0.1677	13.1135	82.9169	83.2502	89.9091	92.9091	473.91	1.192E-33	5.873E-09	0.099	4.391E-01	3.885E-01
PGA	TD	7-VSI	27	0.930	0.863	0.864	0.4172	0.1741	13.4679	84.7787	84.9431	89.4401	91.4401	472.11	7.563E-34			7.122E-03	4.702E-01
PGA	TD	30-PGV, t5-95	28		0.854	0.858	0.4295	0.1844	14.7008	90.1405	90.4739	97.1327	100.1327	424.32	3.857E-32	3.089E-05	0.009	6.495E-01	7.679E-01
PGA	TD	3-AI	29	0.922	0.849	0.851	0.4377	0.1916	14.9646	92.0627	92.2271	96.7242	98.7242	422.20	2.643E-32			7.842E-03	7.937E-01
PGA	TD	29-PGA, t5-95	30		0.845	0.849	0.4436	0.1968	15.7472	95.0577	95.3910	102.0499	105.0499	393.16	4.114E-31	9.048E-02	-0.286	6.329E-02	7.132E-01
PGA	TD	1-PGA	31	0.918	0.841	0.843	0.4494	0.2019	15.7979	96.0616	96.2260	100.7231	102.7231	396.77	1.861E-31			1.336E-03	6.366E-01
PGA	TD	14-EPV	32	0.917	0.839	0.841	0.4513	0.2036	15.8083	96.7079	96.8723	101.3694	103.3694	392.78	2.550E-31			3.363E-02	6.672E-01
PGA	TD	2-PGV	33	0.906	0.818	0.820	0.4808	0.2312	17.9325	106.3383	106.5027	110.9998	112.9998	337.23	2.807E-29			2.287E-02	4.914E-01
PGA	TD	12-HI	34	0.891	0.792	0.795	0.5138	0.2639	20.5467	116.4182	116.5826	121.0797	123.0797	286.15	3.856E-27			6.913E-03	8.609E-01
PGA	TD	16-IEPV	35	0.880	0.772	0.775	0.5580	0.2895	22.3909	123.4321	123.5965	128.0936	130.0936	254.40	1.187E-25			2.403E-02	3.987E-01
PGA	TD	8-IF	36	0.853	0.725	0.728	0.5906	0.3488	27.2015	137.6129	137.7773	142.2744	144.2744	198.50	1.218E-22			2.002E-03	1.381E-01
PGA	TD	5-CAV	37	0.813	0.657	0.661	0.6594	0.4348	34.4072	154.3625	154.5269	159.0240	161.0240	144.60	4.458E-19			5.335E-04	9.712E-02
PGA	TD	4-SED	38	0.804	0.642	0.647	0.6733	0.4533	35.5952	157.5149	157.6793	162.1764	164.1764	135.72	2.081E-18			3.492E-03	4.787E-03
PGA	TD	9-Iv	39	0.778	0.600	0.606	0.7118	0.5066	39.9885	165.9719	166.1363	170.6334	172.6334	113.63	1.319E-16			4.501E-03	2.145E-02

5.9.1 Summary for Efficiency Performances for Frame F2S2B2

When the *TD-based result set for F2S2B2 frame (T_1=0.30 s, as a typical short period system)* analyzed under the *PGA-based GM subset* is examined in detail, ordinary scalar IMs (in decreasing order) PGA, EPV, PGV, HI, IEPV, I_F, CAV, SED and I_v ranked in the worst 10 with R^2-adjusted values below 0.85. Acceleration-related parameters AI and PGA performed slightly better than velocity-related parameters listed above. The correlation performances of spectrum-based IMs ASI, EPA, IEPA, ASI*, and VSI turned out to be much better, with R^2-adjusted values between 0.93-0.86. The structure-specific S_a-based novel scalar and vector IMs (i.e., ASA$_{40}$, Sa$_{CM}$, $\langle S_a, R(T_1, T_2) \rangle$, $\langle S_a, S_{dN} \rangle$, $\langle S_a, S_a/DSI \rangle$, $\langle S_a, N_p \rangle$, I_{N_p}), on the other hand, ranked in the top 10 with R^2-adjusted values above 0.96. The *MIDR-based result set for F2S2B2 frame* analyzed under the *PGA-based GM subset* has revealed similar observations with minor differences in rankings. In contrast, *BS-based results* yielded slightly lower R^2-adjusted values for top-performing IM candidates and slightly higher R^2-adjusted values for poor-performing ordinary scalar IMs.

The *TD-based result set for F2S2B2 frame (T_1=0.30 s)* analyzed under the *PGV-based GM subset* has revealed that ordinary scalar IMs (in decreasing order) VSI, HI, CAV, PGV, IEPV, I_F, I_v, and SED ranked in the worst 10 with R^2-adjusted values below 0.87. Acceleration-related parameters ASI, EPA, IEPA, PGA and ASI* showed much better performance with respect to other ordinary scalar IMs with R^2-adjusted values between 0.98-0.91, while the performance of PGA has noticeably improved with respect to the PGA-based GM subset. The structure-specific S_a-based novel scalar and vector IMs ranked in the top 10 with R^2-adjusted values above 0.98. The *MIDR-based R^2-adjusted results for F2S2B2 frame* analyzed under the *PGV-based GM subset* are similar in general with minor differences in rankings, whereas *BS-based results* yielded slightly lower R^2-adjusted values for top-performing IM candidates and slightly higher R^2-adjusted values for poor-performing ordinary scalar IMs (in decreasing order).

When the *TD-based result set for F2S2B2 frame (T₁=0.30 s)* analyzed under the *ASI*-based GM subset* is evaluated, ordinary scalar IMs (in decreasing order) VSI, EPV, PGV, IEPV, HI, CAV, I_F, I_v, and SED ranked in the worst 10 with R^2-adjusted values below 0.90. Acceleration-related parameters ASI, EPA, IEPA, PGA, and ASI* showed much better performance with respect to other ordinary scalar IMs with R^2-adjusted values between 0.98-0.93, while the performance of PGA is much higher with respect to PGA-based GM subset case. The structure-specific S_a-based novel scalar and vector IMs ranked in the top 10 with R^2-adjusted values above 0.98. The *MIDR-based R^2-adjusted results for F2S2B2 frame* analyzed under the *ASI*-based GM subset* are similar in general with minor differences in rankings, while *BS-based results* yielded slightly lower R^2-adjusted values for top-performing IM candidates and slightly higher R^2-adjusted values for poor-performing ordinary scalar IMs.

The *TD-based results for F2S2B2 frame (T₁=0.30 s)* analyzed under the *VSI-based GM subset* has exhibited that ordinary scalar IMs (in decreasing order) EPV, VSI, PGV, HI, IEPV, CAV, I_F, I_v, and SED ranked in the worst 10 with R^2-adjusted values below 0.85. Acceleration-related parameters ASI, EPA, IEPA, PGA, and ASI* showed much better performance with respect to the above-listed ordinary scalar IMs with R^2-adjusted values between 0.97-0.89, while the performance of PGA has noticeably improved with respect to the PGA-based GM subset. The structure-specific S_a-based novel scalar and vector IMs ranked in the top 10 with R^2-adjusted values above 0.97. The *MIDR-based R^2-adjusted results for F2S2B2 frame* analyzed under the *VSI-based GM subset* are similar in general with minor differences in rankings, whereas *BS-based results* yielded slightly lower R^2-adjusted values for top-performing IM candidates and slightly higher R^2-adjusted values for poor-performing ordinary scalar IMs.

When the *TD-based result set for F2S2B2 frame (T₁=0.30 s)* analyzed under the *S_a-based GM subset* is examined, ordinary scalar IMs (in decreasing order) VSI, EPV, PGV, HI, IEPV, I_F, CAV, SED, and I_v ranked in the worst 10 with R^2-adjusted values below 0.86. Acceleration-related parameters IEPA, EPA, ASI, PGA, and ASI*

performed better with respect to other ordinary scalar IMs with R^2-adjusted values between 0.95-0.91. The structure-specific S_a-based novel scalar and vector IMs ranked in the top 10 with R^2-adjusted values above 0.95. The *MIDR-based R^2-adjusted results for F2S2B2 frame* analyzed under the *S_a-based GM subset* are similar in general with minor differences in rankings, while the *BS-based set* resulted in slightly lower R^2-adjusted values.

When the results of *F2S2B2 frame* under all alternative GM subsets are holistically examined, it has been observed that the vector IMs formed with frequency-related PGV/PGA or duration-related t_{5-95} generally improved the individual performances of scalar forms, where PGV/PGA-based vector IMs performed slightly better. Supplementary statistical metrics (i.e., RMSE, MSE, PRESS, AIC, AICc, BIC, CAIC, and F-value) have confirmed the R^2-adjusted value-based rankings, where RMSE, MSE, PRESS, AIC, AICc, BIC, CAIC values decrease with increasing R^2-adjusted values, while F-values generally increase in parallel with increasing R^2-adjusted values. However, there exists violating cases in these result sets noticed, especially for $\langle S_a, S_{dN} \rangle$, and for particular cases of $\langle IM_1, t_{5-95} \rangle$ and $\langle IM_1, PGV/PGA \rangle$ forms. It has been observed that even weak-to-moderate inter-correlations between the primary and secondary parameters (as revealed with rho(1,2) statistics) are affecting the significance of the regression models, thus leading to lower F-values. Additionally, specific cases have been observed where p-values computed for the second parameters of some vector IMs are larger than the 0.05 limit, marking the insignificance of the second IM in the regression models.

5.9.2   Summary for Efficiency Performances for Frame F3S2B

When the *TD-based result set for F3S2B frame (T_1=0.45 s)* analyzed under the *PGA-based GM subset* is evaluated, ordinary scalar IMs (in decreasing order) EPA, ASI, IEPA, AI, I_F, PGA, SED, CAV, and I_v ranked in the worst 10 with R^2-adjusted values below 0.78. Scalar indices EPV, ASI*, VSI, HI, and PGV showed much better performance with respect to other ordinary scalar IMs with R^2-adjusted values

between 0.92-0.79. The structure-specific S_a-based novel scalar and vector IMs ranked in the top 10 with R^2-adjusted values above 0.96. The *MIDR-based R^2-adjusted results for F3S2B frame* analyzed under the *PGA-based GM subset* are similar in general with minor differences in rankings, while *BS-based results* yielded slightly lower R^2-adjusted values for top-performing IM candidates and slightly higher R^2-adjusted values for poor-performing ordinary scalar IMs.

The *TD-based result set for F3S2B frame (T_1=0.45 s)* analyzed under the *PGV-based GM subset* has revealed that ordinary scalar IMs (in decreasing order) AI, HI, PGV, CAV, IEPV, I_F, I_v, and SED ranked in the worst 10 with R^2-adjusted values below 0.91. Alternative scalar IMs IEPA, ASI*, ASI, EPA, EPV, PGA, and VSI showed much better performance with respect to the above-mentioned ordinary scalar IMs with R^2-adjusted values between 0.95-0.91, while the performance of PGA has noticeably improved with respect to PGA-based GM subset. The structure-specific S_a-based novel scalar and vector IMs ranked in the top 10 with R^2-adjusted values above 0.97. The *MIDR-based R^2-adjusted results for F3S2B frame* analyzed under the *PGV-based GM subset* are similar in general with minor differences in rankings, whereas *BS-based results* yielded slightly lower R^2-adjusted values for top-performing IM candidates and slightly higher R^2-adjusted values for poor-performing ordinary scalar IMs.

When the *TD-based result set for F3S2B frame (T_1=0.45 s)* analyzed under the *ASI*-based GM subset* is evaluated, ordinary scalar IMs (in decreasing order) PGA, IEPV, HI, PGV, I_F, CAV, SED, and I_v ranked in the worst 10 with R^2-adjusted values below 0.90. Alternative scalar indices ASI*, IEPA, VSI, EPV, EPA, AI, and ASI showed better performance with respect to the above-listed ordinary scalar IMs with R^2-adjusted values between 0.94-0.91, while the performance of PGA is much higher with respect to PGA-based GM subset case. The structure-specific S_a-based novel scalar and vector IMs ranked in the top 10 with R^2-adjusted values above 0.97. The *MIDR-based R^2-adjusted results for F3S2B frame* analyzed under the *ASI*-based GM subset* are similar in general with minor differences in rankings, while *BS-based*

results yielded slightly lower R^2-adjusted values for top-performing IM candidates and slightly higher R^2-adjusted values for poor-performing ordinary scalar IMs.

The *TD-based results for F3S2B frame (T_1=0.45 s)* analyzed under the *VSI-based GM subset* has exhibited that ordinary scalar IMs (in decreasing order) EPA, ASI, HI, PGV, IEPV, I_F, CAV, I_v, and SED ranked in the worst 10 with R^2-adjusted values of 0.90 and lower. Alternative scalar IMs IEPA, ASI*, EPV, AI, VSI, and PGA showed better performance with respect to the listed ordinary scalar IMs with R^2-adjusted values between 0.95-0.90, while the performance of PGA has noticeably improved with respect to the PGA-based GM subset. The structure-specific S_a-based novel scalar and vector IMs ranked in the top 10 with R^2-adjusted values above 0.97. The *MIDR-based R^2-adjusted results for F3S2B frame* analyzed under the *VSI-based GM subset* are similar in general with minor differences in rankings, whereas *BS-based results* yielded slightly lower R^2-adjusted values for top-performing IM candidates and slightly higher R^2-adjusted values for poor-performing ordinary scalar IMs.

When the *TD-based result set for F3S2B frame (T_1=0.45 s)* analyzed under the *S_a-based GM subset* is examined, ordinary scalar IMs (in decreasing order) EPA, ASI, PGA, HI, I_F, SED, CAV, and I_v ranked in the worst 10 with R^2-adjusted values below 0.85. Alternative indices ASI*, IEPA, AI, VSI, EPV, PGV, and IEPV performed better with respect to other ordinary scalar IMs with R^2-adjusted values between 0.93-0.86. The structure-specific S_a-based novel scalar and vector IMs ranked in the top 10 with R^2-adjusted values above 0.96. The *MIDR-based R^2-adjusted results for F3S2B frame* analyzed under the *S_a-based GM subset* are similar in general with minor differences in rankings, while the *BS-based set* resulted in slightly lower R^2-adjusted values.

When the results of *F3S2B frame* under all alternative GM subsets are examined as a whole, it has been observed that the vector IMs formed with PGV/PGA or t_{5-95} generally enhanced the individual performances of scalar forms, where PGV/PGA-based vector IMs performed slightly better. Supplementary statistical metrics have

generally confirmed the R^2-adjusted value-based rankings with the exception of irregular F-values observed especially for $\langle S_a, S_{dN} \rangle$, and for particular cases of $\langle IM_1, t_{5-95} \rangle$ and $\langle IM_1, PGV/PGA \rangle$ forms. Additionally, specific cases have been observed where p-values computed for the second parameters of particular vector IMs are larger than the 0.05 limit, marking the insignificance of the second IM in the regression models.

5.9.3 Summary for Efficiency Performances for Frame F2S2B

When the *TD-based result set for F2S2B frame ($T_1=0.59$ s)* analyzed under the *PGA-based GM subset* is evaluated, ordinary scalar IMs (in decreasing order) AI, SED, I_v, IEPA, EPA, ASI, CAV, and PGA ranked in the worst 10 with R^2-adjusted values below 0.78. Scalar indices EPV, VSI, ASI*, HI, IEPV, PGV, and I_v showed much better performance with respect to other ordinary scalar IMs with R^2-adjusted values between 0.94-0.81. The structure-specific S_a-based novel scalar and vector IMs ranked in the top 10 with R^2-adjusted values above 0.96. The *MIDR-based R^2-adjusted results for F2S2B frame* analyzed under the *PGA-based GM subset* are similar in general with minor differences in rankings, while *BS-based results* yielded slightly lower R^2-adjusted values for top-performing IM candidates and slightly higher R^2-adjusted values for poor-performing ordinary scalar IMs.

The *TD-based result set for F2S2B frame ($T_1=0.59$ s)* analyzed under the *PGV-based GM subset* has revealed that ordinary scalar IMs (in decreasing order) ASI, EPA, PGV, CAV, IEPV, I_F, I_v, and SED ranked in the worst 10 with R^2-adjusted values below 0.89. Alternative scalar IMs ASI*, EPV, VSI, IEPA, HI, AI, and PGA showed much better performance with respect to the above-mentioned ordinary scalar IMs with R^2-adjusted values between 0.97-0.90, while the performance of PGA has noticeably improved with respect to PGA-based GM subset. The structure-specific S_a-based novel scalar and vector IMs generally ranked in the top 10 with R^2-adjusted values above 0.97. The *MIDR-based R^2-adjusted results for F2S2B frame* analyzed

under the *PGV-based GM subset* are similar in general with minor differences in rankings, whereas *BS-based results* yielded slightly lower R^2-adjusted values.

When the *TD-based result set for F2S2B frame (T_1=0.59 s)* analyzed under the *ASI*-based GM subset* is evaluated, ordinary scalar IMs (in decreasing order) IEPA, I_F, PGA, SED, EPA, ASI, I_v, and CAV ranked in the worst 10 with R^2-adjusted values below 0.91. Alternative scalar indices VSI, EPV, ASI*, HI, IEPV, PGV, and AI showed better performance with respect to the above-listed ordinary scalar IMs with R^2-adjusted values between 0.97-0.91. The structure-specific S_a-based novel scalar and vector IMs generally ranked in the top 15 with R^2-adjusted values above 0.96. The *MIDR-based R^2-adjusted results for F2S2B frame* analyzed under the *ASI*-based GM subset* are similar in general with minor differences in rankings, while *BS-based results* yielded slightly lower R^2-adjusted values.

The *TD-based results for F2S2B frame (T_1=0.59 s)* analyzed under the *VSI-based GM subset* have exhibited that ordinary scalar IMs (in decreasing order) AI, IEPA, I_v, PGA, CAV, EPA, ASI, and SED ranked in the worst 10 with R^2-adjusted values below 0.89. Alternative scalar IMs ASI*, EPV, VSI, HI, PGV, IEPV, and I_F showed better performance with respect to the listed ordinary scalar IMs with R^2-adjusted values between 0.95-0.89. The structure-specific S_a-based novel scalar and vector IMs generally ranked in the top 20 with R^2-adjusted values above 0.94. The *MIDR-based R^2-adjusted results for F2S2B frame* analyzed under the *VSI-based GM subset* are similar in general with minor differences in rankings, whereas *BS-based results* yielded slightly lower R^2-adjusted values for top-performing IM candidates and slightly higher R^2-adjusted values for poor-performing ordinary scalar IMs.

When the *TD-based result set for F2S2B frame (T_1=0.59 s)* analyzed under the *S_a-based GM subset* is examined, ordinary scalar IMs (in decreasing order) AI, IEPA, PGA, SED, I_v, CAV, EPA, and ASI ranked in the worst 10 with R^2-adjusted values below 0.85. Alternative indices EPV, ASI*, VSI, PGV, HI, IEPV, and I_F performed better with respect to other ordinary scalar IMs with R^2-adjusted values between 0.94-0.85. The structure-specific S_a-based novel scalar and vector IMs ranked in the

top 10 with R^2-adjusted values above 0.95. The *MIDR-based R^2-adjusted results for F2S2B frame* analyzed under the *S_a-based GM subset* are similar in general with minor differences in rankings, while the *BS-based set* resulted in slightly lower R^2-adjusted values

When the results of *F2S2B frame* under all alternative GM subsets are examined as a whole, it has been observed that the vector IMs formed with PGV/PGA or $t_{5\text{-}95}$ generally enhanced the individual performances of scalar forms, where PGV/PGA-based vector IMs performed slightly better. Supplementary statistical metrics have generally confirmed the R^2-adjusted value-based rankings with the exception of irregular F-values observed especially for $\langle S_a, S_{dN} \rangle$, and for particular cases of $\langle IM_1, t_{5-95} \rangle$ and $\langle IM_1, PGV/PGA \rangle$ forms. Additionally, specific cases have been observed where p-values computed for the second parameters of particular vector IMs are larger than the 0.05 limit, marking the insignificance of the second IM in the regression models.

5.9.4 Summary for Efficiency Performances for Frame F5S7B

When the *TD-based result set for F5S7B frame (T_1=0.66 s)* analyzed under the *PGA-based GM subset* is evaluated, ordinary scalar IMs (in decreasing order) SED, AI, I_v, CAV, IEPA, EPA, ASI, and PGA ranked in the worst 10 with R^2-adjusted values below 0.78. Scalar indices EPV, HI, VSI, ASI*, IEPV, PGV, and I_F showed much better performance with respect to other ordinary scalar IMs with R^2-adjusted values between 0.95-0.81. The structure-specific S_a-based novel scalar and vector IMs ranked in the top 10 with R^2-adjusted values above 0.97. The *MIDR-based R^2-adjusted results for F5S7B frame* analyzed under the *PGA-based GM subset* are similar in general with minor differences in rankings, while *BS-based results* yielded slightly lower R^2-adjusted values for top-performing IM candidates and slightly higher R^2-adjusted values for poor-performing ordinary scalar IMs.

The *TD-based result set for F5S7B frame (T$_1$=0.66 s)* analyzed under the *PGV-based GM subset* has revealed that ordinary scalar IMs (in decreasing order) PGA, PGV, IEPV, CAV, I$_F$, I$_v$, and SED ranked in the worst 10 with R^2-adjusted values below 0.90. Alternative scalar IMs ASI*, EPV, VSI, HI, AI, IEPA, ASI, and EPA showed better performance with respect to the above-mentioned ordinary scalar IMs with R^2-adjusted values between 0.97-0.90. The structure-specific S$_a$-based novel scalar and vector IMs ranked in the top 10 with R^2-adjusted values above 0.98. The *MIDR-based R^2-adjusted results for F5S7B frame* analyzed under the *PGV-based GM subset* are similar in general with minor differences in rankings, whereas *BS-based results* yielded slightly lower R^2-adjusted values.

When the *TD-based result set for F5S7B frame (T$_1$=0.66 s)* analyzed under the *ASI*-based GM subset* is evaluated, ordinary scalar IMs (in decreasing order) AI, IEPA, SED, I$_v$, PGA, CAV, EPA, and ASI ranked in the worst 10 with R^2-adjusted values below 0.92. Alternative scalar indices EPV, VSI, HI, ASI*, IEPV, PGV, and I$_F$ showed better performance with respect to above-listed ordinary scalar IMs with R^2-adjusted values between 0.98-0.92. The structure-specific S$_a$-based novel scalar and vector IMs generally ranked in the top 10 with R^2-adjusted values above 0.98. The *MIDR-based R^2-adjusted results for F5S7B frame* analyzed under the *ASI*-based GM subset* are similar in general with minor differences in rankings, while *BS-based results* yielded slightly lower R^2-adjusted values.

The *TD-based results for F5S7B frame (T$_1$=0.66 s)* analyzed under the *VSI-based GM subset* have exhibited that ordinary scalar IMs (in decreasing order) AI, CAV, IEPA, I$_v$, PGA, SED, EPA, and ASI ranked in the worst 10 with R^2-adjusted values below 0.91. Alternative scalar IMs VSI, ASI*, EPV, HI, PGV, IEPV, and I$_F$ showed better performance with respect to the listed ordinary scalar IMs with R^2-adjusted values between 0.96-0.92. The structure-specific S$_a$-based novel scalar and vector IMs ranked in the top 10 with R^2-adjusted values above 0.97. The *MIDR-based R^2-adjusted results for F5S7B frame* analyzed under the *VSI-based GM subset* are similar in general with minor differences in rankings, whereas *BS-based results* yielded slightly lower R^2-adjusted values.

When the *TD-based result set for F5S7B frame (T₁=0.66 s)* analyzed under the *S_a-based GM subset* is examined, ordinary scalar IMs (in decreasing order) IEPA, AI, PGA, EPA, ASI, I_v, SED, and CAV ranked in the worst 10 with R^2-adjusted values below 0.91. Alternative indices ASI*, EPV, VSI, HI, IEPV, PGV, and I_F performed better with respect to other ordinary scalar IMs with R^2-adjusted values between 0.97-0.91. The structure-specific S_a-based novel scalar and vector IMs ranked in the top 10 with R^2-adjusted values above 0.97. The *MIDR-based R^2-adjusted results for F5S7B frame* analyzed under the *S_a-based GM subset* are similar in general with minor differences in rankings, while the *BS-based set* resulted in slightly lower R^2-adjusted.

When the results of *F5S7B frame* under all alternative GM subsets are examined as a whole, it has been observed that the vector IMs formed with PGV/PGA or t_{5-95} generally enhanced the individual performances of scalar forms, where PGV/PGA-based vector IMs performed slightly better. Supplementary statistical metrics have generally confirmed the R^2-adjusted value-based rankings with the exception of irregular F-values observed especially for $\langle S_a, S_{dN} \rangle$, and for particular cases of $\langle IM_1, t_{5-95} \rangle$ and $\langle IM_1, PGV/PGA \rangle$ forms. Additionally, specific cases have been observed where p-values computed for the second parameters of particular vector IMs are larger than the 0.05 limit, marking the insignificance of the second IM in the regression models.

5.9.5   Summary for Efficiency Performances for Frame F5S2B

When the *TD-based result set for F5S2B frame (T₁=0.75 s)* analyzed under the *PGA-based GM subset* is evaluated, ordinary scalar IMs (in decreasing order) SED, AI, I_v, CAV, IEPA, EPA, ASI, and PGA ranked in the worst 10 with R^2-adjusted values below 0.79. Scalar indices EPV, VSI, HI, ASI*, IEPV, PGV, and I_F showed much better performance with respect to other ordinary scalar IMs with R^2-adjusted values between 0.94-0.82. The structure-specific S_a-based novel scalar and vector IMs ranked in the top 10 with R^2-adjusted values above 0.94. The *MIDR-based R^2-*

adjusted results for F5S2B frame analyzed under the *PGA-based GM subset* are similar in general with minor differences in rankings, while *BS-based results* yielded slightly lower R^2-adjusted values for top-performing IM candidates and higher R^2-adjusted values for poor-performing ordinary scalar IMs.

The *TD-based result set for F5S2B frame ($T_1=0.75$ s)* analyzed under the *PGV-based GM subset* has revealed that ordinary scalar IMs (in decreasing order) EPA, PGA, PGV, IEPV, CAV, I_F, I_v, and SED ranked in the worst 10 with R^2-adjusted values below 0.86. Alternative scalar IMs EPV, VSI, ASI*, HI, AI, IEPA, and ASI showed better performance with respect to the above-mentioned ordinary scalar IMs with R^2-adjusted values between 0.96-0.85. The structure-specific S_a-based novel scalar and vector IMs ranked in the top 15 with R^2-adjusted values above 0.94. The *MIDR-based R^2-adjusted results for F5S2B frame* analyzed under the *PGV-based GM subset* are similar in general with minor differences in rankings, whereas *BS-based results* yielded slightly lower R^2-adjusted values for top-performing IM candidates and higher R^2-adjusted values for poor-performing ordinary scalar IM.

When the *TD-based result set for F5S2B frame ($T_1=0.75$ s)* analyzed under the *ASI*-based GM subset* is evaluated, ordinary scalar IMs (in decreasing order) SED, AI, IEPA, I_v, PGA, CAV, EPA, and ASI ranked in the worst 10 with R^2-adjusted values below 0.89. Alternative scalar indices EPV, HI, VSI, ASI*, IEPV, PGV, and I_F showed better performance with respect to the above-listed ordinary scalar IMs with R^2-adjusted values between 0.97-0.90. The structure-specific S_a-based novel scalar and vector IMs generally ranked in the top 10 with R^2-adjusted values above 0.96. The *MIDR-based R^2-adjusted results for F5S2B frame* analyzed under the *ASI*-based GM subset* are similar in general with minor differences in rankings, while *BS-based results* yielded slightly lower R^2-adjusted values.

The *TD-based results for F5S2B frame ($T_1=0.75$ s)* analyzed under the *VSI-based GM subset* have exhibited that ordinary scalar IMs (in decreasing order) AI, I_v, SED, CAV, IEPA, PGA, EPA, and ASI ranked in the worst 10 with R^2-adjusted values below 0.86. Alternative scalar IMs VSI, HI, EPV, ASI*, PGV, IEPV, and I_F showed

better performance with respect to the listed ordinary scalar IMs with R^2-adjusted values between 0.96-0.90. The structure-specific S_a-based novel scalar and vector IMs ranked in the top 15 with R^2-adjusted values above 0.94. The *MIDR-based R^2-adjusted results for F5S2B frame* analyzed under the *VSI-based GM subset* are slightly higher in general with minor differences in rankings, whereas *BS-based results* yielded slightly lower R^2-adjusted values for top-performing IM candidates and slightly higher R^2-adjusted values for some of the poor-performing ordinary scalar IMs.

When the *TD-based result set for F5S2B frame (T_1=0.75 s)* analyzed under the *S_a-based GM subset* is examined, ordinary scalar IMs (in decreasing order) SED, I_v, AI, IEPA, PGA, EPA, ASI, and CAV ranked in the worst 10 with R^2-adjusted values below 0.93. Alternative indices EPV, HI, VSI, PGV, IEPV, ASI*, and I_F performed better with respect to other ordinary scalar IMs with R^2-adjusted values between 0.98-0.95. The structure-specific S_a-based novel scalar and vector IMs ranked in the top 10 with R^2-adjusted values above 0.97. The *MIDR-based R^2-adjusted results for F5S2B frame* analyzed under the *S_a-based GM subset* are similar in general with minor differences in rankings, while the *BS-based set* resulted in slightly lower R^2-adjusted values.

When the results of *F5S2B frame* under all alternative GM subsets are examined as a whole, it has been observed that the vector IMs formed with PGV/PGA or $t_{5\text{-}95}$ generally enhanced the individual performances of scalar forms, where PGV/PGA-based vector IMs performed slightly better. Supplementary statistical metrics usually have confirmed the R^2-adjusted value-based rankings with the exception of irregular F-values observed, especially for $\langle S_a, S_{dN} \rangle$, and for particular cases of $\langle IM_1, t_{5-95} \rangle$ and $\langle IM_1, PGV/PGA \rangle$ forms. Additionally, specific cases have been observed where p-values computed for the second parameters of particular vector IMs are larger than the 0.05 limit, marking the insignificance of the second IM in the regression models.

5.9.6   Summary for Efficiency Performances for Frame F5S4B

When the *TD-based result set for F5S4B frame (T₁=0.95 s, as a relatively long period system)* analyzed under the *PGA-based GM subset* is evaluated, ordinary scalar IMs (in decreasing order) I_v, AI, CAV, IEPA, EPA, ASI, and PGA ranked in the worst 10 with R^2-adjusted values below 0.84. Scalar indices HI, EPV, VSI, ASI*, IEPV, I_F, PGV, and SED showed much better performance with respect to other ordinary scalar IMs with R^2-adjusted values between 0.97-0.88. The structure-specific S_a-based novel scalar and vector IMs ranked in the top 10 with R^2-adjusted values above 0.98. The *MIDR-based R^2-adjusted results for F5S4B frame* analyzed under the *PGA-based GM subset* are similar in general with minor differences in rankings, while *BS-based results* yielded slightly lower R^2-adjusted values for top-performing IM candidates and higher R^2-adjusted values for poor-performing ordinary scalar IMs.

The *TD-based result set for F5S4B frame (T₁=0.95 s)* analyzed under the *PGV-based GM subset* has revealed that ordinary scalar IMs (in decreasing order) I_F, IEPA, PGA, CAV, ASI, EPA, I_v, and SED ranked in the worst 10 with R^2-adjusted values below 0.86. Alternative scalar IMs HI, VSI, EPV, ASI*, PGV, AI, and IEPV showed better performance with respect to the above-mentioned ordinary scalar IMs with R^2-adjusted values between 0.97-0.88. The structure-specific S_a-based novel scalar and vector IMs ranked in the top 10 with R^2-adjusted values above 0.98. The *MIDR-based R^2-adjusted results for F5S4B frame* analyzed under the *PGV-based GM subset* are similar in general with minor differences in rankings, whereas *BS-based results* yielded slightly lower R^2-adjusted values for top-performing IM candidates.

When the *TD-based result set for F5S4B frame (T₁=0.95 s)* analyzed under the *ASI*-based GM subset* is evaluated, ordinary scalar IMs (in decreasing order) SED, AI, I_v, CAV, IEPA, PGA, EPA, and ASI ranked in the worst 10 with R^2-adjusted values below 0.90. Alternative scalar indices HI, EPV, VSI, ASI*, IEPV, PGV, and I_F showed better performance with respect to the above-listed ordinary scalar IMs with R^2-adjusted values between 0.98-0.92. The structure-specific S_a-based novel scalar

and vector IMs generally ranked in the top 10 with R^2-adjusted values above 0.98. The *MIDR-based R^2-adjusted results for F5S4B frame* analyzed under the *ASI*-based GM subset* are similar in general with minor differences in rankings, while *BS-based results* generally yielded slightly lower R^2-adjusted values.

The *TD-based results for F5S4B frame (T_1=0.95 s)* analyzed under the *VSI-based GM subset* have exhibited that ordinary scalar IMs (in decreasing order) AI, I_v, SED, IEPA, CAV, PGA, EPA, and ASI ranked in the worst 10 with R^2-adjusted values below 0.88. Alternative scalar IMs VSI, HI, EPV, ASI*, PGV, IEPV, and I_F showed better performance with respect to the listed ordinary scalar IMs with R^2-adjusted values between 0.97-0.91. The structure-specific S_a-based novel scalar and vector IMs ranked in the top 10 with R^2-adjusted values above 0.97. The *MIDR-based R^2-adjusted results for F5S4B frame* analyzed under the *VSI-based GM subset* are similar in general with minor differences in rankings, whereas *BS-based results* yielded lower R^2-adjusted values.

When the *TD-based result set for F5S4B frame (T_1=0.95 s)* analyzed under the *S_a-based GM subset* is examined, ordinary scalar IMs (in decreasing order) I_v, AI, IEPA, PGA, CAV, EPA, and ASI ranked in the worst 10 with R^2-adjusted values below 0.90. Alternative indices VSI, HI, EPV, ASI*, IEPV, PGV, I_F, and SED performed better with respect to other ordinary scalar IMs with R^2-adjusted values between 0.98-0.93. The structure-specific S_a-based novel scalar and vector IMs ranked in the top 10 with R^2-adjusted values above 0.98. The *MIDR-based R^2-adjusted results for F5S4B frame* analyzed under the *S_a-based GM subset* are similar in general with minor differences in rankings, while the *BS-based set* resulted in lower R^2-adjusted values.

When the results of *F5S4B frame* under all alternative GM subsets are examined as a whole, it has been observed that the vector IMs formed with PGV/PGA or t_{5-95} generally enhanced the individual performances of scalar forms, where PGV/PGA-based vector IMs performed slightly better. Supplementary statistical metrics have generally confirmed the R^2-adjusted value-based rankings with the exception of

irregular F-values observed, especially for $\langle S_a, S_{dN} \rangle$, and for particular cases of $\langle IM_1, t_{5-95} \rangle$ and $\langle IM_1, PGV/PGA \rangle$ forms. Additionally, specific cases have been observed where p-values computed for the second parameters of particular vector IMs are larger than the 0.05 limit, marking the insignificance of the second IM in the regression models.

5.9.7 Summary for Efficiency Performances for Frame F8S3B

When the *TD-based result set for F8S3B frame (T₁=1.20 s, as a typical long-period system)* analyzed under the *PGA-based GM subset* is evaluated, ordinary scalar IMs (in decreasing order) I_v, CAV, AI, IEPA, EPA, ASI, and PGA ranked in the worst 10 with R^2-adjusted values below 0.88. Scalar indices HI, VSI, I_F, EPV, IEPV, SED, ASI*, and PGV showed much better performance with respect to other ordinary scalar IMs with R^2-adjusted values between 0.97-0.88. The structure-specific S_a-based novel scalar and vector IMs ranked in the top 10 with R^2-adjusted values above 0.97. The *MIDR-based R^2-adjusted results for F8S3B frame* analyzed under the *PGA-based GM subset* exhibited noticeable differences for some IMs leading to improvement in rankings, while *BS-based results* yielded slightly lower R^2-adjusted values for top-performing IM candidates and higher R^2-adjusted values for poor-performing ordinary scalar IMs.

The *TD-based result set for F8S3B frame (T₁=1.20 s)* analyzed under the *PGV-based GM subset* has revealed that ordinary scalar IMs (in decreasing order) AI, I_v, SED, CAV, IEPA, PGA, ASI, and EPA ranked in the worst 10 with R^2-adjusted values below 0.85. Alternative scalar IMs HI, VSI, PGV, ASI*, IEPV, I_F, and EPV showed better performance with respect to the above-mentioned ordinary scalar IMs with R^2-adjusted values between 0.96-0.88. The structure-specific S_a-based novel scalar and vector IMs ranked in the top 10 with R^2-adjusted values above 0.96. The *MIDR-based R^2-adjusted results for F8S3B frame* analyzed under the *PGV-based GM subset* are similar in general with minor differences in rankings, whereas *BS-based*

results yielded lower R^2-adjusted values for top-performing IM candidates and slightly higher R^2-adjusted values for poor-performing ordinary scalar IMs.

When the *TD-based result set for F8S3B frame (T_1=1.20 s)* analyzed under the *ASI*-based GM subset* is evaluated, ordinary scalar IMs (in decreasing order) I_v, AI, CAV, IEPA, PGA, EPA, and ASI ranked in the worst 10 with R^2-adjusted values below 0.92. Alternative scalar indices HI, VSI, I_F, SED, IEPV, EPV, PGV, and ASI* showed better performance with respect to the above-listed ordinary scalar IMs with R^2-adjusted values between 0.97-0.93. The structure-specific S_a-based novel scalar and vector IMs generally ranked in the top 10 with R^2-adjusted values above 0.98. The *MIDR-based R^2-adjusted results for F8S3B frame* analyzed under the *ASI*-based GM subset* exhibited higher values for IM candidates in the worst 10, while *BS-based results* generally yielded slightly lower R^2-adjusted values for top-performing IM candidates and higher R^2-adjusted values for poor-performing ordinary scalar IMs.

The *TD-based results for F8S3B frame (T_1=1.20 s)* analyzed under the *VSI-based GM subset* have exhibited that ordinary scalar IMs (in decreasing order) SED, AI, CAV, IEPA, PGA, EPA, and ASI ranked in the worst 10 with R^2-adjusted values below 0.90. Alternative scalar IMs HI, VSI, PGV, I_F, IEPV, ASI*, EPV, and I_v showed better performance with respect to the listed ordinary scalar IMs with R^2-adjusted values between 0.97-0.91. The structure-specific S_a-based novel scalar and vector IMs ranked in the top 10 with R^2-adjusted values above 0.97. The *MIDR-based R^2-adjusted results for F8S3B frame* analyzed under the *VSI-based GM subset* exhibited noticeable differences for some IMs leading to improvement in rankings, whereas *BS-based results* generally yielded slightly lower R^2-adjusted values for top-performing IM candidates and higher R^2-adjusted values for poor-performing ordinary scalar IMs.

When the *TD-based result set for F8S3B frame (T_1=1.20 s)* analyzed under the *S_a-based GM subset* is examined, ordinary scalar IMs (in decreasing order) EPV, AI, CAV, IEPA, PGA, EPA, and ASI ranked in the worst 10 with R^2-adjusted values

below 0.90. Alternative indices HI, IEPV, VSI, I_F, SED, PGV, ASI*, and I_v performed better with respect to other ordinary scalar IMs with R^2-adjusted values between 0.97-0.90. The structure-specific S_a-based novel scalar and vector IMs generally ranked in the top 10 with R^2-adjusted values above 0.97. The *MIDR-based R^2-adjusted results for F8S3B frame* analyzed under the *S_a-based GM subset* are similar in general with minor differences in rankings, while the *BS-based set* generally resulted in lower R^2-adjusted values with the exception of the worst 4 IMs, which have higher R^2-adjusted values.

When the results of *F8S3B frame* under all alternative GM subsets are examined as a whole, it has been observed that the vector IMs formed with PGV/PGA or $t_{5\text{-}95}$ generally enhanced the individual performances of scalar forms, where PGV/PGA-based vector IMs performed slightly better. Supplementary statistical metrics have generally confirmed the R^2-adjusted value-based rankings with the exception of irregular F-values observed, especially for $\langle S_a, S_{dN} \rangle$, and for particular cases of $\langle IM_1, t_{5-95} \rangle$ and $\langle IM_1, PGV/PGA \rangle$ forms. Additionally, specific cases have been observed where p-values computed for the second parameters of particular vector IMs are larger than the 0.05 limit, marking the insignificance of the second IM in the regression models.

5.9.8   Overall Evaluation of Efficiency Performances

To facilitate the interpretations, summary tables have been prepared to display the R^2-adjusted values for 7 frames, 5 DB IMs (as PGA, PGV, ASI*, VSI and $S_a(T_1)$) and selected IMs (i.e., the widely used scalar IMs *-PGA and PGV-*, the better candidates *-ASI*, VSI, $S_a(T_1)$, ASI, HI-* and a qualifying list of S_a-based scalar and/or vector intensity measures *-S_{aC}, S_{aCM}, ASA_{40}, I_{N_p}, $\langle S_a, R(T_1, T_2) \rangle$, $\langle S_a, N_p \rangle$, $\langle S_a, S_{dN} \rangle$, $\langle S_a, S_a/DSI \rangle$*). Table A.3 thru Table A.6, correspondingly, present the relative rankings of these IMs in the following format "## - ####" (which corresponds to "rank ## - R^2-adjusted value"). In these tables, the IMs ranking in the **Top 5** are highlighted with **bold fonts**, whereas the IMs ranking in the succeeding group (Top

6th to Top 10th) are marked with *italic fonts*. The tabulated R^2-adjusted results of the 15-monitored IMs are graphically re-presented in Figure 5.18 - Figure 5.20 for TD, Figure 5.21 - Figure 5.23 for MIDR, and Figure 5.24 - Figure 5.26 for BS to display the period-wise variation of the efficiency performances.

Foremost, TD- and MIDR-based charts have marked the superiority of the novel scalar and vector IM candidates over the ordinary scalar indices, which was expected due to the fact that these more recent candidates are S_a-based and structure-specific. When the evaluations are comparatively made among the TD- and MIDR-based results of ordinary scalar IMs, S_a is the best parameter in most of the cases. PGA and ASI turned out to be relatively more efficient for the short period system, ASI being slightly superior. The relatively high efficiency of these two parameters rapidly diminished with increasing periods. PGV exhibited comparably low performance at short periods, while its performance has much improved beyond the short period range. As opposed to PGA, PGV, and ASI, spectrum-based (but structure-independent) ASI* and VSI turned out to be much more stable in terms of efficiency in the entire period range considered. ASI* was slightly superior at short periods, while VSI enhanced its performance at longer periods. HI also showed a high correlation at long periods, but its performance is lower with respect to VSI at short-to-medium periods, but outperforms VSI at long periods. The less preferred parameter EPA has shown a slightly higher correlation with respect to PGA for the short-period system, but did not outperform ASI. The modified version of EPA, IEPA, exhibited higher efficiency with respect to PGA, but failed to perform better as opposed to the original EPA, while for medium-to-long period systems, IEPA showed relatively higher efficiency. The results for medium period systems have revealed the superiority of the velocity-based EPV with respect to PGV (even VSI in specific cases), whereas the performance of IEPV was mostly close to PGV. Correspondingly, IEPV, as a recommendation of Yang et al. (2009) for near-fault ground motions, did not bring in additional improvement to the efficiency with respect to its counterparts. The performances of AI, SED, CAV, I_F, and I_v will not be

re-discussed here, as interpretations about these alternative scalar IMs have already been made in Section 5.6.
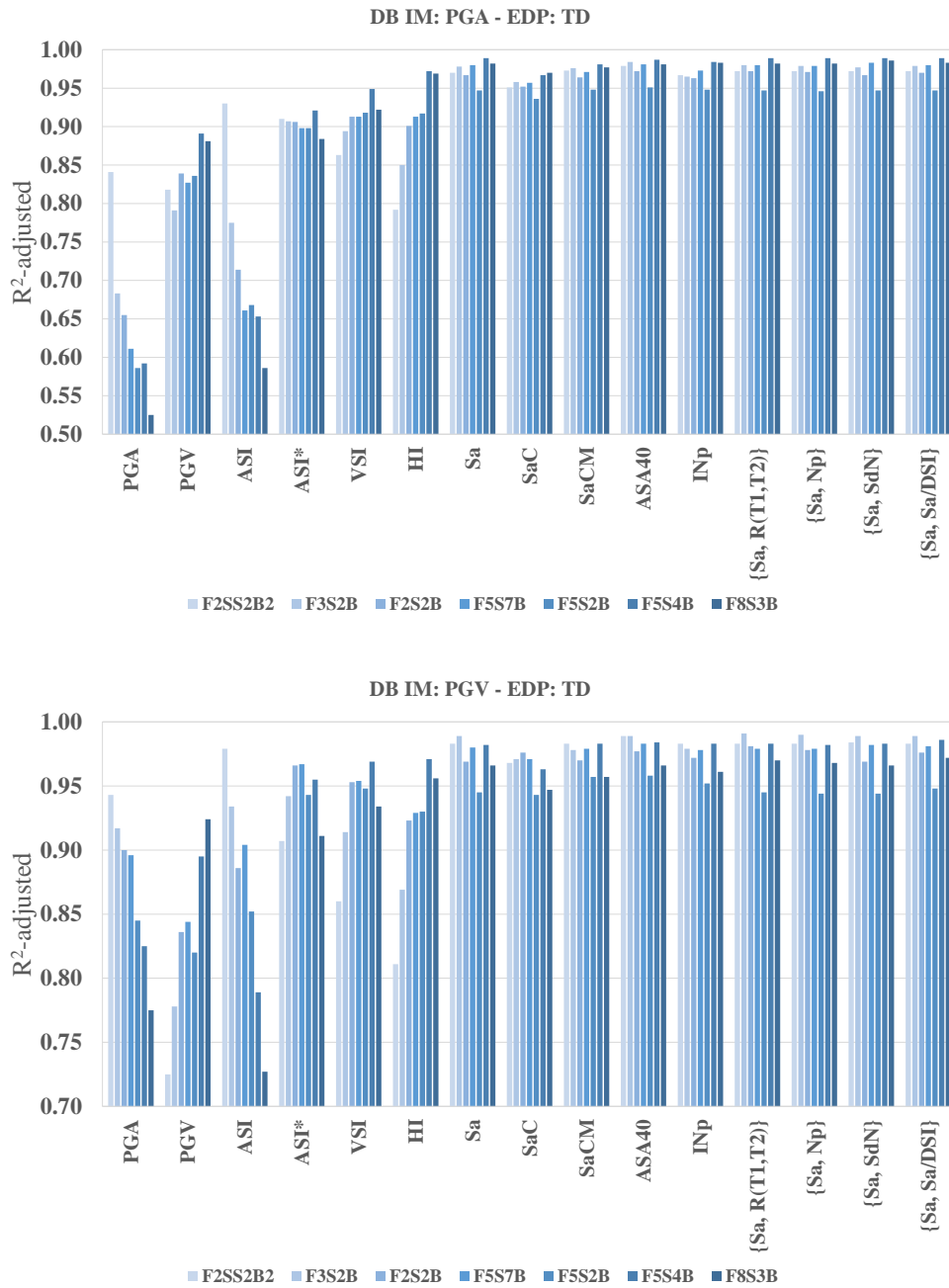
Figure 5.18. Period-wise variation of R^2-adjusted values for EDP: TD under GM subsets with DB IM: PGA and PGV
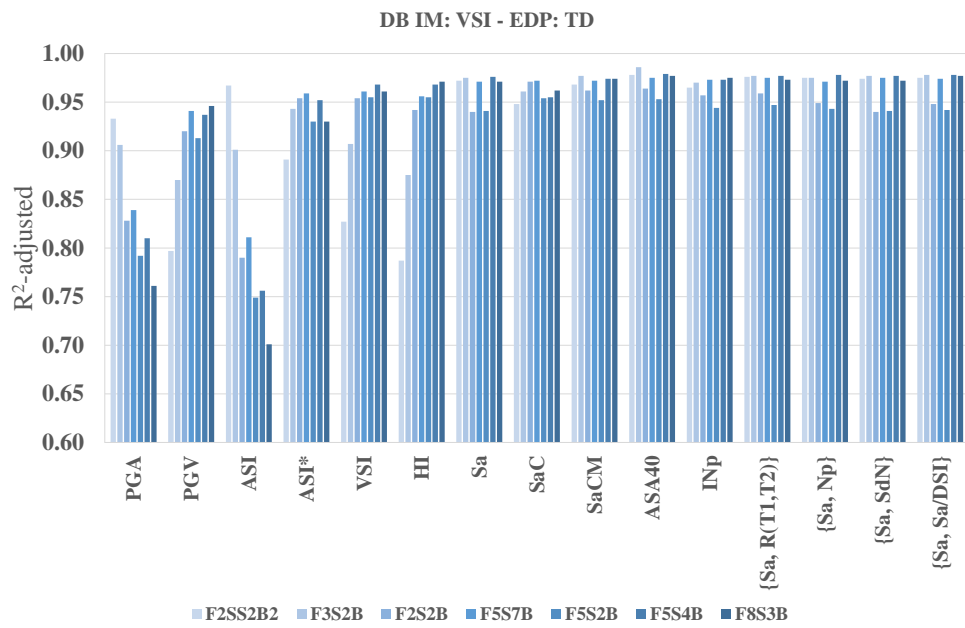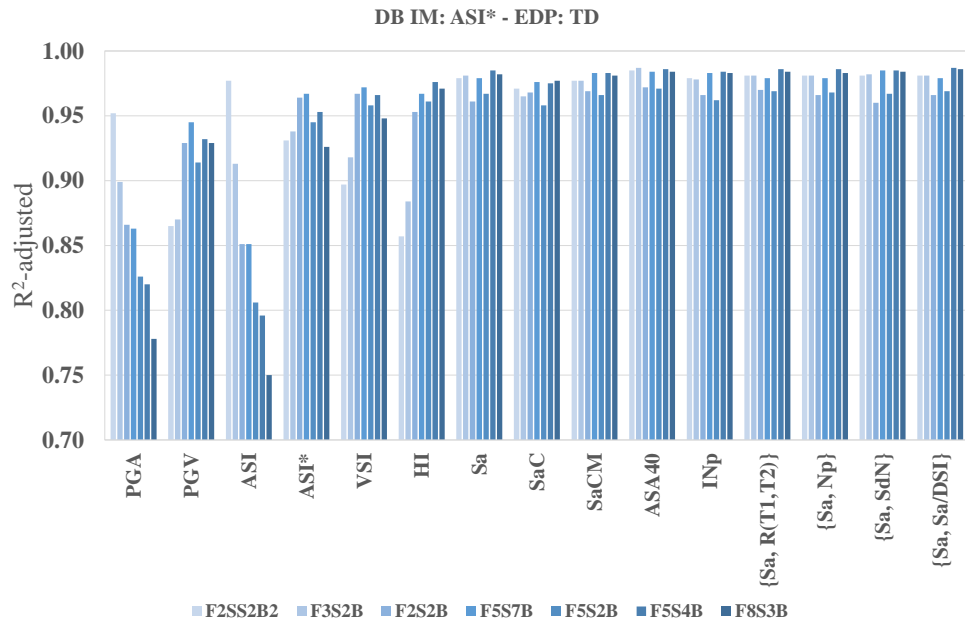
Figure 5.19. Period-wise variation of R^2-adjusted values for EDP: TD under GM subsets with DB IM: ASI* and VSI
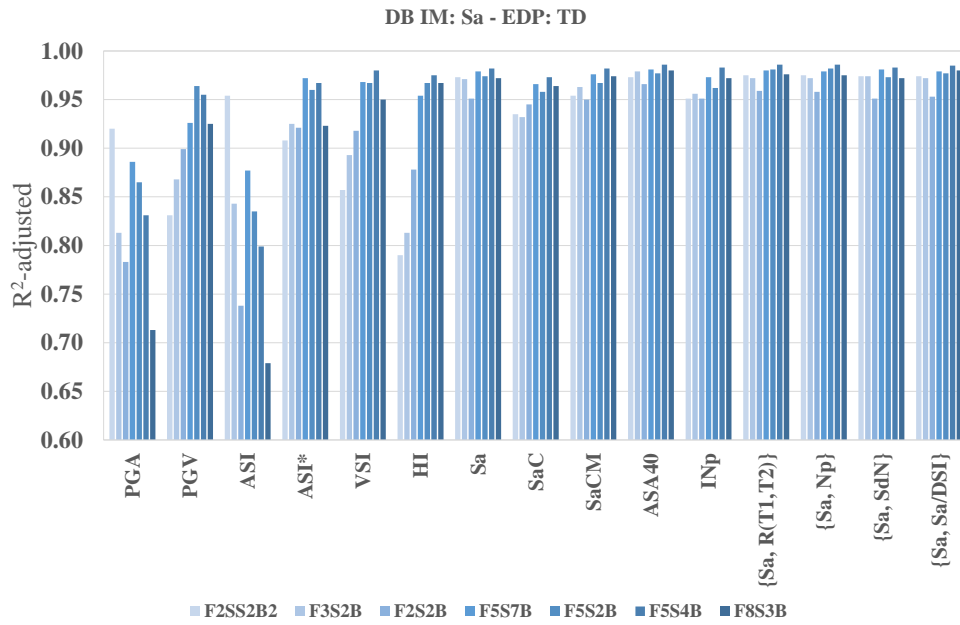
Figure 5.20. Period-wise variation of R^2-adjusted values for EDP: TD under GM subset with DB IM: $S_a(T_1)$
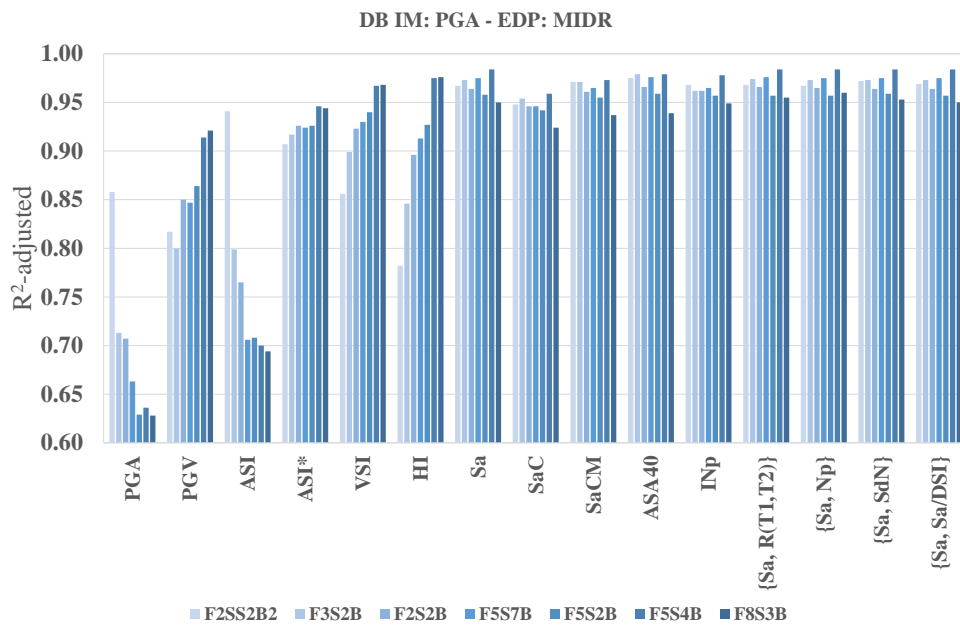
Figure 5.21. Period-wise variation of R^2-adjusted values for EDP: MIDR under GM subset with DB IM: PGA

DB IM: PGV - EDP: MIDR

DB IM: ASI* - EDP: MIDR

Legend: F2SS2B2, F3S2B, F2S2B, F5S7B, F5S2B, F5S4B, F8S3B
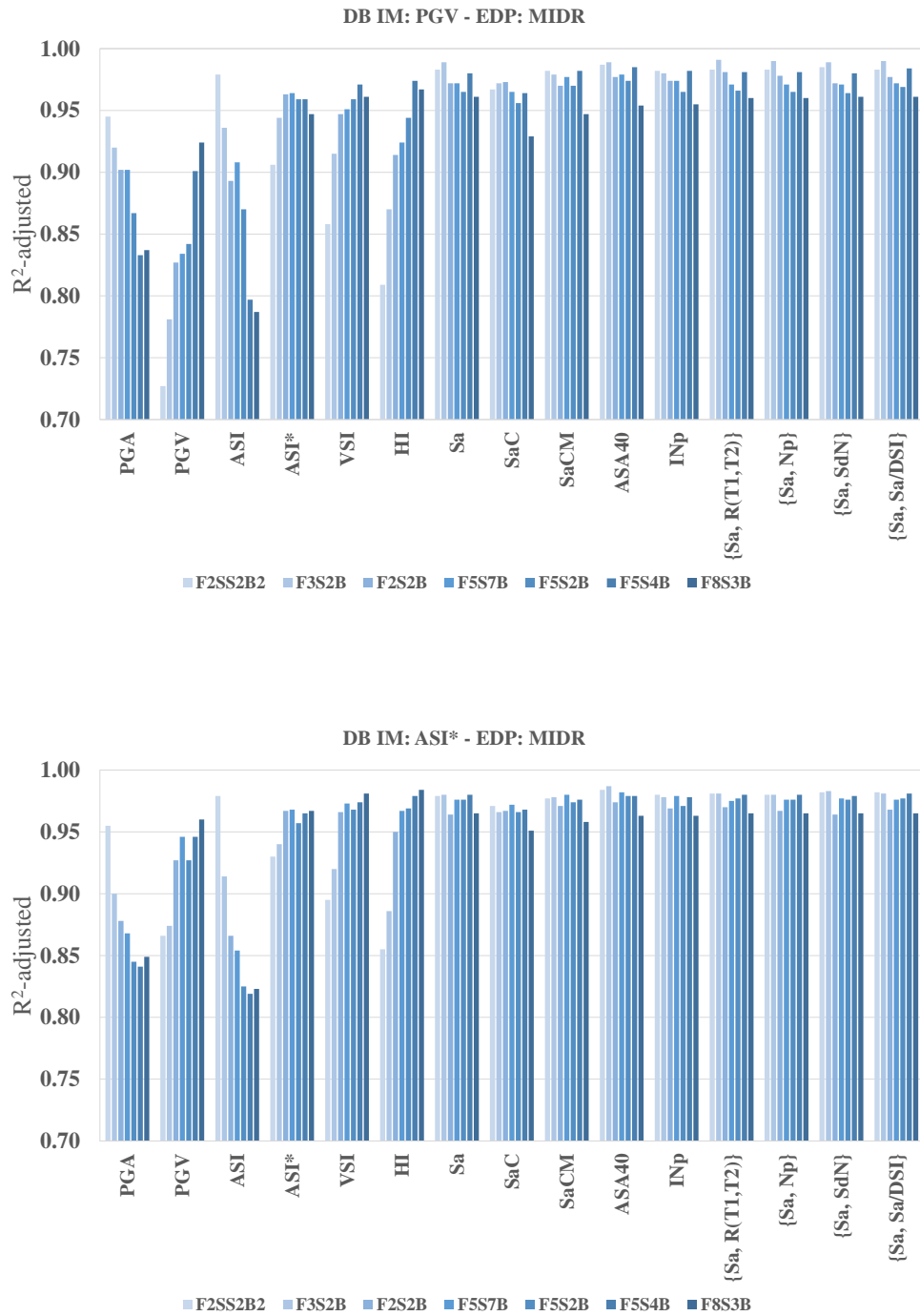
Figure 5.22. Period-wise variation of R^2-adjusted values for EDP: MIDR under GM subsets with DB IM: PGV and ASI*
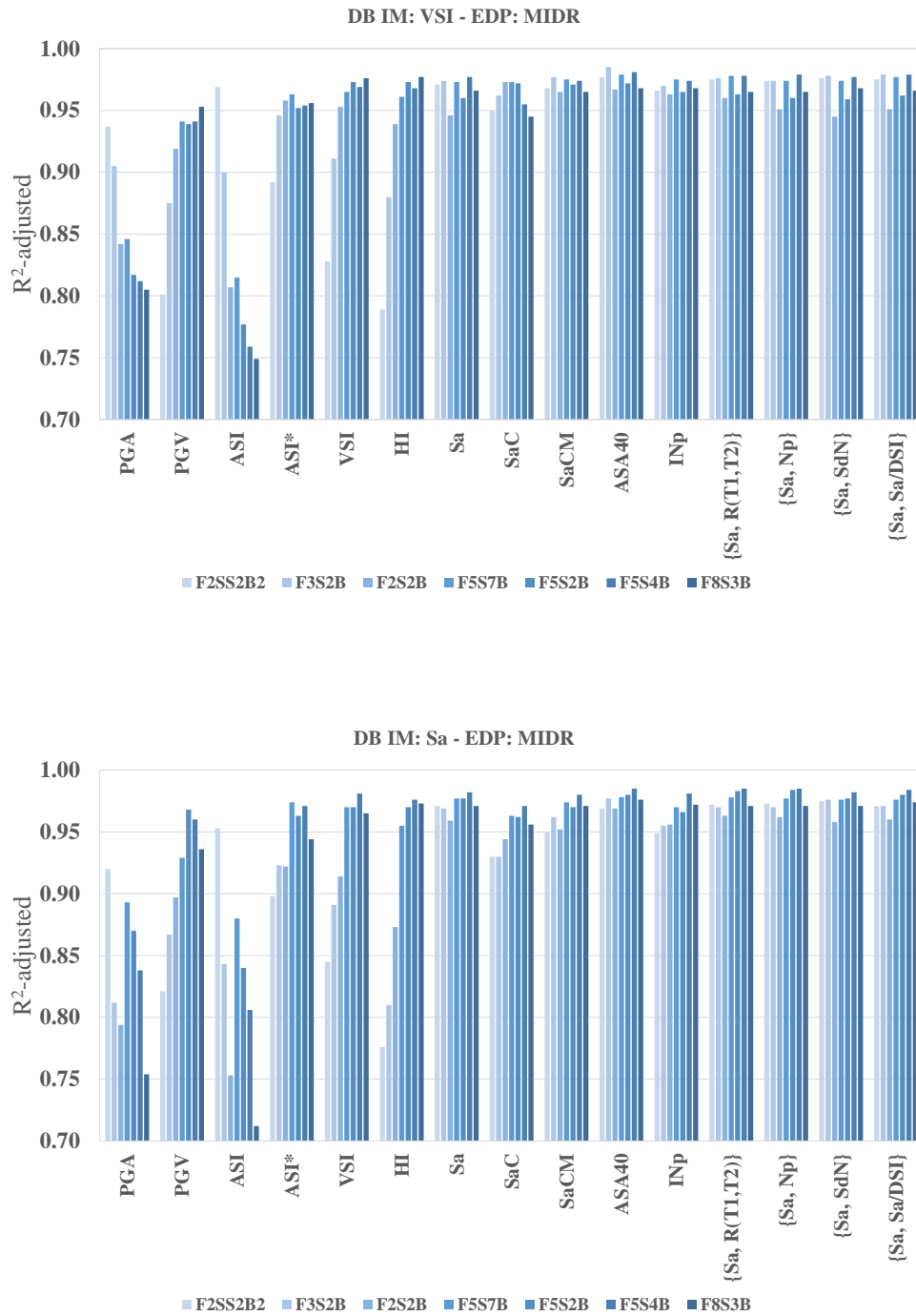
Figure 5.23. Period-wise variation of R^2-adjusted values for EDP: MIDR under GM subsets with DB IM: VSI and $S_a(T_1)$
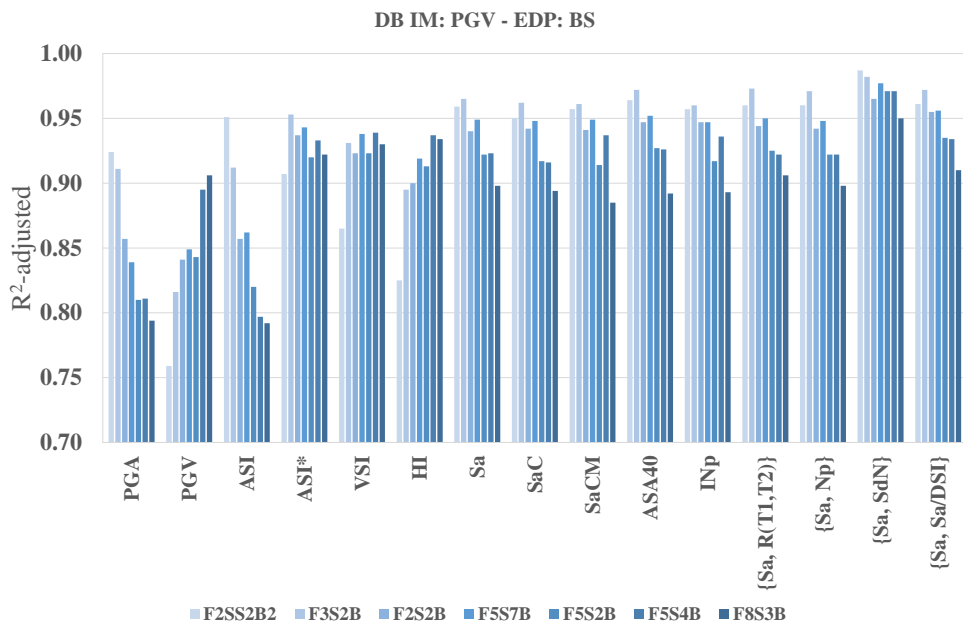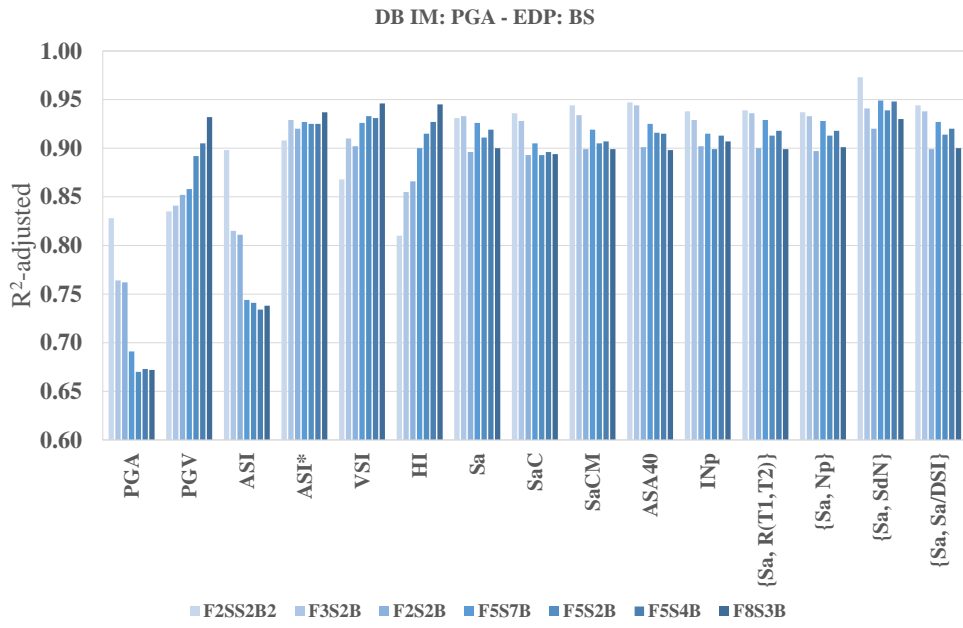
Figure 5.24. Period-wise variation of R^2-adjusted values for EDP: BS under GM subsets with DB IM: PGA and PGV
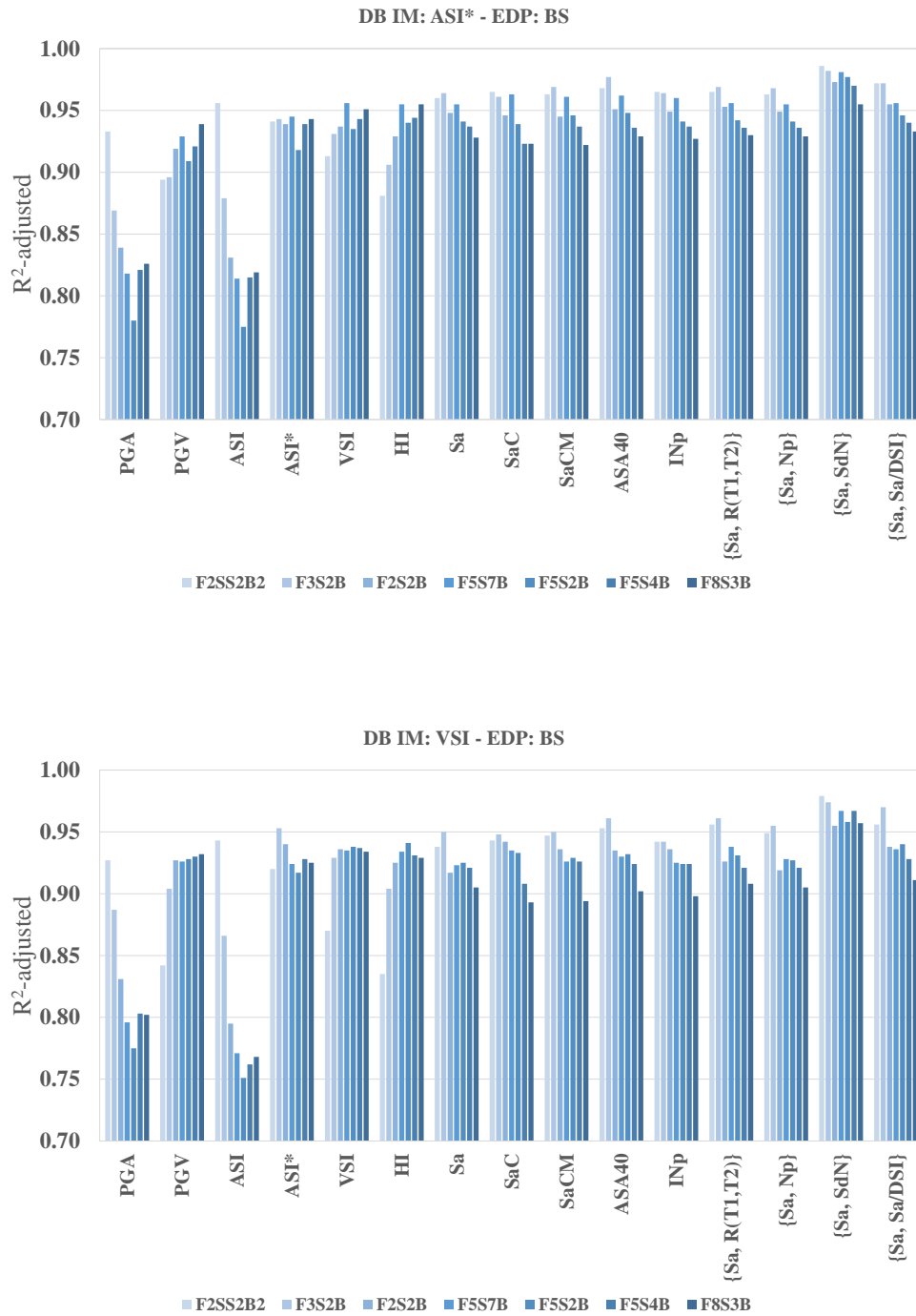
Figure 5.25. Period-wise variation of R^2-adjusted values for EDP: BS under GM subsets with DB IM: ASI* and VSI
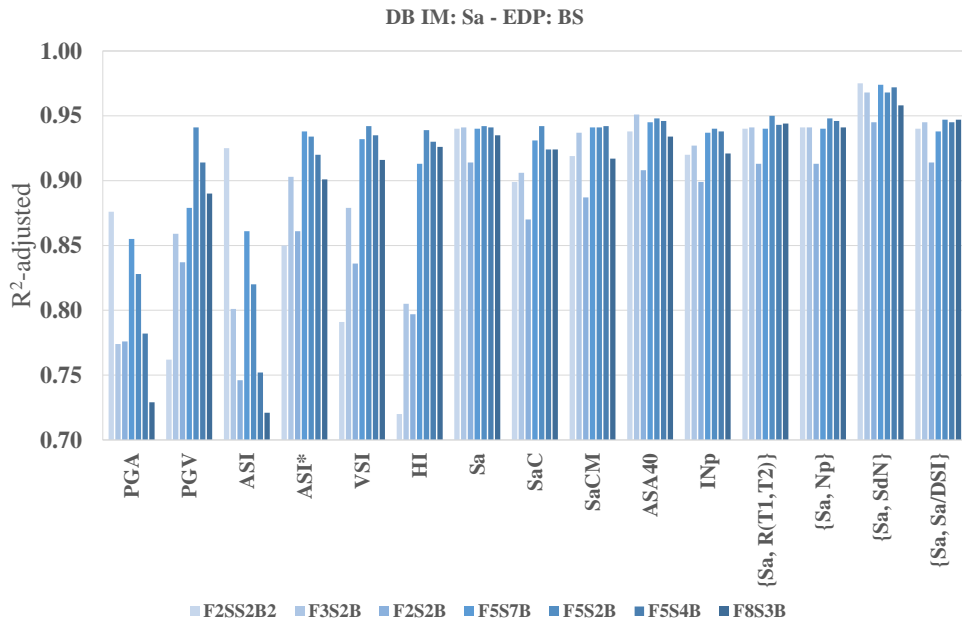
DB IM: Sa - EDP: BS

Figure 5.26. Period-wise variation of R^2-adjusted values for EDP: BS under GM subset with DB IM: $S_a(T_1)$

When the R^2-adjusted based evaluations are extended to the spectrum based novel IMs, it has been observed that these more advanced parameters mostly ranked in the top 15 with R^2-adjusted values above 0.94 and generally close to each other, and the performances seemed to be comparatively constant in the period range of consideration. The numerical values for TD- and MIDR-based results have marked the superiority of ASA_{40} with respect to both scalar and vector forms, yet there are few cases where other novel candidates took the lead as well. The relatively better performance of ASA_{40} has confirmed the suitability of R=40 assumption for the structure set used herein. On the contrary, S_{aC} and S_{agm} yielded slightly lower values with respect to original S_a in general (with particular exceptions), pointing to the inappropriate period assumptions for cT_1 and $T^{(n)}$ input parameters in these IMs. S_{aCM}, in contrast, performed comparably better with respect to S_{aC}, indicating that the input parameters (c and α) recommended by Lin et al. (2011) are more appropriate for the systems analyzed (and for the IM formulation). In the vectorial forms $\langle S_a, N_p \rangle$ and $\langle S_a, R(T_1, T_2) \rangle$, the same T_2 was assumed (i.e., $T_2 = 2T_1$) and the

155

performance metrics had the same order of magnitude. Although $\langle S_a, N_p \rangle$ had been proposed as a better indicator of the spectral shape (for the period range defined) as opposed to $\langle S_a, R(T_1, T_2) \rangle$ (Bojórquez and Iervolino; 2010, 2011), this phenomenon was not observed numerically herein. However, both IMs performed better than the scalar S$_{aC}$. Even the scalar alternative of $\langle S_a, N_p \rangle$, I_{N_p}, generally performed relatively better than S$_{aC}$, while this simpler version yielded slightly lower values in general with respect to the original form. The last two IMs in the summary list, $\langle S_a, S_{dN} \rangle$ and $\langle S_a, S_a/DSI \rangle$), require more complex calculations with respect to $\langle S_a, R(T_1, T_2) \rangle$ and other advanced scalar indices as they employ displacement spectrum as well, but generally yielded higher R^2-adjusted values.

It would be beneficial to re-express that all these S$_a$-based advanced scalar and vector parameters rely on assumed input parameters to calculate the defined indices, and further calibration of these numerical inputs (for each structural system or for the whole building set) might lead to increased efficiencies (i.e., R^2-adjusted values) and eventually, modify rankings of the top IMs. Nevertheless, it can be principally stated that $\langle S_a, R(T_1, T_2) \rangle$ and $\langle S_a, N_p \rangle$ are the most efficient vector IMs herein along with their relative simplicity as opposed to $\langle S_a, S_{dN} \rangle$ and $\langle S_a, S_a/DSI \rangle$. The significance checks for the second parameter of these vector IMs, on the other hand, have occasionally raised concerns about the statistical significance of the secondary indices within the regression models.

When the vector IMs with consideration of frequency content or significant duration (i.e., $\langle IM_1, PGV/PGA \rangle$ or $\langle IM_1, t_{5-95} \rangle$ classes) are examined (though not presented in summary tables), it has been frequently observed that PGV/PGA or t$_{5-95}$ seem to slightly enhance the R^2-adjusted based efficiency performance of vector IMs with respect to their corresponding scalar IM$_1$ cases, yet supplementary statistical parameters (i.e., F-values showing the significance of the regression model and p-values(2) revealing the statistical significance of the second IM parameter in the regression model) did not always confirm that these improvements are statistically significant. PGV/PGA turned out to be more influential while supplementing poor-

performing PGA or ASI, while remained with limited impact in vector forms with PGV, VSI, HI, ASI* and $S_a(T_1)$. The duration-related parameter t_{5-95}, in contrast, was relatively less effective for the structural systems considered.

In comparison with TD- and MIDR-based evaluations, BS-based performance metrics mostly turned out to be lower for top-performing scalar or vector IMs, whereas for poor-performing IMs, some improvements with respect to TD- or MIDR-based statistics have been observed especially for the PGA-based GM subset. Among the IMs presented in the summary tables, the vector IM $\langle S_a, S_{dN} \rangle$ mostly outperformed in BS-based cases, while the detailed examination of F-values corresponding to this IM has raised concerns about the validity of its superior performance.

GM subset-wise comparative evaluation of efficiency metrics (as presented in the summary tables) has revealed that the performance of acceleration-related indices improved with the utilization of PGV- based GM subset with respect to the PGA-based results. On the contrary, PGV-based subset yielded lower values for PGV (with the exception of the case for the long-period system) when compared with the PGA-based results. It has also been observed that choosing ASI* and VSI as DB IM improved the R^2-adjusted statistics of PGA, PGV, ASI*, and VSI where the improvement for PGA case remained limited with respect to others. When the efficiency metrics for S_a and other novel scalar-vector IMs are examined, DB IM did not seem to change the performance of these candidates significantly.

As an additional evaluation to investigate the efficiency of alternative IMs in linear and nonlinear response ranges, the NTH results for two typical frames (F3S2B frame as a medium-period system and F5S4B frame as a relatively long-period system) have been differentiated as linear and nonlinear sets. Afterwards, MIDR-based regression studies have been re-performed for these two distinct sets of results, and the statistical outputs corresponding to this stage are provided in the supplementary file of Appendix E, where the complete set of results are summarized in Table A.7. The linear response-based sample sets of results have clearly marked the superiority

of scalar IM S_a and S_a-based vector IMs with vector alternatives having slightly higher R^2-adjusted values. This outcome was expected, as the structures utilized generally exhibit first mode dominant behavior. The nonlinear response case, on the other hand, has revealed that S_a and S_a-based scalar and vector IMs generally performed better than the rest, but R^2-adjusted values always remained below 0.90.

5.9.9 Overall Evaluation of Sufficiency against M_w and R_{JB}

Detailed evaluation of the sufficiency of all IMs considering different frame, EDP, and GM subset cases is very complicated to reach simple conclusions. For this reason, summary tables for the abovementioned IM alternatives have been prepared for M_w and R_{JB} cases, but are not presented herein within the text. The reader may refer to Appendix E for the complete set of summary tables (Table A.8 - Table A.11 for M_w and Table A.12 – Table A.15 for R_{JB}) presented before the detailed tables.

Table A.8 thru Table A.11 emphasize the general M_w dependence of ordinary scalar IMs especially observed for short and long period structural systems, where PGA and ASI turned out to be insufficient in most of the cases examined. Other scalar IMs exhibited better performance in terms of sufficiency (with fewer number of "insufficient" cases), as observed for medium period systems. S_a and PGV seem to be the most robust parameters with limited "insufficient" cases. Additionally, it has been clearly observed for the ordinary scalar IMs that the DB IM also affects the sufficiency performance of parameters. PGA- and VSI-based GM subsets generally yielded "insufficient" cases; in contrast, PGV-based GM subsets yielded relatively few unfavorable cases. When the results for novel scalar and vector IMs are examined, it has been noticed that these candidates are generally sufficient against M_w when the EDP is TD or MIDR; however, BS-based results seem to be more sensitive to M_w-dependency.

Table A.12 – Table A.15 set, on the other hand, clearly reveals that monitored IMs are generally sufficient against R_{JB}, when the EDP is TD or MIDR. BS-based results

have conversely shown the dependence of particular IMs on R_{JB}, especially observed for the medium-to-long period systems analyzed.

As a general outcome of this stage of the study, the comprehensive sufficiency evaluations have marked the significance of moment magnitude M_w (as compared to source-to-site distance R_{JB}) on the seismic demands estimated as functions of candidate IMs.

5.10 Discussion of Results

To briefly summarize the steps followed within the scope of this chapter; MDOF-based evaluation stage has inherited a shortlist of ordinary scalar IMs (PGA, PGV, AI, SED, CAV, ASI*, VSI, I_F, I_v) from the SDOF-based evaluation stage and has exercised two different sampling methods (i.e., Stratified Random Sampling and Cluster Sampling) at first to form alternative GM subsets. These alternative record sets have been utilized to perform NTH analyses employing the simplified ESDOF models of a set of reinforced concrete frame systems, and correlations between the shortlisted IMs and major seismic demands have been computed, accordingly. Preliminary comparison of the Pearson correlation coefficients has revealed that Stratified Random and Cluster Sampling-based subsets generally yield similar rankings for the shortlisted scalar IMs, fallaciously confirming the usability of Cluster Sampling Set in further stages of the study as well. However, accumulation of the response data in low-to-moderate intensity levels, as graphically represented, has clearly shown that Stratified Random Sampling approach is more appropriate to obtain a relatively uniform distribution of results along the intensity levels. After this step, MDOF system-based NTH analyses have been performed employing the Stratified Random Sampling-based GM subsets based on the shortlisted IMs and structure-specific S_a's.

The correlation studies from both ESDOF and MDOF systems have revealed the comparative performances of the shortlisted IMs in the entire period range of

consideration (T=0.3-1.2 sec), which is the fundamental period range for the structural systems utilized. The period-wise variation of the correlation coefficients (based on TD, MIDR and BS demands) consolidated the conclusions from the SDOF-based evaluations, with Pearson correlation coefficients slightly lower. Among the shortlisted 10 ordinary scalar IMs, SED turned out to be the worst with highest dispersion in the results. I_F and I_v comparably performed better, but showed moderate correlation for short-to-medium periods. PGA, proved to be efficient only for short periods, had lower performance with respect to AI and CAV. The structure-specific S_a turned out to be the most efficient parameter among the list, especially observed in TD- and MIDR-based results, whereas correlation results have shown that spectrum-based but structure-independent ASI* and VSI exhibit a comparably high performance for the frames employed. ESDOF-based results supported with strongly correlating MDOF-based interpretations have also led to the recommendation that an analyst could form a hazard-independent GM subset considering ASI* or VSI as the conditioning IM. Such an attempt would make the record set structure-independent as well, as opposed to structure-specific S_a-based sets.

The next stage of the MDOF-based evaluations utilized the PGA and PGV subsets (as the simplest approach to a form record set), ASI* and VSI subsets (as per the abovementioned recommendation), and S_a-based subsets corresponding to the frames employed. The NTH analysis-based EDP demands obtained under these alternative record subsets have been further used to develop linear regression models (based on ln-ln transformed data indeed) following the Cloud Analysis approach. The predictors for these regression equations have been alternatively chosen from an expanded list of IMs (39 candidates) that constitute the shortlisted IMs, additional ordinary scalar IMs such as EPA, EPV, IEPA, IEPV, novel scalar and vector IMs recently proposed in the literature, and additionally, vector IM alternatives formed either with frequency-related PGV/PGA or significant duration-related t_{5-95}. The efficiency (as the major criterion for selecting IMs) of each IM alternative has been quantified via the R^2-adjusted value (accompanied with several supplementary

metrics to validate the statistical interpretations) and the IM candidates have been ranked according to this metric.

Overall examination of the efficiency metrics has highlighted that the superiority of structure-specific S_a and S_a-based scalar/vector IMs while predicting frame-based TD, MIDR and BS demands. The detailed ranking tables have also confirmed for ordinary scalar IMs that the Pearson correlation coefficient-based rankings are in accordance with the R^2-adjusted value-based rankings. The results have displayed particular situations where EPA-IEPA and EPV are superior to their counterparts PGA and PGV. Nevertheless, spectrum-based but structure-independent ASI* and VSI generally outperform ordinary scalar IMs considering the entire period range, with the exceptional case that HI performs slightly better at longer periods. The period-wise stable performance of ASI* and VSI marks them as "efficient" IMs among the ordinary scalar indices. GM subset-wise evaluations have also displayed that these two parameters improve the efficiency metrics of other ordinary scalar IMs.

When the focus is directed to S_a and S_a-based novel IMs, S_a clearly exhibited higher efficiency with respect to ordinary scalar IMs. In the meantime, among the more advanced forms, ASA$_{40}$, $\langle S_a, R(T_1, T_2) \rangle$, $\langle S_a, S_{dN} \rangle$, $\langle S_a, S_a/DSI \rangle$, and $\langle S_a, N_p \rangle$ generally performed better than S_a, while introducing additional computational cost. It has been displayed for particular cases that supplementary statistical metrics raise concerns about the statistical significance of the secondary IM in these vectorial forms. The high performance of ASA$_{40}$ along with its simplicity (though necessitates the consideration of the period elongation) puts forward this IM among the novel IM candidates.

The vector IMs in combination with ordinary scalar IMs and PGV/PGA or t$_{5-95}$ have occasionally performed slightly better than their corresponding scalar forms, while PGV/PGA-based alternatives seemed to be more effective with respect to duration related t$_{5-95}$.

161

In addition to the evaluations regarding the efficiency performance of candidate IMs, sufficiency checks against moment magnitude-M_w and source-to-site distance R_{JB} have been performed as well. The numerical results of statistical significance checks have displayed the dependence on M_w of some ordinary scalar IMs, while some particular BS-based cases have also been observed for R_{JB} dependency.

CHAPTER 6

EVALUATION OF THE EFFECT OF INTENSITY MEASURES ON GROUND MOTION SELECTION FOR FRAGILITY ANALYSES

6.1 Introduction

This chapter mainly examines the sensitivity of seismic fragility curves to the intensity measure considered in the ground motion selection stage of fragility analyses. Additionally, the effect of the number of bins and ground motion records selected from each bin is questioned in detail. For this purpose, two frame cases, one representative for short-to-medium period range and the other for medium-to-long period range, are utilized. New GM subsets covering a narrower but more realistic range of intensity levels corresponding to five different conditioning IMs are formed to achieve a uniform distribution of GM data as well. Employing these GM records, nonlinear time history analyses are performed on the ESDOF models of the selected frames to obtain MIDR estimations. Alternative linear seismic demand models corresponding to selected scalar IMs are generated with full and reduced datasets with different binning and number of records considerations. These demand models are later utilized to obtain the probability of exceedances leading to fragility curves which are compared to elaborate on the effects of conditioning IM, the number of bins considered and the number of records employed.

6.2 Concept of Fragility Curves

The fragility is simply the exceedance probability of a prescribed limit state at a specific seismic hazard level generally defined through a ground motion intensity measure or an intensity scale (Shinozuka et al., 2000). The development of the fragility information can be either empirically based on expert opinion, actual post-seismic event damage information, experimental data, or analytically established on

the structural simulations performed on the mathematical models (Ay, 2006). The last option naturally provides any risk-oriented analyst to collect as much information as possible from particular cases that can be carefully evaluated in a simulated environment. Correspondingly, the resulting fragility information, generally in the form of fragility functions, is conveyed as key ingredients into earthquake loss estimation studies (Ugurhan et al., 2011).

Generally, in combination of the ground motion variability, variability of the structural capacity, and the modelling uncertainty, the mathematical formulation forming the fragility functions can be illustrated as (Wen et al., 2004):

$$P(EDP \geq LS_i | IM_j) = 1 - \Phi \left(\frac{\ln(\hat{C}) - \ln(\widehat{EDP})}{\sqrt{\beta_C^2 + \beta_{EDP|IM}^2 + \beta_M^2}} \right) \tag{6.1}$$

where $P(EDP \geq LS_i | IM_j)$ stands for the probability of exceeding the limit state LS_i at the defined intensity level IM_j. Φ denotes the cumulative standard normal distribution. $\hat{C}$ and $\widehat{EDP}$ represent the median capacity and demand, respectively, and β_C, $\beta_{EDP|IM}$ and β_M stand for the variability in capacity, variability in demand at the defined intensity level, and the epistemic uncertainty due to modeling (Azari Sisi, 2016). If, in this reliability function, the ground motion variability (i.e., record-to-record variability) is considered to be dominant with respect to the capacity-related and epistemic uncertainties (i.e., when these two uncertainties are neglected), the formulation simplifies into:

$$P(EDP \geq LS_i | IM_j) = 1 - \Phi \left(\frac{\ln(\hat{C}) - \ln(\widehat{EDP})}{\beta_{EDP|IM}} \right) \tag{6.2}$$

The resulting formulation, indeed, signifies the importance of the selected intensity measure reflected through the increased or reduced dispersion in the calculated demands. The superiority of any candidate IM reveals itself here in this part of the fragility-based approach where the efficiency criterion comes into the picture.

There exist several studies in the literature employing different IMs in the derivation of fragility functions, as a whole portraying the evolution of the use of simple scalar to more advanced vector IMs, which lead to fragility surfaces indeed (Shinozuka et al., 2000; Erberik and Elnashai, 2004; Akkar et al., 2005; Ay, 2006; Hancılar, 2009; Celik and Ellingwood, 2010; Avşar et al., 2011; Gehl et al., 2013; Mazılıgüney et al., 2013; Modica and Stafford, 2014; Mazılıgüney et al., 2019). The fundamental point in these studies is that calculating the probability of exceeding a prescribed limit state necessitates the availability of a sufficiently sized set of analysis results at each intensity level, later generally utilized to form the cumulative distribution function to compute the corresponding exceedance probability. Alternatively, counting the number of exceeding cases at the intensity level of consideration might also be used to determine the proportion (Karimzadeh et al., 2020). Obtaining the values of probability of exceedance (dependent on the limit state considered) at generally equally-spaced intensity levels over the entire range of the conditioning IM considered, a log-normal function is commonly fitted to the data to finalize the fragility curve. Figure 6.1 illustrates the stages for convenient comprehension.
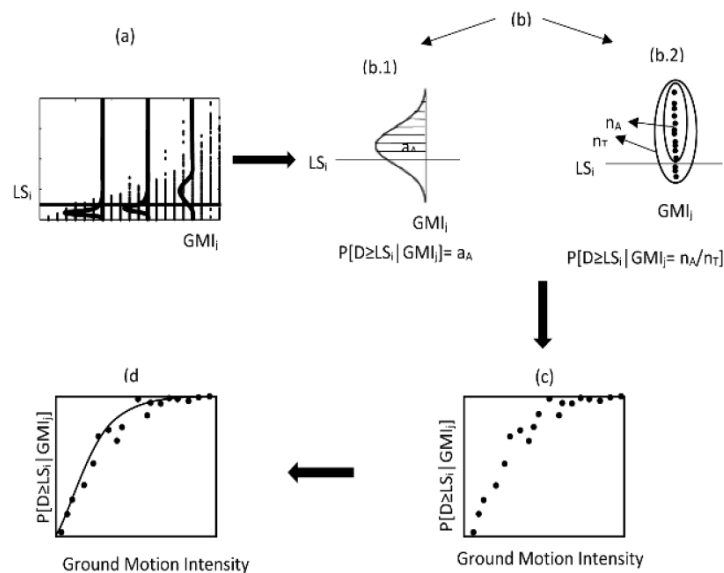
Figure 6.1. Schematic representation of the derivation of a fragility curve
(Karimzadeh et al., 2020)

165

6.3   Derivation of Fragility Curves

This study extends the endeavor of evaluating the efficiency and sufficiency of the IMs to fragility analyses with the aim of investigating the effect of selected IMs on the resulting curves. For this purpose, two frames, F3S2B and F5S4B, have been utilized to derive the MIDR-based fragility curves as a function of selected IMs (i.e., PGA, PGV, ASI*, VSI, $S_a(T_1)$, and ASA_{40}) with consideration of different GM subsets (PGA-, PGV-, ASI*-, VSI- and S_a-based datasets). The reason for selecting ASA_{40} is solely based on the relatively superior performance of this advanced scalar IM, as displayed in Chapter 5. The structure-specific IM $S_a(T_1)$, which has lower performance, yet easier to compute with respect to ASA_{40}, has also been considered in the list due to its ever-increasing use in fragility studies. Other advanced scalar IMs such as Sa_C, Sa_{CM}, S_{agm} or I_{Np} have not been considered in the fragility stage due to their inferior performance with respect to ASA_{40}. Of the structure independent IMs, PGA and PGV have been included as the simplest IMs and due to their common use as well, whereas ASI* and VSI have been incorporated due to their superior performance over PGA and PGV, as revealed in Chapter 4 and Chapter 5. The vector IMs have also been kept out of considerations, as the study is focused on single IM-dependent fragility curves, which are more practical to generate and interpret.

The five distinct GM subsets (each conditioned to PGA, PGV, ASI*, VSI, and S_a) have been re-formed on the basis of the former observations pointing at the uneven distribution of the GM records. Following intensity bounds have been defined accordingly for more realistic upper limits:

For the common sets;

- PGA: 0-1.50 g
- PGV: 0-150 cm/s
- ASI*: 0-3 g*s
- VSI: 0-400 cm

166

For F3S2B frame-specific S_a-set;

- S_a: 0-2.00 g

For F5S4B frame-specific S_a-set;

- S_a: 0-2.00 g

With reference to the statement by Cimellaro et al. (2011) presented in Appendix Section C.2, more than 20 records are needed for fragility studies. Here in this stage, 30 records for each bin have been aimed, while the number of bins has been kept as 10. The total number of records to be utilized as each GM subset (conditioned to different DB IM) eventually reaches 300 records, where the sample set size target with 110 records has already failed. As a solution to this problem, the scaling of the records is allowed for this part of the study, and records from lower intensity levels have been up-scaled by amplitude scaling to complete the GM datasets to target 300. The maximum limit for scaling factors considered during the modification of the records is 2.0 and 2.5 for F3S2B and F5S4B, respectively, where these limits are roughly in alignment with the latest recommendations of Dávalos and Miranda (2019).

The resulting uniformly distributed GM subsets have been employed to perform nonlinear time history analyses on the ESDOF models of the frames, which were shown to yield sufficiently reliable estimates of MDOF models' demand parameters. Consequently, ESDOF-based MIDR estimations have been obtained from the transient analysis results, where the MIDR values for collapsing cases have been taken as the assumed CP limit state-based values.

The complete MIDR result set corresponding to each GM subset (i.e., with different DB IM) has been processed for each frame to calculate the exceedance probabilities of IO, LS, and CP limit states for each bin (i.e., at the mid-values of the bins) with a counting methodology. The total number of bins is considered as 10, as illustrated in Figure 6.2. A cumulative lognormal distribution function has been fitted to the set of scattered probabilities employing the probit regression method by Baker (2015). This

set of IO, LS, and CP fragility curves is considered as "Original data-based" results. Alternatively, the transient analysis results have been utilized to construct the seismic demand models as previously exercised in Chapter 5. The probabilities of exceedance of IO, LS, and CP limit states have been re-calculated based on these regression models assuming a constant variance along the entire intensity range, and a different set of cumulative lognormal distribution functions has been fitted to the set of new scattered probabilities. The resulting set of IO, LS, and CP fragility curves is considered as "Regression Equation based" results, and will be termed as "benchmark curves" hereinafter.
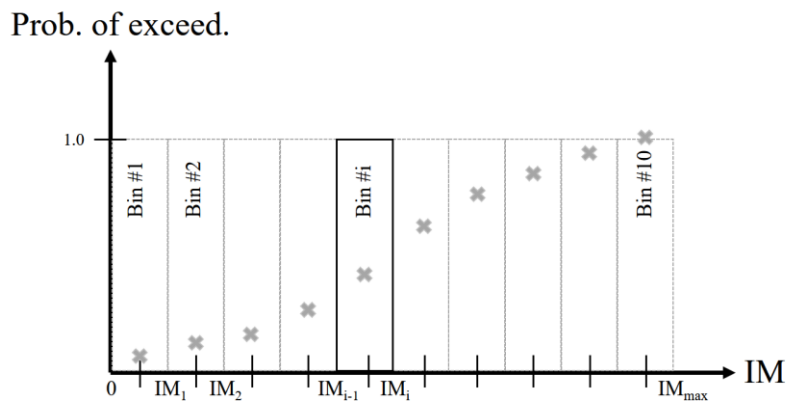
Figure 6.2. Schematic representation of binning with generic probability of exceedance distribution

In addition to the GM subset effects, the effect of ground motion set size on the fragility curves has been evaluated through the variation of the number of bins and the number of records. Four different cases for both the number of bins (i.e., 10, 8, 5, and 3 bins) and the number of records from each bin (i.e., 30-, 20-, 11- and 7-record samples from each bin) have been examined leading to 16 different cases in total. Since this approach poses a combinatorial problem, the formation of the downsized sample sets has been repeated 1000 times, yielding 1000 resamples in the

end for each inspected fragility curve. To exemplify, in a case with 5 bins and 7 records, the entire IM range is divided into 5 groups equally spaced with a step size ΔIM equal to $IM_{max}/5$, the whole dataset of results is partitioned into these 5 bins. Afterwards, 7 records from each bin are randomly selected without replacement yielding 5x7=35 records in total, forming the downsized sample set. This record selection procedure is repeated 1000 times to obtain different reduced dataset resamples.

At this point, it is crucial to note here that the reduced datasets are not directly used in the calculation of exceedance probabilities; on the contrary, they are utilized to develop regression models that are used to compute exceedance probabilities later on. The mean and mean± one sigma curves from each set of 1000 resamples are computed accordingly to facilitate the evaluation of variations in resulting probability estimations.

Figure 6.3 illustrates a sample case for F3S2B frame (with alternative cases for the number of bins and number of records) where the DB IM is PGA and the IO-, LS- and CP-based fragility curves have been derived as a function of PGA (i.e., IM=PGA). The plotting of resample-based curves together with the collection of "Original data-based", "Regression Equation based", mean and mean±1 sigma band curves gives a clue for the scatter in the final curves (and thus, probability estimations); however, it is hard to interpret several DB IM-IM cases collectively.

The above-mentioned procedure has been repeated several times for alternative IM cases (i.e., PGA, PGV, ASI*, VSI, $S_a(T_1)$ and ASA_{40}) together with different GM subsets (PGA-, PGV-, ASI*-, VSI- and S_a-based datasets) results, to reveal the effect of GM subsets and the number of bins/records on the resulting curves. Figure A.152 thru Figure A.163 represent the resulting fragility curves for F3S2B frame under 5 different GM subsets (DB IM=PGA, PGV, ASI*, VSI, and Sa, respectively) with various binning and number of records cases. Similarly, Figure A.169 thru Figure A.180 display the resulting fragility curves for F5S4B frame.
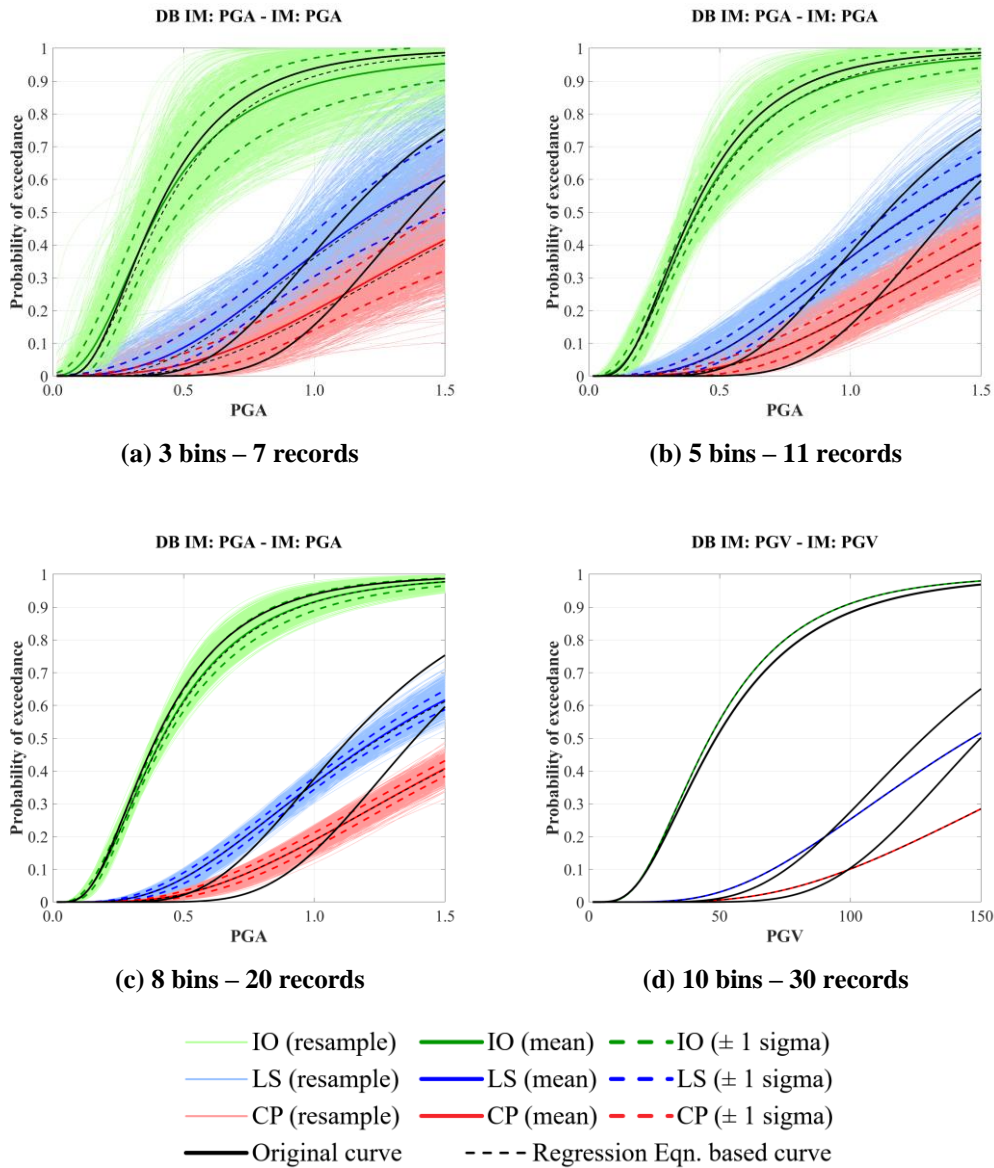
Figure 6.3. PGA-based fragility curves for F3S2B (MIDR) under PGA-based set

It is clear from this set of figures that the scatter in the final fragility curves (of the resamples) increases with decreasing number of bins and records as opposed to the original 10 bins-30 records case. Widening of the mean±1 sigma bands is a natural result of the observed scatters.

6.4   Comparison of Fragility Curves Considering Alternative Intensity Measures

The comparison of the MIDR-based fragility curves considering alternative intensity measures with different bin-number of records cases is evaluated in three stages. First, the effect of the conditioning IM is examined on various fragility curves defined as a function of alternative IMs. Next, the sensitivity of the fragility curve estimations is evaluated on the basis of the number of records employed. Finally, the effect of the number of bins to partition the whole dataset is investigated. The following sub-sections present the relevant materials and corresponding observations accordingly.

6.4.1   The Effect of Intensity Measures Defining the GM Set

The essential purpose of looking at the effect of IMs defining the GM set (i.e., DB IM) on the alternative IM-based fragility curves is that an analyst might have utilized a ground motion dataset formed with a consideration of an IM, while he/she might consider another IM to derive the corresponding fragility functions. The observations in Chapter 5 have already commented on the effect of the GM subset on the efficiency and sufficiency evaluations. Similar concerns have directed the study to evaluate this possibility and, if it exists, to quantify its effect. To facilitate the evaluations, Figure A.164-Figure A.168 for F3S2B frame and Figure A.181-Figure A.185 for F5S4B frame have been prepared to reveal the effects of DB IM. The data of the mean curves from separate DB IM-based sets have been collected for each specific IM case to compare the curves accordingly. For F3S2B, Figure 6.4-Figure 6.9 set presents the PGA-, PGV-, ASI*-, VSI-, S_a- and ASA_{40}-based fragility curves obtained under GM subsets conditioned to different DB IMs. Similar sets of figures for F5S4B are presented in Appendix F (please refer to Figure A.186-Figure A.191). In these figures, the left, middle, and right panes display the IO, LS, and CP fragility curves, respectively.
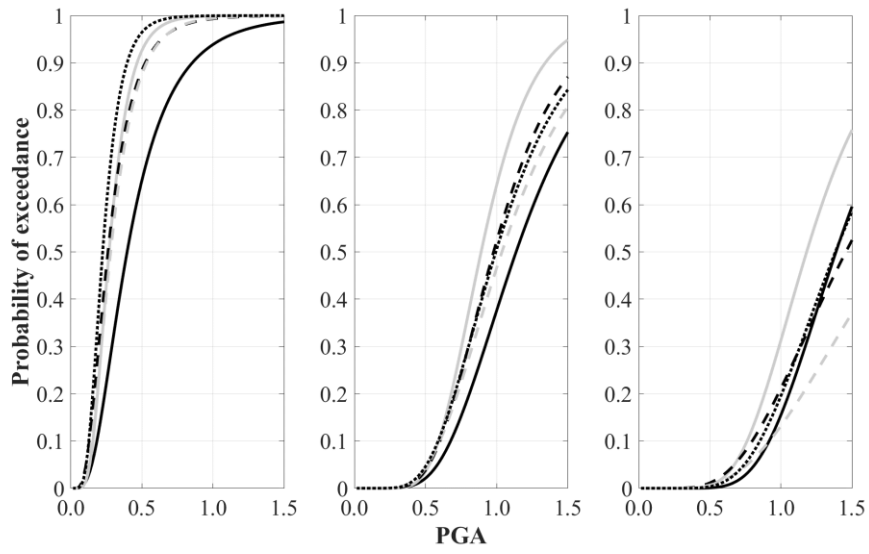
(a) Original Data Based
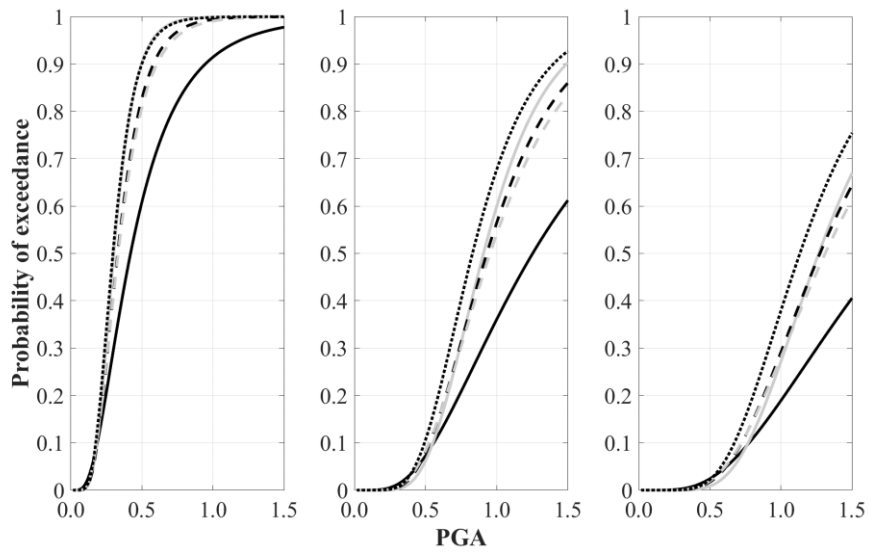
(b) Regression Equation Based

PGA ——— PGV ——— ASI* ‒ ‒ ‒ VSI ‒ ‒ ‒ Sa ⋯⋯⋯

Figure 6.4. PGA-based fragility curves for F3S2B (MIDR) under different GM record sets (10 bins – 30 records)
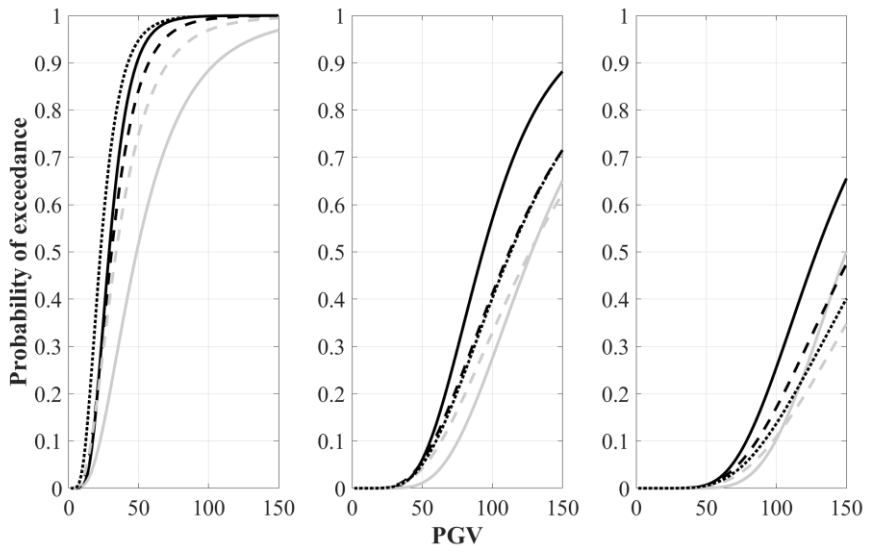
(a) Original Data Based
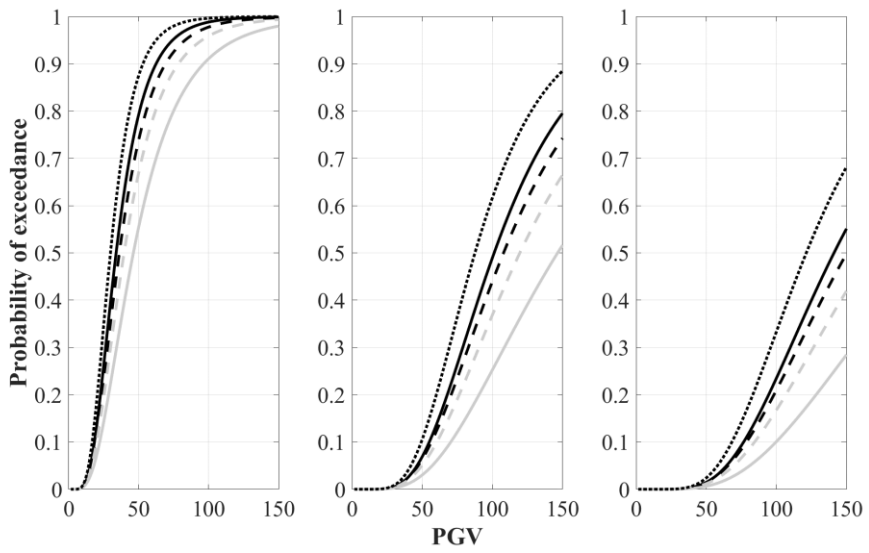
(b) Regression Equation Based

——— PGA ——— PGV – – – ASI* – – – VSI ········ Sa

Figure 6.5. PGV-based fragility curves for F3S2B (MIDR) under different GM record sets (10 bins – 30 records)
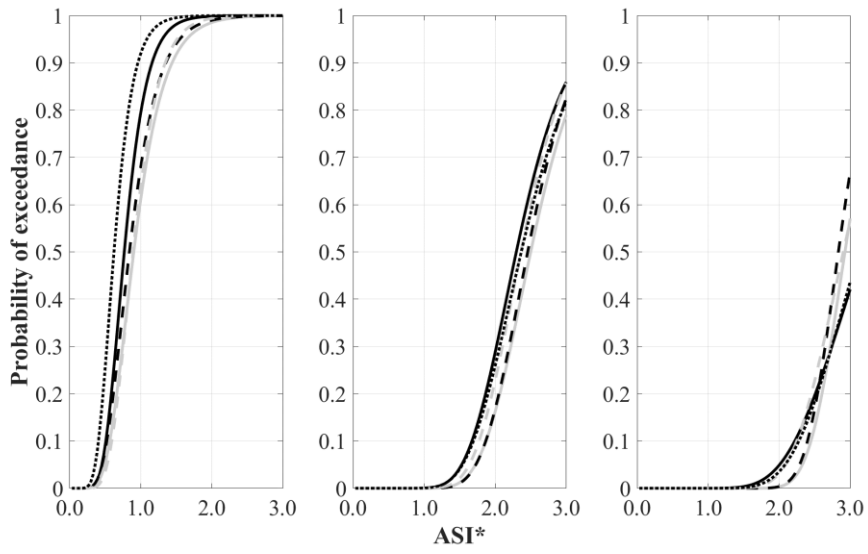
(a) Original Data Based
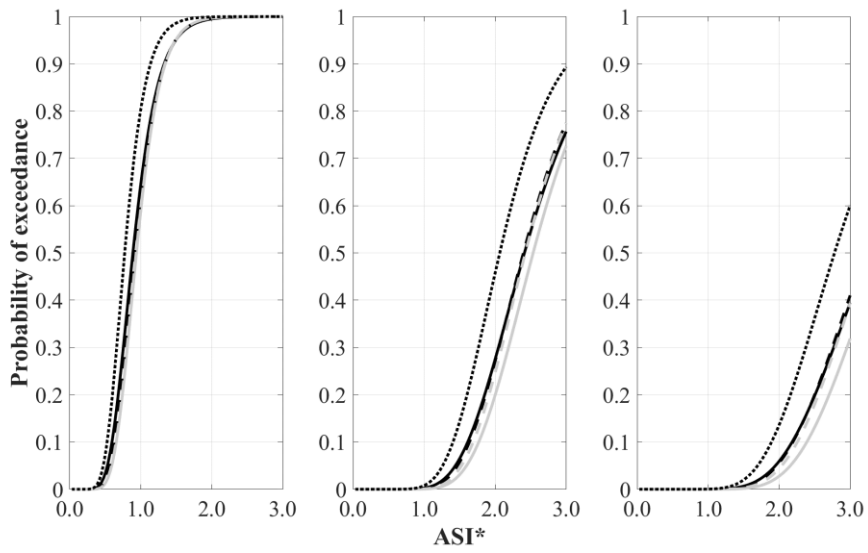
(b) Regression Equation Based

PGA ——— PGV – – –ASI* – – –VSI ········ Sa

Figure 6.6. ASI*-based fragility curves for F3S2B (MIDR) under different GM record sets (10 bins – 30 records)

174
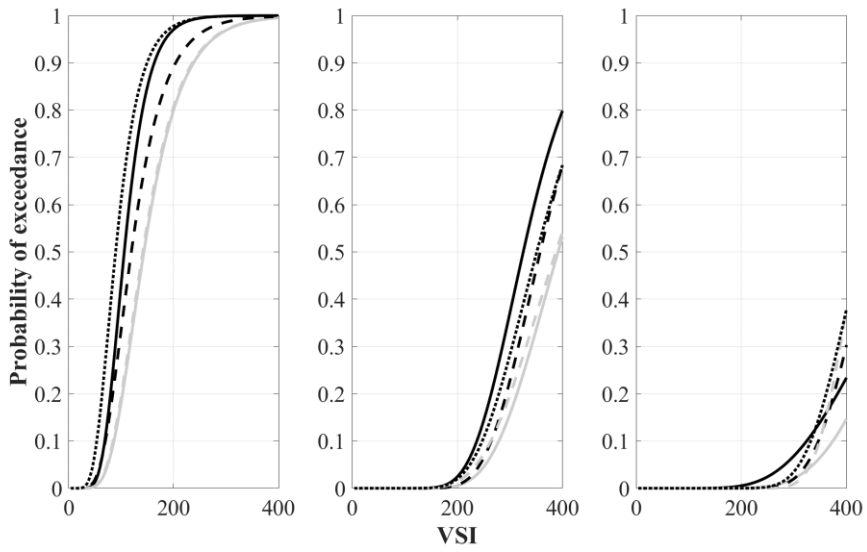
(a) Original Data Based
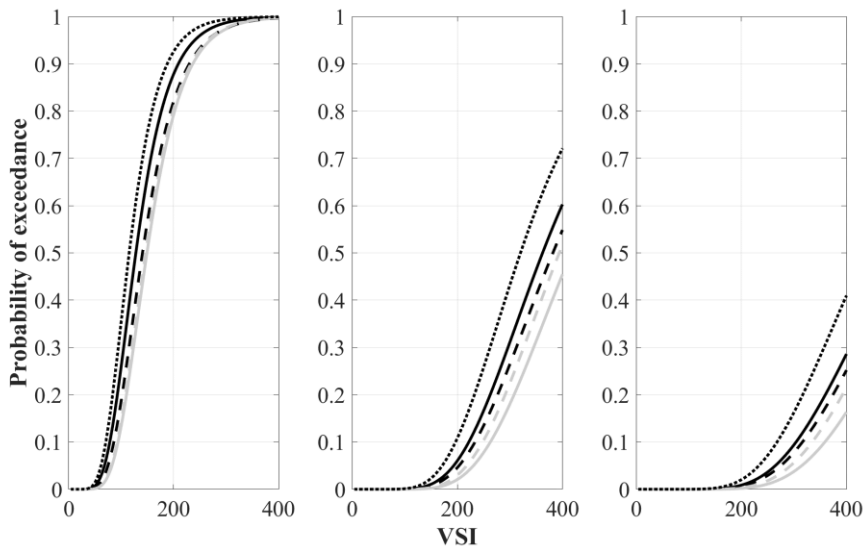
(b) Regression Equation Based

——— PGA ——— PGV – – – ASI* – – – VSI ········ Sa

Figure 6.7. VSI-based fragility curves for F3S2B (MIDR) under different GM record sets (10 bins – 30 records)
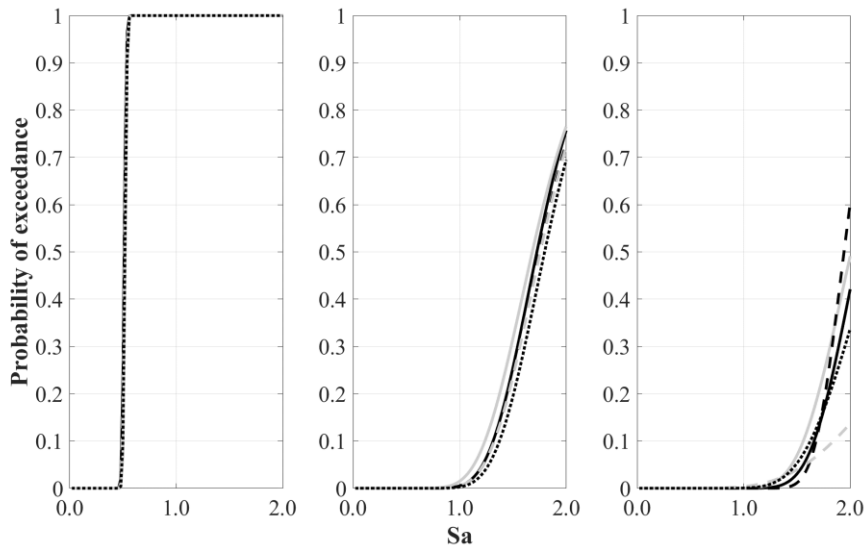
(a) Original Data Based
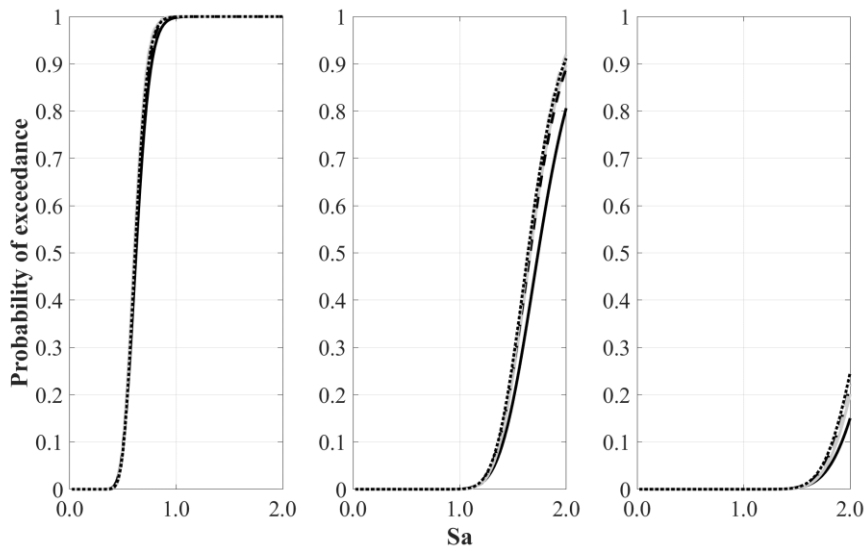
(b) Regression Equation Based

PGA   PGV   ASI*   VSI   Sa

Figure 6.8. S_a-based fragility curves for F3S2B (MIDR) under different GM record sets (10 bins – 30 records)
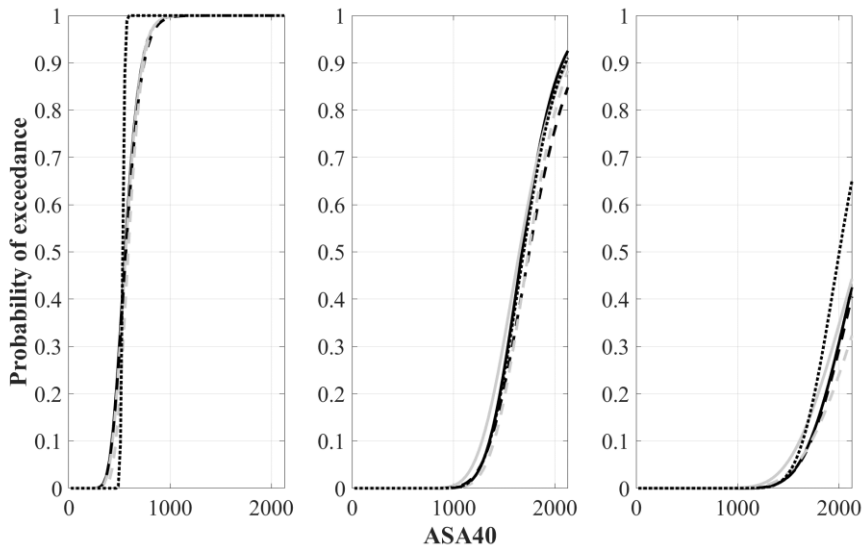
(a) Original Data Based
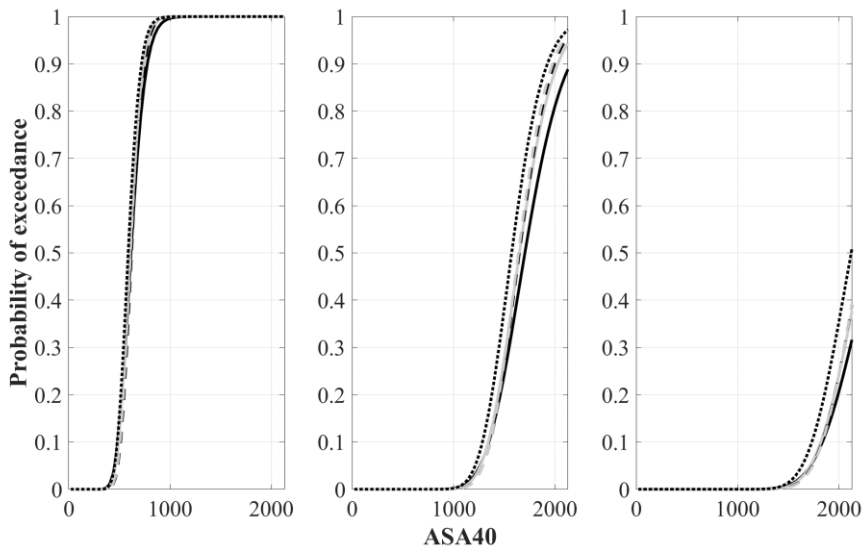
(b) Regression Equation Based

PGA ⎯⎯⎯ PGV ⎯⎯⎯ ASI* ⎯ ⎯ ⎯ VSI ⎯ ⎯ ⎯ Sa ·········

Figure 6.9. ASA$_{40}$-based fragility curves for F3S2B (MIDR) under different GM record sets (10 bins – 30 records)

For F3S2B frame; Figure 6.4 has revealed that the effect of GM subset conditioned to different DB IM is substantial in the resulting PGA-based curves. Considering "Original Data-Based" cases, the differences in IO-based curves exceeded 0.50 (in probability of exceedance-PoE terms) at low-to-moderate PGA levels, probably due to sharply increasing nature of IO curves. The maximum difference in LS-based curves is observed around 0.25 at a PGA level of 1.0g. On the other hand, the maximum difference observed in CP-based curves is around 0.40 at PGA_{max}=1.5g. The PGA curves under GM subsets other than DB IM=PGA case generally yielded higher PoE's in IO and LS curves (with respect to DB IM=PGA case), whereas VSI remained the lowest among CP curves considering the moderate-to-high intensity levels. "Regression Equation-Based" cases yielded slightly smaller differences for IO curves. However, the maximum differences with respect to PGA for both LS and CP curves are around 0.30 at PGA_{max}.

Considering "Original Data-Based" case of Figure 6.5, the variations reached up to 0.70 for IO curves, with PGV-based curves yielding the lowest values. This substantial difference is attributed to the sharply increasing PoE values of IO curves. The maximum differences between LS- and CP-based curves are around 0.30 at a PGV level of 150 cm/s, where PGA gave the highest PoE values. In comparison with "Original Data-Based" case, "Regression Equation-Based" cases displayed a similar trend in IO curves, while the maximum variances in LS and CP curves reached up to a PoE value of 0.40 at PGV_{max} level.

Figure 6.6 presents a relatively more compact set of ASI*-based curves with less scatter as opposed to former IM cases. Although the maximum difference in "Original Data-Based" IO curves is around 0.5, the variances are very limited in LS curves, and around 0.20 in CP curves. "Regression Equation-Based" LS and CP curves, in contrast, showed a maximum variance of 0.20 and 0.30, respectively, S_a-based curves noticeably deviating from the rest.

VSI-based curves, as presented in Figure 6.7, have yielded the maximum differences as 0.50, 0.30, and 0.25 for "Original Data-Based" IO, LS, and CP curves, respectively.

As displayed in Figure 6.8, S_a-based curves evaluated under different DB IM-based sets yielded much limited scatter (with a maximum PoE difference of 0.10) in the curves with the exceptional case of "Original Data-Based" CP curves (with maximum difference exceeding 0.45). S_a-based curves seemed to be less sensitive to alternating GM subsets.

Figure 6.9 portrays the cases for ASA_{40}-based fragility curves, where a maximum PoE difference of 0.50 has been observed for the specific "Original Data-Based" IO curves. This extreme difference is due to the S_a-based subset, which has led to an unusual fragility function as opposed to other resulting functions. The variances in LS and CP curves remained at 0.10 and 0.35 levels, respectively, observed at $ASA_{40,max}$. "Regression Equation-Based" IO curves yielded very close PoE estimates, whereas the maximum differences in LS and CP curves were observed as 0.10 and 0.20, respectively.

Overall evaluation of the above-listed figures has revealed that when the same IM is considered for both fragility function defining IM and the GM subset conditioning IM (i.e., DB IM=IM), the "Regression Equation-Based" PoEs turned out to be lower with respect to "Original Data-Based" PoE, as in the cases of PGA, PGV, and ASI*. This observation, indeed, marks the effect of modelling error due to regression models (i.e., seismic demand models) utilized. In addition to this observation, S_a-based GM subsets generally yielded higher PoE values, which is indeed observed in "Regression Equation-Based" curve sets.

When the evaluations are extended to the frame F5S4B, "Original Data-Based" IO, LS, and CP curves turned out to be more scattered, as displayed in Figure A.186, leading to maximum PoE differences of 0.5 in all three cases. The "Regression Equation-Based" curves have yielded slightly smaller differences (in the order of 0.40) between PoE estimates, where PGA gave the lowest.

In Figure A.187, which displays the PGV-based fragilities, the maximum differences observed in "Original Data-Based" curves are around 0.65 for IO (at low intensity levels), 0.35 for LS, and 0.45 for CP (at PGV_{max}), whereas the maximum values are slightly smaller for "Regression Equation-Based" cases (0.40 for IO, approximately 0.25 for LS and 0.30 for CP).

"Original Data-Based" ASI* curves, as illustrated in Figure A.188, yielded maximum differences of 0.40, 0.30, and 0.30 for IO, LS, and CP, respectively. In contrast, "Regression Equation-Based" curves yielded maximum PoE differences as 0.35, 0.30, and 0.20 for IO, LS, and CP, respectively.

Figure A.189 has revealed for VSI-based curves that the maximum differences are generally in the order of 0.30 as extreme, while the unusual "Original Data-Based" curve obtained from the S_a-based GM subset is neglected.

As presented in Figure A.190, S_a-based curves have been less affected from the alternative subsets, where the maximum differences have been observed as 0.15 and 0.35 for "Original Data-Based" LS and CP curves, respectively. The maximum variance is smaller for "Regression Equation-Based" PoE estimations from CP curves with a value of 0.20.

Finally, Figure A.191 displays the cases for ASA_{40}-based curves, where the maximum PoE difference is in the order of 0.10 (neglecting the abruptly changing "Original Data-Based" IO curves).

Overall evaluation of the figures particular to F5S4B frame has similarly revealed that when the same IM is considered for both fragility function defining IM and the GM subset conditioning IM (i.e., DB IM=IM), the "Regression Equation-Based" PoEs turned out to be lower with respect to "Original Data-Based" PoE, as in the cases of PGA and PGV. In addition to this observation, S_a-based GM subsets generally yielded higher PoE values, which is indeed observed in "Regression Equation-Based" curve sets.

180

The overall observation for this section is the pronounced effect of the GM subsets (conditioned to alternative DB IMs) on the resulting fragility curves, especially noticed for PGA- and PGV-based fragility curves, and for ASI*- and VSI-based curves to a lesser extent. Although S_a- and ASA_{40}-based fragilities seem to be less sensitive to the GM subsets, the effect of intensity measures used in the formation of a GM subset might lead to large discrepancies in PoE values which will eventually affect the loss estimation studies in the end.

6.4.2 The Effect of Number of Records Employed

A relatively large GM dataset with 300 records might be preferable for a researcher from the earthquake engineering community, unfortunately, complicates the task for practising engineers. The practising engineer will obviously attempt to reduce the dataset to tolerable numbers acknowledging trade-off, but providing computational economy. Taking its motivation from the dilemma between the accuracy and the economy, this section looks over the effect of the number of records to be sampled within each bin on the derived fragility curves.

It would be explanatory to note here that for a GM subset considering 10 bins, the number of records available in each bin is 30 (which is valid only for DB IM=IM case), leading to 300 records in total, while the number of records in each bin increases to 100 when the number of bins is considered as 3. The selection of n records from these partitioned sets naturally leads to a combination problem.

The steps to derive alternative fragility curves with different GM subset sizes (due to the selection of n records from a larger bin-wise set) have already been presented in Section 6.3. The mean and mean±1 sigma band curves corresponding to different "number of records" cases (as presented in Appendix F) are collected into new sets of figures comparing the resulting fragility curves. Figure 6.10 thru Figure 6.14 represent the cases for F3S2B frame, whereas the figures for F5S4B frame (Figure A.192 thru Figure A.196) are presented in Appendix F.

DB IM: PGA - IM: PGA - 5 bins

DB IM: PGA - IM: PGA - 10 bins

——— 30 ——— 20 – – ·11 – – ·7

(thinner lines are ± 1 sigma bands)

Figure 6.10. Alternative PGA-based fragility curves for F3S2B (MIDR) under PGA-based record sets formed with different number of records in each bin

DB IM: PGV - IM: PGV - 5 bins

DB IM: PGV - IM: PGV - 10 bins

————30   ————20   — — ·11   — — ·7

(thinner lines are ± 1 sigma bands)

Figure 6.11. Alternative PGV-based fragility curves for F3S2B (MIDR) under PGV-based record sets formed with different number of records in each bin
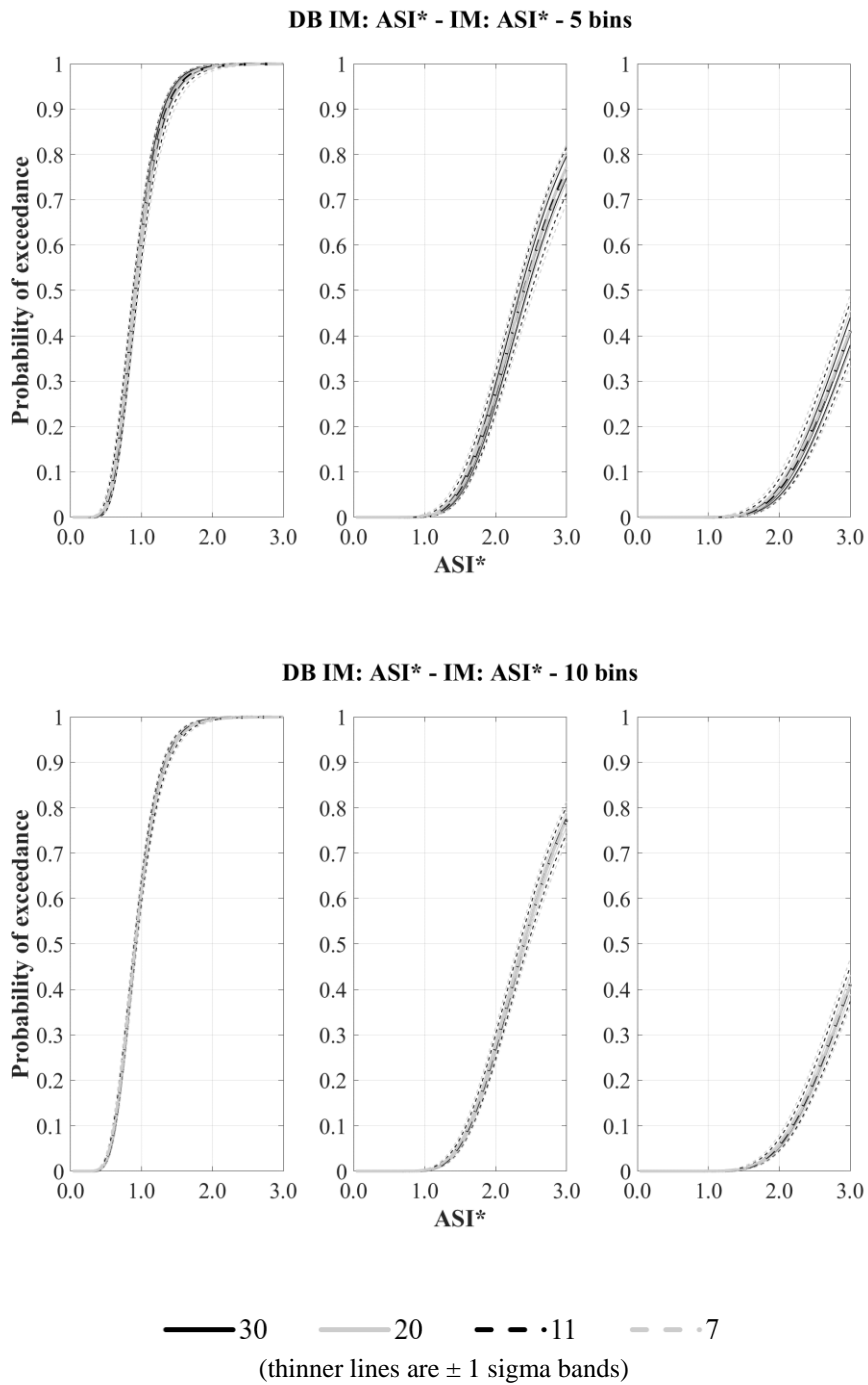
Figure 6.12. Alternative ASI*-based fragility curves for F3S2B (MIDR) under ASI*-based record sets formed with different number of records in each bin

DB IM: VSI - IM: VSI - 5 bins

DB IM: VSI - IM: VSI - 10 bins

30 ——— 20 ——— ·11 – – ·7

(thinner lines are ± 1 sigma bands)

Figure 6.13. Alternative VSI-based fragility curves for F3S2B (MIDR) under VSI-based record sets formed with different number of records in each bin

185
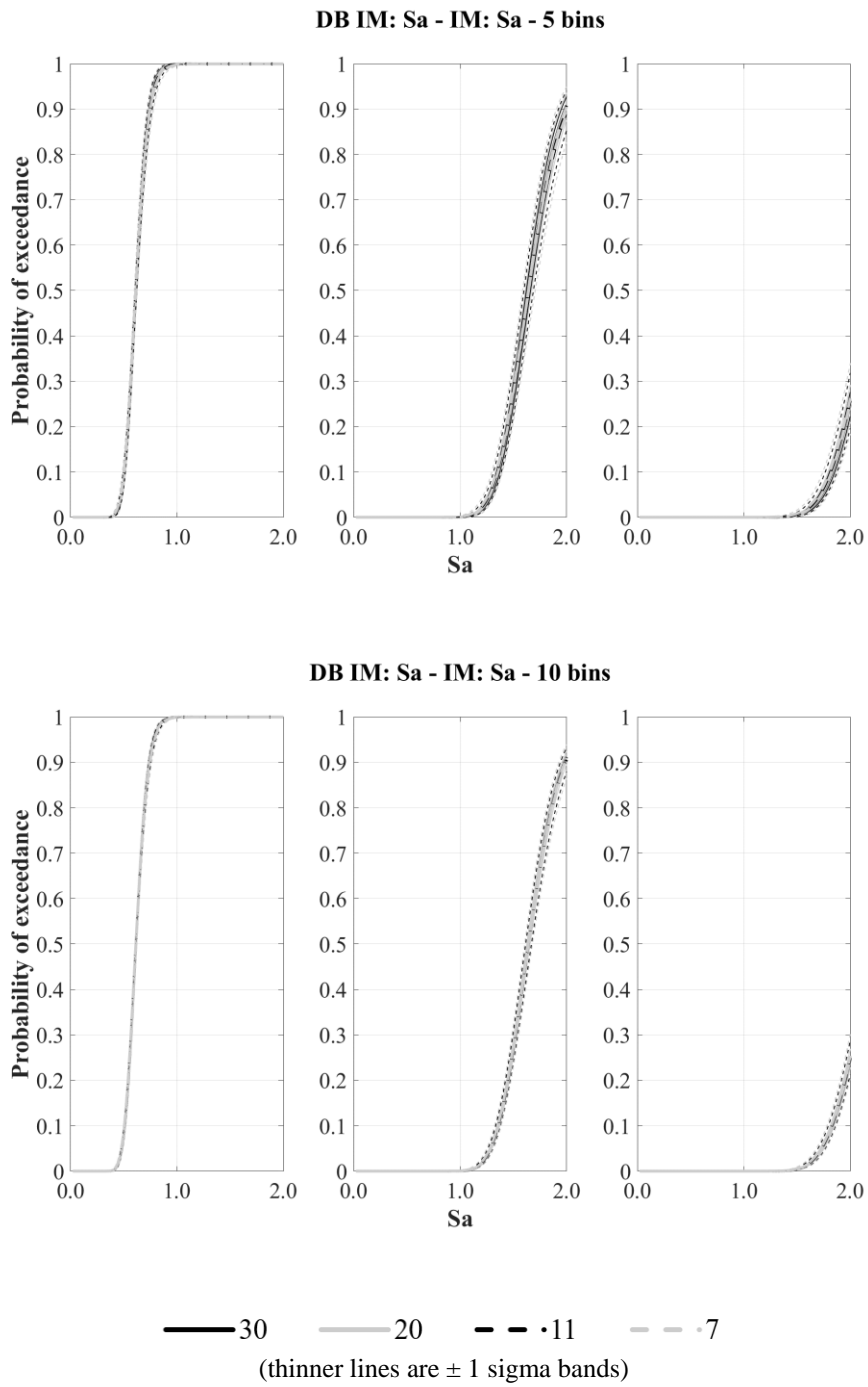
Figure 6.14. Alternative S_a-based fragility curves for F3S2B (MIDR) under S_a-based record sets formed with different number of records in each bin

Considering the set of Figure 6.10-Figure 6.14, the mean curves obtained from the resamples corresponding to each examined case (particularly evaluated for each DB IM=IM case) have converged to the "benchmark curves" (obtained from the "Regression Equation-Based" fragility calculations), as expected with reference to inferential statistics. Considering the individual cases with 10 bins, the mean±1 sigma band curves for PGA and PGV have yielded a PoE range of 0.05 at maximum, when 20 records are randomly selected out of 30 records. The PoE ranges have relatively widened to 0.10 for the cases when 7 records are randomly selected (leading to a GM set size of 70 records considering 10 bins). The PoE ranges for ASI*-, VSI- and S_a-based curves turned out to be slightly narrower with respect to PGA- and PGV-based curves. As compared to the cases with consideration of 10 bins, the fragility curves formed with 5 bins exhibited wider PoE ranges, as expected, reaching up to 0.15 level for PGA and PGV-based curves, when 7 records are sampled from each bin (thus, leading to a GM set size of 35 records). The improvement through the use of ASI*, VSI, and Sa, which was observed in 10-bin case, has not been identified in the 5-bin case.

The examination of the figure set for F5S4B frame (Figure A.192 thru Figure A.196) has led to similar observations, which resulted in a general recommendation that 20 records could be considered as the minimum number of records for each bin (i.e., intensity level) to obtain reliable PoE results with limited variation.

6.4.3   The Effect of Number of Bins

Similar to the evaluation stage with the number of records, the effect of the number of bins to partition the GM dataset, thus, corresponding number of intensity levels to form the seismic demand model which will be utilized to form the fragility curves, has also been investigated through the comparison of mean and mean±1 sigma band curves for different DB IM=IM cases. The figure set Figure 6.15-Figure 6.19 corresponds to F3S2B frame, whereas the set Figure A.197-Figure A.201 is for F5S4B.

DB IM: PGA - IM: PGA - 11 records

DB IM: PGA - IM: PGA - 30 records
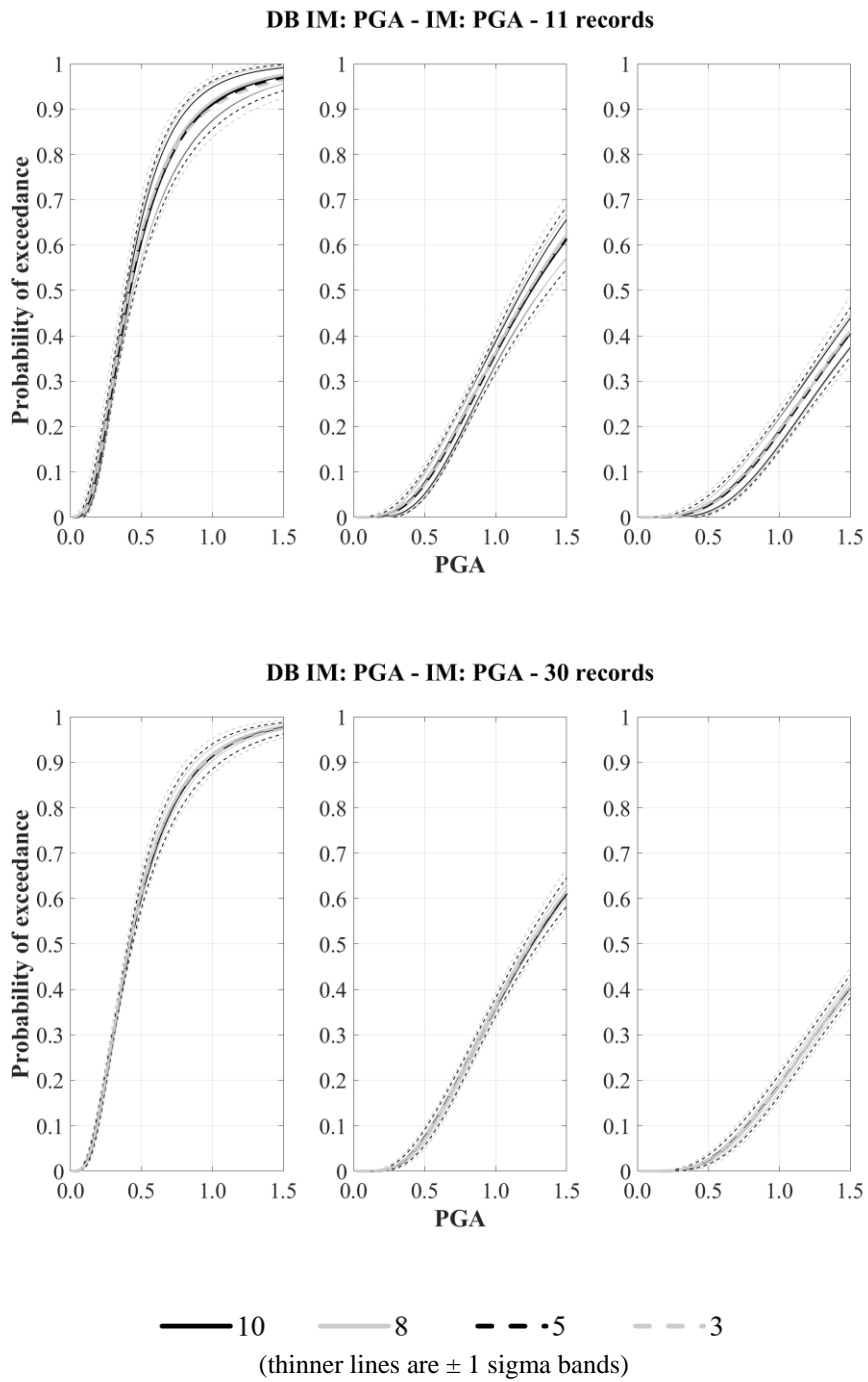
Figure 6.15. Alternative PGA-based fragility curves for F3S2B (MIDR) under PGA-based record sets formed with different number of bins

DB IM: PGV - IM: PGV - 11 records

DB IM: PGV - IM: PGV - 30 records

———— 10　　———— 8　　— — ·5　　— — · 3
(thinner lines are ± 1 sigma bands)
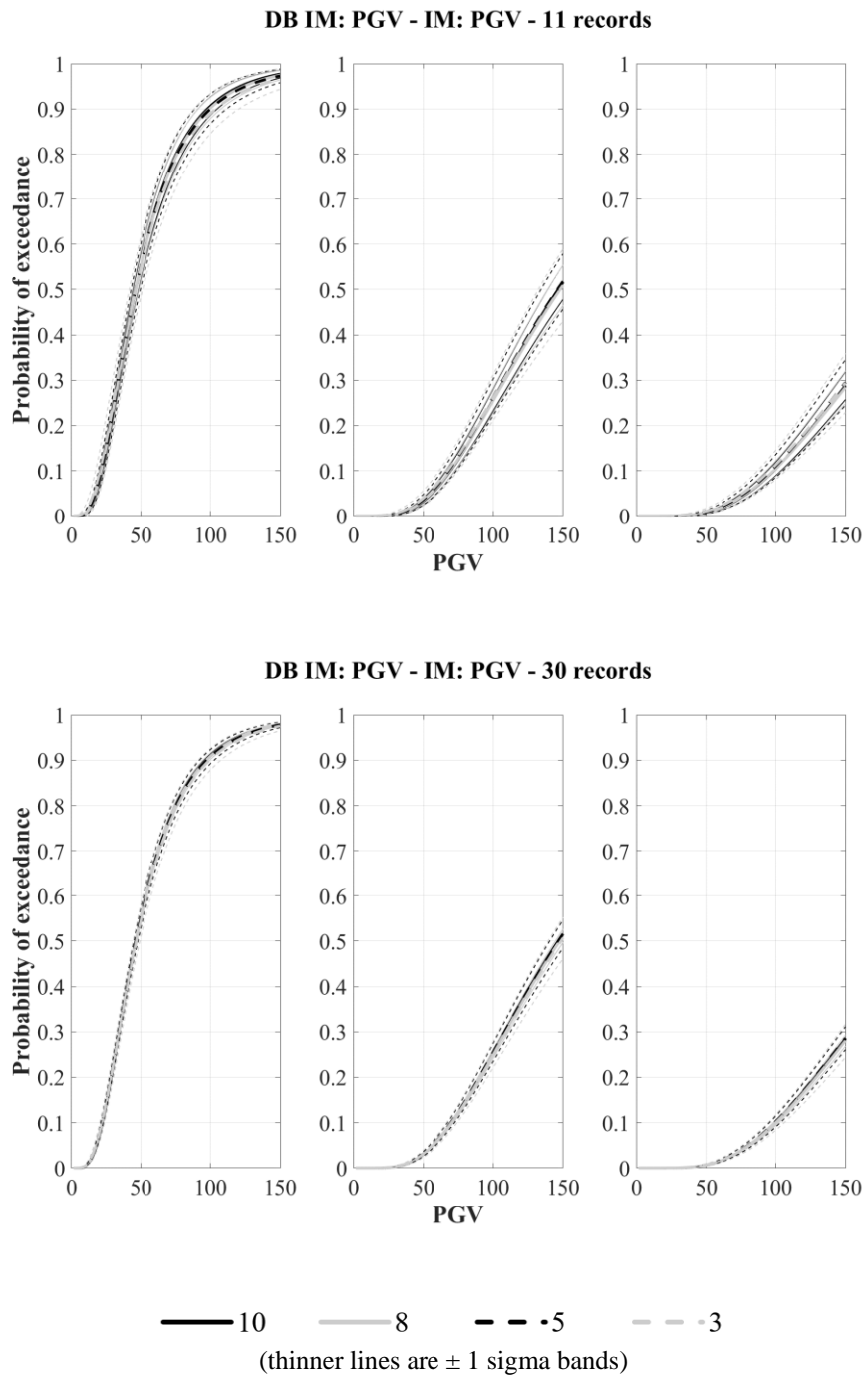
Figure 6.16. Alternative PGV-based fragility curves for F3S2B (MIDR) under PGV-based record sets formed with different number of bins

189

DB IM: ASI* - IM: ASI* - 11 records

DB IM: ASI* - IM: ASI* - 30 records

———10   ———8   – – ·5   – – ·3

(thinner lines are ± 1 sigma bands)
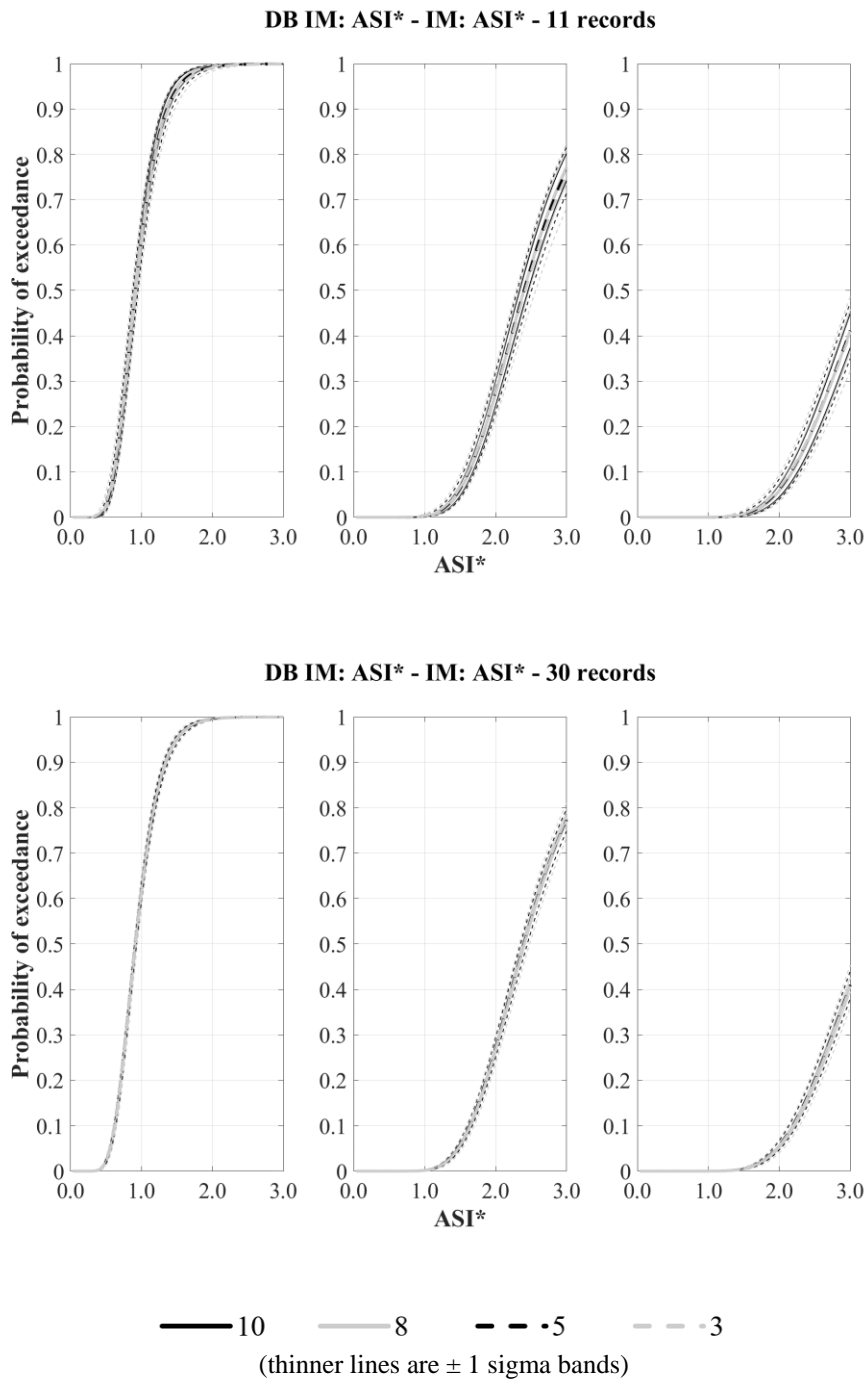
Figure 6.17. Alternative ASI*-based fragility curves for F3S2B (MIDR) under ASI*-based record sets formed with different number of bins

190

DB IM: VSI - IM: VSI - 11 records

DB IM: VSI - IM: VSI - 30 records

———10 ———8 — — ·5 — — ·3

(thinner lines are ± 1 sigma bands)
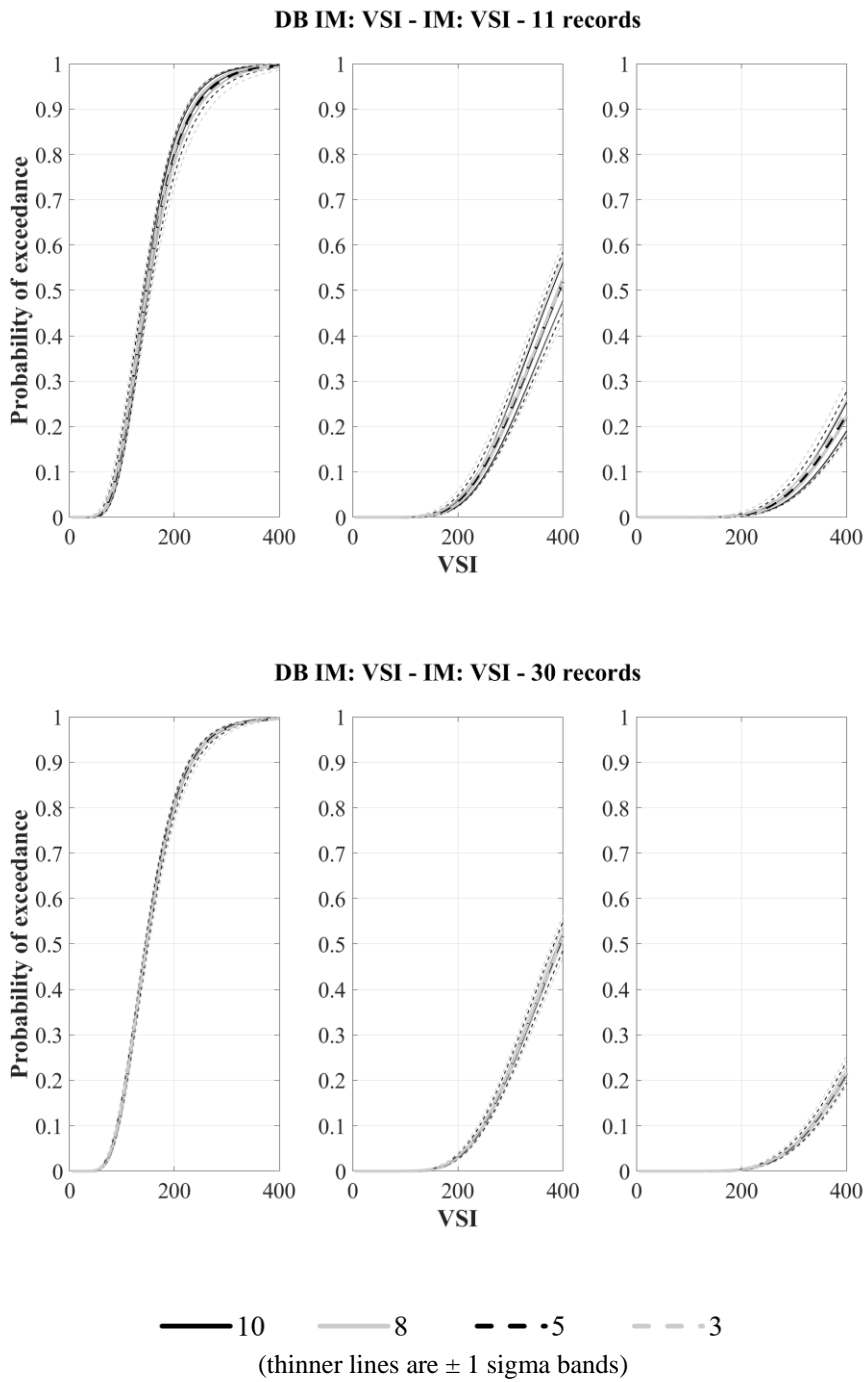
Figure 6.18. Alternative VSI-based fragility curves for F3S2B (MIDR) under VSI-based record sets formed with different number of bins

DB IM: Sa - IM: Sa - 11 records

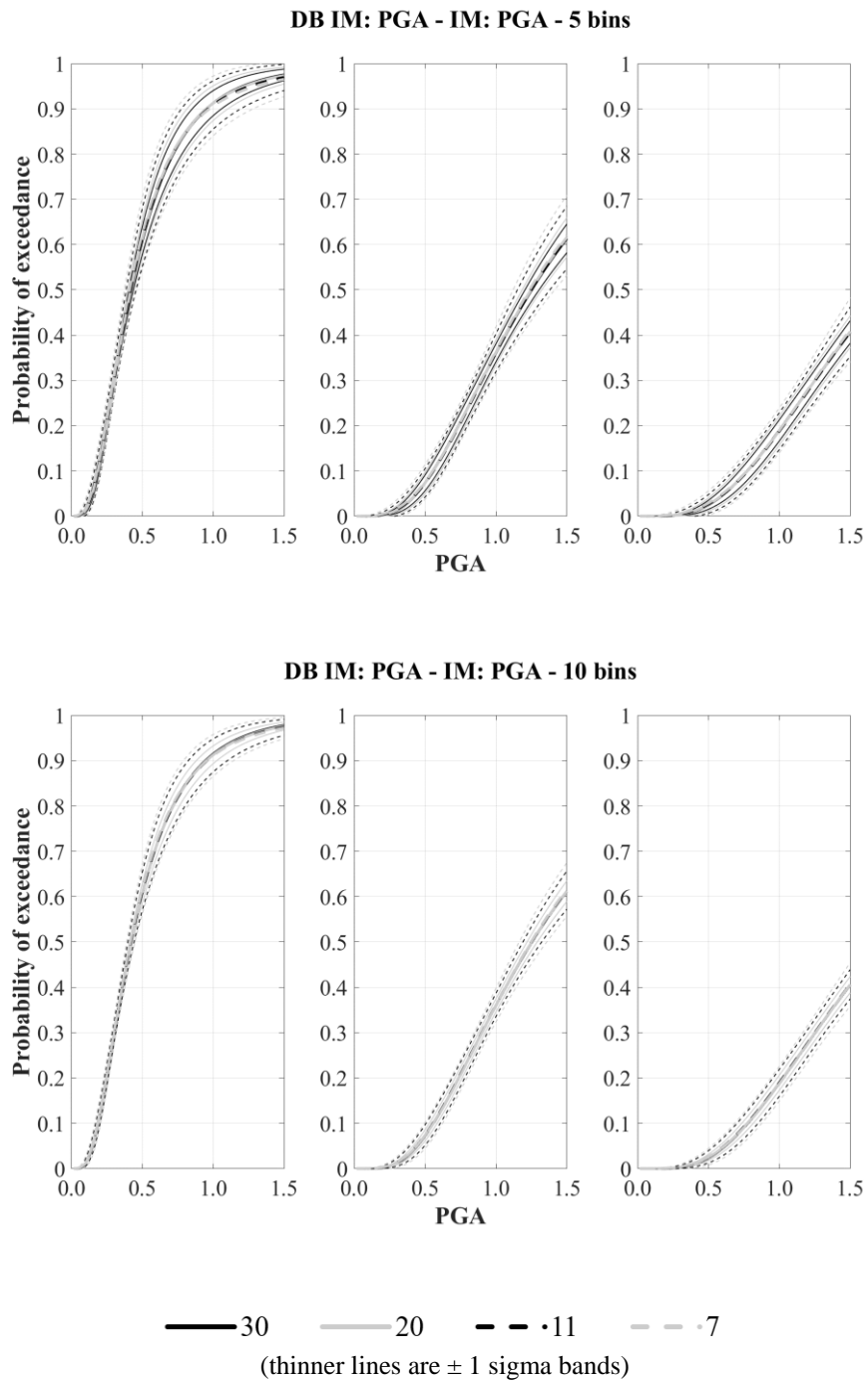**DB IM: Sa - IM: Sa - 30 records**

(thinner lines are ± 1 sigma bands)
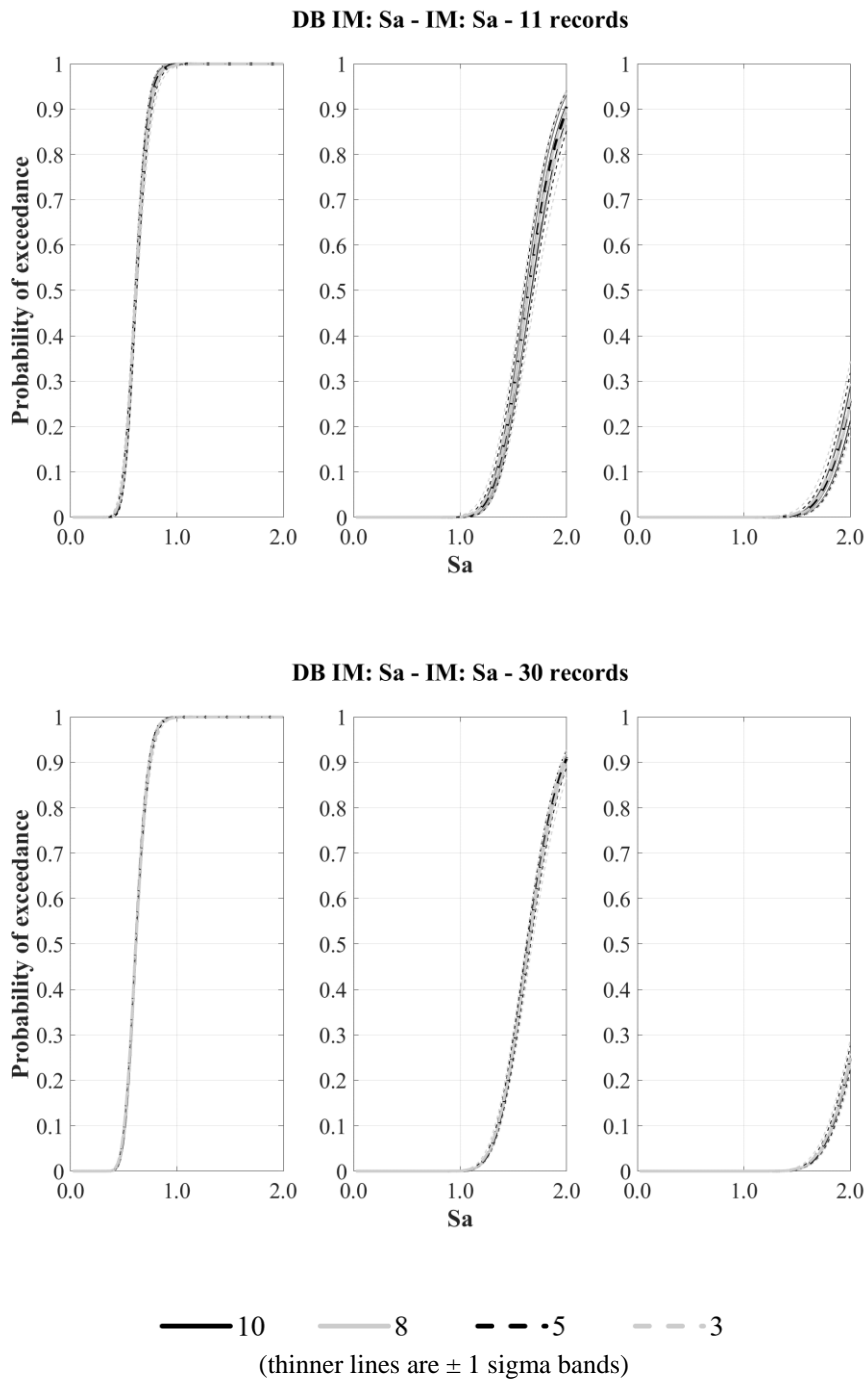
Figure 6.19. Alternative S_a-based fragility curves for F3S2B (MIDR) under S_a-based record sets formed with different number of bins
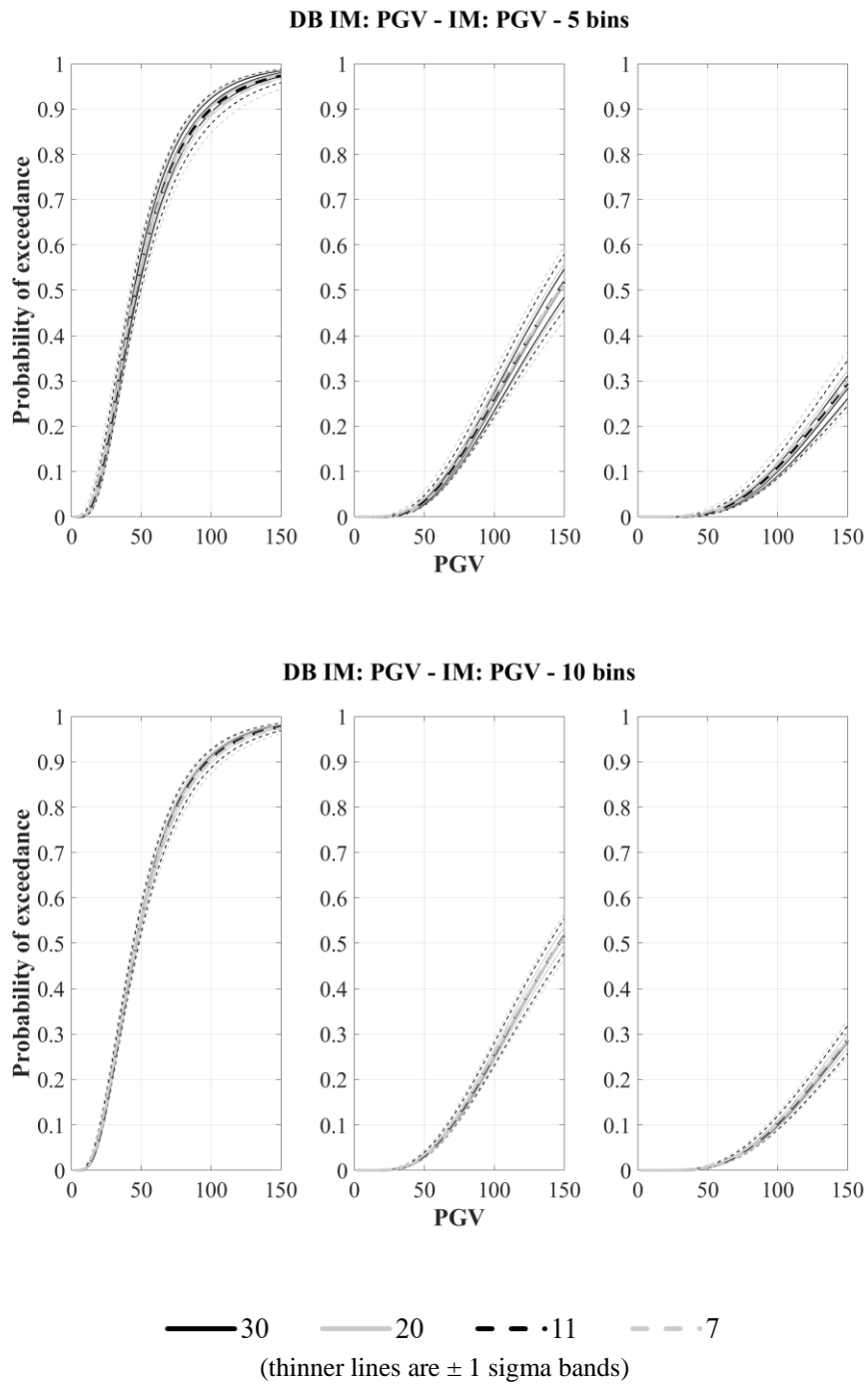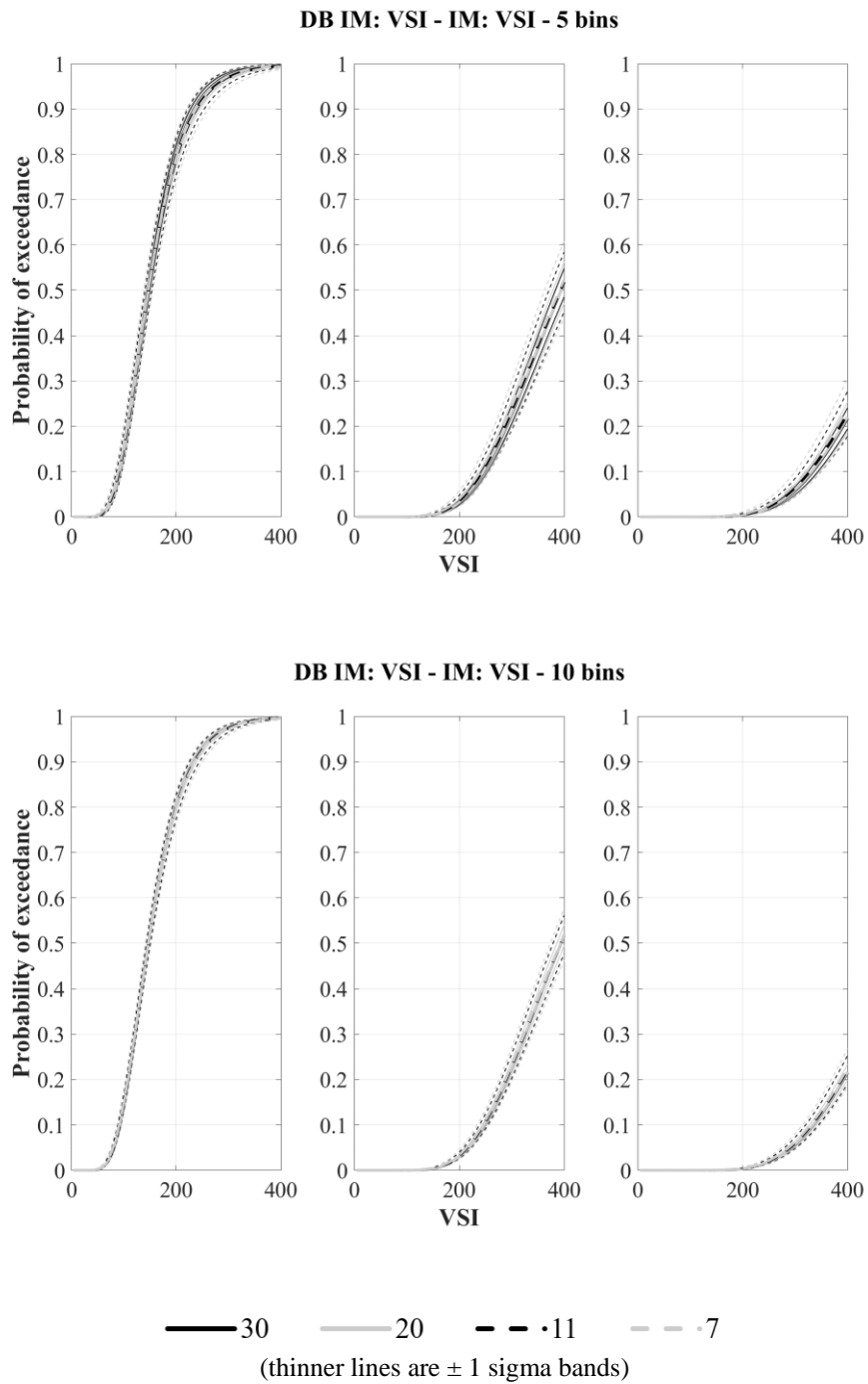
In comparison with the former section's observations, the figure set for F3S2B (Figure 6.15-Figure 6.19) has revealed that the fragility curves are less sensitive to the number of bins considered, when 30 records are employed in each bin. However, when 11 records are sampled from each bin, the effect of the number of bins is much more significant. The PoE variance reached up to a level of 0.20 with 11 records in the case of PGA-based curves, while ASI*, VSI, and S_a have provided comparably limited PoE variance. The figure set for F5S4B has exhibited similar trends.

The examination of the overall figure set might lead to consideration of fewer number of bins (i.e., less than 10 bins) to form the GM dataset and obtain reliable fragility curves; however, comprehensive evaluation of resulting fragility curves from individual resample sets has led to the recommendation of keeping the number of bins as 10.

6.5   Discussion of Results

The detailed evaluation of the effect of IMs along with the effect of the number of bins and records employed (in each bin) on the resulting fragility curves has marked the significance of the selected IM, particularly when considered as the conditioning IM to form the GM subset. Besides, the noticeable differences observed from the fragility curves, when the IM (as the input variable of the fragility function) is not the same as the DB IM, calls for further evaluation of the validity of these alternating fragilities with observed damages of the structures.

Comparative studies questioning the effect of the number of bins and number of records have led to a recommendation of 10 bins (i.e., corresponding to 10 intensity levels) with 20 records randomly selected for each bin for fragility curves almost covering the entire response range with consideration of 3 different performance limit states. This study differentiates from recent studies generally concentrating on probabilistic collapse estimations.

193

CHAPTER 7

SUMMARY, CONCLUSIONS AND FUTURE WORK RECOMMENDATIONS

7.1   Summary and Contributions

The performance-based earthquake engineering approach has featured the importance of intensity measures both in quantifying the hazard at a site and in selection of ground motion records compatible with these quantified metrics in order to obtain reliable estimates of the structural and/or non-structural responses under expected seismic hazards. Correspondingly, the timeline portrays the development of several intensity indices; basic scalar parameters generally with the aim of characterizing the damage potential of strong ground motions and more advanced scalar or vectorial forms with the ultimate goal of reducing dispersions in the response predictions. Although there exist several studies examining the correlation performance, efficiency, and sufficiency of the intensity measures, recent research studies have focused on the performance of the examined parameters to predict the collapse capacities for a pre-defined hazard level in general. This study approaches to the problem from a broader perspective, and evaluates the efficiency and sufficiency of a long list of scalar and vector intensity measures considering the entire response range of typical structures without adhering to a specific hazard level.

Chapter 1 presents a list of scalar to vector intensity measures displaying the transition into spectrum-based (i.e., structure-specific) scalar or vector forms and allegorically establishes a bridge between essential articles on the subject and the research problem and motivation.

Chapter 2 introduces a large ground motion record database inherited from the former NGA-West database of PEER, and demonstrates the main seismological features of this set. Besides, the concept of correlation is presented along with two key correlation metrics; Pearson's product-moment correlation and Spearman's

rank-order correlation. These two metrics have been utilized to reveal the inter-correlational characteristics of the fundamental intensity measures calculated from the records of the main set formed.

Chapter 3 is devoted to the description of the structural systems employed throughout the research study. The structural and modelling details of the selected reinforced concrete frames are explained in detail, and types of analyses performed on mathematical models of complete or simplified equivalents are explained.

In Chapter 4, the efficiency of the fundamental intensity measures, which are available from Chapter 2, is evaluated via a single-degree-of-freedom system-based approach. Generic structures with varying fundamental periods, strength, ductility, and base shear coefficient levels are formed and subjected to the full record set to compute the correlation of intensity measures with top drift demands. The correlation performance of each intensity measure is discussed accordingly for changing levels of strength, ductility, base shear coefficient and fundamental period. The chapter recommends a shortlist of intensity parameters to be employed within the next section.

Established on the findings of the previous section, Chapter 5 utilizes the shortlisted indices to form alternative ground motion record subsets employing two different sampling methods: (i) Stratified random sampling and (ii) Cluster sampling. The section demonstrates the characteristics of these subsets and explains the analyses performed with these record sets. Based on the correlation results of the shortlisted intensity measures obtained from the analyses of simplified equivalents of the complex multi-degree-of-freedom systems under random and cluster sampling-based sets, preliminary observations for the parameters are discussed, leading to a conclusion to continue with the random sampling-based subsets. The results from the analyses of multi-degree-of-freedom systems under random sampling-based subsets are presented and evaluated afterwards, to further reduce the number of subsets to consider for the next stage. Besides, the correlation of the responses obtained from more complex multi-degree-of-freedom systems and their simplified

196

equivalents are evaluated to check the suitability of employing simplified models to estimate global seismic demands. Following this step, a larger list of parameters incorporating novel scalar and vector intensity measures is formed, and the regression equation-based methodology is presented in detail for the evaluation of efficiency and sufficiency of the new intensity measure list. The statistical metrics computed from this stage are evaluated in detail to identify the "best candidate" intensity measures for the structural systems employed.

Chapter 6 links the importance of intensity measures to the fragility curve concept, where the intensity parameter is considered in the ground motion selection stage of fragility analyses. This section utilizes the ground motion subsets from the previous chapter, and derives fragility curves as a function of alternative intensity measures either as a choice of practicality or based on the efficiency and sufficiency-based highlights of the former chapter. The effect of the number of bins and the number of records in each bin is evaluated in detail to make recommendations on the subject that would lead to reliable fragility curves.

The contributions of this research study can be highlighted as follows:

- Comprehensive evaluation of a long list of scalar and vector intensity measures has been made considering efficiency and sufficiency criteria.
- Both SDOF and MDOF-based evaluations have been made to reveal the correlation performance of candidate intensity parameters.
- A regression parameter (R^2-adjusted) based efficiency evaluation has been considered in contrast to the studies in the literature generally relying on correlation coefficients and dispersion metrics.
- Efficient scalar and vector intensity measures have been identified. Sufficiency against moment magnitude and source-to-site distance have been checked and reported.
- The effect of ground motion record subsets formed on the basis of alternative intensity measures has been observed in correlation and regression-based studies.

- "Best candidate" intensity measures have been identified with their trade-offs.
- The effect of intensity measures on the ground motion selection stage of the fragility studies has been identified along with the consideration of the number of bins and the number of records in each bin.

7.2   Conclusions

The conclusions of this dissertation can be compiled under following items:

- *Pearson -Spearman correlations and inter-correlational evaluations*
  - Pearson correlation coefficient is sensitive to the distribution of data, heteroscedasticity, and outliers, whereas the Spearman correlation coefficient is more robust with respect to Pearson.
  - Ln-transformation of intensity data is appropriate prior to the calculation of Pearson correlation coefficients, and generally yields similar coefficient values with Spearman calculations performed on non-transformed data.
  - Acceleration-related, velocity-related, and displacement-related IMs correlate better among their own classes, whereas inter-class correlations are lower with respect to intra-class correlations.
  - PGV/PGA ratio, as an indicator of frequency content, generally displays weak forms of both negative and positive correlation with acceleration- and velocity- related parameters, and can supplement scalar intensity measures as the second intensity measure to improve the performance in seismic demand prediction equations. This proposal has been investigated within the context of this study, and relevant conclusions will be presented under related items.
  - The pulse period T_P generally shows weak forms of positive and negative correlations with the remaining IM set, and can supplement scalar intensity

measures as the second intensity measure to be utilized for records with significant pulse effects. This proposal has not been examined within the context of this study, and remains as a future study recommendation.

- The duration-related parameter t_r does not have a significant correlation with other intensity parameters, and can supplement scalar intensity measures as the second intensity measure for specific consideration of ground motion duration effects on particular damage indices. This proposal has been partially evaluated within the context of this study, and relevant conclusions will be presented under related items.

- *SDOF-based evaluations*
  - There is no single IM that is efficient at all periods. Acceleration-related indices are efficient at short periods, whereas velocity-related parameters are correlating well with the drift demands of medium-to-long period SDOF systems. For long period systems, displacement-related IMs become effective.
  - PGA is the simplest acceleration-related scalar IM that is relatively efficient for short period systems; however, its correlation performance immediately diminishes as the period of the system enters into medium or long period range. For these periods, PGV becomes the simplest relatively efficient alternative.
  - PGV/PGA is not an efficient parameter due to its weak correlation performance for short-to-medium period systems, but exhibits moderate correlation performance for long period systems. This parameter can be regarded as a supplementary (i.e., secondary) index in vector IMs.
  - Arias Intensity, AI, and Characteristic Intensity, I_C, include duration information of the ground motion as well, and are similar to PGA at short periods, yet they are more efficient at long periods.
  - The spectrum-based, but structure-independent ASI is effective for short period systems, but is not an efficient IM for medium-to-long period systems.

The modified version of this parameter, ASI*, on the other hand, is relatively inferior at very short periods, but correlate much better in the entire period range considered. Consequently, ASI* is suggested to be preferred against ASI.

- SED and CAV include duration information as well, and correlate better at long periods. However, they are relatively inefficient for short period systems.

- The spectrum-based, but structure-independent VSI perform better at medium-to-long periods, as compared to PGV.

- The spectrum-based structure-independent IMs, EPA and EPV, correlate slightly better than their counterparts, PGA and PGV, while EPV is much superior at intermediate period range.

- Ground motion period-related parameters T_P, T_m, and duration-related index, t_r, poorly correlate with the drift demands and could not be regarded as efficient intensity measures. Nevertheless, they could assist efficient parameters in vector IM forms.

- Fajfar Intensity, I_F and Riddell and Garcia's velocity-related index, I_v, show a stable and good correlation with the displacement demands of SDOF systems at a wide period range.

- The spectrum-based and structure-specific parameters S_a, S_v and S_d show strong correlations with the drift demands of SDOF systems, and thus, remain as the 'best' candidates in terms of efficiency. Nonetheless, they require period-related information about the structural system or the collection of structures to be analyzed.

- The effect of strength reduction factor (R) level on the correlation results seems to be significant up to a period limit of T=1.5 sec; in contrast, the effect of ductility (μ) or yield base shear coefficient (η) level does not seem to affect the period-wise variations significantly. This observation is generally valid for all IMs.

- With regards to the hysteretic behavior considered for the systems, SDOF system-based correlation results seem to be more sensitive to R factors for EPP systems as opposed to SDOF systems with bi-linear hardening hysteretic behavior. This observation is valid for periods up to a limiting value of T=1.5 sec. However, the general trends do not differ significantly.

- As a final refining conclusion of this stage, acceleration-based IMs PGA, AI, ASI, and ASI* could be considered as qualifying structure-independent indices for short-period systems, whereas, for medium-to-long periods, IMs such as PGV, SED, CAV, VSI, I_F, and I_v could be considered as these parameters exhibit high and stable correlation performance at these period levels. The latter IM set is also considered to be efficient for structural systems that are expected to undergo various degrees of inelasticity.

- *Sampling Methods*
  - Cluster Sampling is considered to be a more objective method of forming a GM subset with respect to Stratified Random Sampling; however, Cluster Sampling yields a set of records concentrating at low-to-moderate intensity levels. In contrast, Stratified Random Sampling is clearly a better method to obtain an almost uniform distribution of records covering a wide range of intensity levels particular to the intensity measure considered.

  - The efficiency evaluation of ordinary scalar IMs with two different GM subsets (Cluster Sampling-based subset versus Stratified Random Sampling-Combined based subset) has revealed that the general conclusions about the superiority of specific IMs are the same regardless of the record sampling method. However, the interpretations made for ordinary scalar parameters have not been investigated for novel scalar or vector IMs.

- *ESDOF vs. MDOF compatibility*
  - For the structural systems with first mode dominant behavior, engineering demand parameters calculated from ESDOF and MDOF models, and

resulting correlation coefficients are almost in the same order of magnitude, neglecting the extremes. Consequently, simpler ESDOF systems are suitable for quick yet accurate estimations of global demands and performances.

- *MDOF-based evaluations*
  - The efficiency of any candidate IM can be computed via a regression equation-based (Cloud Analysis-based approach) to comparatively display the performances of both scalar and vector IMs considering the whole intensity range. The R^2-adjusted value-based rankings are in accordance with Pearson correlation coefficient-based ranking for scalar IMs.
  - The general conclusion of SDOF-based evaluations regarding the well known scalar IMs is valid for MDOF-based evaluations as well. That is; acceleration-related parameters are efficient at short periods, whereas velocity-related indices correlate better with the seismic demands of systems with medium-to-long periods. However, among the structure-independent scalar IMs, ASI* and VSI exhibit relatively stable performance considering the short-to-relatively long period range. When the GM subsets are formed according to these indices, the efficiency performances of other simple scalar IMs generally improve as well. Considering these two favorable properties of these IMs, ASI* and VSI are recommended to considered as "best candidates" for the period range considered (T=0.3-1.2 sec). For periods higher than 1.0 sec, HI can be utilized as well, since the performance of HI becomes noticeable at this period range.
  - Although AI, SED, CAV, I_F and I_v might have showed sufficient efficiency performance at certain periods or limited period ranges, considering the overall response range of the frames employed, they are considered as inefficient, thus recommended to be not used.
  - Among ordinary scalar IMs, the structure-specific IM S_a seems to be highly efficient for the structures with periods up to 1.20 sec and showing first mode

202

dominant behavior. This observation is valid for both TD and MIDR-based evaluations.

- The novel scalar and vector IMs, mostly based on S_a, show strong correlations with the global seismic demands of the structural systems. But, they generally necessitate certain input parameters that need to be calibrated for their computations, or require even more complex calculations with the vectorial forms utilizing displacement spectrum. However, ASA_{40} with its simpler form with respect to other candidates is recommended to be considered as the "best candidate" among the novel advanced IMs.

- $\langle S_a, S_{dN} \rangle$ and $\langle S_a, S_a/DSI \rangle$ seem to exhibit high efficiency according to R^2-adjusted values. However, supplementary statistical metrics do not confirm their performance, which calls for further investigations.

- When supplemented with PGV/PGA or t_{5-95}, the efficiency performance of vector IM seems to improve with respect to the solo performance of the primary IM, but the significance of the secondary parameter cannot be verified for particular cases.

- Sufficiency checks against M_w and R_{JB} shows that scalar IMs PGA and ASI (and ASI*-VSI-HI in fewer situations) are dependent on M_w. Besides, BS demands show dependency on R_{JB} in particular cases.

- *Fragility Analyses*
  - The effect of conditioning IM for the formation of GM subsets which will be utilized to derive fragility curves is highly pronounced for PGA- and PGV-based fragility curves, whereas ASI*- and VSI-based curves are less affected. Although S_a- and ASA_{40}-based fragilities seem to be less sensitive to the GM subsets, the effect of intensity measures used in the formation of a GM subset might lead to large discrepancies in PoE values which will eventually affect the loss estimation studies in the end.

- The minimum number of records to be selected for each intensity level is recommended as 20 in order to obtain reliable PoE estimates with limited dispersion.
- The minimum number of intensity levels (i.e., bins or stripes) is recommended as 10 to accurately derive fragility curves for three common performance levels IO, LS, and CP.

7.3 Limitations of This Study and Future Work Recommendations

This study utilizes a set of seven reinforced concrete frames with fundamental periods covering short- to relatively long periods; however, the structural systems generally exhibit a dominant first mode behavior. The evaluation of intensity measures can be improved with consideration of systems that show higher mode effects as well.

The structural systems turned out to be "not susceptible" to duration effects. Additional structural systems that have potential sensitivity to ground motion duration (i.e., as in the case of specific steel structures) can be incorporated in further studies to examine the increased effect of duration-related intensity parameters.

The efficiency and sufficiency examinations have been made on the basis of 2D frames, which could be improved with more complex 3D models having both regular and irregular structural plans as well. In this way, the effect of the directionality of the ground motions on the performance of candidate IMs could also be studied.

The ground motion record subsets have been formed without any consideration of specific seismological properties, and the evaluations have been made solely on resulting intensity measures. The study can be further elaborated with detailed consideration of seismological characteristics which may affect the performance of intensity measures examined or the significance of secondary intensity measures in the vector-formed alternatives. This perspective may clarify the effect of the interaction between site characteristics and site-specific motions on the resulting

intensity measures, and their efficiency and sufficiency performances. Similarly, the pulse effects can be examined in detail.

Scaling robustness and practicality of candidate intensity indices have not been evaluated within the context of the study. These criteria are worthwhile to investigate further. Especially, the scaling issue needs to be thoroughly examined, since the lack of records at high intensity levels forces the analysts to employ scaled records.

Top displacement, maximum inter-story drift ratio, and maximum base shear have been considered as key engineering demand parameters revealing the global performance of examined structures. Component-level engineering demand parameters or damage indices can also be considered to evaluate the efficiency and sufficiency of intensity measures.

The fragility analysis part has focused on fragility curves which are functions of single intensity measures. The evaluation steps followed herein can be extended to fragility surfaces dependent on vector intensity measures, and guidelines for these more complex vulnerability functions can be developed.

REFERENCES

Adam, C., Tsantaki, S., Ibarra, L. F., & Kampenhuber, D. (2014). Record-to-record variability of the collapse capacity of multi-story frame structures vulnerable to P-delta. *Proceedings of the Second European Conference on Earthquake Engineering and Seismology (2ECEES)*.

Akaike, H. (1998). Information theory and an extension of the maximum likelihood principle. *In Selected papers of Hirotugu Akaike* (pp. 199-213). Springer, New York, NY.

Akkar, S., & Küçükdoğan, B. (2008). Direct use of PGV for estimating peak nonlinear oscillator displacements. *Earthquake Engineering & Structural Dynamics*, *37*(12), 1411-1433.

Akkar, S., & Özen, Ö. (2005). Effect of peak ground velocity on deformation demands for SDOF systems. *Earthquake Engineering & Structural Dynamics*, *34*(13), 1551-1571.

Akkar, S., Sucuoğlu, H., & Yakut, A., (2005). Displacement-based fragility functions for low- and mid-rise ordinary concrete buildings. *Earthquake Spectra*, *21*(4), 901–927.

Alimoradi, A., Pezeshk, S., Naeim, F., & Frigui, H. (2005). Fuzzy pattern classification of strong ground motion records. *Journal of Earthquake Engineering*, *9*(03), 307-332.

Ang, A. H. S. (1990). Reliability bases for seismic safety assessment and design. *Proceedings of the 4th US National Conf. on Earthquake Engineering,* Oakland, California. Vol. 1, pp. 29-45.

Antoniou, S., & Pinho, R. (2004a). Advantages and limitations of adaptive and non-adaptive force-based pushover procedures. *Journal of Earthquake Engineering*, *8*(04), 497-522.

Antoniou, S., & Pinho, R. (2004b). Development and verification of a displacement-based adaptive pushover procedure. *Journal of Earthquake Engineering*, *8*(05), 643-661.

Applied Technology Council (ATC) (1978). Tentative provisions for the development of seismic regulations for buildings. ATC-3, California.

Applied Technology Council (ATC) (1996). Seismic evaluation and retrofit of concrete buildings, ATC-40, Volume 1-2, Redwood City, California.

Applied Technology Council (ATC), (2007). ATC-58 35% Draft, Guidelines for seismic performance assessment of buildings, Redwood City, CA.

Applied Technology Council (ATC), (2009). ATC-58 50% Draft, Guidelines for seismic performance assessment of buildings, Redwood City, CA.

Applied Technology Council (ATC), (2011). ATC-58-1 75% Draft, Seismic performance assessment of buildings, Redwood City, CA.

Applied Technology Council (ATC), (2011). ATC-58-1 90% Draft, Seismic performance assessment of buildings, Redwood City, CA.

Araya, R., & Saragoni, R. (1984). Earthquake accelerogram destructiveness potential factor. *Proceedings of the 8th World Conference of Earthquake Engineering*, San Francisco, USA. vol. 2: 835–841.

Arias, A. (1970). A measure of earthquake intensity, Seismic Design for Nuclear Power Plants. R.J. Hansen (ed.), Massachusetts Institute of Technology Press, Cambridge, MA, 438–483.

Aslani, H., & Miranda, E. (2005). Probability-based seismic response analysis. *Engineering Structures*, *27*(8), 1151-1163.

ASCE/SEI 7-16 (2016). *Minimum design loads and associated criteria for buildings and other structures*. American Society of Civil Engineers, Reston, VA, USA.

Avşar, Ö., Yakut, A., & Caner, A. (2011). Analytical fragility curves for ordinary highway bridges in Turkey. *Earthquake Spectra*, *27*(4), 971-996.

Ay, B. Ö. (2006). *Fragility based assessment of low-rise and mid-rise reinforced concrete frame buildings in Turkey*. MSc Thesis, Middle East Technical University, Ankara.

Ay, B. Ö. (2012). *A proposed ground motion selection and scaling procedures for structural systems*. PhD Thesis, Middle East Technical University, Ankara.

Azari Sisi, A. (2016). *Derivation of site-specific UHS based on simulated ground motions and its parametric effects on building fragility*. PhD Thesis, Middle East Technical University, Ankara.

Bai, J.-W., Gardoni, P., & Hueste, M. B. (2011). Story-specific demand models and seismic fragility estimates for multi-story buildings. *Structural Safety*, *33*, 96-107.

Baker, J. W., & Cornell, C. A. (2004). Choice of a vector of ground motion intensity measures for seismic demand hazard analysis. *Proceedings of the 13th World Conference on Earthquake Engineering*, Vancouver, Canada, Paper No. 3384.

Baker, J.W., & Cornell, C.A., (2005). A vector-valued ground motion intensity measure consisting of spectral acceleration and epsilon. *Earthquake Engineering & Structural Dynamics*, *34*(10), 1193–1217.

Baker, J. W., & C. A. Cornell (2006). *Vector-valued ground motion intensity measures for probabilistic seismic demand analysis*. PEER Report 2006/08,

Pacific Earthquake Engineering Research Center, College of Engineering, University of California, Berkeley.

Baker, J. W. (2015). Efficient analytical fragility function fitting using dynamic structural analysis. *Earthquake Spectra*, *31*(1), 579-599.

Benjamin J.R. and Associates (1988). *A criterion for determining exceedance of the Operating Basis Earthquake*. EPRI Report NP-5930, Electric Power Research Institute, Palo Alto, California.

Bhasker, R., & Menon, A. (2020). Characterization of ground motion intensity for the seismic fragility assessment of plan-irregular RC buildings. *Structures*, *27*, 1763-1776.

Bianchini, M. (2008). *Improved scalar intensity measures in performance-based earthquake engineering*. Nota Tecnica n. 215, Università degli Studi di Bologna, Bologna, Italy.

Bianchini, M., Diotallevi, P., & Baker, J. W. (2009). Prediction of inelastic structural response using an average of spectral accelerations. *Proceedings of the 10th International Conference on Structural Safety and Reliability (ICOSSAR 09)*, Osaka, Japan, 13-19 September.

Bojórquez, E., & Iervolino, I. (2010). A spectral shape-based scalar ground motion intensity measure for maximum and cumulative structural demands. *Proceedings of the 14th European Conference on Earthquake Engineering*.

Bojórquez, E., & Iervolino, I. (2011). Spectral shape proxies and nonlinear structural response. *Soil Dynamics and Earthquake Engineering*, *31*(7), 996-1008.

Bommer, J. J., & Martinez-Pereira, A. (1999). The effective duration of earthquake strong motion. *Journal of Earthquake Engineering*, *3*(02), 127-172.

Bozdogan, H. (1987). Model selection and Akaike's information criterion (AIC): The general theory and its analytical extensions. *Psychometrika*, *52*(3), 345-370.

Bradley, B. A. (2010). A generalized conditional intensity measure approach and holistic ground-motion selection. *Earthquake Engineering & Structural Dynamics*, *39*(12), 1321-1342.

Bradley, B. A. (2013). A comparison of intensity-based demand distributions and the seismic demand hazard for seismic performance assessment. *Earthquake Engineering & Structural Dynamics*, *42*(15), 2235-2253.

Bradley, B. A., Burks, L. S., & Baker, J. W. (2015). Ground motion selection for simulation-based seismic hazard and structural reliability assessment. *Earthquake Engineering & Structural Dynamics*, *44*(13), 2321-2340.

Buratti, N., Stafford, P. J., & Bommer, J. J., (2011). Earthquake accelerogram selection and scaling procedures for estimating the distribution of drift response. *Journal of Structural Engineering (ASCE)*, *137*(3), 345-357.

Buratti, N. (2012). A comparison of the performances of various ground–motion intensity measures. *Proceedings of the 15th World Conference on Earthquake Engineering*, Lisbon, Portugal.

Burnham, K. P., & Anderson, D. R. (2002). *Model selection and multimodel inference: a practical information-theoretic approach* (2nd ed.), Springer-Verlag.

Cabanas, L., Benito, & B. Herraiz, M. (1997). An approach to the measurement of the potential structural damage of earthquake ground motions. *Earthquake Engineering & Structural Dynamics*, *26*, 79-92.

Cantagallo, C., Camata, G., Spacone, E., & Corotis, R. (2012). The variability of deformation demand with ground motion intensity. *Probabilistic engineering mechanics*, *28*, 59-65.

Cavanaugh, J. E. (1997). Unifying the derivations for the Akaike and corrected Akaike information criteria. *Statistics & Probability Letters*, *33*(2), 201-208.

Celik, O. C., & Ellingwood, B. R. (2010). Seismic fragilities for non-ductile reinforced concrete frames–Role of aleatoric and epistemic uncertainties. *Structural Safety*, *32*(1), 1-12.

Chen, P. Y., & Popovich, P. M. (2002). *Correlation: Parametric and nonparametric measures*. (Sage University Papers Series on Quantitative Applications in the Social Sciences, series no. 07-139). Thousand Oaks, CA, USA: Sage Publications.

Chopra, A. K., & Goel, R. K. (2002). A modal pushover analysis procedure for estimating seismic demands for buildings. *Earthquake Engineering & Structural Dynamics*, *31*(3), 561-582.

Chopra, A. K., & Chinatanapakdee, C. (2004). Inelastic deformation ratios for design and evaluation of structures: Single-degree-of-freedom bilinear systems. *Journal of Structural Engineering (ASCE)*, *130*(9), 1309–1319.

Chiou, B., Darragh, R., Gregor, N., & Silva, W. (2008). NGA project strong-motion database. *Earthquake Spectra*, *24*(1), 23-44.

Cimellaro, G. P., Reinhorn, A. M., D'Ambrisi, A., & De Stefano, M. (2011). Fragility analysis and seismic record selection. *Journal of Structural Engineering (ASCE)*, *137*(3), 379–390.

Cordova, P. P., Deierlein, G. G., Mehanny, S. S. F., & Cornell, C. A. (2000). Development of a two-parameter seismic intensity measure and probabilistic assessment procedure. The Second U.S.-Japan Workshop on Performance-Based Earthquake Engineering Methodology for Reinforced Concrete Building Structures, Sapporo, Hokkaido, Japan.

Dávalos, H., & Miranda, E. (2019). Evaluation of the scaling factor bias influence on the probability of collapse using $S_a(T_1)$ as the intensity measure. *Earthquake Spectra*, 35(2), 679-702.

De Biasio, M., Grange, S., Dufour, F., Allain, F., & Petre-Lazar, I. (2014). A simple and efficient intensity measure to account for nonlinear structural behavior. *Earthquake Spectra*, *30*(4), 1403-1426.

Ding, Y., Peng, Y., & Li, J. (2020). Cluster analysis of earthquake ground-motion records and characteristic period of seismic response spectrum. *Journal of Earthquake Engineering*, *24*(6), 1012-1033.

Elenas, A. (2000). Correlation between seismic acceleration parameters and overall structural damage indices of buildings. *Soil Dynamics and Earthquake Engineering*, *20*, 93-100.

Elenas, A., & Meskouris, K. (2001). Correlation study between seismic acceleration parameters and damage indices of structure. *Engineering Structures*, *23*, 698-704.

Erberik, M. A., & Çullu, S. (2006). Assessment of seismic fragility curves for low- and mid-rise reinforced concrete frame buildings using Duzce field database. *In Advances in earthquake engineering for urban risk reduction* (pp. 151-166). Springer, Dordrecht.

EPRI (Electrical Power Research Institute) (1998). *A criterion for determining exceedance of the operating basis earthquake*. EPRI NP-5930, Palo Alto, CA.

Erberik, M. A., & Elnashai, A. S. (2004). Fragility analysis of flat-slab structures. *Engineering Structures*, *26*(7), 937-948.

Fajfar, P., Vidic, T., & Fischinger., M. (1990). A measure of earthquake motion capacity to damage medium-period structures. *Soil Dynamics and Earthquake Engineering*, *9*(5), 236–242.

Federal Emergency Management Agency (FEMA) (2000). *Prestandard: Commentary for seismic rehabilitation of buildings (FEMA-356)*. Washington, DC.

Federal Emergency Management Agency (FEMA) (2012). *Seismic performance assessment of buildings, Volume 1-Methodology*. Rep. No. FEMA P-58-1.

Garson, G. D. (2013). *Correlation (Statistical associates "Blue Book" series)*. Asheboro, NC, USA: Statistical Publishing Associates.

Gehl, P., Seyedi, D. M., & Douglas, J. (2013). Vector-valued fragility functions for seismic risk evaluation. *Bulletin of Earthquake Engineering*, 11(2), 365-384.

Giovenale, P., Cornell, C. A., & Esteva, L. (2004). Comparing the adequacy of alternative ground motion intensity measures for the estimation of structural responses. *Earthquake Engineering & Structural Dynamics*, *33*(8), 951–975.

Goel, R. K., & Chopra, A. K. (2005). Extension of modal pushover analysis to compute member forces. *Earthquake Spectra*, *21*(1), 125-139.

Gupta, B. C., & Guttman, I. (2014). *Statistics and probability with applications for engineers and scientists*. John Wiley & Sons.

Gülkan, P. (2020). *Mete A. Sözen: A Brief Life Story. Call Me 'Mete'*. TMMOB Turkish Chamber of Civil Engineers, Istanbul Branch, 1-15.

Hancılar, U. (2009). *Correlations between ground motion intensity measures and structural response parameters through nonlinear dynamic analyses*. PhD Thesis, Kandilli Observatory and Earthquake Research Institute, Boğaziçi University, İstanbul.

Hancock, J., Bommer, J. J., & Stafford, P.J., (2008). Numbers of scaled and matched accelerograms required for inelastic dynamic analyses. *Earthquake Engineering & Structural Dynamics*, *37*(14), 1585–1607.

Haselton, C. B., Fry, A., Baker, J. W., Hamburger, R. O., Whittaker, A. S., Stewart, J. P., ..., & Pekelnicky, R. G. (2014). Response-history analysis for the design of new buildings: a fully revised chapter 16 methodology proposed for the 2015 NEHRP Provisions and the ASCE/SEI 7-16 Standard. *Proceedings of the Tenth US National Conference on Earthquake Engineering*. Alaska, United States of America.

Hernandez-Montes, E., Kwon, O. S., & Aschheim, M. A. (2004). An energy-based formulation for first-and multiple-mode nonlinear static (pushover) analyses. *Journal of Earthquake Engineering*, *8*(01), 69-88.

Housner, G. W. (1952). Spectrum intensity of strong-motion earthquakes. *Proceedings of the Symposium on Earthquakes and Blast Effects on Structures*, Earthquake Engineering Research Institute, Los Angeles, CA, 20–36.

Housner, G. W., & Jennings, P. C. (1977). *Earthquake design criteria for structures*. California Institute of Technology, Earthquake Engineering Research Laboratory.

Huang, Y. N. (2008). *Performance assessment of conventional and base-isolated nuclear power plants for earthquake and blast loadings*. PhD Thesis, Department of Civil, Structural and Environmental Engineering, State University of New York at Buffalo.

International Conference on Building Officials (ICBO) (1982). *Uniform Building Code*, Whittier, CA.

Kadaş, K. (2006). *Influence of idealized pushover curves on seismic response*. MSc Thesis, Department of Civil Engineering, Middle East Technical University, Ankara.

Kadaş, K., Yakut, A., & Kazaz, İ. (2011). Spectral ground motion intensity based on capacity and period elongation. *Journal of Structural Engineering (ASCE)*, *137*(3), 401–409.

Kalkan, E., & Chopra, A. K. (2010). *Practical guidelines to select and scale earthquake records for nonlinear response history analysis of structures*, USGS Open-File Report 2010-1068, U.S. Geological Survey, Reston, Virginia, 126pp.

Kalkan, E., Chopra, A.K. (2011). Modal-pushover-based ground motion scaling procedure, Journal of Structural Engineering (ASCE), 137 (3), 298–310.

Karimzadeh, S., Kadas, K., Askan, A., Erberik, M. A., & Yakut, A. (2020). Derivation of analytical fragility curves using SDOF models of masonry structures in Erzincan (Turkey). *Earthquakes and Structures*, *18*(2), 249-261.

Karimzadeh, S., Kadas, K., Askan, A., & Yakut, A. (2021). Comparison of real and simulated records using ground motion intensity measures. *Soil Dynamics and Earthquake Engineering*, *147*, 106796.

Katsanos, E. I., Sextos, A. G., & Manolis, G. D. (2010). Selection of earthquake ground motion records: a state-of-the-art review from a structural engineering perspective. *Soil Dynamics and Earthquake Engineering*, *30*(4), pp. 157-169.

Kazantzi, A. K., & Vamvatsikos, D. (2015). Intensity measure selection for vulnerability studies of building classes. *Earthquake Engineering & Structural Dynamics*, *44*(15), 2677-2694.

Kohrangi, M., Bazzurro, P., & Vamvatsikos, D. (2016a). Vector and scalar IMs in structural response estimation, Part I: Hazard analysis. *Earthquake Spectra*, *32*(3), 1507-1524.

Kohrangi, M., Bazzurro, P., & Vamvatsikos, D. (2016b). Vector and scalar IMs in structural response estimation, part II: building demand assessment. *Earthquake Spectra*, *32*(3), 1525-1543.

Kohrangi, M., Bazzurro, P., Vamvatsikos, D., & Spillatura, A. (2017). Conditional spectrum-based ground motion record selection using average spectral acceleration. *Earthquake Engineering & Structural Dynamics*, *46*(10), 1667-1685.

Kostinakis, K., Athanatopoulou, A., & Morfidis, K. (2015). Correlation between ground motion intensity measures and seismic damage of 3D R/C buildings. *Engineering Structures*, *82*, 151-167.

Kowalski, C. (1972). On the effects of non-normality on the distribution of the sample product-moment correlation coefficient. *Journal of the Royal Statistical Society. Series C (Applied Statistics)*, *21*(1), 1-12. doi:10.2307/2346598

Kramer, S. L. (1996). *Geotechnical earthquake engineering*. Pearson Education India.

Kurama, Y. C., & Farrow, K. T. (2003). Ground motion scaling methods for different site conditions and structure characteristics. *Earthquake Engineering & Structural Dynamics*, *32*(15), 2425-2450.

Kwong, N. S., & Chopra, A. K. (2015). *Selection and scaling of ground motions for nonlinear response history analysis of buildings in performance-based earthquake engineering*. PEER Report 2015/11, PEER Center, Berkeley, CA.

Liao, W., Loh, C., & Wan, S. (2001). Earthquake responses of RC moment frames subjected to near-fault ground motions. *Structural Design of Tall Buildings*, *10*, 219-229.

Lin, L., Naumoski, N., Saatcioglu, M., & Foo, S. (2011). Improved intensity measures for probabilistic seismic demand analysis. Part 1: development of improved intensity measures. *Canadian Journal of Civil Engineering*, *38*(1), 79-88.

Lin, T. (2012). *Advancement of hazard-consistent ground motion selection methodology*. PhD Thesis, Stanford University.

Luco, N. (2002). *Probabilistic seismic demand analysis: SMRF connection fractures, and near-source effects*. PhD Thesis, Department of Civil and Environmental Engineering, June 2002, Stanford University, Stanford, CA.

Luco, N., & Cornell, C.A. (2007). Structure-specific scalar intensity measures for near-source and ordinary earthquake ground motions. *Earthquake Spectra*, *23*(2), 357–392.

MATLAB (2018). 9.4.0.813654 (R2018a). Natick, Massachusetts: The MathWorks Inc.

Mazılıgüney, L., Yakut, A., Kadaş, K., & Kalem, İ. (2013). Fragility analysis of reinforced concrete school buildings using alternative intensity measure-based ground motion sets. *Proceedings of the 2nd Turkish Conference on Earthquake Engineering and Seismology*, pp. 25-27.

Mazılıgüney, L., Akansel, V. H., Soysal, B. F., Kadaş, K., & Yakut, A. (2019). Seismic risk assessment of school buildings on the basis of recent Turkish seismic hazard map. *Proceedings of the 6th International Earthquake Symposium Kocaeli*.

Mazılıgüney, L. (2020). *Seismic vulnerability assessment of reinforced concrete school buildings in Turkey*. PhD Thesis, Middle East Technical University, Ankara.

McKenna, F., Fenves, G. L, & Scott, M. H. (2000). *Open system for earthquake engineering simulation*. University of California, Berkeley, http://opensees.berkeley.edu.

Miranda, E. (2001). Estimation of inelastic deformation demands of SDOF systems. *Journal of Structural Engineering*, *127*(9), 1005-1012.

Modica, A., & Stafford, P. J. (2014). Vector fragility surfaces for reinforced concrete frames in Europe. *Bulletin of Earthquake Engineering*, *12*(4), 1725-1753.

Narisetty, N. N. (2020). Bayesian model selection for high-dimensional data. *In Handbook of Statistics Vol. 43: Principles and Methods for Data Science*, Editors: Arni S.R. Srinivasa Rao, C.R. Rao, 207-248.

Nau, J. M., & Hall, W. J. (1982). *An evaluation of scaling methods for earthquake response spectra*. Structural Research Series No. 499, Department of Civil Engineering, University of Illinois: Urbana, IL.

NIST (2011). *Selecting and scaling earthquake ground motions for performing response-history analyses*, NEHRP Consultants Joint Venture, NIST GCR 11-917-15.

Nuttli, O. W. (1979). *The relation of sustained maximum ground acceleration and velocity to earthquake intensity and magnitude*. Miscellaneous Paper S-71-1, Report 16, U.S. Army Corps of Engineers, Waterways Experiment Station, Vicksburg, Mississippi.

Oğuz, S. (2005). *Evaluation of pushover analysis procedures for frame structures*. MSc Thesis, Department of Civil Engineering, Middle East Technical University, Ankara.

OpenSees (Version 2.4.5) [Computer Software]. University of California, Berkeley, CA. Retrieved from http://opensees.berkeley.edu, [last visited on December 2014]

O'Reilly, G. J., Kohrangi, M., Bazzurro, P., & Monteiro, R. (2018). Intensity measures for the collapse assessment of infilled RC frames. *Proceedings of the 16th European Conference on Earthquake Engineering*. Thessaloniki, Greece.

O'Reilly, G. J., & Monteiro, R. (2019). Probabilistic models for structures with bilinear demand-intensity relationships. *Earthquake Engineering & Structural Dynamics*, *48*(2), 253-268.

Ozmen, H. B., & Inel, M. (2016). Damage potential of earthquake records for RC building stock. *Earthquakes and Structures*, *10*, 1315-1330.

Ozmen, H. B. (2017). Developing hybrid parameters for measuring damage potential of earthquake records: case for RC building stock. *Bulletin of Earthquake Engineering*, *15*(7), 3083-3101.

Palanci, M., & Senel, S. M. (2019). Correlation of earthquake intensity measures and spectral displacement demands in building type structures. *Soil Dynamics and Earthquake Engineering*, *121*, 306-326.

Papanikolaou, V. K., Elnashai, A. S., & Pareja, J. F. (2005). Evaluation of conventional and adaptive pushover analysis I: Methodology. *Journal of Earthquake Engineering*, *09*(06), 923-941.

Papanikolaou, V. K., Elnashai, A. S., & Pareja, J. F. (2006). Evaluation of conventional and adaptive pushover analysis II: Comparative results. *Journal of Earthquake Engineering*, *10*(01), 127-151.

Park, Y. J., Ang, A. H. S., & Wen, Y. K. (1985). Seismic damage analysis of reinforced concrete buildings. *Journal of Structural Engineering*, *111*(4), 740-757.

Pearson, K. (1901). *Principal components analysis*. The London, Edinburgh, and Dublin Philosophical Magazine and Journal of Science, 6 (2), 559.

Porter, K. A. (2003). An overview of PEER's performance-based earthquake engineering methodology. *Proceedings of the Ninth International Conference on Applications of Statistics and Probability in Civil Engineering*, 1-8.

Power, M., Chiou, B., Abrahamson, N., Bozorgnia, Y., Shantz, T., & Roblee, C. (2008). An overview of the NGA project. *Earthquake Spectra*, *24*(1), 3–21.

Priestley, M. J. N. (2000). Performance based seismic design. *Bulletin of the New Zealand Society for Earthquake Engineering*, *33*(3), 325-346.

Ramamoorthy, S. K., Gardoni, P., & Bracci, J. M. (2006). Probabilistic demand models and fragility curves for reinforced concrete frames. *Journal of Structural Engineering*, *132*(10), 1563-1572.

Ramamoorthy, S. K., Gardoni, P., & Bracci, J. M. (2008). Seismic fragility and confidence bounds for gravity load designed reinforced concrete frames of varying height. *Journal of Structural Engineering*, *134*(4), 639-650.

Rathje, E. M., Abrahamson, N. A., & Bray, J. D. (1998) Simplified frequency content estimates of earthquake ground motions. *Journal of Geotechnical and Geoenvironmental Engineering*, *124*(2), 150-159.

Riddell, R. (2007). On ground motion intensity indices. *Earthquake Spectra*, *23*(1), 147-173.

Riddell, R., & Garcia, J. E. (2001). Hysteretic energy spectrum and damage control. *Earthquake Engineering & Structural Dynamics*, *30*(12), 1791-1816.

Rencher, A. C., & Christensen, W. F. (2012). *Methods of multivariate analysis*. 3rd Edition, John Wiley & Sons.

Romao, X., Delgado, R., & Costa, A. (2011). Assessment of the statistical distributions of structural demand under earthquake loading. *Journal of Earthquake Engineering*, *15*(5), 724-753.

Ryan, T. P. (2008). *Modern regression methods* (Vol. 655). John Wiley & Sons.

Sarma, S. K., & Yang K. S. (1987). An evaluation of strong motion records and a new parameter A95. *Earthquake Engineering & Structural Dynamics*, *15*, 119-132.

Schwarz, G. (1978). Estimating the dimension of a model. *Annals of statistics*, *6*(2), 461-464.

Shome, N., Cornell, C. A., Bazzurro, P., & Carballo, J. E. (1998). Earthquakes, records, and nonlinear responses. *Earthquake Spectra*, *14*(3), 469-500.

Sriramula, S., Menon, D., & Prasad, A. M. (2007). Correlation measures: Robustness and performance in simulations. *Proceedings of the 10th International Conference on Applications of Statistics and Probability in Civil Engineering (ICASP10)*, Tokyo, Japan.

Sucuoğlu, H., & Nurtuğ, A. (1995). Earthquake ground motion characteristic and seismic energy dissipation. *Earthquake Engineering & Structural Dynamics*, *24*, 1195-1213.

Sucuoğlu, H. (1997). Discussion of "An approach to the measurement of the potential structural damage of earthquake ground motions". *Earthquake Engineering & Structural Dynamics*, *26*, 1283-1285.

Sucuoğlu, H., Yücemen, S., Gezer, A., & Erberik, A. (1998). Statistical evaluation of the damage potential of earthquake ground motions. *Structural Safety*, *20*(4), 357-378.

Seismosoft (2016). SeismoSignal 2016 –A computer program for signal processing of strong-motion data. Available from URL:http://www.seismosoft.com/.

Shinozuka, M., Feng, M. Q., Lee, J., & Naganuma, T. (2000). Statistical analysis of fragility curves. *Journal of Engineering Mechanics*, *126*(12), 1224-1231.

Shome, N., Cornell, C. A., Bazzurro, P., & Carballo, J. E. (1998). Earthquakes, records, and nonlinear responses. *Earthquake Spectra*, *14*(3), 469–500.

TBEC (2018). *Turkish Building Earthquake Code*. Disaster and Emergency Management Authority, Ankara.

Theophilou, A. A. I., Chryssanthopoulos, M. K., & Kappos, A. J. (2017). A vector-valued ground motion intensity measure incorporating normalized spectral area. *Bulletin of Earthquake Engineering*, *15*(1), 249-270.

Thompson, S. K. (2012). *Sampling*. 3rd Edition, John Wiley & Sons.

Trifunac, M. D., & Brady, A. G. (1975). A study on the duration of strong earthquake ground motion. *Bulletin of the Seismological Society of America*, *65*(3), 581-626.

Tso, W. K., Zhu, T. J., & Heidebrecht, A. C. (1992). Engineering implication of ground motion A/V ratio. *Soil Dynamics and Earthquake Engineering*, *11*(3), 133-144.

Uang, C.H., & Bertero V.V. (1988). *Implications of recorded earthquake ground motions on seismic design of buildings structures*, UCB/EERC-88/13, California.

Ugurhan, B., Askan, A., & Erberik, M. A. (2011). A methodology for seismic loss estimation in urban regions based on ground-motion simulations. *Bulletin of the Seismological Society of America*, *101*(2), 710-725.

Utility Software for Data Processing (USDP) (2008). Department of Civil Engineering, Middle East Technical University, Ankara, Turkey, currently available from URL: http://web.boun.edu.tr/sinan.akkar/index.php/usdp, (accessed January 2012).

Van Cao, V., & Ronagh, H. R. (2014a). Correlation between parameters of pulse-type motions and damage of low-rise RC frames. *Earthquakes and Structures*, *7*(3), 365-384.

Van Cao, V., & Ronagh, H. R. (2014b). Correlation between seismic parameters of far-fault motions and damage indices of low-rise reinforced concrete frames. *Soil Dynamics and Earthquake Engineering*, *66*, 102-112.

Von Thun, J. L., Roehim, L. H., Scott, G. A., & Wilson, J. A. (1988). Earthquake ground motions for design and analysis of dams. *Earthquake Engineering and Soil Dynamics II-Recent Advances in Ground Motion Evaluation*, Geotechnical Special Publication, 20, 463-481.

Wen, Y. K., Ellingwood, B. R., & Bracci, J. M. (2004). *Vulnerability function framework for consequence-based engineering*. MAE Center Report 04-04.

Wu, Y.M., Hsiao, N.C., & Teng, T.L., (2004). Relationship between strong motion peak values and seismic loss during the 1999 Chi-Chi, Taiwan earthquake. *Natural Hazards*, *32*, 357-373.

Yaghmaei-Sabegh, S. (2017). A novel approach for classification of earthquake ground-motion records. *Journal of Seismology*, *21*(4), 885-907.

Yakhchalian, M., Nicknam, A., & Amiri, G. G. (2015). Optimal vector-valued intensity measure for seismic collapse assessment of structures. *Earthquake Engineering and Engineering Vibration*, *14*(1), 37-54.

Yakhchalian, M., Yakhchalian, M., & Yakhchalian, M. (2019). Reliable fragility functions for seismic collapse assessment of reinforced concrete special moment resisting frame structures under near-fault ground motions. *The Structural Design of Tall and Special Buildings*, *28*(9), e1608.

Yakut, A., & Yılmaz, H. (2008). Correlation of deformation demands with ground motion intensity. *Journal of Structural Engineering*, *134*(12), 1818-1828.

Yang, D., Pan, J., & Li, G., (2009). Non-structure-specific intensity measure parameters and characteristic period of near-fault ground motions, *Earthquake Engineering & Structural Dynamics*, *38*(11), 1257–1280.

Ye, L., Ma, Q., Miao, Z., Guan, H., & Zhuge, Y. (2013). Numerical and comparative study of earthquake intensity indices in seismic analysis. *The Structural Design of Tall and Special Buildings*, *22*(4), 362-381.

Yılmaz, H. (2007). *Correlation of deformation demands with ground motion intensity*. MSc Thesis, Department of Civil Engineering, Middle East Technical University, Ankara.

Zacharenaki, A., Fragiadakis, M., Assimaki, D., & Papadrakakis, M. (2014). Bias assessment in incremental dynamic analysis due to record scaling. *Soil Dynamics and Earthquake Engineering*, *67*, 158-168.

Zengin, E. (2016). *A proposed ground motion selection and scaling procedure for nonlinear response history analysis*. PhD Thesis, Kandilli Observatory and Earthquake Research Institute, Boğaziçi University, İstanbul.

Zhu, T. J., Tso, W. K., & Heidebrecht, A. C. (1988). Effect of peak ground a/v ratio on structural damage. *ASCE Journal of Structural Engineering*, *114*(5), pp. 1019- 1037.

APPENDICES

A. Additional Histogram Plots for IMs (for Chapter 2)
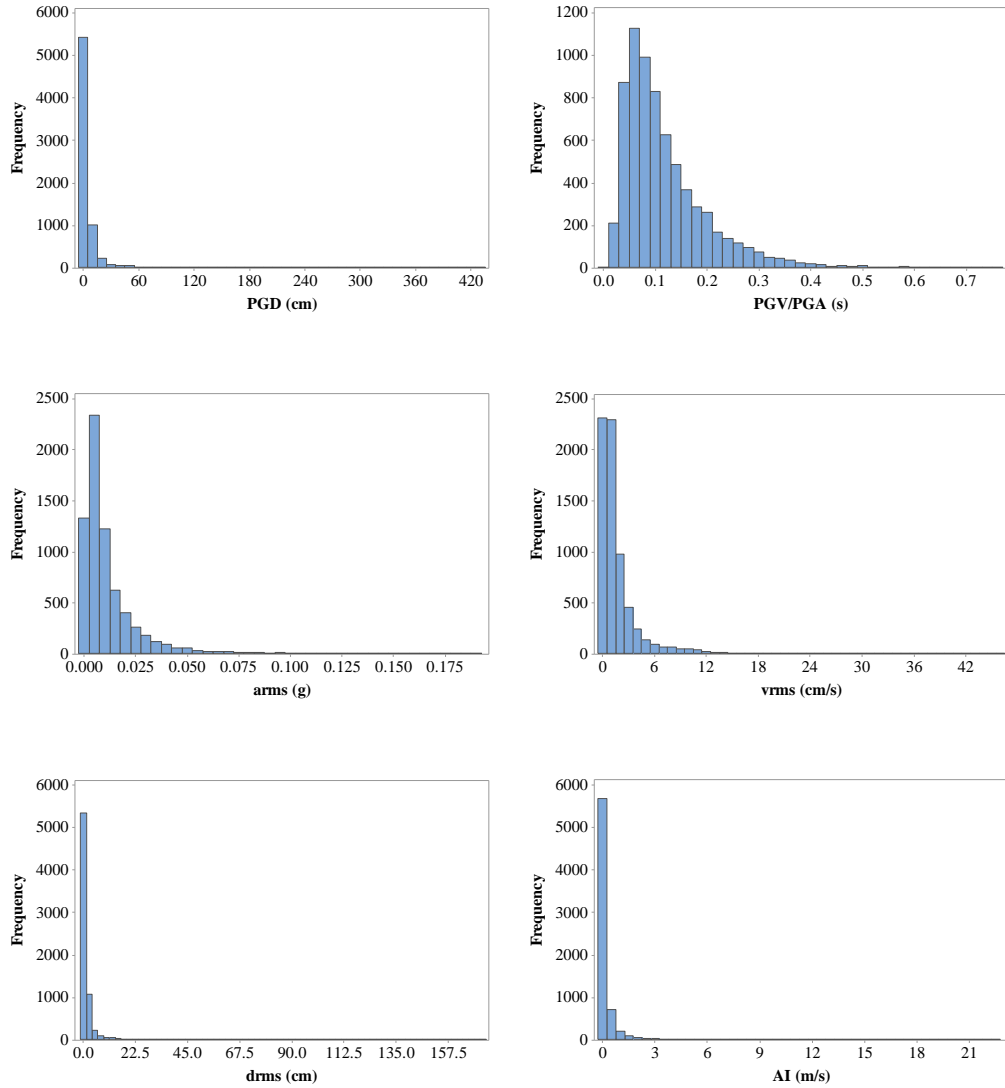
Figure A.1. Histogram plots for PGD, PGV/PGA, a_{rms}, v_{rms}, d_{rms} and AI
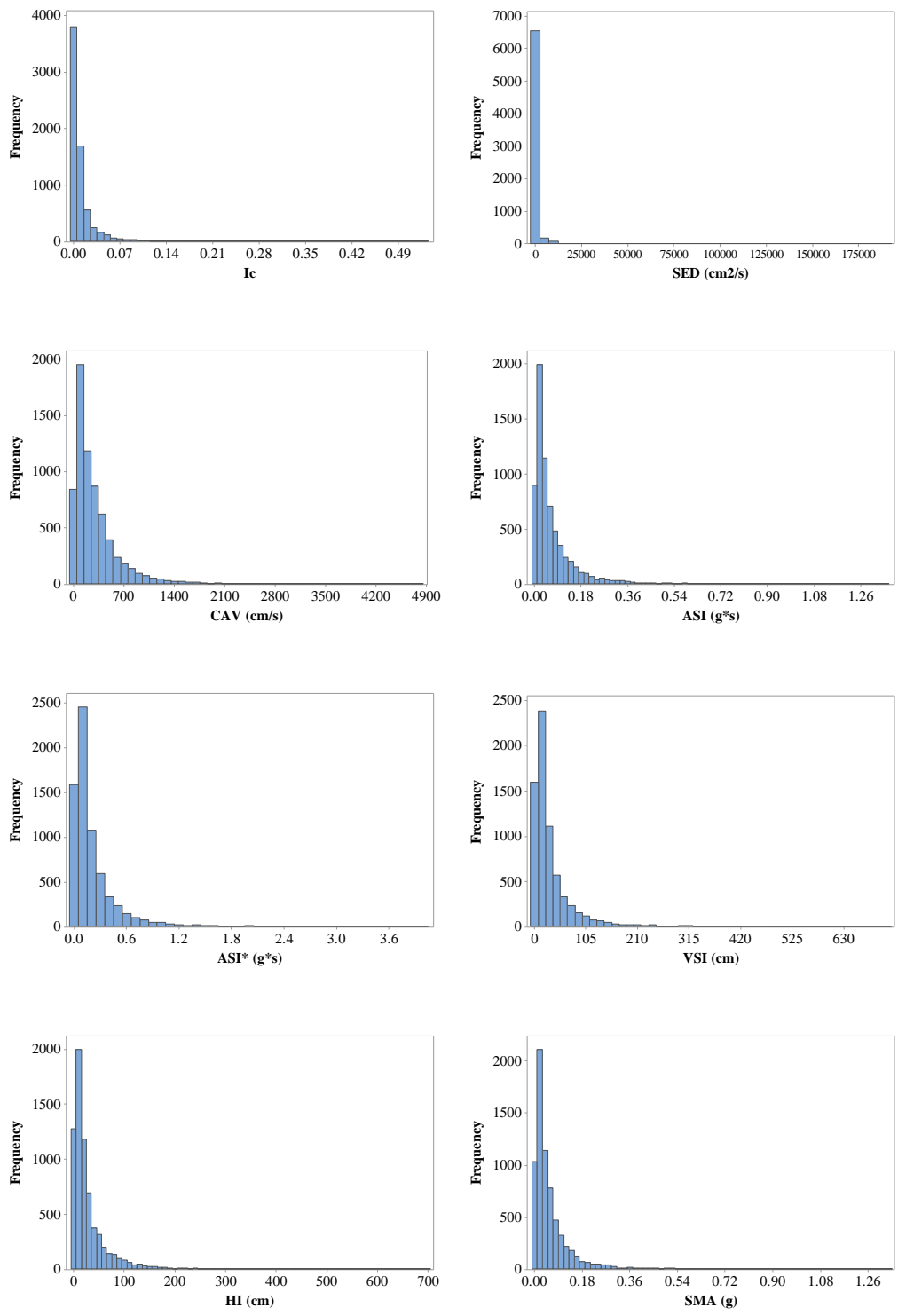
Figure A.2. Histogram plots for Ic, SED, CAV, ASI, ASI*, VSI, HI and SMA
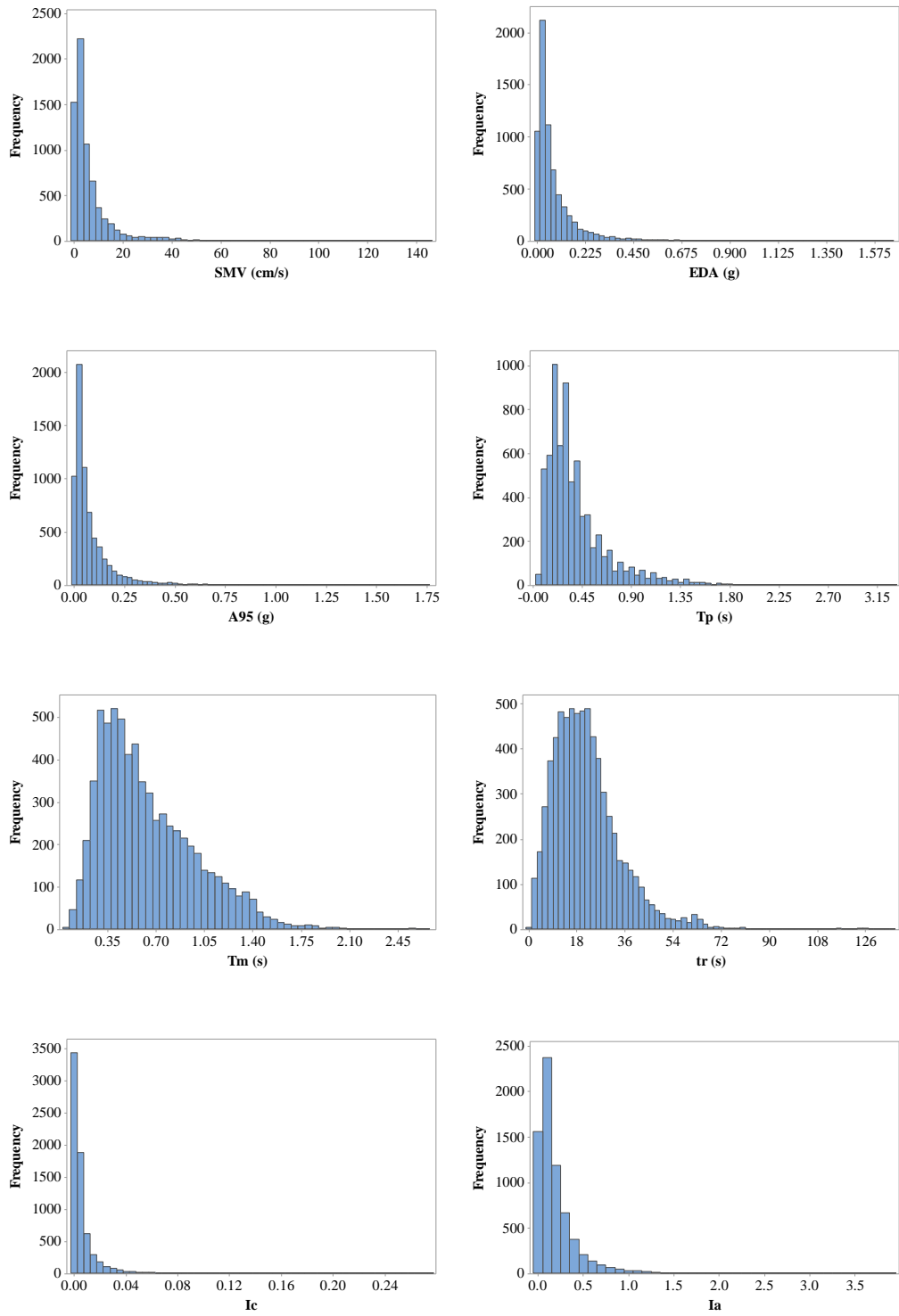
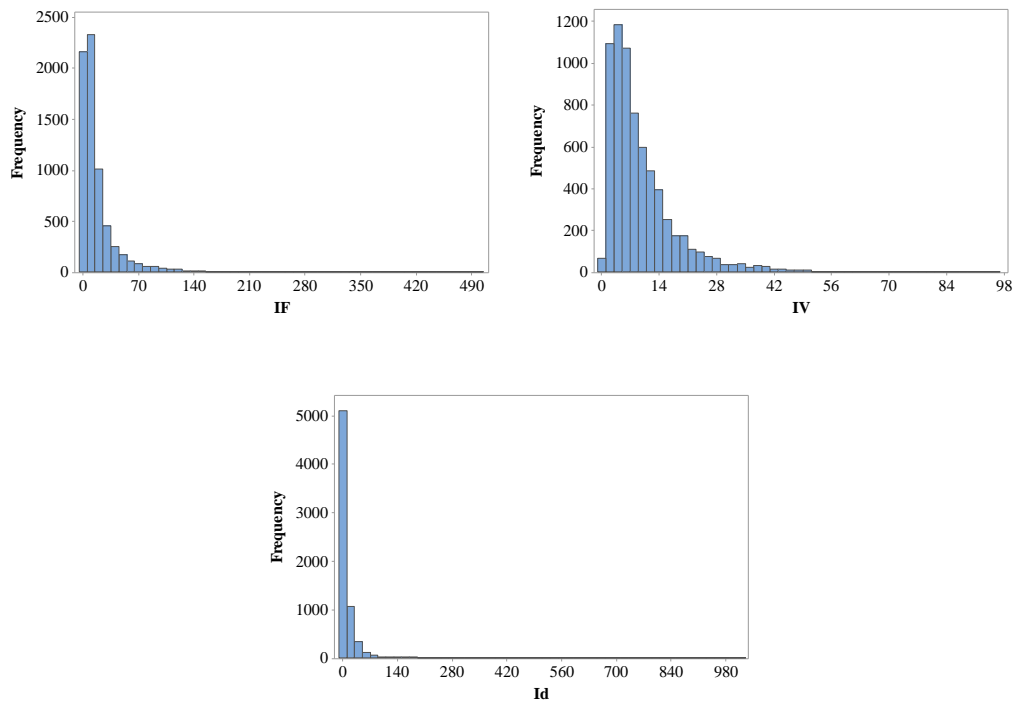Figure A.3. Histogram plots for SMV, EDA, A95, Tp, Tm, tr, Ic and Ia

Figure A.4. Histogram plots for I_F, I_V and I_d

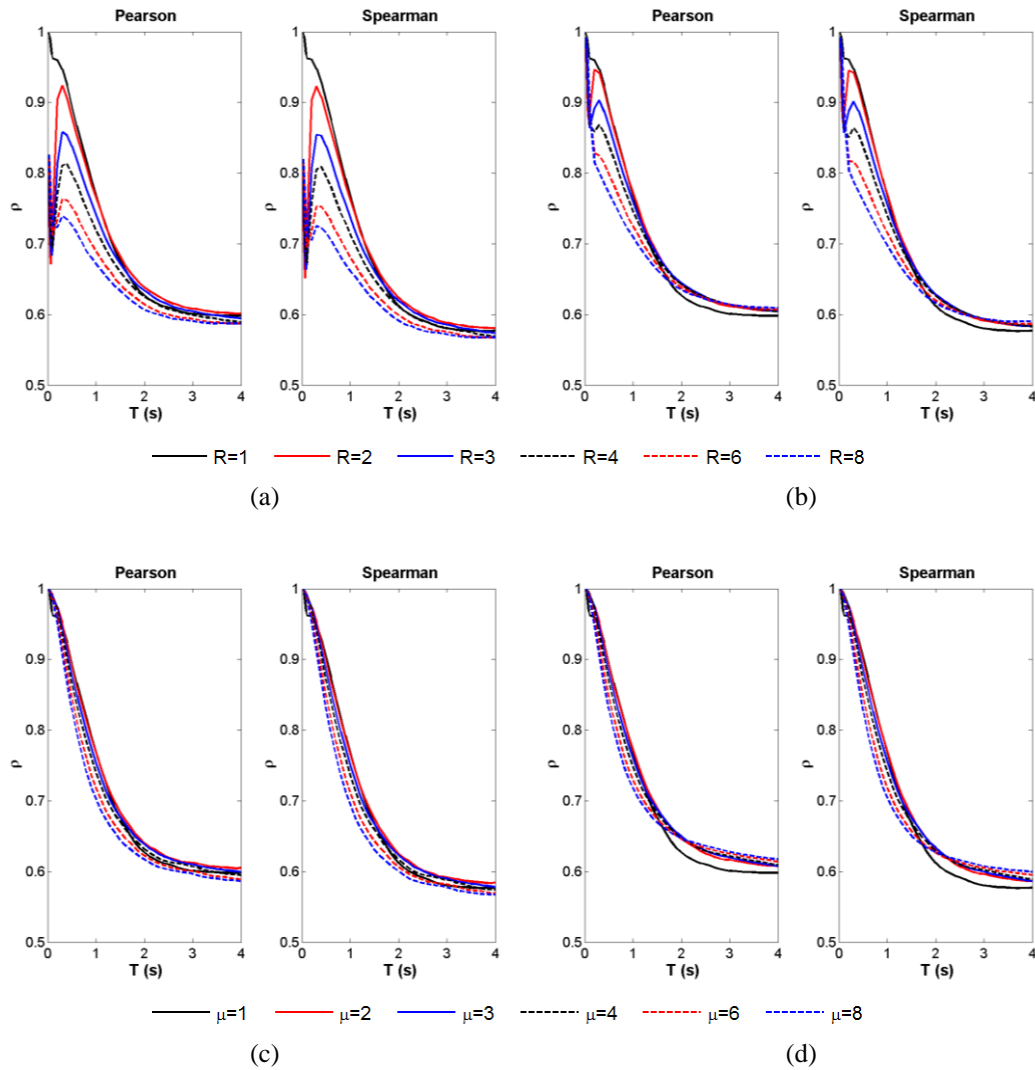## B. Additional Correlation Coefficient Variation Plots (for Chapter 4)

Figure A.5. Variation of correlation coefficient values with period (correlation of IM **PGA** with EDP **SDOF top drift** for different R and μ cases (a) Elastic-Perfectly-Plastic, (b) Bilinear Hardening (α=5%), (c) Elastic-Perfectly-Plastic, (d) Bilinear Hardening (α=5%))
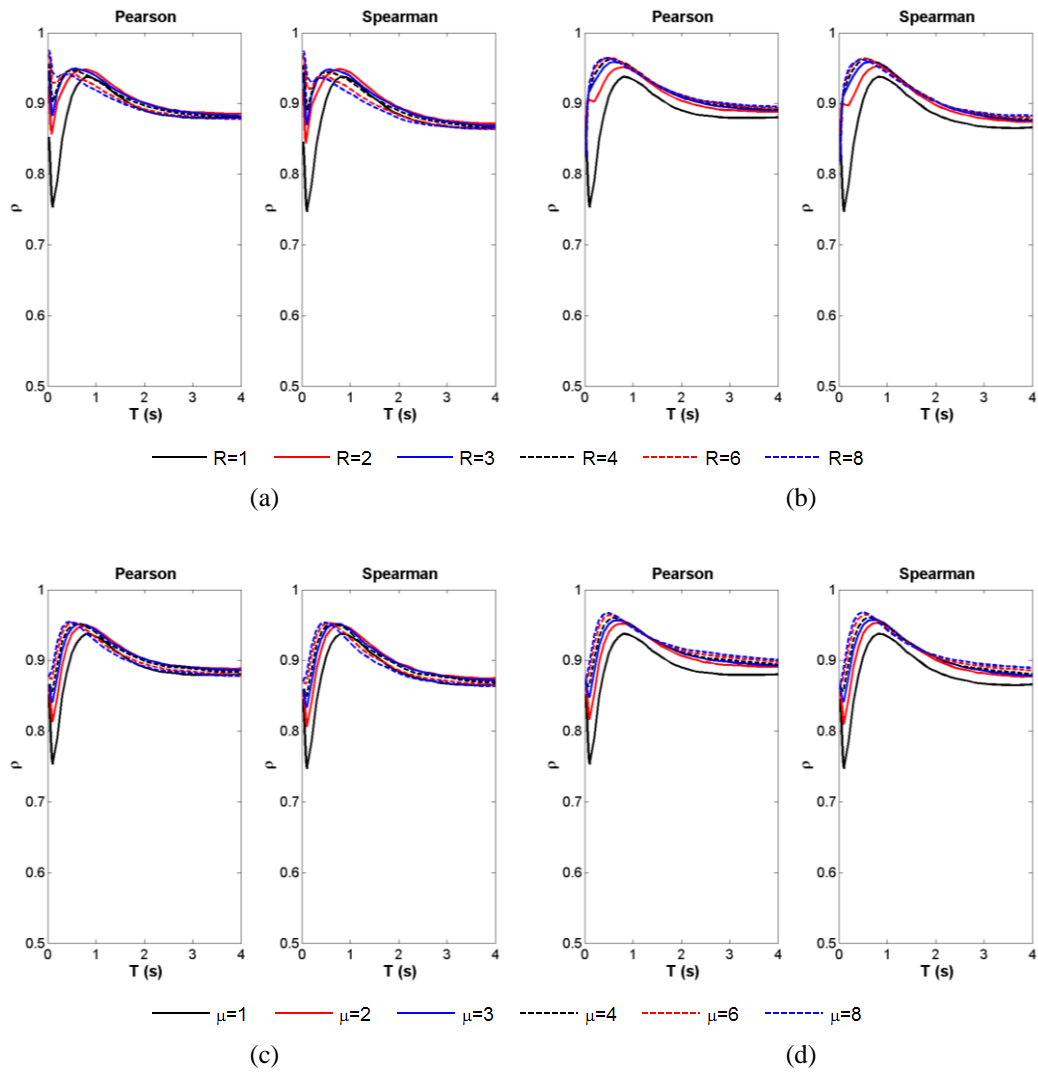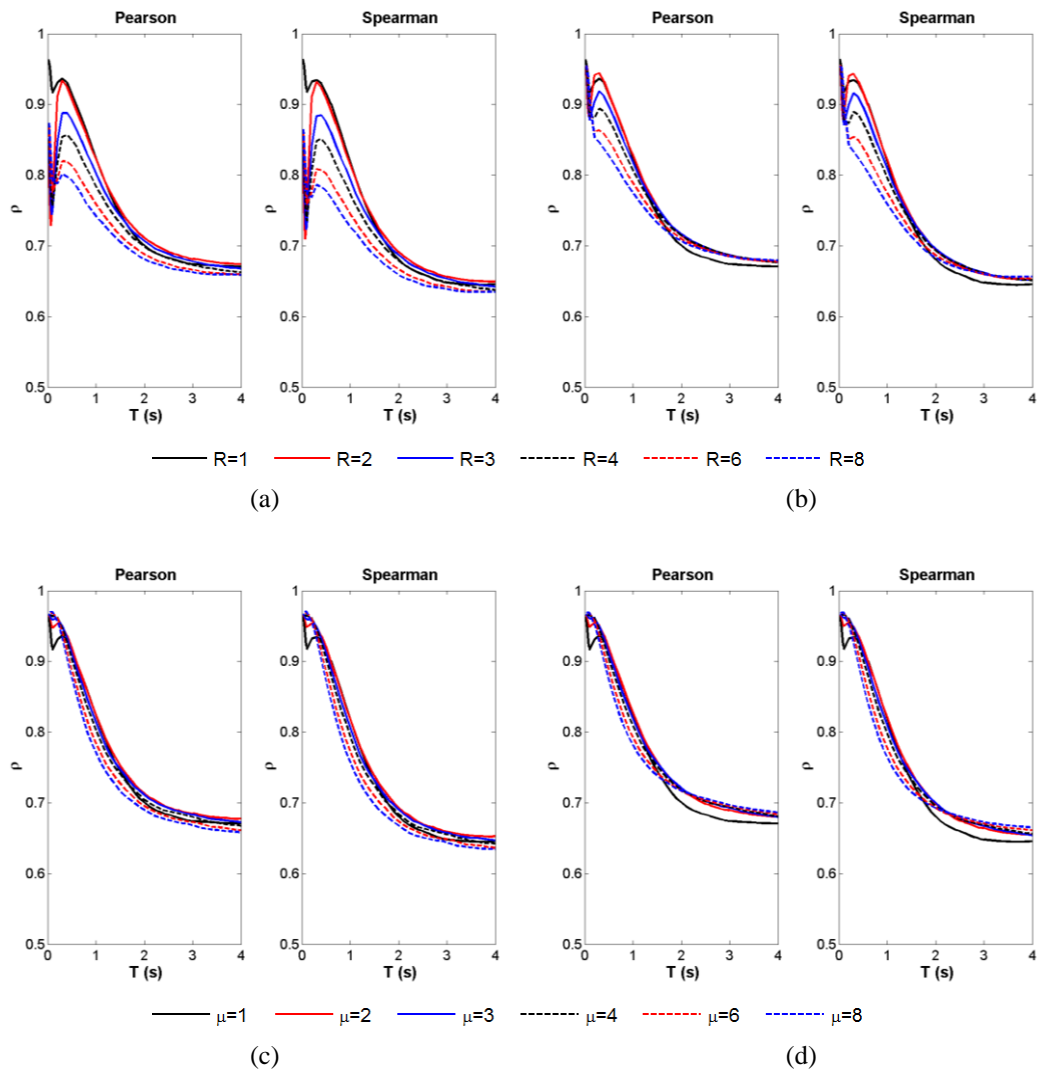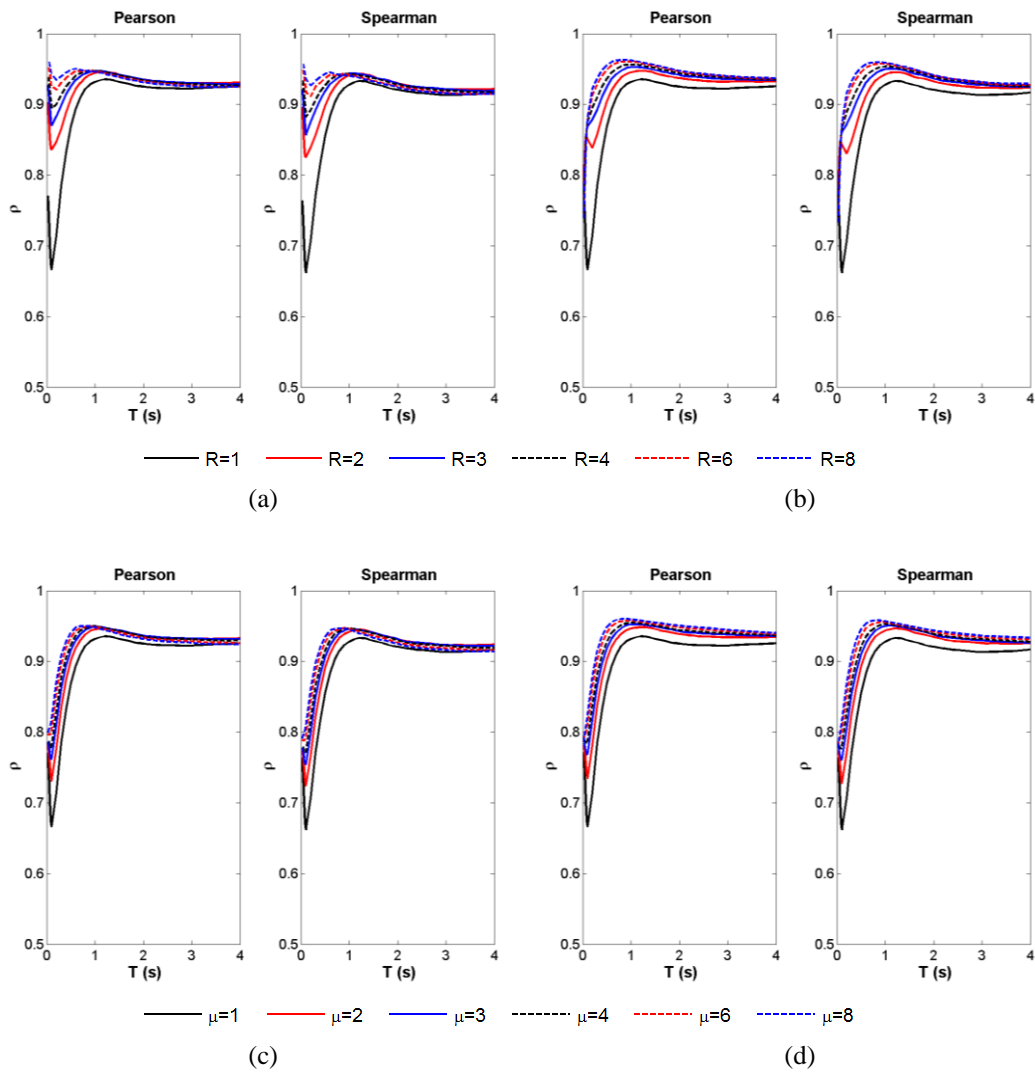
Figure A.6. Variation of correlation coefficient values with period (correlation of IM **PGV** with EDP **SDOF top drift** for different R and μ cases (a) Elastic-Perfectly-Plastic, (b) Bilinear Hardening (α=5%), (c) Elastic-Perfectly-Plastic, (d) Bilinear Hardening (α=5%))
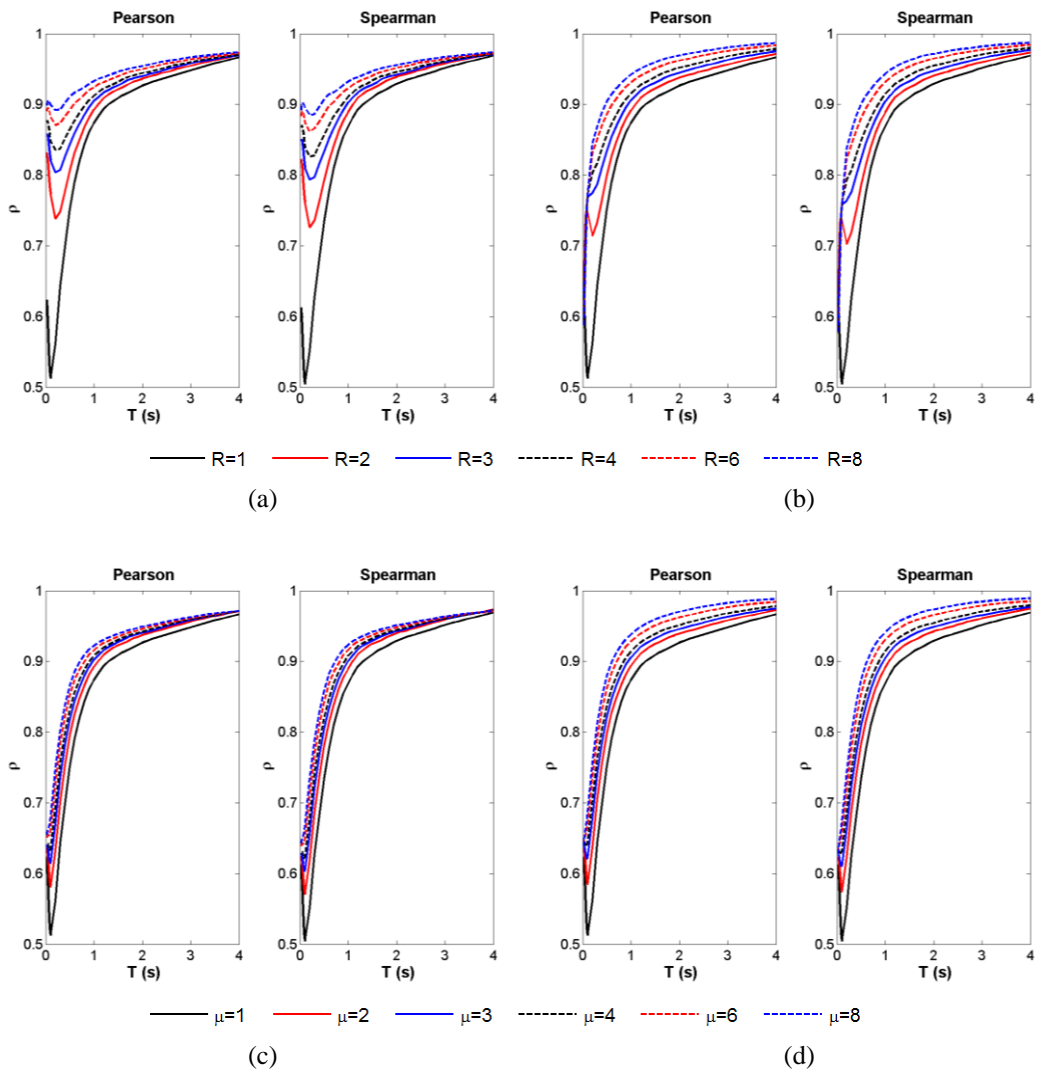
Figure A.7. Variation of correlation coefficient values with period (correlation of IM **PGD** with EDP **SDOF top drift** for different R and μ cases (a) Elastic-Perfectly-Plastic, (b) Bilinear Hardening (α=5%), (c) Elastic-Perfectly-Plastic, (d) Bilinear Hardening (α=5%))

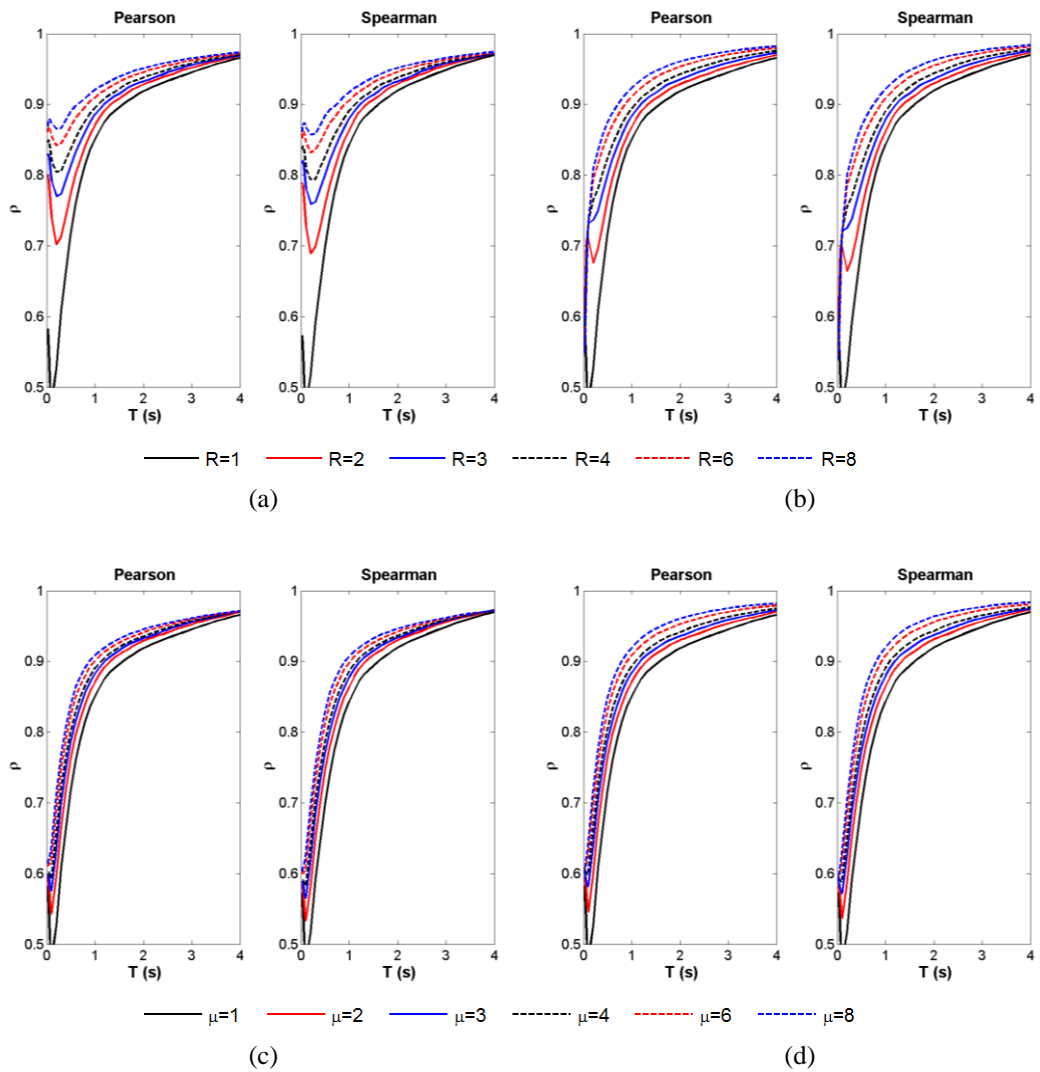Figure A.8. Variation of correlation coefficient values with period (correlation of IM **PGV/PGA** with EDP **SDOF top drift** for different R and μ cases (a) Elastic-Perfectly-Plastic, (b) Bilinear Hardening (α=5%), (c) Elastic-Perfectly-Plastic, (d) Bilinear Hardening (α=5%))

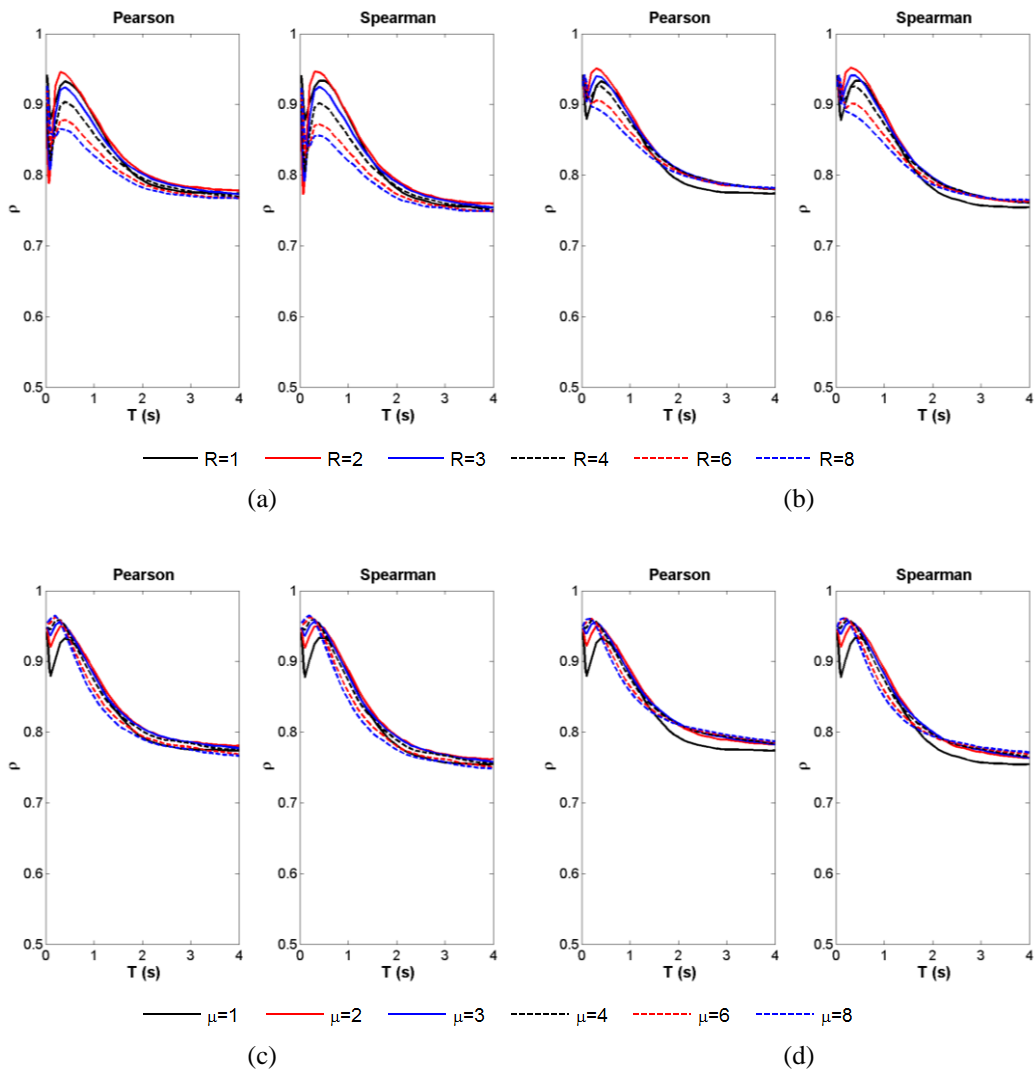Figure A.9. Variation of correlation coefficient values with period (correlation of IM a_{rms} with EDP **SDOF top drift** for different R and μ cases (a) Elastic-Perfectly-Plastic, (b) Bilinear Hardening (α=5%), (c) Elastic-Perfectly-Plastic, (d) Bilinear Hardening (α=5%))

Figure A.10. Variation of correlation coefficient values with period (correlation of IM $\mathbf{v_{rms}}$ with EDP **SDOF top drift** for different R and μ cases (a) Elastic-Perfectly-Plastic, (b) Bilinear Hardening (α=5%), (c) Elastic-Perfectly-Plastic, (d) Bilinear Hardening (α=5%))
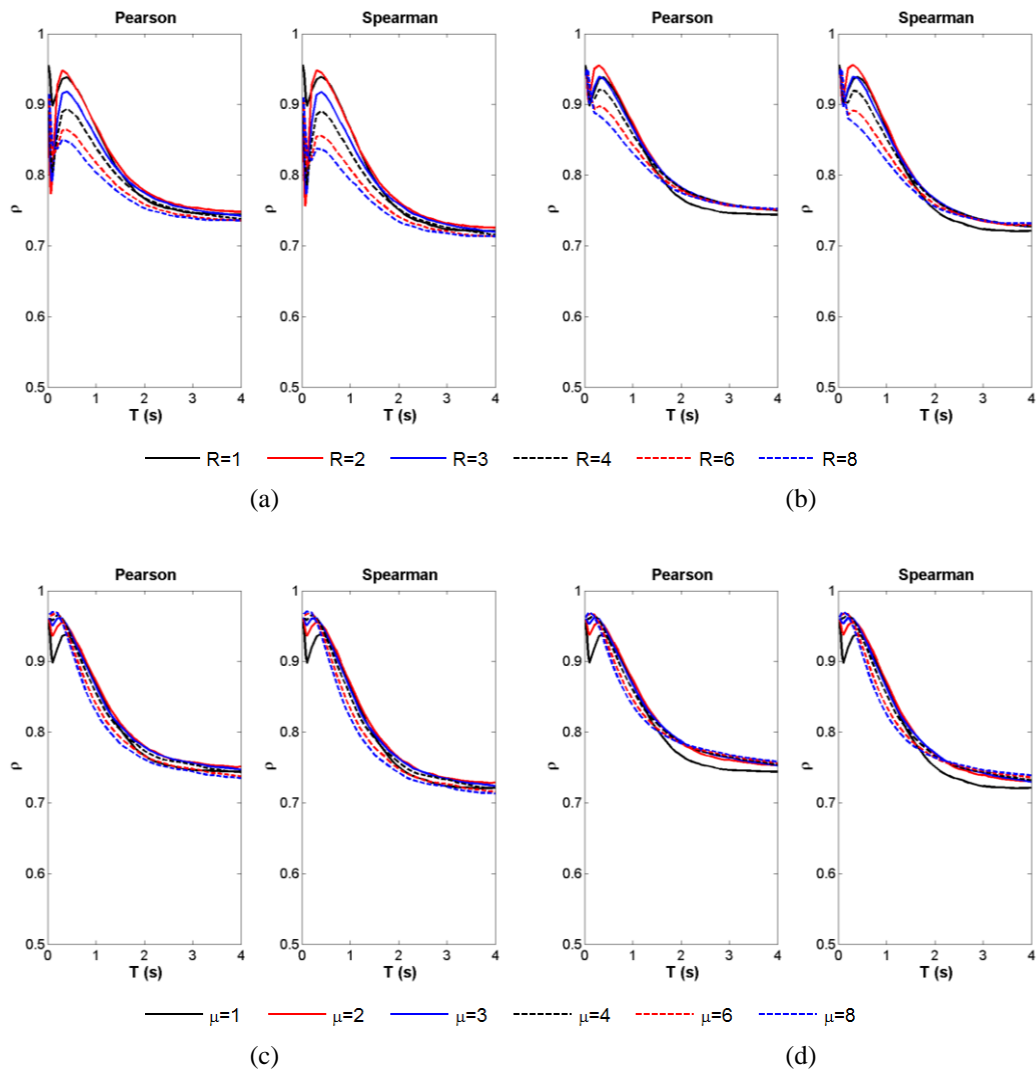
Figure A.11. Variation of correlation coefficient values with period (correlation of IM **d$_{rms}$** with EDP **SDOF top drift** for different R and μ cases (a) Elastic-Perfectly-Plastic, (b) Bilinear Hardening (α=5%), (c) Elastic-Perfectly-Plastic, (d) Bilinear Hardening (α=5%))
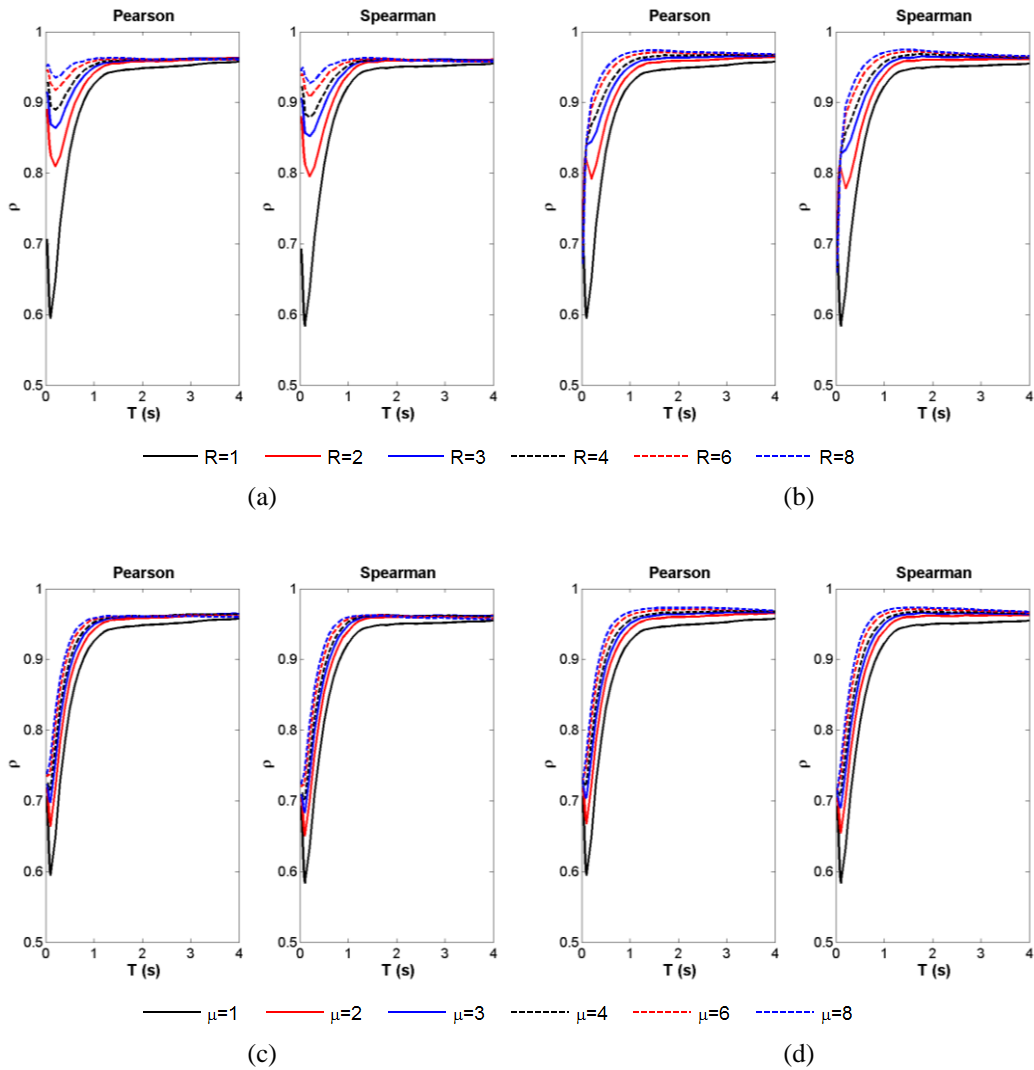
Figure A.12. Variation of correlation coefficient values with period (correlation of IM **AI** with EDP **SDOF top drift** for different R and μ cases (a) Elastic-Perfectly-Plastic, (b) Bilinear Hardening (α=5%), (c) Elastic-Perfectly-Plastic, (d) Bilinear Hardening (α=5%))

Figure A.13. Variation of correlation coefficient values with period (correlation of IM **Ic***** with EDP **SDOF top drift** for different R and μ cases (a) Elastic-Perfectly-Plastic, (b) Bilinear Hardening (α=5%), (c) Elastic-Perfectly-Plastic, (d) Bilinear Hardening (α=5%))

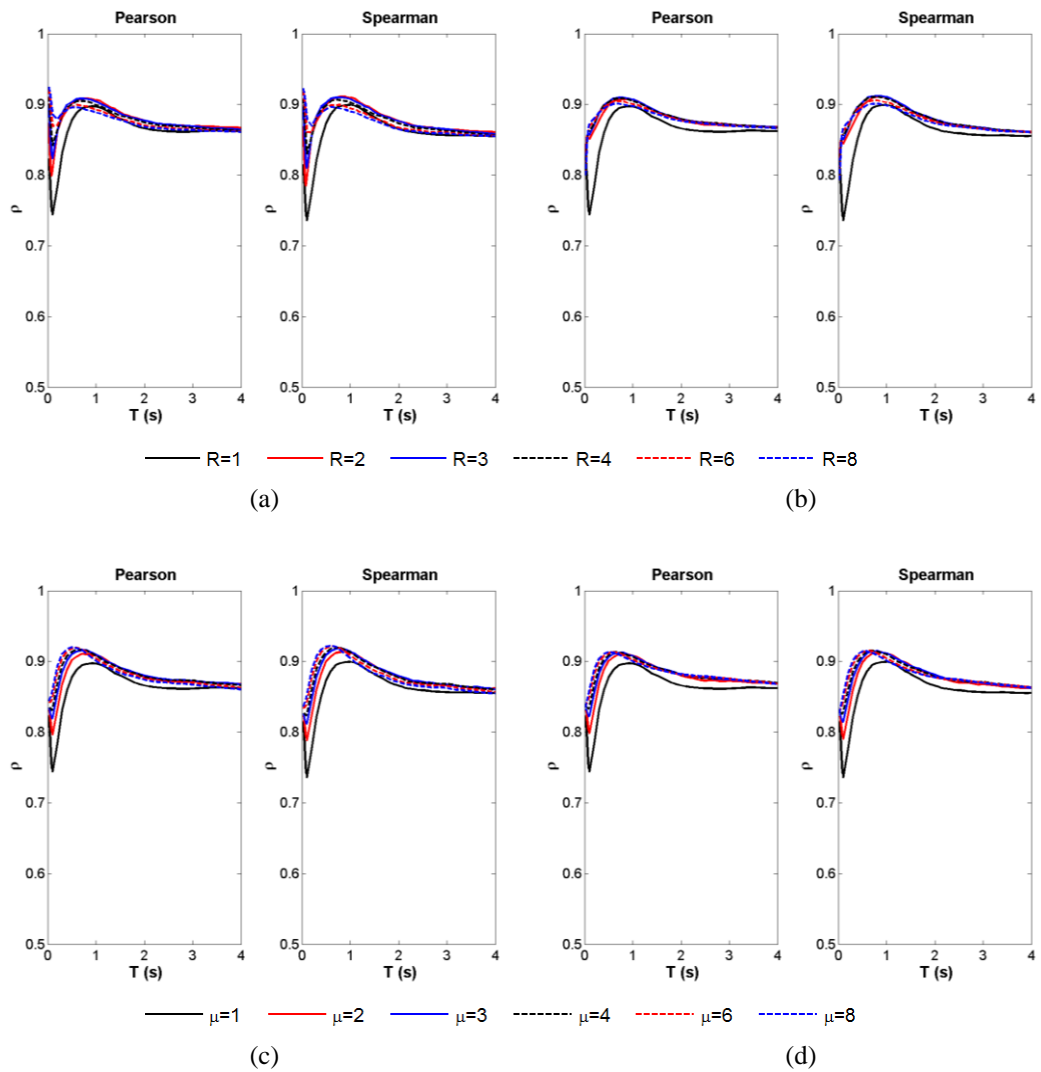Figure A.14. Variation of correlation coefficient values with period (correlation of IM **SED** with EDP **SDOF top drift** for different R and μ cases (a) Elastic-Perfectly-Plastic, (b) Bilinear Hardening (α=5%), (c) Elastic-Perfectly-Plastic, (d) Bilinear Hardening (α=5%))

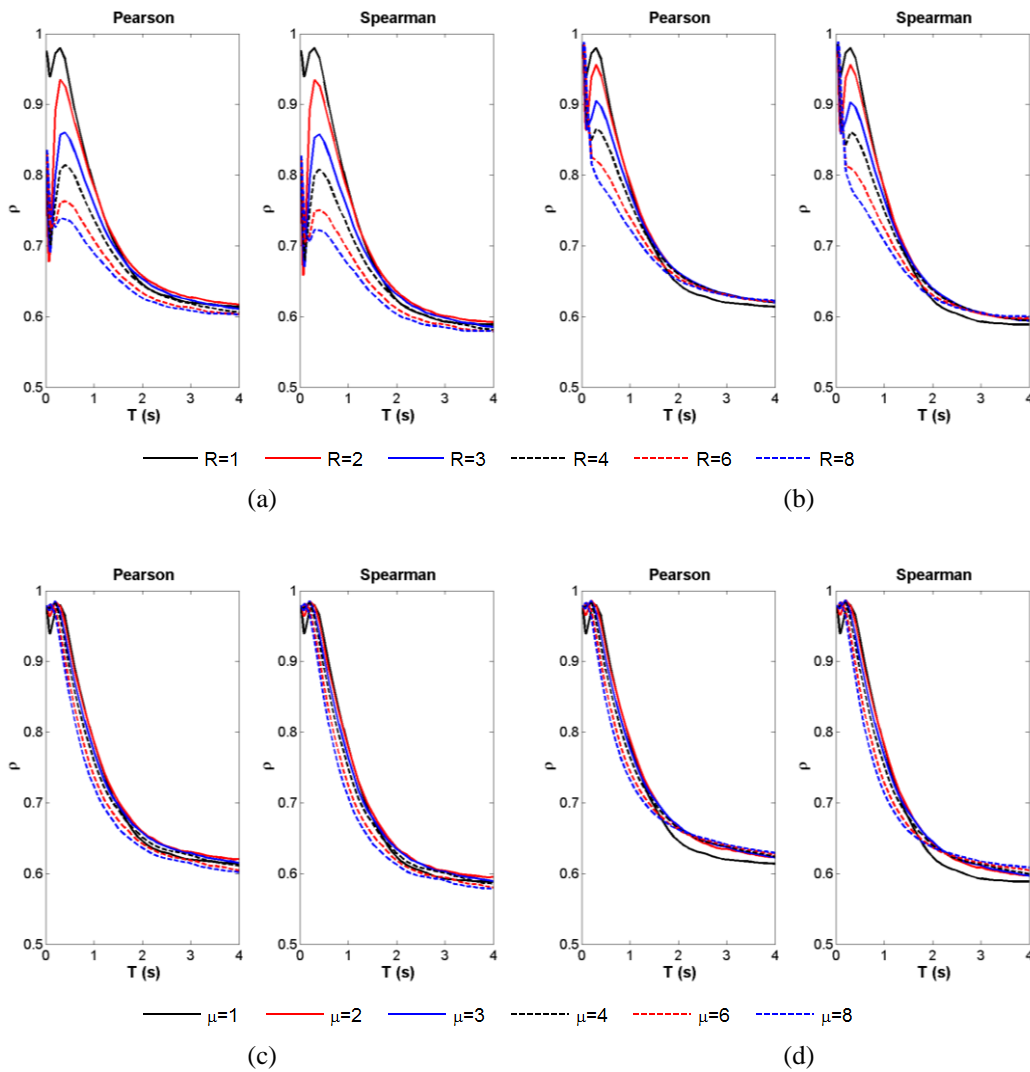Figure A.15. Variation of correlation coefficient values with period (correlation of IM **CAV** with EDP **SDOF top drift** for different R and μ cases (a) Elastic-Perfectly-Plastic, (b) Bilinear Hardening (α=5%), (c) Elastic-Perfectly-Plastic, (d) Bilinear Hardening (α=5%))
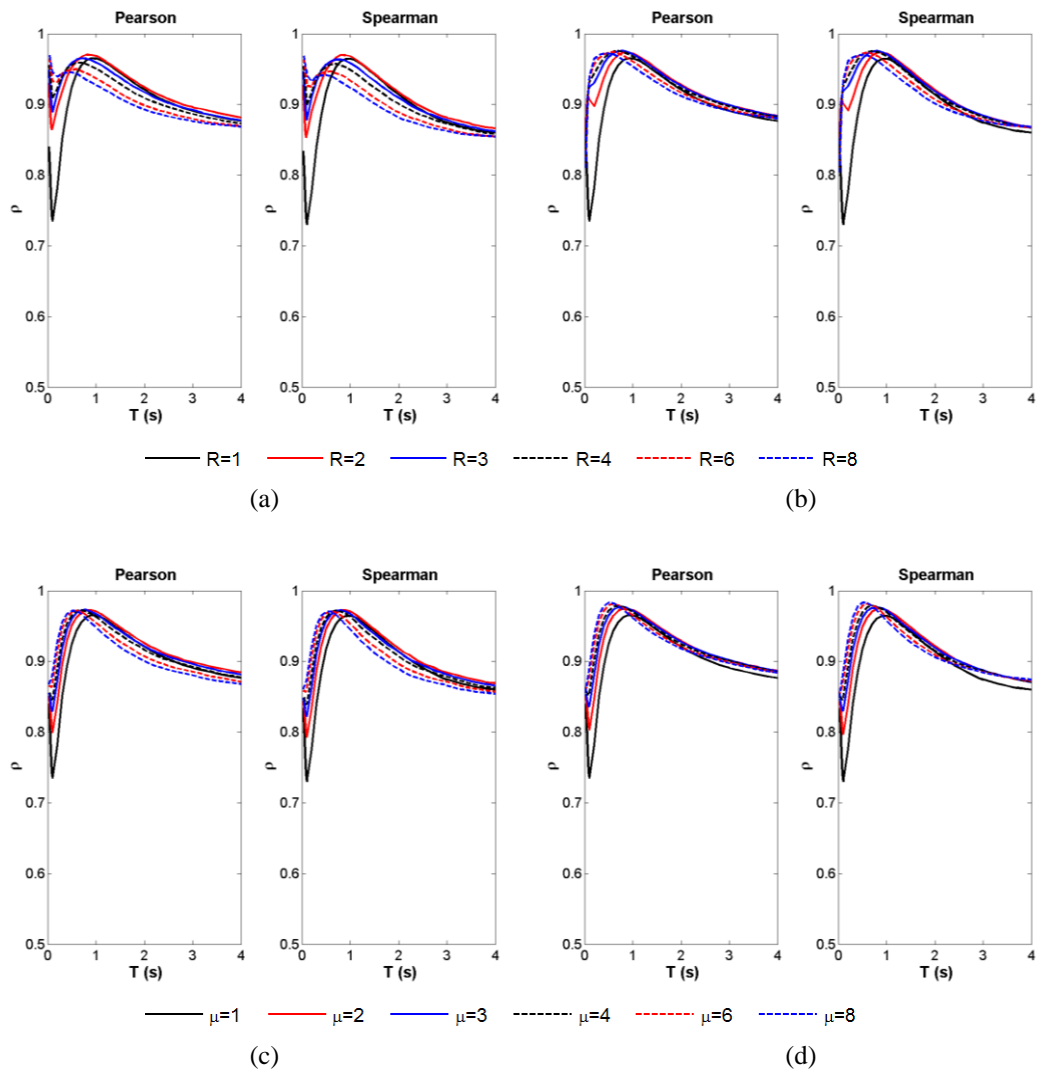
Figure A.16. Variation of correlation coefficient values with period (correlation of IM **ASI** with EDP **SDOF top drift** for different R and μ cases (a) Elastic-Perfectly-Plastic, (b) Bilinear Hardening (α=5%), (c) Elastic-Perfectly-Plastic, (d) Bilinear Hardening (α=5%))

Figure A.17. Variation of correlation coefficient values with period (correlation of IM **VSI** with EDP **SDOF top drift** for different R and μ cases (a) Elastic-Perfectly-Plastic, (b) Bilinear Hardening (α=5%), (c) Elastic-Perfectly-Plastic, (d) Bilinear Hardening (α=5%))

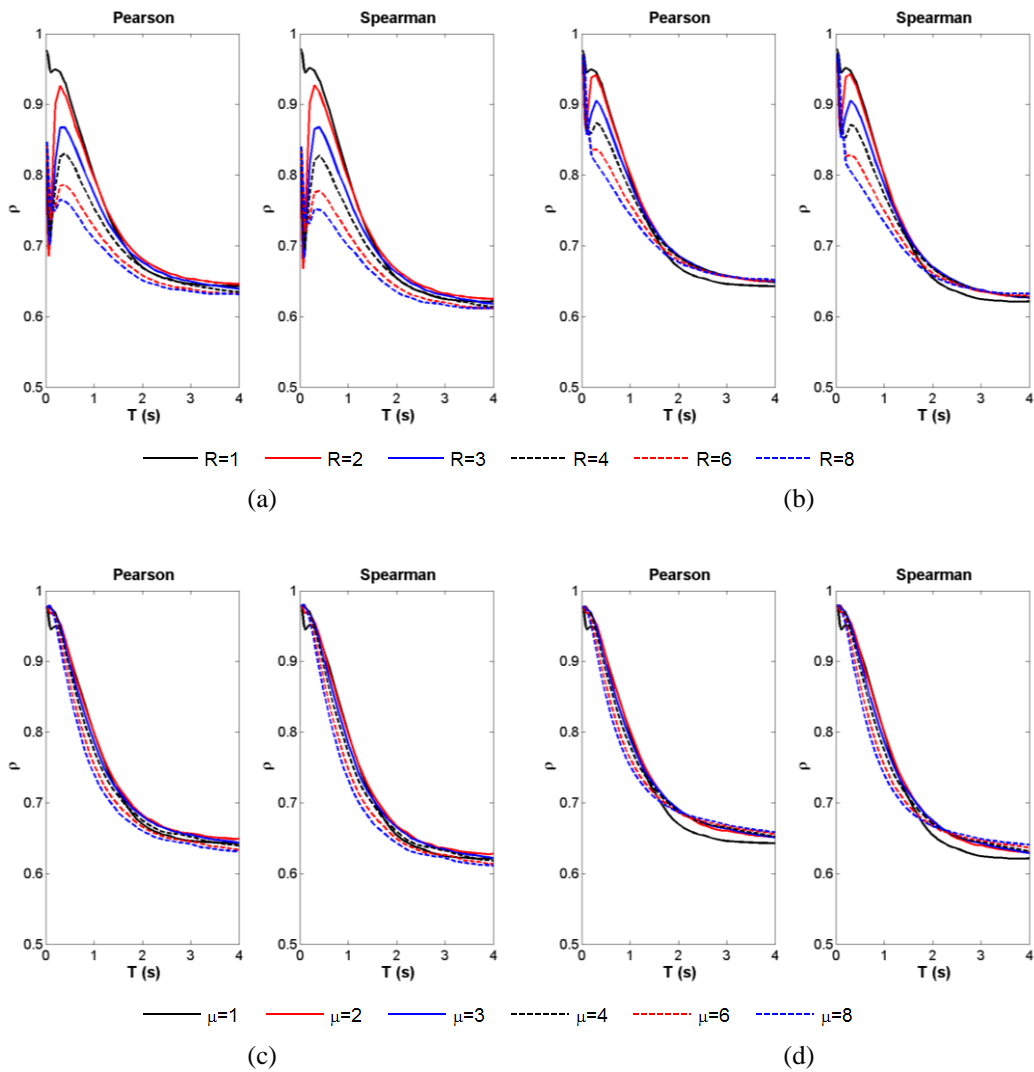Figure A.18. Variation of correlation coefficient values with period (correlation of IM **SMA** with EDP **SDOF top drift** for different R and μ cases (a) Elastic-Perfectly-Plastic, (b) Bilinear Hardening (α=5%), (c) Elastic-Perfectly-Plastic, (d) Bilinear Hardening (α=5%))
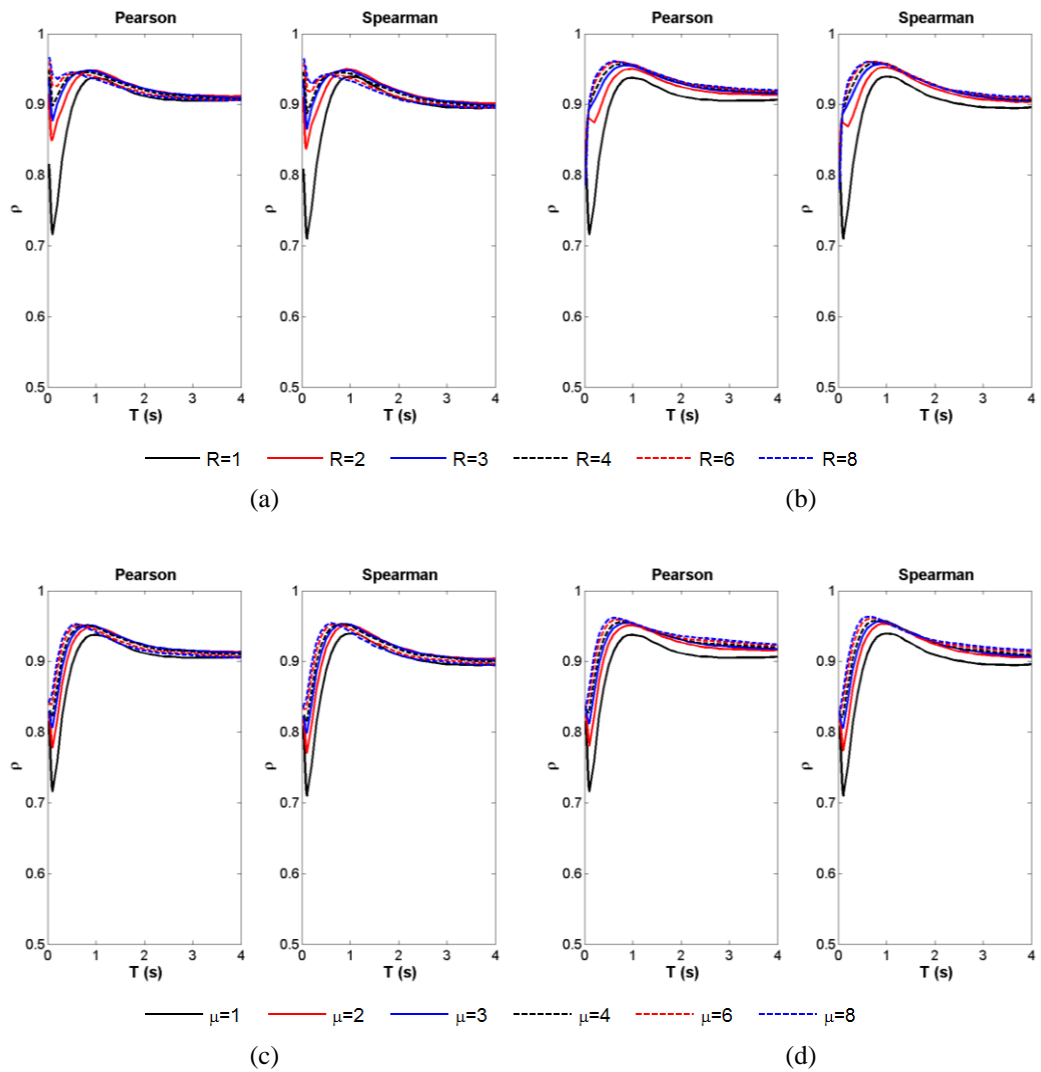
Figure A.19. Variation of correlation coefficient values with period (correlation of IM **SMV** with EDP **SDOF top drift** for different R and μ cases (a) Elastic-Perfectly-Plastic, (b) Bilinear Hardening (α=5%), (c) Elastic-Perfectly-Plastic, (d) Bilinear Hardening (α=5%))
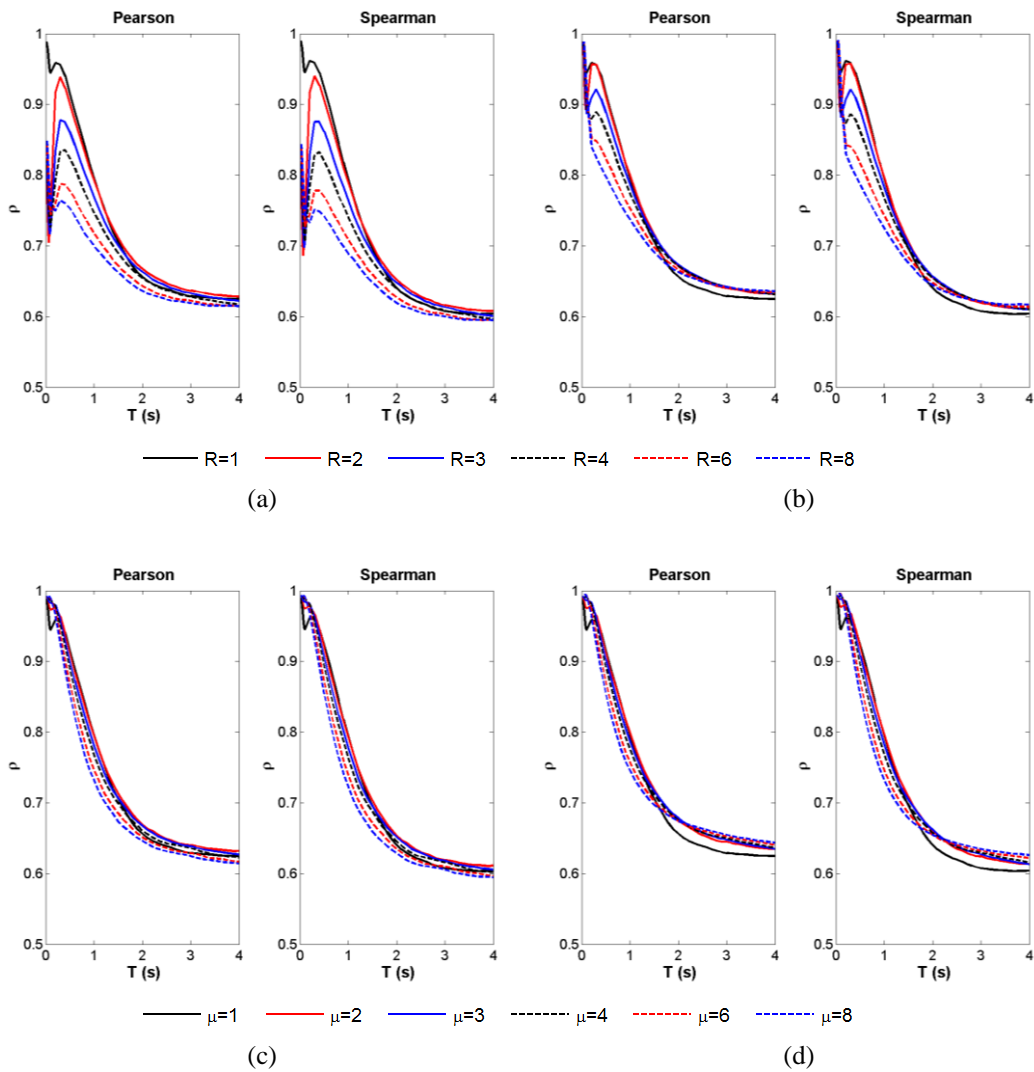
Figure A.20. Variation of correlation coefficient values with period (correlation of IM **EDA** with EDP **SDOF top drift** for different R and μ cases (a) Elastic-Perfectly-Plastic, (b) Bilinear Hardening (α=5%), (c) Elastic-Perfectly-Plastic, (d) Bilinear Hardening (α=5%))

238

Figure A.21. Variation of correlation coefficient values with period (correlation of IM A_{95} with EDP **SDOF top drift** for different R and μ cases (a) Elastic-Perfectly-Plastic, (b) Bilinear Hardening (α=5%), (c) Elastic-Perfectly-Plastic, (d) Bilinear Hardening (α=5%))
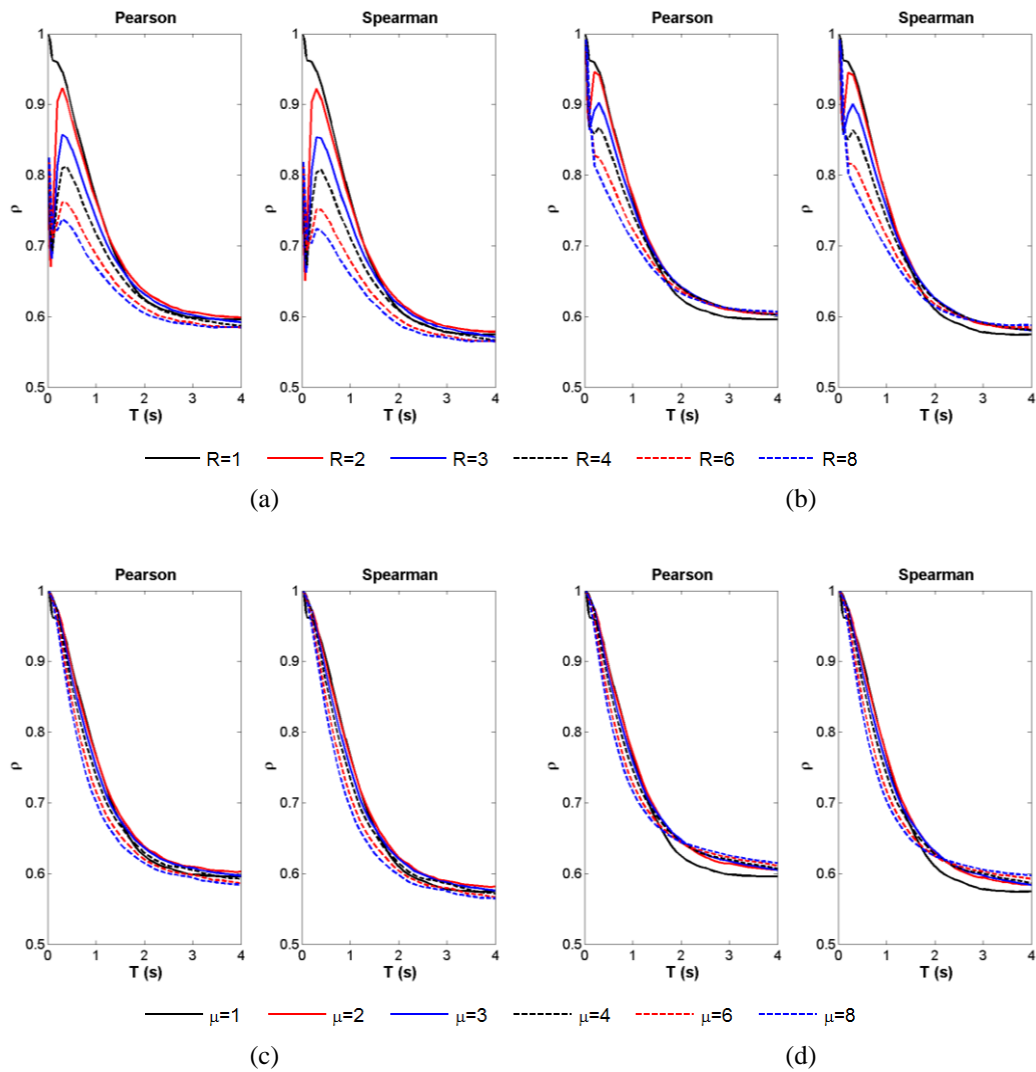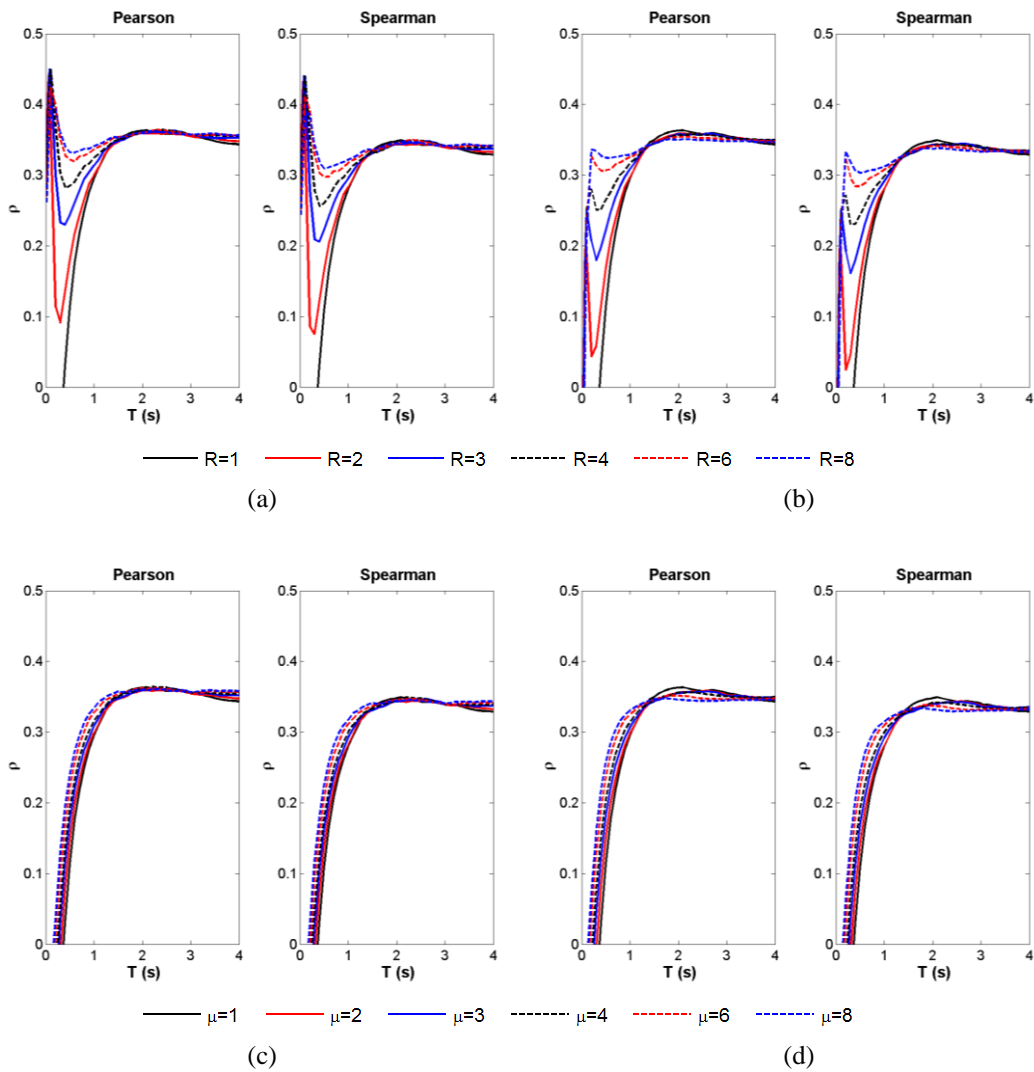
Figure A.22. Variation of correlation coefficient values with period (correlation of IM T_p with EDP **SDOF top drift** for different R and μ cases (a) Elastic-Perfectly-Plastic, (b) Bilinear Hardening (α=5%), (c) Elastic-Perfectly-Plastic, (d) Bilinear Hardening (α=5%))

Figure A.23. Variation of correlation coefficient values with period (correlation of IM $\mathbf{T_m}$ with EDP **SDOF top drift** for different R and μ cases (a) Elastic-Perfectly-Plastic, (b) Bilinear Hardening (α=5%), (c) Elastic-Perfectly-Plastic, (d) Bilinear Hardening (α=5%))

Figure A.24. Variation of correlation coefficient values with period (correlation of IM t_r with EDP **SDOF top drift** for different R and μ cases (a) Elastic-Perfectly-Plastic, (b) Bilinear Hardening ($\alpha=5\%$), (c) Elastic-Perfectly-Plastic, (d) Bilinear Hardening ($\alpha=5\%$))
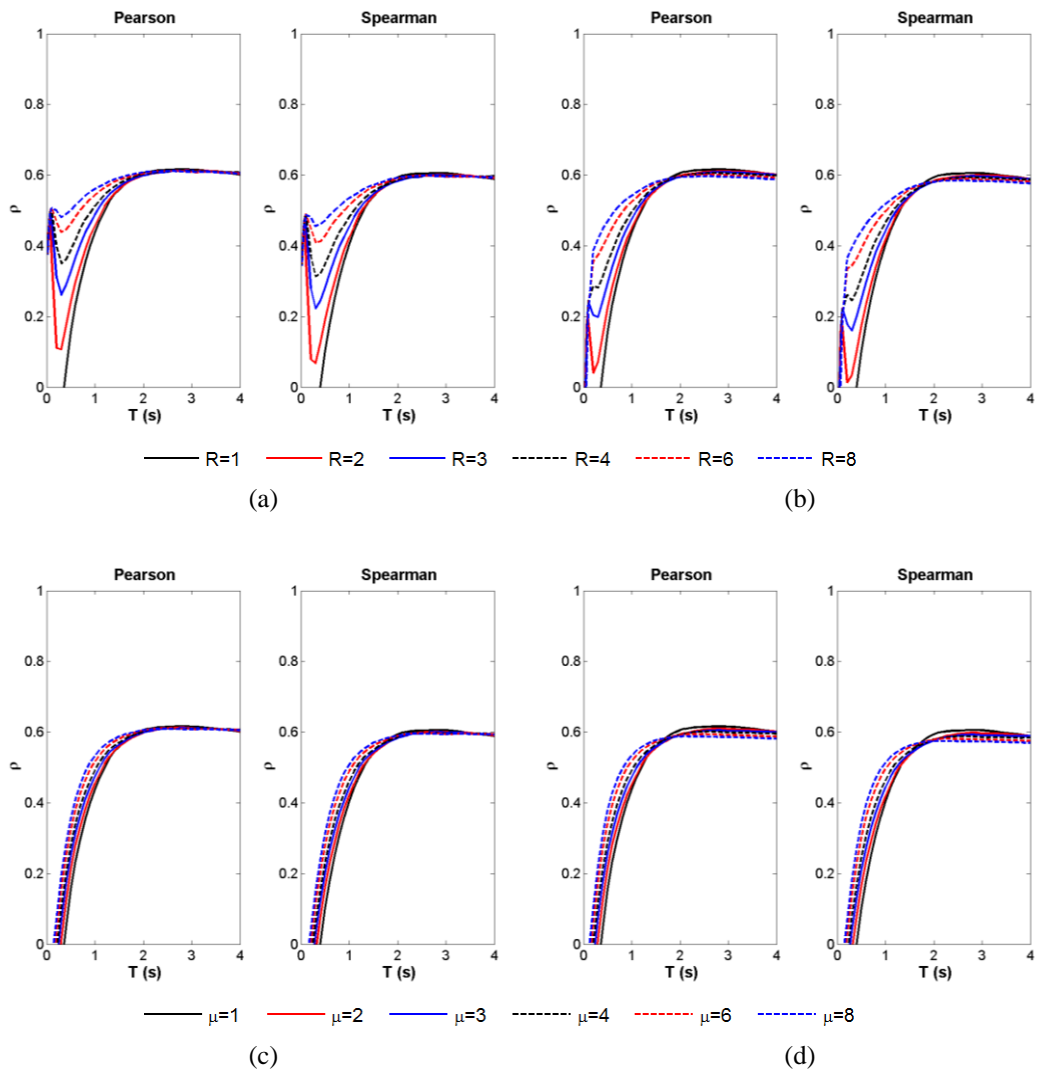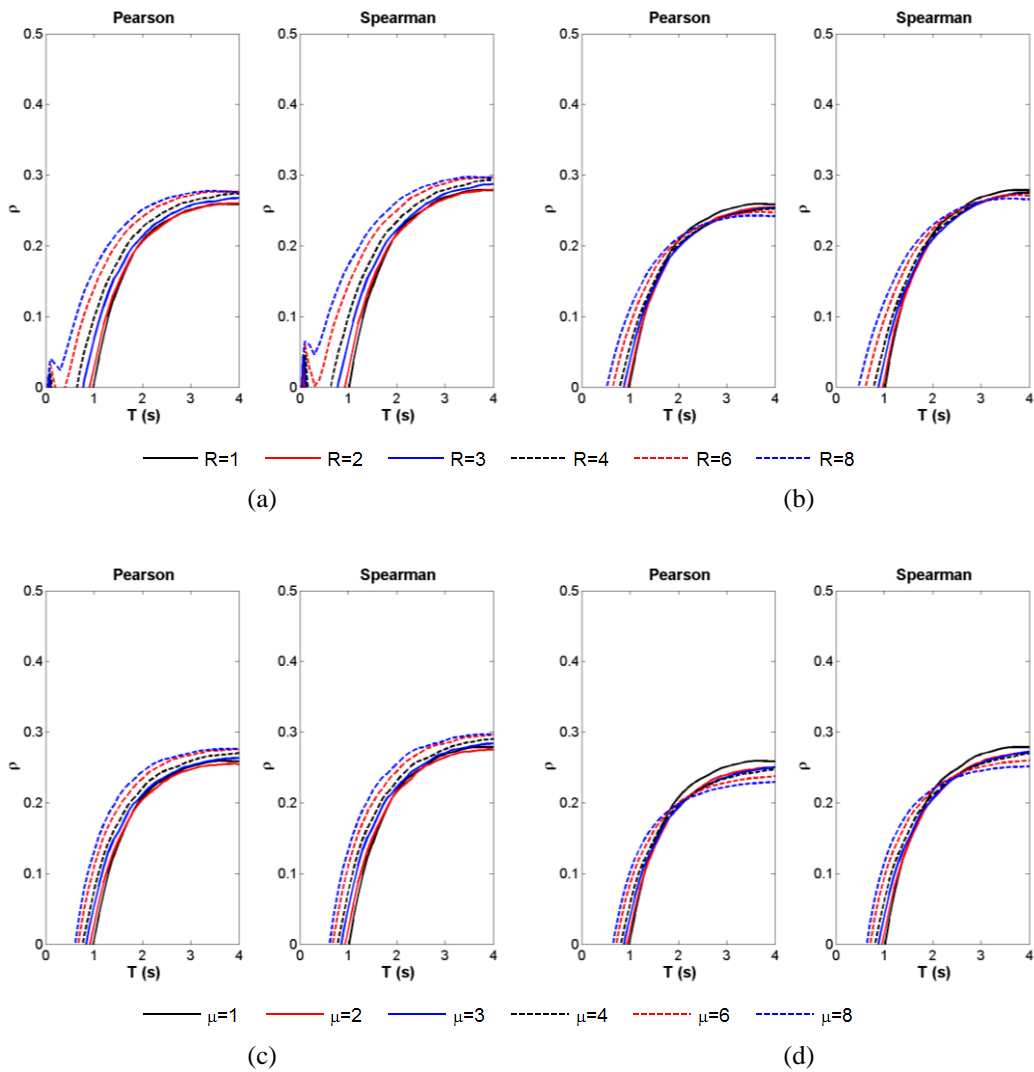
Figure A.25. Variation of correlation coefficient values with period (correlation of IM $\mathbf{I_C}$ with EDP **SDOF top drift** for different R and μ cases (a) Elastic-Perfectly-Plastic, (b) Bilinear Hardening (α=5%), (c) Elastic-Perfectly-Plastic, (d) Bilinear Hardening (α=5%))

Figure A.26. Variation of correlation coefficient values with period (correlation of IM I_a with EDP **SDOF top drift** for different R and μ cases (a) Elastic-Perfectly-Plastic, (b) Bilinear Hardening (α=5%), (c) Elastic-Perfectly-Plastic, (d) Bilinear Hardening (α=5%))
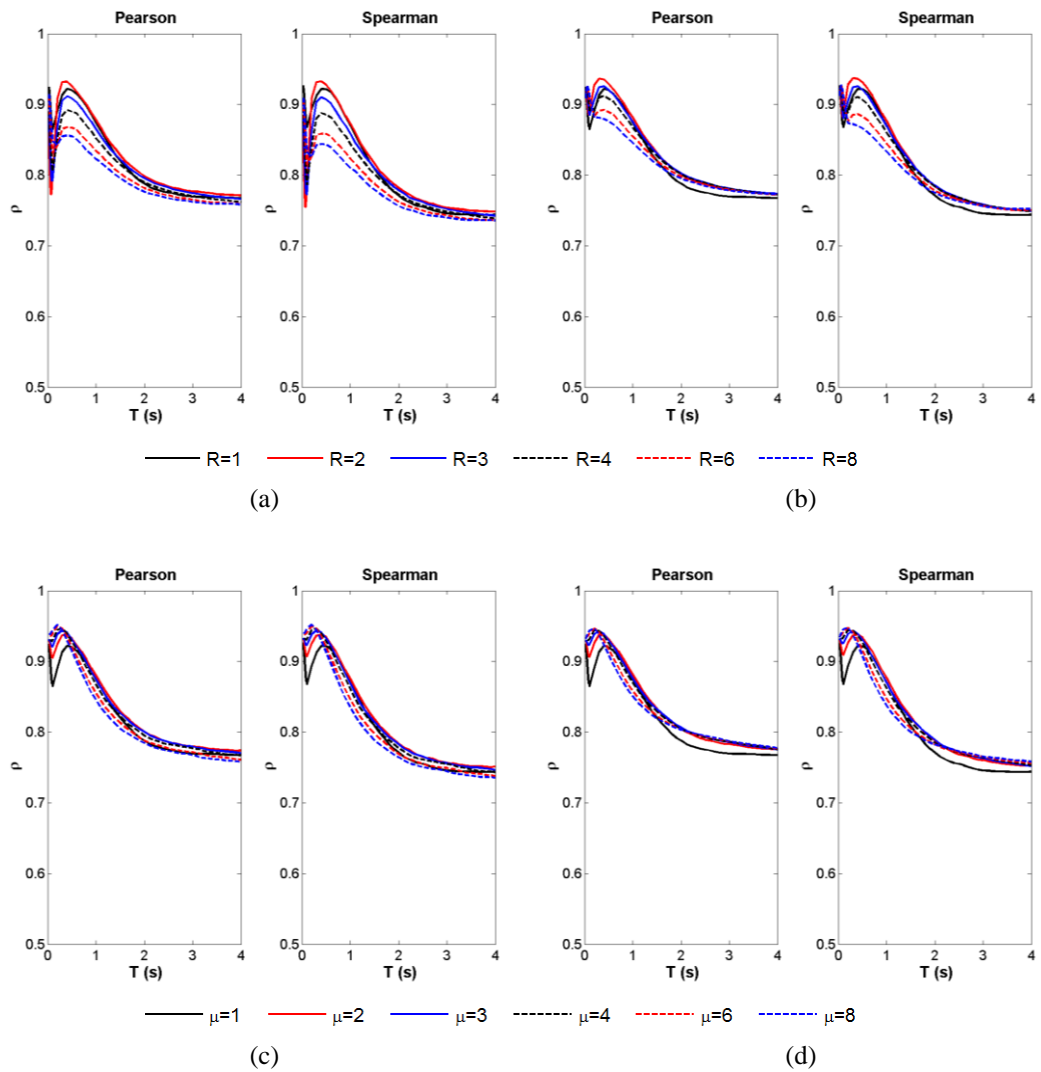
Figure A.27. Variation of correlation coefficient values with period (correlation of IM I_F with EDP **SDOF top drift** for different R and μ cases (a) Elastic-Perfectly-Plastic, (b) Bilinear Hardening (α=5%), (c) Elastic-Perfectly-Plastic, (d) Bilinear Hardening (α=5%))

Figure A.28. Variation of correlation coefficient values with period (correlation of IM I_v with EDP **SDOF top drift** for different R and μ cases (a) Elastic-Perfectly-Plastic, (b) Bilinear Hardening (α=5%), (c) Elastic-Perfectly-Plastic, (d) Bilinear Hardening (α=5%))
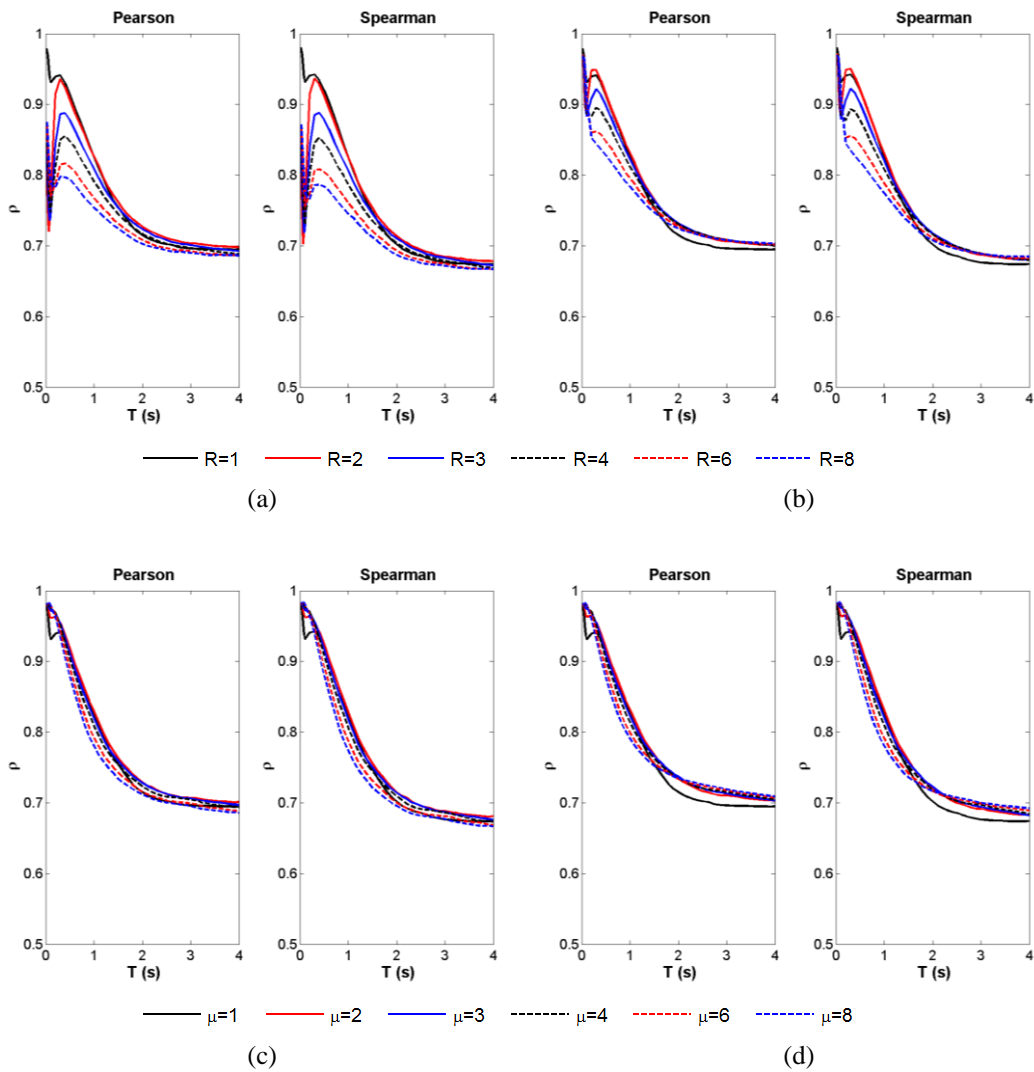
Figure A.29. Variation of correlation coefficient values with period (correlation of IM I_d with EDP **SDOF top drift** for different R and μ cases (a) Elastic-Perfectly-Plastic, (b) Bilinear Hardening (α=5%), (c) Elastic-Perfectly-Plastic, (d) Bilinear Hardening (α=5%))

Figure A.30. Variation of correlation coefficient values with period (correlation of IM **ASI*** with EDP **SDOF top drift** for different R and μ cases (a) Elastic-Perfectly-Plastic, (b) Bilinear Hardening (α=5%), (c) Elastic-Perfectly-Plastic, (d) Bilinear Hardening (α=5%))
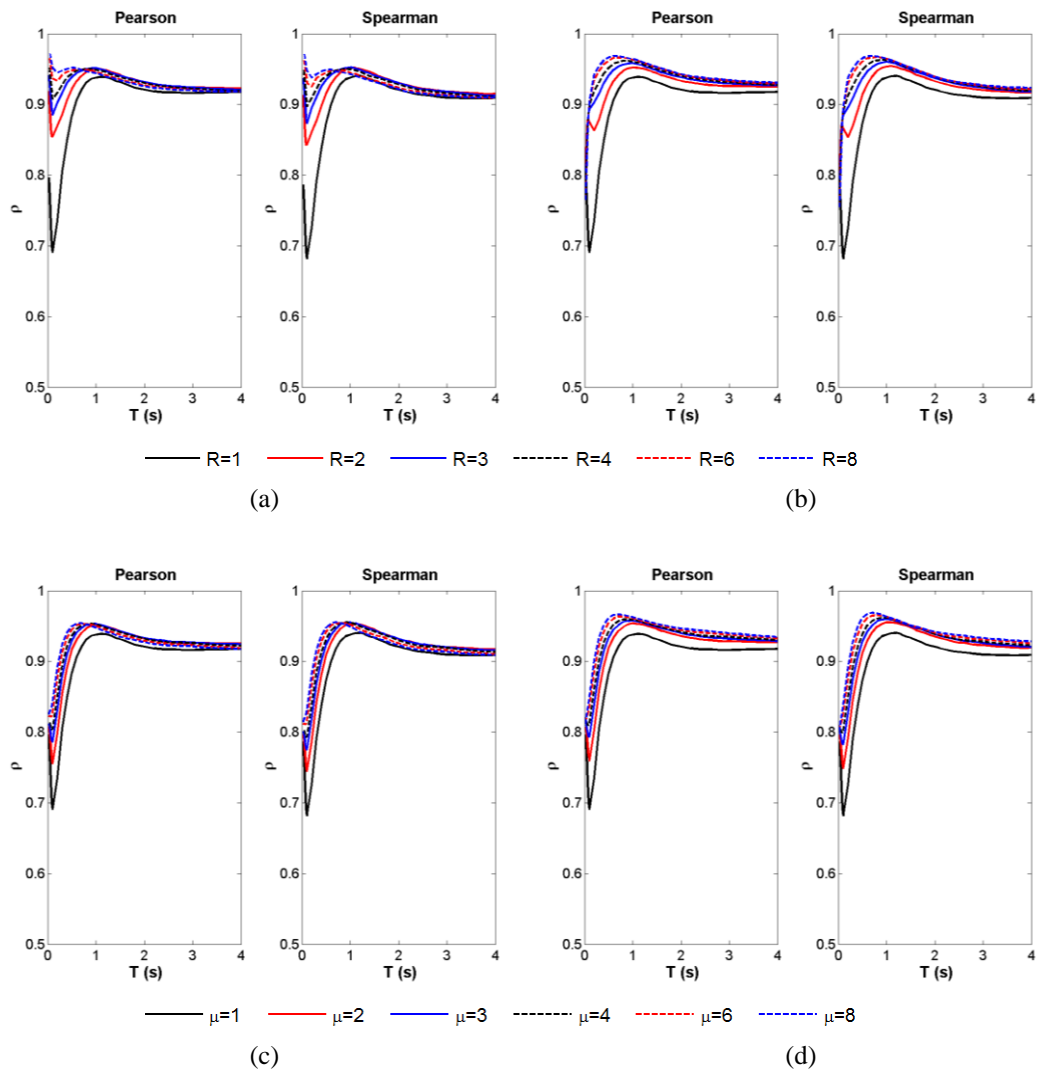
Figure A.31. Variation of correlation coefficient values with period (correlation of IM **EPA** with EDP **SDOF top drift** for different R and μ cases (a) Elastic-Perfectly-Plastic, (b) Bilinear Hardening (α=5%), (c) Elastic-Perfectly-Plastic, (d) Bilinear Hardening (α=5%))
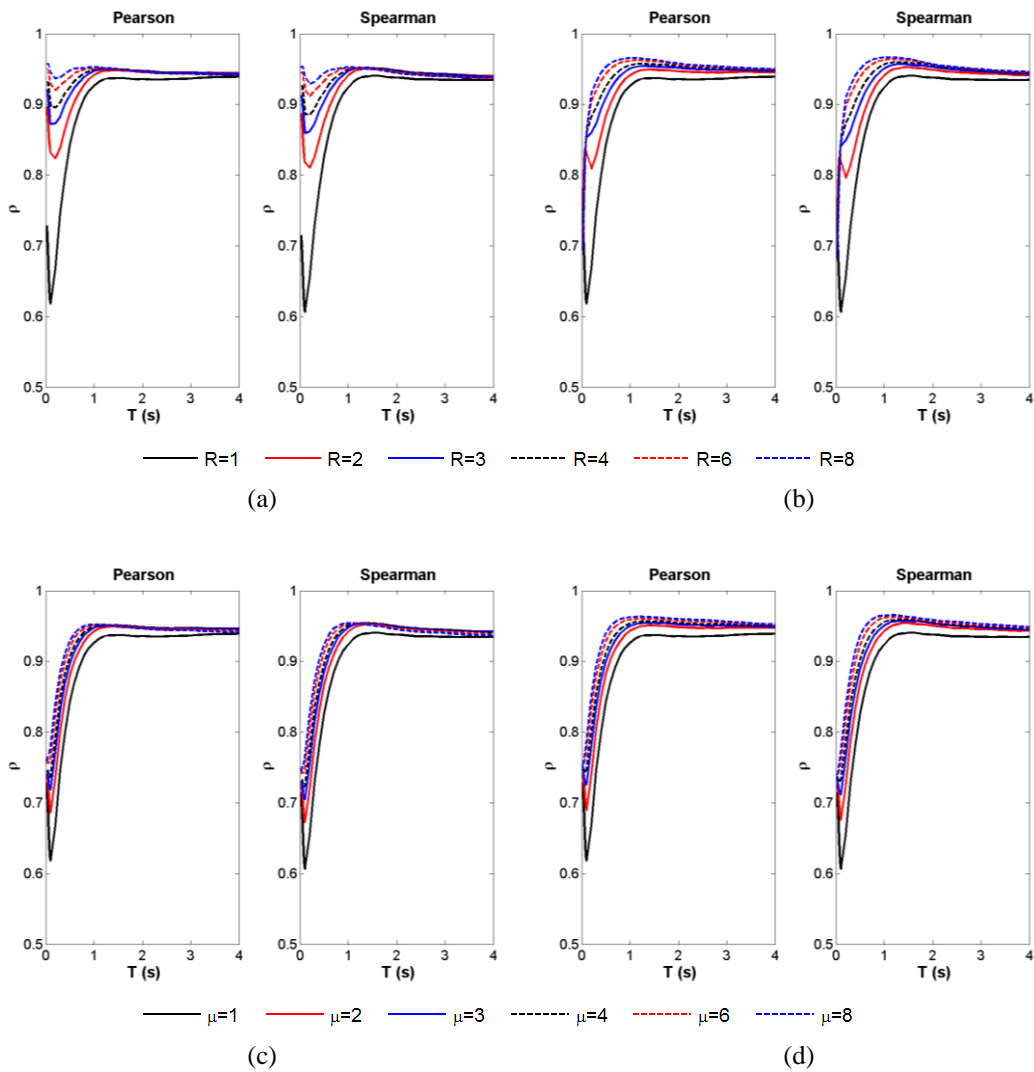
Figure A.32. Variation of correlation coefficient values with period (correlation of IM **EPV** with EDP **SDOF top drift** for different R and μ cases (a) Elastic-Perfectly-Plastic, (b) Bilinear Hardening (α=5%), (c) Elastic-Perfectly-Plastic, (d) Bilinear Hardening (α=5%))
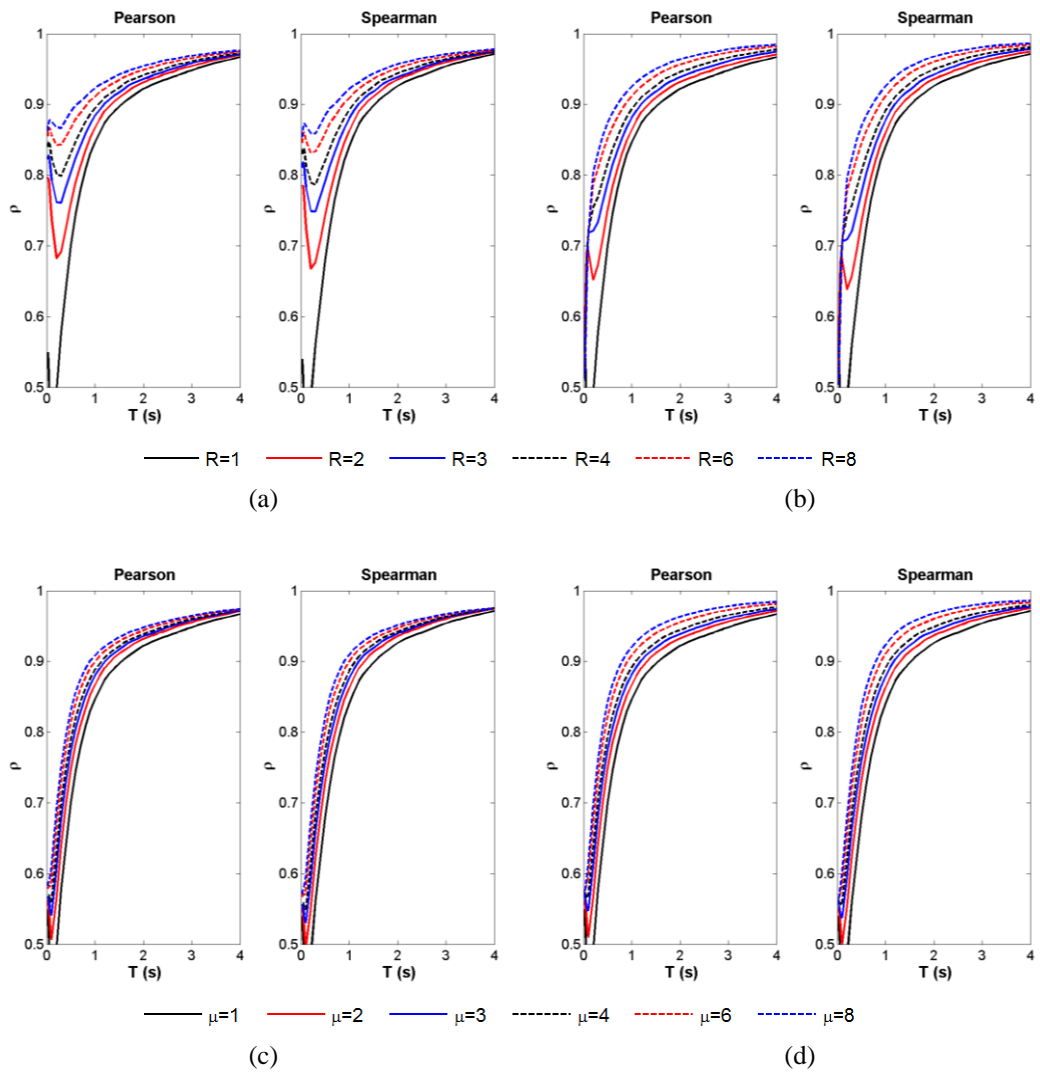
Figure A.33. Variation of correlation coefficient values with period (correlation of IM S_a with EDP **SDOF top drift** for different R and μ cases (a) Elastic-Perfectly-Plastic, (b) Bilinear Hardening (α=5%), (c) Elastic-Perfectly-Plastic, (d) Bilinear Hardening (α=5%))

Figure A.34. Variation of correlation coefficient values with period (correlation of IM S_v with EDP **SDOF top drift** for different R and μ cases (a) Elastic-Perfectly-Plastic, (b) Bilinear Hardening (α=5%), (c) Elastic-Perfectly-Plastic, (d) Bilinear Hardening (α=5%))
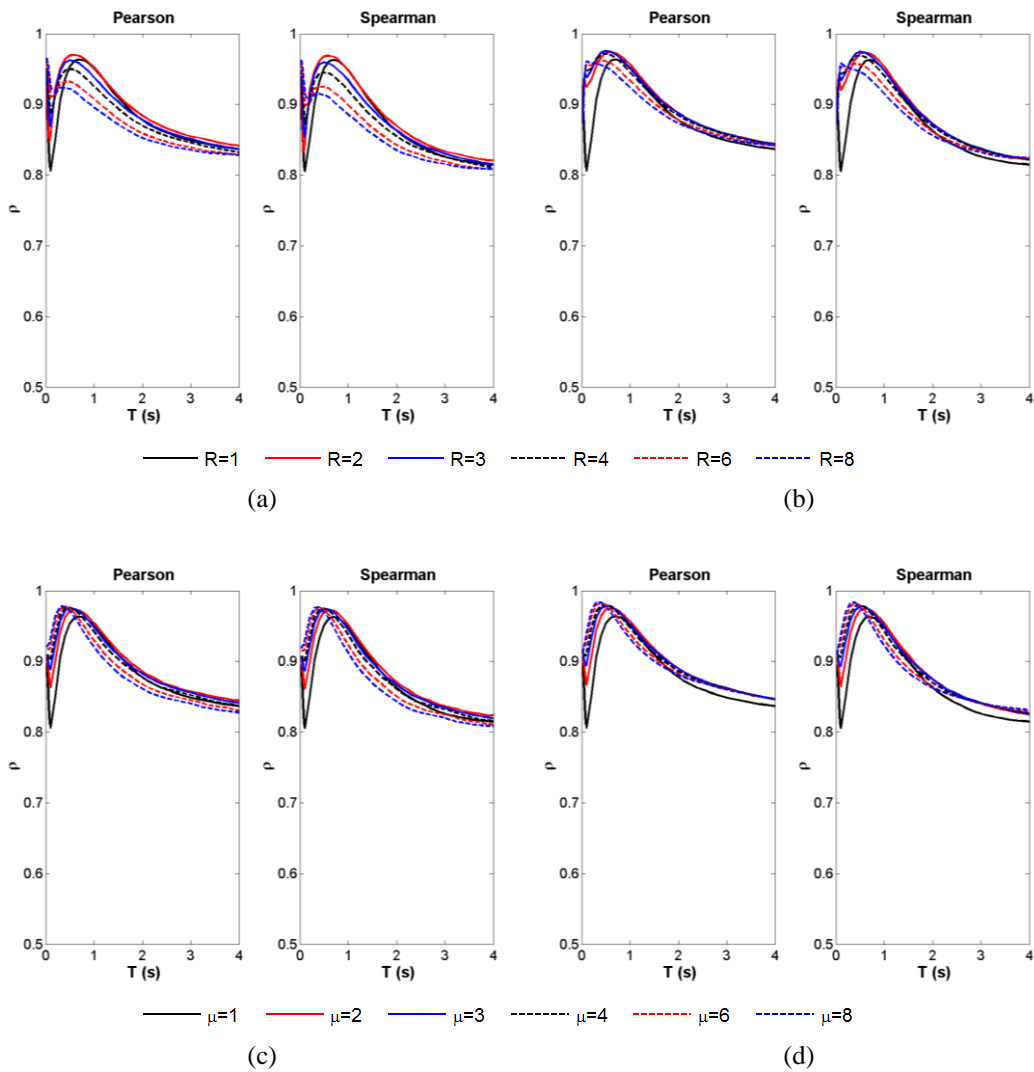
252

Figure A.35. Variation of correlation coefficient values with period (correlation of IM S_d with EDP **SDOF top drift** for different R and μ cases (a) Elastic-Perfectly-Plastic, (b) Bilinear Hardening (α=5%), (c) Elastic-Perfectly-Plastic, (d) Bilinear Hardening (α=5%))
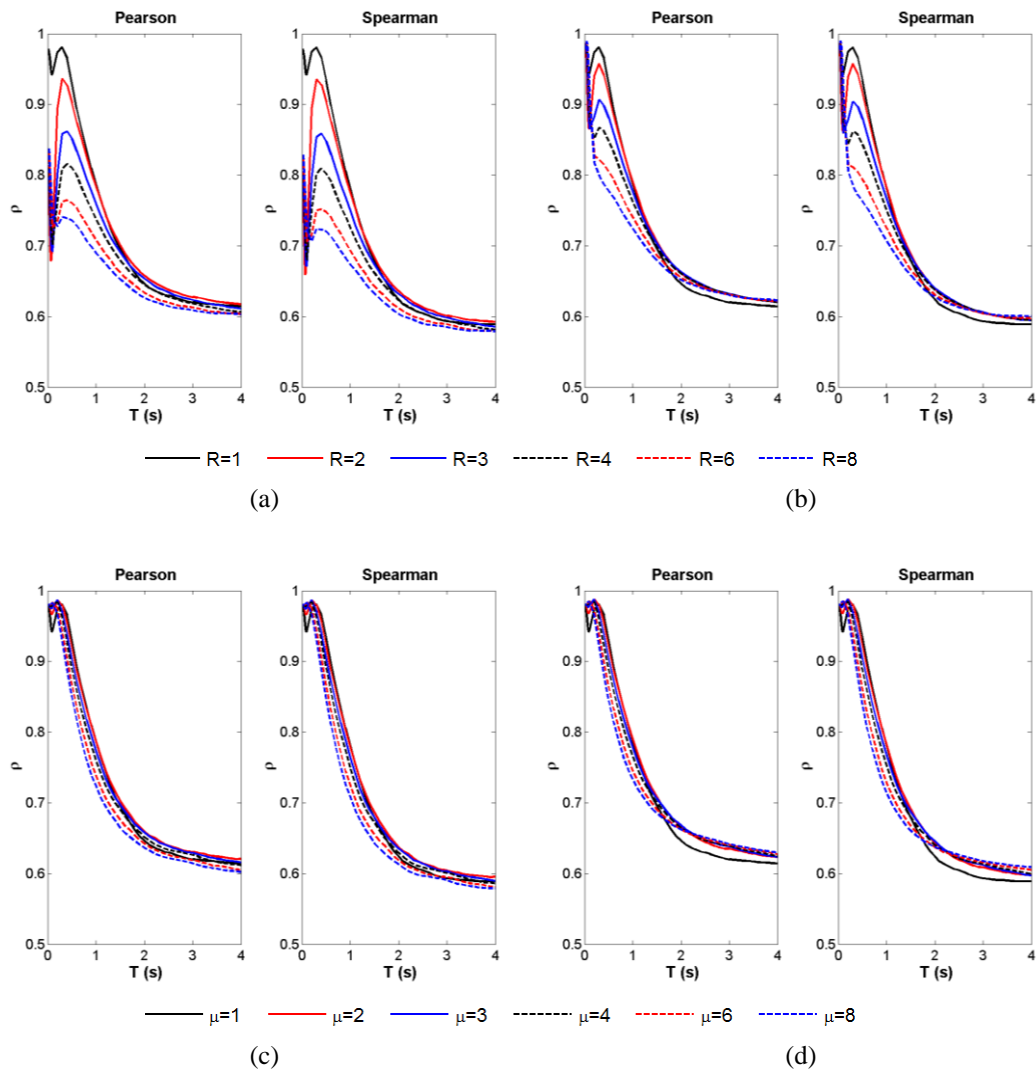
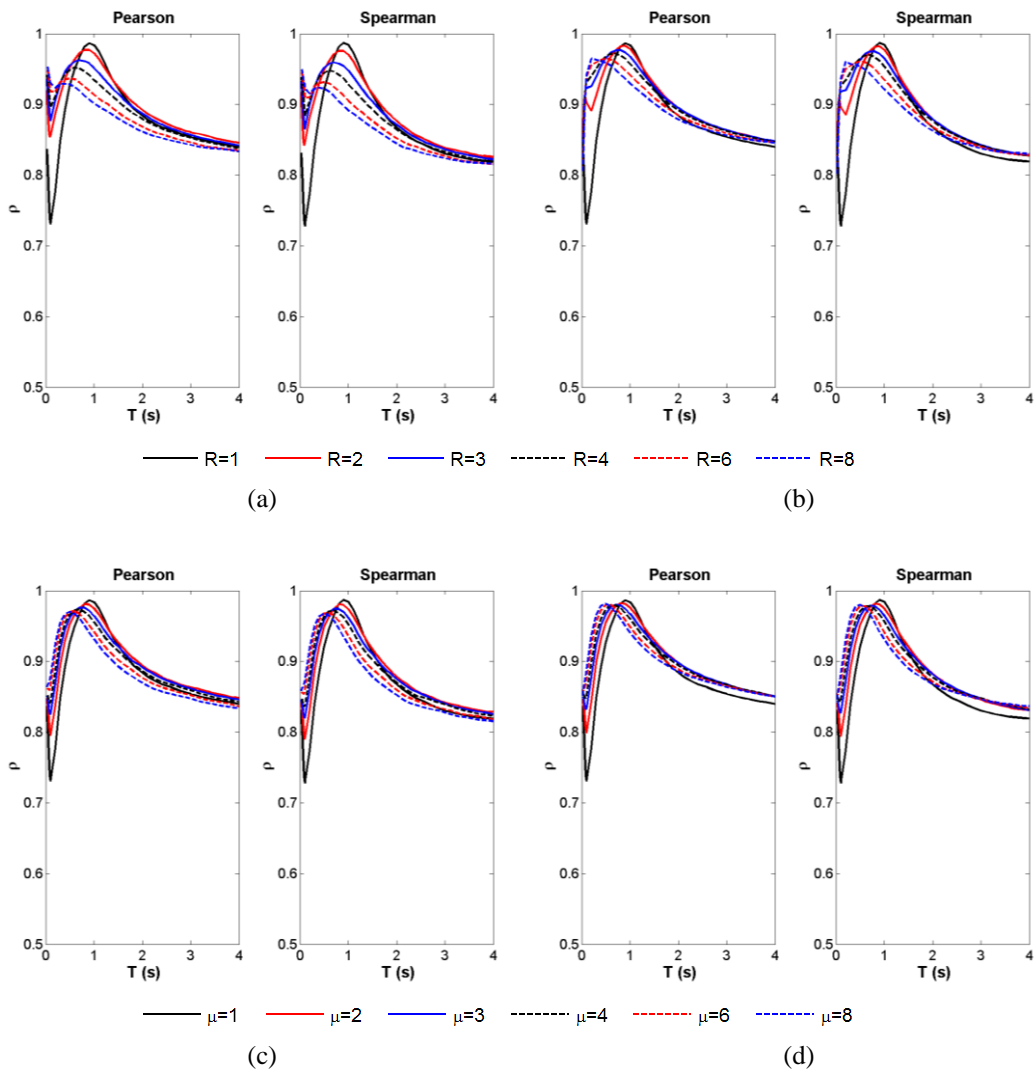Figure A.36. Variation of correlation coefficient values with period (correlation of IM **PGA** with EDP **SDOF top drift** for different η cases (a) Elastic-Perfectly-Plastic and (b) Bilinear Hardening (α=5%))

Figure A.37. Variation of correlation coefficient values with period (correlation of IM **PGV** with EDP **SDOF top drift** for different η cases (a) Elastic-Perfectly-Plastic and (b) Bilinear Hardening (α=5%))

Figure A.38. Variation of correlation coefficient values with period (correlation of IM **PGD** with EDP **SDOF top drift** for different η cases (a) Elastic-Perfectly-Plastic and (b) Bilinear Hardening (α=5%))

Figure A.39. Variation of correlation coefficient values with period (correlation of IM **PGV/PGA** with EDP **SDOF top drift** for different η cases (a) Elastic-Perfectly-Plastic and (b) Bilinear Hardening (α=5%))
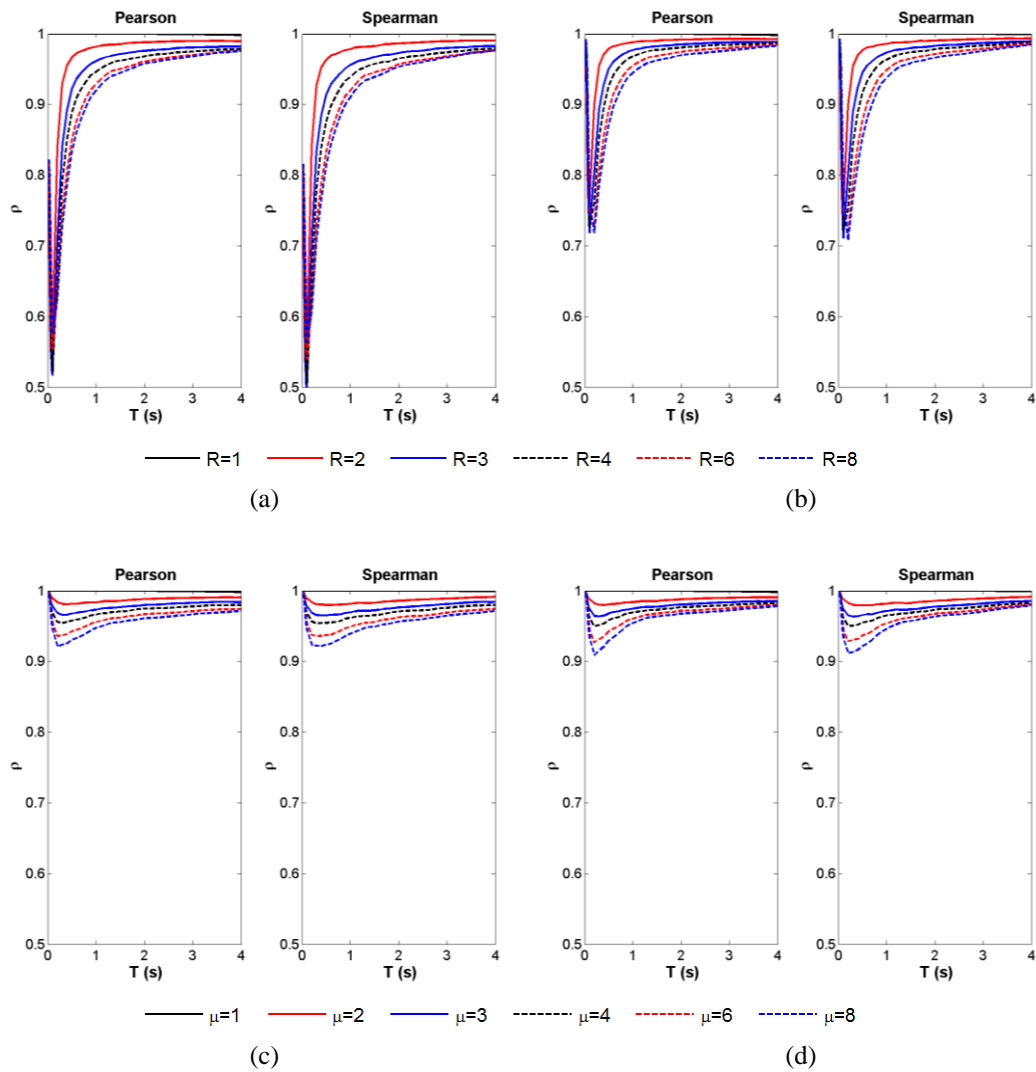
Figure A.40. Variation of correlation coefficient values with period (correlation of IM **a_rms** with EDP **SDOF top drift** for different η cases (a) Elastic-Perfectly-Plastic and (b) Bilinear Hardening (α=5%))

Figure A.41. Variation of correlation coefficient values with period (correlation of IM **v_rms** with EDP **SDOF top drift** for different η cases (a) Elastic-Perfectly-Plastic and (b) Bilinear Hardening (α=5%))
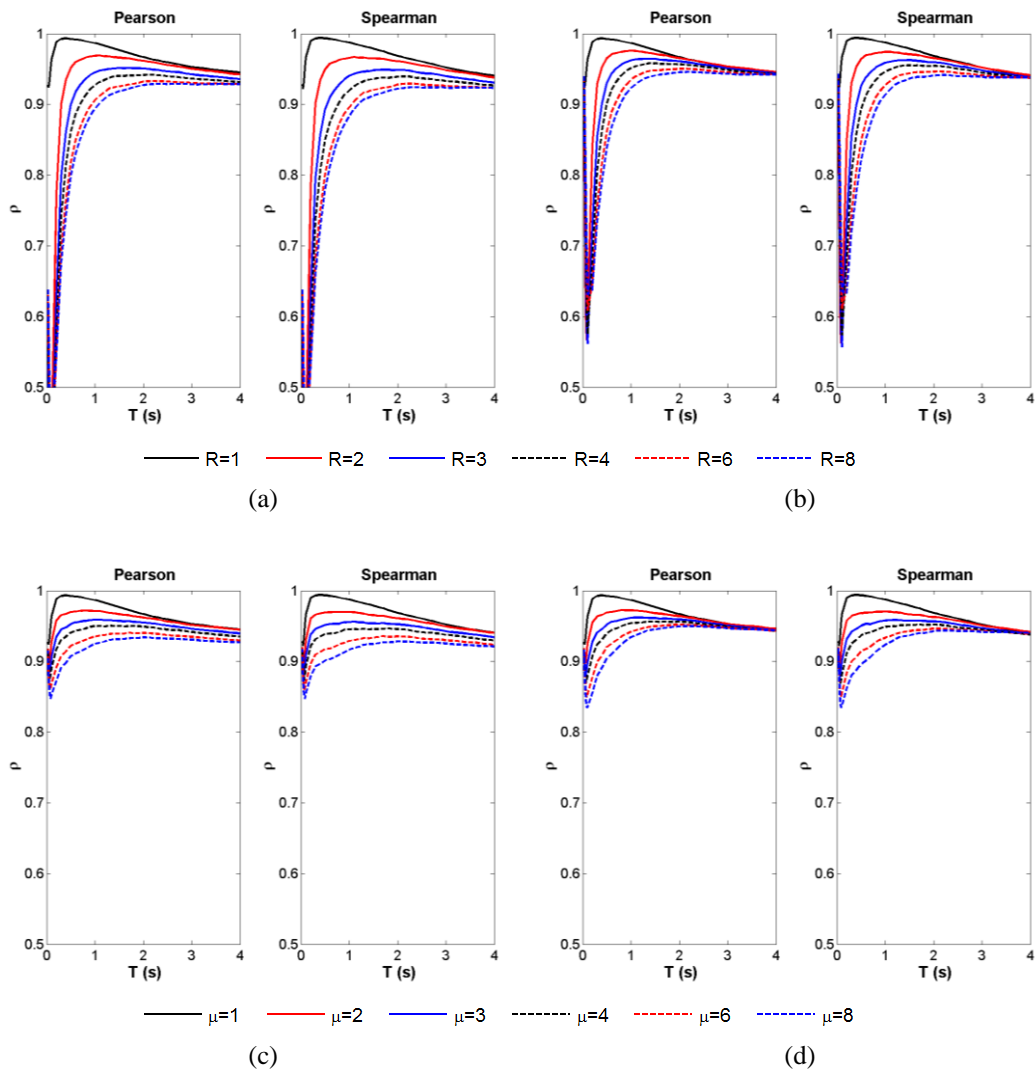
Figure A.42. Variation of correlation coefficient values with period (correlation of IM **d_{rms}** with EDP **SDOF top drift** for different η cases (a) Elastic-Perfectly-Plastic and (b) Bilinear Hardening (α=5%))

Figure A.43. Variation of correlation coefficient values with period (correlation of IM **AI** with EDP **SDOF top drift** for different η cases (a) Elastic-Perfectly-Plastic and (b) Bilinear Hardening (α=5%))
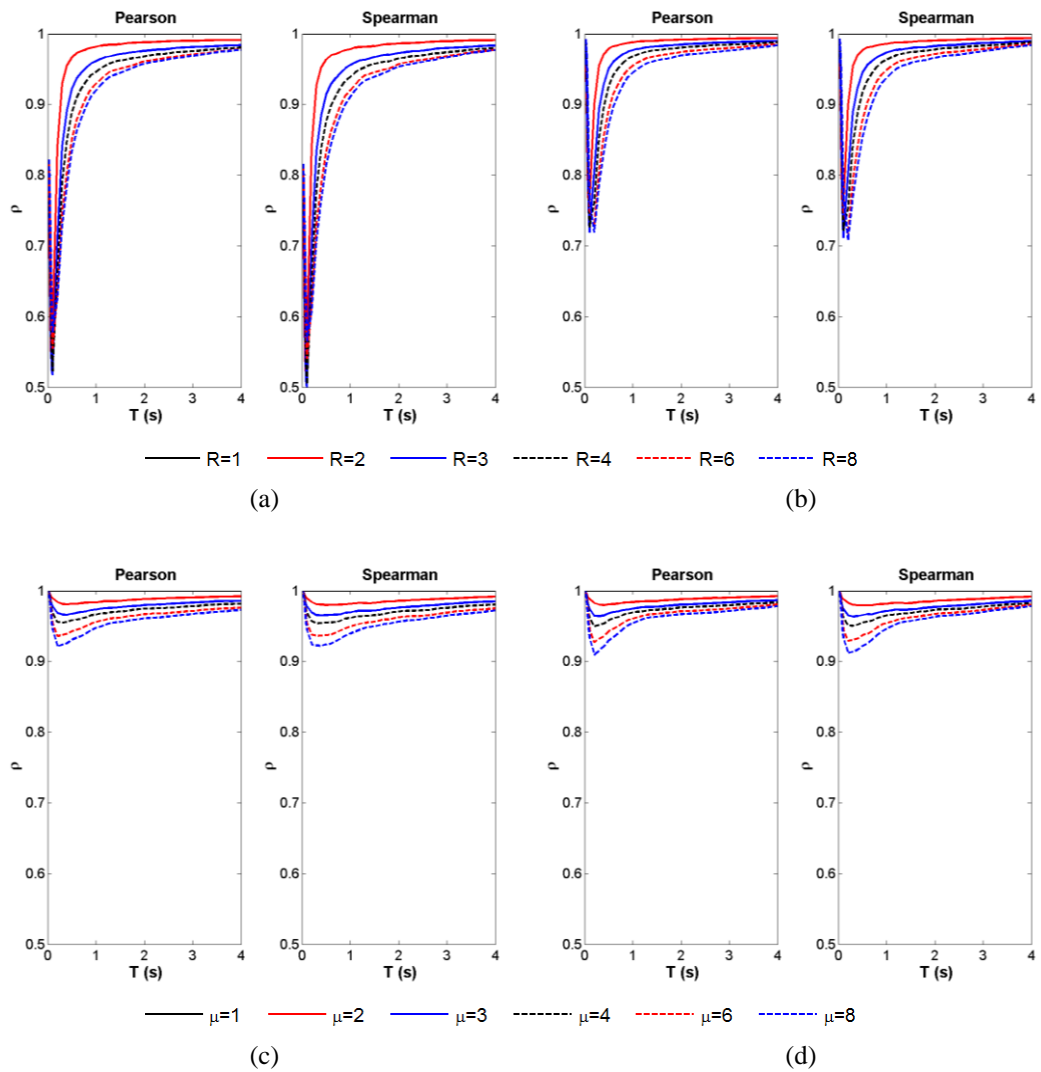
Figure A.44. Variation of correlation coefficient values with period (correlation of IM **Ic*** with EDP **SDOF top drift** for different η cases (a) Elastic-Perfectly-Plastic and (b) Bilinear Hardening (α=5%))

Figure A.45. Variation of correlation coefficient values with period (correlation of IM **SED** with EDP **SDOF top drift** for different η cases (a) Elastic-Perfectly-Plastic and (b) Bilinear Hardening (α=5%))
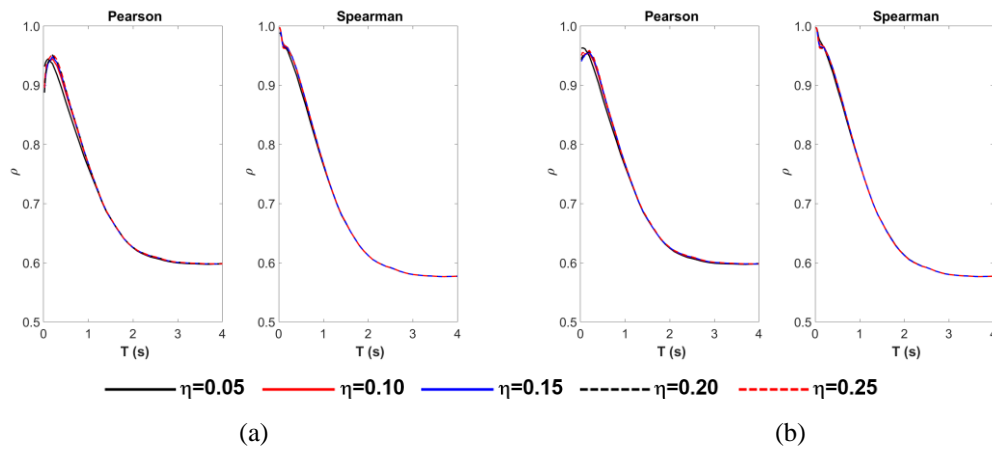
Figure A.46. Variation of correlation coefficient values with period (correlation of IM **CAV** with EDP **SDOF top drift** for different η cases (a) Elastic-Perfectly-Plastic and (b) Bilinear Hardening (α=5%))
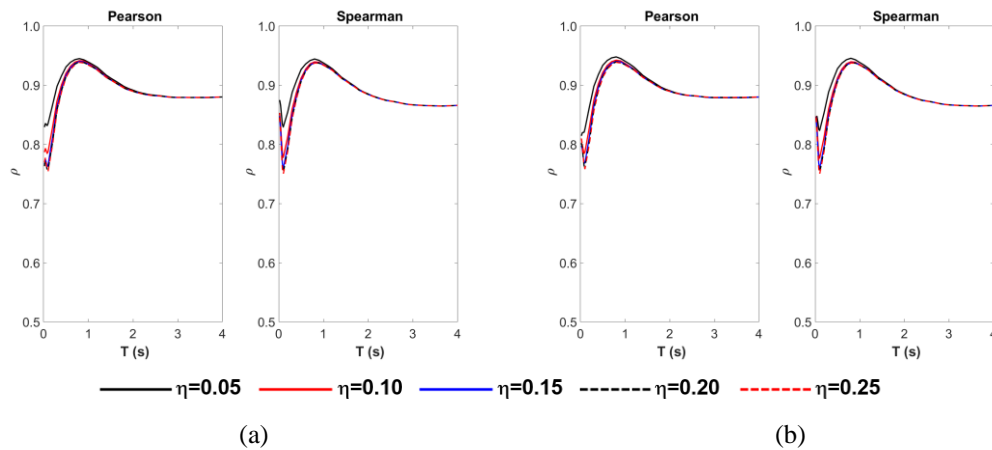

Figure A.47. Variation of correlation coefficient values with period (correlation of IM **ASI** with EDP **SDOF top drift** for different η cases (a) Elastic-Perfectly-Plastic and (b) Bilinear Hardening (α=5%))

259

Figure A.48. Variation of correlation coefficient values with period (correlation of IM **VSI** with EDP **SDOF top drift** for different η cases (a) Elastic-Perfectly-Plastic and (b) Bilinear Hardening (α=5%))
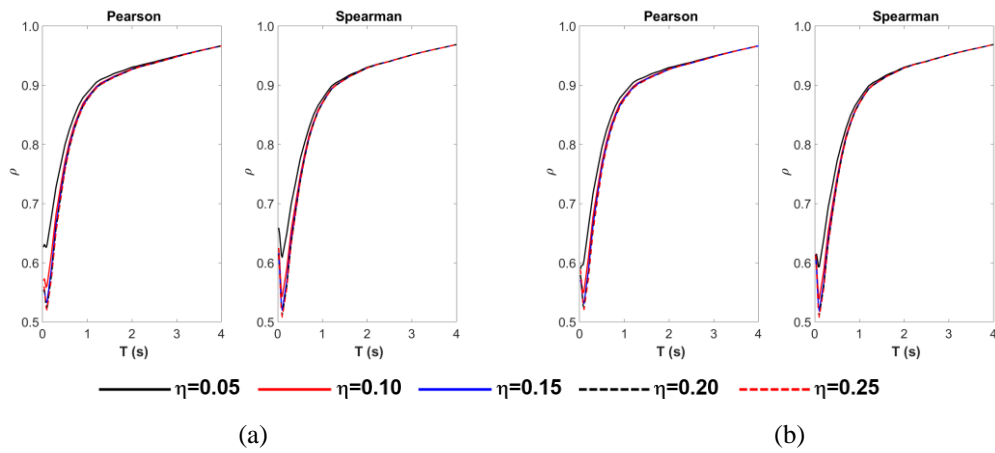

Figure A.49. Variation of correlation coefficient values with period (correlation of IM **SMA** with EDP **SDOF top drift** for different η cases (a) Elastic-Perfectly-Plastic and (b) Bilinear Hardening (α=5%))

260
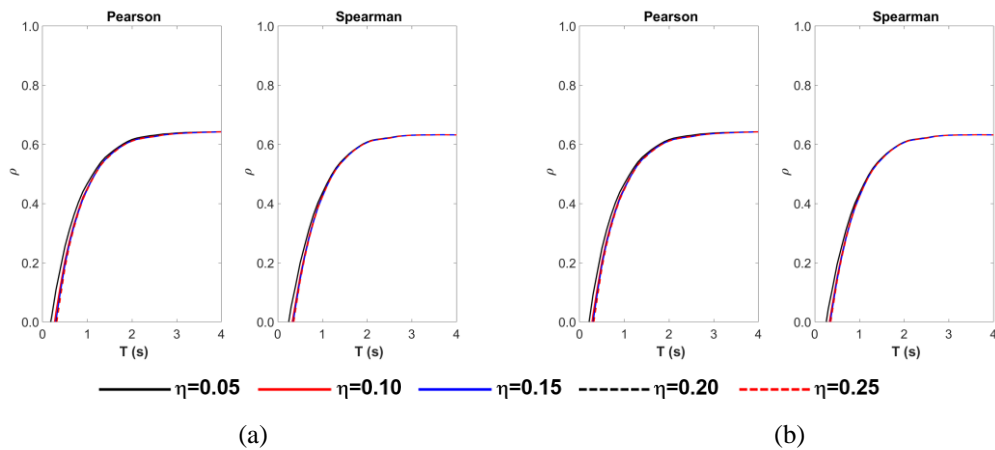
Figure A.50. Variation of correlation coefficient values with period (correlation of IM **SMV** with EDP **SDOF top drift** for different η cases (a) Elastic-Perfectly-Plastic and (b) Bilinear Hardening (α=5%))

Figure A.51. Variation of correlation coefficient values with period (correlation of IM **EDA** with EDP **SDOF top drift** for different η cases (a) Elastic-Perfectly-Plastic and (b) Bilinear Hardening (α=5%))
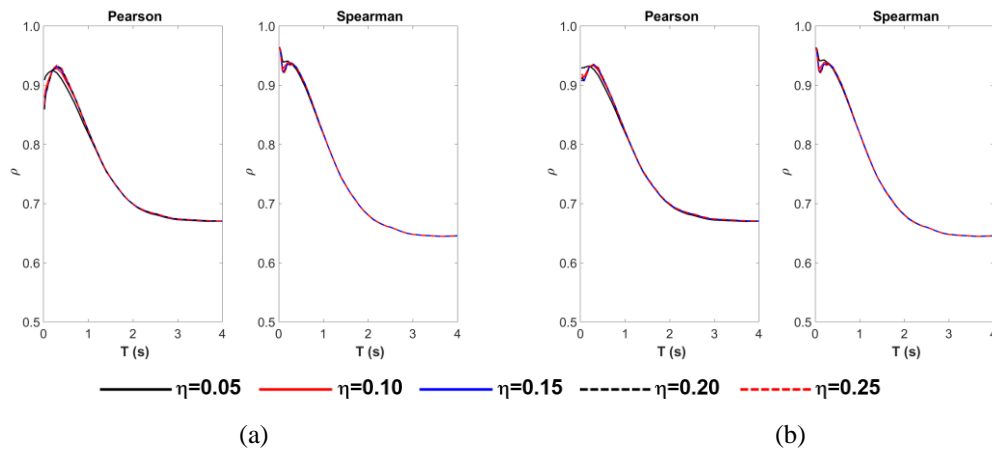
Figure A.52. Variation of correlation coefficient values with period (correlation of IM A_{95} with EDP **SDOF top drift** for different η cases (a) Elastic-Perfectly-Plastic and (b) Bilinear Hardening (α=5%))

Figure A.53. Variation of correlation coefficient values with period (correlation of IM T_p with EDP **SDOF top drift** for different η cases (a) Elastic-Perfectly-Plastic and (b) Bilinear Hardening (α=5%))
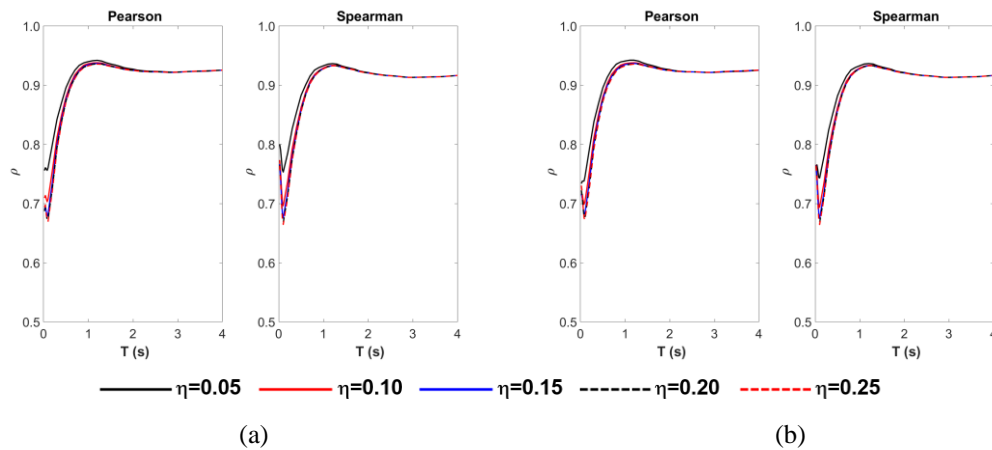
Figure A.54. Variation of correlation coefficient values with period (correlation of IM $\mathbf{T_m}$ with EDP **SDOF top drift** for different η cases (a) Elastic-Perfectly-Plastic and (b) Bilinear Hardening (α=5%))

Figure A.55. Variation of correlation coefficient values with period (correlation of IM $\mathbf{t_r}$ with EDP **SDOF top drift** for different η cases (a) Elastic-Perfectly-Plastic and (b) Bilinear Hardening (α=5%))
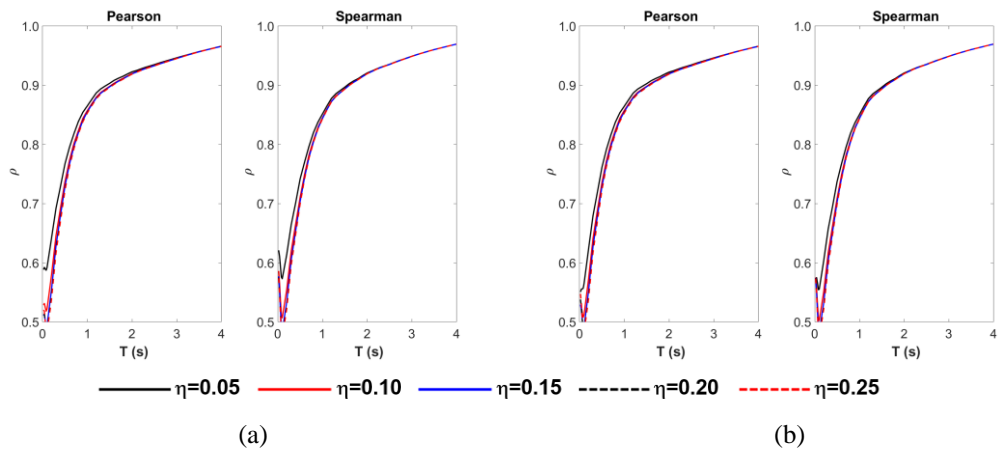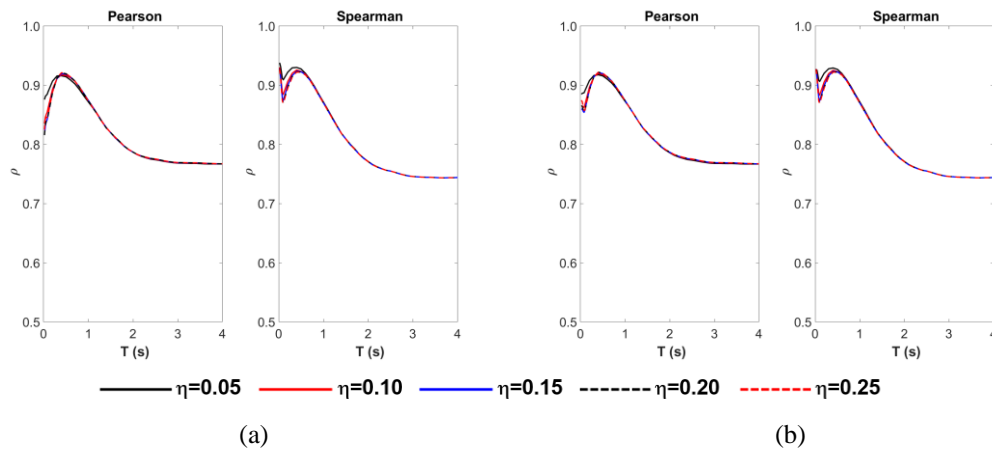
Figure A.56. Variation of correlation coefficient values with period (correlation of IM I_C with EDP **SDOF top drift** for different η cases (a) Elastic-Perfectly-Plastic and (b) Bilinear Hardening (α=5%))
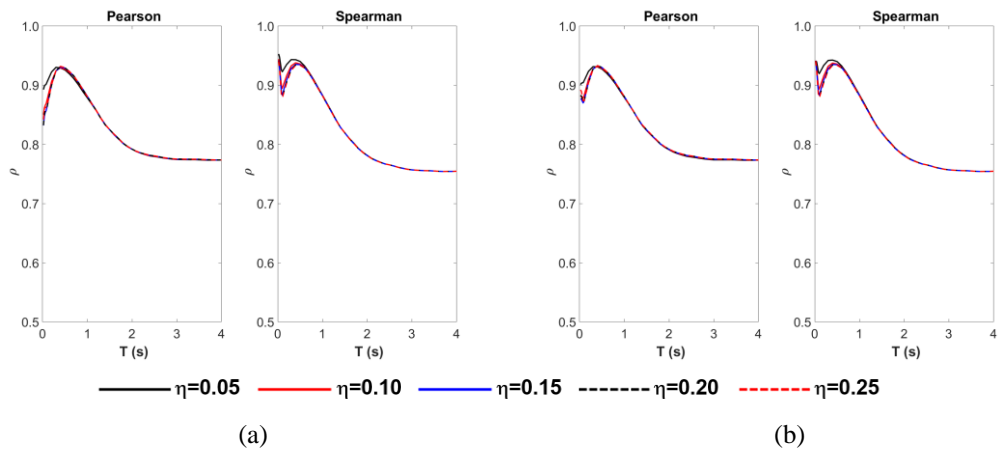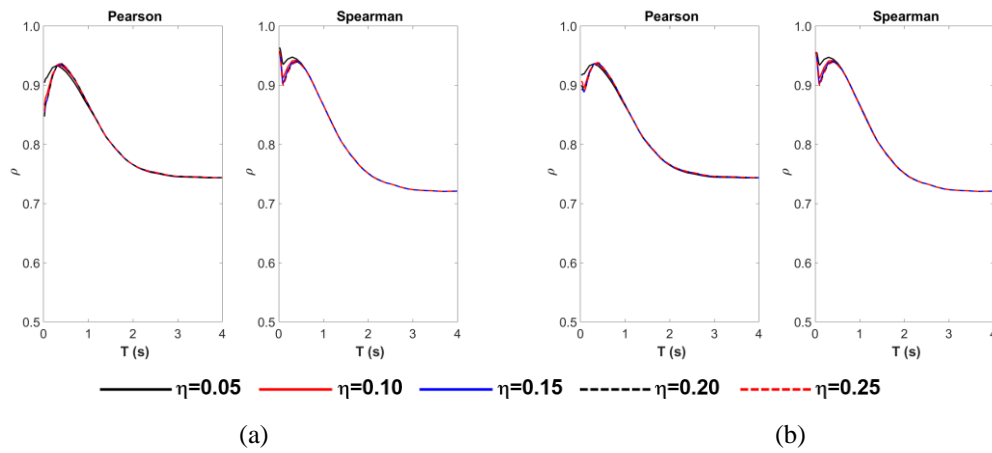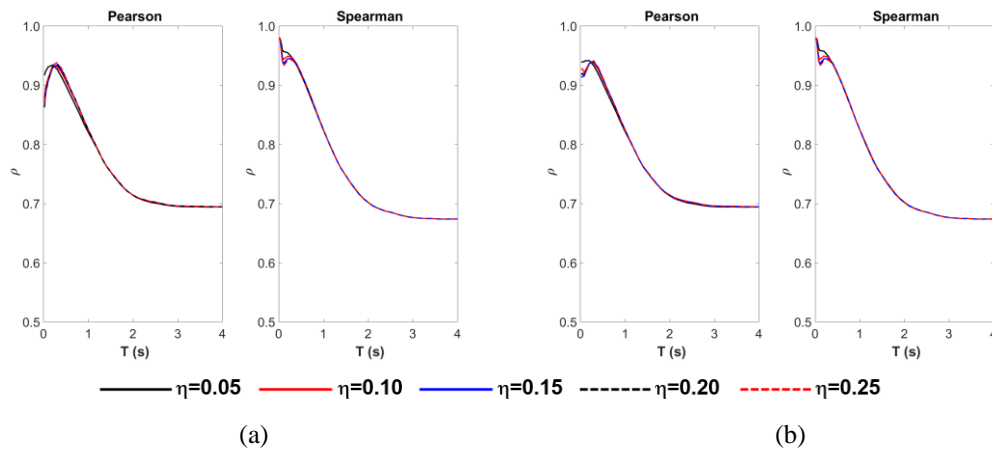

Figure A.57. Variation of correlation coefficient values with period (correlation of IM I_a with EDP **SDOF top drift** for different η cases (a) Elastic-Perfectly-Plastic and (b) Bilinear Hardening (α=5%))
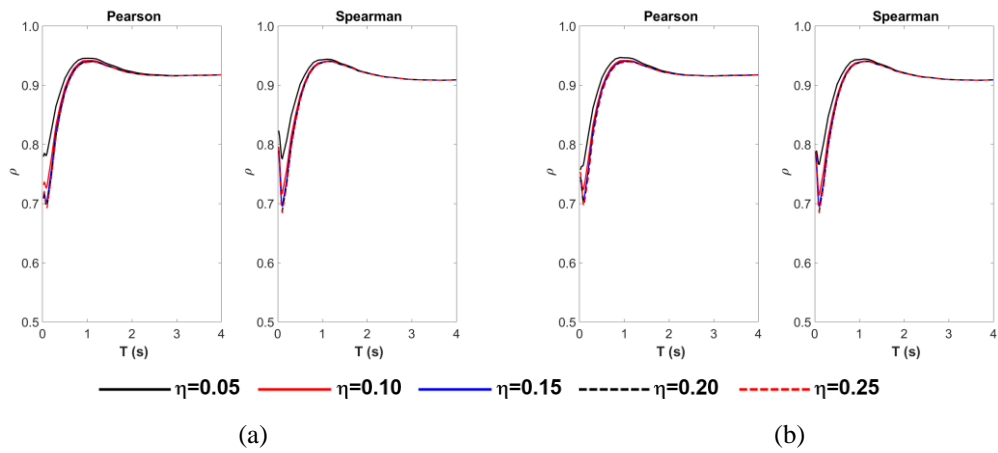
Figure A.58. Variation of correlation coefficient values with period (correlation of IM $\mathbf{I_F}$ with EDP **SDOF top drift** for different η cases (a) Elastic-Perfectly-Plastic and (b) Bilinear Hardening (α=5%))
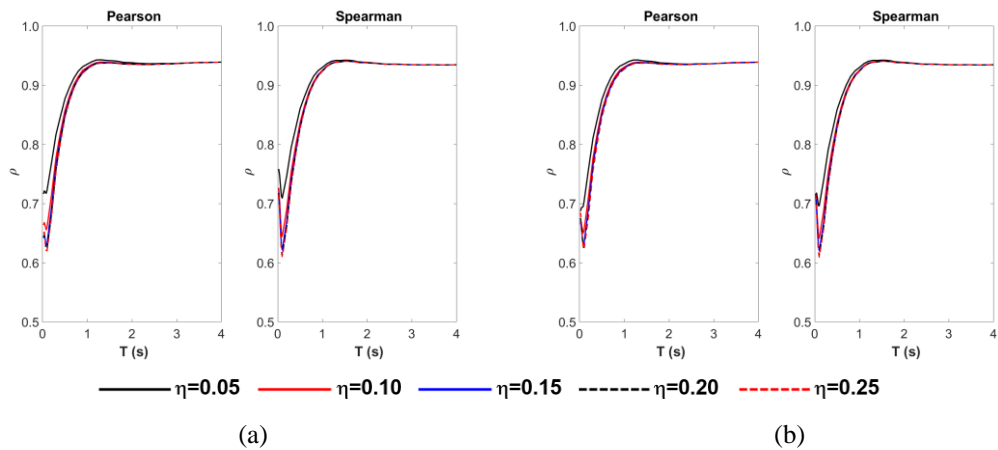
Figure A.59. Variation of correlation coefficient values with period (correlation of IM $\mathbf{I_V}$ with EDP **SDOF top drift** for different η cases (a) Elastic-Perfectly-Plastic and (b) Bilinear Hardening (α=5%))
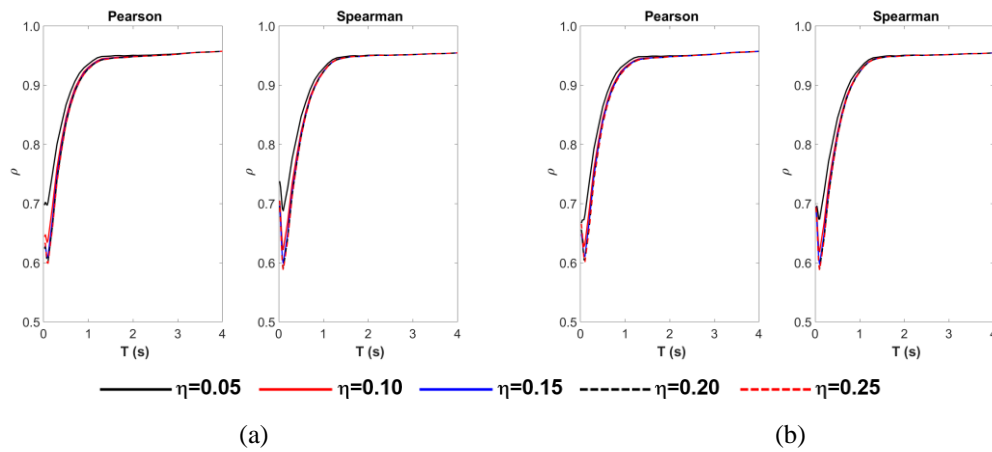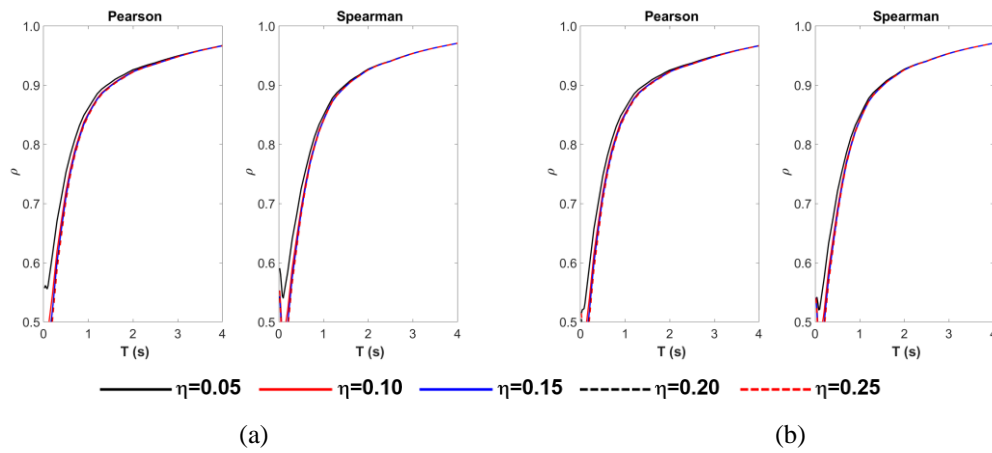
Figure A.60. Variation of correlation coefficient values with period (correlation of IM I_d with EDP **SDOF top drift** for different η cases (a) Elastic-Perfectly-Plastic and (b) Bilinear Hardening (α=5%))
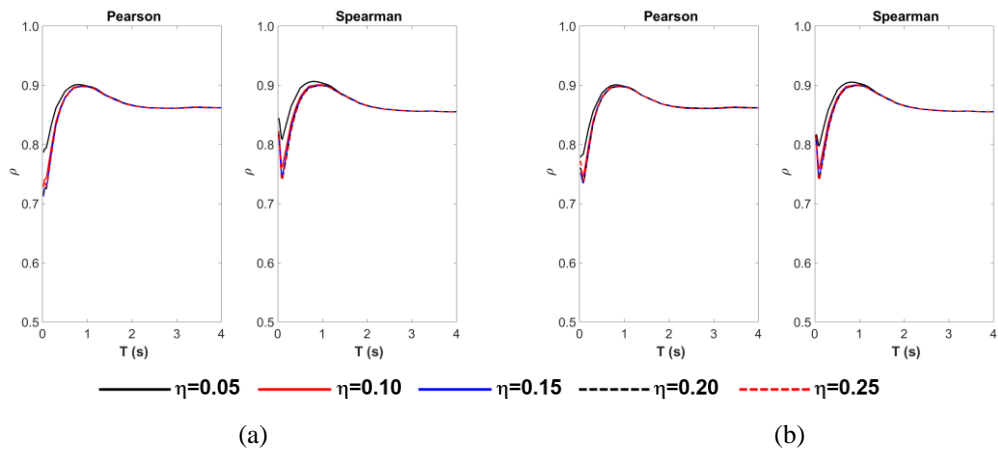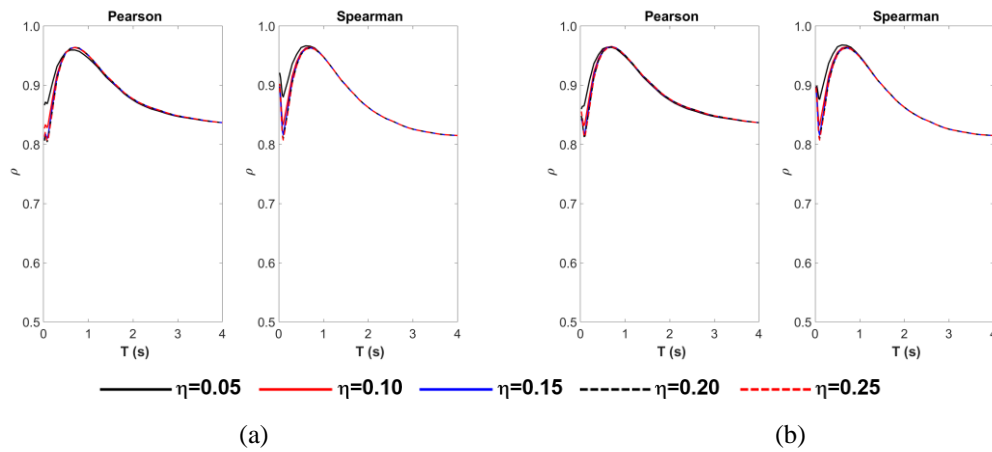

Figure A.61. Variation of correlation coefficient values with period (correlation of IM **ASI*** with EDP **SDOF top drift** for different η cases (a) Elastic-Perfectly-Plastic and (b) Bilinear Hardening (α=5%))
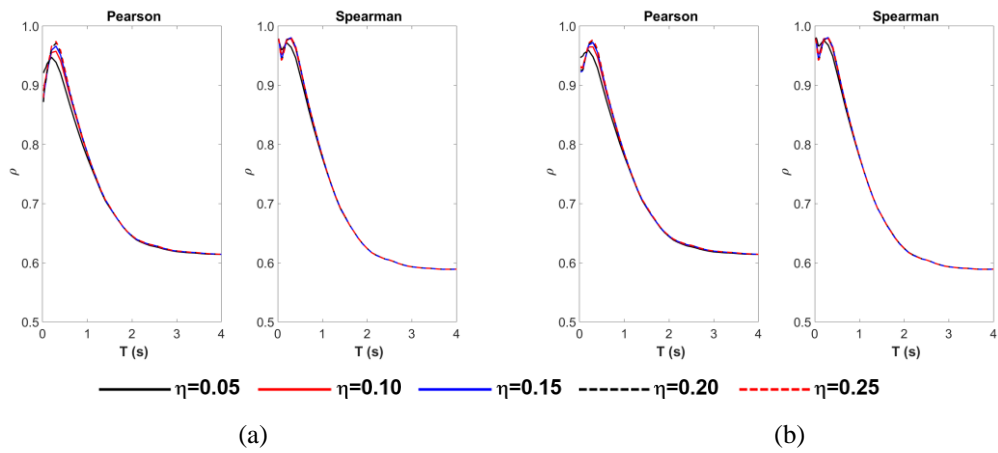
Figure A.62. Variation of correlation coefficient values with period (correlation of IM **EPA** with EDP **SDOF top drift** for different η cases (a) Elastic-Perfectly-Plastic and (b) Bilinear Hardening (α=5%))
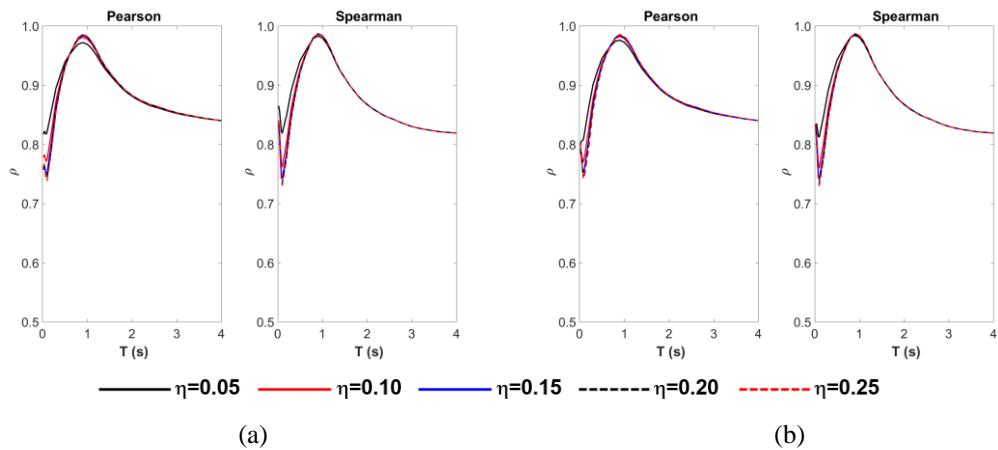
Figure A.63. Variation of correlation coefficient values with period (correlation of IM **EPV** with EDP **SDOF top drift** for different η cases (a) Elastic-Perfectly-Plastic and (b) Bilinear Hardening (α=5%))
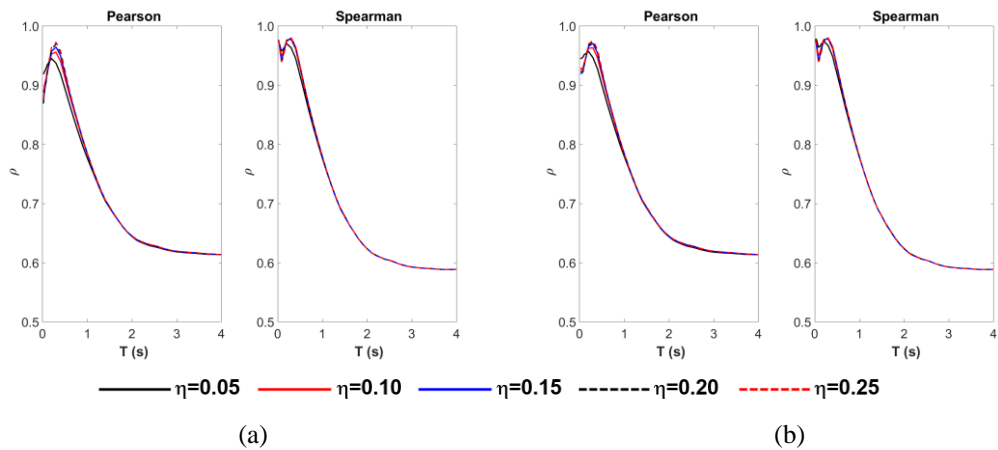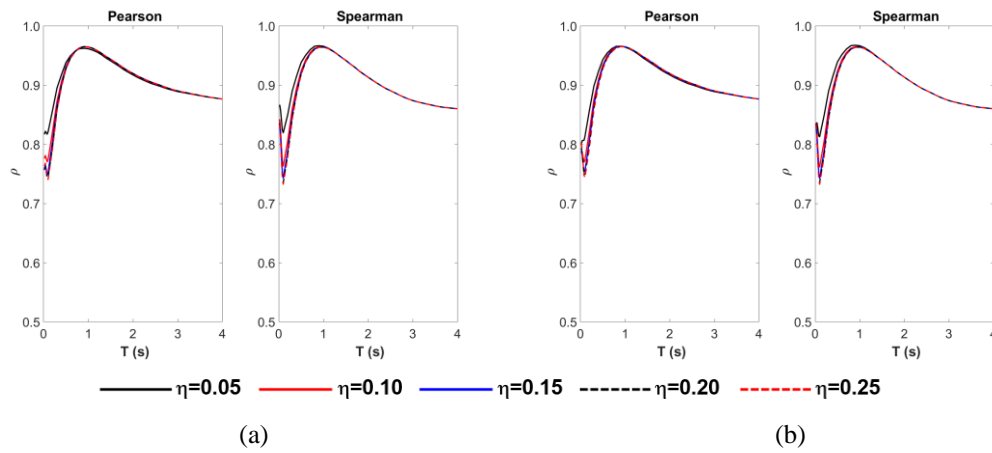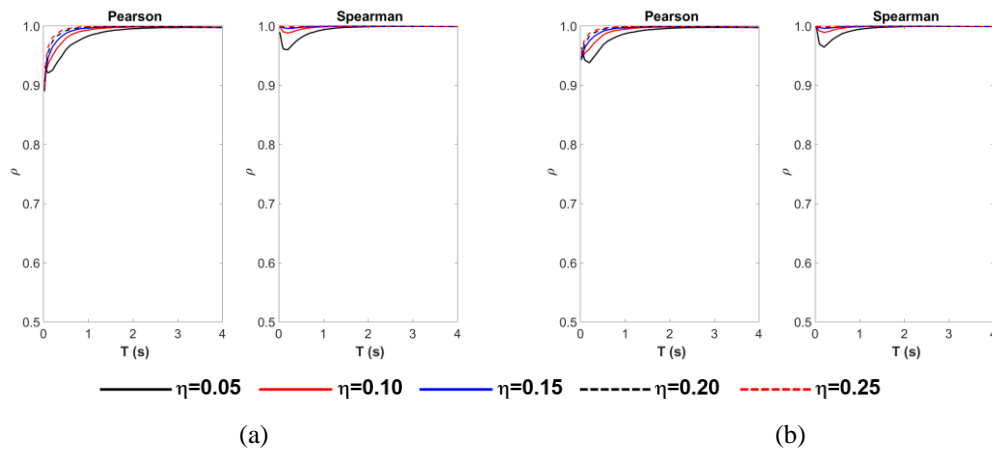
Figure A.64. Variation of correlation coefficient values with period (correlation of IM S_a with EDP **SDOF top drift** for different η cases (a) Elastic-Perfectly-Plastic and (b) Bilinear Hardening (α=5%))
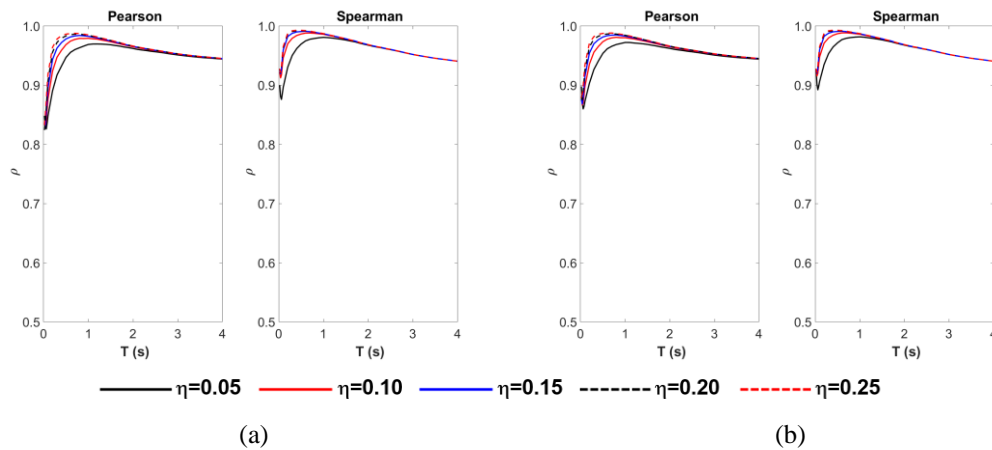
Figure A.65. Variation of correlation coefficient values with period (correlation of IM S_v with EDP **SDOF top drift** for different η cases (a) Elastic-Perfectly-Plastic and (b) Bilinear Hardening (α=5%))
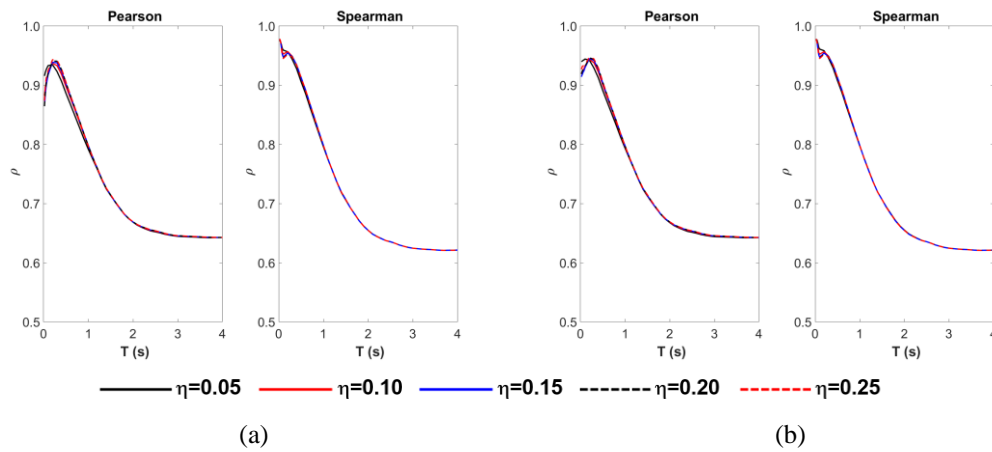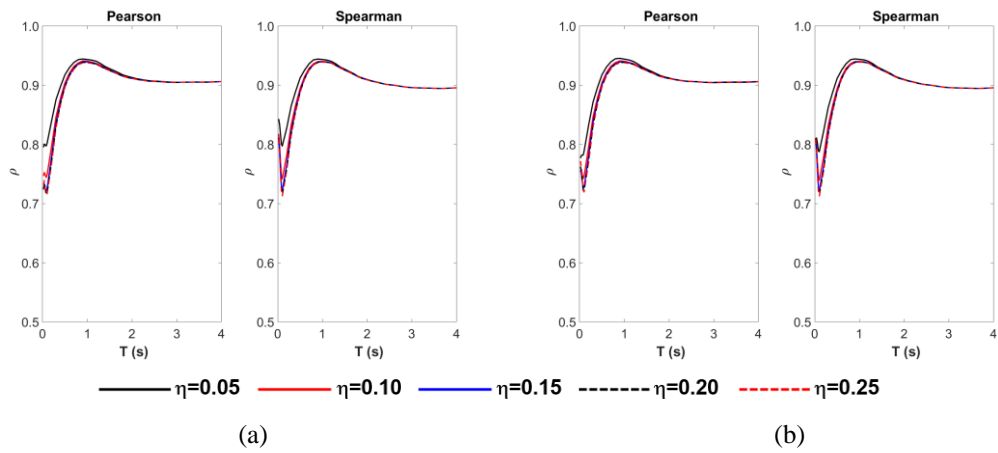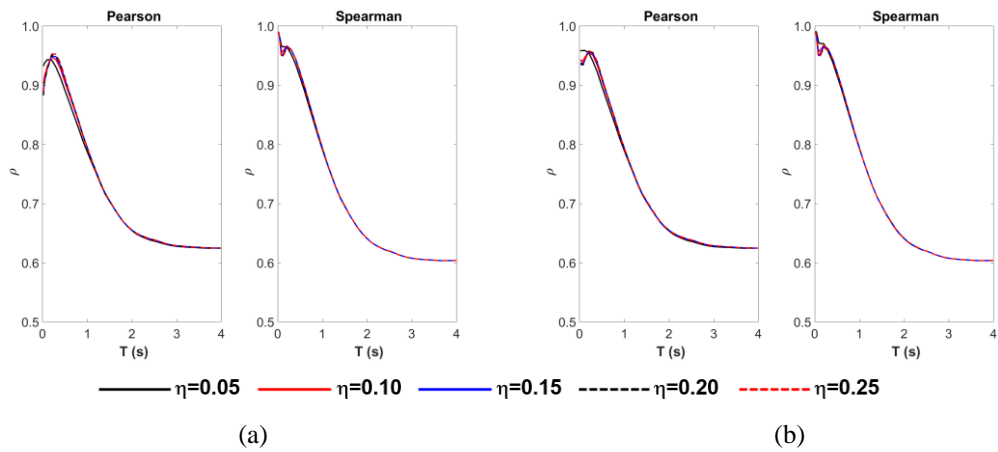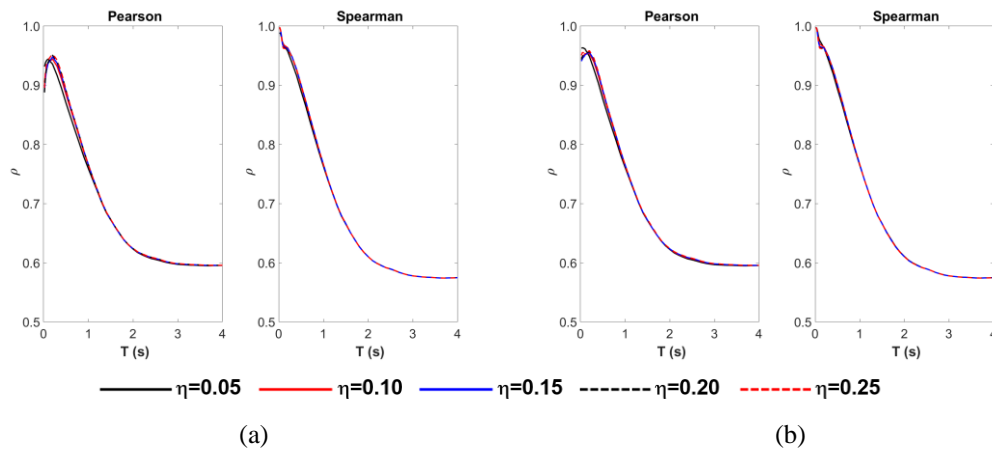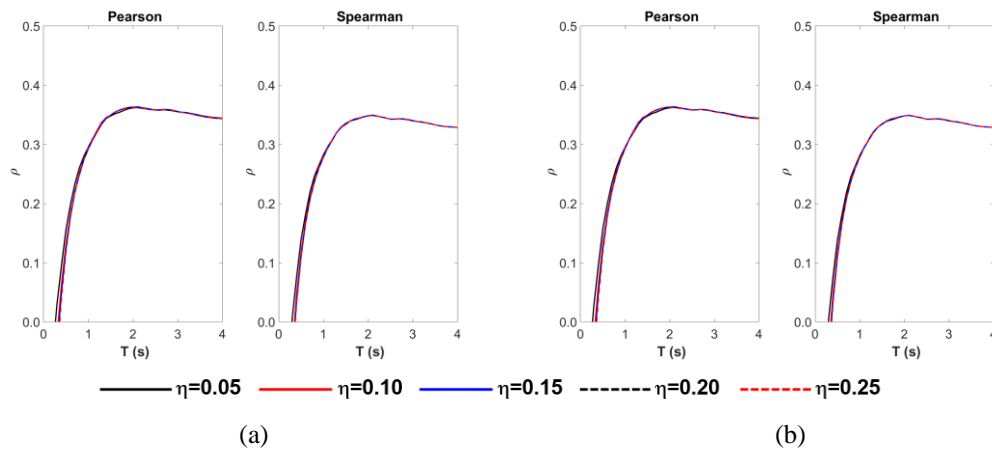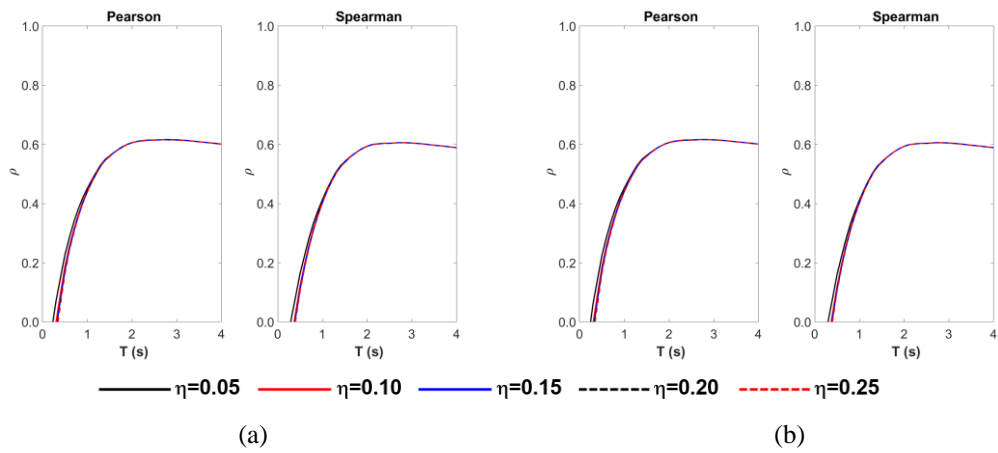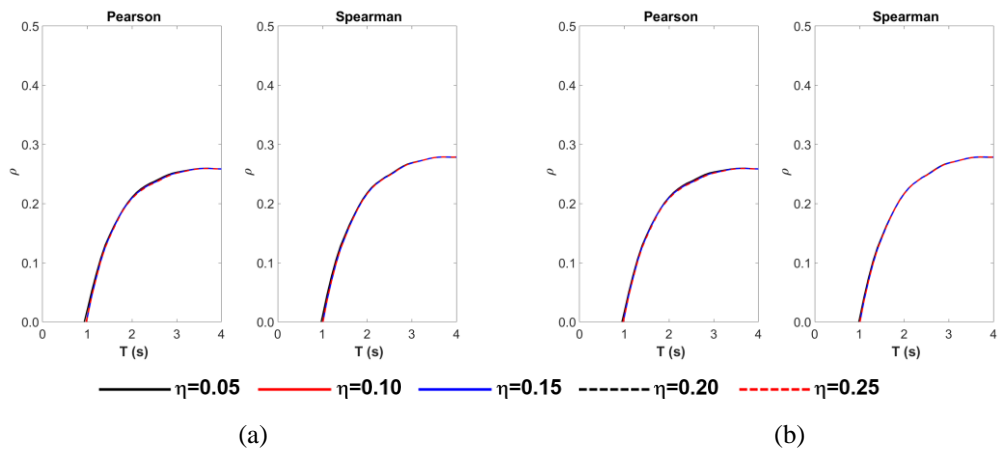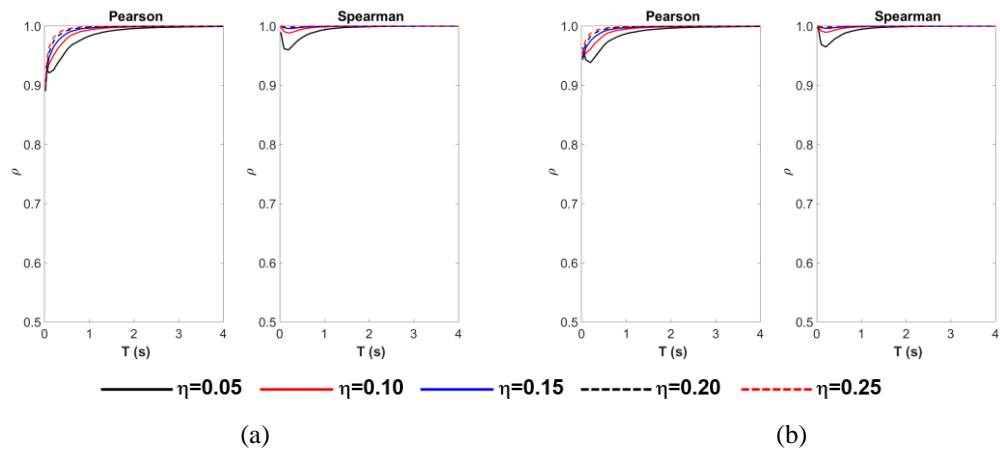
Figure A.66. Variation of correlation coefficient values with period (correlation of IM S_d with EDP **SDOF top drift** for different η cases (a) Elastic-Perfectly-Plastic and (b) Bilinear Hardening (α=5%))

C. Detailed Information about Stratified Random Sampling- and Cluster Sampling-based GM Subsets

This supplementary section presents brief information about stratified random and cluster sampling methods, and explains in detail the application of these sampling methods to form alternative GM subsets that have been utilized in MDOF-based analyses.

C.1.   Stratified Random and Cluster Sampling Methods

In statistics, random sampling is simply drawing n samples from a finite population of N objects, without replacement, in a completely random manner, where the sample mean and variance are generally utilized to make statistical predictions about the population mean and variance, which is comprehensively elaborated in the context of inferential statistics (Gupta and Guttman, 2014). In stratified random sampling, in contrast, the population is divided into a specified number of groups, generally referred as strata, and samples are randomly selected from each stratum. A stratified sample set with desired number of samples from each stratum will tend to represent the population with greater precision as opposed to a simple random sample set with the same size (Thompson, 2012).

Alternatively, in cluster sampling, the population is partitioned into different groups, generally termed as clusters, where the number of clusters is determined via an iterative approach and is generally dependent on the pattern characteristics of the population. Each item in the population is assigned to one cluster only, despite the fact that more advanced fuzzy clustering approaches discard this rule. The items in the same cluster have properties as similar as possible, where the items from different clusters are expected to exhibit dissimilar properties. Similarity and dissimilarity are defined in terms of specific statistical metrics. The cluster analysis involves two approaches; hierarchical and non-hierarchical clustering; the first one is generally preferred for categorical data analysis, whereas the latter is utilized for data having

defined properties in n-dimensional space. After the finalization of the clusters and assignment of individual elements to those clusters, a two-stage sampling approach could be followed to select a subset of elements from each cluster randomly to form the main sample set. The interested reader is referred to Rencher and Christensen (2012) for a detailed explanation of the mathematical procedures in the background of the cluster sampling method.

The cluster sampling method is considered to provide less precision with respect to simple random sampling or stratified random sampling, which requires an increased sample set size to compensate for its drawback. However, the advantage to eliminate the subjectivity in the classification of data (which is generally based on pre-defined criteria) via an unsupervised data classification approach makes this analysis and sampling method statistically preferable as well. As a result of this promising feature, the analysis method has also taken place in the earthquake engineering and engineering seismology community, especially utilized in the classification of strong ground motion records. Alimoradi et al. (2005) proposed and applied a fuzzy c-means approach to classify GM records. In their study, a set of 1470 accelerograms was partitioned into 6 clusters considering a short list of IMs; PGA, EPA, EPV, Maximum Incremental Velocity (MIV), Maximum Incremental Displacement (MID), and 0.05g bracketed duration. Similarly, Yaghmaei-Sabegh (2017) utilized k-means approach to classify 49 as-recorded and 36 artificial GM records considering different indicators. Taking its motivation from these two studies, Ding et al. (2020) has recently applied k-means clustering on a set of 7692 GMs and introduced a new seismic response spectrum and an associated characteristic period based on a 3-cluster dataset individually formed for 4 different site classes. These studies have encouraged the utilization of cluster sampling with k-means clustering approach to objectively classify the records from the main database and to form a sample set that would represent the wide range of ground motion characteristics represented by alternative IM definitions herein. The following section describes the application of these two sampling methods on the main dataset to form GM record subsets for MDOF-bases analyses.

C.2. Application of the Stratified Random Sampling Method

The stratified random sampling (will be shortly referred as random sampling hereinafter) method had been implicitly applied, indeed, in a former study by Erberik and Çullu (2006) forming a set of GM records with a uniform distribution of PGV as much as possible with consideration of the fact that this IM is generally a better index for representation of damage potential of ground motions. The GM set formed therein was later utilized by Kadaş (2006) and Yılmaz (2007) in their nonlinear time history analysis-based research endeavors. This study is following the same logic to obtain a uniform distribution of records from a larger dataset, yet differentiating from the PGV-based selection approach by considering alternative IMs as well. Along with the spectral acceleration $S_a(T_1)$ which is specific to the structure examined, the IMs shortlisted in Chapter 4 have been considered as the conditioning IM (will be referred as DB IM hereinafter) for the formation of alternative GM subsets. It is important to note here that no seismological criteria have been enforced on the main dataset to eliminate records, as the essential purpose of this study to evaluate the IMs from a hazard-independent perspective.

The stratification, as part of this method, has been applied in a way that the entire population is divided into 10 groups/strata (the term "bin" is also used hereinafter) where the cut-off levels are the equally-spaced intensity levels in accordance with the maximum value of the conditioning IM (DB IM) observed in the main dataset (Figure A.67).
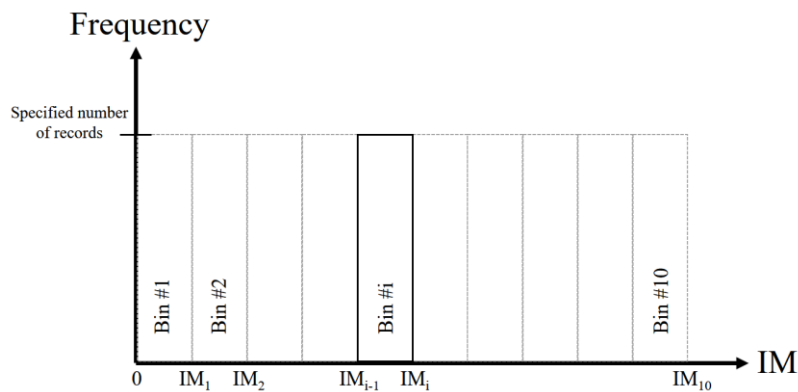
Figure A.67. Schematic representation of stratification/binning in stratified sampling approach

Limiting the number of strata/bins to 10 was not based on any statistical foundation, yet considered as sufficient as the initial step to limit the record-to-record variability within the bins. Considering the increased number of bins (with equal number of records in each bin, thus increasing the sample set size) might improve the results at the end to a certain extent; however, stratifying the population with fewer intensity levels (thus, reducing the sample set size) would yield much-increased record-to-record variability in each bin and is expected to affect the numerical interpretations eventually.

The determination of the number of records to be sampled from each strata/bin, on the other hand, constitutes a much more crucial step in this sampling method while this "minimum number of records required" problem has already motivated researchers worldwide to examine the phenomenon from a different (i.e., code-based and/or hazard-consistency) perspective. The fundamental study by Shome et al. (1998) had emphasized the need for decreasing the dispersion (by a factor of 2) about the median target response spectrum in order to achieve a decrease (by a factor of 4) in the computational effort in terms of NLTHA. Hancock et al. (2008) presented their own "required number of records" proposal to estimate the median maximum drift within ±10% of the median at a confidence level of 64%. Referring to 35% draft of ATC-58-1 (2007) (which was the basis for FEMA P-58-1), Huang (2008) investigated the recommendation on the use of 11 GM records for intensity-based assessment and explicitly showed the statistics based-relationship between the required level of confidence, the required level of accuracy, the dispersion in the response and the required number of records. A list of sample values is also provided in that study to show the resulting numbers (Table A.1).

Table A.1 The required number of records (n) as a function of dispersion, confidence level and tolerance range (adopted from Huang, 2008)

Dispersion	Confidence (%)	Tolerance (%)	n
0.5	75	0.1, 0.2, 0.3	36, 10, 5
	85	0.1, 0.2, 0.3	57, 16, 8
	95	0.1, 0.2, 0.3	106, 29, 14
0.55	75	0.1, 0.2, 0.3	44, 12, 6
	85	0.1, 0.2, 0.3	69, 19, 9
	95	0.1, 0.2, 0.3	128, 35, 17
0.6	75	0.1, 0.2, 0.3	52, 14, 7
	85	0.1, 0.2, 0.3	82, 22, 11
	95	0.1, 0.2, 0.3	152, 42, 20
0.65	75	0.1, 0.2, 0.3	62, 17, 8
	85	0.1, 0.2, 0.3	96, 26, 13
	95	0.1, 0.2, 0.3	179, 49, 24

Buratti et al. (2011) put emphasis on the need for an increased number of records to accurately determine the full distribution of the response as opposed to the prediction of the median response only. In parallel with this remark, Cimellaro et al. (2011) proposed that at least 20 records should be used for fragility analyses. The NIST GCR 11-917-15 document (NIST, 2011) even reported the use of 40 records at different intensity levels. The building codes ASCE 7-16 (ASCE, 2016) and TBEC-2018 have recently increased the minimum number of records from 7 to 11. Considering the technical basis discussed by Shome et al. (1998) and Huang (2008), the required number of records should be determined on the level of resulting response dispersion at each intensity level of the subject IM (especially for higher intensity levels). However, this approach is impractical to follow; therefore, this study is conforming to the recently prescribed code requirement and considers 11 records for each bin. With a dispersion of 0.52, the expected tolerance range for an

11-record-based estimate of any median response parameter with 75% confidence is ±20%, as explicitly calculated by Huang (2008).

Taking the recommendations of the previous chapter into account, PGA-, PGV-, AI-, SED-, CAV-, ASI*, VSI, I_F and I_v-based alternative GM subsets (structure-independent subsets, indeed) have been formed with the random sampling methodology described above. The neglection of ASI during the subset formation step is solely based on the fact that the acceleration-related PGA and AI couple, and the modified version of ASI, ASI*, are already in the DB IM list, and ASI has not been considered necessary for subset formation. The maximum values of the conditioning DB IMs are considered as follows:

- PGA: 0-1.78g
- PGV: 0-263 cm/s
- AI: 0-22.8 m/s
- SED: 20504 cm^2/s
- CAV: 0-4814 cm/s
- ASI*: 0-4 g*s
- VSI: 0-717 cm
- I_F: 0-501 cm/s*$s^{0.25}$
- I_v: 0-97 $(cm/s)^{2/3}*s^{(1/3)}$

The scatter of the IMs obtained from the GM records against the conditioning IM (DB IM) of each alternative subset has been presented in Figure A.69 thru Figure A.86. In accordance with the numerical results of Table 2.2 and Table 2.3, these figures support the fact that the degree of correlations among specific IM couples (i.e., if both considered within the similar group) are expected to be stronger visualized by much less scatter in data. Besides, the frequency distributions of the conditioning IMs (DB IMs) illustrated in Figure A.68 have revealed that the uniformity of GM data at low-to-moderate intensity levels could be achieved with 11 records, but the lack of large magnitude events resulting in high intensities is

apparent. The option of scaling records to these levels to complete the subsets was not considered at this stage of the study to keep potential scaling-based effects out.
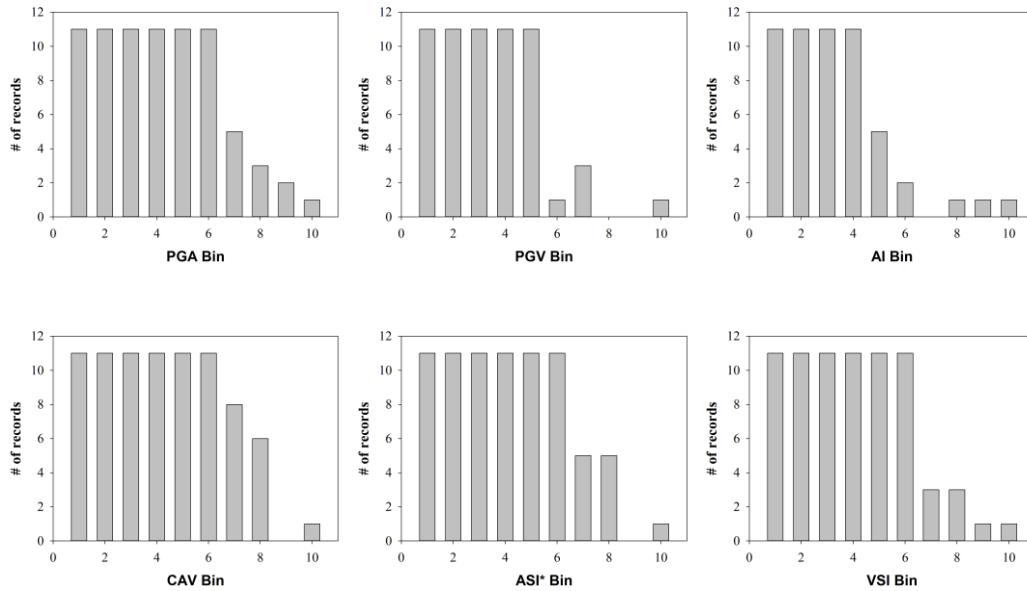
Figure A.68. Distribution of representative DB IMs corresponding to stratified sampling-based GM subsets

In addition to the above-described non-structure specific GM subsets, a final alternative subset for each of the structural models (which are presented in Chapter 3) has been formed considering the structure-specific spectral acceleration $S_a(T_1)$ for the model. The maximum values of $S_a(T_1)$ considered for the employed models are as follows:

- $S_a(T_1)$ – F2S2B2 (T_1=0.30 s): 0-4.36g
- $S_a(T_1)$ – F3S2B (T_1=0.45 s): 0-2.53g
- $S_a(T_1)$ – F2S2B (T_1=0.59 s): 0-2.19g
- $S_a(T_1)$ – F5S7B (T_1=0.66 s): 0-2.75g
- $S_a(T_1)$ – F5S2B (T_1=0.75 s): 0-3.48g

276

- $S_a(T_1)$ – F5S4B (T_1=0.95 s): 0-2.01g
- $S_a(T_1)$ – F8S3B (T_1=1.20 s): 0-1.71g

The scatter of key IMs (against the conditioning IM, DB IM=S_a) obtained from the GM records of each alternative S_a-based subset has been presented in Figure A.87 thru Figure A.93. The S_a-based frequency distributions have also revealed that the uniformity of GM data at low-to-moderate levels could be attained with 11 records, but the lack of large magnitude events causing high intensities is noticeable. The option of scaling records to these levels was not considered either.

Together with the subsets of different non-structure specific IMs (PGA, PGV, AI, SED, CAV, ASI*, VSI, I_F, and I_v) and the structure-specific IM ($S_a(T_1)$), 10 alternative GM record subsets have been formed for each structural model nearly yielding ~420-450 GM records in total. The marginal plots for moment magnitude (M_w) versus source-to-site distances (R_{JB}) displayed in Figure A.94-Figure A.96 have exhibited the dominancy of near-fault (R_{JB}=0-20 km) records in the subsets with varying M_w distribution characteristics.
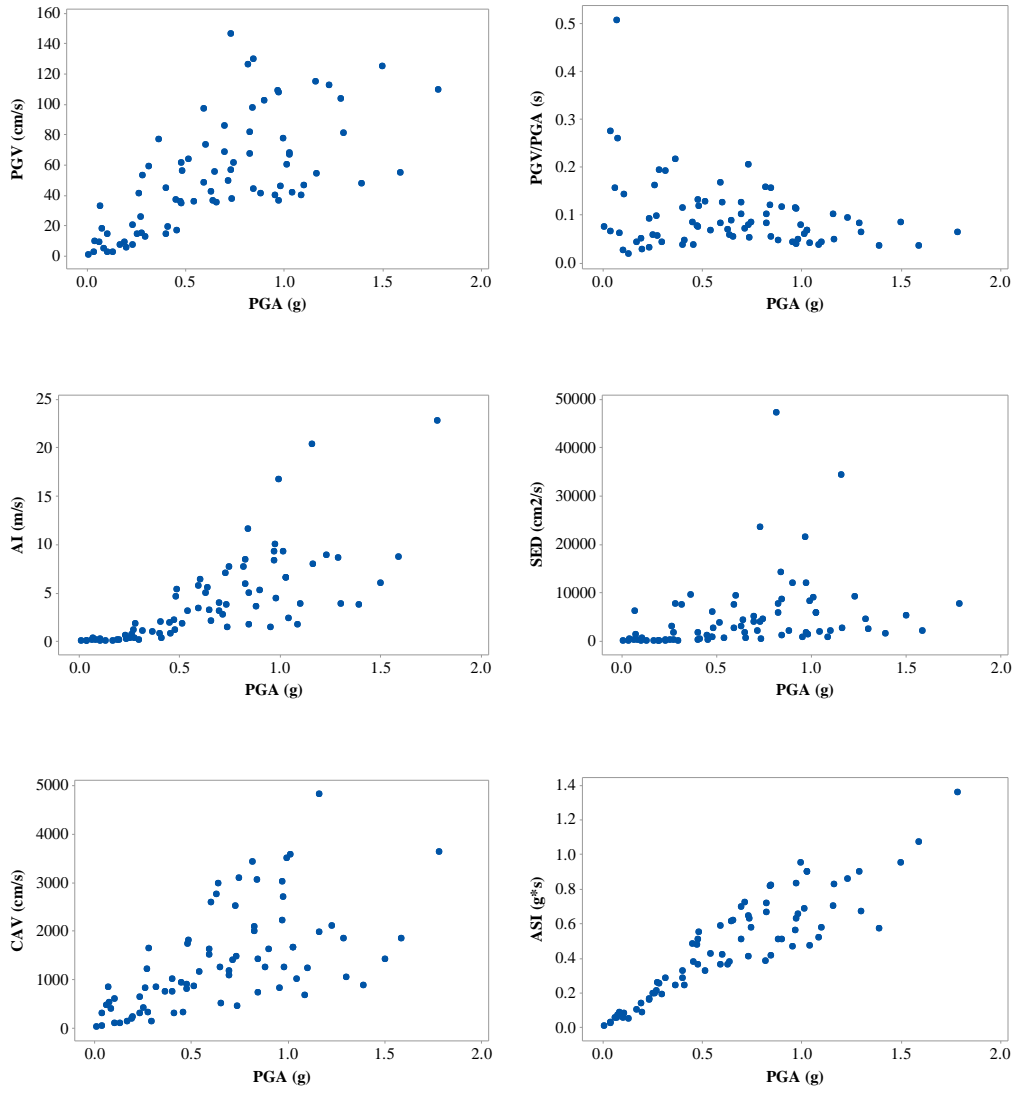
Figure A.69. Scatter plots for selected IMs against PGA (PGA-set)
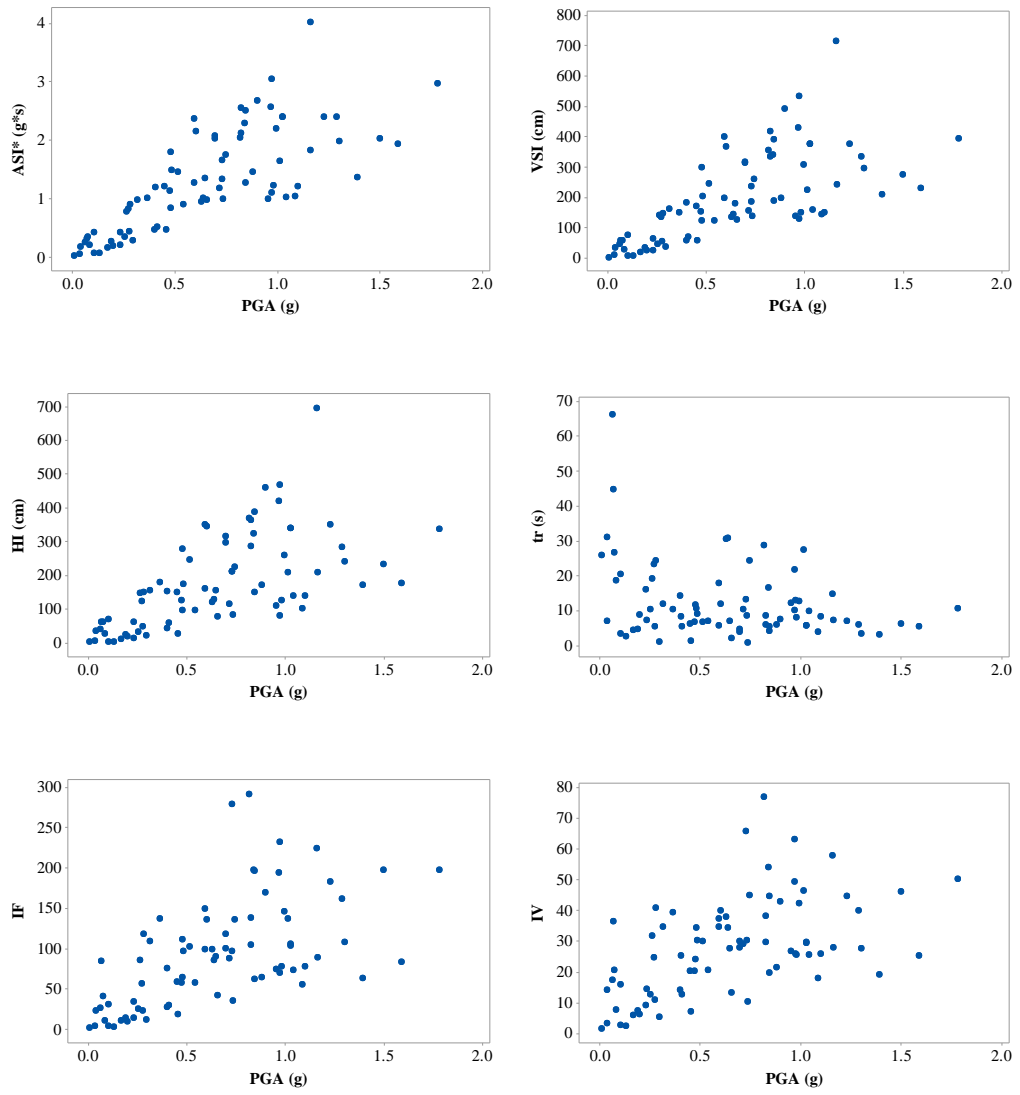
Figure A.70. Additional scatter plots for selected IMs against PGA (PGA-set)
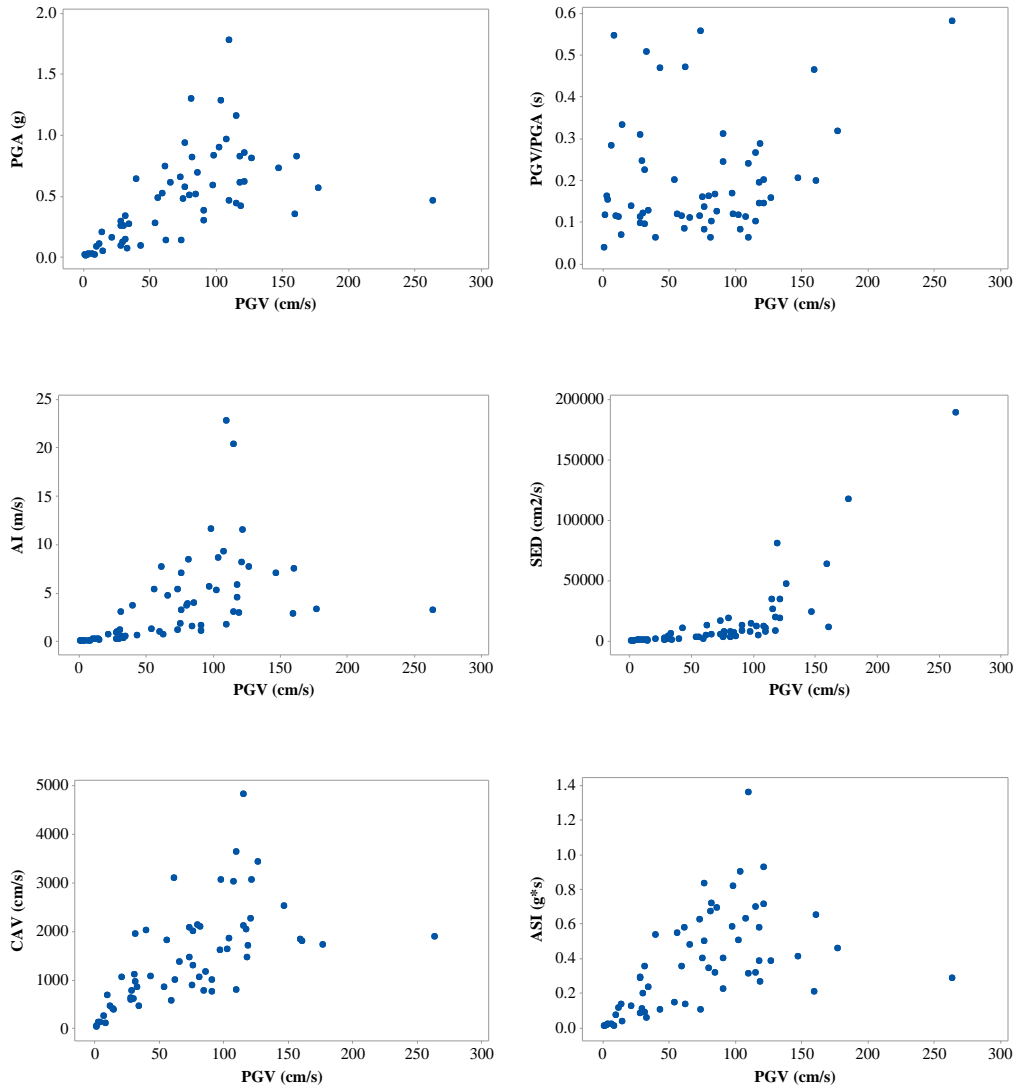
Figure A.71. Scatter plots for selected IMs against PGV (PGV-set)
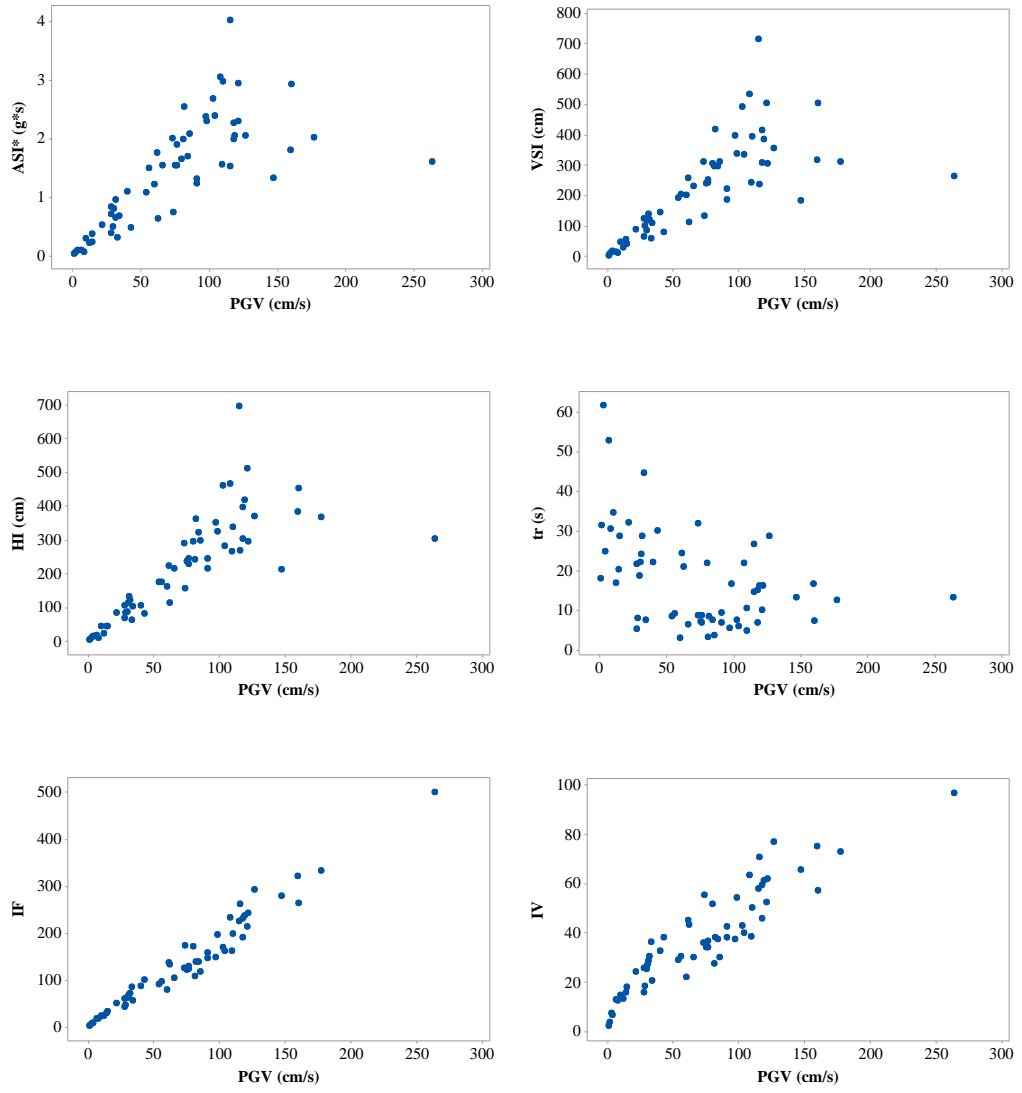
Figure A.72. Additional scatter plots for selected IMs against PGV (PGV-set)
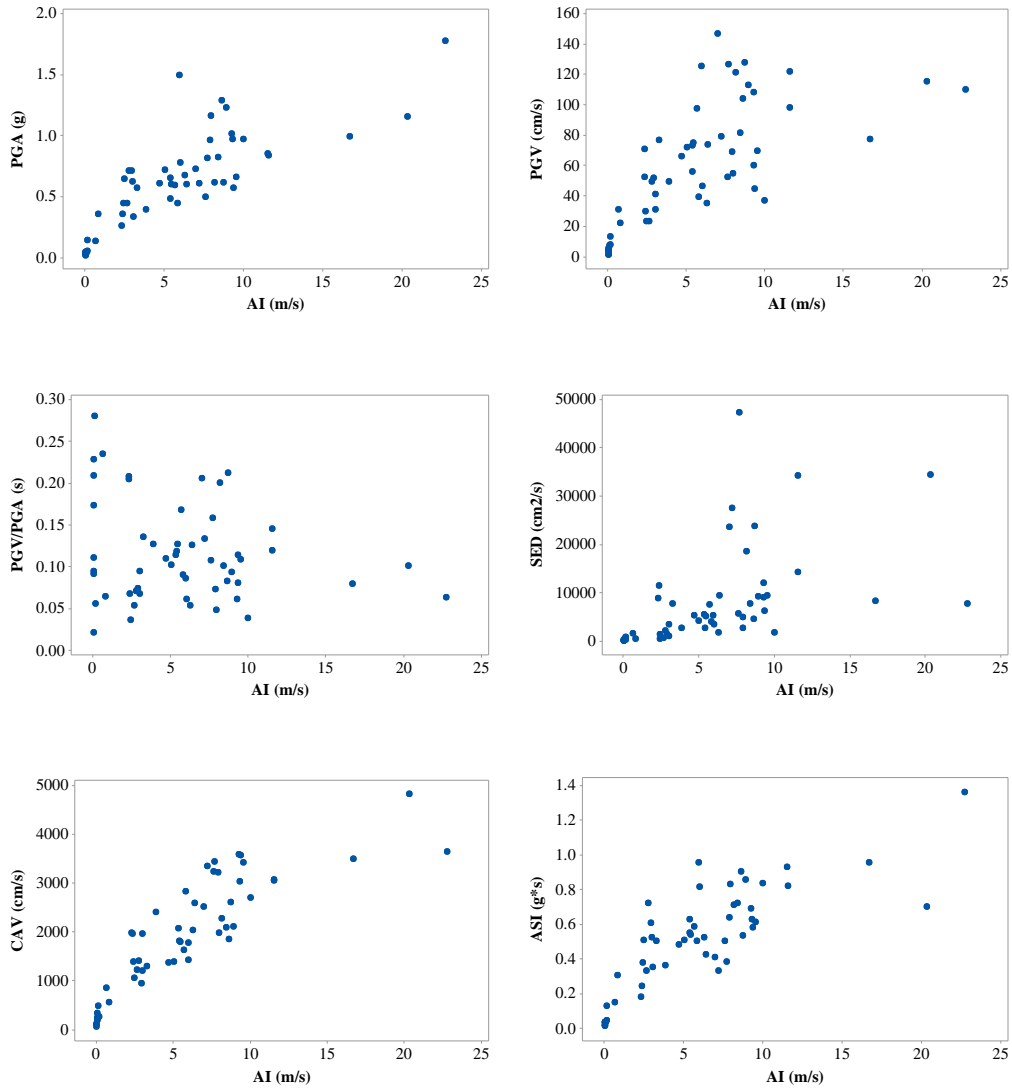
Figure A.73. Scatter plots for selected IMs against AI (AI-set)
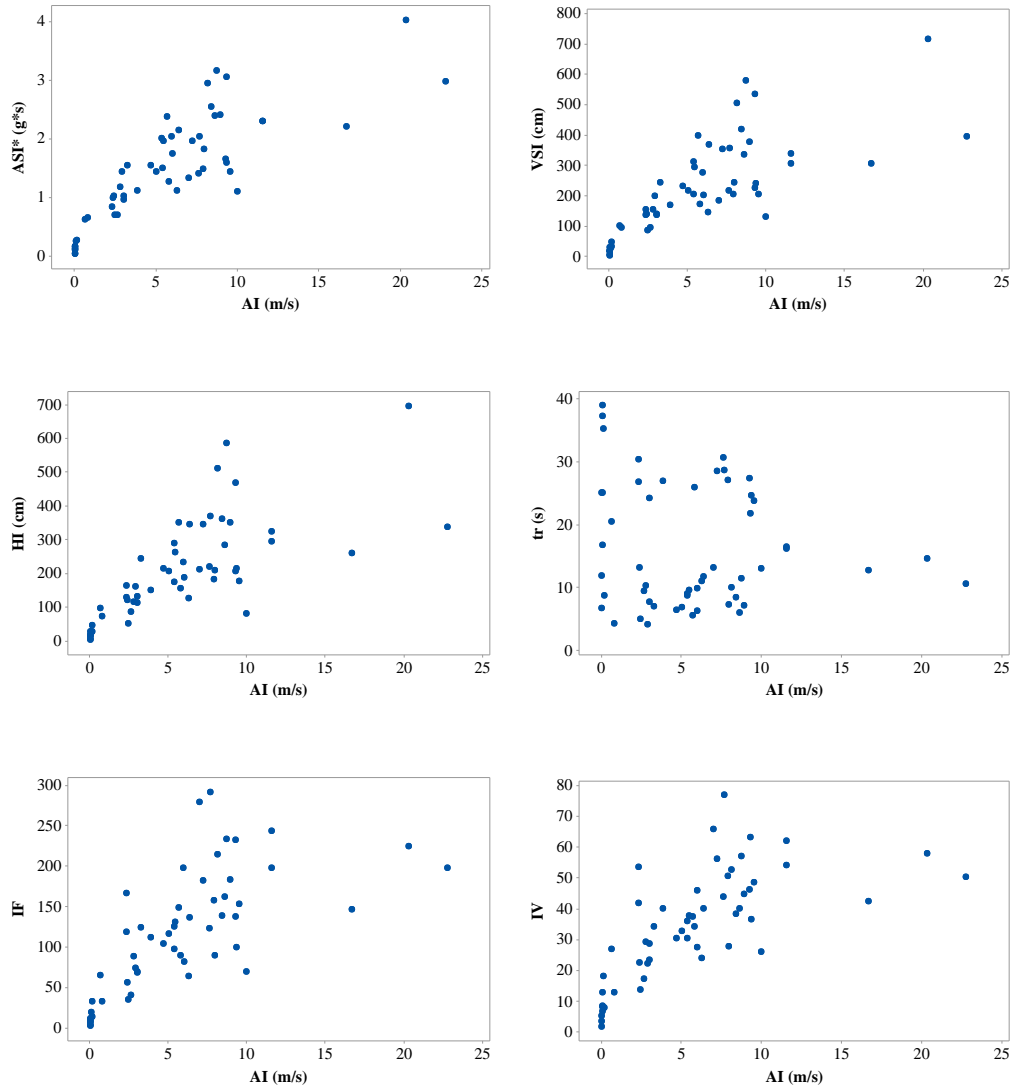
Figure A.74. Additional scatter plots for selected IMs against AI (AI-set)
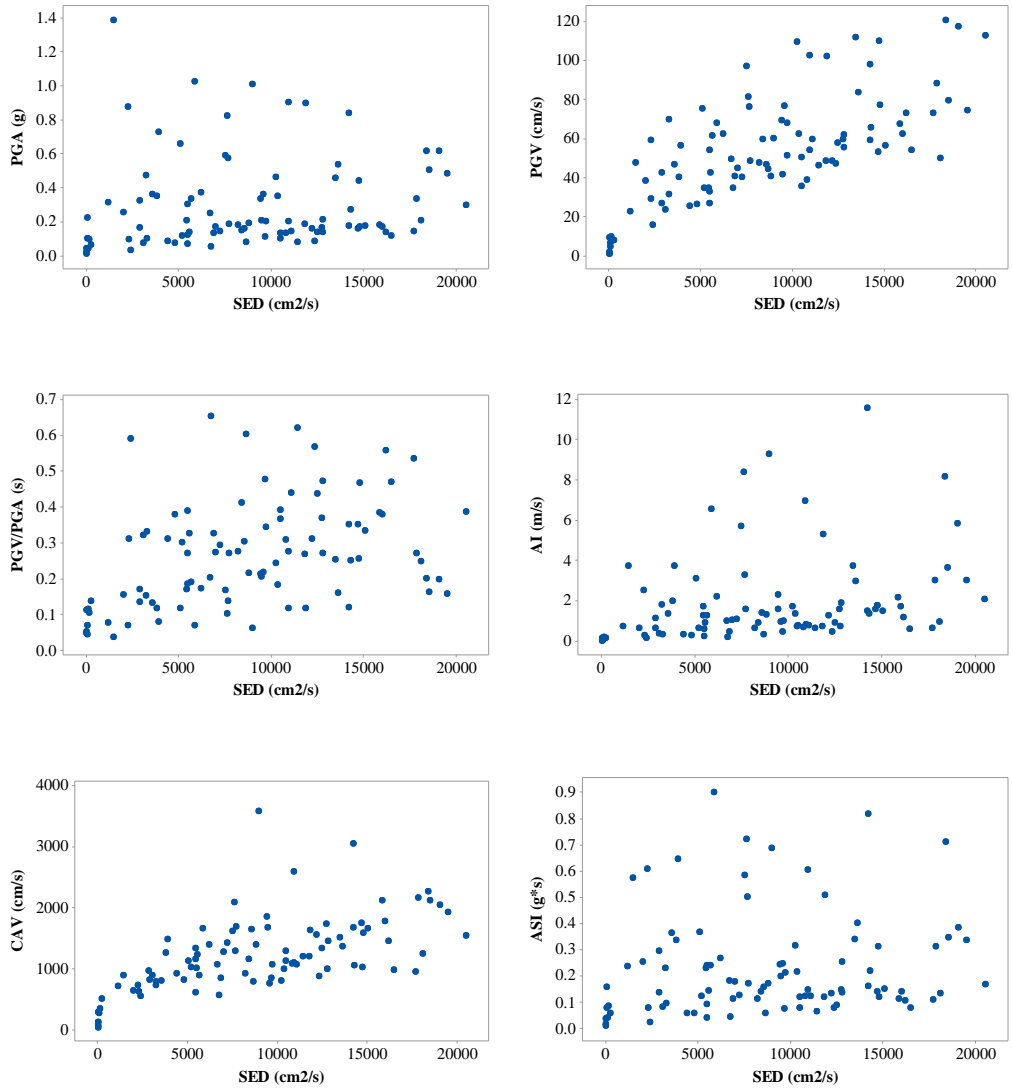
Figure A.75. Scatter plots for selected IMs against SED (SED-set)
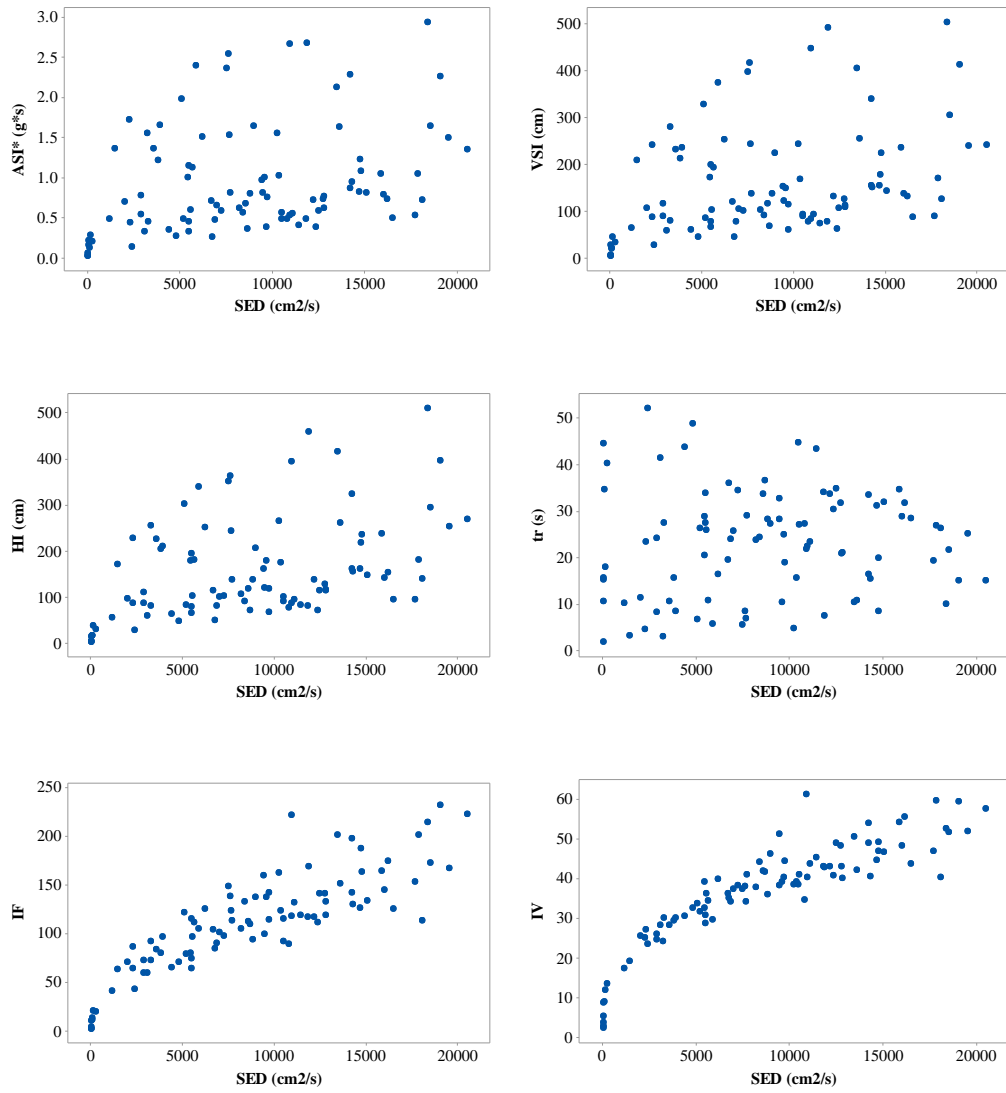
Figure A.76. Additional scatter plots for selected IMs against SED (SED-set)
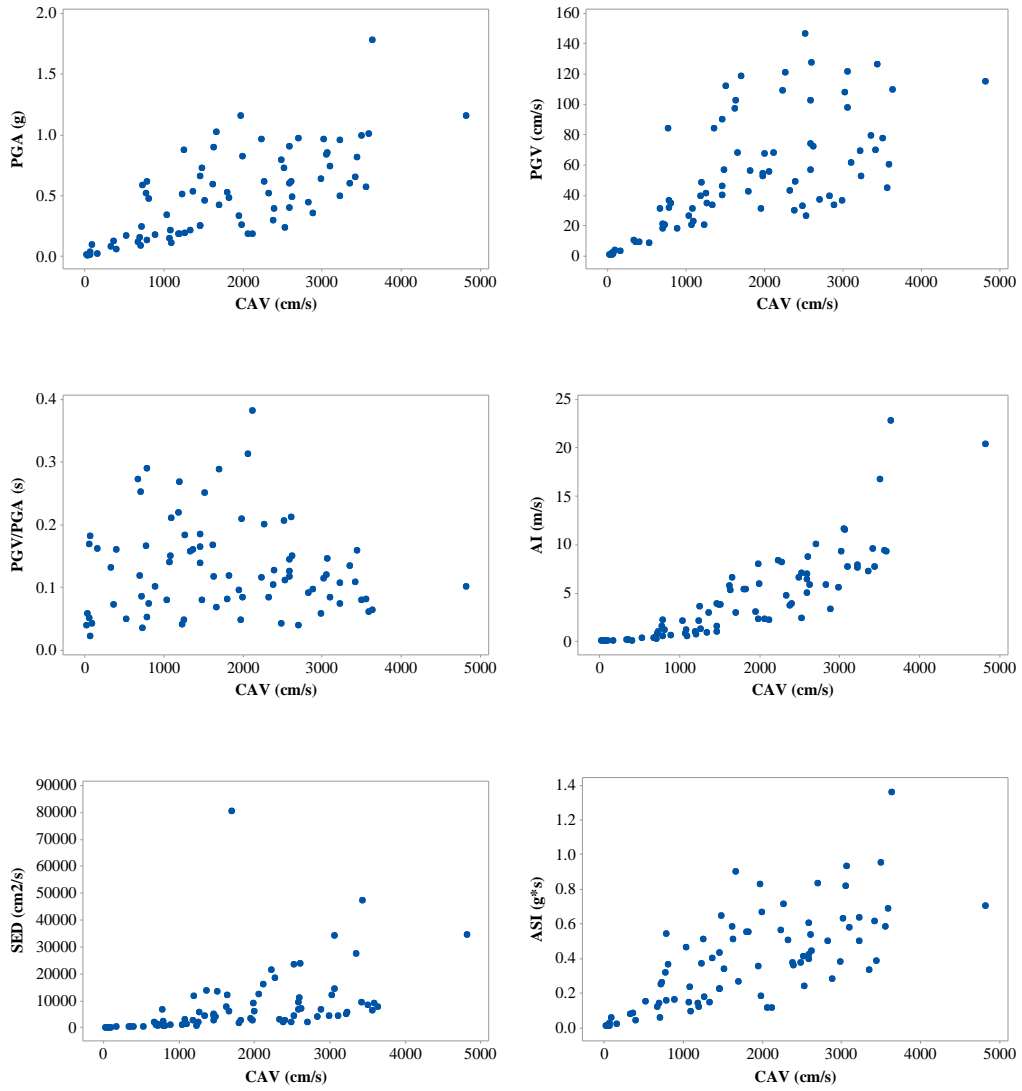
Figure A.77. Scatter plots for selected IMs against CAV (CAV-set)
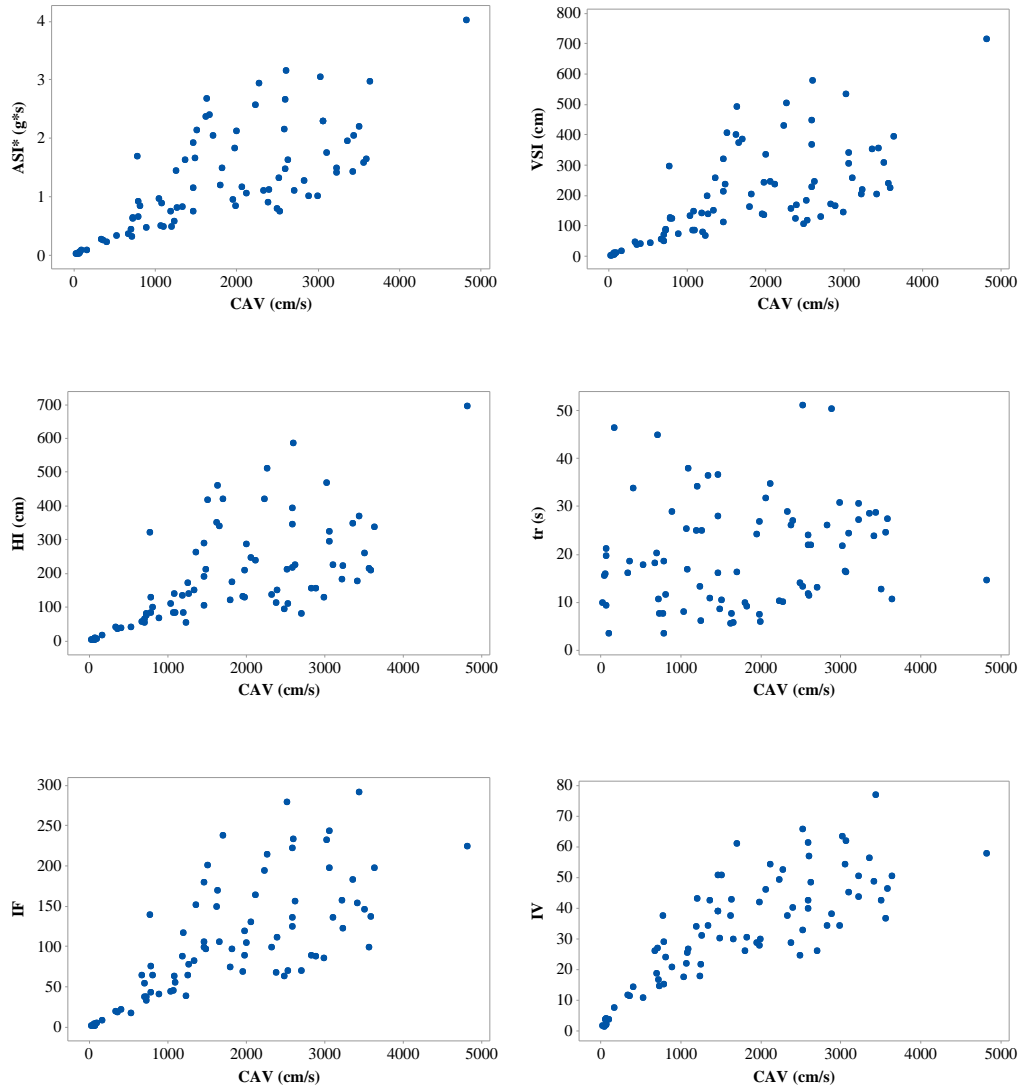
Figure A.78. Additional scatter plots for selected IMs against CAV (CAV-set)
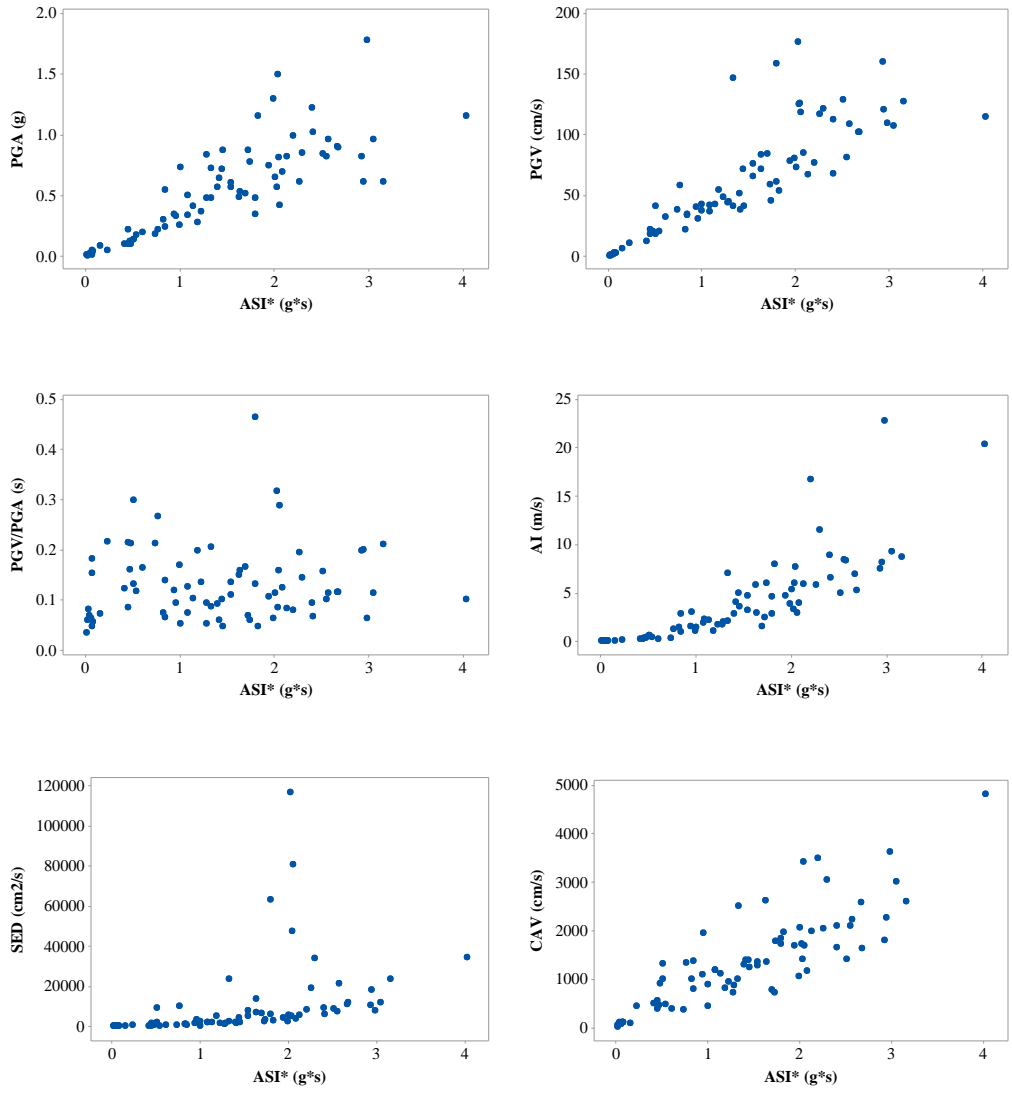
Figure A.79. Scatter plots for selected IMs against ASI* (ASI*-set)
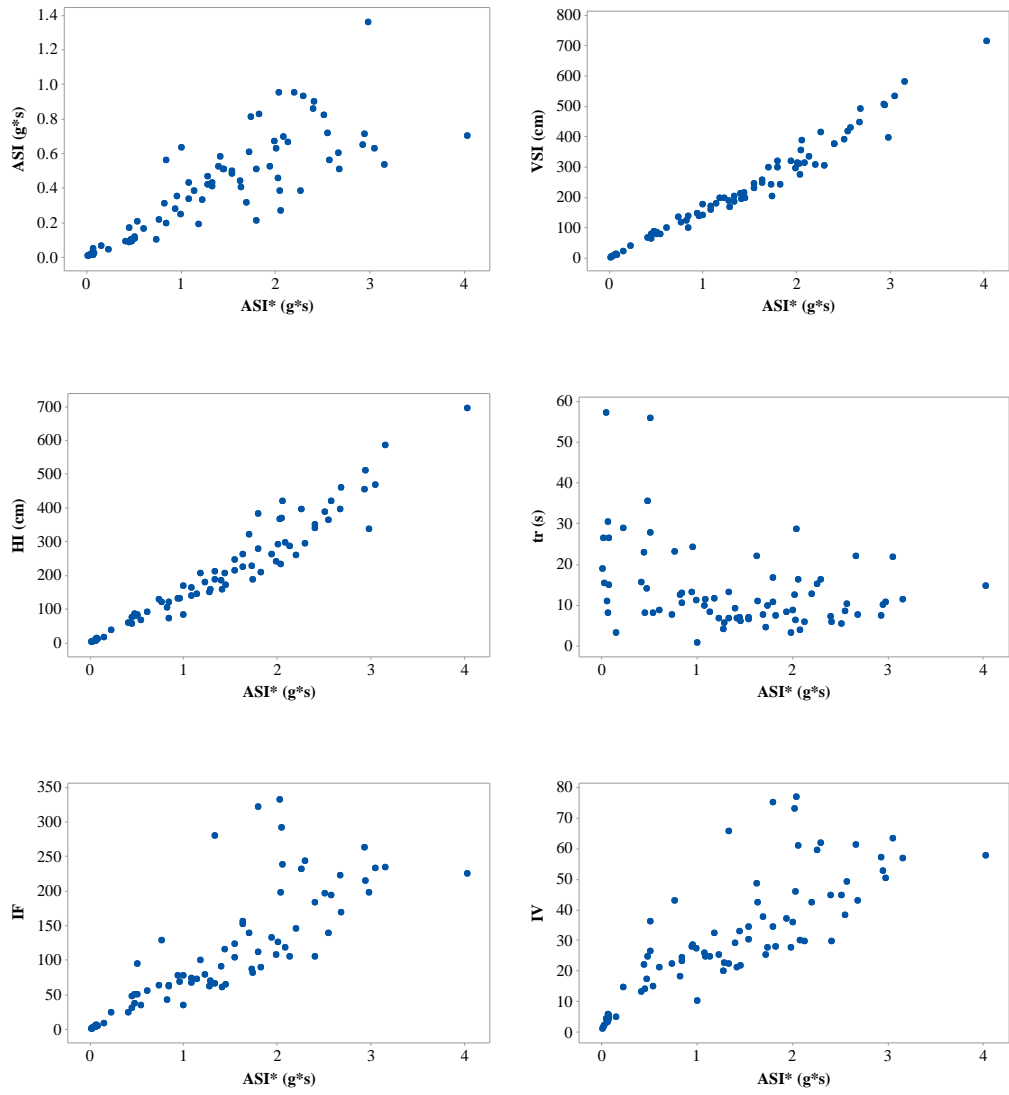
Figure A.80. Additional scatter plots for selected IMs against ASI* (ASI*-set)
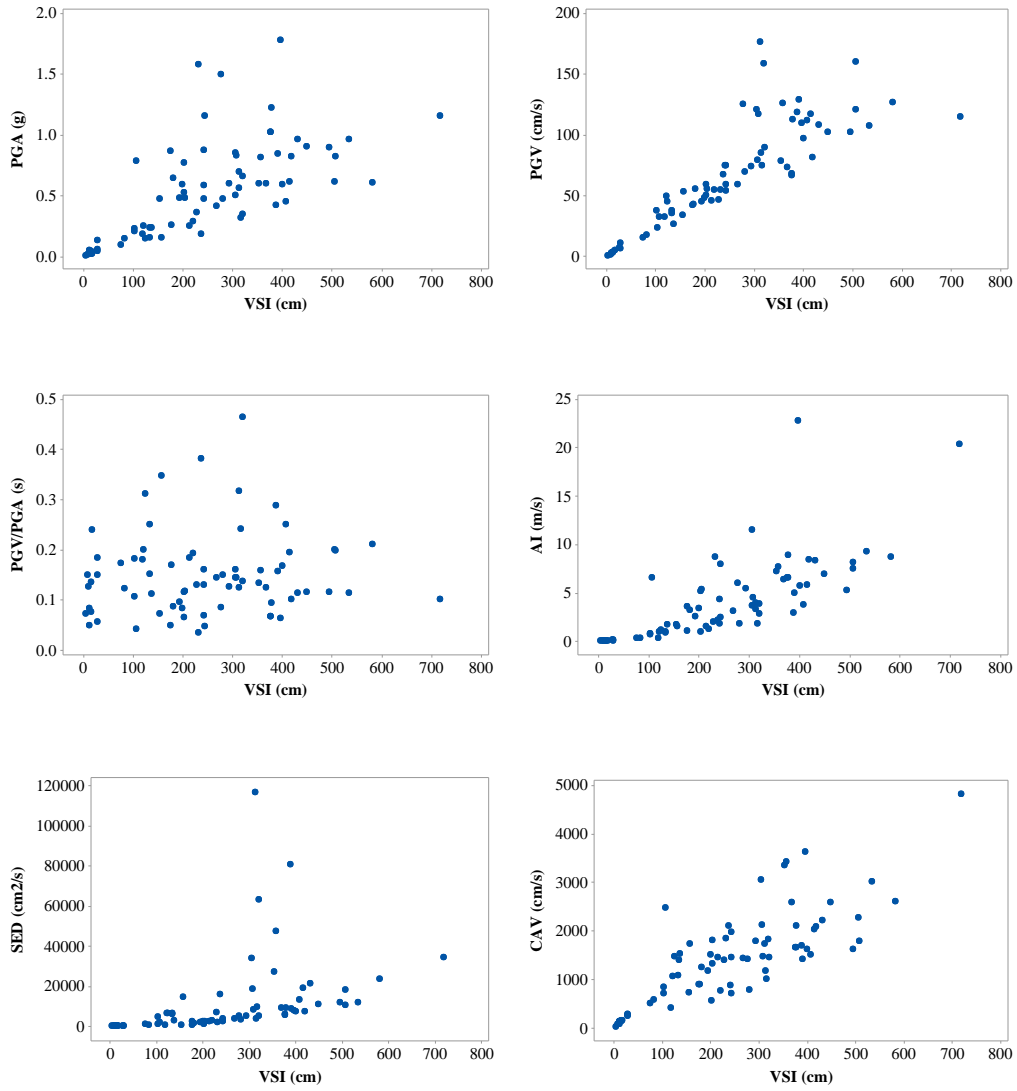
Figure A.81. Scatter plots for selected IMs against VSI (VSI-set)
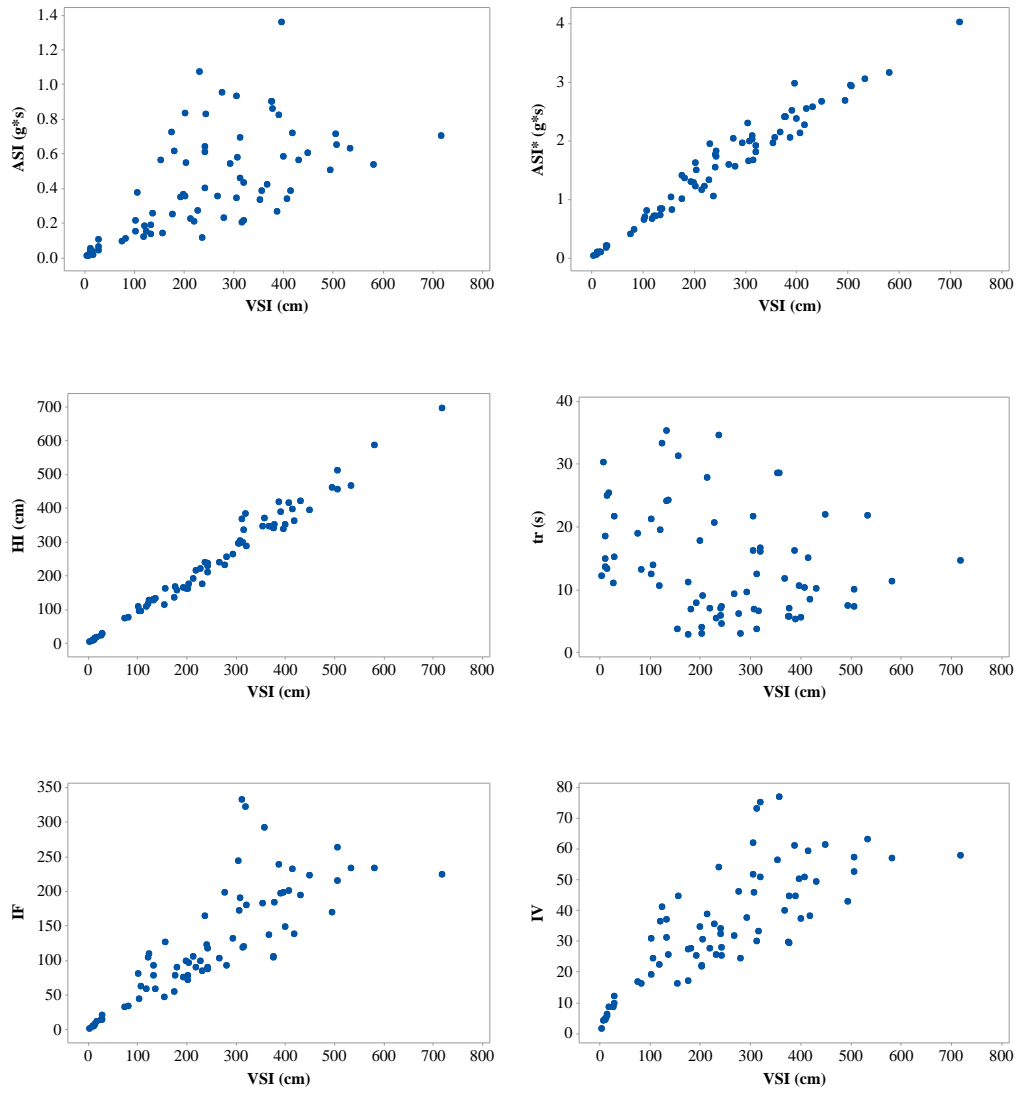
Figure A.82. Additional scatter plots for selected IMs against VSI (VSI-set)
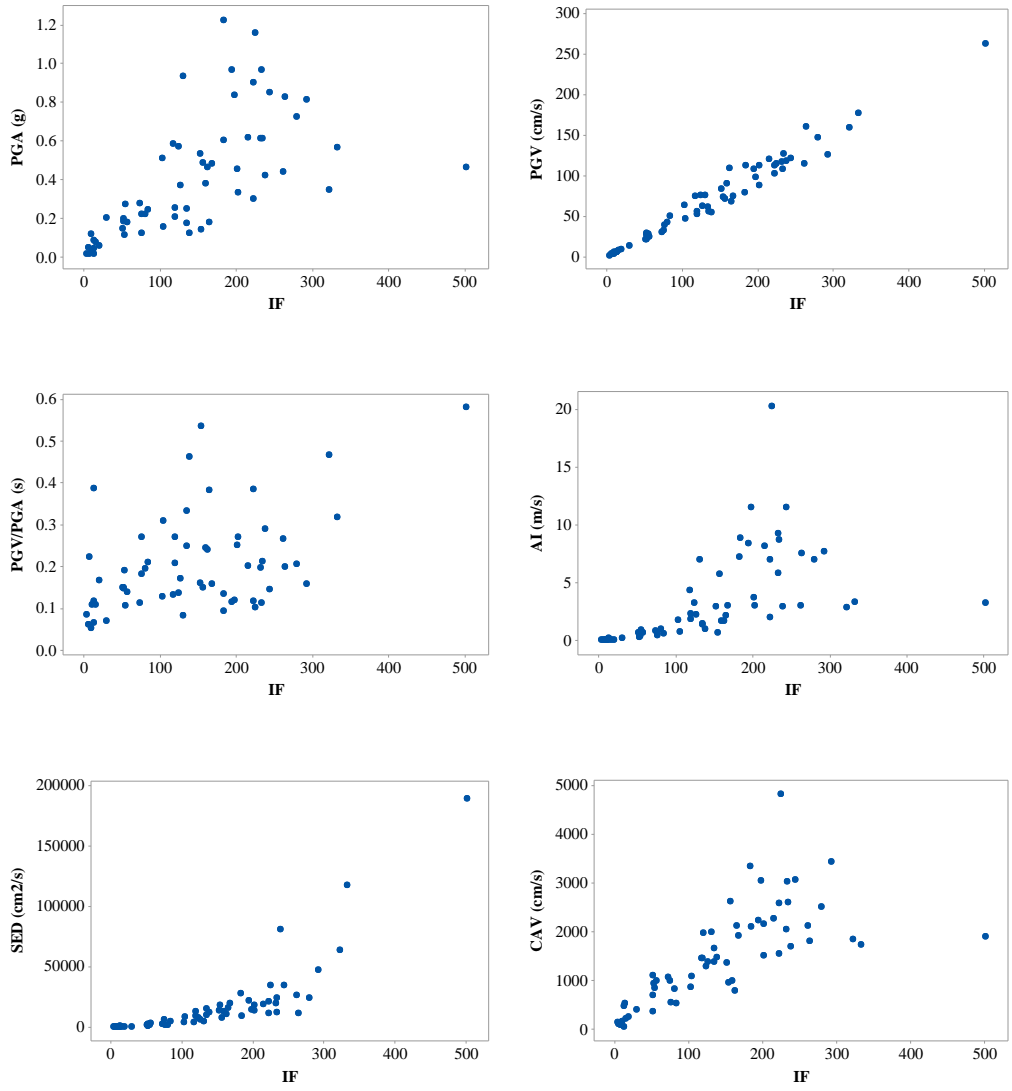
Figure A.83. Scatter plots for selected IMs against I$_F$ (I$_F$-set)
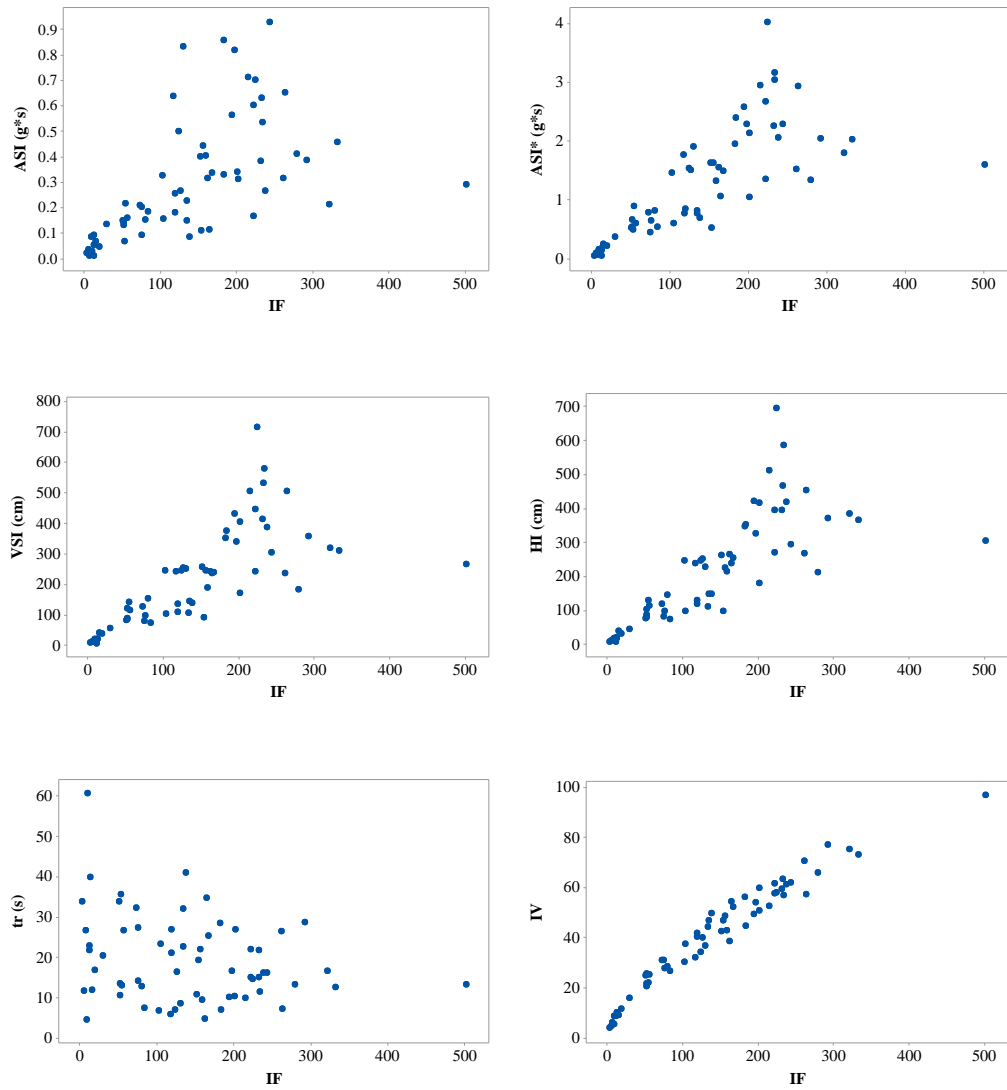
Figure A.84. Additional scatter plots for selected IMs against I_F (I_F-set)
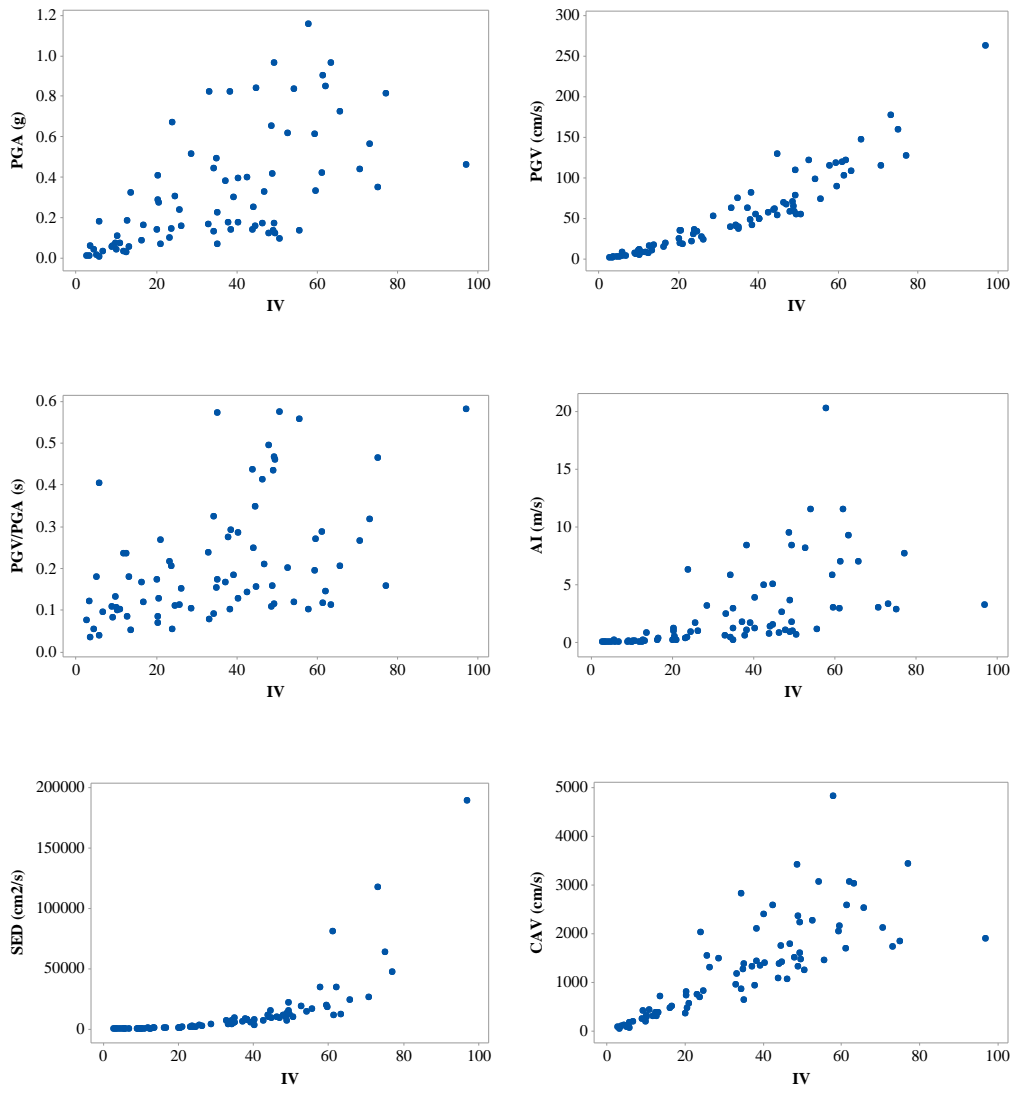
Figure A.85. Scatter plots for selected IMs against Iᵥ (Iv-set)
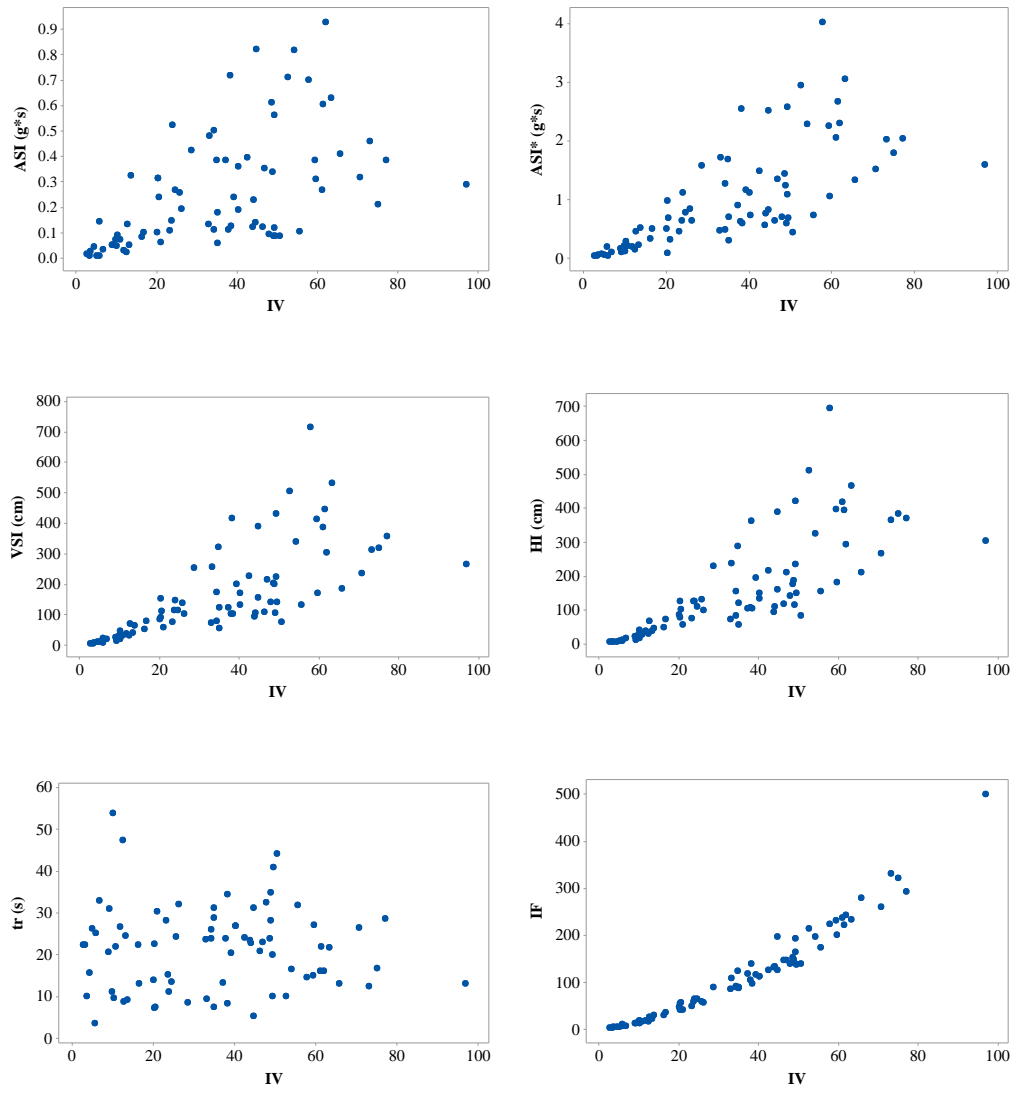
Figure A.86. Additional scatter plots for selected IMs against Iv (Iv-set)
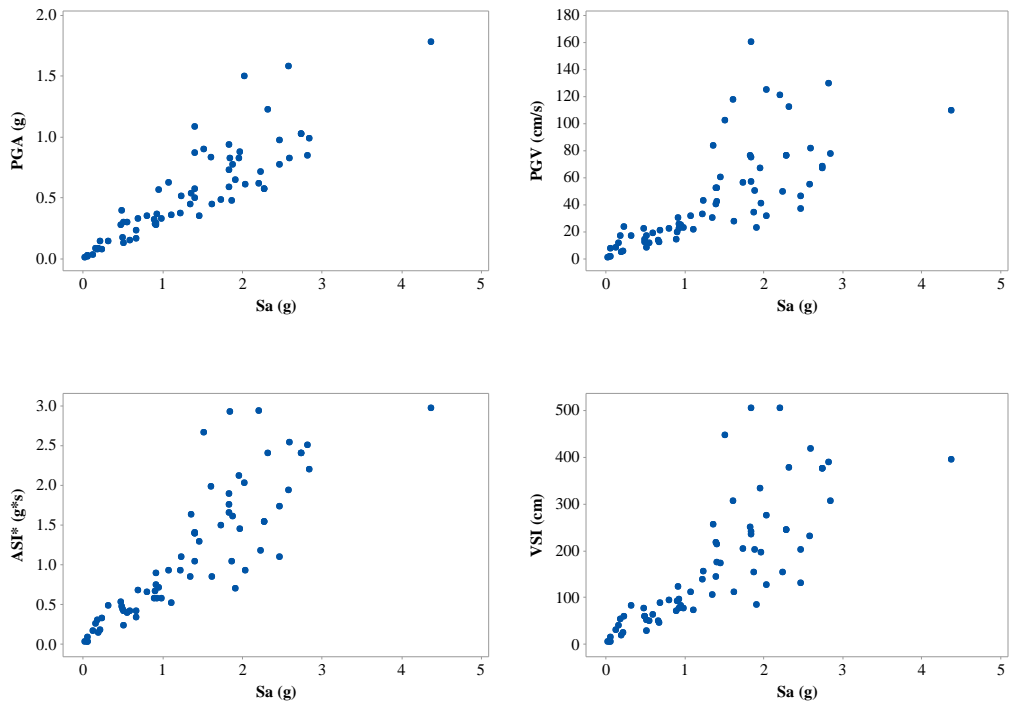
Figure A.87. Scatter plots for selected IMs against S_a (F2S2B2-T_1=0.30s, S_a-set)
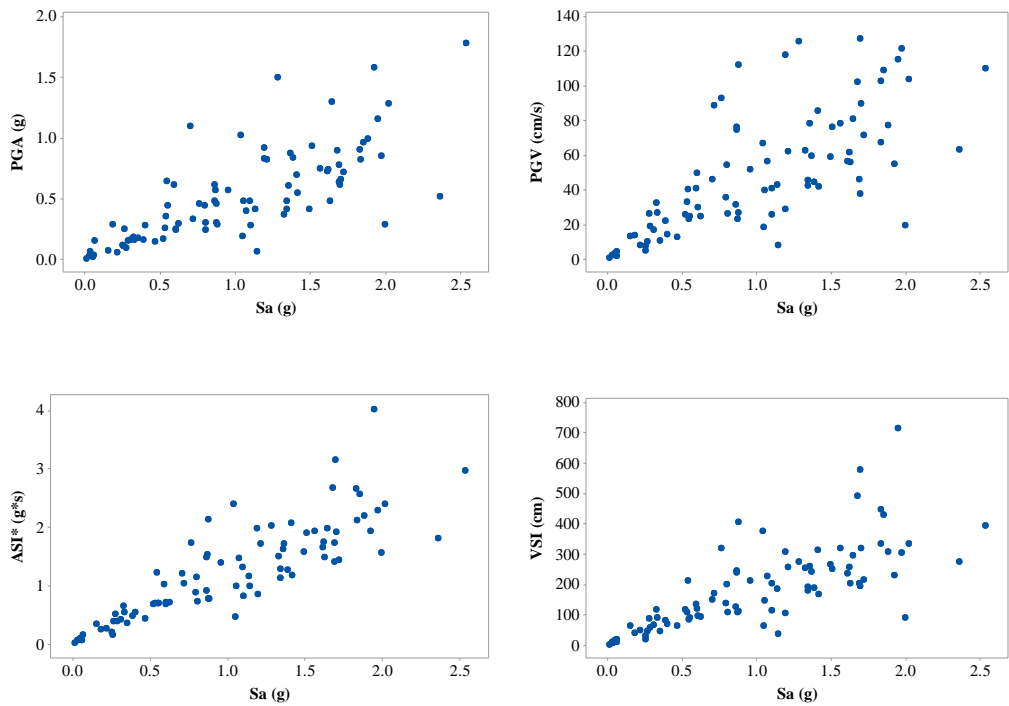
Figure A.88. Scatter plots for selected IMs against S_a (F3S2B-T_1=0.45s, S_a-set)
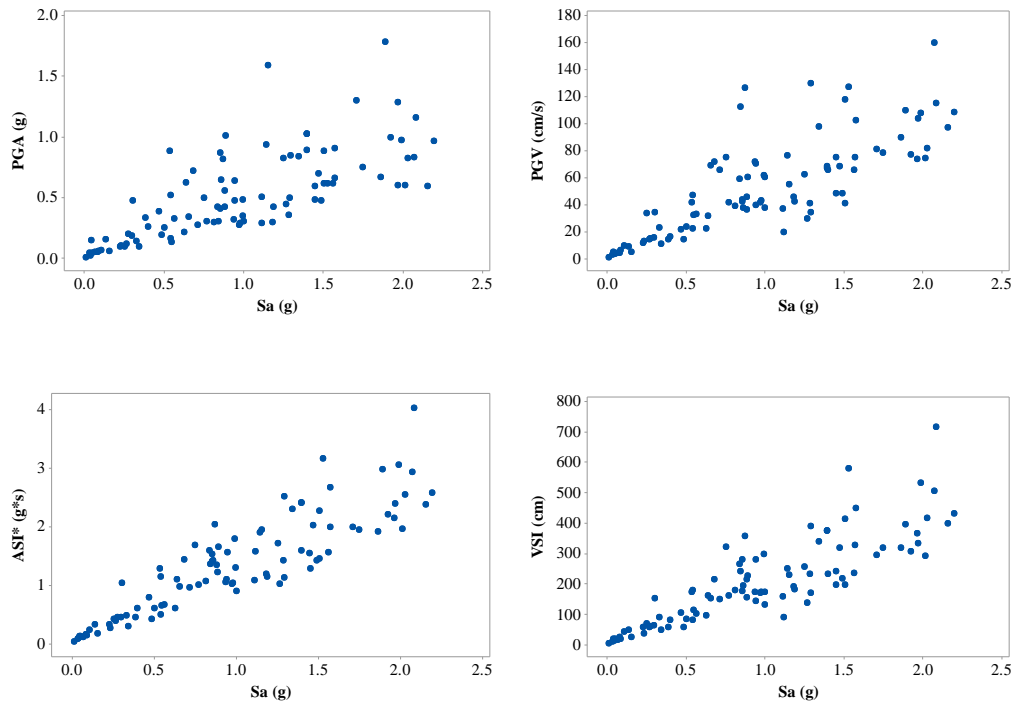
Figure A.89. Scatter plots for selected IMs against S_a (F2S2B-T_1=0.59s, S_a-set)
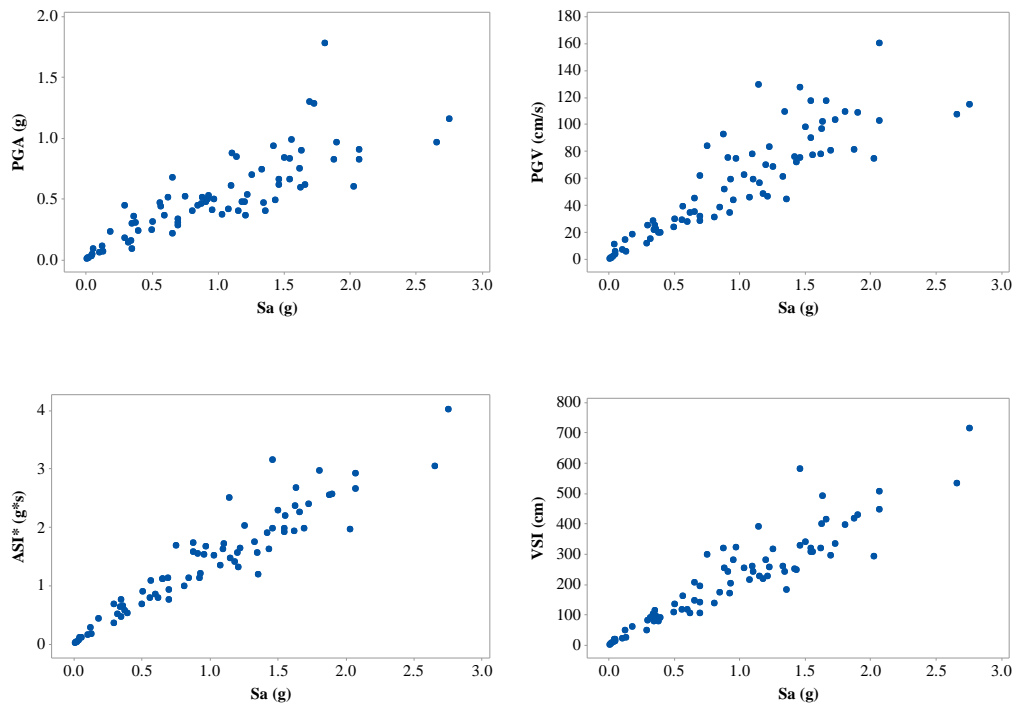
Figure A.90. Scatter plots for selected IMs against S_a (F5S7B-T_1=0.66s, S_a-set)
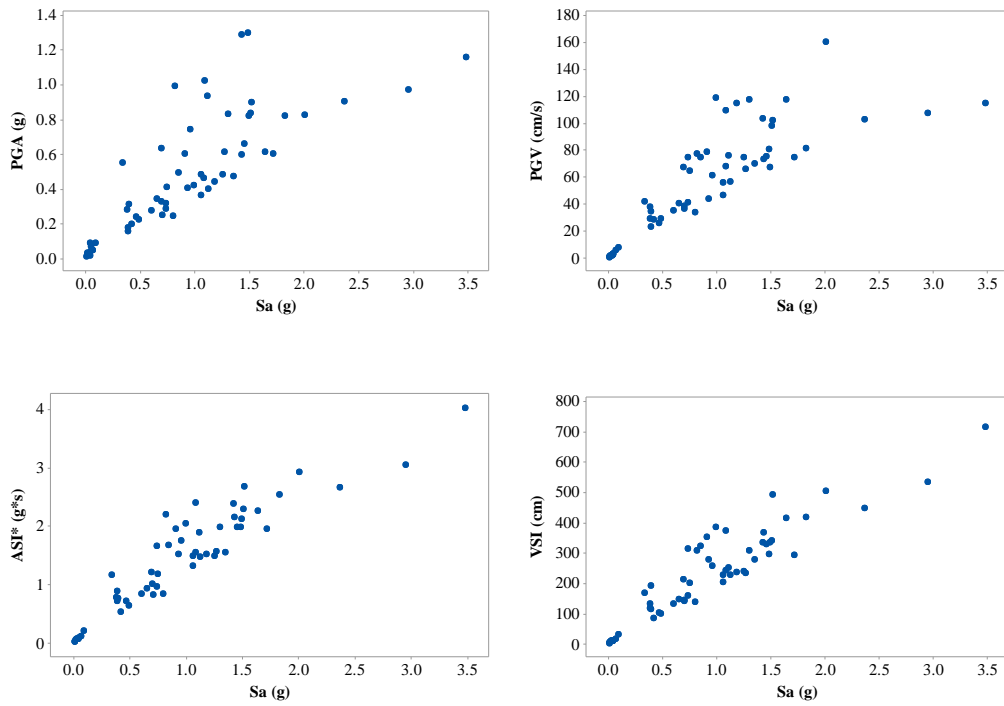
Figure A.91. Scatter plots for selected IMs against S_a (F5S2B-T_1=0.75s, S_a-set)
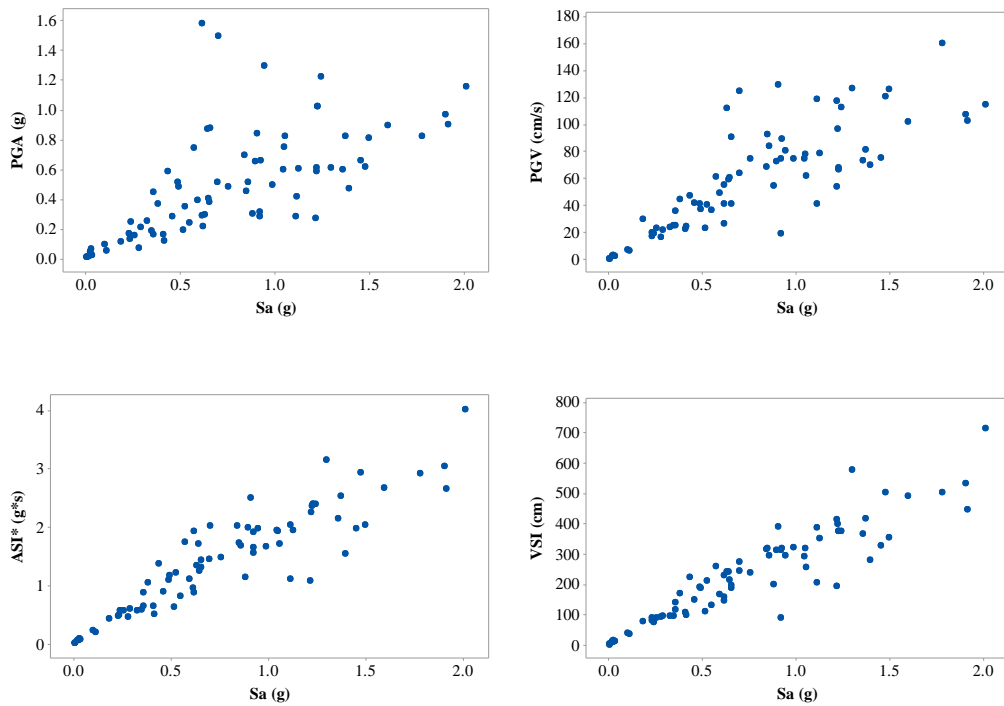
Figure A.92. Scatter plots for selected IMs against S_a (F5S4B-T_1=0.95s, S_a-set)
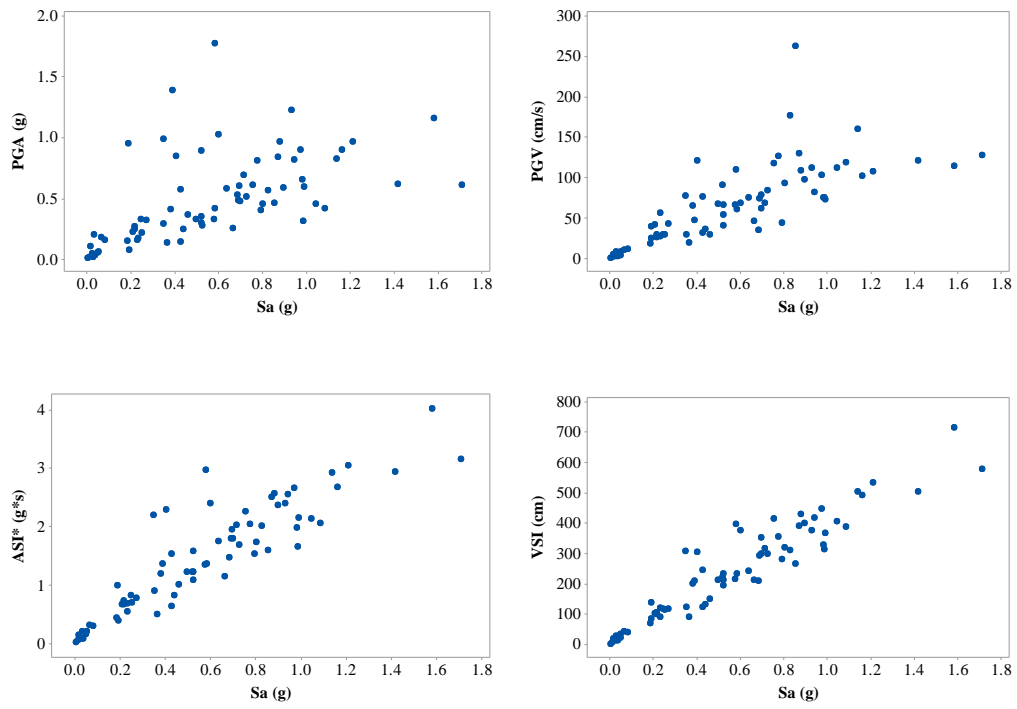
Figure A.93. Scatter plots for selected IMs against S_a (F8S3B-T_1=1.20s, S_a-set)

(a) PGA-set

(b) PGV-set

(c) AI-set

(d) SED-set

(e) CAV-set

(f) ASI*-set
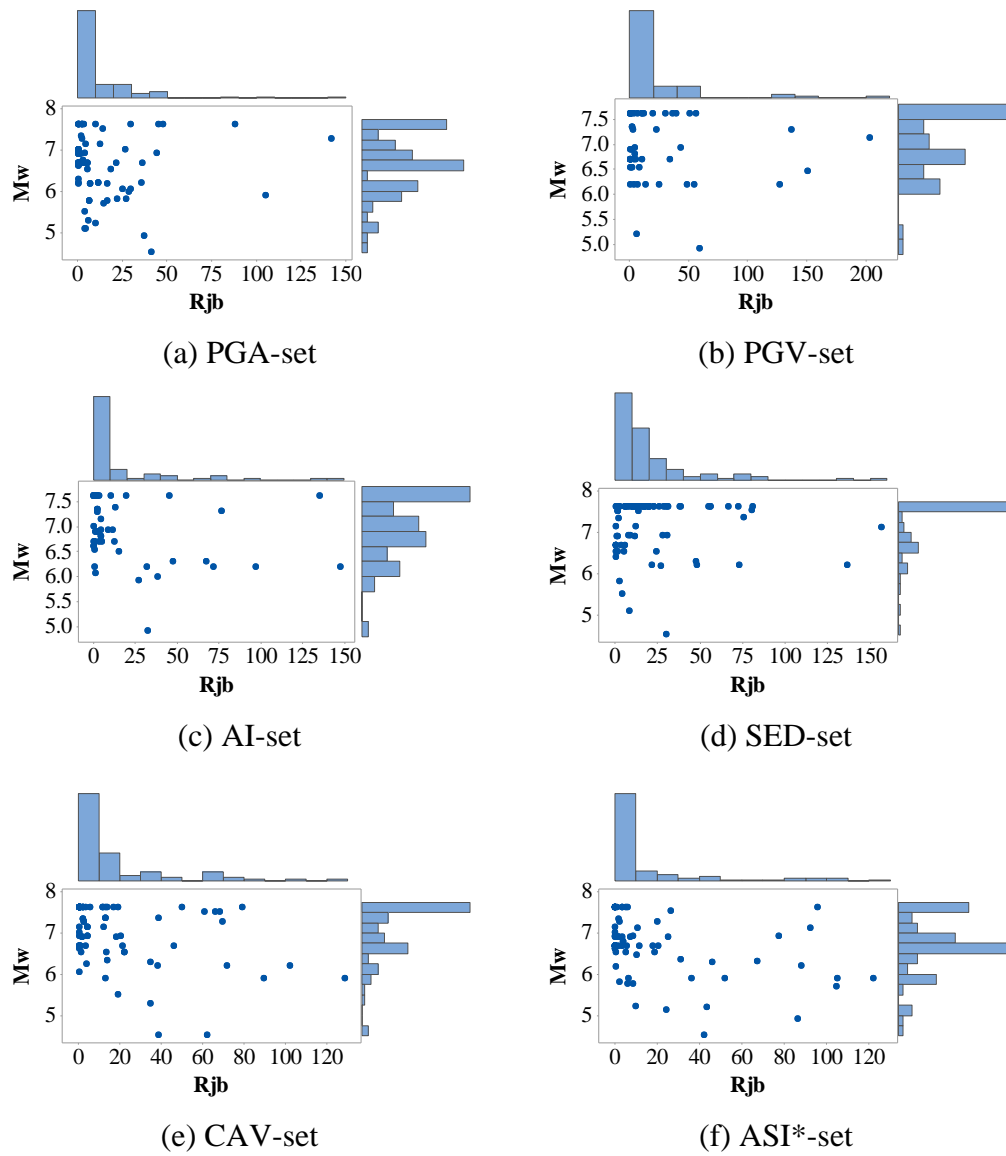
Figure A.94. Marginal plots for M_w vs R_{JB} for selected sets (PGA, PGV, AI, SED, CAV, ASI*)

(a) VSI-set

(b) I$_F$-set

(c) I$_v$-set

(d) S$_a$-set (F2S2B)

(e) S$_a$-set (F2S2B2)

(f) S$_a$-set (F3S2B)
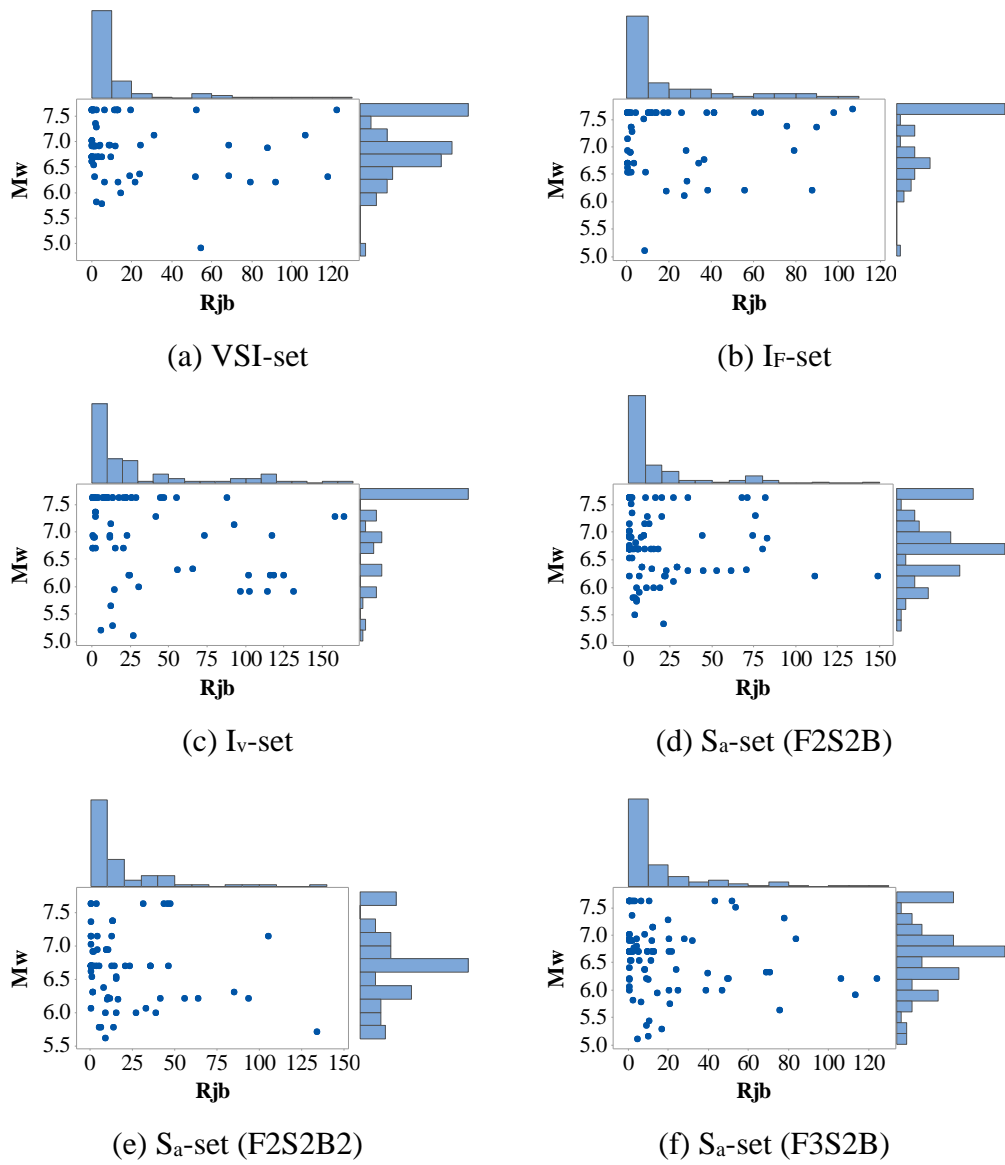
Figure A.95. Marginal plots for M$_w$ vs R$_{JB}$ for selected sets (VSI, I$_F$, I$_v$, S$_a$ alternatives)
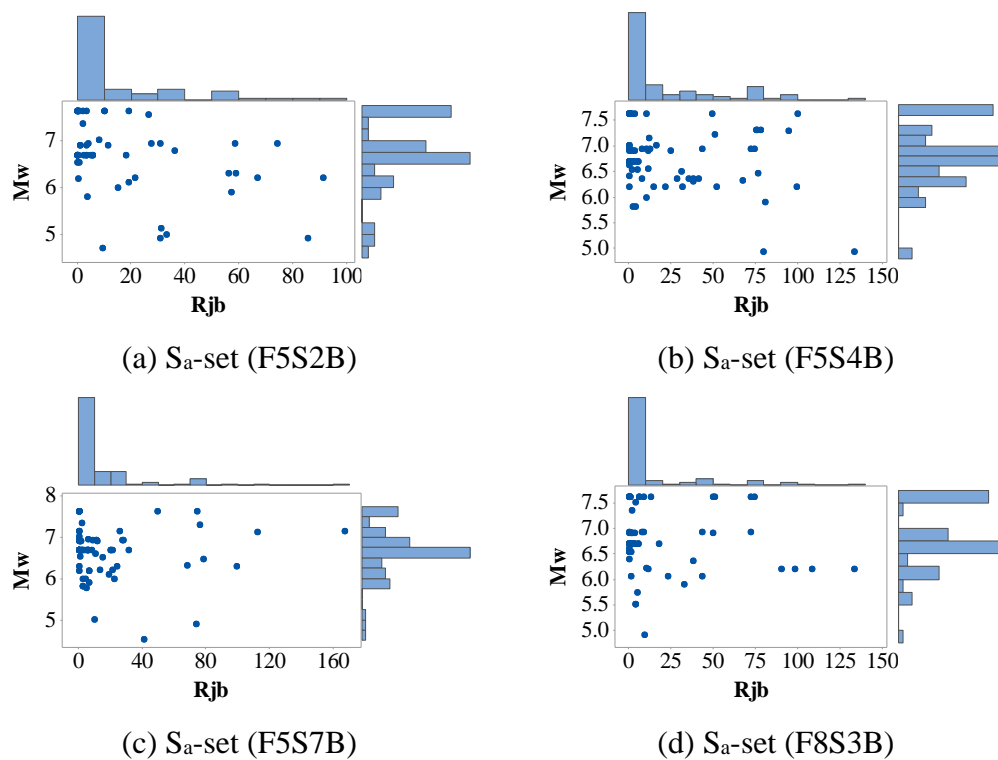
Figure A.96. Marginal plots for M_w vs R_{JB} for selected sets (S_a alternatives)

C.3.   Application of the Cluster Sampling Method

The need for objective classification of the GM records with respect to their individual GM characteristics (represented with a long list of IMs) and to facilitate the formation of a dataset as a downsized subset of the main database with all key characteristics implicitly included has directed this study to follow a cluster sampling method. To classify 6'883 records (made available in Chapter 2) reliably; of the non-hierarchical clustering approach, k-means clustering (i.e., hard clustering) algorithm has been utilized to assign one record to only one group/cluster. The ground motion characteristics reflected through IMs (as previously calculated and examined in Chapter 2) showing moderate-to-strong inter-correlation; however, required a data preparation/modification stage to be applied in advance of the clustering stage.

The principal component analysis (PCA) (after Karl Pearson, 1901), effective in dealing with highly inter-dependent data, simply reduces the dimensionality of a dataset with a large number of inter-related variables, yet retaining as much of the variation in the dataset as possible. Generally, the first principal component is a linear combination of the original variables and explains much of the variation under the condition that it is uncorrelated with the previous components. Besides, the first few principal components provide a simpler picture of the data than trying to understand all the original variables. Figure A.97 presents a sample case with a group of two-dimensional data, where the first principal component (i.e., eigenvector and its corresponding eigenvalue) is shown to explain the largest proportion of the variance inherent in the data. In this study, the PCA has been performed on the original dataset via MATLAB (2018), and the proportions of the total variance explained by each principal component have been calculated.
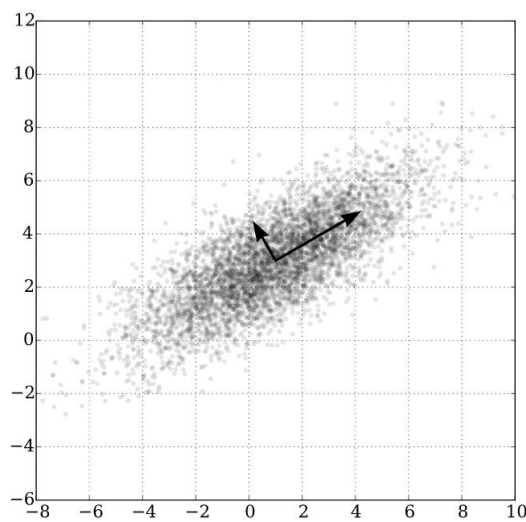
Figure A.97. A sample representation of the principal components after PCA (taken from Wikimedia Commons)

Table A.2 presents the numerical results for the first 5 principal components, concluding that the first two eigenvectors are sufficient to define the whole set. In simple terms, the 25-dimensional dataset with 6'883 items has been transformed in a way that two-dimensional re-representation of the set could be utilized in the cluster analysis stage as a sufficiently simpler equivalent.

Table A.2 Proportion of variance explained by the first 5 principal components

Eigenvector #	Proportion of Variance
1	0.9362
2	0.0625
3	0.0008
4	0.0003
5	0.0002
Total	~1.0000

The cluster analysis, following the PCA stage, has been performed utilizing the k-means function readily available in MATLAB software with the following options:

- Distance metric has been defined as "Cityblock" with a trial-and-error procedure. This measure considers the sum of absolute differences where each centroid is the component-wise median of the points in the cluster.

- The k-means partitioning is sensitive to the initial choice of seeds which are considered in the calculations of the centroids, thus leading to inaccurate clustering of the sample space. The solution to this potential problem is considering replicates, in other words, repetitions to re-apply partitioning with new initial centroid positions. This parameter has been taken as 20 in the analyses.

- The clustering solution has been evaluated using Calinski-Harabasz Criterion with consideration of 20 clusters.

The numerical evaluations have recommended the optimal number of clusters as 10, as shown in Figure A.98, where the resulting clusters are displayed in Figure A.99.

After the finalization of the k-means oriented classification stage, 40 records have been sampled from each cluster leading to a 400-record cluster sampling-based subset. The reason for keeping the number of samples from each cluster so high is to compensate for the precision loss in cluster sampling, and additionally, to keep the cluster sampling-based set size almost equivalent to the combined set of random sampling-based sample subsets.

The scatter of key IMs against PGA or PGV for the cluster sampling-based subset has been presented in Figure A.100 and Figure A.101. The distribution of the shortlisted IMs from this subset has also been checked considering the bin-wise intensity ranges defined in the random sampling stage. Figure A.102 shows the corresponding frequency distributions for alternative IMs and has displayed the accumulation of records at low intensity levels leading to a conclusion that the cluster sampling-based GM subset might not be suitable for intensity-based assessments to be performed at various intensity levels. The marginal plot for moment magnitude (M_w) versus source-to-site distances (R_{JB}) displayed in Figure A.103 has exhibited that R_{JB} distribution for cluster sampling-based subset is positively skewed, but not squeezed as the random sampling-based subset.
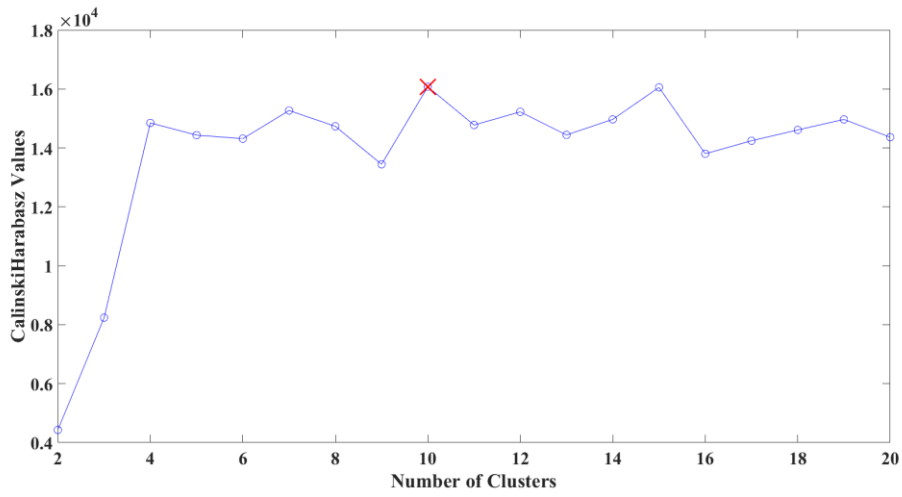
Figure A.98. Variation of Calinski-Harabasz values with number of clusters
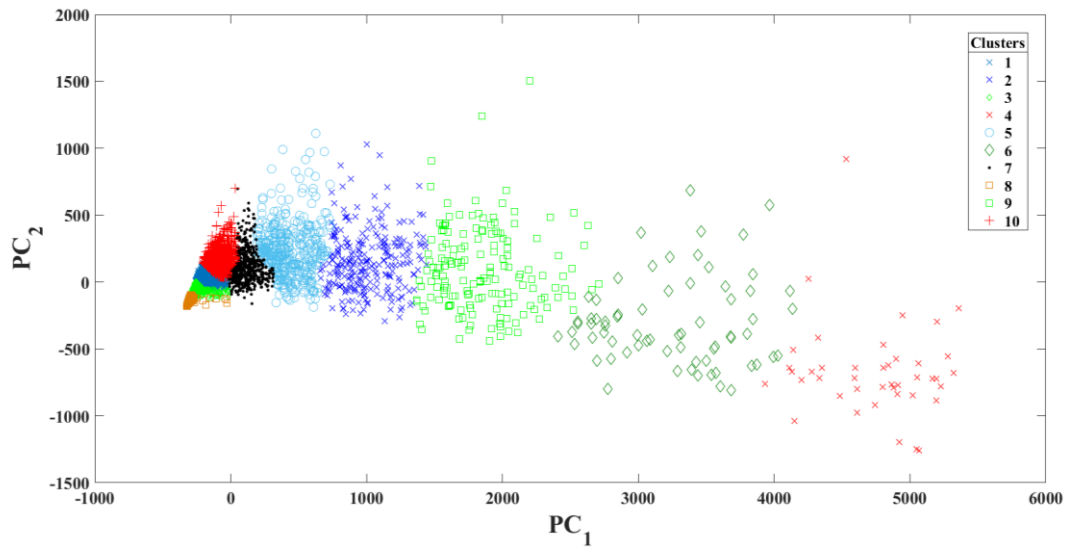
Figure A.99. Resulting clusters for the GM data based on the first two principal components
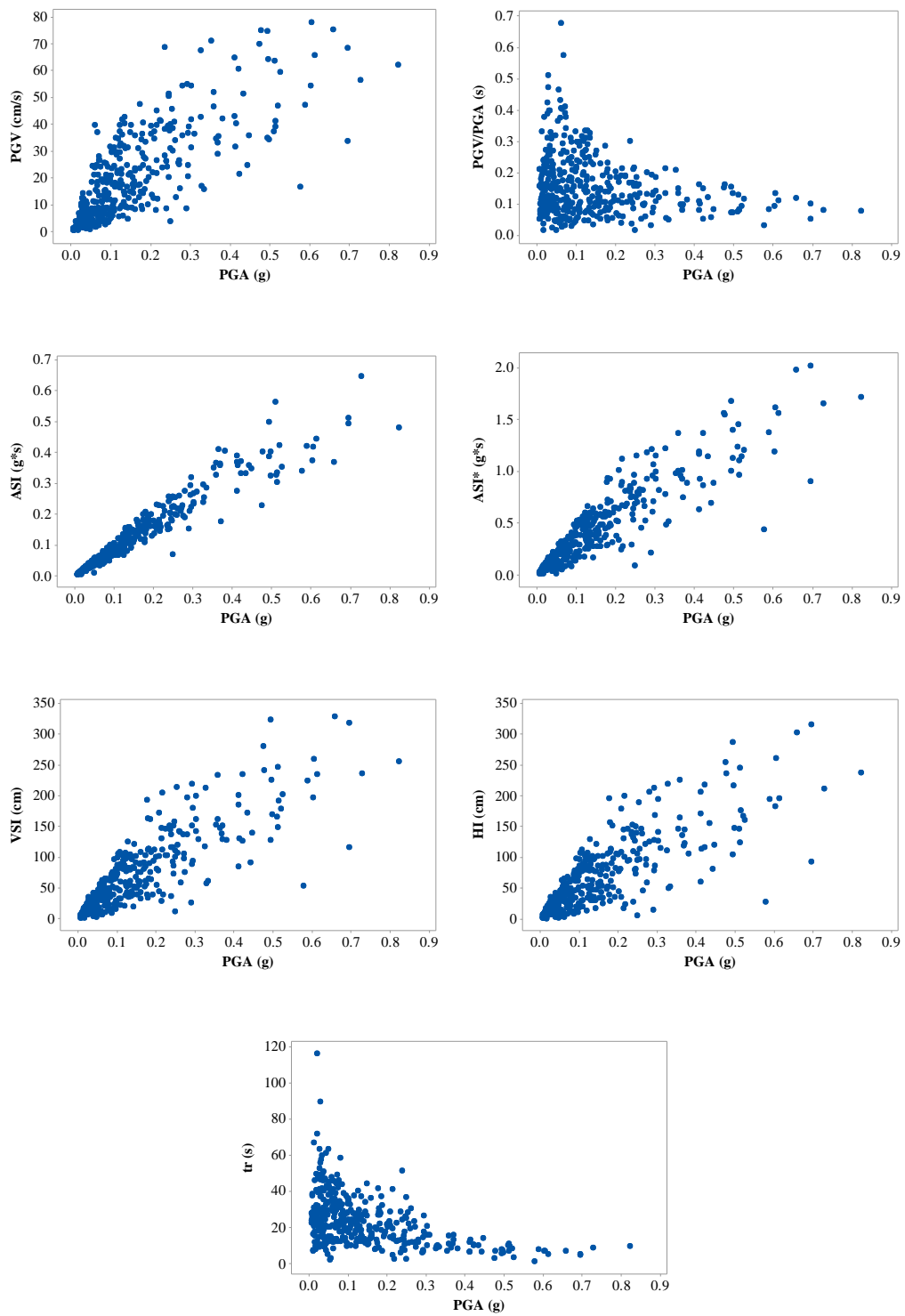
Figure A.100. Scatter plots for selected IMs against PGA (Cluster Sampling Set)
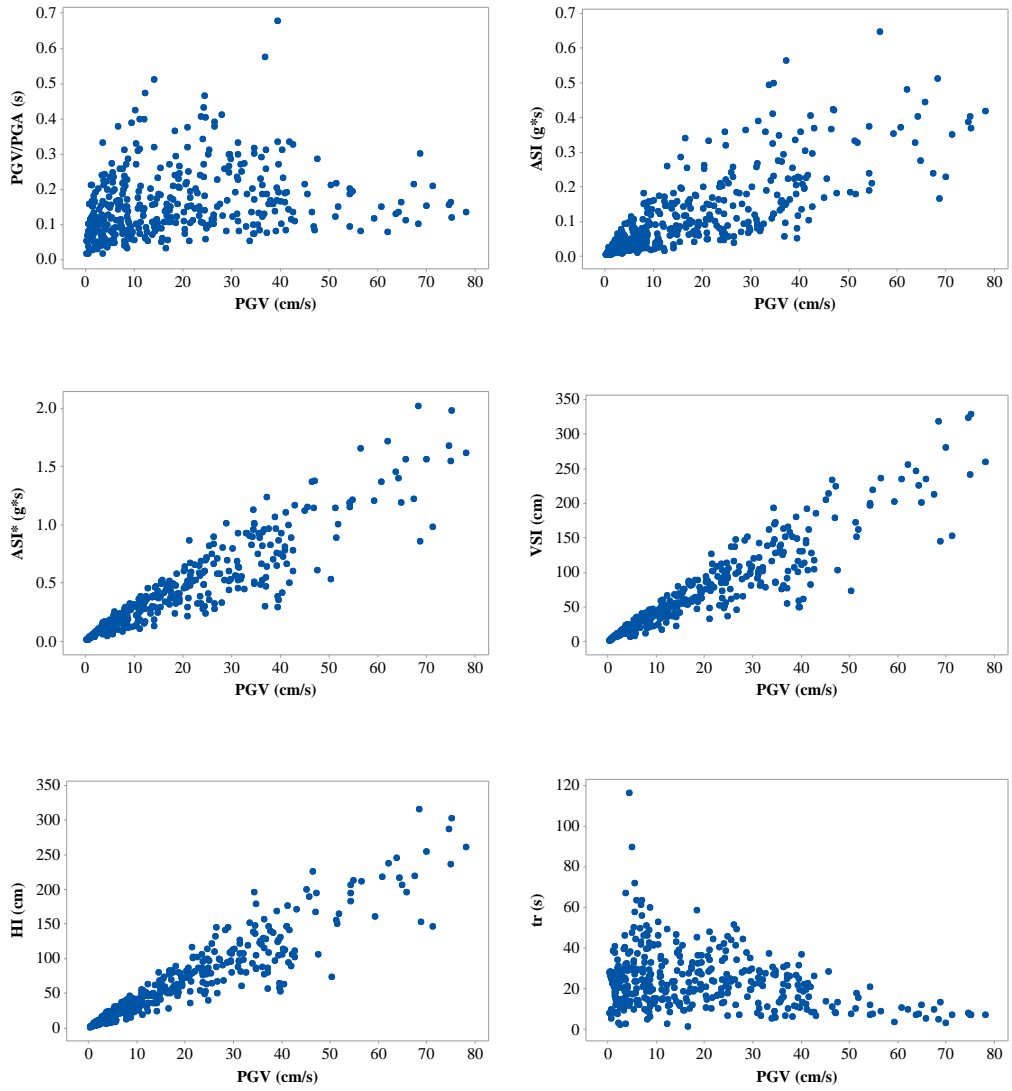
Figure A.101. Scatter plots for selected IMs against PGV (Cluster Sampling Set)
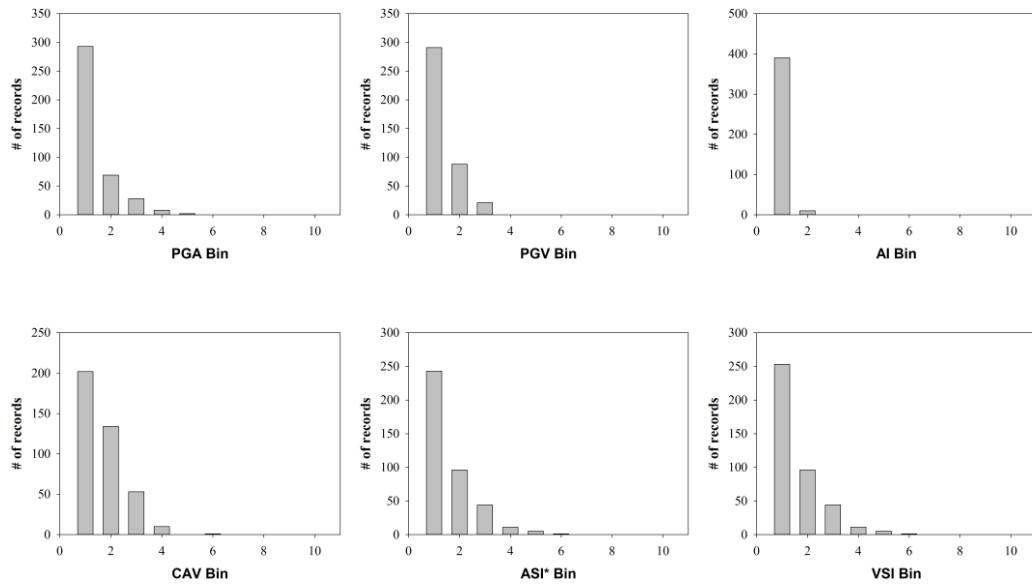
Figure A.102. Distribution of IMs corresponding to cluster sampling-based GM subset
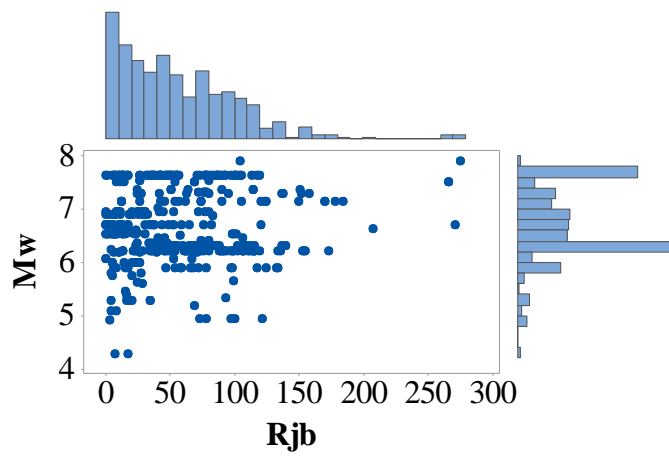
Figure A.103. Marginal plot for M_w vs R_{JB} for Cluster Sampling-set

D. Additional Scatter Plots (for Chapter 5)

○ Random Sampling-Combined Set   + Cluster Sampling Set
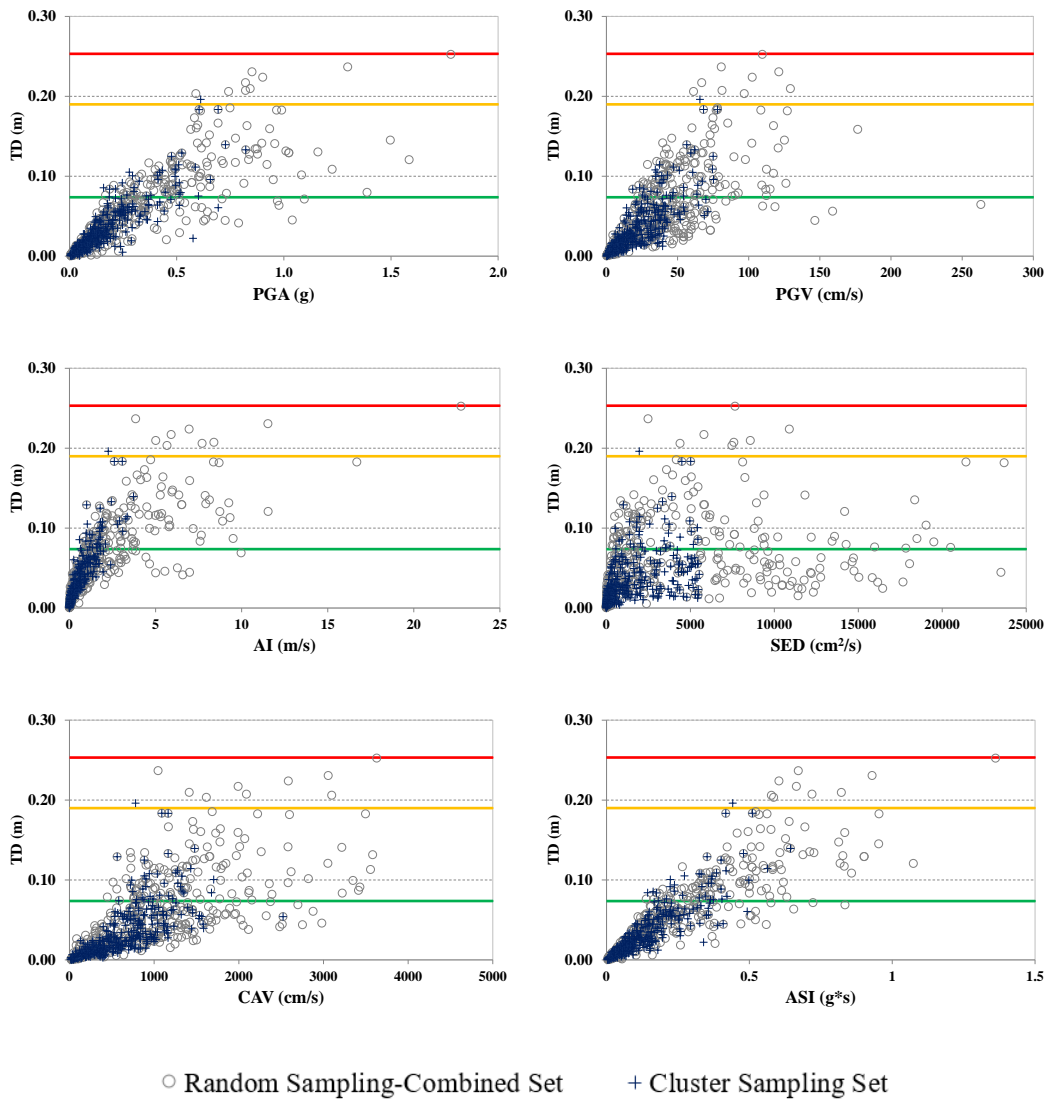
Figure A.104. Scatter plots for selected IMs (PGA, PGV, AI, SED, CAV, ASI) versus Top Drift for F3S2B (T_1=0.45 s) (ESDOF)
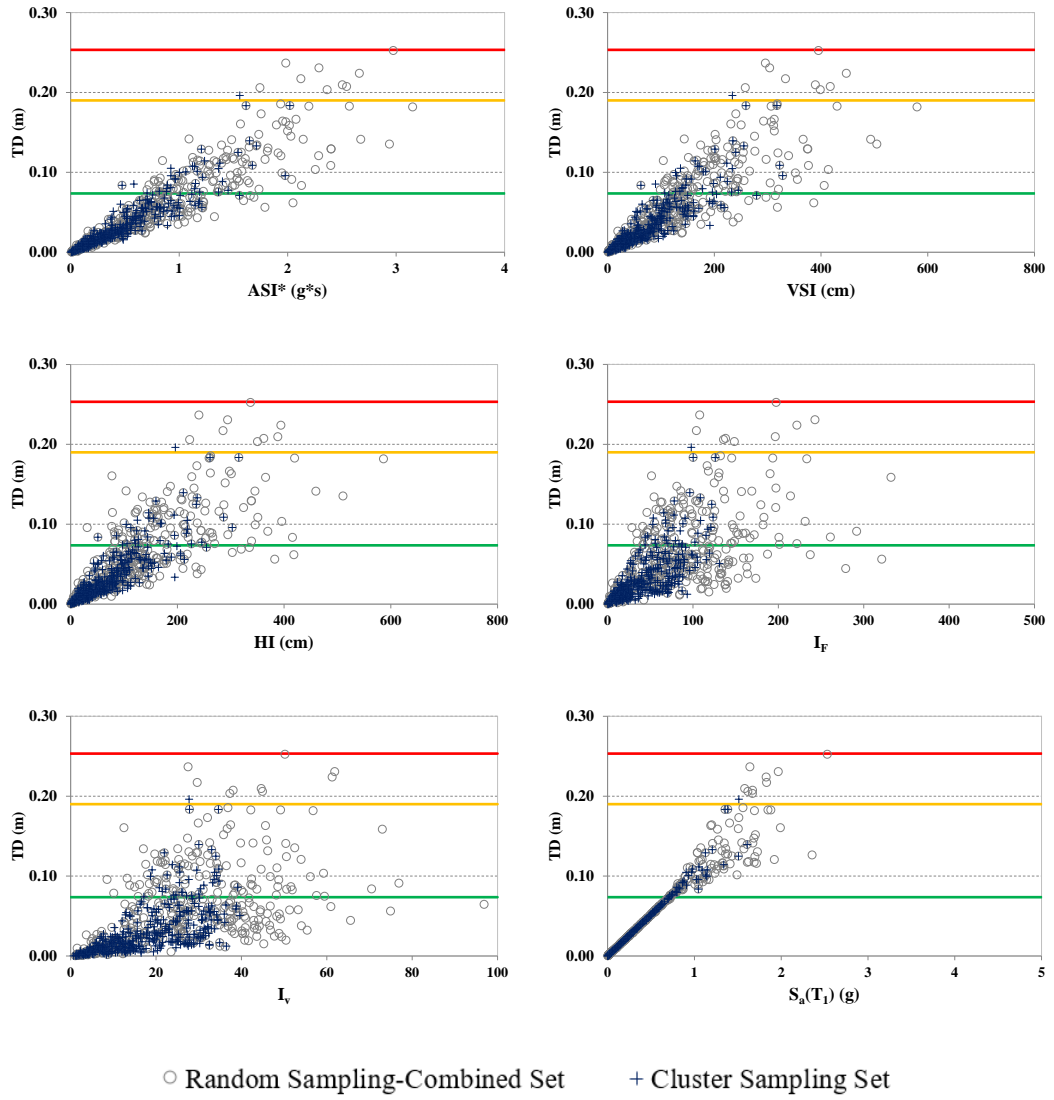
Figure A.105. Scatter plots for selected IMs (ASI*, VSI, HI, I_F, I_V, $S_a(T_1)$) versus Top Drift for F3S2B (T_1=0.45 s) (ESDOF)
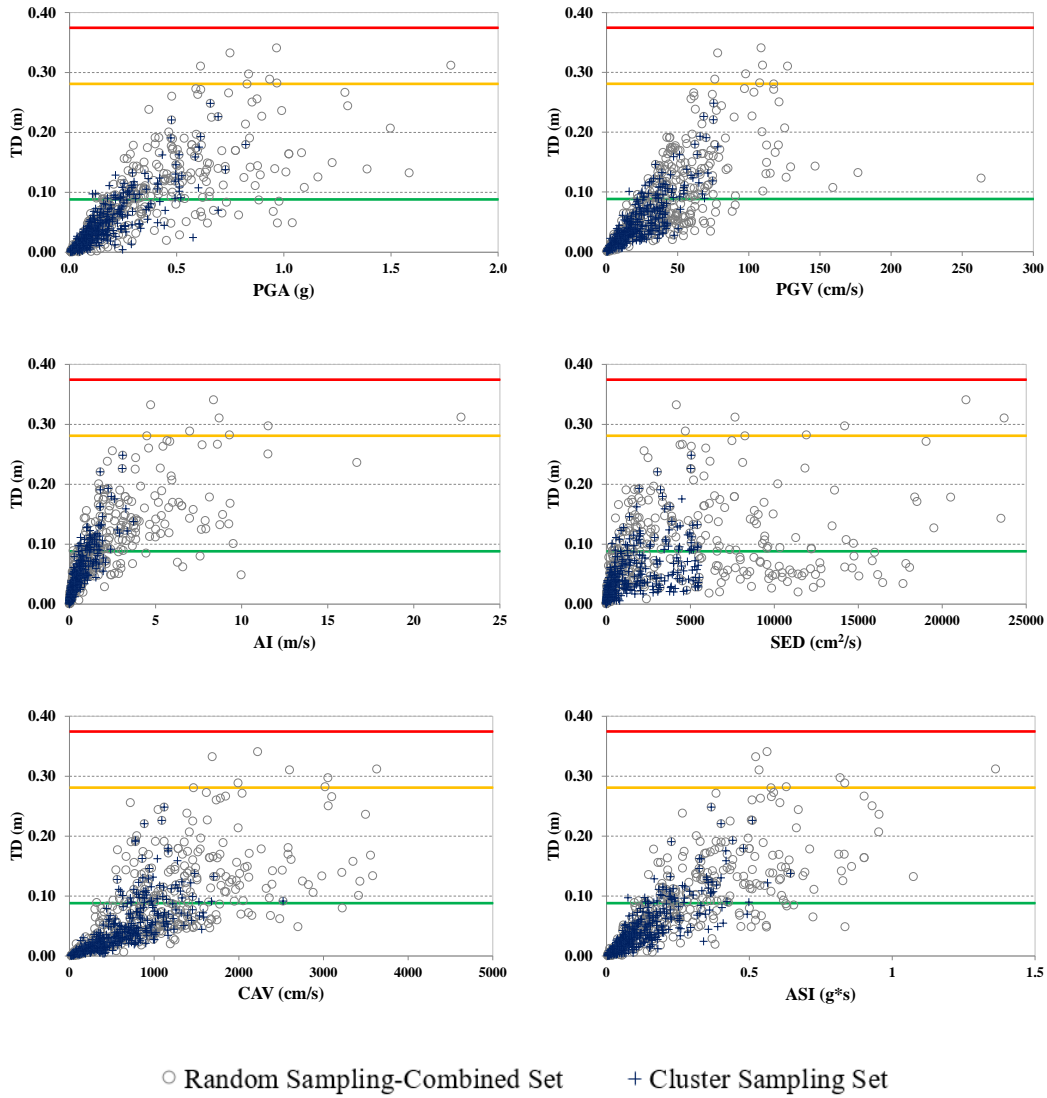
Figure A.106. Scatter plots for selected IMs (PGA, PGV, AI, SED, CAV, ASI) versus Top Drift for F2S2B (T_1=0.59 s) (ESDOF)
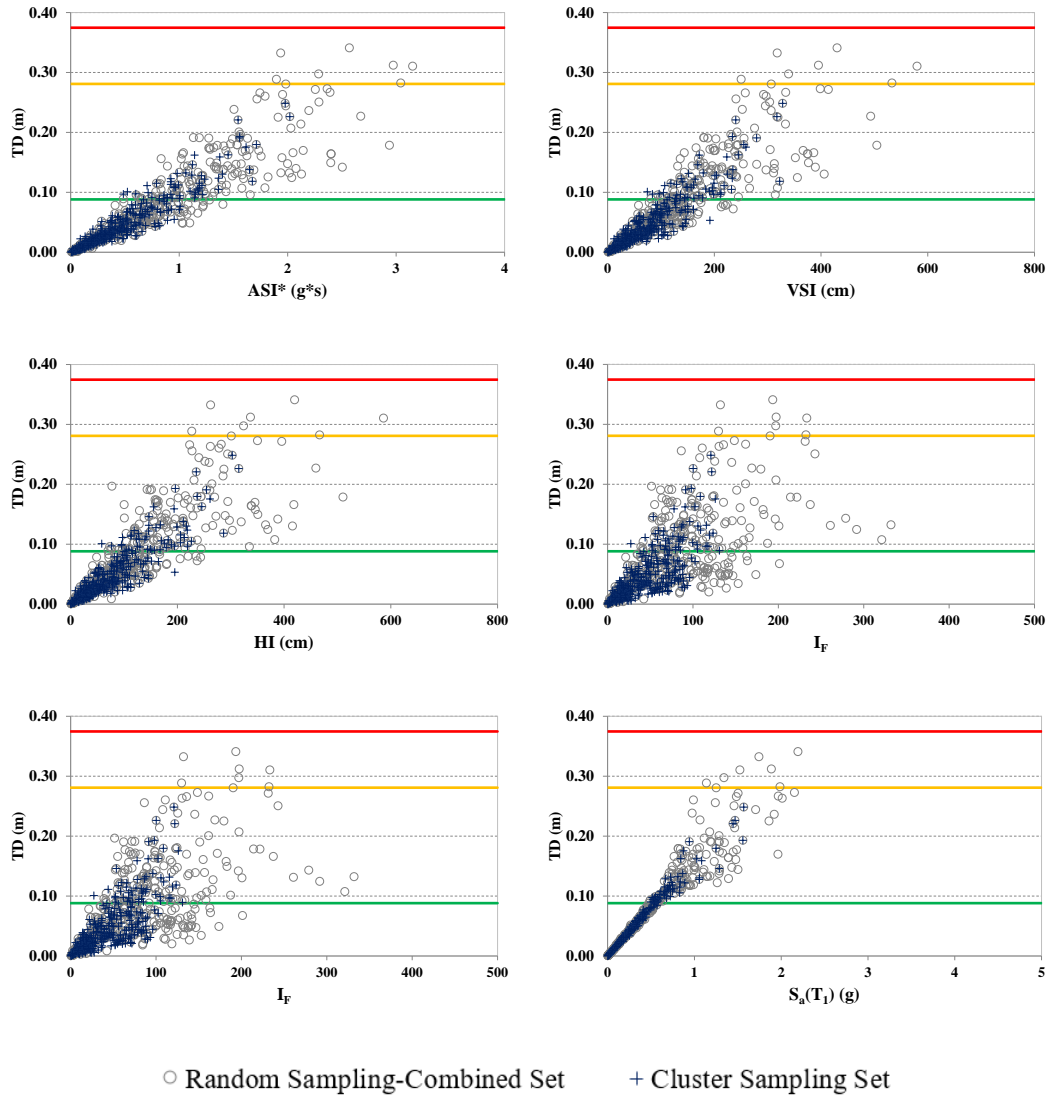
Figure A.107. Scatter plots for selected IMs (ASI*, VSI, HI, I_F, I_V, $S_a(T_1)$) versus Top Drift for F2S2B (T_1=0.59 s) (ESDOF)
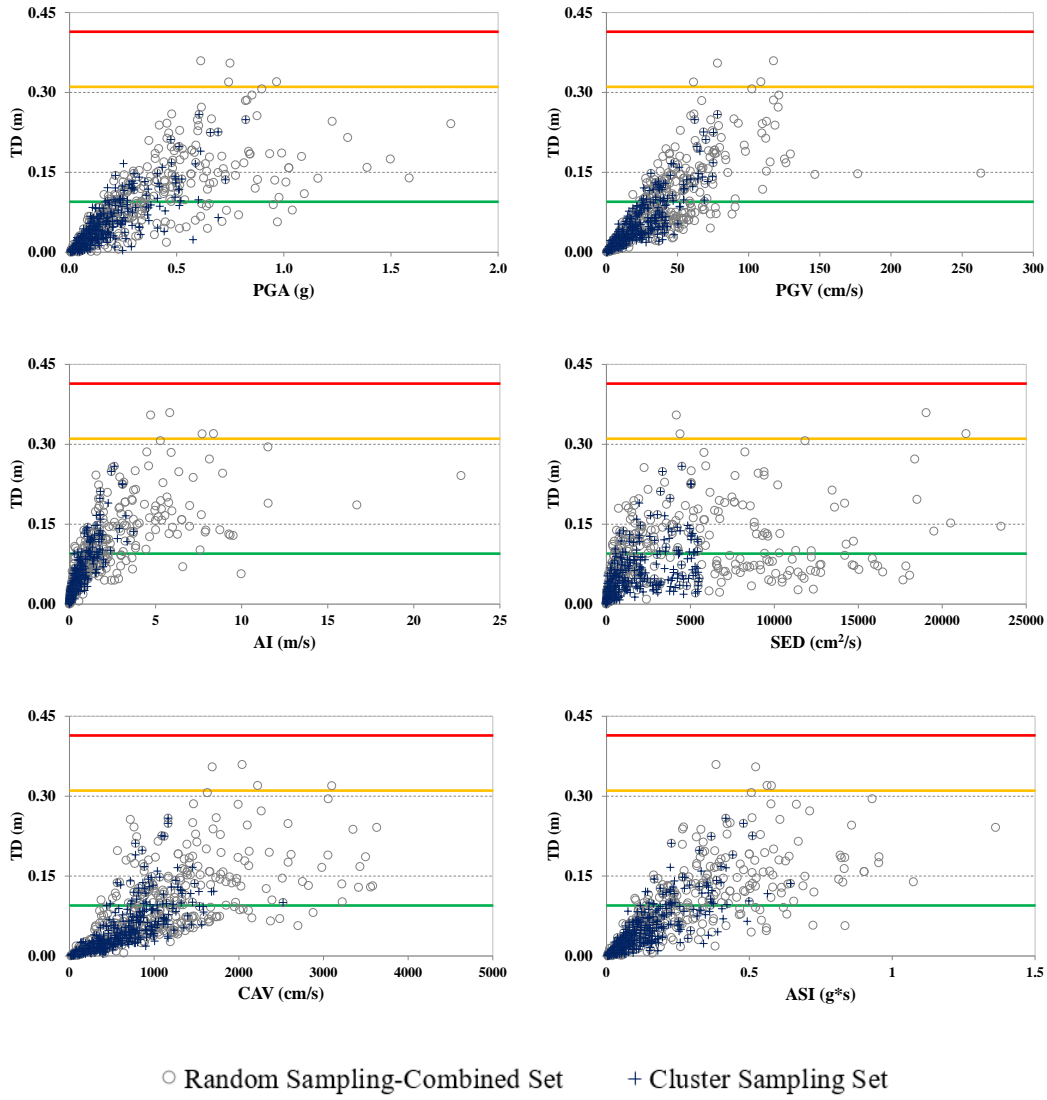
Figure A.108. Scatter plots for selected IMs (PGA, PGV, AI, SED, CAV, ASI) versus Top Drift for F5S7B (T_1=0.66 s) (ESDOF)
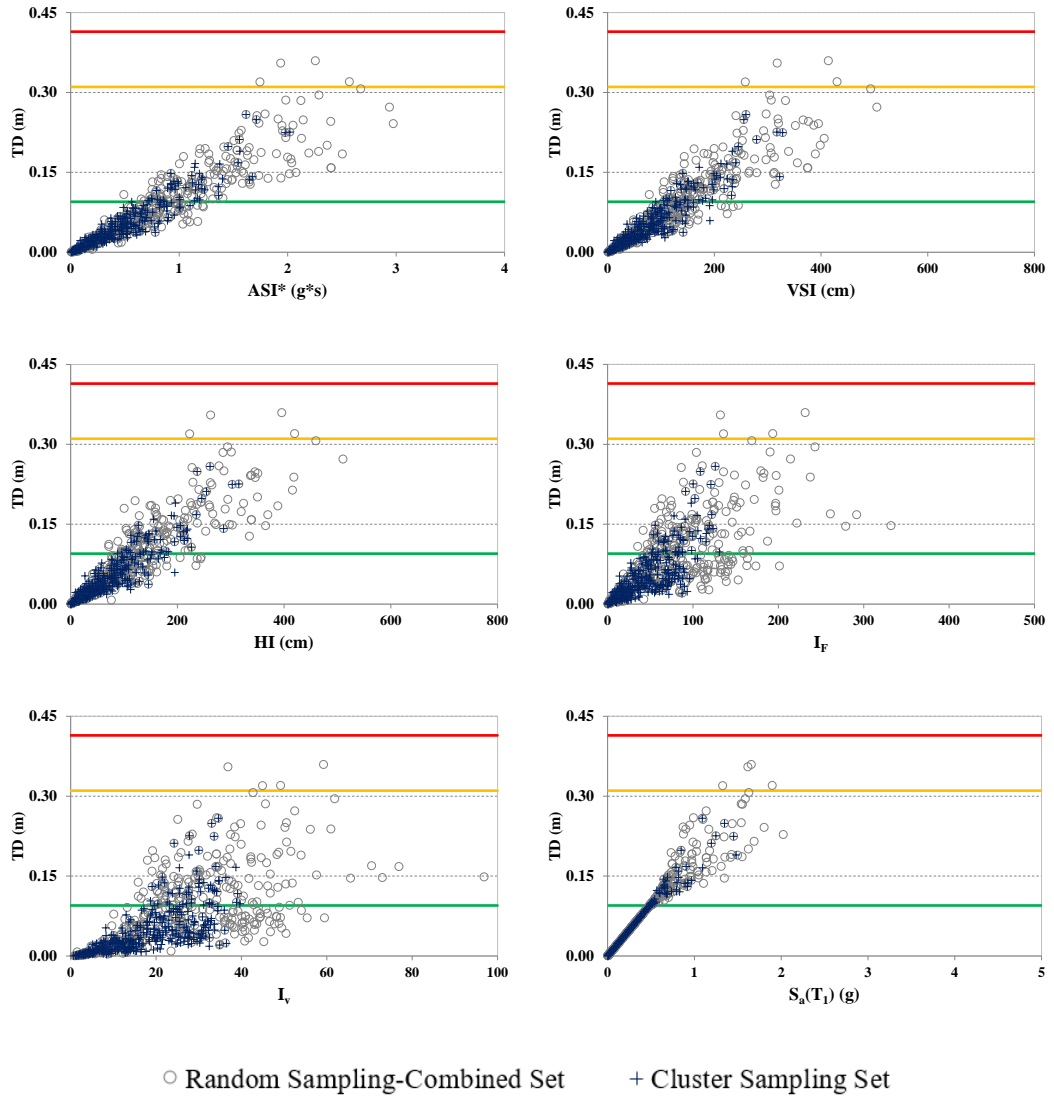
Figure A.109. Scatter plots for selected IMs (ASI*, VSI, HI, I_F, I_V, $S_a(T_1)$) versus Top Drift for F5S7B (T_1=0.66 s) (ESDOF)
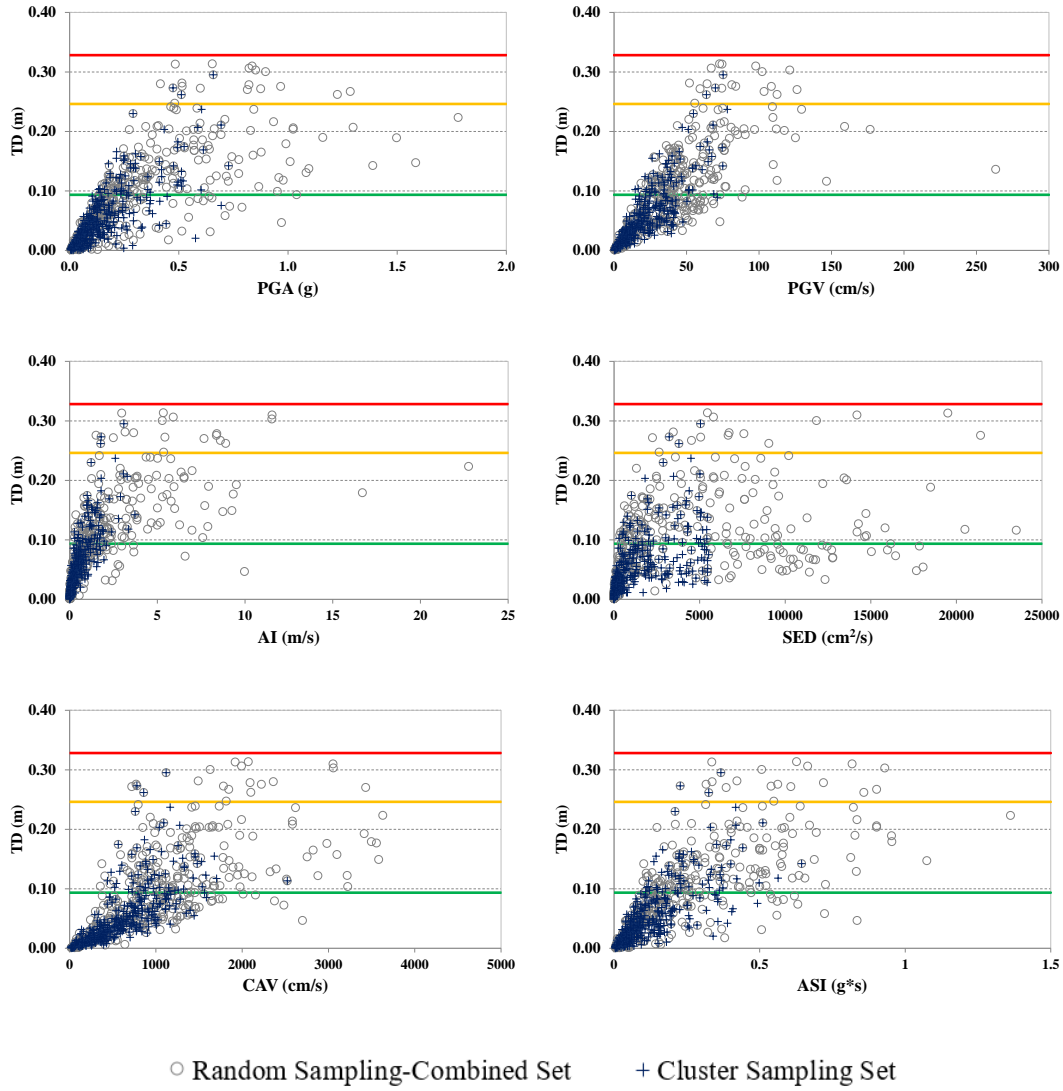
Figure A.110. Scatter plots for selected IMs (PGA, PGV, AI, SED, CAV, ASI) versus Top Drift for F5S2B (T$_1$=0.75 s) (ESDOF)

○ Random Sampling-Combined Set   + Cluster Sampling Set
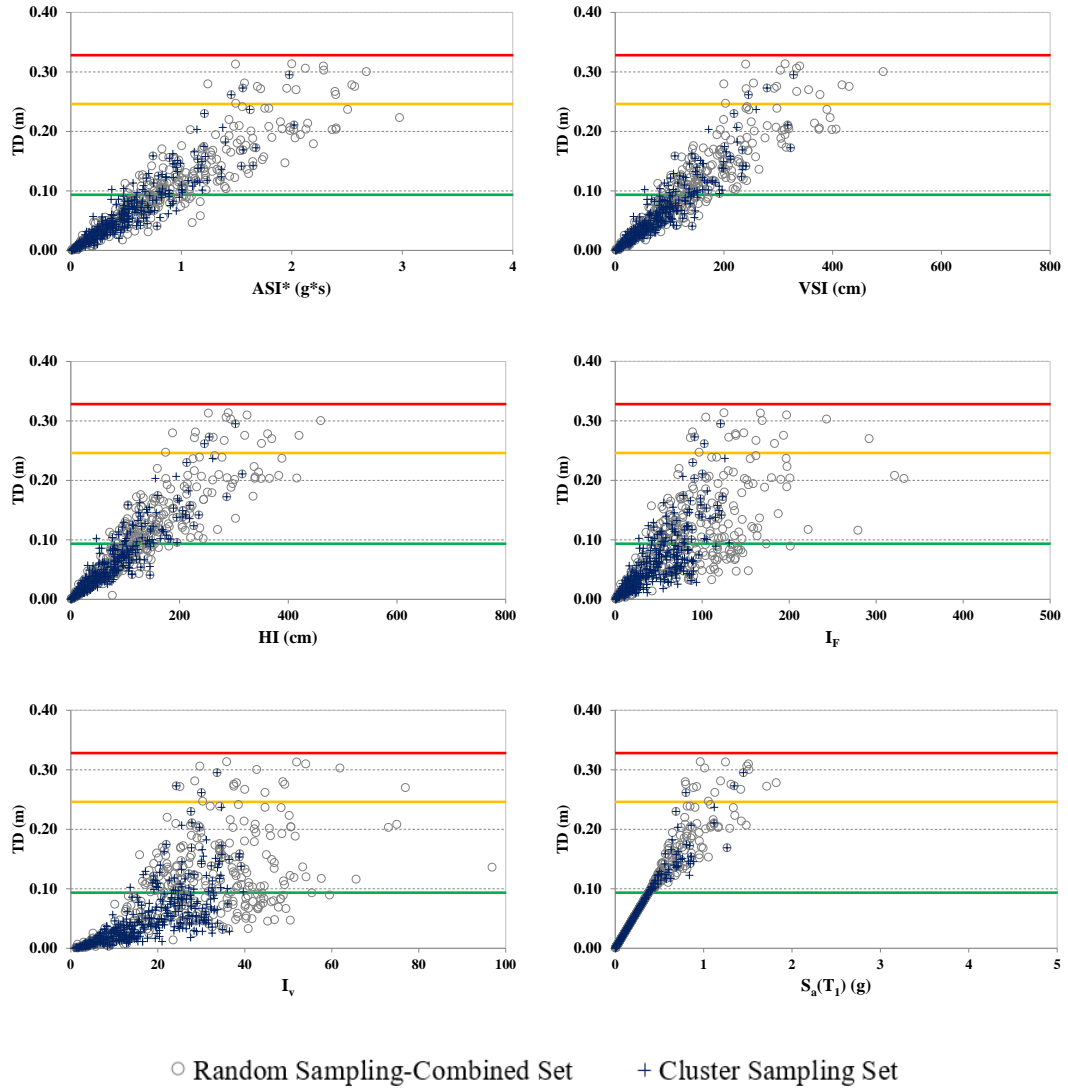
Figure A.111. Scatter plots for selected IMs (ASI*, VSI, HI, I_F, I_V, $S_a(T_1)$) versus Top Drift for F5S2B (T_1=0.75 s) (ESDOF)
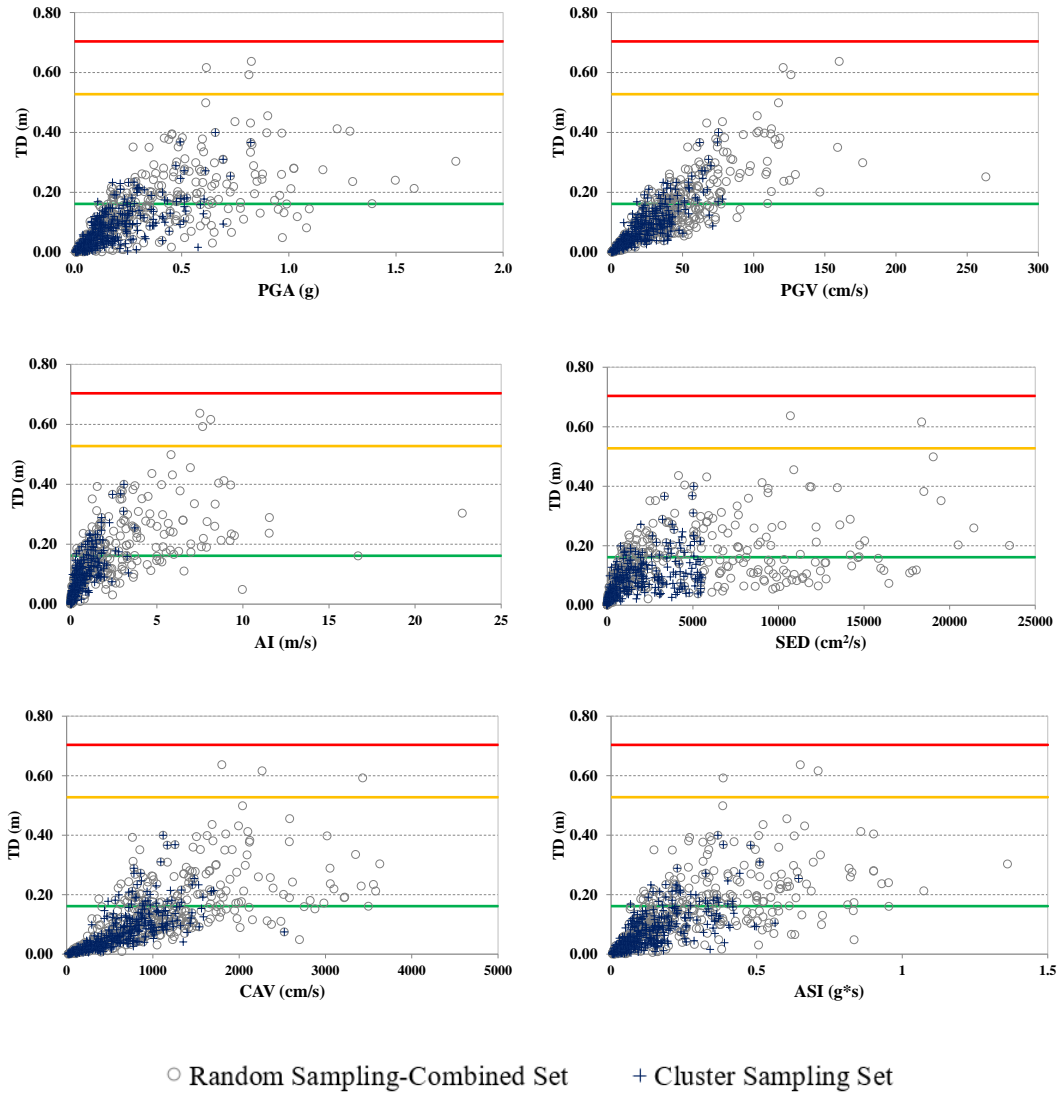
Figure A.112. Scatter plots for selected IMs (PGA, PGV, AI, SED, CAV, ASI) versus Top Drift for F5S4B (T_1=0.95 s) (ESDOF)
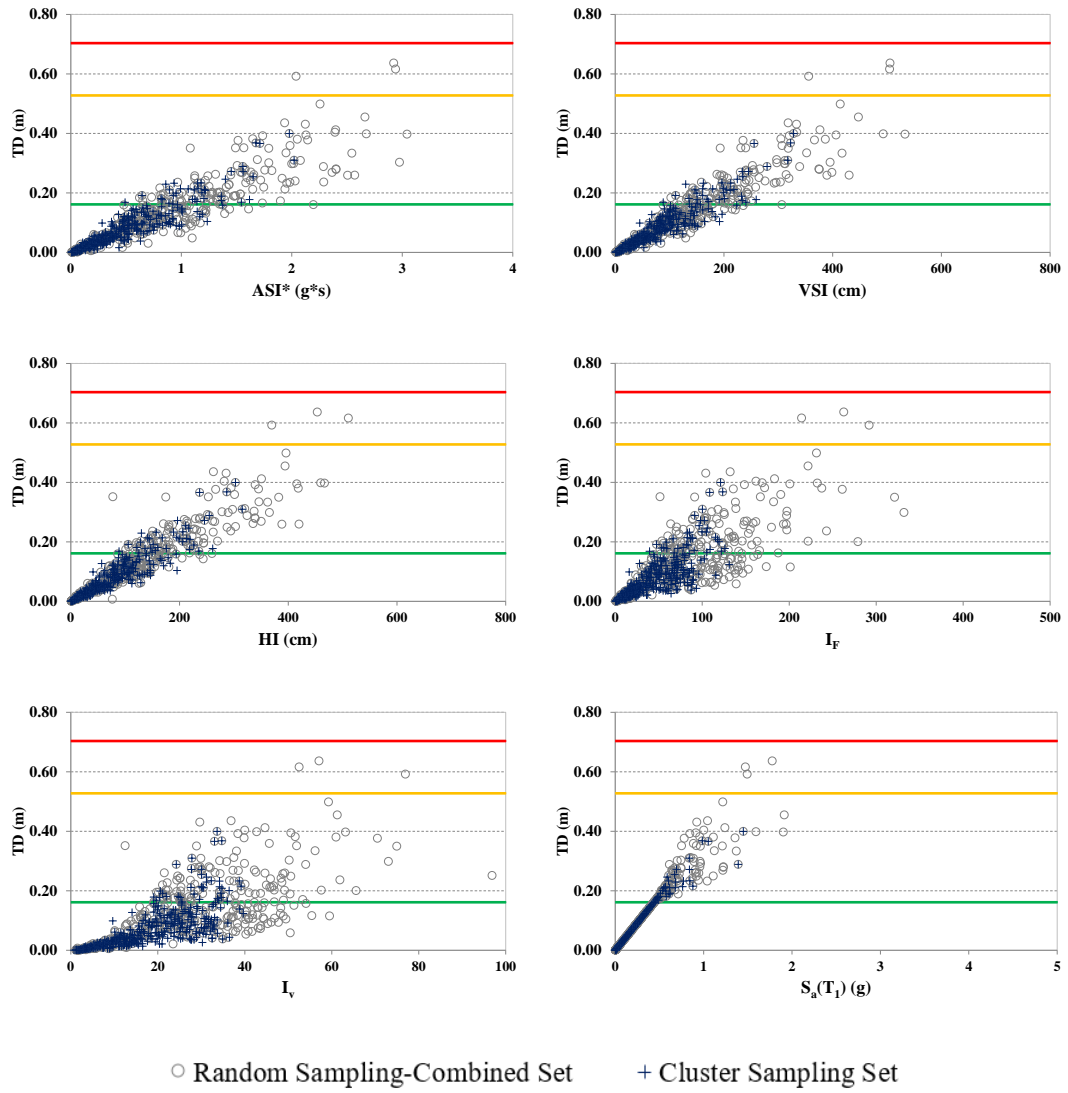
Figure A.113. Scatter plots for selected IMs (ASI*, VSI, HI, I_F, I_V, $S_a(T_1)$) versus Top Drift for F5S4B (T_1=0.95 s) (ESDOF)
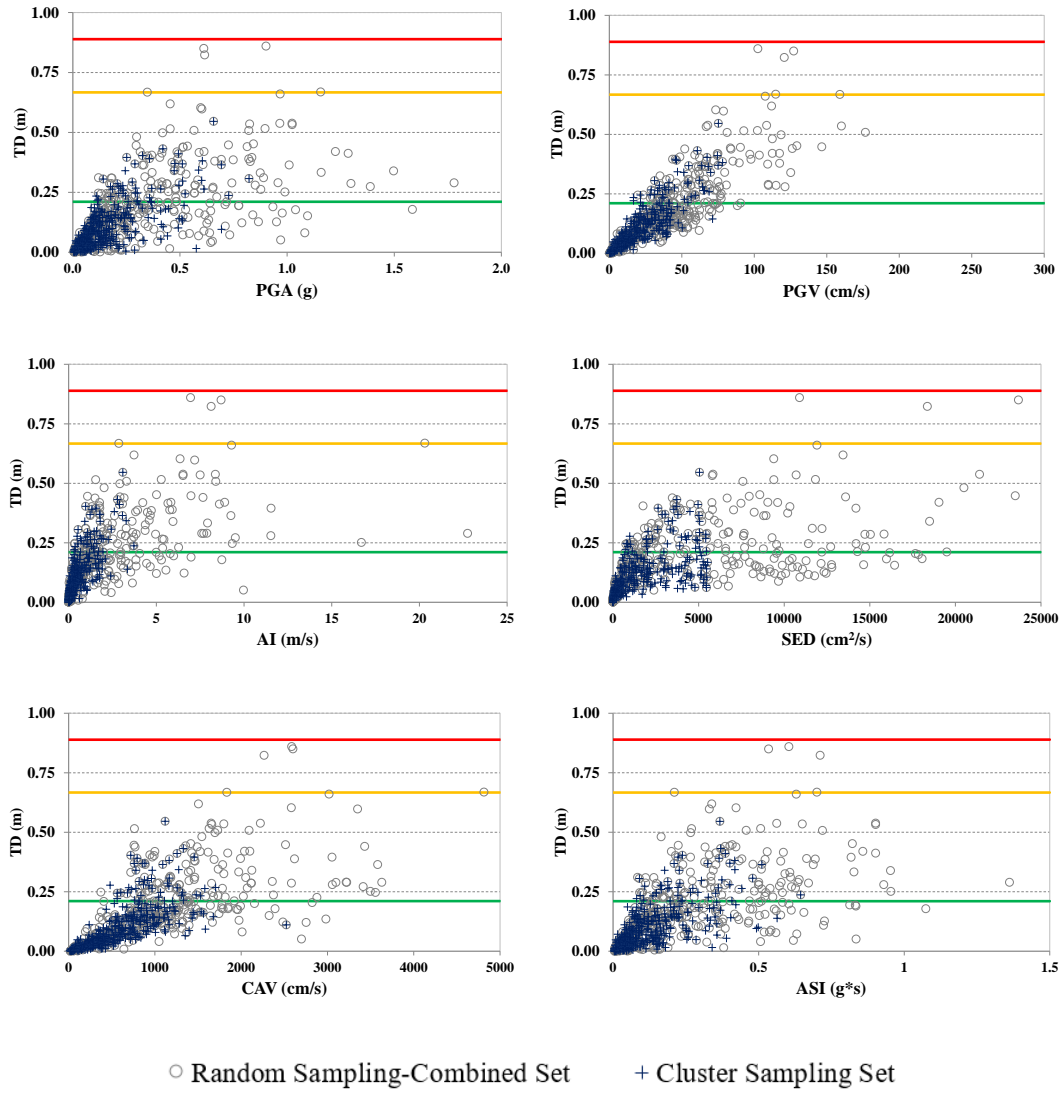
Figure A.114. Scatter plots for selected IMs (PGA, PGV, AI, SED, CAV, ASI) versus Top Drift for F8S3B (T_1=1.20 s) (ESDOF)
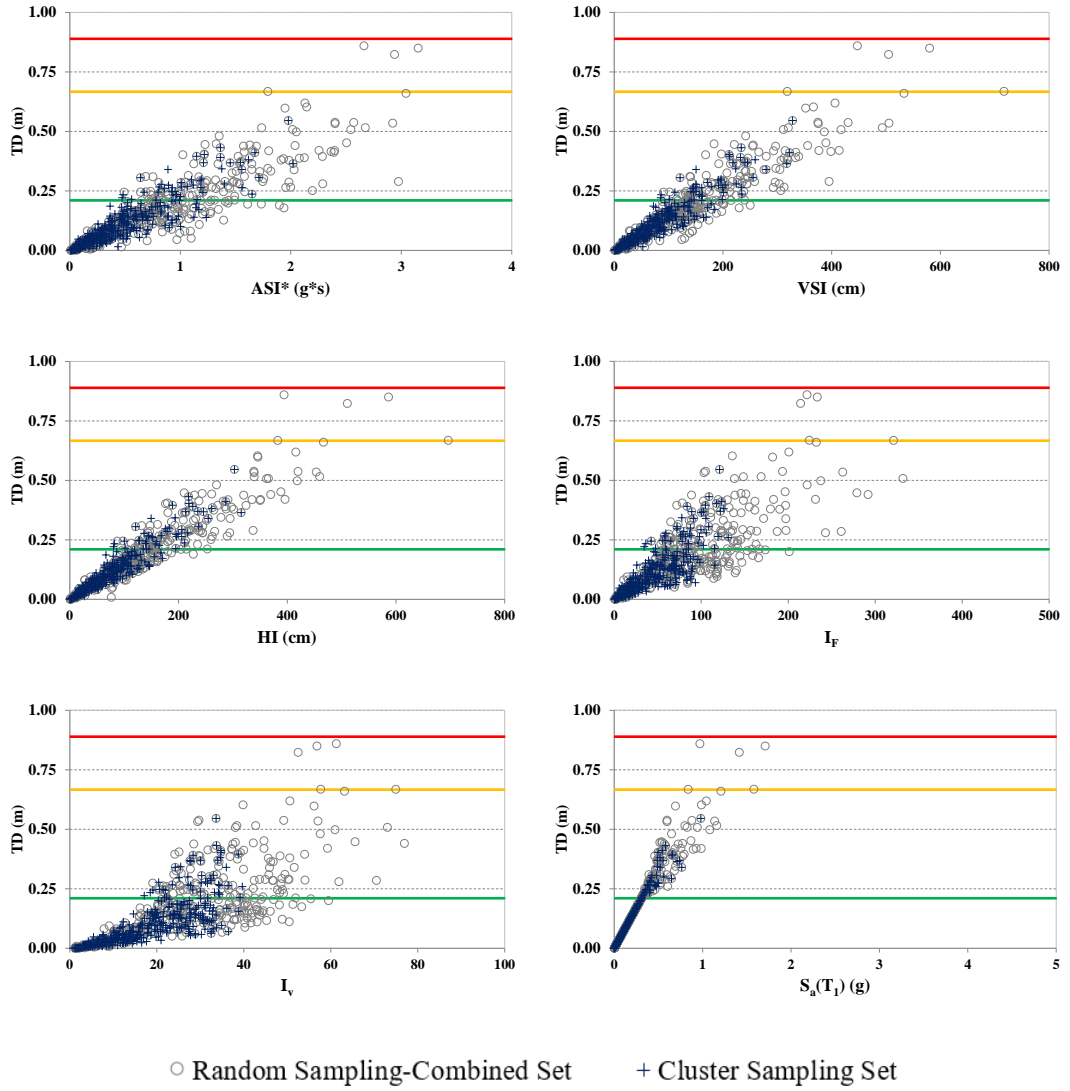
Figure A.115. Scatter plots for selected IMs (ASI*, VSI, HI, I_F, I_V, $S_a(T_1)$) versus Top Drift for F8S3B (T_1=1.20 s) (ESDOF)
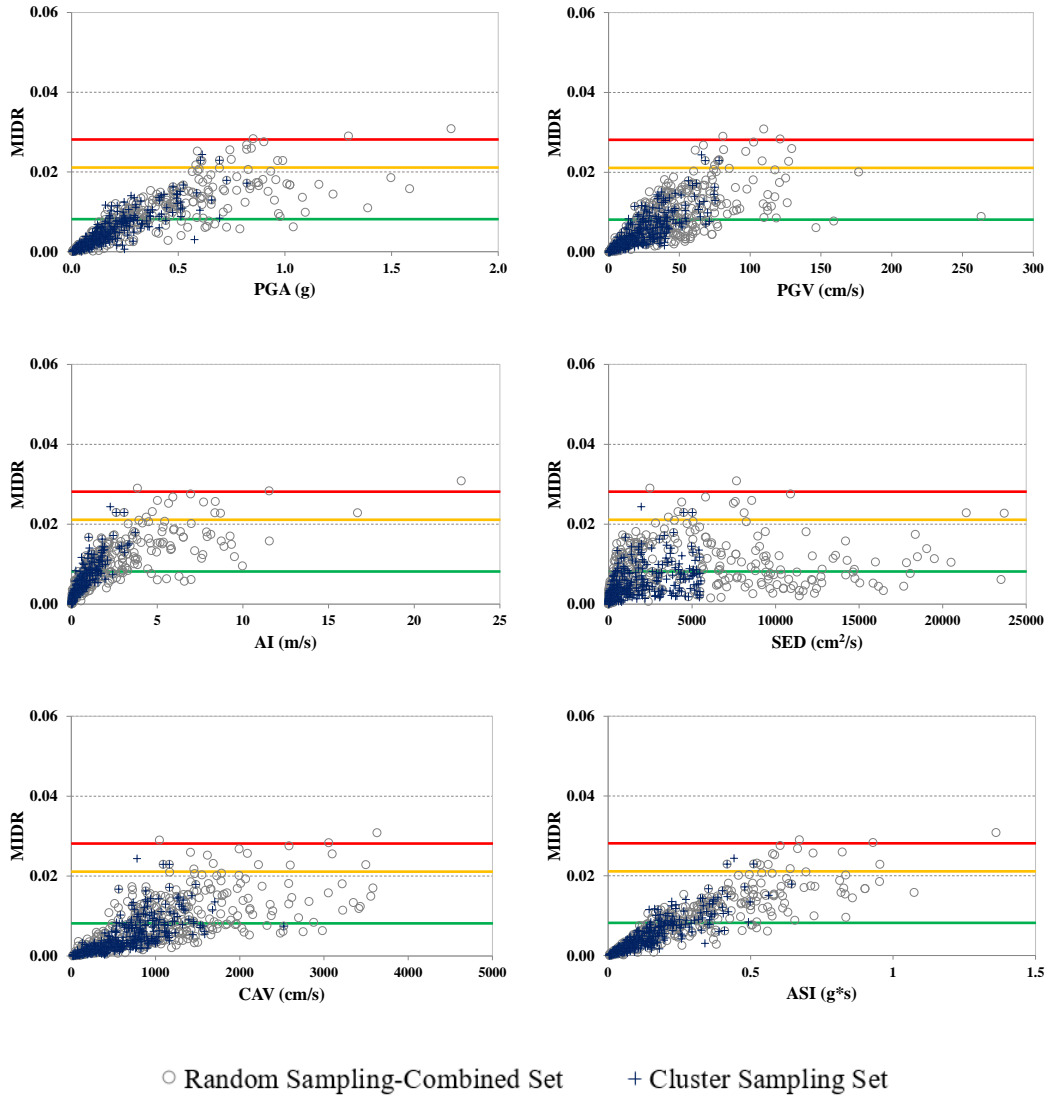
Figure A.116. Scatter plots for selected IMs (PGA, PGV, AI, SED, CAV, ASI) versus MIDR for F3S2B (T_1=0.45 s) (ESDOF)
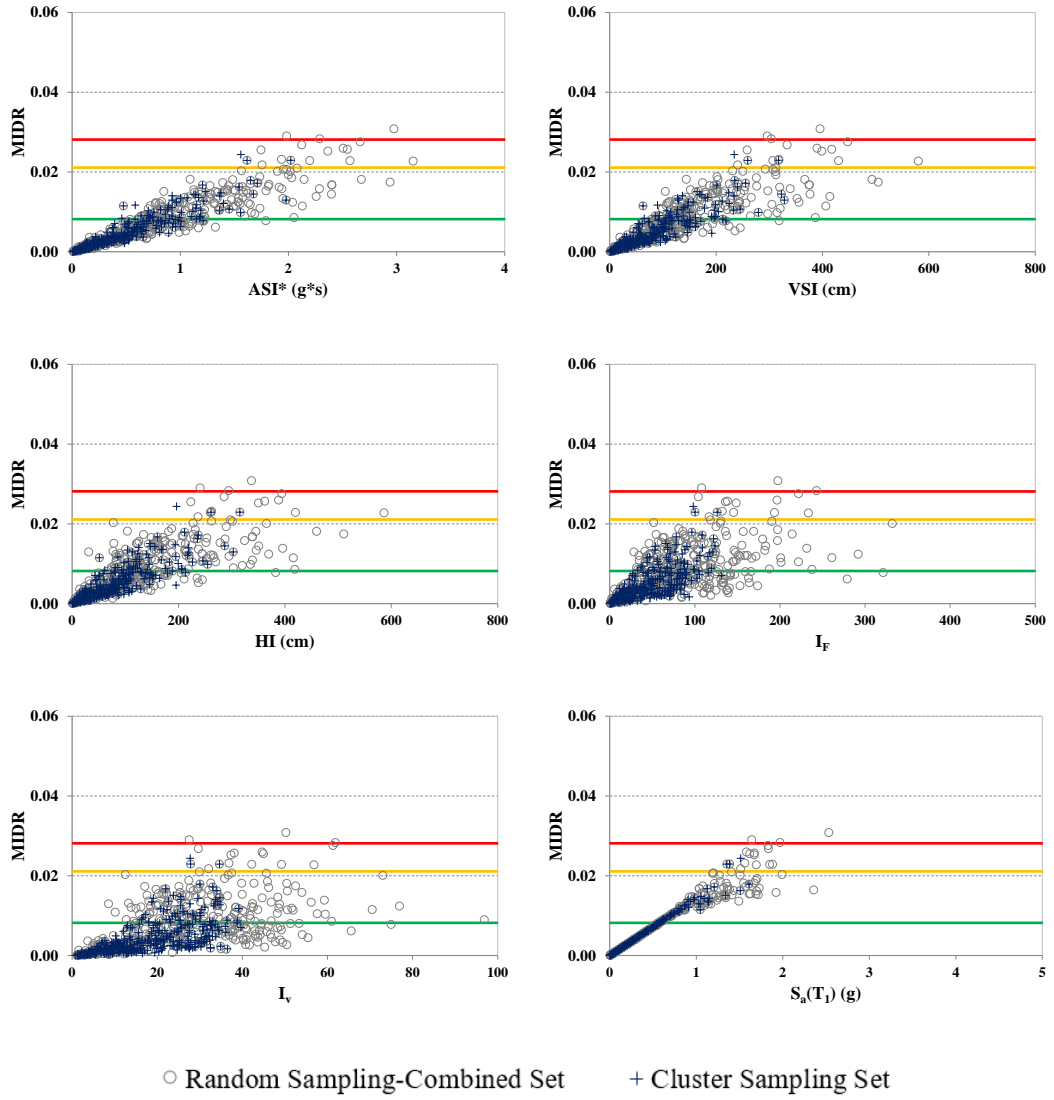
Figure A.117. Scatter plots for selected IMs (ASI*, VSI, HI, I_F, I_V, $S_a(T_1)$) versus MIDR for F3S2B (T_1=0.45 s) (ESDOF)
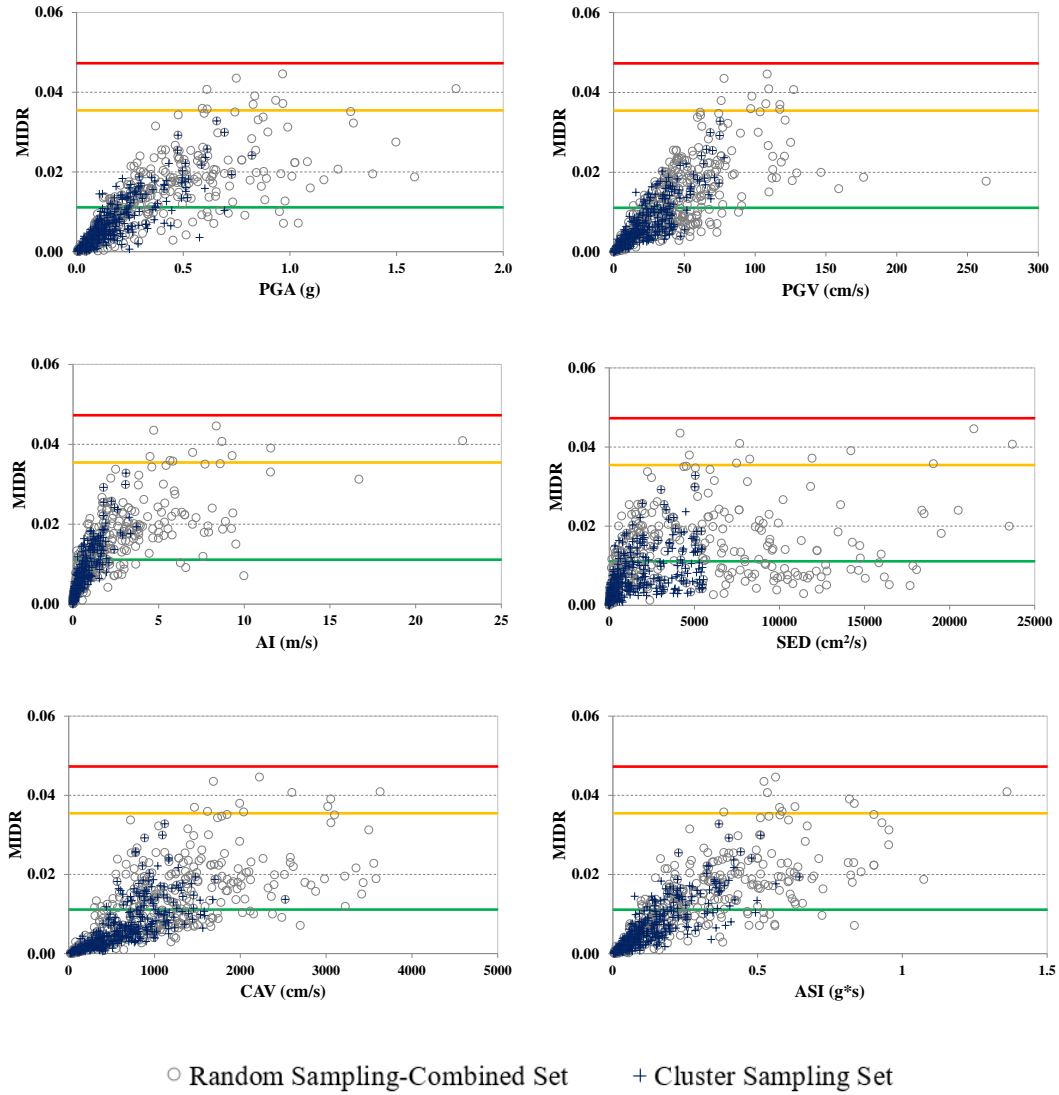
Figure A.118. Scatter plots for selected IMs (PGA, PGV, AI, SED, CAV, ASI) versus MIDR for F2S2B (T_1=0.59 s) (ESDOF)

324
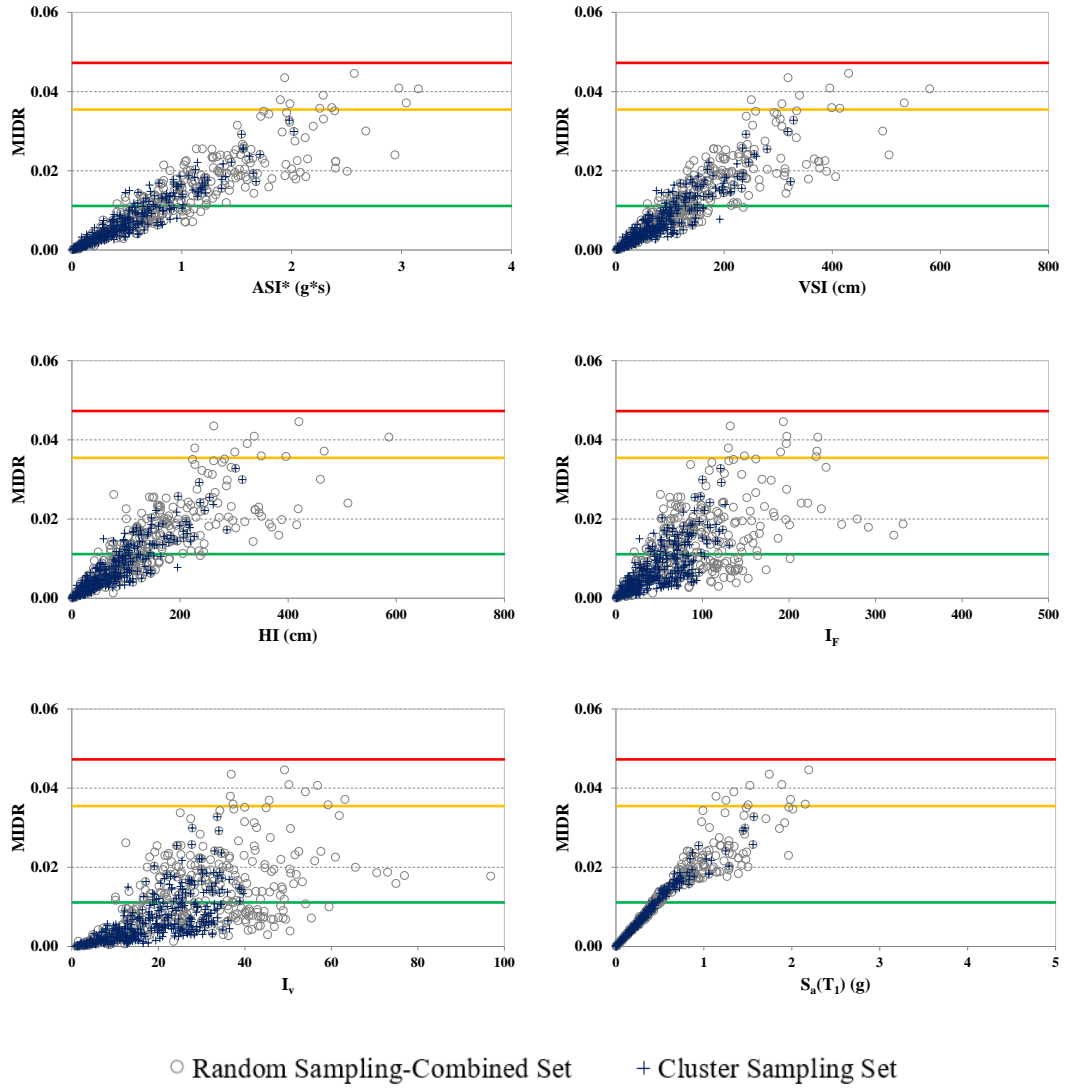
Figure A.119. Scatter plots for selected IMs (ASI*, VSI, HI, I_F, I_V, $S_a(T_1)$) versus MIDR for F2S2B (T_1=0.59 s) (ESDOF)
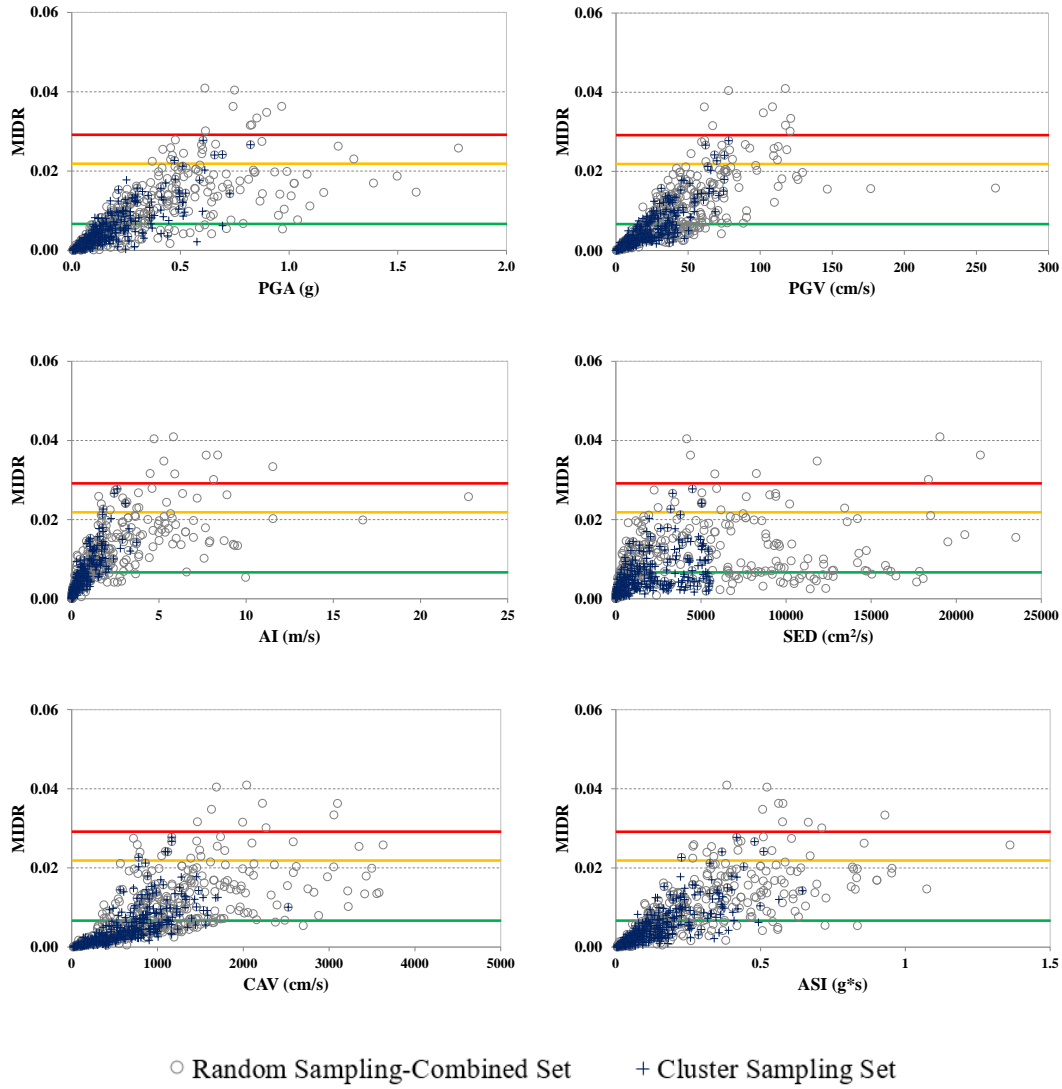
Figure A.120. Scatter plots for selected IMs (PGA, PGV, AI, SED, CAV, ASI) versus MIDR for F5S7B (T_1=0.66 s) (ESDOF)

○ Random Sampling-Combined Set   + Cluster Sampling Set
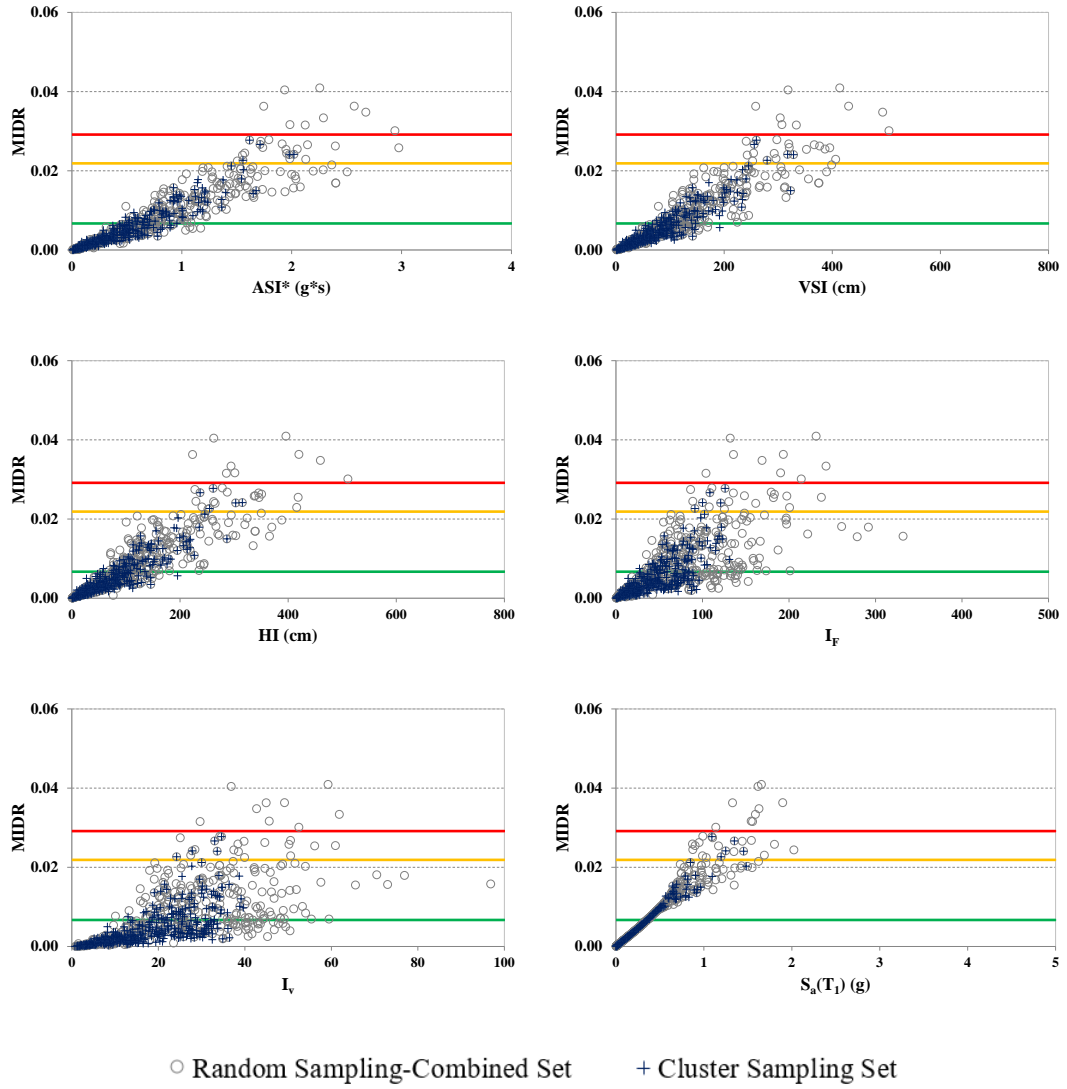
Figure A.121. Scatter plots for selected IMs (ASI*, VSI, HI, I_F, I_V, $S_a(T_1)$) versus MIDR for F5S7B (T_1=0.66 s) (ESDOF)
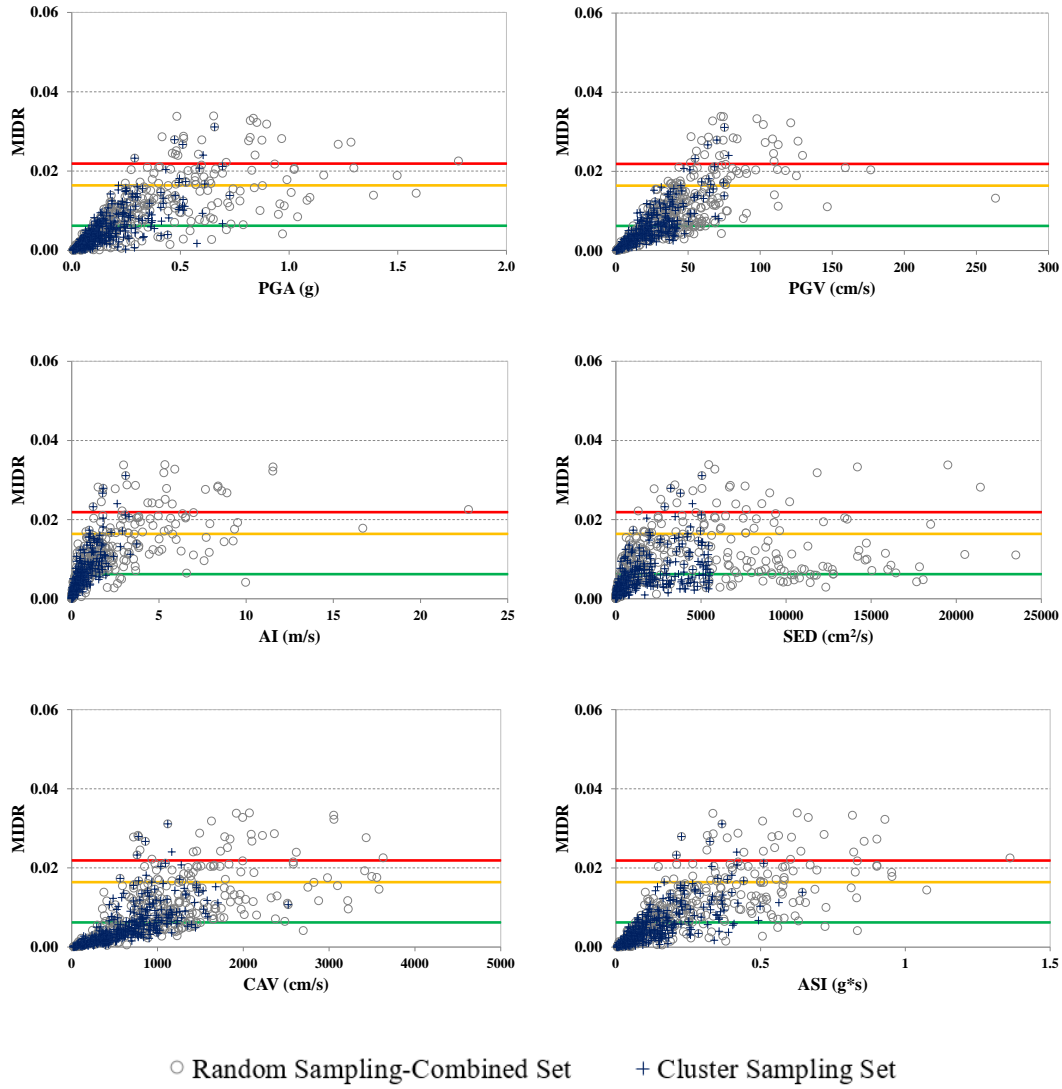
Figure A.122. Scatter plots for selected IMs (PGA, PGV, AI, SED, CAV, ASI) versus MIDR for F5S2B (T_1=0.75 s) (ESDOF)
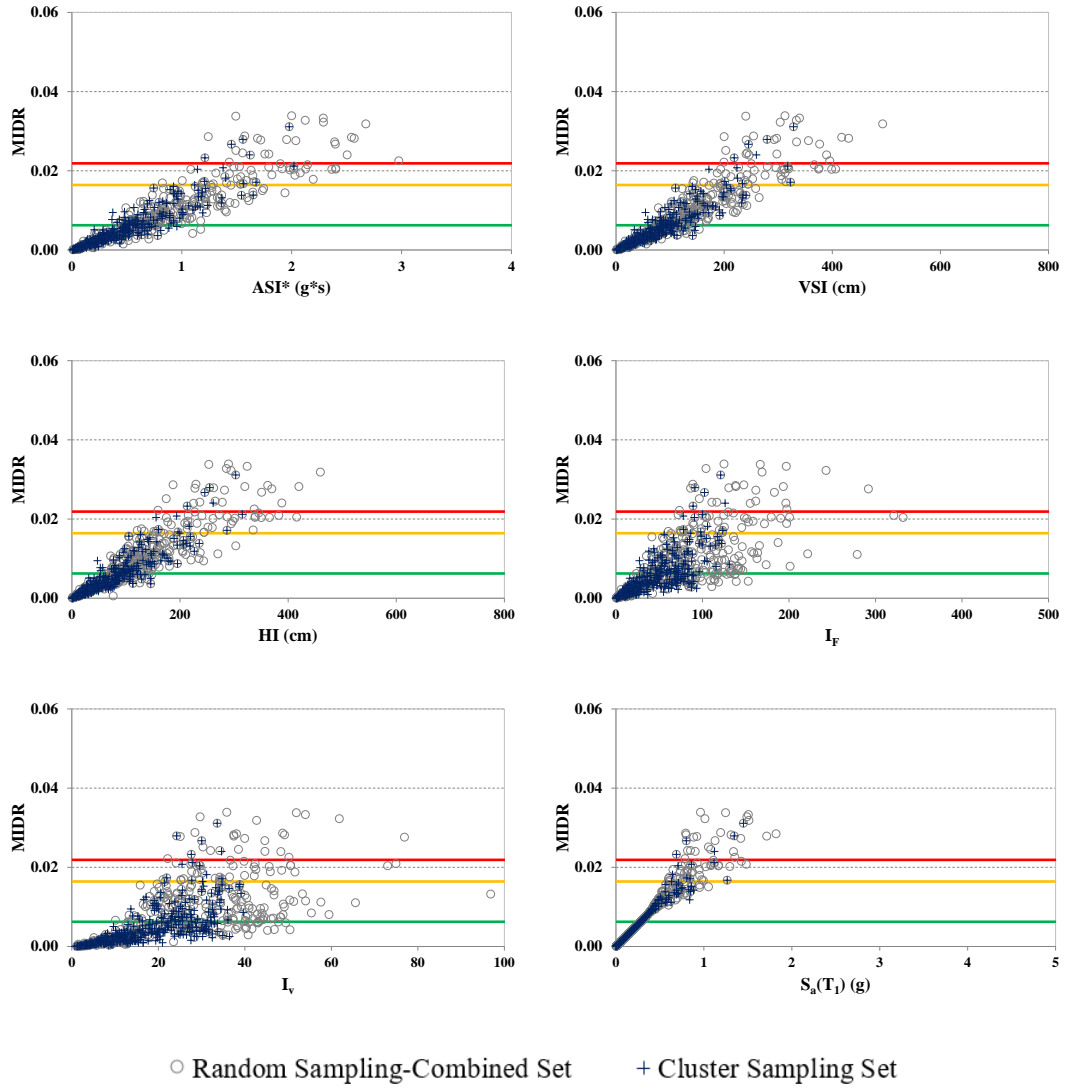
Figure A.123. Scatter plots for selected IMs (ASI*, VSI, HI, I_F, I_V, $S_a(T_1)$) versus MIDR for F5S2B (T_1=0.75 s) (ESDOF)
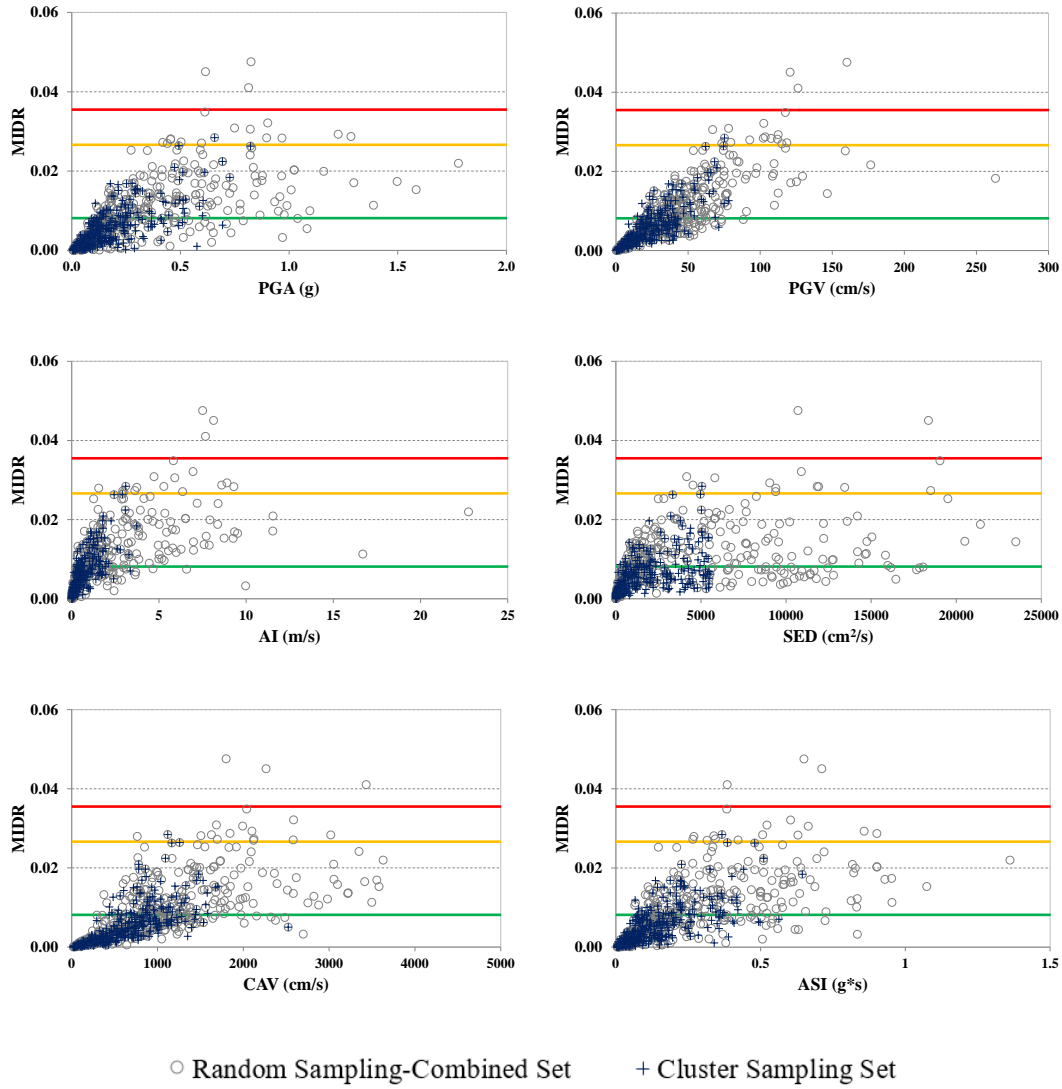
Figure A.124. Scatter plots for selected IMs (PGA, PGV, AI, SED, CAV, ASI) versus MIDR for F5S4B (T_1=0.95 s) (ESDOF)
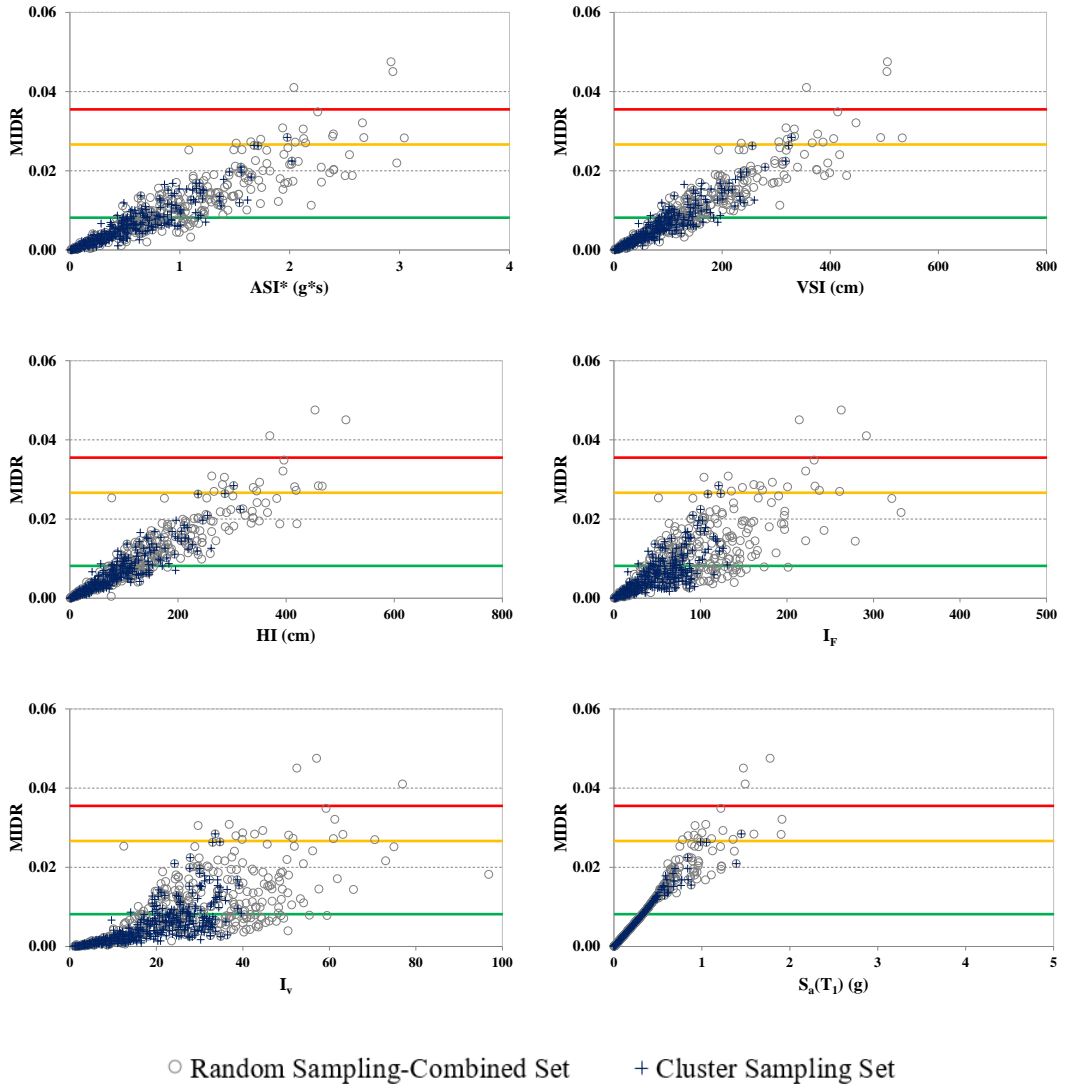
Figure A.125. Scatter plots for selected IMs (ASI*, VSI, HI, I_F, I_V, $S_a(T_1)$) versus MIDR for F5S4B (T_1=0.95 s) (ESDOF)
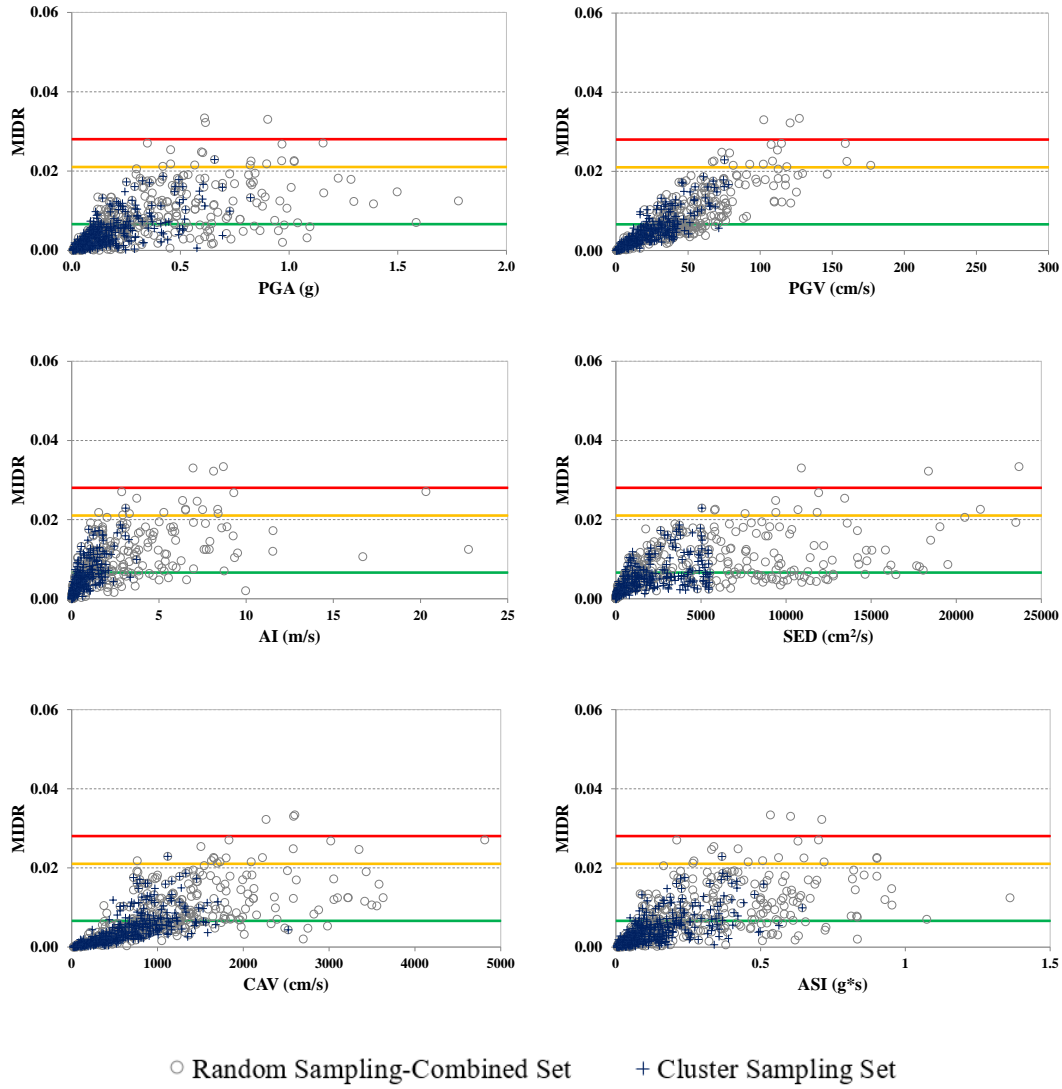
Figure A.126. Scatter plots for selected IMs (PGA, PGV, AI, SED, CAV, ASI) versus MIDR for F8S3B (T_1=1.20 s) (ESDOF)
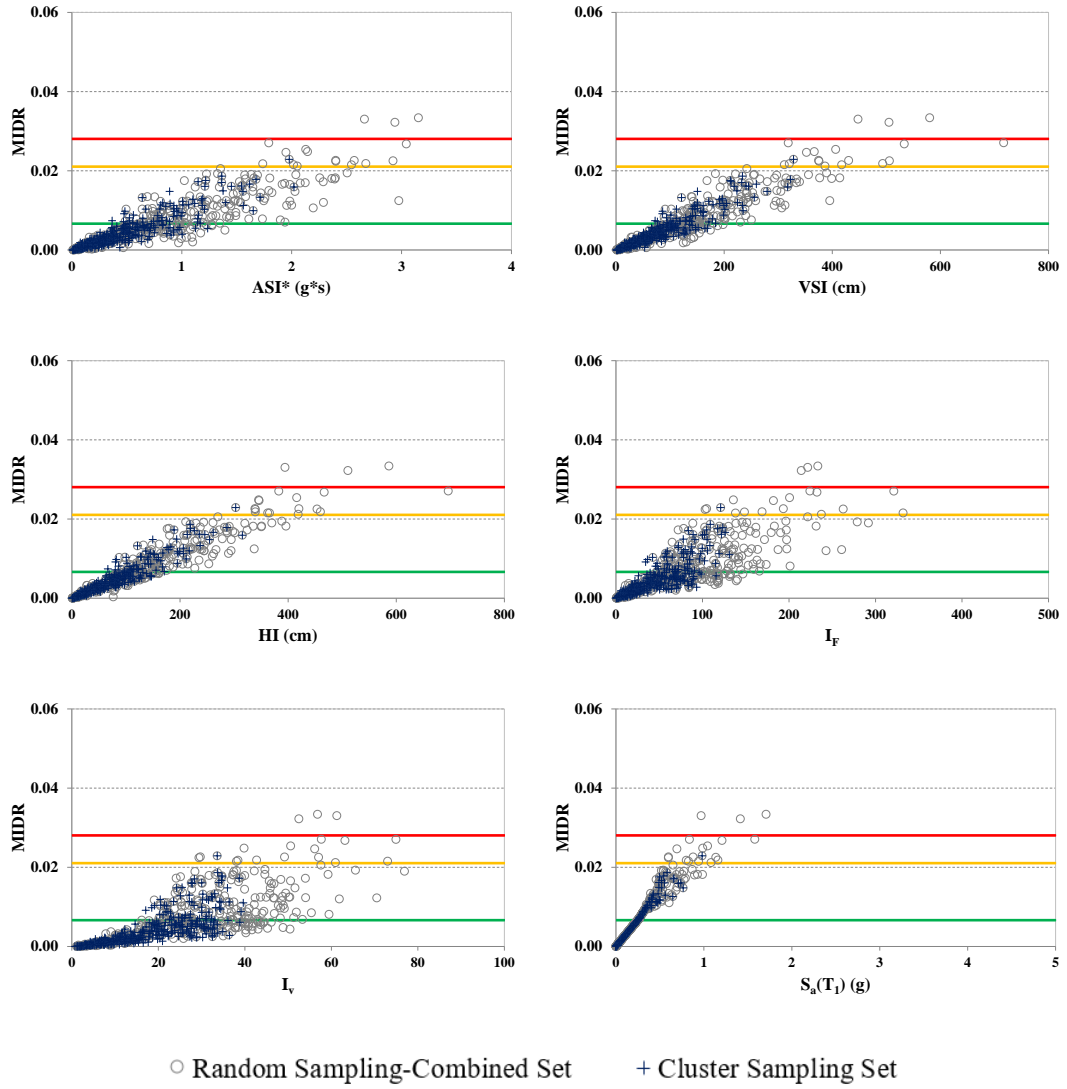
Figure A.127. Scatter plots for selected IMs (ASI*, VSI, HI, I_F, I_V, $S_a(T_1)$) versus MIDR for F8S3B (T_1=1.20 s) (ESDOF)
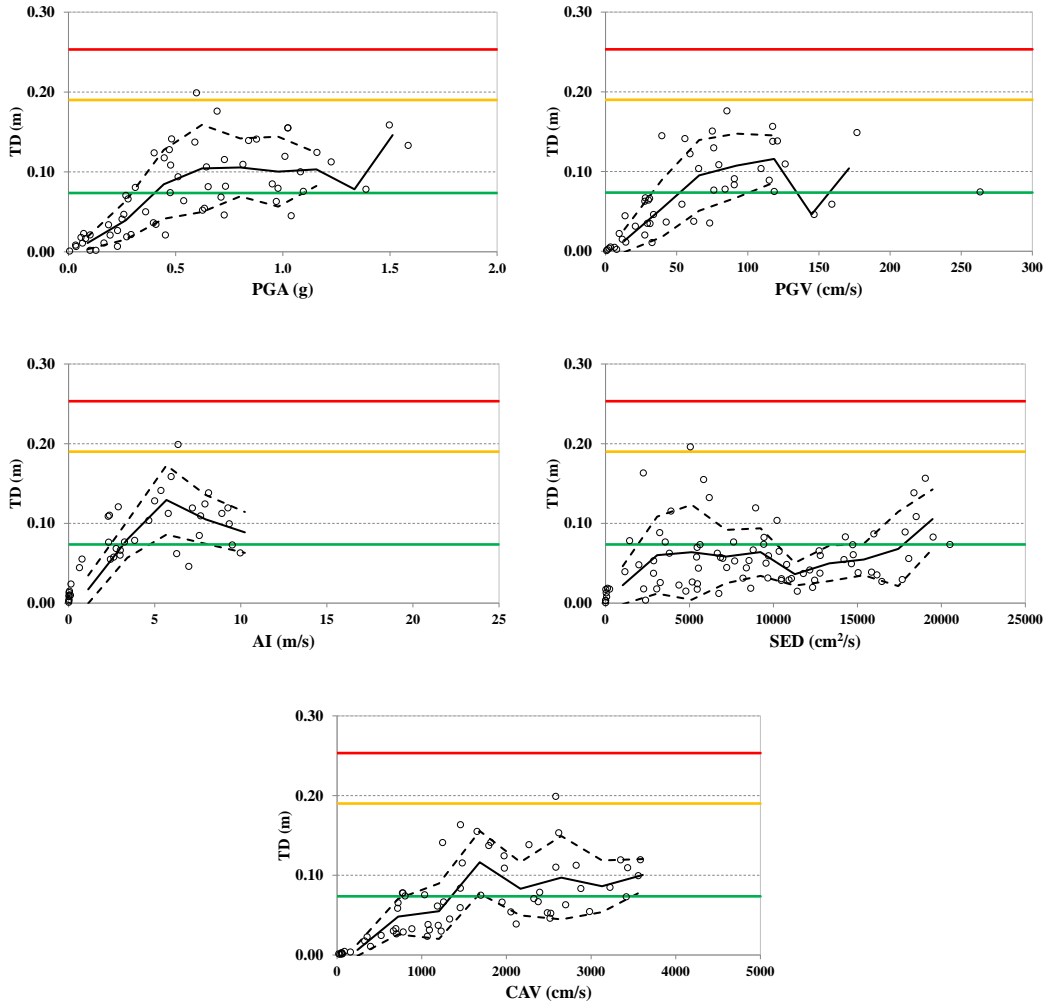
Figure A.128. Scatter plots for selected IMs (PGA, PGV, AI, SED, CAV) versus Top Drift for F3S2B (T_1=0.45 s) (MDOF)
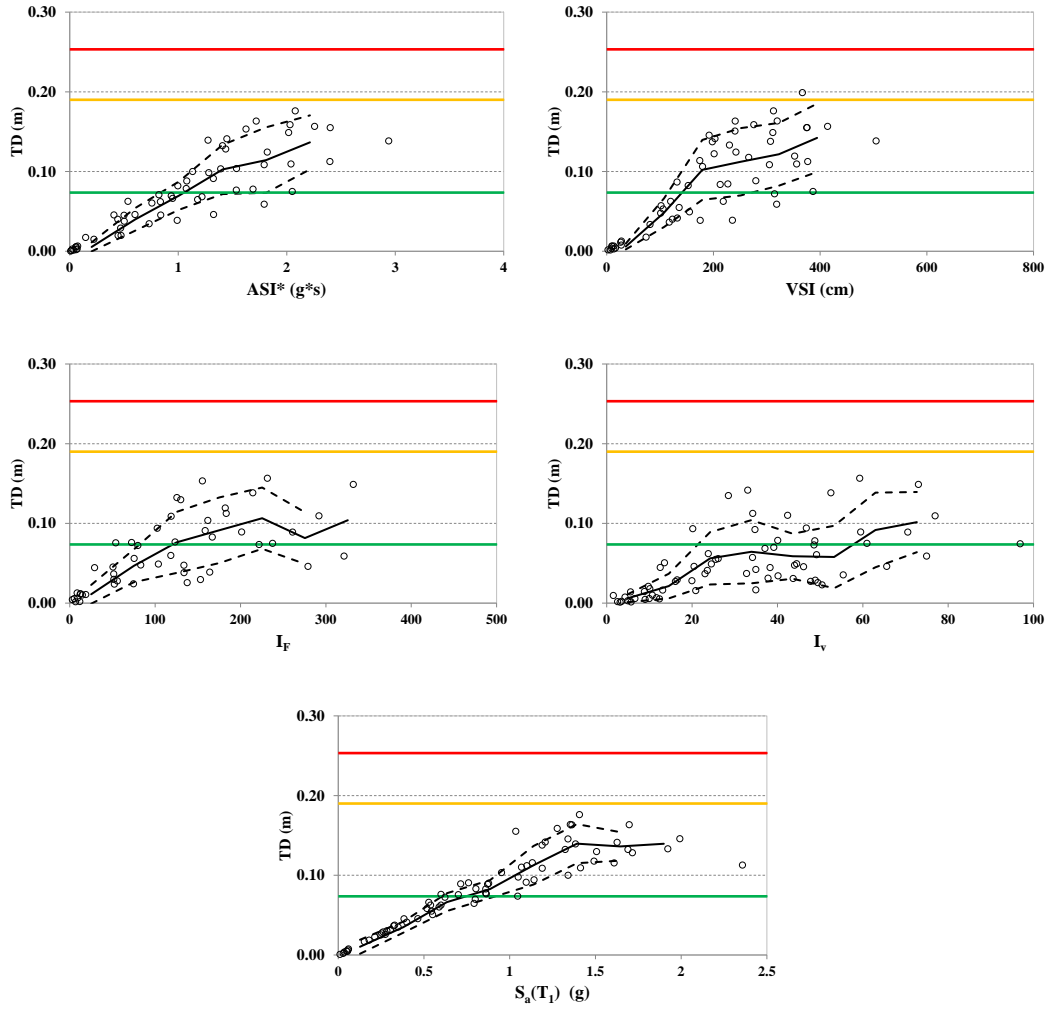
Figure A.129. Scatter plots for selected IMs (ASI*, VSI, I_F, I_V, $S_a(T_1)$) versus Top Drift for F3S2B (T_1=0.45 s) (MDOF)
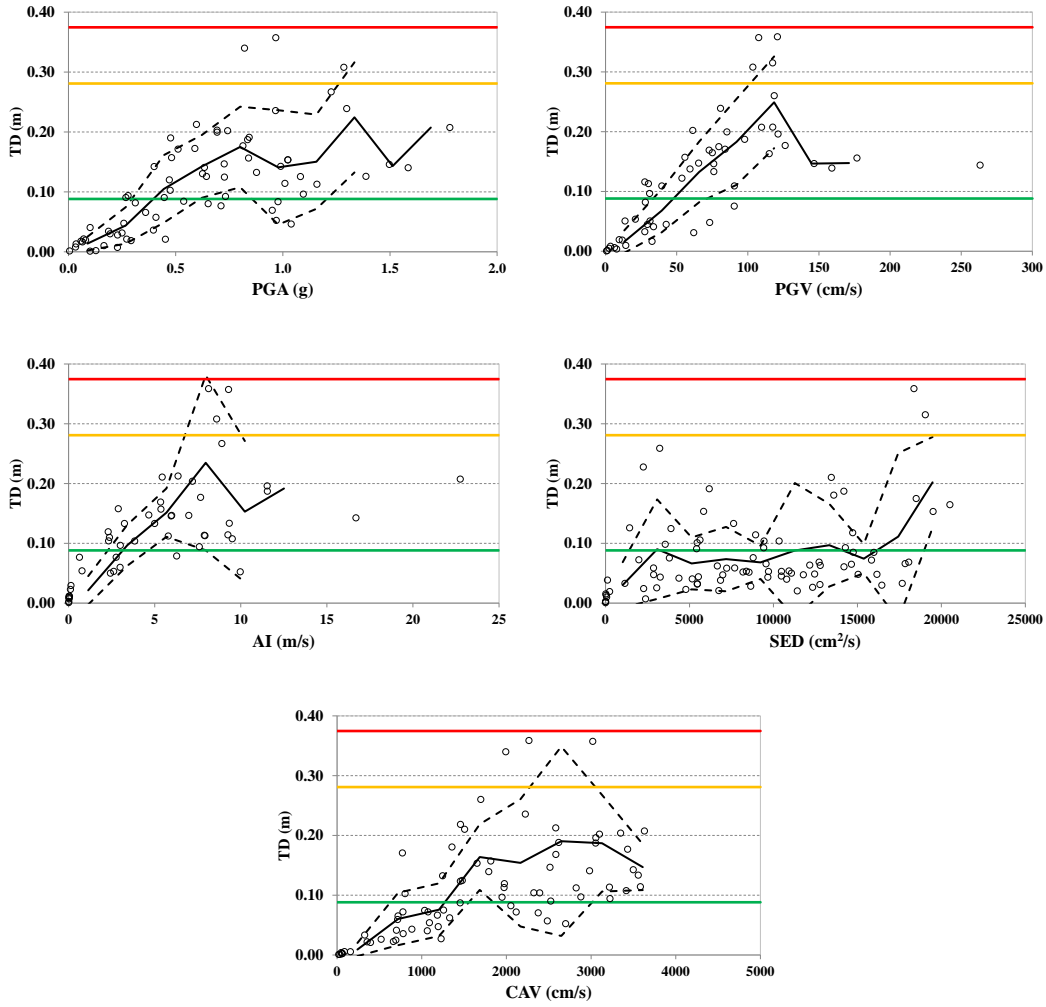
Figure A.130. Scatter plots for selected IMs (PGA, PGV, AI, SED, CAV) versus Top Drift for F2S2B (T_1=0.59 s) (MDOF)
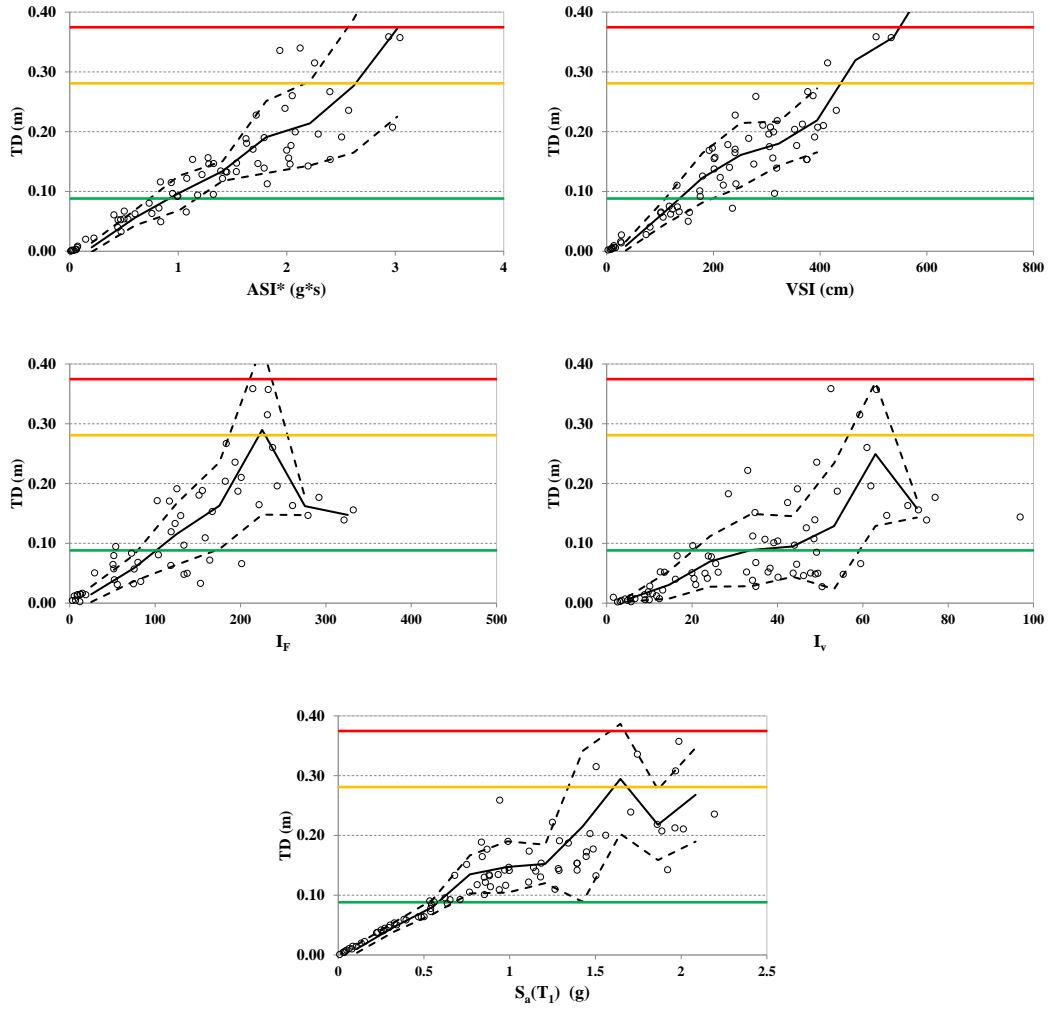
Figure A.131. Scatter plots for selected IMs (ASI*, VSI, I_F, I_V, $S_a(T_1)$) versus Top Drift for F2S2B (T_1=0.59 s) (MDOF)
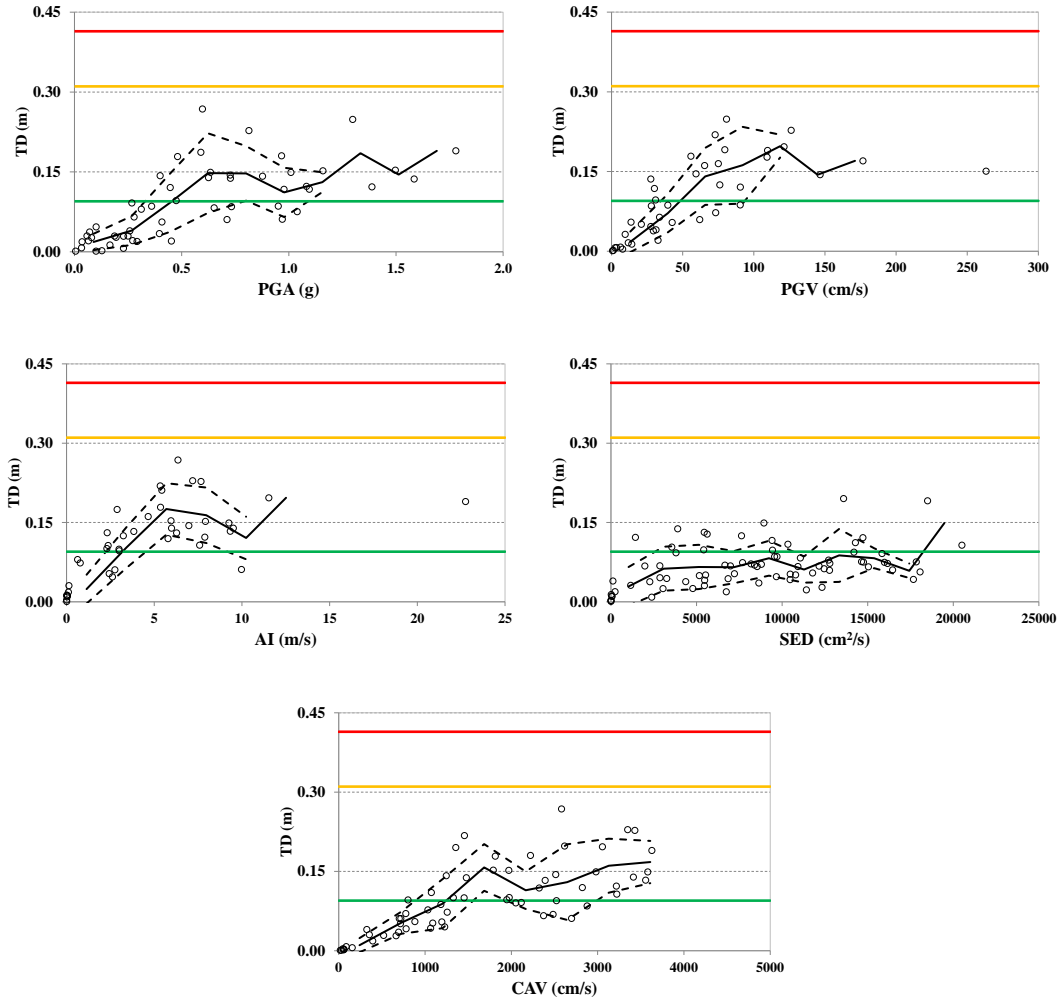
Figure A.132. Scatter plots for selected IMs (PGA, PGV, AI, SED, CAV) versus
Top Drift for F5S7B (T_1=0.66 s) (MDOF)
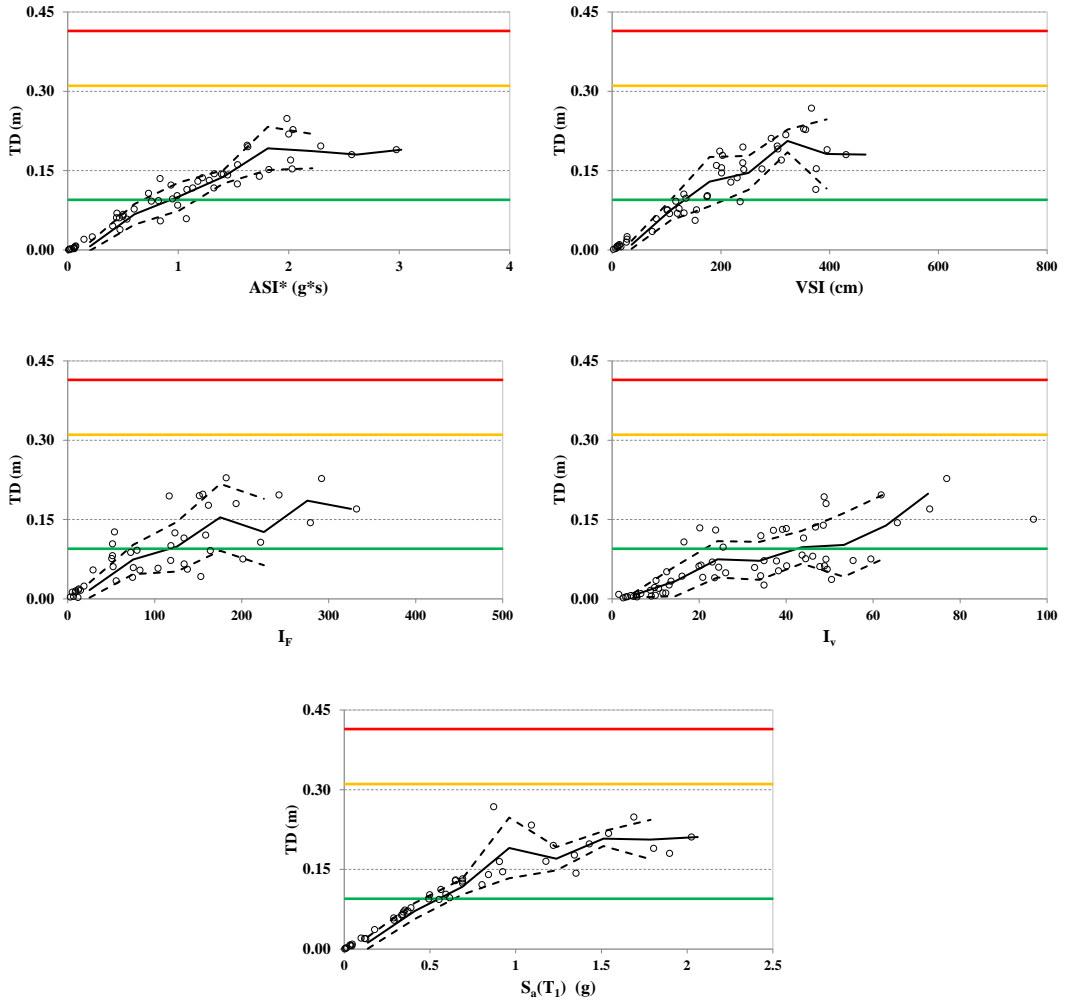
Figure A.133. Scatter plots for selected IMs (ASI*, VSI, I_F, I_v, $S_a(T_1)$) versus Top Drift for F5S7B (T_1=0.66 s) (MDOF)
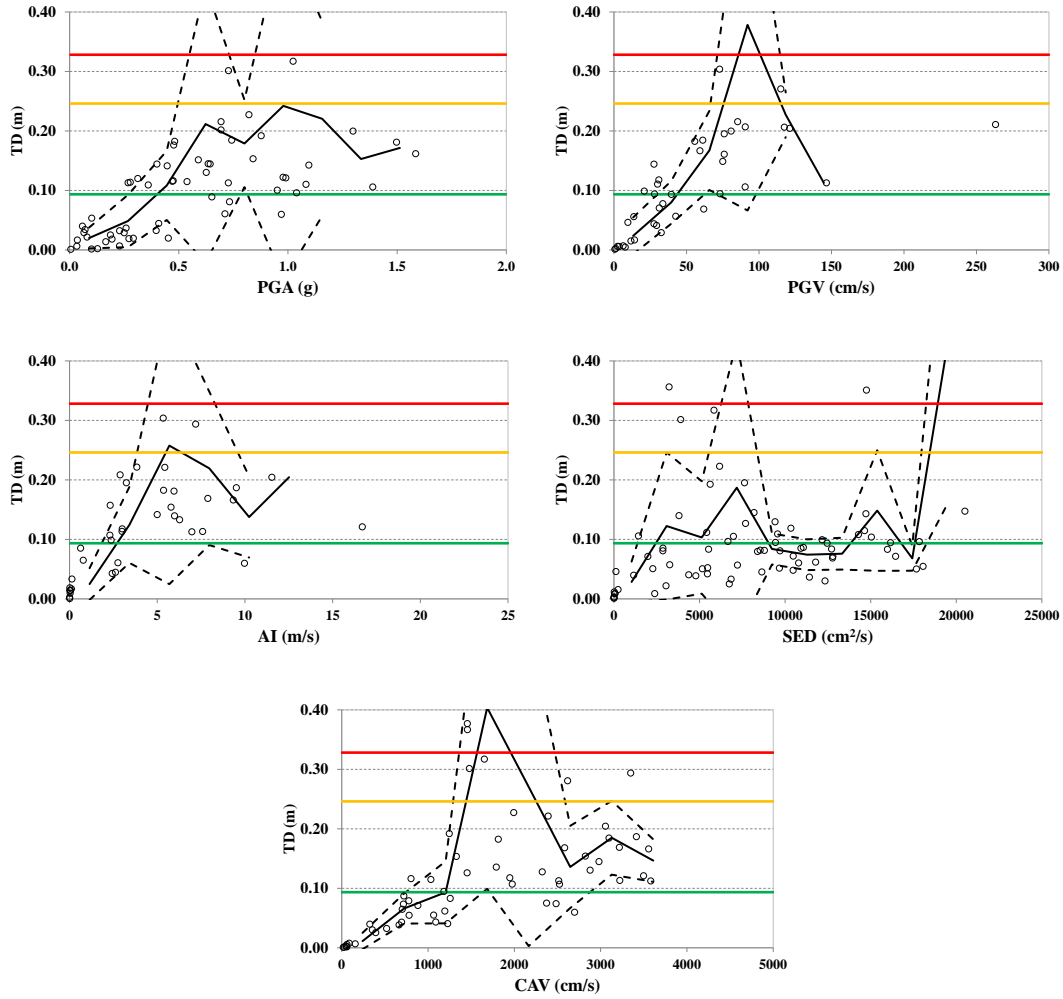
Figure A.134. Scatter plots for selected IMs (PGA, PGV, AI, SED, CAV) versus Top Drift for F5S2B (T_1=0.75 s) (MDOF)
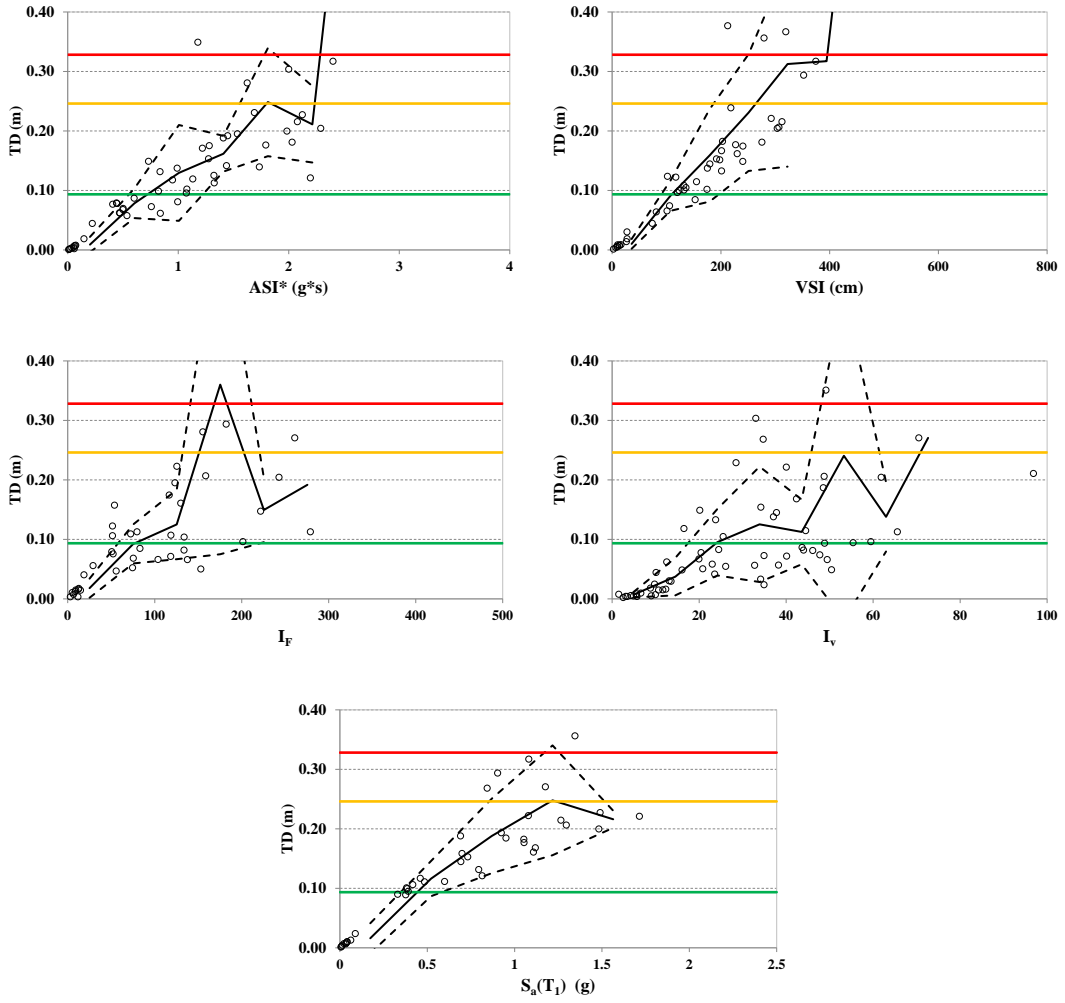
Figure A.135. Scatter plots for selected IMs (ASI*, VSI, I_F, I_V, $S_a(T_1)$) versus Top Drift for F5S2B (T_1=0.75 s) (MDOF)
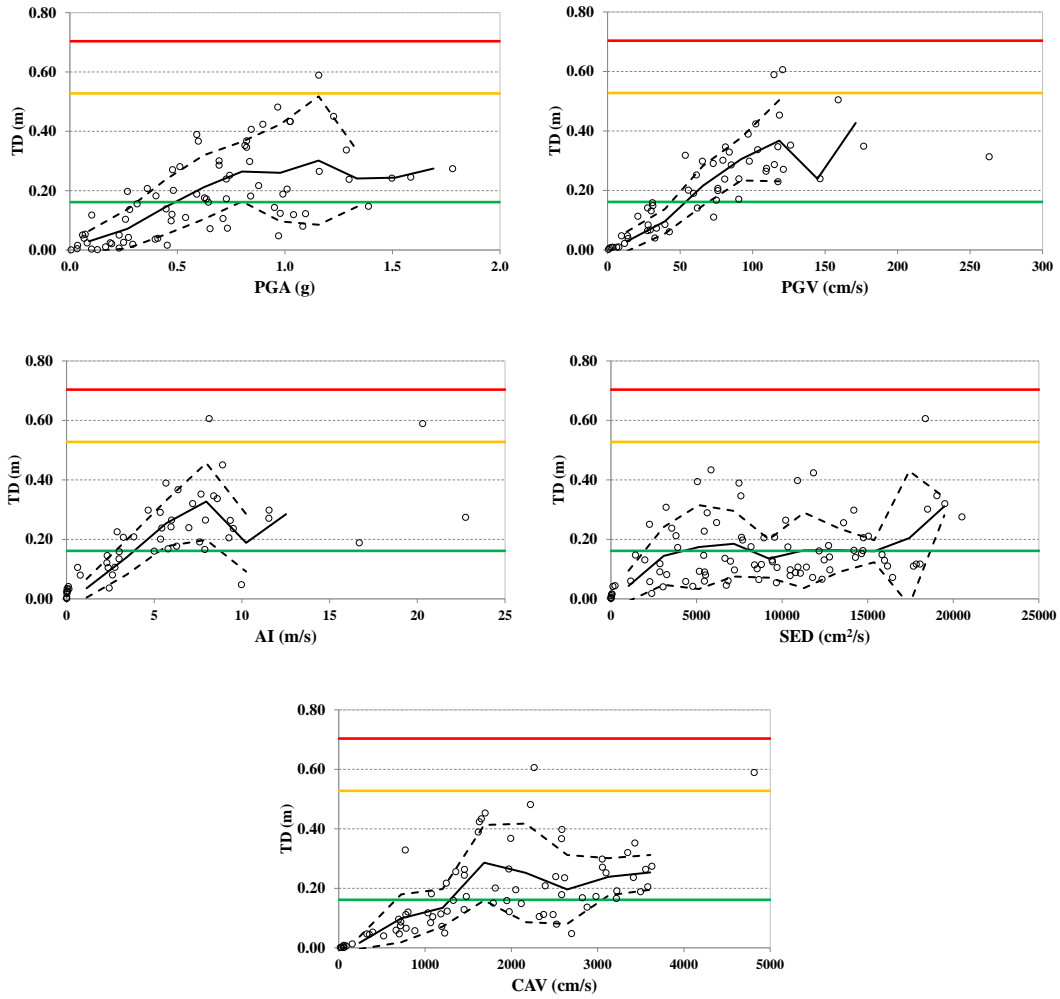
Figure A.136. Scatter plots for selected IMs (PGA, PGV, AI, SED, CAV) versus Top Drift for F5S4B (T_1=0.95 s) (MDOF)
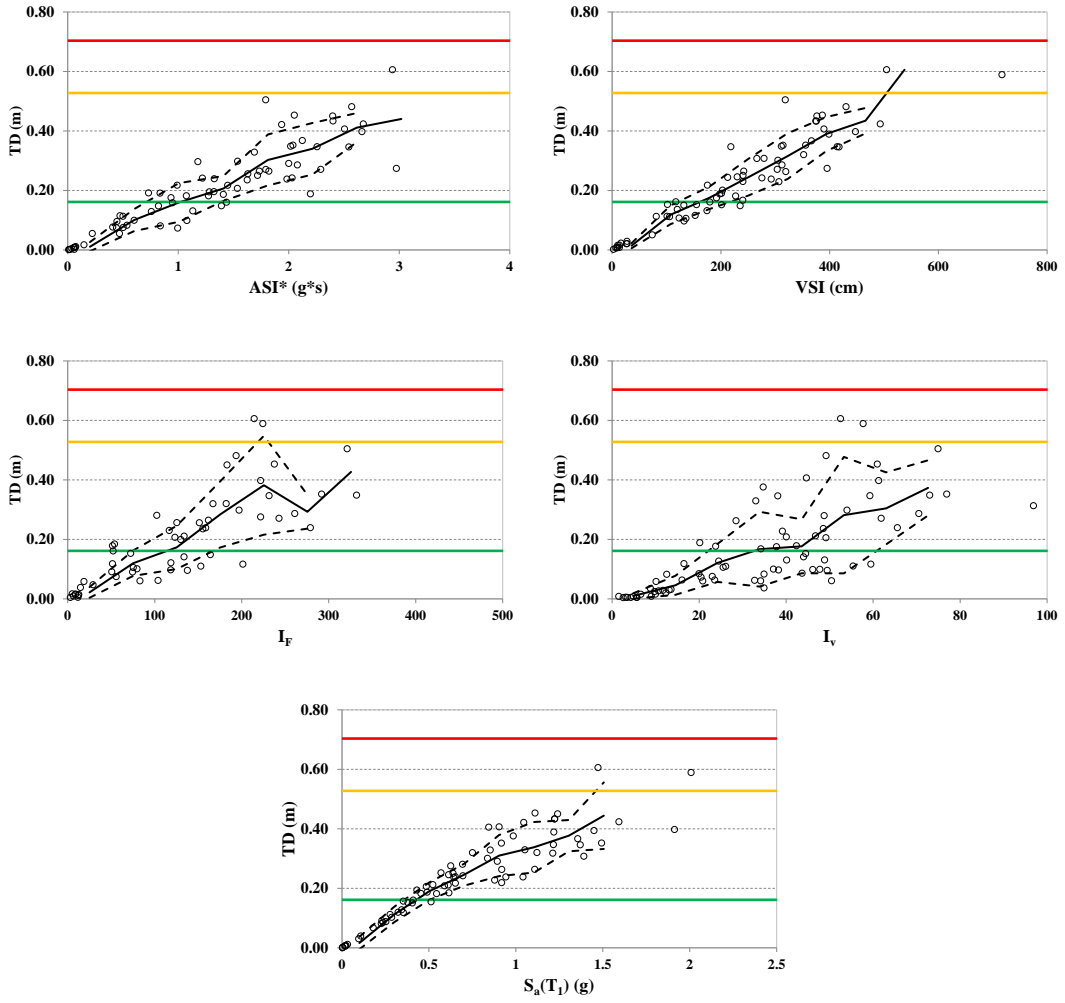
Figure A.137. Scatter plots for selected IMs (ASI*, VSI, I_F, I_V, $S_a(T_1)$) versus Top Drift for F5S4B (T_1=0.95 s) (MDOF)
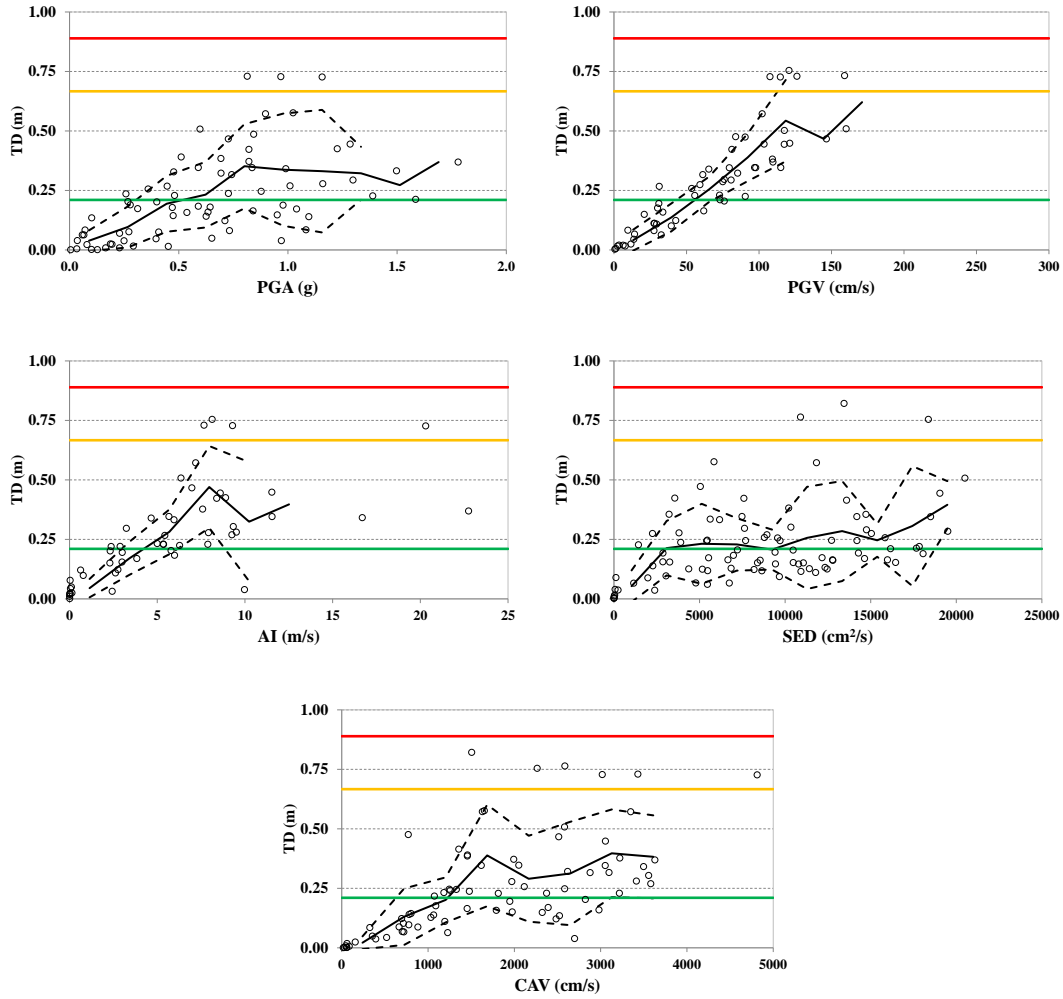
Figure A.138. Scatter plots for selected IMs (PGA, PGV, AI, SED, CAV) versus Top Drift for F8S3B (T_1=1.20 s) (MDOF)
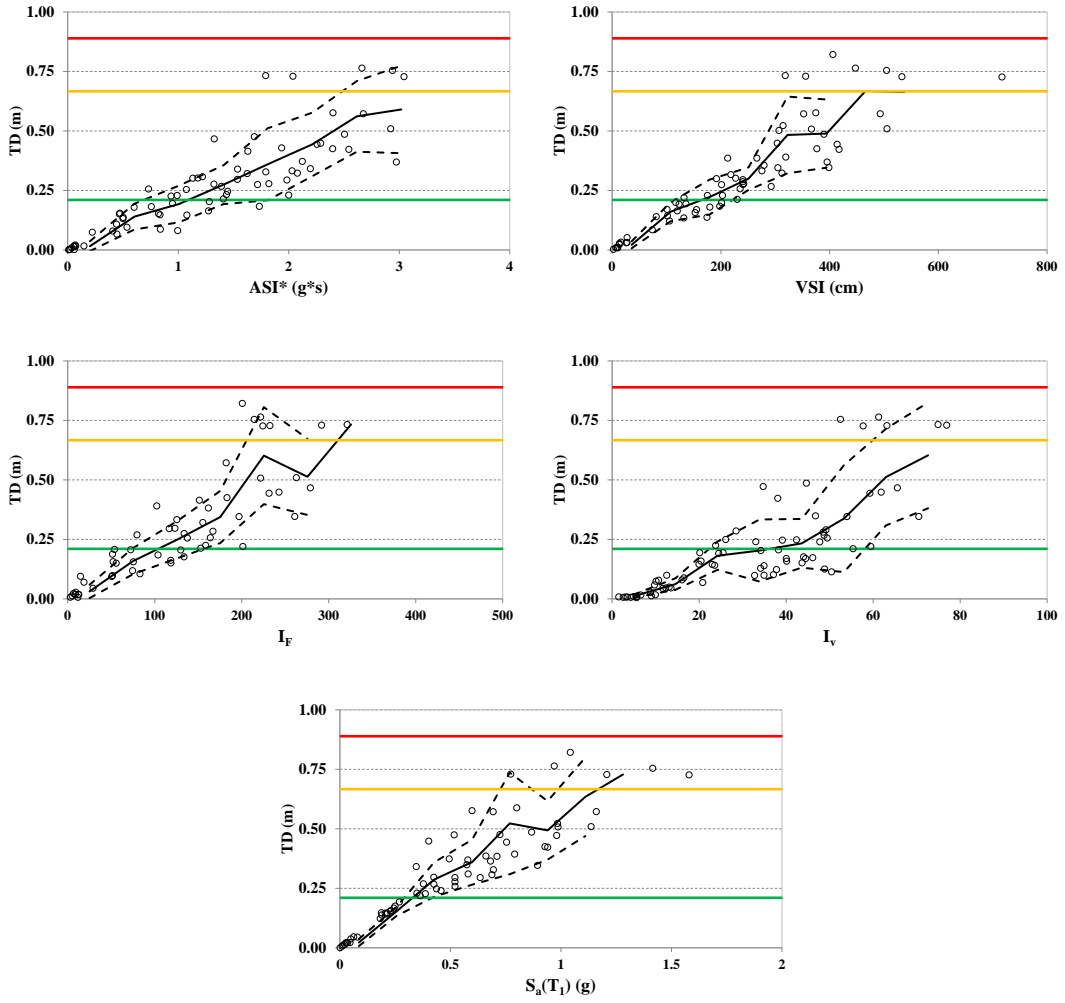
Figure A.139. Scatter plots for selected IMs (ASI*, VSI, I_F, I_V, $S_a(T_1)$) versus Top Drift for F8S3B (T_1=1.20 s) (MDOF)
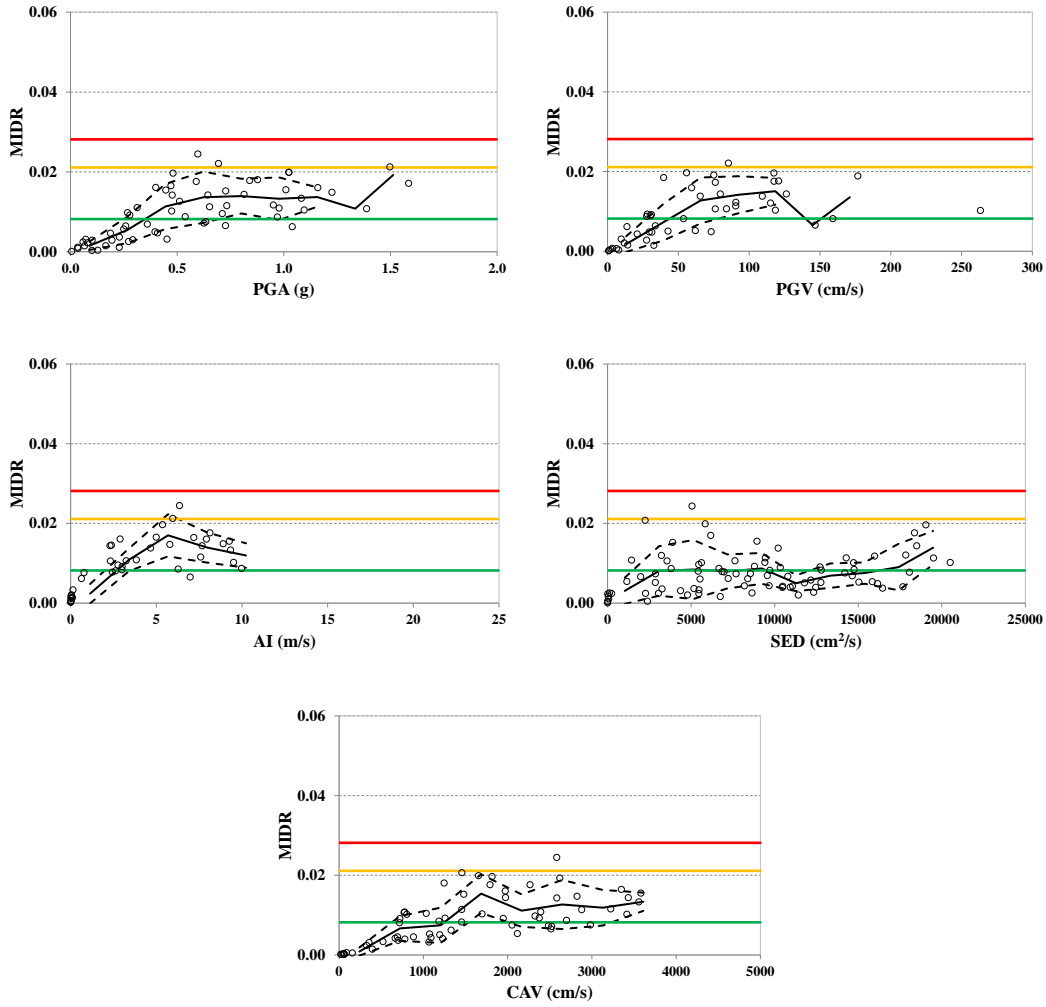
Figure A.140. Scatter plots for selected IMs (PGA, PGV, AI, SED, CAV) versus MIDR for F3S2B (T_1=0.45 s) (MDOF)

346
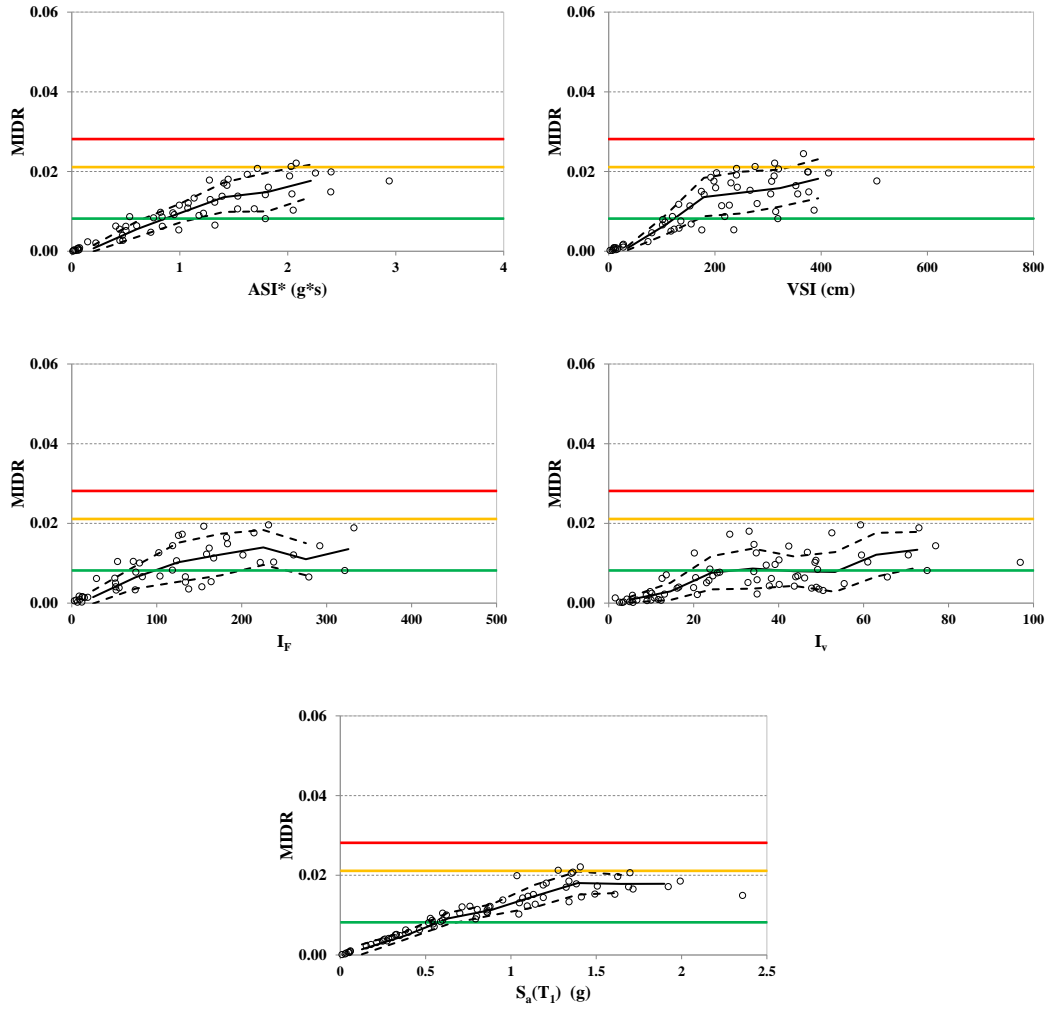
Figure A.141. Scatter plots for selected IMs (ASI*, VSI, I_F, I_v, $S_a(T_1)$) versus MIDR for F3S2B (T_1=0.45 s) (MDOF)
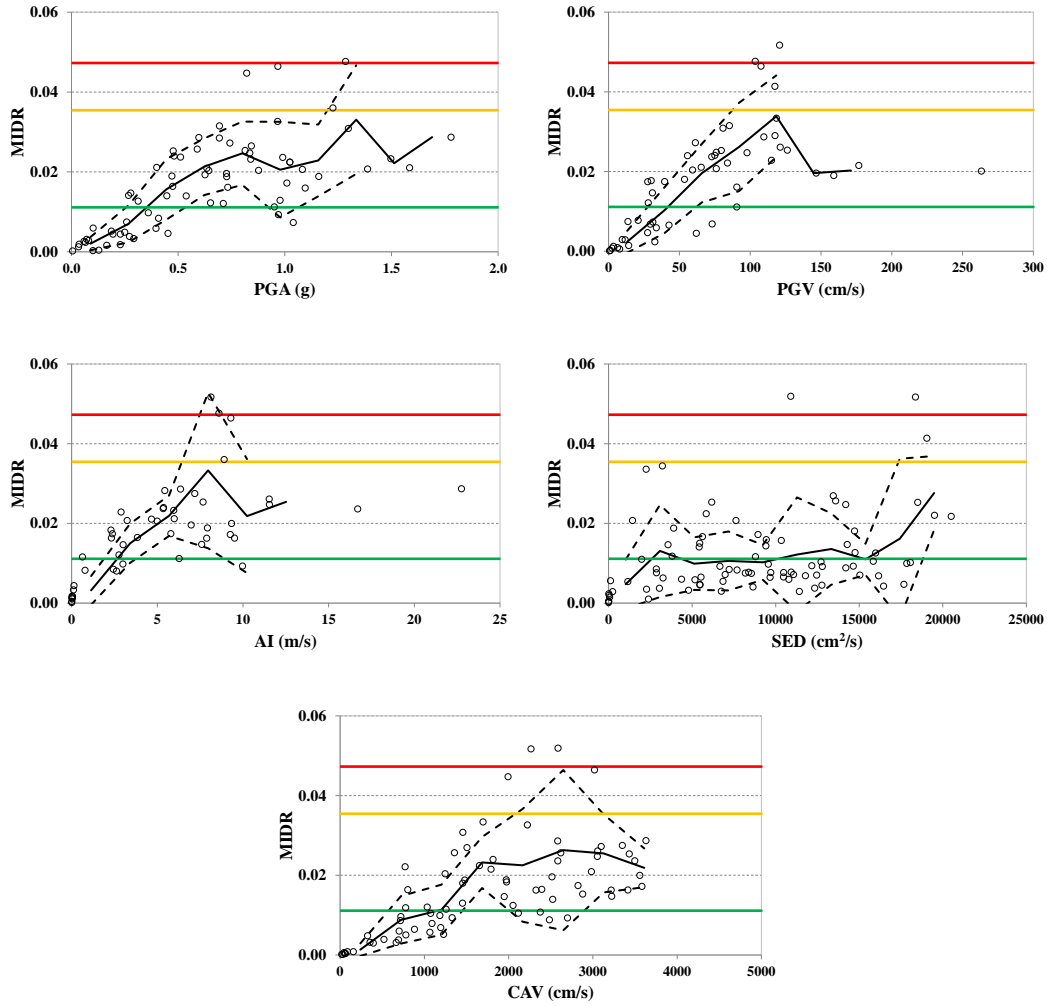
Figure A.142. Scatter plots for selected IMs (PGA, PGV, AI, SED, CAV) versus MIDR for F2S2B (T_1=0.59 s) (MDOF)
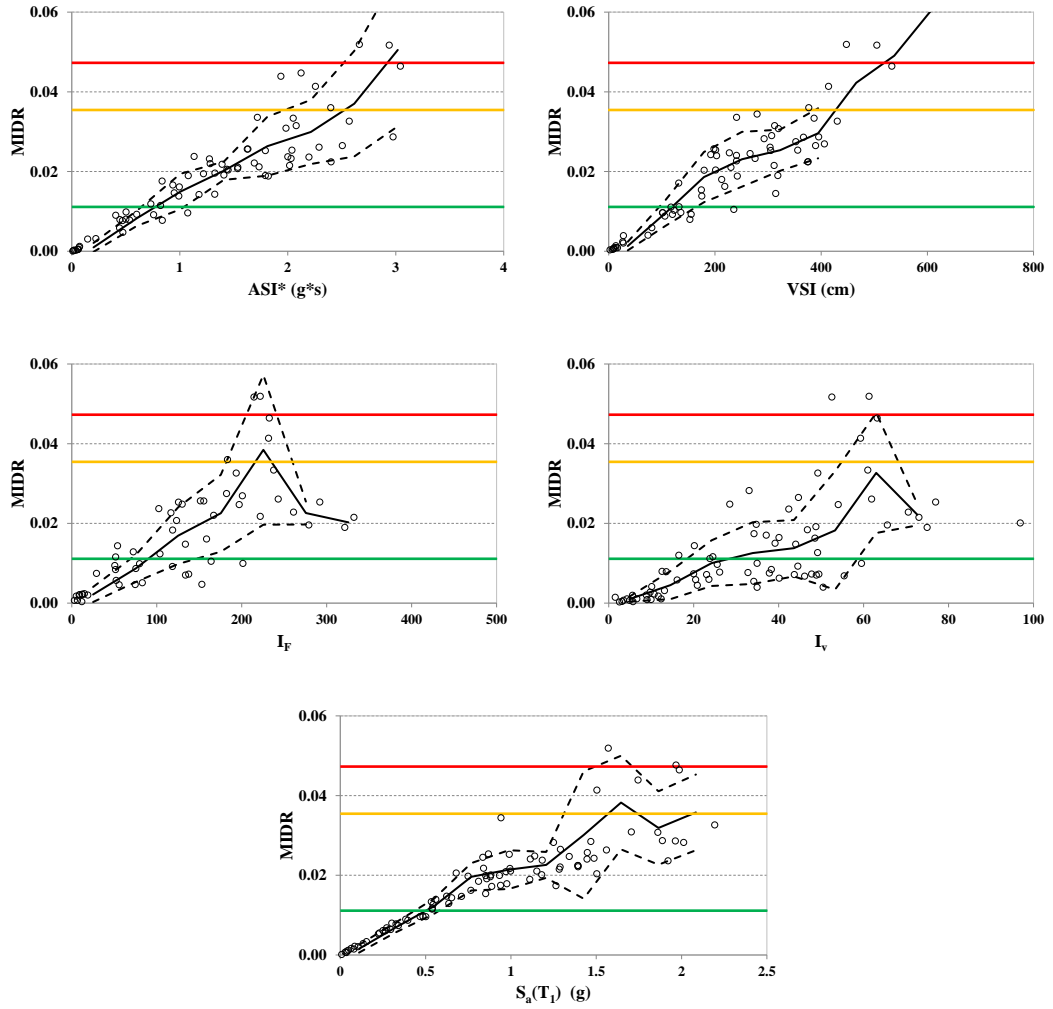
Figure A.143. Scatter plots for selected IMs (ASI*, VSI, I_F, I_v, $S_a(T_1)$) versus MIDR for F2S2B (T_1=0.59 s) (MDOF)
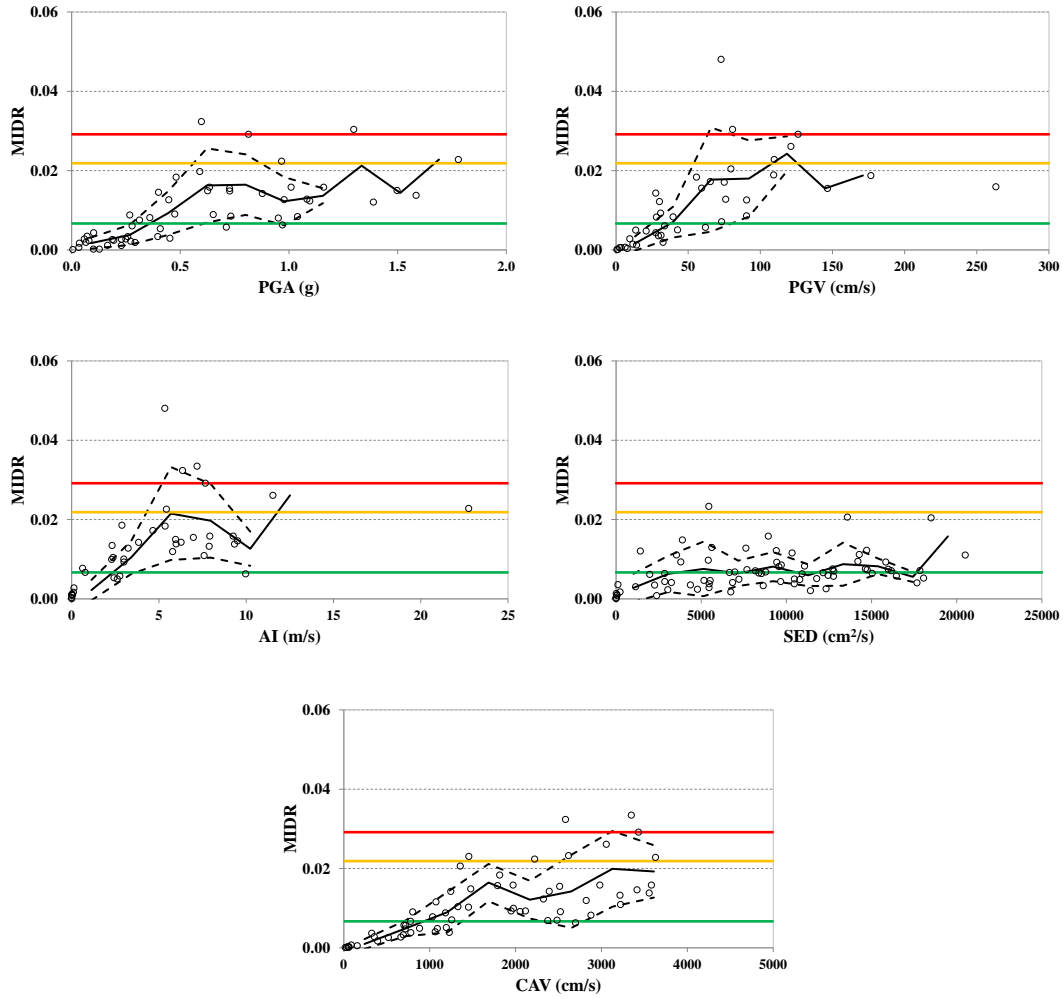
Figure A.144. Scatter plots for selected IMs (PGA, PGV, AI, SED, CAV) versus MIDR for F5S7B (T_1=0.66 s) (MDOF)
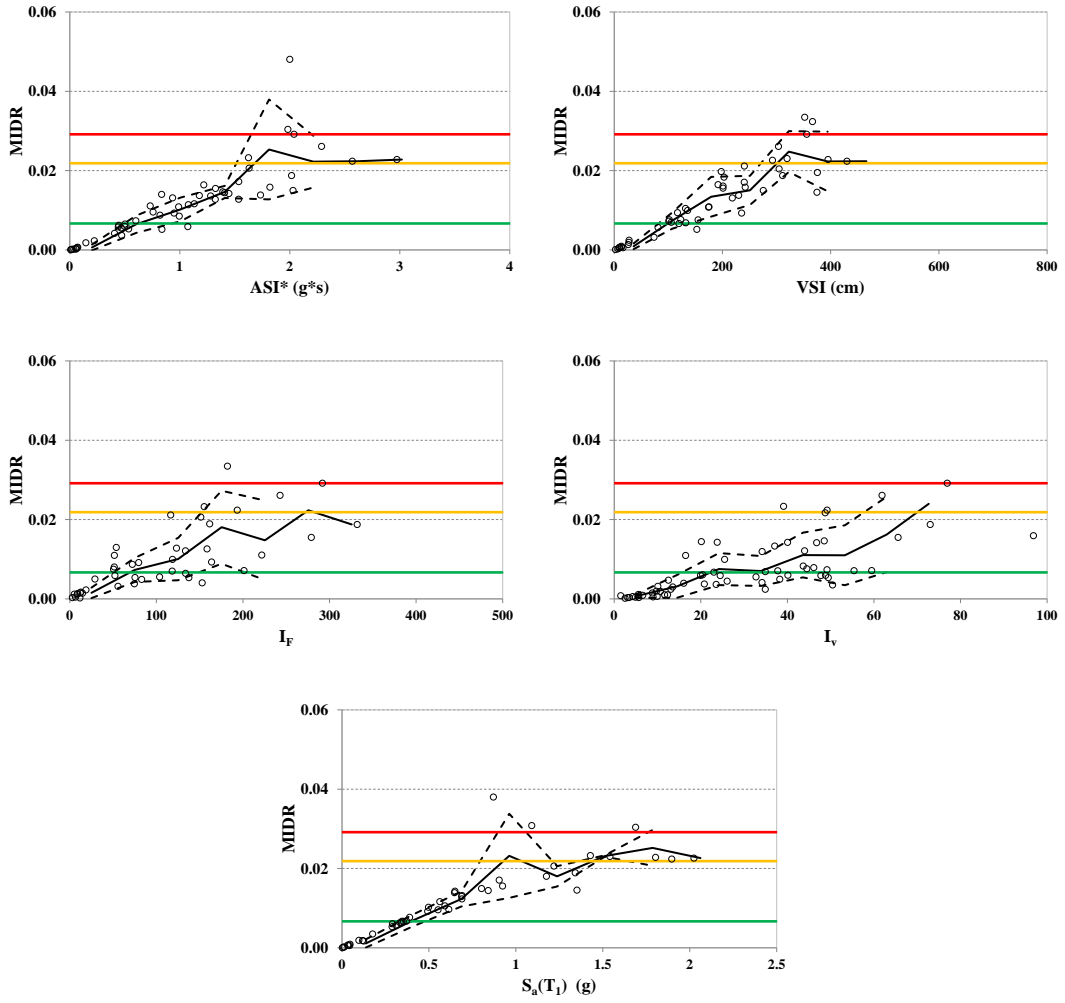
Figure A.145. Scatter plots for selected IMs (ASI*, VSI, I_F, I_V, $S_a(T_1)$) versus MIDR for F5S7B (T_1=0.66 s) (MDOF)
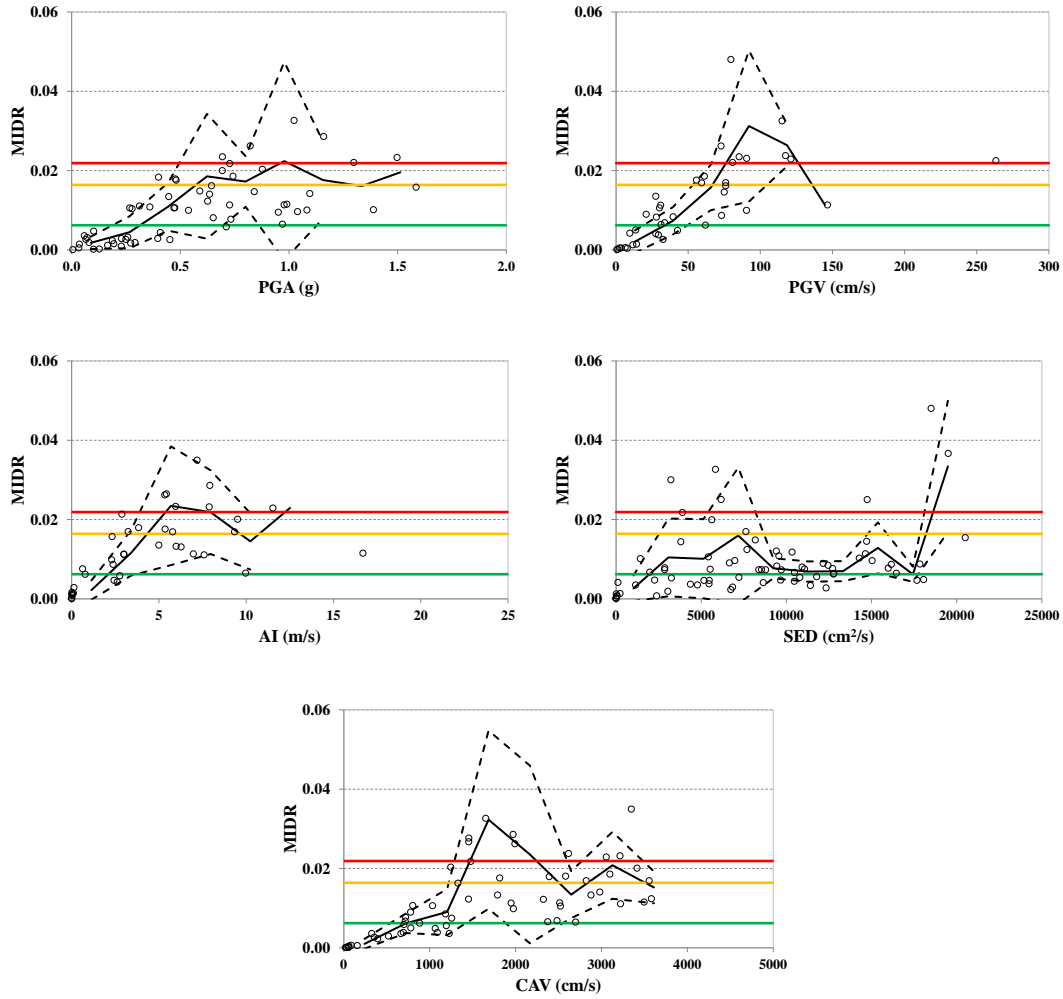
Figure A.146. Scatter plots for selected IMs (PGA, PGV, AI, SED, CAV) versus MIDR for F5S2B (T_1=0.75 s) (MDOF)
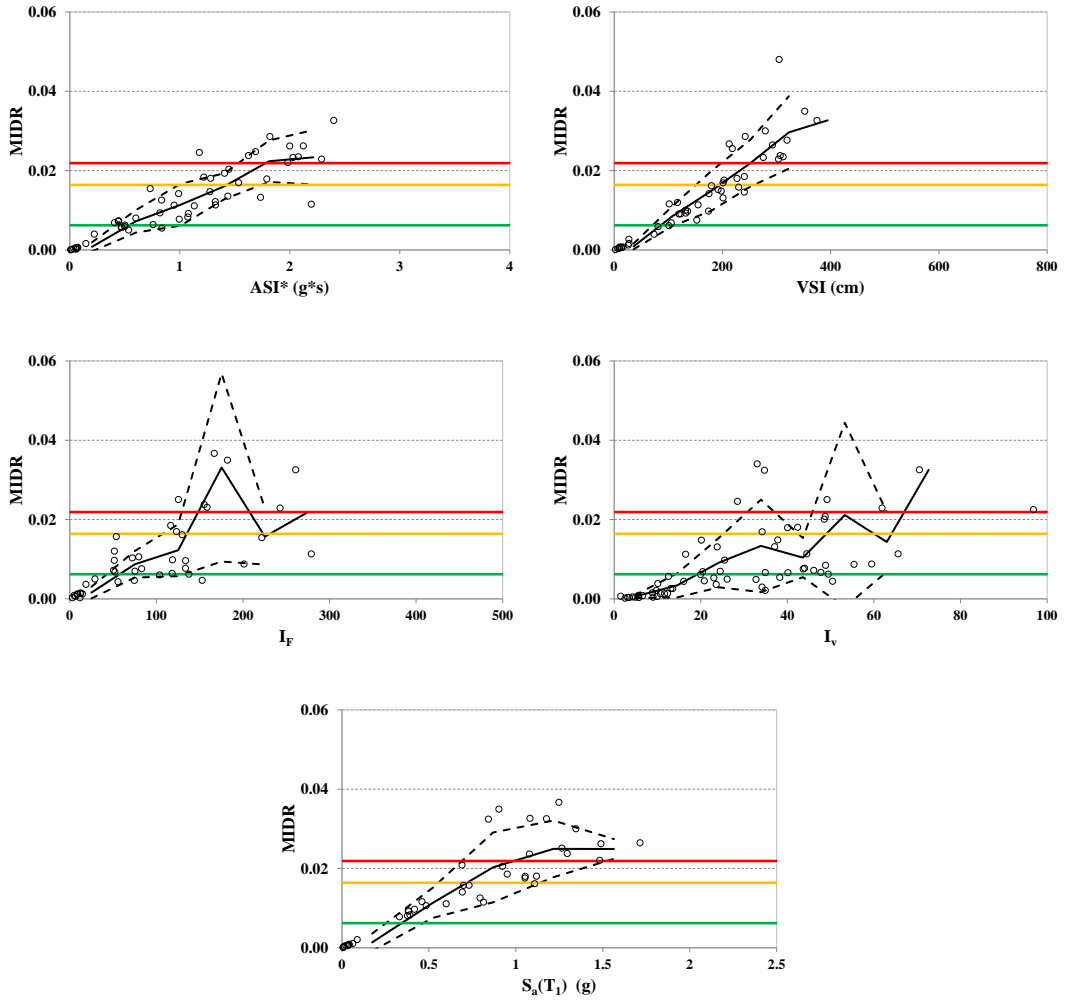
Figure A.147. Scatter plots for selected IMs (ASI*, VSI, I_F, I_V, $S_a(T_1)$) versus MIDR for F5S2B (T_1=0.75 s) (MDOF)
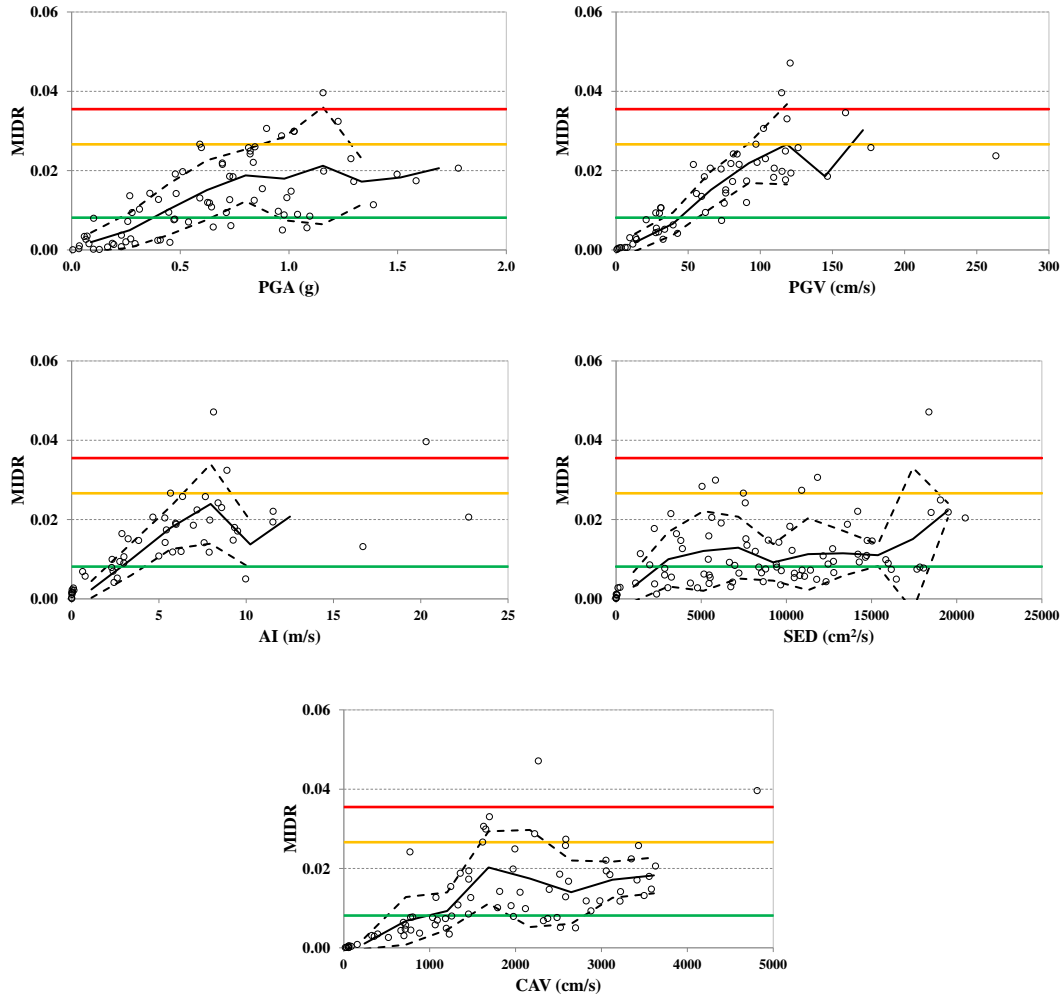
Figure A.148. Scatter plots for selected IMs (PGA, PGV, AI, SED, CAV) versus MIDR for F5S4B (T_1=0.95 s) (MDOF)
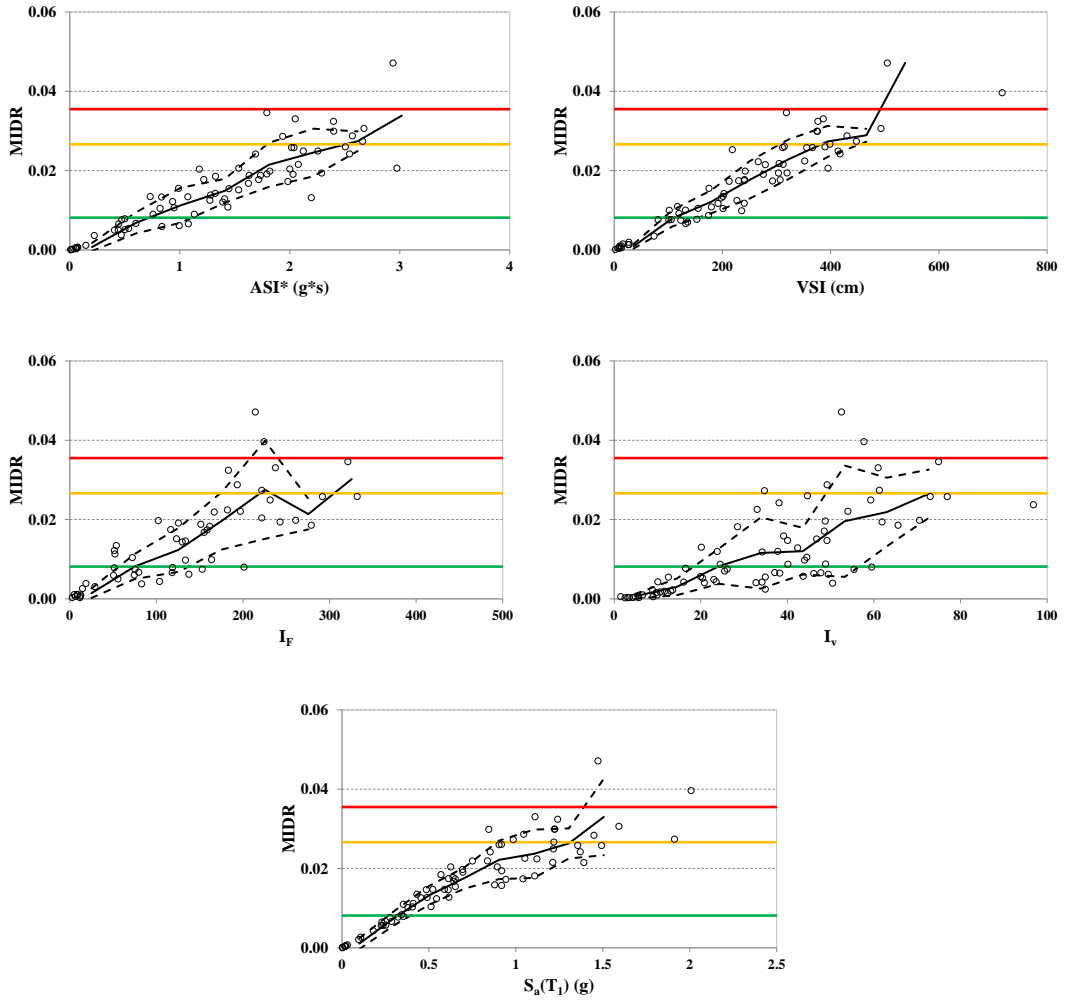
Figure A.149. Scatter plots for selected IMs (ASI*, VSI, I_F, I_V, $S_a(T_1)$) versus MIDR for F5S4B (T_1=0.95 s) (MDOF)
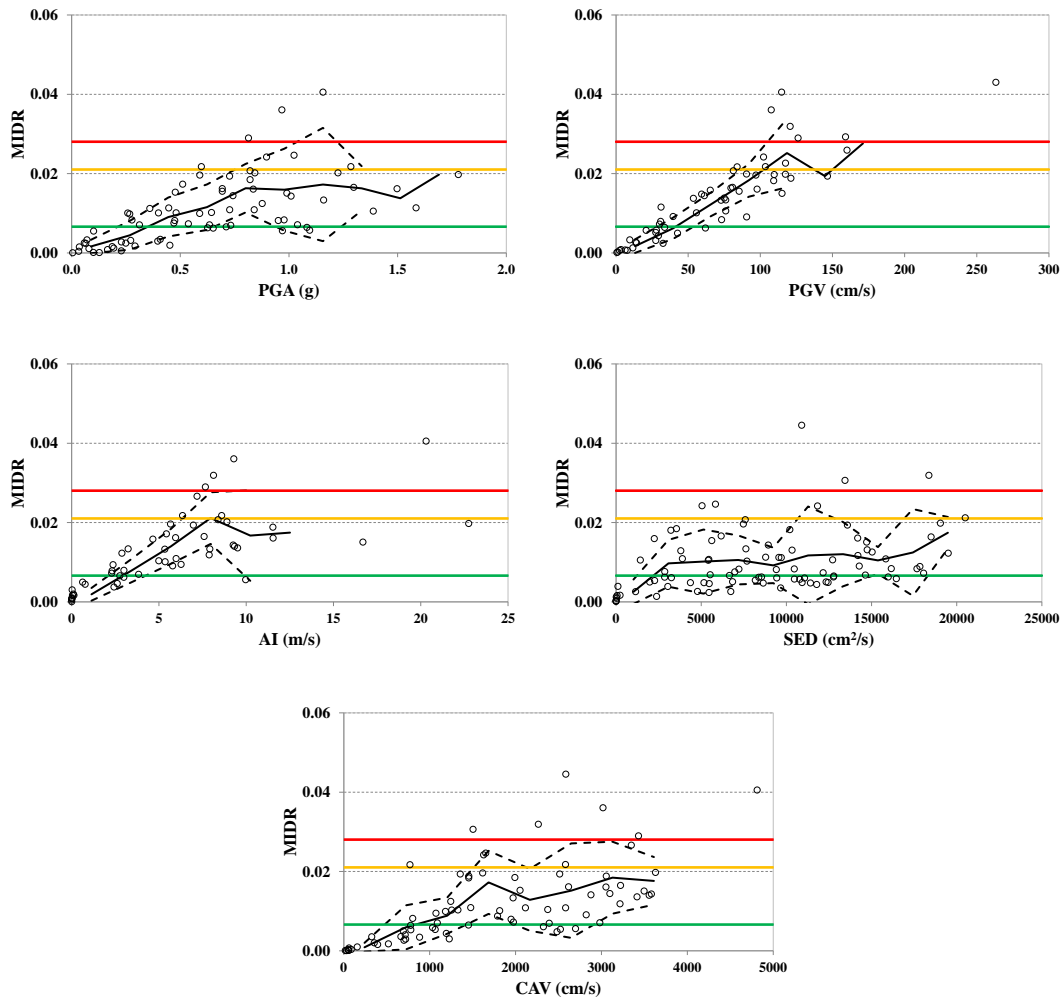
Figure A.150. Scatter plots for selected IMs (PGA, PGV, AI, SED, CAV) versus MIDR for F8S3B (T_1=1.20 s) (MDOF)
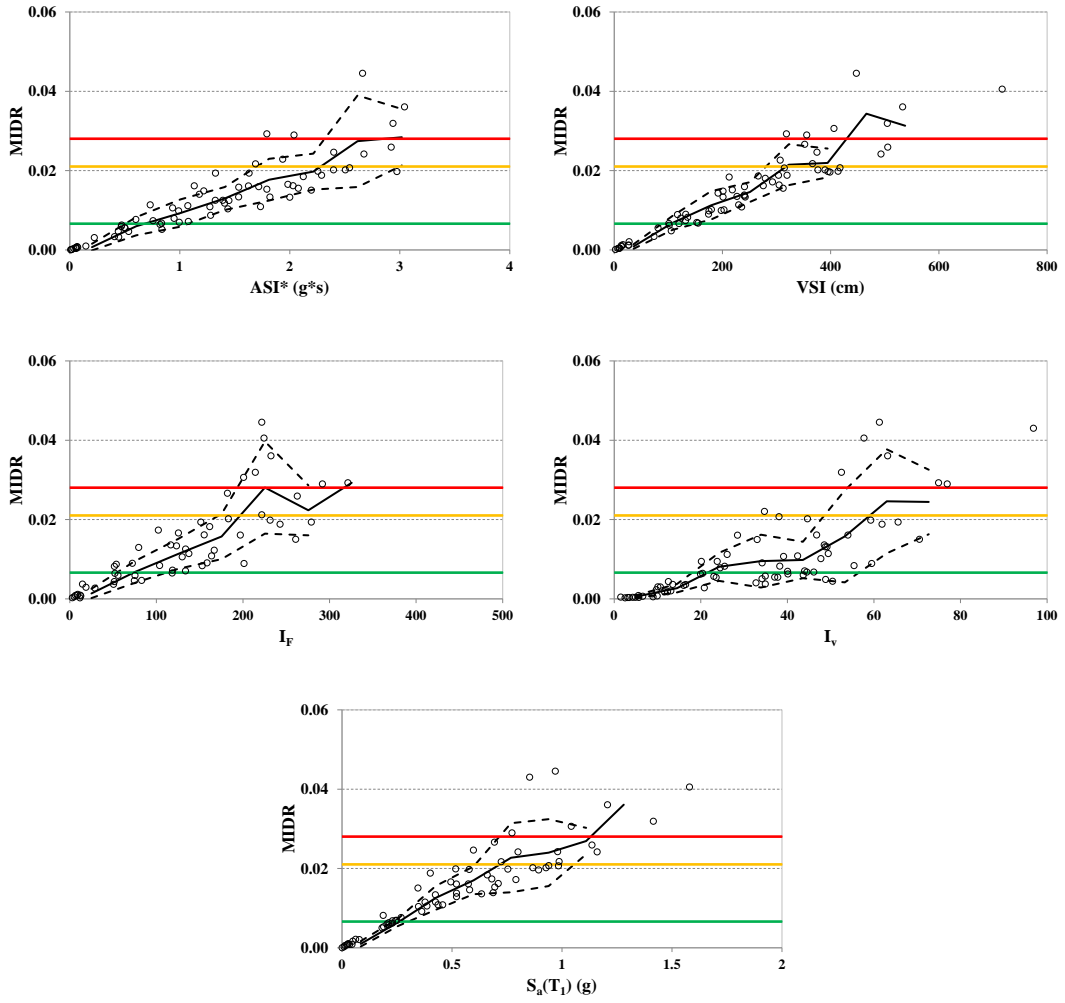
Figure A.151. Scatter plots for selected IMs (ASI*, VSI, I_F, I_V, $S_a(T_1)$) versus MIDR for F8S3B (T_1=1.20 s) (MDOF)

E. Tables for IM Rankings and Sufficiency Checks (for Chapter 5)

The individual tables for IM rankings and sufficiency checks for different frame, DB IM, and EDP cases are not presented herein, but provided as a digital pdf file in the attached CD. However, the summary tables for IM rankings and sufficiency checks are presented on the following pages.

Table A.3 Overall summary of efficiency rankings with respect to R²-adjusted values (frames F2S2B2 and F3S2B)

F2S2B2 (0.30s)

EDP	DB IM	1-PGA	2-PGV	6-ASI*	7-VSI	10-Sa	11-ASI	12-HI	17-SaC	18-SaCM	20-ASA40	21-INp	36-Sa, R(T1,T2)	37-Sa, Np	38-Sa, SdN	39-Sa, Sa/DSI
														Adjusted-R² Summary		
TD	PGA	31-0.841	33-0.818	21-0.91	27-0.863	8-0.97	17-0.93	34-0.792	12-0.951	2-0.973	1-0.979	10-0.967	3-0.972	6-0.972	4-0.972	5-0.972
	PGV	19-0.943	35-0.725	26-0.907	30-0.86	6-0.983	11-0.979	32-0.811	16-0.968	3-0.983	1-0.989	7-0.983	5-0.983	4-0.983	2-0.984	10-0.983
	ASI*	21-0.952	33-0.865	26-0.931	30-0.897	10-0.979	12-0.977	35-0.857	17-0.971	14-0.977	1-0.985	9-0.979	3-0.981	4-0.981	5-0.981	2-0.981
	VSI	21-0.933	33-0.797	27-0.891	32-0.827	8-0.972	12-0.967	34-0.787	17-0.948	10-0.968	1-0.978	15-0.965	2-0.976	3-0.975	5-0.974	4-0.975
	Sa	22-0.92	33-0.831	25-0.908	31-0.857	7-0.973	13-0.954	34-0.79	19-0.935	11-0.954	6-0.973	15-0.951	2-0.975	1-0.975	3-0.974	5-0.974
MIDR	PGA	29-0.858	33-0.817	23-0.907	30-0.856	9-0.967	15-0.941	34-0.782	13-0.948	3-0.971	1-0.975	5-0.968	6-0.968	8-0.967	2-0.972	4-0.969
	PGV	19-0.945	35-0.727	27-0.906	30-0.858	3-0.983	11-0.979	32-0.809	16-0.967	10-0.982	1-0.987	9-0.982	6-0.983	5-0.983	2-0.985	8-0.983
	ASI*	21-0.955	33-0.866	26-0.93	31-0.895	11-0.979	12-0.979	35-0.855	17-0.971	15-0.977	1-0.984	6-0.98	5-0.981	8-0.98	3-0.982	4-0.982
	VSI	21-0.937	33-0.801	27-0.892	32-0.828	9-0.971	12-0.969	34-0.789	17-0.95	13-0.968	1-0.977	15-0.966	3-0.975	5-0.974	2-0.976	4-0.975
	Sa	22-0.92	33-0.821	25-0.898	31-0.845	6-0.971	11-0.953	34-0.776	19-0.93	15-0.95	8-0.969	16-0.949	3-0.972	2-0.973	1-0.975	5-0.971
BS	PGA	33-0.828	31-0.835	17-0.908	27-0.868	11-0.931	21-0.898	34-0.81	8-0.936	3-0.944	2-0.947	6-0.938	5-0.939	7-0.937	1-0.973	4-0.944
	PGV	21-0.924	34-0.759	24-0.907	29-0.865	8-0.959	12-0.951	32-0.825	15-0.95	10-0.957	2-0.964	9-0.957	4-0.96	6-0.96	1-0.987	3-0.961
	ASI*	26-0.933	32-0.894	23-0.941	31-0.913	12-0.96	15-0.956	35-0.881	8-0.965	9-0.963	5-0.968	9-0.965	7-0.965	10-0.963	1-0.986	3-0.972
	VSI	22-0.927	33-0.842	25-0.92	31-0.87	18-0.938	13-0.943	34-0.835	14-0.943	9-0.947	5-0.953	16-0.942	4-0.956	8-0.949	1-0.979	3-0.956
	Sa	22-0.876	33-0.762	27-0.85	31-0.791	3-0.94	10-0.925	34-0.72	17-0.899	16-0.919	8-0.938	14-0.92	4-0.94	2-0.941	1-0.975	6-0.94

F3S2B (0.45s)

EDP	DB IM	1-PGA	2-PGV	6-ASI*	7-VSI	10-Sa	11-ASI	12-HI	17-SaC	18-SaCM	20-ASA40	21-INp	36-Sa, R(T1,T2)	37-Sa, Np	38-Sa, SdN	39-Sa, Sa/DSI
														Adjusted-R² Summary		
TD	PGA	36-0.683	29-0.791	14-0.907	20-0.894	5-0.978	31-0.775	23-0.85	11-0.958	9-0.976	1-0.984	10-0.965	2-0.98	3-0.979	6-0.977	4-0.979
	PGV	27-0.917	34-0.778	18-0.942	29-0.914	4-0.989	19-0.934	32-0.869	11-0.971	10-0.978	8-0.989	9-0.979	1-0.991	2-0.99	5-0.989	3-0.989
	ASI*	31-0.899	35-0.87	16-0.938	21-0.918	5-0.981	29-0.913	34-0.884	11-0.965	10-0.977	1-0.987	9-0.978	4-0.981	7-0.981	2-0.982	3-0.981
	VSI	28-0.906	34-0.87	16-0.943	27-0.907	9-0.975	31-0.901	33-0.875	11-0.961	3-0.977	1-0.986	10-0.97	4-0.977	7-0.975	5-0.977	2-0.978
	Sa	34-0.813	27-0.868	15-0.925	23-0.893	6-0.971	32-0.843	35-0.813	12-0.932	9-0.963	1-0.979	10-0.956	5-0.972	4-0.972	2-0.974	3-0.972
MIDR	PGA	36-0.917	28-0.8	16-0.917	20-0.899	5-0.973	23-0.846	30-0.799	11-0.954	9-0.971	1-0.979	10-0.962	2-0.974	3-0.973	6-0.973	4-0.973
	PGV	27-0.92	34-0.781	18-0.944	29-0.915	6-0.989	19-0.936	32-0.87	11-0.972	10-0.979	5-0.989	9-0.98	1-0.991	2-0.99	4-0.989	3-0.99
	ASI*	31-0.9	35-0.874	15-0.94	21-0.92	6-0.98	29-0.914	34-0.886	11-0.966	10-0.978	1-0.987	9-0.978	4-0.981	7-0.98	2-0.983	3-0.981
	VSI	29-0.905	34-0.875	15-0.946	26-0.911	9-0.974	31-0.9	33-0.88	11-0.962	4-0.977	1-0.985	10-0.97	5-0.976	7-0.974	3-0.978	2-0.979
	Sa	34-0.812	27-0.867	15-0.923	23-0.891	6-0.969	32-0.843	35-0.81	12-0.93	9-0.962	1-0.977	10-0.955	4-0.97	5-0.97	2-0.976	3-0.971
BS	PGA	36-0.764	28-0.841	14-0.929	20-0.91	7-0.933	31-0.815	25-0.855	16-0.928	5-0.934	4-0.944	15-0.929	2-0.936	6-0.933	2-0.941	3-0.938
	PGV	30-0.911	34-0.816	13-0.953	20-0.931	7-0.965	27-0.912	32-0.895	9-0.962	10-0.961	4-0.972	11-0.96	2-0.973	5-0.971	1-0.982	3-0.972
	ASI*	35-0.869	30-0.896	13-0.943	18-0.931	10-0.964	33-0.879	29-0.906	11-0.961	5-0.969	2-0.977	9-0.964	6-0.969	7-0.968	1-0.982	4-0.972
	VSI	33-0.887	28-0.904	9-0.953	22-0.929	12-0.95	35-0.866	29-0.904	13-0.948	11-0.95	3-0.961	15-0.942	4-0.961	6-0.955	1-0.974	2-0.97
	Sa	36-0.774	26-0.859	13-0.903	19-0.879	7-0.941	33-0.801	30-0.805	11-0.906	9-0.937	2-0.951	10-0.927	5-0.941	6-0.941	1-0.968	3-0.945

Table A.4 Overall summary of efficiency rankings with respect to R²-adjusted values (frames F2S2B and F5S7B)

F2S2B (0.59s)

EDP	DB IM	1-PGA	2-PGV	6-ASI*	7-VSI	10-Sa	11-ASI	12-HI	17-SaC	18-SaCM	20-ASA40	21-INp	36-Sa, R(T1,T2)	37-Sa, Np	38-Sa, SdN	39-Sa, Sa/DSI
TD	PGA	39-0.655	26-0.839	21-0.906	15-0.913	7-0.967	37-0.714	22-0.901	11-0.952	9-0.964	2-0.972	10-0.963	1-0.972	3-0.971	6-0.967	4-0.97
TD	PGV	29-0.9	34-0.836	13-0.966	19-0.953	9-0.969	31-0.886	25-0.923	5-0.976	8-0.97	3-0.977	7-0.972	1-0.981	2-0.978	11-0.969	4-0.976
TD	ASI*	33-0.866	27-0.929	14-0.964	7-0.967	17-0.961	37-0.851	21-0.953	4-0.968	3-0.969	1-0.972	10-0.966	2-0.97	11-0.966	19-0.96	12-0.966
TD	VSI	34-0.828	26-0.92	8-0.954	11-0.954	19-0.94	38-0.79	18-0.942	1-0.971	3-0.962	2-0.964	5-0.957	4-0.959	14-0.949	21-0.94	16-0.948
TD	Sa	33-0.783	23-0.899	14-0.921	17-0.918	8-0.951	39-0.738	26-0.878	11-0.945	9-0.95	1-0.966	6-0.951	2-0.959	3-0.958	7-0.951	5-0.953
MIDR	PGA	39-0.707	27-0.85	15-0.926	20-0.923	7-0.964	34-0.765	22-0.896	13-0.946	10-0.961	1-0.966	9-0.962	2-0.966	3-0.965	4-0.964	5-0.964
MIDR	PGV	29-0.902	34-0.827	13-0.963	20-0.947	8-0.972	30-0.893	27-0.914	7-0.973	11-0.97	3-0.977	6-0.974	1-0.981	2-0.978	9-0.972	4-0.977
MIDR	ASI*	33-0.878	28-0.927	11-0.967	14-0.966	16-0.964	36-0.866	22-0.95	12-0.967	2-0.971	1-0.974	4-0.969	3-0.97	10-0.967	18-0.964	7-0.968
MIDR	VSI	33-0.842	26-0.919	7-0.958	11-0.953	17-0.946	38-0.807	21-0.939	1-0.973	3-0.965	2-0.967	4-0.963	5-0.96	14-0.951	20-0.945	15-0.951
MIDR	Sa	33-0.794	23-0.897	14-0.922	18-0.914	6-0.959	37-0.753	26-0.873	11-0.944	10-0.952	1-0.969	9-0.956	2-0.963	3-0.962	8-0.958	5-0.96
BS	PGA	36-0.762	27-0.852	3-0.92	10-0.902	19-0.896	32-0.811	25-0.866	20-0.893	16-0.899	11-0.901	9-0.902	13-0.9	17-0.897	4-0.92	15-0.899
BS	PGV	30-0.857	34-0.841	12-0.937	17-0.923	10-0.94	31-0.857	26-0.9	7-0.942	9-0.941	4-0.947	5-0.947	6-0.944	8-0.942	1-0.965	3-0.955
BS	ASI*	35-0.839	27-0.919	13-0.939	16-0.937	8-0.948	38-0.831	21-0.929	10-0.946	11-0.945	5-0.951	7-0.949	4-0.953	6-0.949	1-0.973	3-0.955
BS	VSI	35-0.831	18-0.927	5-0.94	7-0.936	24-0.917	39-0.795	21-0.925	3-0.942	13-0.936	14-0.935	8-0.936	20-0.926	22-0.919	1-0.955	6-0.938
BS	Sa	33-0.776	21-0.837	13-0.861	23-0.836	3-0.914	36-0.746	30-0.797	12-0.87	10-0.887	8-0.908	9-0.899	5-0.913	4-0.913	1-0.945	2-0.914

Adjusted-R² Summary: columns 36–39.

F5S7B (0.66s)

EDP	DB IM	1-PGA	2-PGV	6-ASI*	7-VSI	10-Sa	11-ASI	12-HI	17-SaC	18-SaCM	20-ASA40	21-INp	36-Sa, R(T1,T2)	37-Sa, Np	38-Sa, SdN	39-Sa, Sa/DSI
TD	PGA	39-0.611	26-0.827	22-0.898	18-0.913	6-0.98	38-0.661	17-0.913	11-0.957	10-0.971	2-0.981	9-0.973	3-0.98	7-0.979	1-0.983	4-0.98
TD	PGV	31-0.896	34-0.844	13-0.967	19-0.954	6-0.98	28-0.904	25-0.929	11-0.971	9-0.979	1-0.983	10-0.978	7-0.979	8-0.979	2-0.982	3-0.981
TD	ASI*	36-0.863	27-0.945	20-0.967	14-0.972	6-0.979	39-0.851	19-0.967	12-0.976	3-0.983	2-0.984	10-0.979	10-0.979	9-0.979	1-0.985	8-0.979
TD	VSI	36-0.839	26-0.941	17-0.959	14-0.961	10-0.971	39-0.811	21-0.956	6-0.972	8-0.972	3-0.975	5-0.973	2-0.975	9-0.971	1-0.975	4-0.974
TD	Sa	33-0.886	27-0.926	11-0.972	18-0.968	5-0.979	36-0.877	22-0.954	20-0.966	9-0.976	2-0.981	10-0.973	3-0.98	4-0.979	1-0.981	6-0.979
MIDR	PGA	39-0.663	26-0.847	20-0.924	16-0.93	5-0.975	38-0.706	22-0.913	13-0.946	9-0.965	2-0.976	10-0.965	1-0.976	4-0.975	8-0.975	6-0.975
MIDR	PGV	31-0.902	34-0.834	14-0.964	20-0.951	5-0.972	28-0.908	25-0.924	12-0.965	2-0.977	1-0.979	3-0.974	9-0.971	10-0.971	8-0.971	4-0.972
MIDR	ASI*	35-0.868	27-0.946	19-0.968	12-0.973	7-0.976	39-0.854	20-0.967	15-0.972	2-0.98	3-0.982	3-0.979	11-0.975	10-0.976	4-0.977	8-0.976
MIDR	VSI	36-0.846	26-0.941	18-0.963	14-0.965	9-0.973	39-0.815	21-0.961	11-0.973	4-0.975	4-0.975	5-0.975	2-0.978	6-0.974	8-0.974	3-0.977
MIDR	Sa	33-0.893	27-0.929	12-0.938	14-0.97	4-0.977	36-0.88	22-0.955	20-0.963	12-0.974	2-0.981	16-0.97	2-0.978	3-0.977	6-0.976	5-0.976
BS	PGA	39-0.691	26-0.858	10-0.927	12-0.926	14-0.926	35-0.744	22-0.9	21-0.905	18-0.919	17-0.925	19-0.915	5-0.929	7-0.928	1-0.949	9-0.927
BS	PGV	34-0.839	32-0.849	13-0.943	15-0.938	8-0.949	29-0.863	23-0.919	9-0.948	7-0.949	5-0.952	11-0.947	6-0.95	10-0.948	1-0.977	3-0.956
BS	ASI*	37-0.818	24-0.929	20-0.945	12-0.956	14-0.955	39-0.814	17-0.955	2-0.963	4-0.961	3-0.962	6-0.96	11-0.956	16-0.955	1-0.981	13-0.956
BS	VSI	37-0.796	16-0.926	22-0.924	6-0.935	23-0.923	39-0.771	9-0.934	7-0.935	17-0.926	13-0.93	20-0.925	3-0.938	15-0.928	1-0.967	4-0.936
BS	Sa	36-0.855	29-0.879	12-0.938	17-0.932	8-0.94	35-0.861	21-0.913	18-0.931	4-0.941	2-0.945	14-0.937	5-0.94	6-0.94	1-0.974	11-0.938

Adjusted-R² Summary: columns 36–39.

Table A.5 Overall summary of efficiency rankings with respect to R^2-adjusted values (frames F5S2B and F5S4B)

F5S2B (0.75s)

EDP	DB IM	1-PGA	2-PGV	6-ASI*	7-VSI	10-Sa	11-ASI	12-HI	17-SaC	18-SaCM	20-ASA40	21-INp	36-Sa,R(T1,T2)	37-Sa,Np	38-Sa,SdN	39-Sa,Sa/DSI
																Adjusted-R^2 Summary
TD	PGA	39-0.586	24-0.836	22-0.898	17-0.918	5-0.947	38-0.668	19-0.917	12-0.936	3-0.948	1-0.951	2-0.948	8-0.947	9-0.946	4-0.947	6-0.947
	PGV	32-0.845	34-0.82	16-0.943	6-0.948	11-0.945	29-0.852	21-0.93	18-0.943	3-0.957	1-0.958	4-0.952	10-0.945	13-0.944	14-0.944	7-0.948
	ASI*	35-0.826	24-0.914	22-0.945	18-0.958	7-0.967	39-0.806	13-0.961	15-0.958	10-0.966	1-0.971	11-0.962	3-0.969	5-0.968	9-0.967	4-0.969
	VSI	36-0.792	23-0.913	21-0.93	2-0.955	16-0.941	39-0.749	39-0.955	6-0.954	9-0.952	8-0.953	12-0.944	11-0.947	13-0.943	17-0.941	14-0.942
	Sa	34-0.865	18-0.964	24-0.96	15-0.967	7-0.974	37-0.835	14-0.967	26-0.958	13-0.967	4-0.977	23-0.962	2-0.981	1-0.982	9-0.973	3-0.977
MIDR	PGA	39-0.629	26-0.864	22-0.926	14-0.94	5-0.958	37-0.708	21-0.927	13-0.942	11-0.955	2-0.959	2-0.959	8-0.957	10-0.957	3-0.959	7-0.957
	PGV	32-0.867	34-0.842	14-0.959	13-0.959	8-0.965	30-0.87	22-0.944	19-0.956	3-0.97	1-0.974	10-0.965	6-0.966	9-0.965	11-0.964	4-0.969
	ASI*	35-0.845	26-0.927	22-0.957	15-0.968	6-0.976	39-0.825	14-0.969	18-0.966	10-0.974	2-0.979	11-0.971	4-0.977	7-0.976	9-0.976	3-0.977
	VSI	36-0.817	23-0.939	21-0.952	3-0.973	16-0.96	39-0.777	4-0.973	7-0.972	9-0.971	8-0.972	11-0.965	13-0.963	15-0.96	17-0.959	14-0.962
	Sa	34-0.87	18-0.968	24-0.963	15-0.97	8-0.977	37-0.84	13-0.97	26-0.962	14-0.97	3-0.98	22-0.966	2-0.983	1-0.984	7-0.977	8-0.98
BS	PGA	39-0.67	25-0.892	9-0.925	3-0.933	17-0.911	37-0.741	13-0.915	24-0.893	20-0.905	12-0.916	21-0.899	16-0.913	15-0.913	1-0.939	14-0.914
	PGV	37-0.81	28-0.843	15-0.92	10-0.923	12-0.922	34-0.82	20-0.913	16-0.917	19-0.914	6-0.927	17-0.917	8-0.925	11-0.922	1-0.971	2-0.935
	ASI*	37-0.78	24-0.909	22-0.918	19-0.935	10-0.941	39-0.775	15-0.94	16-0.939	4-0.946	3-0.948	9-0.941	7-0.942	11-0.941	1-0.977	5-0.946
	VSI	37-0.775	17-0.928	27-0.917	9-0.938	23-0.925	39-0.751	4-0.941	10-0.933	15-0.929	11-0.932	25-0.924	13-0.931	18-0.927	1-0.958	8-0.94
	Sa	35-0.828	15-0.941	26-0.934	11-0.942	12-0.942	38-0.82	22-0.939	13-0.942	16-0.941	3-0.948	19-0.94	2-0.95	5-0.948	1-0.968	8-0.947

F5S4B (0.95s)

EDP	DB IM	1-PGA	2-PGV	6-ASI*	7-VSI	10-Sa	11-ASI	12-HI	17-SaC	18-SaCM	20-ASA40	21-INp	36-Sa,R(T1,T2)	37-Sa,Np	38-Sa,SdN	39-Sa,Sa/DSI
																Adjusted-R^2 Summary
TD	PGA	39-0.592	28-0.891	22-0.921	19-0.949	3-0.989	38-0.653	11-0.972	15-0.967	10-0.981	8-0.987	9-0.984	5-0.989	4-0.989	2-0.989	1-0.989
	PGV	33-0.825	26-0.895	22-0.955	15-0.969	9-0.982	35-0.789	12-0.971	18-0.963	7-0.983	2-0.984	5-0.983	6-0.983	8-0.982	4-0.983	1-0.986
	ASI*	37-0.82	24-0.932	22-0.953	20-0.966	8-0.985	39-0.796	11-0.976	14-0.975	10-0.983	2-0.986	9-0.984	4-0.986	3-0.986	6-0.985	1-0.987
	VSI	36-0.81	26-0.937	22-0.952	14-0.968	6-0.976	39-0.756	15-0.968	20-0.955	9-0.974	1-0.979	10-0.973	4-0.977	3-0.978	5-0.977	2-0.978
	Sa	35-0.831	24-0.955	22-0.967	13-0.98	8-0.982	39-0.799	16-0.975	18-0.973	10-0.982	2-0.986	7-0.983	1-0.986	3-0.986	5-0.983	4-0.985
MIDR	PGA	39-0.636	25-0.914	22-0.946	17-0.967	4-0.984	38-0.7	12-0.975	21-0.959	14-0.973	8-0.979	7-0.984	5-0.984	6-0.981	3-0.984	5-0.984
	PGV	33-0.833	26-0.901	20-0.959	15-0.971	9-0.98	35-0.797	13-0.974	18-0.964	3-0.982	1-0.985	9-0.978	5-0.981	6-0.981	8-0.98	2-0.984
	ASI*	37-0.841	26-0.946	22-0.965	17-0.974	5-0.98	39-0.819	8-0.979	21-0.968	14-0.976	10-0.979	12-0.978	4-0.98	3-0.98	7-0.979	2-0.981
	VSI	36-0.812	26-0.941	22-0.954	14-0.969	6-0.977	39-0.759	15-0.968	20-0.955	9-0.974	10-0.979	10-0.974	4-0.978	2-0.979	7-0.977	3-0.979
	Sa	35-0.838	24-0.96	22-0.971	10-0.981	8-0.982	39-0.806	12-0.976	21-0.971	14-0.98	2-0.985	13-0.981	1-0.985	3-0.985	7-0.982	4-0.984
BS	PGA	39-0.673	25-0.905	11-0.925	6-0.931	14-0.919	38-0.734	8-0.927	27-0.896	22-0.907	18-0.915	19-0.913	17-0.918	16-0.918	1-0.948	13-0.92
	PGV	34-0.811	27-0.895	13-0.933	4-0.939	17-0.923	36-0.797	7-0.937	23-0.916	6-0.937	15-0.926	8-0.936	19-0.922	20-0.922	1-0.971	11-0.934
	ASI*	37-0.821	24-0.921	13-0.939	7-0.943	14-0.937	39-0.815	8-0.944	22-0.923	17-0.937	21-0.936	17-0.937	12-0.978	18-0.936	1-0.97	11-0.94
	VSI	36-0.803	13-0.93	16-0.928	3-0.937	22-0.921	39-0.762	9-0.931	27-0.908	17-0.926	19-0.924	20-0.924	23-0.921	24-0.921	1-0.967	15-0.928
	Sa	36-0.782	25-0.914	23-0.92	13-0.935	8-0.941	39-0.752	16-0.93	19-0.924	6-0.942	2-0.946	10-0.938	5-0.943	3-0.946	1-0.972	4-0.945

Table A.6 Overall summary of efficiency rankings with respect to R^2-adjusted values (frame F8S3B)

															Adjusted-R^2 Summary	
EDP	F8S3B (1.20s) DB IM	1-PGA	2-PGV	6-ASI*	7-VSI	10-Sa	11-ASI	12-HI	17-SaC	18-SaCM	20-ASA40	21-INp	36-Sa,R(T1,T2)	37-Sa,Np	38-Sa,SdN	39-Sa,Sa/DSI
TD	PGA	39-0.525	29-0.881	28-0.884	20-0.922	**4-0.982**	38-0.586	15-0.969	14-0.97	*10-0.977*	*9-0.981*	**3-0.983**	*8-0.982*	**5-0.982**	**1-0.986**	**2-0.983**
	PGV	36-0.775	22-0.924	25-0.911	19-0.934	**5-0.966**	38-0.727	13-0.956	16-0.947	11-0.957	6-0.966	*10-0.961*	**2-0.97**	**3-0.968**	*7-0.966*	**1-0.972**
	ASI*	37-0.778	28-0.929	29-0.926	19-0.948	*8-0.982*	39-0.75	14-0.971	11-0.977	*10-0.981*	**2-0.984**	*6-0.983*	**4-0.984**	**5-0.983**	**3-0.984**	**1-0.986**
	VSI	36-0.761	23-0.946	27-0.93	18-0.961	12-0.971	39-0.701	11-0.971	17-0.962	**4-0.974**	**1-0.977**	**3-0.975**	**5-0.973**	*8-0.972*	*10-0.972*	**2-0.977**
	Sa	36-0.713	27-0.925	28-0.923	20-0.95	*9-0.972*	39-0.679	14-0.967	15-0.964	**5-0.974**	**2-0.98**	*10-0.972*	**3-0.976**	**4-0.975**	11-0.972	**1-0.98**
EDP	DB IM	1-PGA	2-PGV	6-ASI*	7-VSI	10-Sa	11-ASI	12-HI	17-SaC	18-SaCM	20-ASA40	21-INp	36-Sa,R(T1,T2)	37-Sa,Np	38-Sa,SdN	39-Sa,Sa/DSI
MIDR	PGA	39-0.628	25-0.921	19-0.944	*7-0.968*	17-0.95	38-0.694	**4-0.976**	23-0.924	21-0.937	20-0.939	18-0.949	12-0.955	*9-0.96*	14-0.953	16-0.95
	PGV	33-0.837	25-0.924	20-0.947	*10-0.961*	11-0.961	38-0.787	**1-0.967**	23-0.929	19-0.947	17-0.954	16-0.955	14-0.96	15-0.96	*9-0.961*	*7-0.961*
	ASI*	37-0.849	23-0.96	12-0.967	*7-0.981*	16-0.965	39-0.823	**2-0.984**	28-0.951	26-0.958	*9-0.968*	*10-0.968*	18-0.965	17-0.965	15-0.965	14-0.965
	VSI	36-0.805	22-0.953	21-0.956	*7-0.976*	14-0.966	39-0.749	**2-0.977**	27-0.945	15-0.965	*9-0.968*	*10-0.968*	16-0.965	18-0.965	12-0.968	13-0.966
	Sa	36-0.754	25-0.936	22-0.944	19-0.965	*10-0.977*	39-0.712	6-0.973	20-0.956	*8-0.971*	**2-0.976**	*7-0.972*	*9-0.971*	11-0.971	14-0.971	**4-0.974**
EDP	DB IM	1-PGA	2-PGV	6-ASI*	7-VSI	10-Sa	11-ASI	12-HI	17-SaC	18-SaCM	20-ASA40	21-INp	36-Sa,R(T1,T2)	37-Sa,Np	38-Sa,SdN	39-Sa,Sa/DSI
BS	PGA	39-0.672	12-0.932	*10-0.937*	*6-0.946*	25-0.9	38-0.738	*7-0.945*	29-0.894	26-0.899	28-0.898	21-0.907	27-0.899	23-0.901	15-0.93	24-0.9
	PGV	35-0.794	16-0.906	11-0.922	*7-0.93*	20-0.898	37-0.792	**5-0.934**	23-0.894	28-0.885	25-0.892	24-0.893	17-0.906	19-0.898	**1-0.95**	15-0.91
	ASI*	37-0.826	12-0.939	11-0.943	*9-0.951*	25-0.928	39-0.819	**3-0.955**	27-0.923	28-0.922	25-0.929	26-0.927	20-0.93	23-0.929	*6-0.955*	18-0.933
	VSI	36-0.802	*8-0.932*	16-0.925	**3-0.934**	23-0.905	39-0.768	11-0.929	29-0.893	28-0.894	25-0.902	26-0.898	20-0.908	22-0.905	**1-0.957**	18-0.911
	Sa	36-0.729	23-0.89	21-0.901	18-0.916	**5-0.935**	39-0.721	*10-0.926*	13-0.924	17-0.917	*8-0.934*	14-0.921	**3-0.944**	**4-0.941**	**1-0.958**	**2-0.947**

362

Table A.7 Overall summary of results in terms of R^2-adjusted values (Linear/Nonlinear response differentiation)

F3S2B (0.45s)

	EDP / DB IM	1-PGA	2-PGV	6-ASI*	7-VSI	10-Sa	11-ASI	12-HI	17-SaC	18-SaCM	20-ASA40	21-INp	36-Sa, R(T1,T2)	37-Sa, Np	38-Sa, SdN	39-Sa, Sa/DSI
OVERALL MIDR	PGA	36-0.713	28-0.8	16-0.917	20-0.899	5-0.973	30-0.799	23-0.846	11-0.954	9-0.971	1-0.979	10-0.962	2-0.974	3-0.973	6-0.973	4-0.973
	PGV	27-0.92	34-0.781	18-0.944	29-0.915	6-0.989	19-0.936	32-0.87	11-0.972	10-0.972	5-0.989	9-0.98	1-0.991	1-0.99	4-0.989	3-0.99
	ASI*	31-0.9	35-0.874	15-0.94	21-0.92	6-0.98	29-0.914	34-0.886	11-0.966	10-0.978	1-0.987	9-0.978	4-0.981	7-0.98	2-0.983	3-0.981
	VSI	29-0.905	34-0.875	15-0.946	26-0.911	9-0.974	31-0.9	33-0.88	11-0.962	4-0.977	1-0.985	10-0.97	5-0.976	7-0.974	3-0.978	2-0.979
	Sa	34-0.812	27-0.867	15-0.923	23-0.891	6-0.969	32-0.843	35-0.81	12-0.93	9-0.962	1-0.977	10-0.955	4-0.97	5-0.97	2-0.976	3-0.971
LINEAR MIDR	PGA	36-0.635	27-0.729	17-0.868	20-0.844	4-0.973	29-0.724	24-0.774	12-0.922	9-0.95	8-0.968	10-0.95	7-0.972	6-0.972	3-0.973	5-0.972
	PGV	32-0.871	35-0.755	15-0.94	22-0.919	4-0.988	24-0.91	31-0.876	11-0.965	10-0.97	8-0.984	9-0.973	3-0.988	6-0.987	1-0.99	7-0.987
	ASI*	34-0.85	32-0.869	15-0.916	20-0.9	6-0.988	28-0.875	33-0.865	11-0.951	10-0.971	8-0.983	9-0.975	3-0.989	2-0.989	5-0.988	4-0.988
	VSI	34-0.883	33-0.89	15-0.94	26-0.906	6-0.981	28-0.9	32-0.89	13-0.946	9-0.972	2-0.984	10-0.97	5-0.981	3-0.982	1-0.985	4-0.98
	Sa	36-0.762	26-0.857	15-0.91	25-0.867	3-0.989	33-0.789	30-0.805	11-0.922	9-0.961	8-0.982	10-0.959	7-0.988	6-0.988	1-0.99	4-0.989
NONLINEAR MIDR	PGA	37-0.05	28-0.202	13-0.532	17-0.466	10-0.591	31-0.131	22-0.366	3-0.707	1-0.794	2-0.789	8-0.612	4-0.67	5-0.635	6-0.631	7-0.618
	PGV	20-0.397	36-0.028	26-0.217	30-0.092	7-0.845	15-0.434	32-0.002	12-0.623	9-0.8	1-0.903	10-0.786	2-0.885	3-0.874	6-0.85	4-0.872
	ASI*	17-0.488	34-0.195	25-0.399	31-0.238	11-0.557	24-0.429	35-0.155	5-0.65	3-0.667	1-0.788	4-0.652	6-0.633	7-0.599	8-0.586	9-0.584
	VSI	19-0.286	31-0.055	24-0.214	32-0.054	9-0.523	16-0.315	35-0.015	12-0.451	2-0.699	1-0.724	10-0.519	4-0.552	6-0.534	5-0.544	3-0.581
	Sa	29-0.373	33-0.284	15-0.514	21-0.421	9-0.573	26-0.399	35-0.228	12-0.538	2-0.668	1-0.746	3-0.618	6-0.59	7-0.585	8-0.58	5-0.594

F5S4B (0.95s)

	EDP / DB IM	1-PGA	2-PGV	6-ASI*	7-VSI	10-Sa	11-ASI	12-HI	17-SaC	18-SaCM	20-ASA40	21-INp	36-Sa, R(T1,T2)	37-Sa, Np	38-Sa, SdN	39-Sa, Sa/DSI
OVERALL MIDR	PGA	39-0.636	25-0.914	22-0.946	17-0.967	4-0.984	38-0.7	12-0.975	21-0.959	14-0.973	8-0.979	9-0.978	7-0.984	6-0.984	3-0.984	5-0.984
	PGV	33-0.833	26-0.901	20-0.959	15-0.971	9-0.98	35-0.797	13-0.974	18-0.964	3-0.982	1-0.985	4-0.982	5-0.981	6-0.981	8-0.98	2-0.984
	ASI*	37-0.841	26-0.946	22-0.965	17-0.974	5-0.98	39-0.819	8-0.979	21-0.968	14-0.976	10-0.979	12-0.978	4-0.98	3-0.98	7-0.979	1-0.981
	VSI	36-0.812	26-0.941	22-0.954	14-0.969	6-0.977	39-0.759	15-0.968	20-0.955	9-0.974	1-0.981	10-0.974	4-0.978	2-0.979	7-0.977	3-0.979
	Sa	35-0.838	24-0.96	22-0.971	10-0.981	8-0.982	39-0.806	16-0.976	21-0.971	14-0.98	2-0.985	13-0.981	1-0.985	3-0.985	7-0.982	4-0.984
LINEAR MIDR	PGA	39-0.539	24-0.898	22-0.922	18-0.959	6-0.983	36-0.635	13-0.968	21-0.937	17-0.961	15-0.964	10-0.971	5-0.983	4-0.984	7-0.983	3-0.985
	PGV	36-0.75	28-0.856	21-0.949	12-0.967	4-0.996	37-0.745	17-0.963	22-0.947	10-0.984	9-0.986	8-0.989	6-0.996	5-0.996	1-0.996	2-0.996
	ASI*	37-0.811	25-0.943	21-0.962	17-0.971	6-0.981	39-0.803	14-0.976	22-0.957	20-0.966	19-0.967	15-0.973	4-0.982	3-0.983	8-0.98	7-0.98
	VSI	37-0.787	25-0.947	27-0.945	13-0.958	3-0.993	39-0.74	19-0.955	21-0.95	11-0.979	10-0.981	9-0.983	4-0.993	2-0.993	1-0.994	5-0.993
	Sa	36-0.857	25-0.963	21-0.981	12-0.986	3-0.995	37-0.852	18-0.983	22-0.973	15-0.986	9-0.989	14-0.989	6-0.995	4-0.995	2-0.996	7-0.995
NONLINEAR MIDR	PGA	33-0.192	26-0.43	20-0.699	14-0.791	11-0.815	36-0.176	8-0.829	17-0.779	5-0.839	1-0.91	10-0.876	4-0.849	2-0.867	3-0.865	6-0.835
	PGV	36-0.016	26-0.295	20-0.471	18-0.626	15-0.706	39--0.025	12-0.718	14-0.713	5-0.777	1-0.846	9-0.731	3-0.787	4-0.779	2-0.797	6-0.776
	ASI*	36-0.096	24-0.525	20-0.583	17-0.717	15-0.743	38-0.042	8-0.784	12-0.765	6-0.801	1-0.863	13-0.763	4-0.826	2-0.838	3-0.827	5-0.804
	VSI	34-0.069	25-0.447	20-0.545	10-0.724	14-0.707	38-0.03	6-0.773	16-0.698	11-0.722	2-0.828	17-0.689	4-0.777	3-0.812	1-0.848	9-0.747
	Sa	34-0.216	22-0.641	20-0.7	5-0.81	19-0.7	37-0.177	10-0.78	15-0.754	12-0.775	2-0.827	14-0.754	3-0.815	8-0.803	9-0.795	13-0.773

Table A.8 Overall summary for M_w-based sufficiency checks (frames F2S2B2 and F3S2B)

F2S2B2 (0.30s)

EDP	DB IM	1-PGA	2-PGV	6-ASI*	7-VSI	10-Sa	11-ASI	12-HI	17-SaC	18-SaCM	20-ASA40	21-INp	36-Sa, R(T1,T2)	37-Sa, Np	38-Sa, SdN	Sufficiency (Mw) 39-Sa, Sa/DSI
TD	PGA	insuff	insuff	insuff	insuff	-	insuff	insuff	-	-	-	-	-	-	-	39-Sa, Sa/DSI
	PGV	-	-	-	-	insuff	-	-	-	-	-	-	-	-	-	
	ASI*	insuff	insuff	insuff	insuff	insuff	insuff	insuff	-	-	insuff	insuff	insuff	insuff	insuff	
	VSI	insuff	insuff	insuff	insuff	insuff	-	insuff	-	-	-	-	-	-	insuff	
	Sa	insuff	insuff	insuff	insuff	-	-	insuff	-	-	-	-	-	-	-	
EDP	DB IM	1-PGA	2-PGV	6-ASI*	7-VSI	10-Sa	11-ASI	12-HI	17-SaC	18-SaCM	20-ASA40	21-INp	36-Sa, R(T1,T2)	37-Sa, Np	38-Sa, SdN	39-Sa, Sa/DSI
MIDR	PGA	insuff	insuff	insuff	insuff	-	insuff	insuff	-	-	-	-	-	-	-	39-Sa, Sa/DSI
	PGV	-	-	-	-	-	-	-	-	-	-	-	-	-	-	
	ASI*	insuff	insuff	insuff	insuff	insuff	insuff	insuff	-	-	insuff	insuff	insuff	insuff	insuff	
	VSI	-	insuff	insuff	insuff	insuff	insuff	insuff	-	-	insuff	insuff	-	insuff	insuff	
	Sa	-	insuff	insuff	insuff	-	-	insuff	-	-	-	-	-	-	-	
EDP	DB IM	1-PGA	2-PGV	6-ASI*	7-VSI	10-Sa	11-ASI	12-HI	17-SaC	18-SaCM	20-ASA40	21-INp	36-Sa, R(T1,T2)	37-Sa, Np	38-Sa, SdN	39-Sa, Sa/DSI
BS	PGA	insuff	insuff	insuff	insuff	-	insuff	insuff	insuff	-	-	-	-	-	-	39-Sa, Sa/DSI
	PGV	-	-	-	-	-	-	-	-	insuff	insuff	insuff	insuff	insuff	-	
	ASI*	insuff	insuff	insuff	insuff	insuff	insuff	insuff	-	insuff	insuff	insuff	insuff	insuff	insuff	
	VSI	-	-	-	insuff	insuff	-	insuff	-	insuff	insuff	insuff	-	insuff	-	
	Sa	-	-	-	-	-	-	-	-	-	-	-	-	-	-	

F3S2B (0.45s)

EDP	DB IM	1-PGA	2-PGV	6-ASI*	7-VSI	10-Sa	11-ASI	12-HI	17-SaC	18-SaCM	20-ASA40	21-INp	36-Sa, R(T1,T2)	37-Sa, Np	38-Sa, SdN	Sufficiency (Mw) 39-Sa, Sa/DSI
TD	PGA	insuff	insuff	insuff	insuff	-	insuff	insuff	insuff	insuff	-	insuff	-	-	-	39-Sa, Sa/DSI
	PGV	-	-	-	-	-	-	-	-	-	-	-	-	-	-	
	ASI*	insuff	-	insuff	insuff	-	insuff	-	-	-	-	-	-	-	-	
	VSI	-	insuff	insuff	insuff	-	insuff	insuff	-	-	-	-	-	-	-	
	Sa	insuff	-	-	-	-	insuff	-	-	-	-	-	-	-	-	
EDP	DB IM	1-PGA	2-PGV	6-ASI*	7-VSI	10-Sa	11-ASI	12-HI	17-SaC	18-SaCM	20-ASA40	21-INp	36-Sa, R(T1,T2)	37-Sa, Np	38-Sa, SdN	39-Sa, Sa/DSI
MIDR	PGA	insuff	insuff	insuff	insuff	-	insuff	insuff	-	insuff	-	insuff	-	-	-	39-Sa, Sa/DSI
	PGV	-	-	-	-	-	-	-	-	-	-	-	-	-	-	
	ASI*	insuff	insuff	-	-	-	insuff	-	-	-	-	-	-	-	-	
	VSI	-	-	-	insuff	insuff	insuff	-	-	-	-	-	-	-	-	
	Sa	insuff	-	-	-	-	insuff	-	-	-	-	-	-	-	-	
EDP	DB IM	1-PGA	2-PGV	6-ASI*	7-VSI	10-Sa	11-ASI	12-HI	17-SaC	18-SaCM	20-ASA40	21-INp	36-Sa, R(T1,T2)	37-Sa, Np	38-Sa, SdN	39-Sa, Sa/DSI
BS	PGA	insuff	insuff	insuff	insuff	-	insuff	insuff	-	insuff	-	insuff	-	-	-	39-Sa, Sa/DSI
	PGV	-	-	-	-	-	insuff	-	-	-	-	-	-	-	-	
	ASI*	insuff	-	-	-	insuff	insuff	-	insuff	insuff	insuff	insuff	insuff	insuff	-	
	VSI	insuff	insuff	-	-	insuff	insuff	-	-	-	-	-	-	-	-	
	Sa	insuff	-	-	-	-	insuff	-	-	-	-	-	-	-	-	

Table A.9 Overall summary for M_w-based sufficiency checks (frames F2S2B and F5S7B)

F2S2B (0.59s) — Sufficiency (M_w)

EDP	DB IM	1-PGA	2-PGV	6-ASI*	7-VSI	10-Sa	11-ASI	12-HI	17-SaC	18-SaCM	20-ASA40	21-INp	36-Sa, R(T1,T2)	37-Sa, Np	38-Sa, SdN	39-Sa, Sa/DSI
TD	PGA	insuff	-	-	-	-	insuff	-	-	-	-	-	-	-	-	-
TD	PGV	insuff	-	-	-	insuff	insuff	-	-	-	-	-	-	-	insuff	-
TD	ASI*	insuff	-	-	insuff	-	insuff	insuff	-	-	-	-	-	-	-	-
TD	VSI	insuff	insuff	-	-	-	insuff	insuff	-	-	-	-	-	-	-	-
TD	Sa	insuff	-	-	-	-	insuff	-	-	-	-	-	-	-	-	-
MIDR	PGA	insuff	-	-	-	-	insuff	-	-	-	-	-	-	-	-	-
MIDR	PGV	insuff	-	-	-	insuff	insuff	insuff	-	-	-	-	-	-	-	-
MIDR	ASI*	insuff	insuff	-	-	-	insuff	insuff	-	-	-	-	-	-	-	-
MIDR	VSI	insuff	-	-	insuff	-	insuff	insuff	-	-	-	-	-	-	-	-
MIDR	Sa	insuff	-	-	-	-	insuff	-	-	-	-	-	-	-	-	-
BS	PGA	insuff	-	-	insuff	insuff	insuff	insuff	-	-	-	-	-	-	-	-
BS	PGV	insuff	-	-	-	-	insuff	-	-	-	-	-	insuff	insuff	-	-
BS	ASI*	insuff	-	-	-	-	insuff	-	-	-	-	insuff	-	-	-	-
BS	VSI	insuff	-	-	-	-	insuff	-	-	-	-	-	-	-	-	-
BS	Sa	insuff	-	-	-	-	insuff	-	-	-	-	-	-	-	-	-

F5S7B (0.66s) — Sufficiency (M_w)

EDP	DB IM	1-PGA	2-PGV	6-ASI*	7-VSI	10-Sa	11-ASI	12-HI	17-SaC	18-SaCM	20-ASA40	21-INp	36-Sa, R(T1,T2)	37-Sa, Np	38-Sa, SdN	39-Sa, Sa/DSI
TD	PGA	insuff	-	-	-	-	insuff	-	-	-	-	-	-	-	-	-
TD	PGV	insuff	-	-	-	-	insuff	-	-	-	-	-	-	-	-	-
TD	ASI*	insuff	-	-	-	-	insuff	-	-	-	-	insuff	-	-	-	-
TD	VSI	insuff	-	-	-	-	insuff	insuff	-	-	-	-	-	-	-	-
TD	Sa	insuff	-	-	-	-	insuff	-	-	-	-	-	-	-	-	-
MIDR	PGA	insuff	-	-	-	-	insuff	-	-	-	-	-	-	-	-	-
MIDR	PGV	insuff	-	-	-	-	insuff	-	-	-	-	-	-	-	-	-
MIDR	ASI*	insuff	-	-	-	-	insuff	-	-	-	-	insuff	-	-	-	-
MIDR	VSI	insuff	-	-	-	-	insuff	-	insuff	-	-	-	-	-	-	-
MIDR	Sa	insuff	-	-	-	-	insuff	insuff	-	-	-	-	-	-	-	-
BS	PGA	insuff	-	-	-	-	insuff	-	-	-	-	-	-	-	-	-
BS	PGV	insuff	-	-	-	-	insuff	-	-	-	-	-	-	-	-	-
BS	ASI*	insuff	-	-	-	-	insuff	-	-	-	-	-	-	-	-	-
BS	VSI	insuff	-	insuff	-	-	insuff	-	-	-	-	insuff	-	-	-	-
BS	Sa	insuff	-	-	-	-	insuff	-	-	-	-	-	-	-	-	-

365

Table A.10 Overall summary for M_w-based sufficiency checks (frames F5S2B and F5S4B)

F5S2B (0.75s)

EDP		DB IM	1-PGA	2-PGV	6-ASI*	7-VSI	10-Sa	11-ASI	12-HI	17-SaC	18-SaCM	20-ASA40	21-INp	36-Sa, R(T1,T2)	37-Sa, Np	38-Sa, SdN	39-Sa, Sa/DSI
TD		PGA	insuff	-	-	-	-	insuff	-	-	-	-	-	-	-	-	-
		PGV	insuff	-	-	-	-	insuff	-	-	-	-	-	-	-	-	-
		ASI*	insuff	-	-	-	-	insuff	-	-	-	-	-	-	-	-	-
		VSI	insuff	-	-	-	-	insuff	-	-	-	-	-	-	-	-	-
		Sa	insuff	-	-	-	-	insuff	-	-	-	-	-	-	-	-	-
MIDR		PGA	insuff	-	-	-	-	insuff	-	-	-	-	-	-	-	-	-
		PGV	insuff	-	-	-	-	insuff	-	-	-	-	-	-	-	-	-
		ASI*	insuff	-	-	-	-	insuff	-	-	-	-	-	-	-	-	-
		VSI	insuff	-	-	-	-	insuff	-	-	-	-	-	-	-	-	-
		Sa	insuff	-	-	-	-	-	-	-	-	-	-	-	-	-	-
BS		PGA	insuff	-	-	-	-	insuff	-	-	-	-	-	-	-	-	-
		PGV	insuff	-	insuff	-	insuff	insuff	-	insuff	insuff	-	insuff	-	insuff	insuff	-
		ASI*	insuff	-	-	-	-	insuff	-	-	-	-	-	-	insuff	-	-
		VSI	insuff	-	insuff	insuff	insuff	insuff	-	insuff	insuff	insuff	insuff	-	-	-	-
		Sa	insuff	-	-	-	-	insuff	-	-	-	-	-	-	-	-	-

F5S4B (0.95s)

EDP		DB IM	1-PGA	2-PGV	6-ASI*	7-VSI	10-Sa	11-ASI	12-HI	17-SaC	18-SaCM	20-ASA40	21-INp	36-Sa, R(T1,T2)	37-Sa, Np	38-Sa, SdN	39-Sa, Sa/DSI
TD		PGA	insuff	-	insuff	insuff	-	insuff	-	-	-	-	-	-	-	-	-
		PGV	insuff	-	insuff	insuff	-	insuff	-	-	-	-	-	-	-	-	-
		ASI*	insuff	-	insuff	-	-	insuff	-	-	-	-	-	-	-	-	-
		VSI	insuff	-	insuff	-	-	insuff	-	-	-	-	-	-	-	-	-
		Sa	insuff	-	-	-	-	insuff	-	-	-	-	-	-	-	-	-
MIDR		PGA	insuff	-	insuff	insuff	-	insuff	-	-	-	-	-	-	-	-	-
		PGV	insuff	-	insuff	insuff	-	insuff	-	-	-	-	-	-	-	-	-
		ASI*	insuff	-	insuff	-	-	insuff	-	-	-	-	-	-	-	-	-
		VSI	insuff	-	insuff	-	-	insuff	-	-	-	-	-	-	-	-	-
		Sa	insuff	-	-	-	-	insuff	-	-	-	-	-	-	-	-	-
BS		PGA	insuff	-	insuff	insuff	-	insuff	-	-	-	-	-	-	-	-	-
		PGV	insuff	-	insuff	insuff	-	insuff	-	-	-	-	-	-	-	-	-
		ASI*	insuff	-	insuff	-	-	insuff	-	-	-	-	-	-	-	-	-
		VSI	insuff	-	insuff	-	-	insuff	-	-	-	-	-	-	-	-	-
		Sa	insuff	-	-	-	-	insuff	-	-	-	-	-	-	-	-	-

366

Table A.11 Overall summary for M_w-based sufficiency checks (frame F8S3B)

EDP	F8S3B (1.20s) DB IM	1-PGA	2-PGV	6-ASI*	7-VSI	10-Sa	11-ASI	12-HI	17-SaC	18-SaCM	20-ASA40	21-INp	36-Sa, R(T1,T2)	37-Sa, Np	38-Sa, SdN	Sufficiency (Mw) 39-Sa, Sa/DSI
TD	PGA	insuff	insuff	-	insuff	-	insuff	-	insuff	-	-	-	-	-	-	-
	PGV	insuff	-	-	-	-	insuff	-	-	-	-	-	-	-	-	-
	ASI*	insuff	insuff	insuff	insuff	-	insuff	insuff	-	-	-	-	-	-	-	-
	VSI	insuff	-	insuff	insuff	insuff	insuff	insuff	-	insuff	-	insuff	-	-	-	-
	Sa	insuff	-	insuff	insuff	-	insuff	insuff	-	-	-	-	-	-	-	-
EDP	**DB IM**	1-PGA	2-PGV	6-ASI*	7-VSI	10-Sa	11-ASI	12-HI	17-SaC	18-SaCM	20-ASA40	21-INp	36-Sa, R(T1,T2)	37-Sa, Np	38-Sa, SdN	39-Sa, Sa/DSI
MIDR	PGA	insuff	-	-	-	insuff	insuff	insuff	insuff	insuff	-	insuff	-	-	-	-
	PGV	insuff	-	insuff	-	-	insuff	-	-	insuff	insuff	insuff	-	-	insuff	-
	ASI*	insuff	-	insuff	insuff	-	insuff	-	-	-	-	-	-	-	-	-
	VSI	insuff	-	insuff	insuff	-	insuff	-	-	-	-	-	-	-	-	-
	Sa	insuff	-	insuff	insuff	-	insuff	insuff	-	-	-	-	-	-	-	-
EDP	**DB IM**	1-PGA	2-PGV	6-ASI*	7-VSI	10-Sa	11-ASI	12-HI	17-SaC	18-SaCM	20-ASA40	21-INp	36-Sa, R(T1,T2)	37-Sa, Np	38-Sa, SdN	39-Sa, Sa/DSI
BS	PGA	insuff	-	insuff	-	-	insuff	-	-	-	-	-	-	-	-	-
	PGV	insuff	-	insuff	-	-	insuff	-	-	-	-	-	-	-	-	-
	ASI*	insuff	-	insuff	insuff	-	insuff	-	-	-	-	-	-	-	-	-
	VSI	insuff	-	insuff	-	-	insuff	-	-	-	-	-	-	-	-	-
	Sa	insuff	-	-	-	-	insuff	-	-	-	-	-	-	-	-	-

Table A.12 Overall summary for R_{JB}-based sufficiency checks (frames F2S2B2 and F3S2B)

F2S2B2 (0.30s)

EDP	DB IM	1-PGA	2-PGV	6-ASI*	7-VSI	10-Sa	11-ASI	12-HI	17-SaC	18-SaCM	20-ASA40	21-INp	36-Sa, R(T1,T2)	37-Sa, Np	38-Sa, SdN	39-Sa, Sa/DSI
TD	PGA	-	-	-	-	-	-	-	-	-	-	-	-	-	-	-
	PGV	-	-	-	-	-	-	-	-	-	-	-	-	-	-	-
	ASI*	-	-	-	-	-	-	-	-	-	-	-	-	-	-	-
	VSI	-	-	-	-	-	-	-	-	-	-	-	-	-	-	-
	Sa	-	-	-	-	-	-	-	-	-	-	-	-	-	-	-
MIDR	PGA	-	-	-	-	-	-	-	-	-	-	-	-	-	-	-
	PGV	-	-	-	-	-	-	-	-	-	-	-	-	-	-	-
	ASI*	-	-	-	-	-	-	-	-	-	-	-	-	-	-	-
	VSI	-	-	-	-	-	-	-	-	-	-	-	-	-	-	-
	Sa	-	-	-	-	-	-	-	-	-	-	-	-	-	-	-
BS	PGA	-	-	-	-	-	-	-	-	-	-	-	-	-	-	-
	PGV	-	-	-	-	-	-	-	-	-	-	-	-	-	-	-
	ASI*	-	-	-	-	-	-	-	-	-	-	-	-	-	-	-
	VSI	-	-	-	-	-	-	-	-	-	-	-	-	-	-	-
	Sa	-	-	-	-	-	-	-	-	-	-	-	-	-	-	-

F3S2B (0.45s)

EDP	DB IM	1-PGA	2-PGV	6-ASI*	7-VSI	10-Sa	11-ASI	12-HI	17-SaC	18-SaCM	20-ASA40	21-INp	36-Sa, R(T1,T2)	37-Sa, Np	38-Sa, SdN	39-Sa, Sa/DSI
TD	PGA	-	-	-	-	insuff	-	-	-	-	-	-	-	insuff	insuff	insuff
	PGV	-	-	-	-	-	-	-	-	-	-	-	-	-	-	-
	ASI*	-	-	-	-	-	-	-	-	-	-	-	-	insuff	insuff	-
	VSI	-	-	-	-	-	-	-	-	-	-	-	-	-	-	-
	Sa	-	-	-	-	-	-	-	-	-	-	-	-	-	-	-
MIDR	PGA	-	-	-	-	-	-	-	-	-	-	-	-	-	insuff	-
	PGV	-	-	-	-	-	-	-	-	-	-	-	-	-	-	-
	ASI*	-	-	-	-	-	-	-	-	-	-	-	-	-	-	-
	VSI	-	-	-	-	-	-	-	-	-	-	-	-	-	-	-
	Sa	-	-	-	-	-	-	-	-	-	-	-	-	-	insuff	-
BS	PGA	-	-	-	-	-	-	-	-	-	-	-	-	-	-	-
	PGV	-	-	insuff	-	-	-	-	insuff	-	-	-	-	-	-	-
	ASI*	-	-	insuff	-	-	-	-	-	-	-	-	-	-	-	-
	VSI	-	-	-	-	-	-	-	-	-	-	-	-	-	insuff	-
	Sa	-	-	-	-	-	-	-	-	-	-	-	-	-	-	-

Table A.13 Overall summary for R_{IB}-based sufficiency checks (frames F2S2B and F5S7B)

F2S2B (0.59s)

EDP		DB IM	1-PGA	2-PGV	6-ASI*	7-VSI	10-Sa	11-ASI	12-HI	17-SaC	18-SaCM	20-ASA40	21-INp	36-Sa, R(T1,T2)	37-Sa, Np	38-Sa, SdN	39-Sa, Sa/DSI
	TD	PGA	-	-	-	-	-	-	-	-	-	-	-	-	-	insuff	-
		PGV	-	-	-	-	-	-	-	-	-	-	-	-	-	-	-
		ASI*	-	-	-	-	-	-	-	-	-	-	-	-	-	-	-
		VSI	-	-	-	-	-	-	-	-	-	-	-	-	-	-	-
		Sa	-	-	-	-	-	-	-	-	-	-	-	-	-	-	-
EDP		DB IM	1-PGA	2-PGV	6-ASI*	7-VSI	10-Sa	11-ASI	12-HI	17-SaC	18-SaCM	20-ASA40	21-INp	36-Sa, R(T1,T2)	37-Sa, Np	38-Sa, SdN	39-Sa, Sa/DSI
	MIDR	PGA	-	-	-	-	-	-	-	-	-	-	-	-	-	-	-
		PGV	-	-	-	-	-	-	-	-	-	-	-	-	-	-	-
		ASI*	-	-	-	-	-	-	-	-	-	-	-	-	-	-	-
		VSI	-	-	-	-	-	-	-	-	-	-	-	-	-	-	-
		Sa	-	-	-	-	-	-	-	-	-	-	-	-	-	-	-
EDP		DB IM	1-PGA	2-PGV	6-ASI*	7-VSI	10-Sa	11-ASI	12-HI	17-SaC	18-SaCM	20-ASA40	21-INp	36-Sa, R(T1,T2)	37-Sa, Np	38-Sa, SdN	39-Sa, Sa/DSI
	BS	PGA	-	-	-	-	-	-	-	-	-	-	-	-	-	-	-
		PGV	-	-	-	-	-	-	insuff	-	-	-	-	-	-	-	-
		ASI*	-	-	insuff	insuff	-	-	-	-	-	-	-	-	-	-	-
		VSI	-	-	insuff	-	-	-	-	-	-	-	-	-	-	-	-
		Sa	-	-	insuff	-	insuff	-	-	-	insuff	insuff	insuff	insuff	insuff	-	insuff

F5S7B (0.66s)

EDP		DB IM	1-PGA	2-PGV	6-ASI*	7-VSI	10-Sa	11-ASI	12-HI	17-SaC	18-SaCM	20-ASA40	21-INp	36-Sa, R(T1,T2)	37-Sa, Np	38-Sa, SdN	39-Sa, Sa/DSI
	TD	PGA	-	-	-	-	-	-	-	-	-	-	-	-	-	-	-
		PGV	-	-	-	-	-	-	-	-	-	-	-	-	-	-	-
		ASI*	-	-	-	-	-	-	-	-	-	-	-	-	-	-	-
		VSI	-	-	-	-	-	-	-	-	-	-	-	-	-	-	-
		Sa	-	-	-	-	-	-	-	-	-	-	-	-	-	-	insuff
EDP		DB IM	1-PGA	2-PGV	6-ASI*	7-VSI	10-Sa	11-ASI	12-HI	17-SaC	18-SaCM	20-ASA40	21-INp	36-Sa, R(T1,T2)	37-Sa, Np	38-Sa, SdN	39-Sa, Sa/DSI
	MIDR	PGA	-	-	-	-	-	-	-	-	-	-	-	-	-	-	-
		PGV	-	-	-	-	-	-	-	-	-	-	-	-	-	-	-
		ASI*	-	-	-	-	-	-	-	-	-	-	-	-	-	-	-
		VSI	-	-	-	-	-	-	-	-	-	-	-	-	-	-	-
		Sa	-	-	-	-	-	-	-	-	-	-	-	-	-	-	-
EDP		DB IM	1-PGA	2-PGV	6-ASI*	7-VSI	10-Sa	11-ASI	12-HI	17-SaC	18-SaCM	20-ASA40	21-INp	36-Sa, R(T1,T2)	37-Sa, Np	38-Sa, SdN	39-Sa, Sa/DSI
	BS	PGA	-	-	-	-	-	-	-	-	-	-	-	-	-	-	-
		PGV	-	-	-	-	-	-	-	-	-	-	-	-	-	-	-
		ASI*	-	-	insuff	insuff	insuff	-	insuff	insuff	insuff	insuff	insuff	insuff	insuff	-	insuff
		VSI	-	-	insuff	insuff	-	-	insuff	insuff	insuff	insuff	insuff	insuff	-	-	insuff
		Sa	-	-	insuff	insuff	insuff	-	-	insuff	insuff	insuff	insuff	insuff	insuff	-	insuff

369

Table A.14 Overall summary for R_{JB}-based sufficiency checks (frames F5S2B and F5S4B)

F5S2B (0.75s) — Sufficiency (R_{jb})

EDP	DB IM	1-PGA	2-PGV	6-ASI*	7-VSI	10-Sa	11-ASI	12-HI	17-SaC	18-SaCM	20-ASA40	21-INp	36-Sa, R(T1,T2)	37-Sa, Np	38-Sa, SdN	39-Sa, Sa/DSI
TD	PGA	-	-	-	-	-	-	-	-	-	-	-	-	-	-	-
	PGV	-	-	-	-	-	-	-	-	-	-	-	-	-	-	-
	ASI*	-	-	-	-	-	-	-	-	-	-	-	-	-	-	-
	VSI	-	-	-	-	-	-	-	-	-	-	-	-	-	-	-
	Sa	-	-	insuff	-	-	-	-	-	insuff	-	-	-	-	-	-
MIDR	PGA	insuff	-	-	-	-	-	-	-	-	-	-	-	-	-	-
	PGV	-	insuff	-	-	-	-	-	-	-	-	-	-	-	-	-
	ASI*	-	-	-	-	-	-	-	-	-	-	-	-	-	-	-
	VSI	-	-	-	-	-	-	-	-	-	-	-	-	-	-	-
	Sa	-	-	-	-	-	-	-	-	-	-	-	-	-	-	-
BS	PGA	-	-	-	-	-	-	-	-	-	-	-	-	-	-	-
	PGV	-	-	-	-	-	-	-	-	-	-	-	-	-	-	-
	ASI*	-	-	insuff	insuff	insuff	-	insuff	insuff	insuff	insuff	insuff	insuff	insuff	-	-
	VSI	-	insuff	insuff	insuff	-	-	insuff	insuff	insuff	insuff	insuff	-	-	-	insuff
	Sa	insuff	insuff	insuff	insuff	-	insuff	insuff	insuff	insuff	insuff	insuff	-	-	-	-

F5S4B (0.95s) — Sufficiency (R_{jb})

EDP	DB IM	1-PGA	2-PGV	6-ASI*	7-VSI	10-Sa	11-ASI	12-HI	17-SaC	18-SaCM	20-ASA40	21-INp	36-Sa, R(T1,T2)	37-Sa, Np	38-Sa, SdN	39-Sa, Sa/DSI
TD	PGA	insuff	-	-	-	-	insuff	-	-	-	-	-	-	-	-	-
	PGV	-	-	-	-	-	-	-	-	-	-	-	-	-	-	-
	ASI*	-	-	-	-	-	-	-	-	-	-	-	-	-	-	-
	VSI	-	-	-	-	-	-	-	-	-	-	-	-	-	-	-
	Sa	-	-	insuff	insuff	-	insuff	insuff	-	-	-	-	-	-	-	-
MIDR	PGA	insuff	-	-	-	-	insuff	-	-	-	-	-	-	-	-	-
	PGV	-	-	-	-	-	-	-	-	-	-	-	-	-	insuff	-
	ASI*	-	-	-	-	-	-	-	-	-	-	-	-	insuff	-	-
	VSI	-	-	-	-	-	-	-	-	-	-	-	-	-	-	-
	Sa	-	-	insuff	insuff	-	insuff	insuff	-	-	-	-	-	-	insuff	-
BS	PGA	-	-	-	-	-	-	-	-	-	-	-	-	-	-	-
	PGV	-	-	-	-	-	-	-	-	-	-	-	-	-	-	-
	ASI*	-	-	insuff	insuff	-	-	insuff	-	-	-	-	-	insuff	insuff	-
	VSI	-	insuff	insuff	insuff	-	-	insuff	insuff	insuff	insuff	-	-	-	-	-
	Sa	insuff	insuff	insuff	insuff	-	-	insuff	insuff	insuff	insuff	insuff	-	-	-	-

Table A.15 Overall summary for R_{JB}-based sufficiency checks (frame F8S3B)

F8S3B (1.20s)																Sufficiency (R_{jb})
EDP	DB IM	1-PGA	2-PGV	6-ASI*	7-VSI	10-Sa	11-ASI	12-HI	17-SaC	18-SaCM	20-ASA40	21-INp	36-Sa, R(T1,T2)	37-Sa, Np	38-Sa, SdN	39-Sa, Sa/DSI
TD	PGA	insuff	-	-	-	-	-	-	-	-	-	-	-	-	-	-
	PGV	-	-	-	-	-	-	-	-	-	-	-	-	-	-	-
	ASI*	-	-	-	-	-	-	-	-	-	-	-	-	-	-	-
	VSI	-	-	-	-	-	-	-	-	-	-	-	-	-	-	-
	Sa	-	-	-	-	-	-	-	-	-	-	-	-	-	-	-
EDP	DB IM	1-PGA	2-PGV	6-ASI*	7-VSI	10-Sa	11-ASI	12-HI	17-SaC	18-SaCM	20-ASA40	21-INp	36-Sa, R(T1,T2)	37-Sa, Np	38-Sa, SdN	39-Sa, Sa/DSI
MIDR	PGA	-	-	-	-	-	-	-	-	-	-	-	-	-	-	-
	PGV	-	-	-	-	-	-	-	-	-	-	-	-	-	-	-
	ASI*	-	-	-	-	-	-	-	-	-	-	-	-	-	-	-
	VSI	-	-	-	-	-	-	-	-	-	-	-	-	-	-	-
	Sa	-	-	-	-	-	-	-	-	-	-	-	-	-	-	-
EDP	DB IM	1-PGA	2-PGV	6-ASI*	7-VSI	10-Sa	11-ASI	12-HI	17-SaC	18-SaCM	20-ASA40	21-INp	36-Sa, R(T1,T2)	37-Sa, Np	38-Sa, SdN	39-Sa, Sa/DSI
BS	PGA	-	-	insuff	insuff	-	-	-	-	-	-	-	-	-	-	-
	PGV	-	-	-	-	-	-	-	-	-	-	-	-	-	-	-
	ASI*	-	insuff	insuff	insuff	-	-	insuff	-	-	-	-	-	-	-	-
	VSI	-	insuff	insuff	insuff	-	-	insuff	-	-	-	-	-	-	-	-
	Sa	-	-	-	-	-	-	-	-	-	-	-	-	-	-	-

371

F. Additional Fragility Charts (for Chapter 6)

(a) 3 bins – 7 records

(b) 3 bins – 11 records

(c) 3 bins – 20 records

(d) 3 bins – 30 records

IO (resample) — IO (mean) – – IO (± 1 sigma)
LS (resample) — LS (mean) – – LS (± 1 sigma)
CP (resample) — CP (mean) – – CP (± 1 sigma)
— Original curve – – – Regression Eqn. based curve
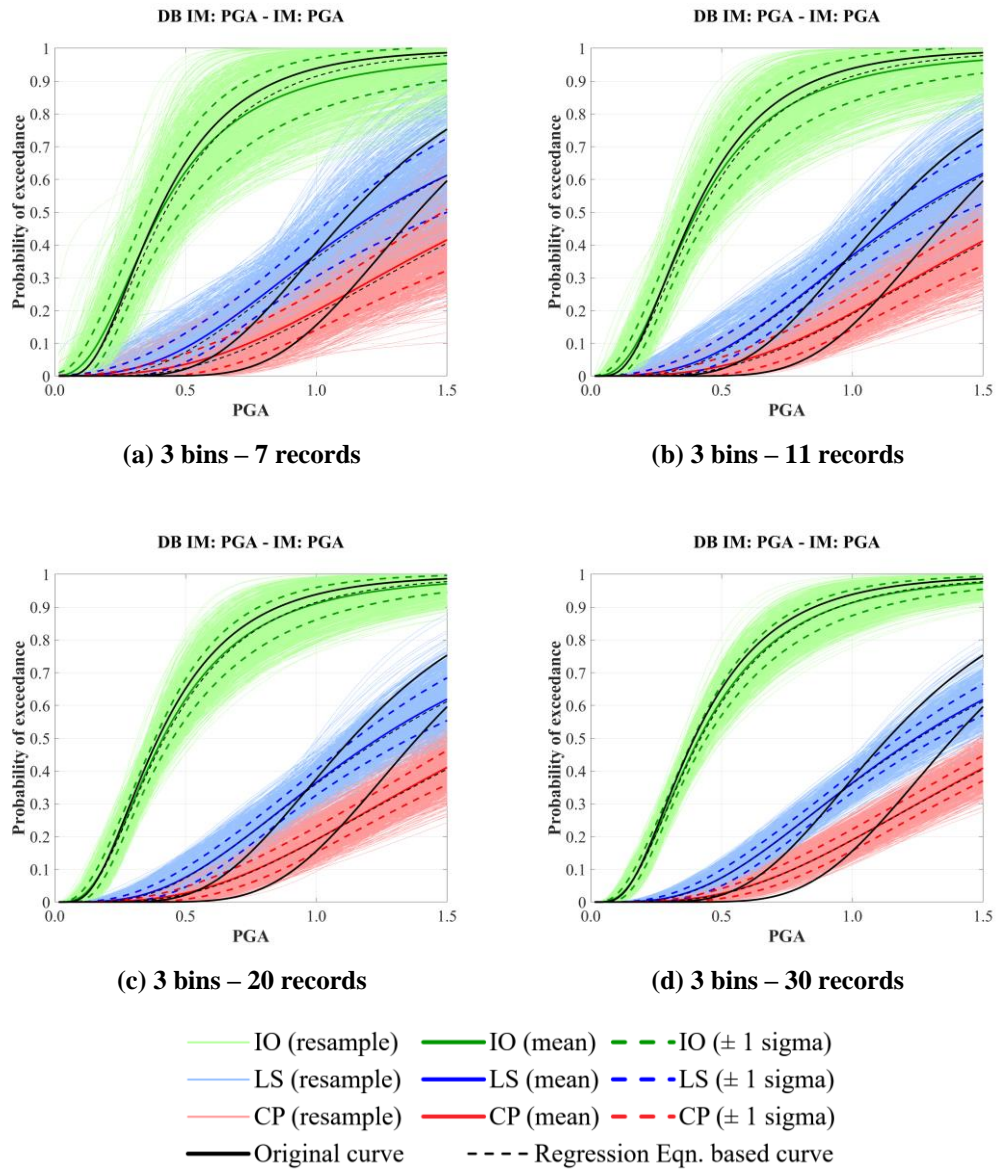
Figure A.152. PGA-based fragility curves for F3S2B (MIDR) under PGA-based set (3 bins considered)

(a) 5 bins – 7 records

**(b) 5 bins – 11 records**

(c) 5 bins – 20 records

(d) 5 bins – 30 records

IO (resample) ⎯⎯ IO (mean) – – – IO (± 1 sigma)

LS (resample) ⎯⎯ LS (mean) – – – LS (± 1 sigma)

CP (resample) ⎯⎯ CP (mean) – – – CP (± 1 sigma)

⎯⎯ Original curve – – – – Regression Eqn. based curve
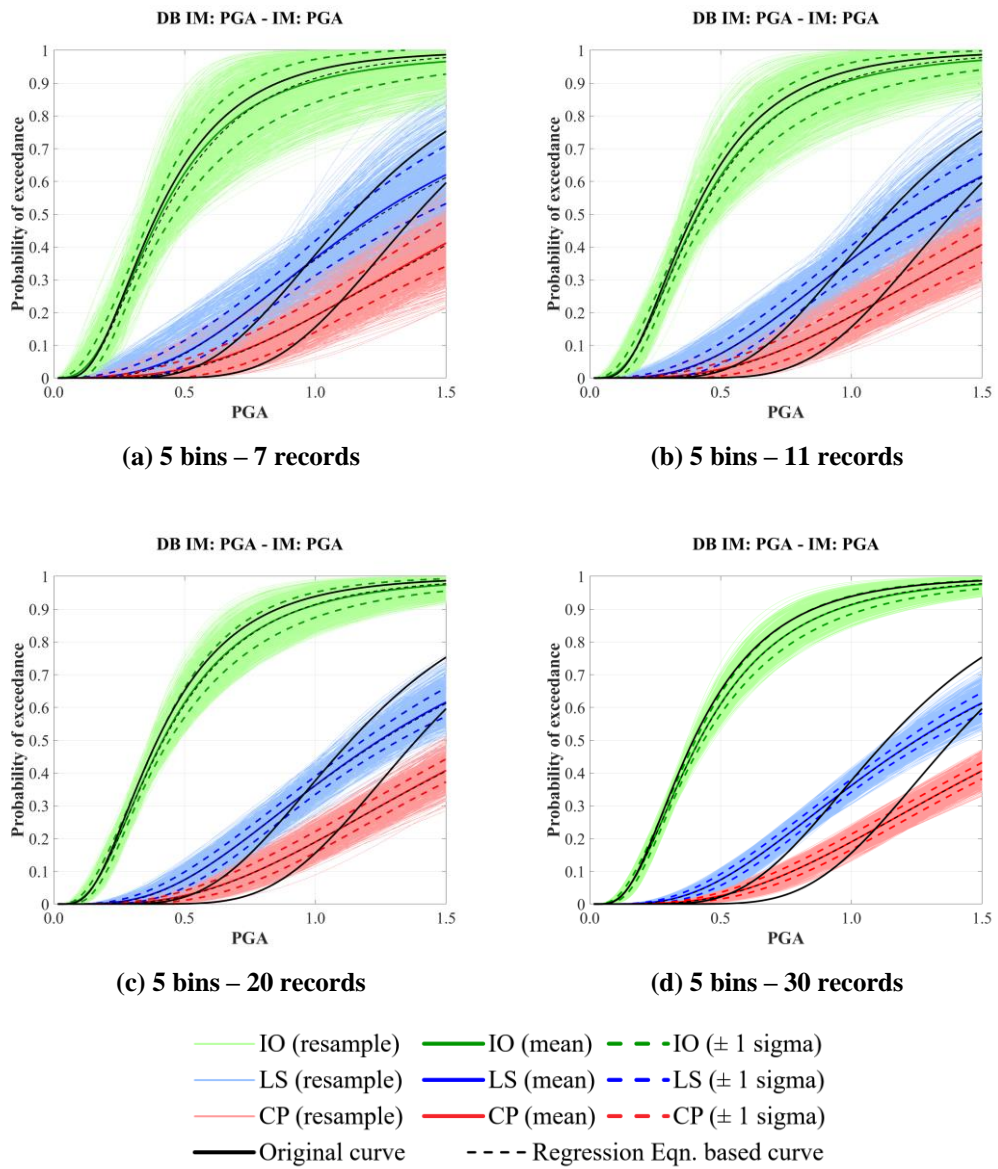
Figure A.153. PGA-based fragility curves for F3S2B (MIDR) under PGA-based set (5 bins considered)

(a) **8 bins – 7 records**

(b) **8 bins – 11 records**

(c) **8 bins – 20 records**

(d) **8 bins – 30 records**
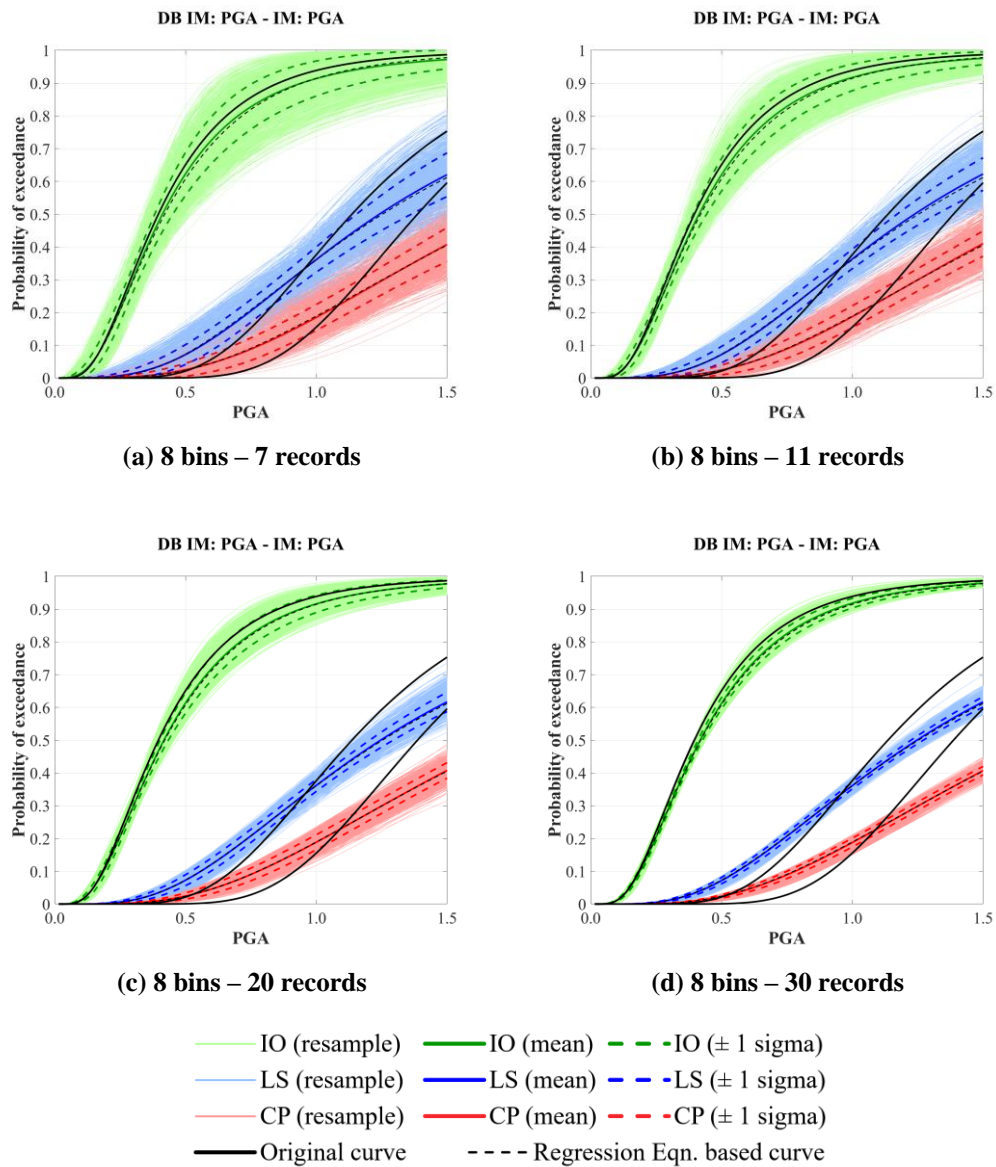
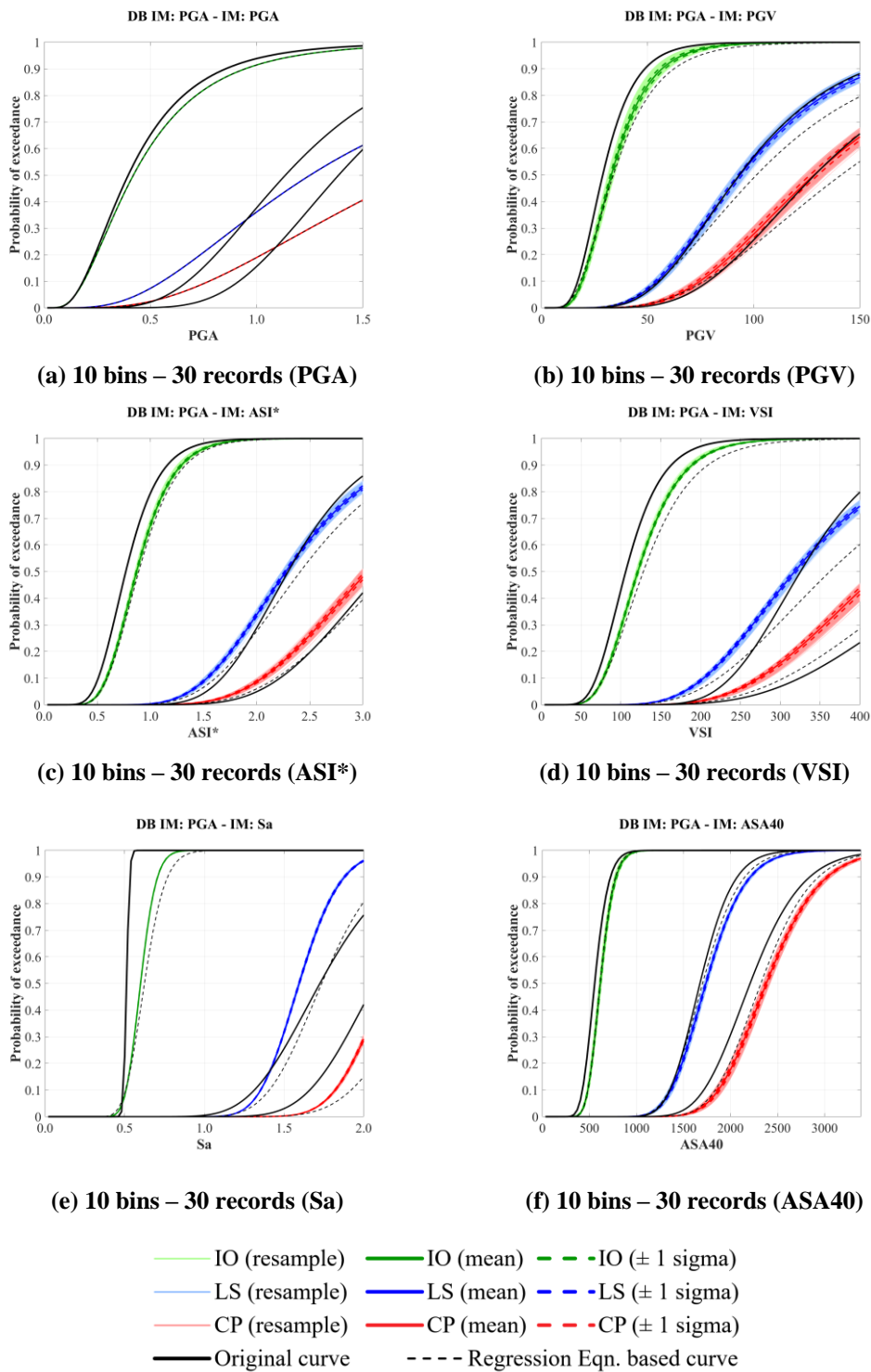Figure A.154. PGA-based fragility curves for F3S2B (MIDR) under PGA-based set (8 bins considered)

(a) 10 bins – 7 records

(b) 10 bins – 11 records

(c) 10 bins – 20 records

(d) 10 bins – 30 records
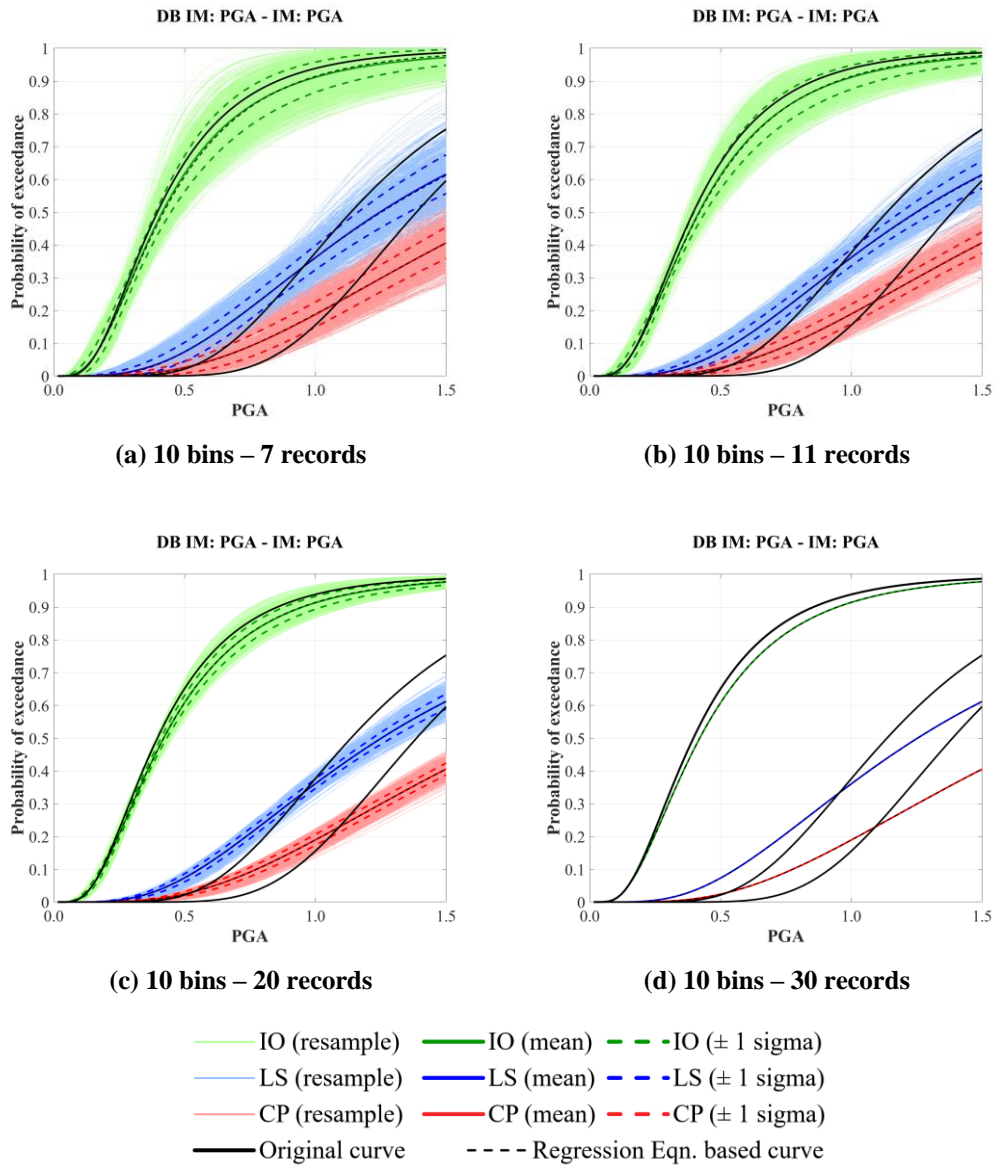
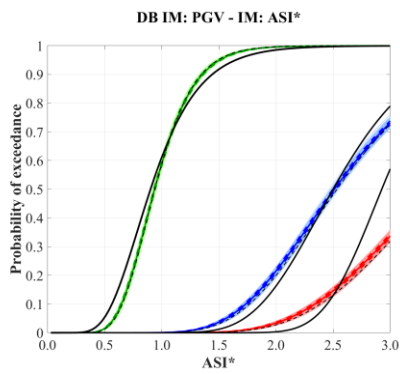Figure A.155. PGA-based fragility curves for F3S2B (MIDR) under PGA-based set (10 bins considered)

(a) 3 bins – 7 records

(b) 3 bins – 11 records

(c) 3 bins – 20 records

(d) 3 bins – 30 records
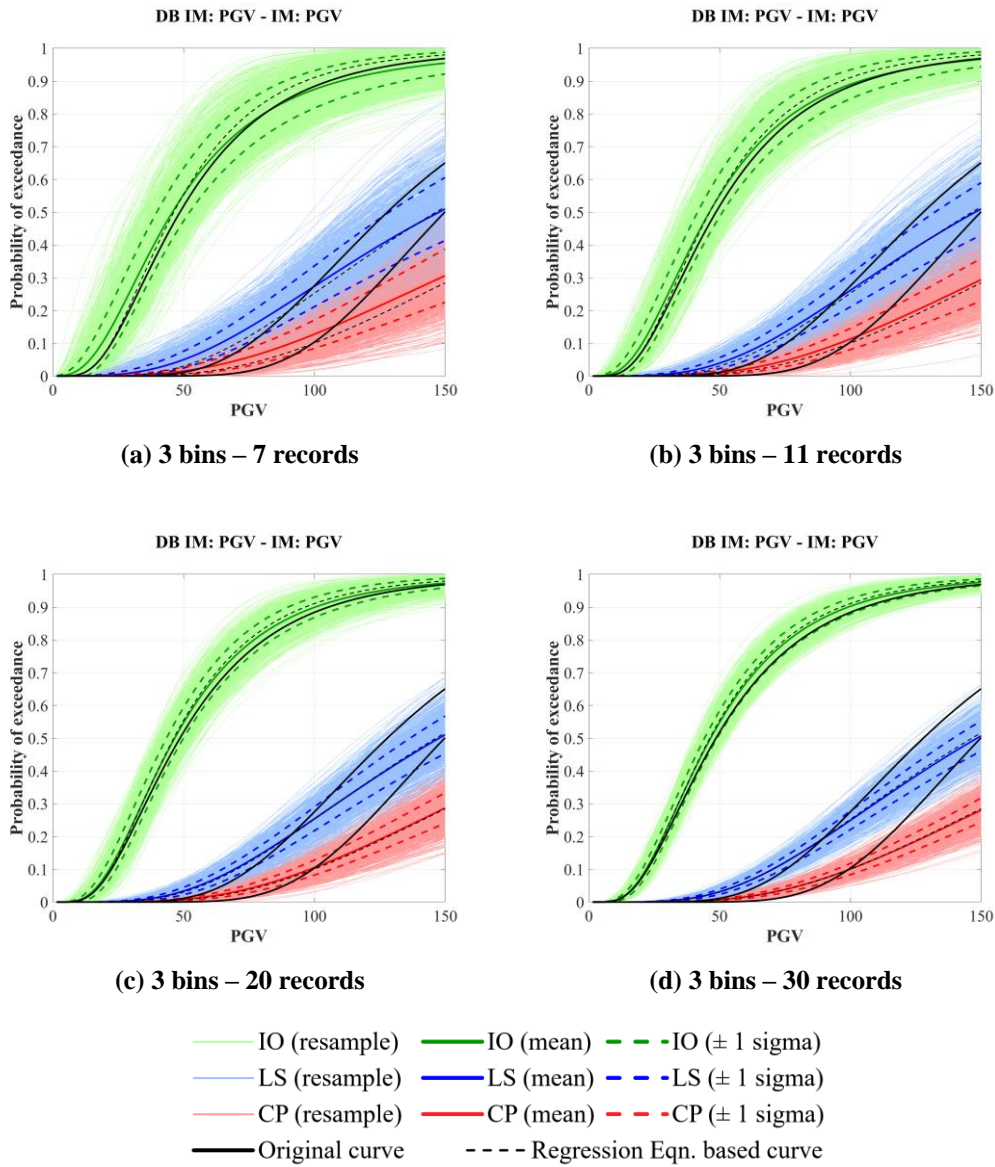
Figure A.156. PGV-based fragility curves for F3S2B (MIDR) under PGV-based set

(3 bins considered)

DB IM: PGV - IM: PGV

(a) 10 bins – 7 records

(b) 10 bins – 11 records

(c) 10 bins – 20 records

(d) 10 bins – 30 records

IO (resample) — IO (mean) — — IO (± 1 sigma)
LS (resample) — LS (mean) — — LS (± 1 sigma)
CP (resample) — CP (mean) — — CP (± 1 sigma)
— Original curve — — — Regression Eqn. based curve
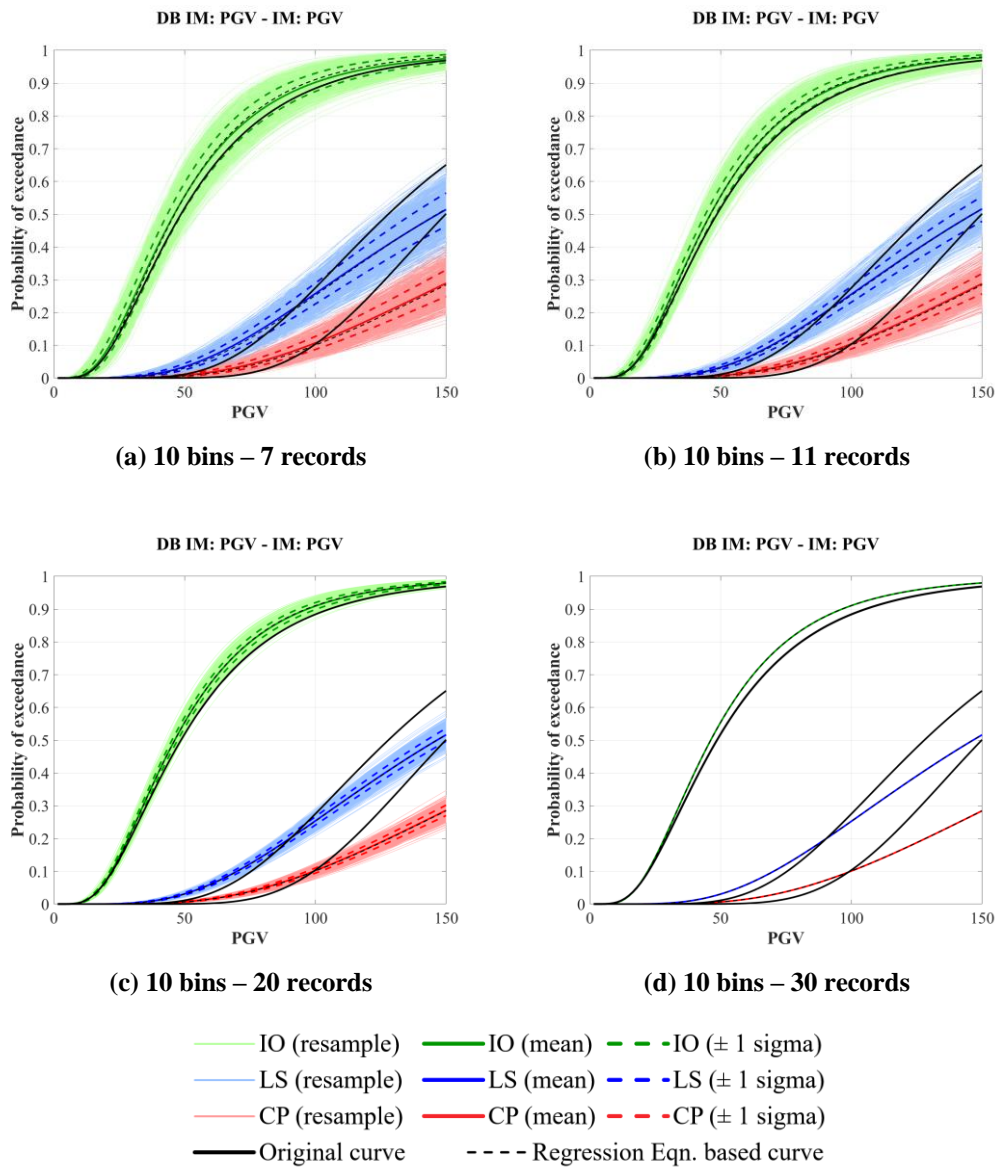
Figure A.157. PGV-based fragility curves for F3S2B (MIDR) under PGV-based set (10 bins considered)

(a) 3 bins – 7 records

(b) 3 bins – 11 records

(c) 3 bins – 20 records

(d) 3 bins – 30 records
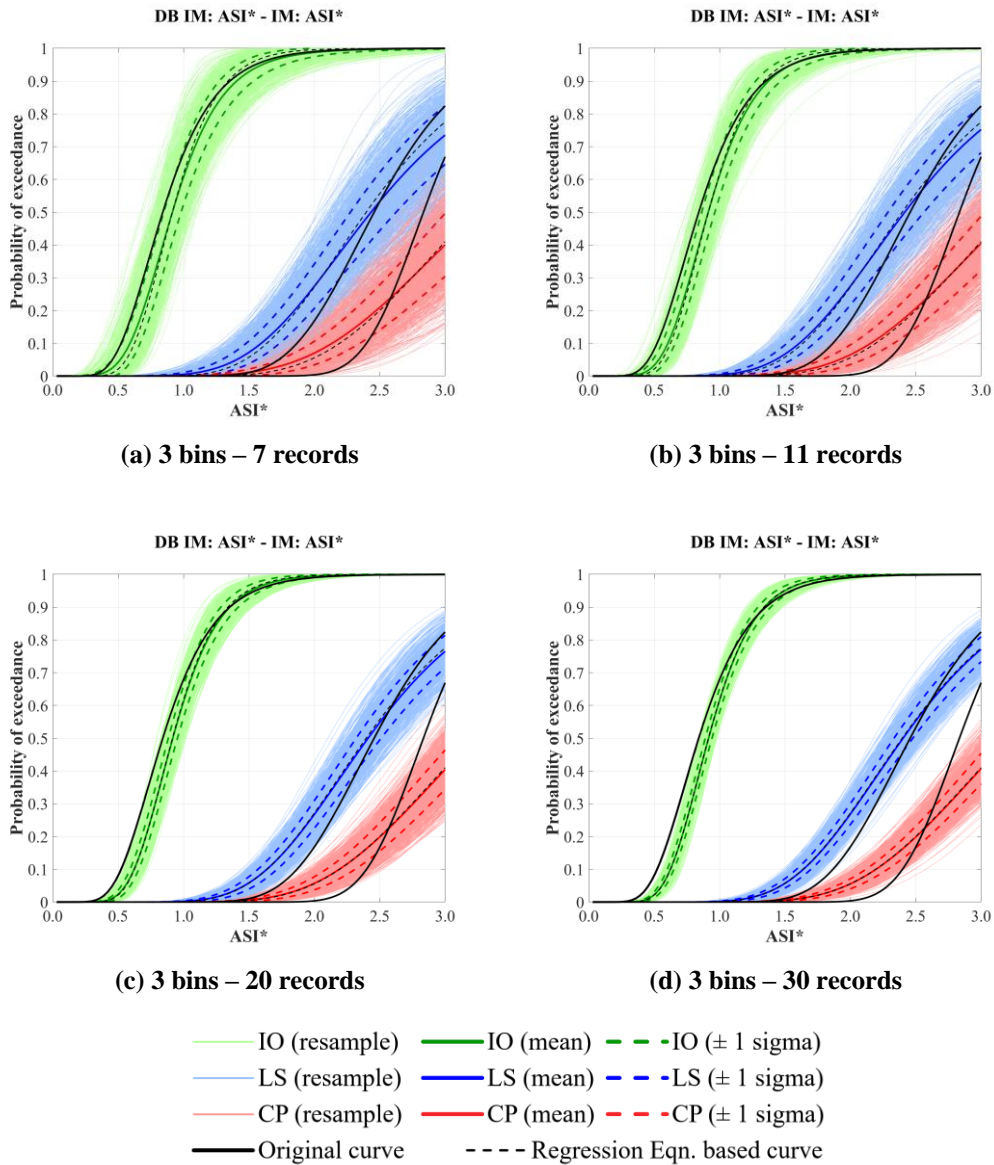
Figure A.158. ASI*-based fragility curves for F3S2B (MIDR) under ASI*-based set (3 bins considered)
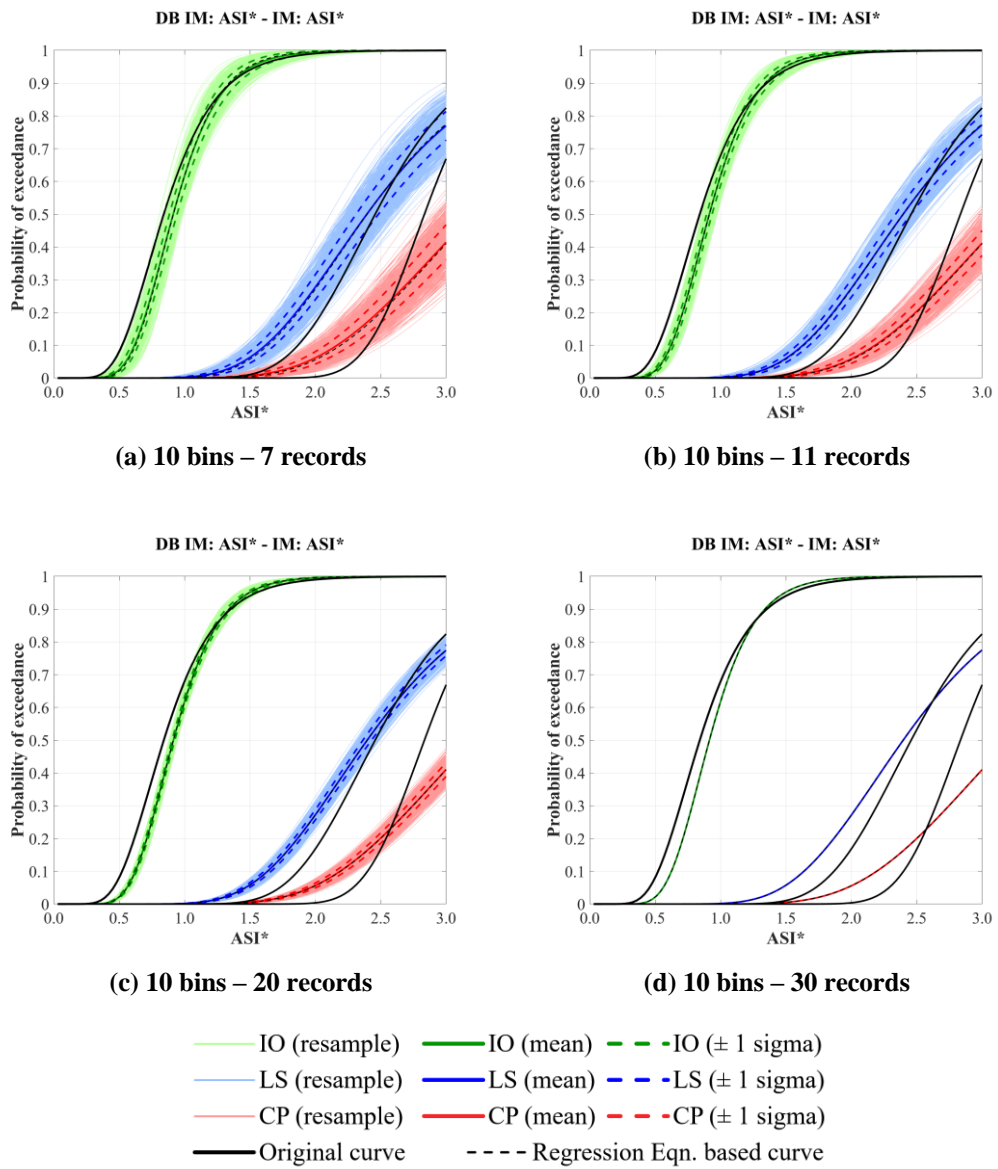
Figure A.159. ASI*-based fragility curves for F3S2B (MIDR) under ASI*-based set (10 bins considered)

(a) 3 bins – 7 records

(b) 3 bins – 11 records

(c) 3 bins – 20 records

(d) 3 bins – 30 records
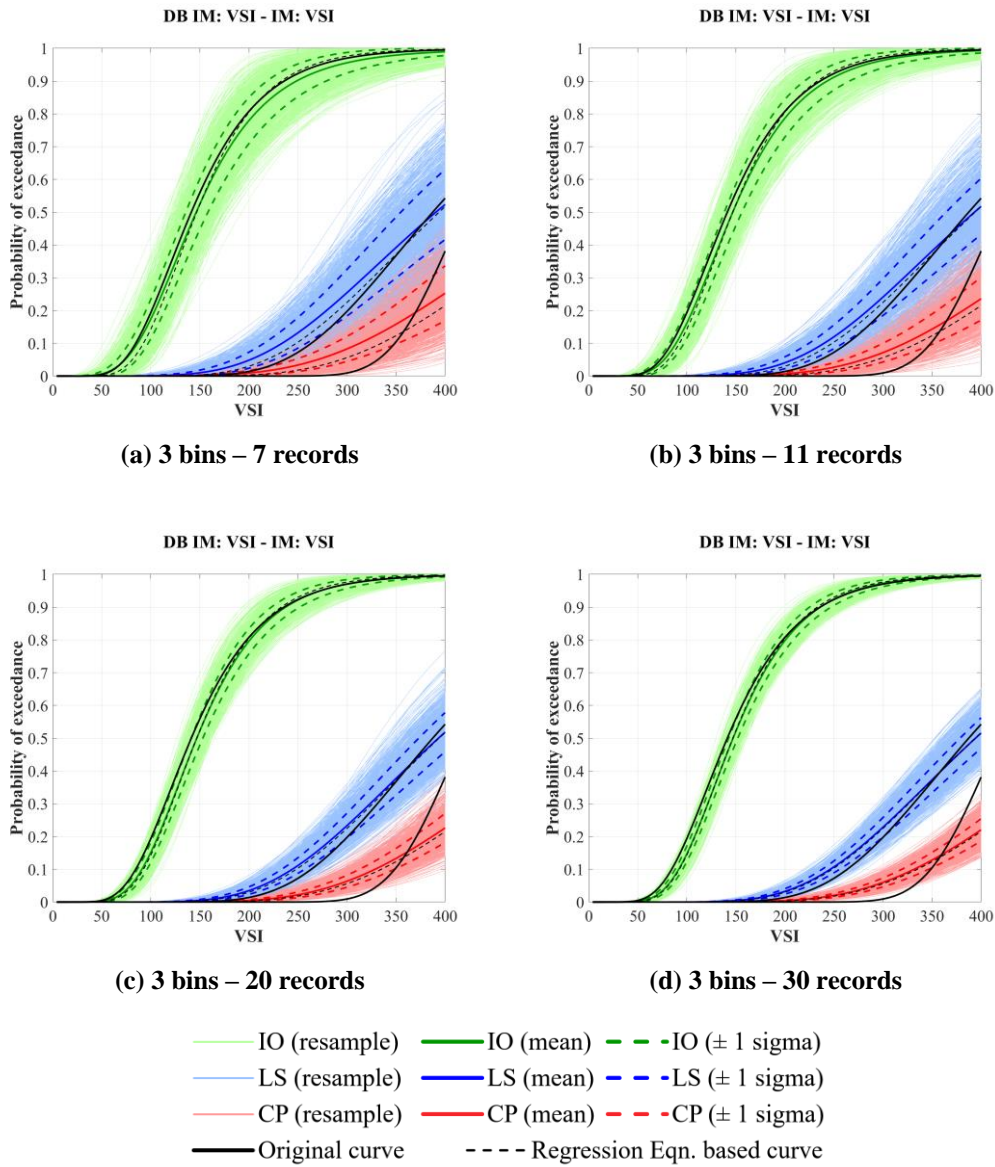
Figure A.160. VSI-based fragility curves for F3S2B (MIDR) under VSI-based set

(3 bins considered)

(a) 10 bins – 7 records

(b) 10 bins – 11 records

(c) 10 bins – 20 records

(d) 10 bins – 30 records
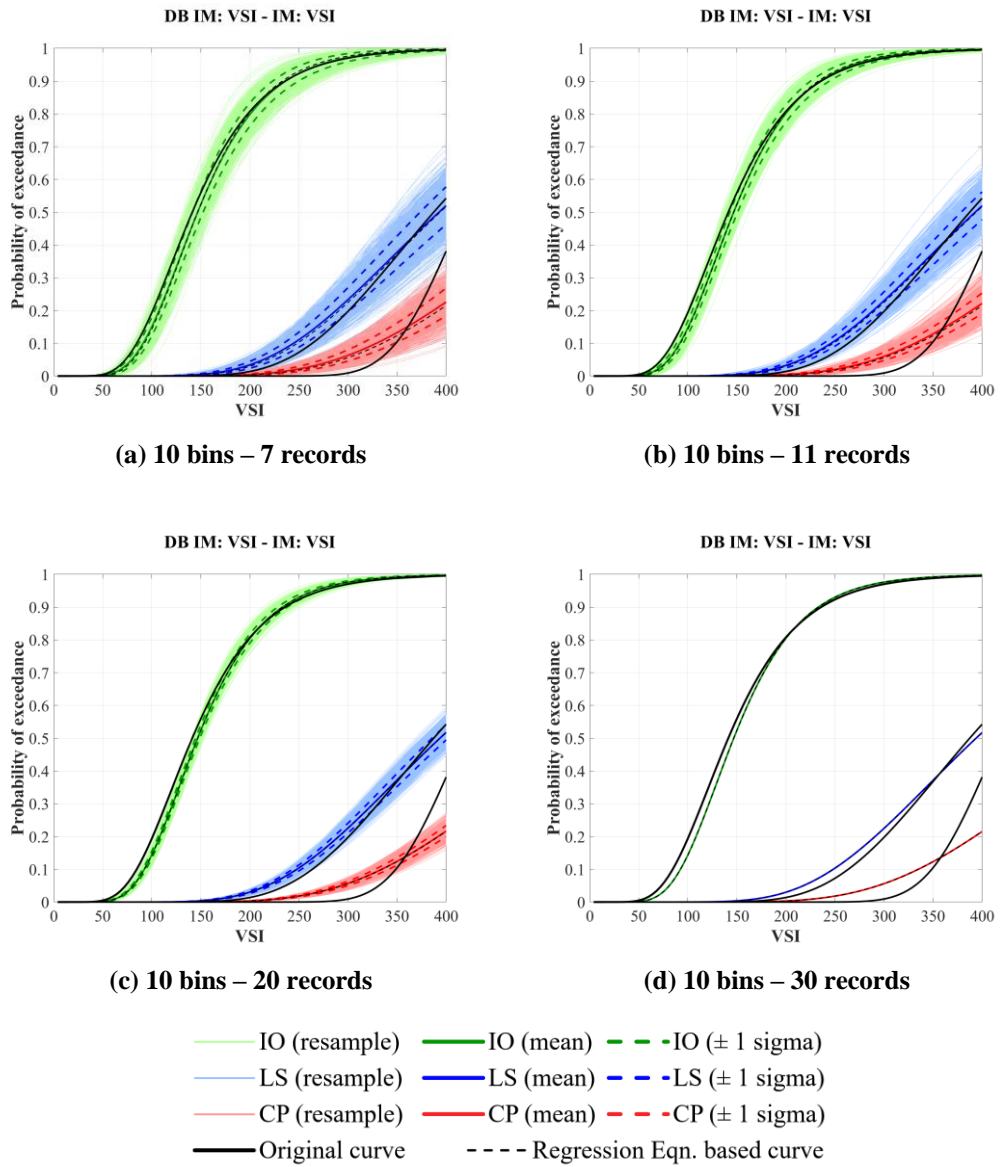
Figure A.161. VSI-based fragility curves for F3S2B (MIDR) under VSI-based set (10 bins considered)

(a) 3 bins – 7 records

(b) 3 bins – 11 records

(c) 3 bins – 20 records

(d) 3 bins – 30 records
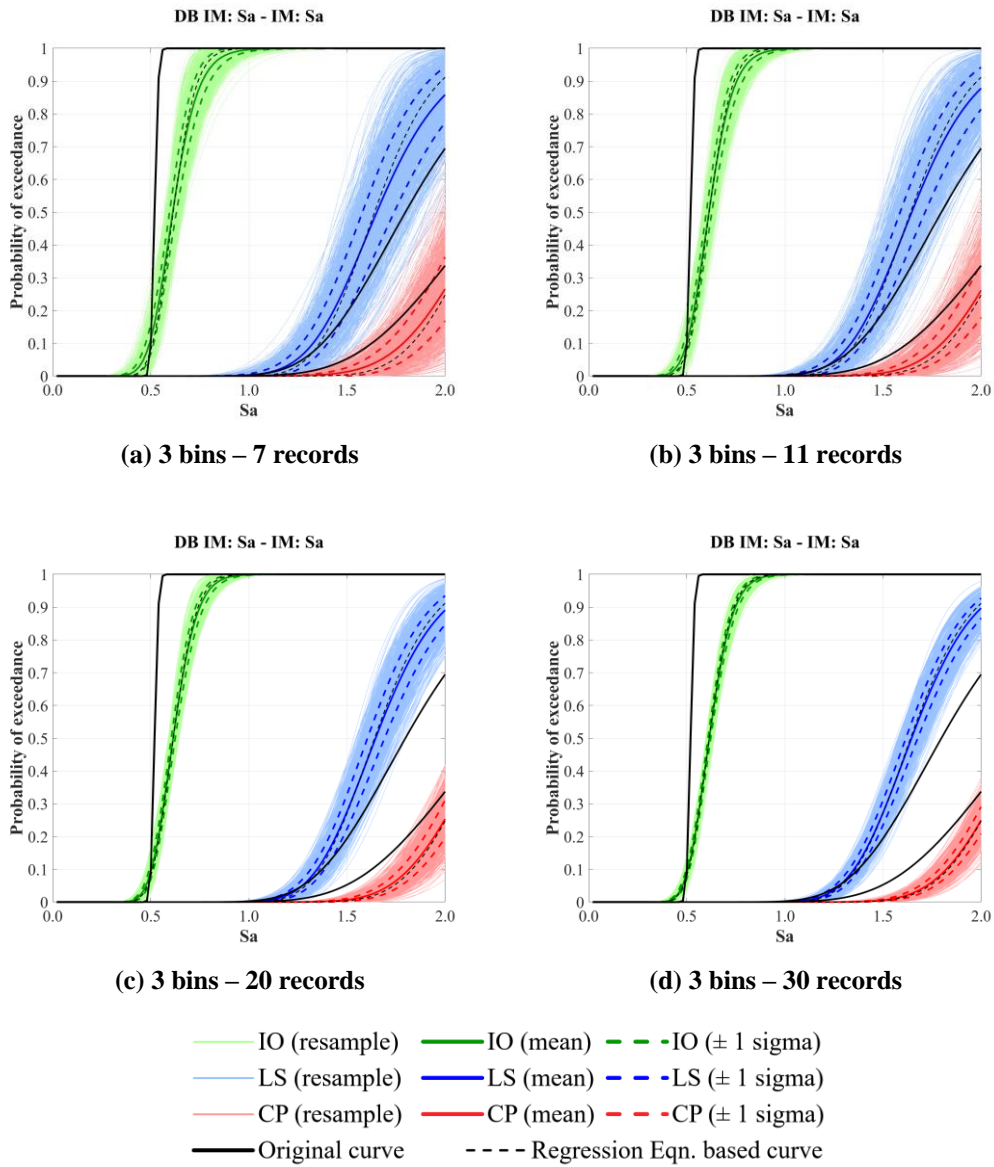
Figure A.162. S_a-based fragility curves for F3S2B (MIDR) under S_a-based set (3 bins considered)

(a) 10 bins – 7 records

(b) 10 bins – 11 records

(c) 10 bins – 20 records
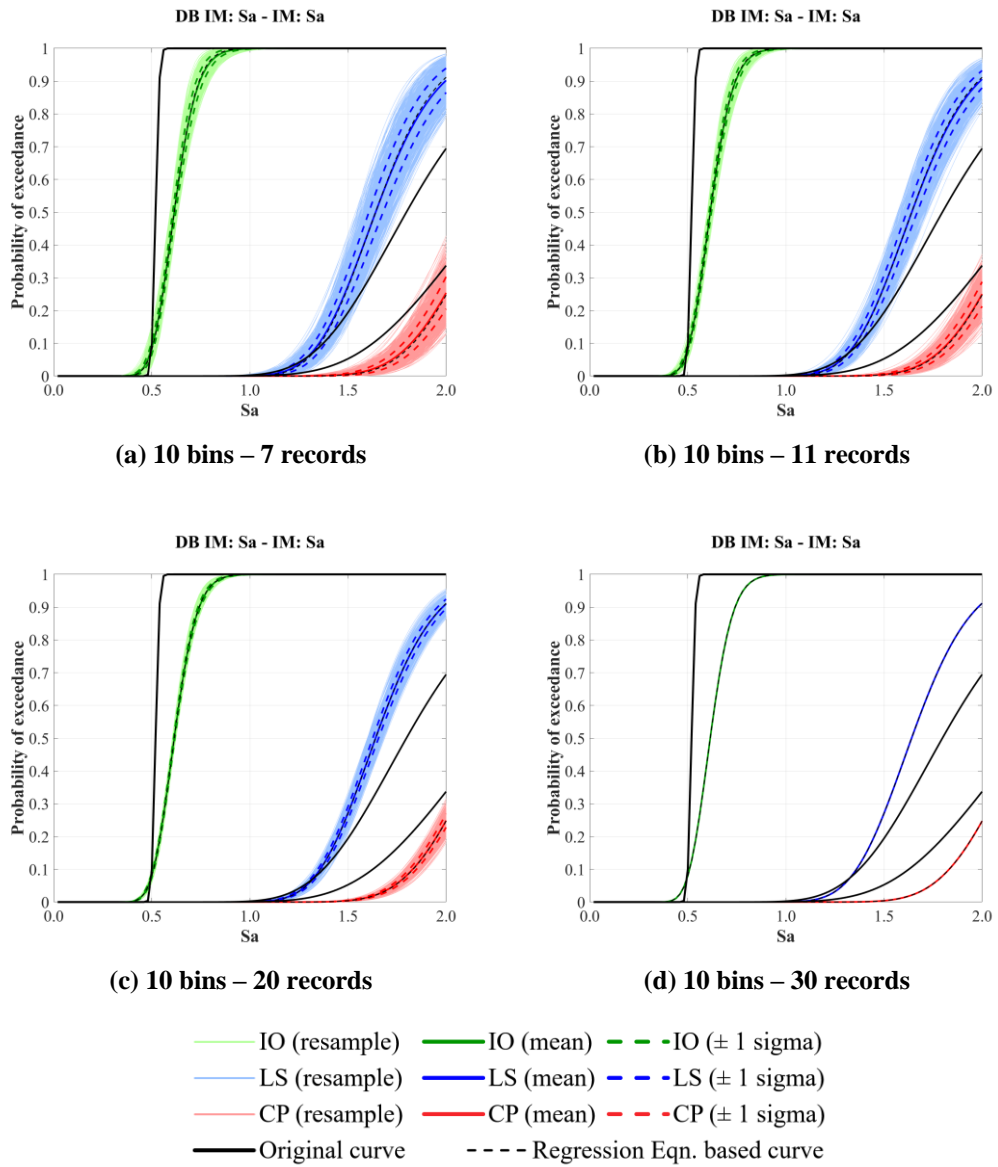
(d) 10 bins – 30 records

Figure A.163. S_a-based fragility curves for F3S2B (MIDR) under S_a-based set (10 bins considered)

(a) 10 bins – 30 records (PGA)

(b) 10 bins – 30 records (PGV)

(c) 10 bins – 30 records (ASI*)

(d) 10 bins – 30 records (VSI)

(e) 10 bins – 30 records (Sa)

(f) 10 bins – 30 records (ASA40)

Figure A.164. Alternative IM-based fragility curves for F3S2B (MIDR) under PGA-based set (10 bins – 30 records considered)

(a) 10 bins – 30 records (PGA)

(b) 10 bins – 30 records (PGV)

(c) 10 bins – 30 records (ASI*)

(d) 10 bins – 30 records (VSI)

(e) 10 bins – 30 records (Sa)

(f) 10 bins – 30 records (ASA40)

IO (resample)   IO (mean)   IO (± 1 sigma)
LS (resample)   LS (mean)   LS (± 1 sigma)
CP (resample)   CP (mean)   CP (± 1 sigma)
Original curve   Regression Eqn. based curve
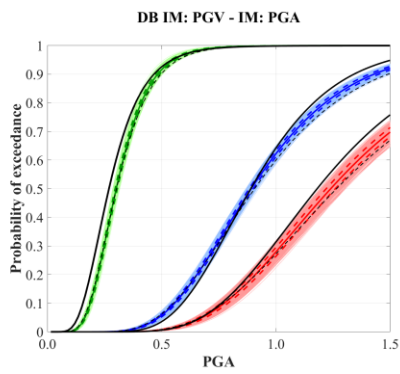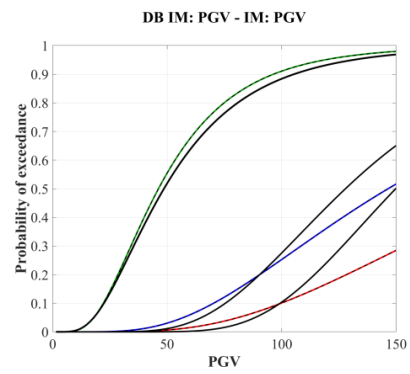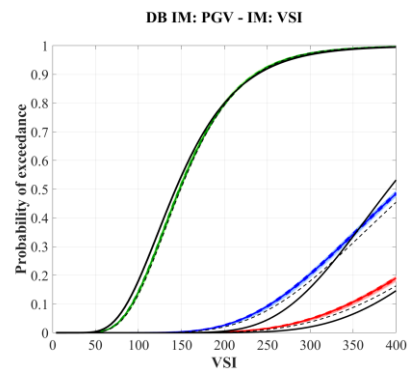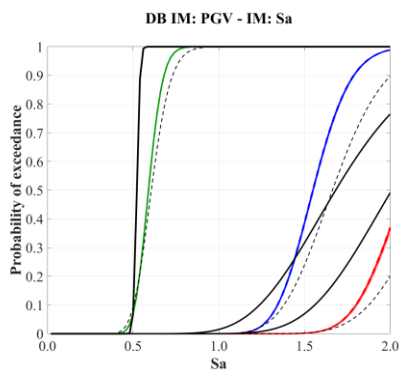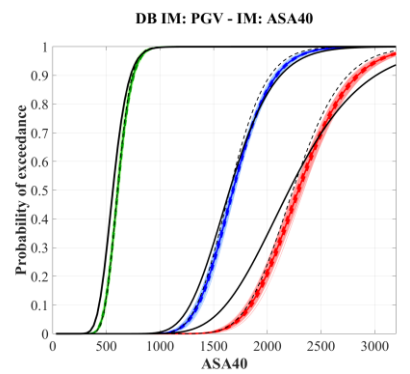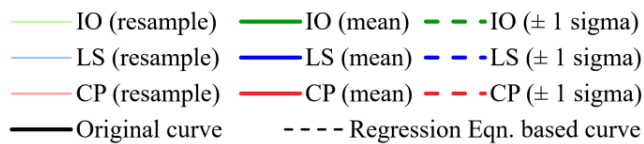
Figure A.165. Alternative IM-based fragility curves for F3S2B (MIDR) under PGV-based set (10 bins – 30 records considered)

DB IM: ASI* - IM: PGA

(a) 10 bins – 30 records (PGA)

DB IM: ASI* - IM: PGV

(b) 10 bins – 30 records (PGV)

DB IM: ASI* - IM: ASI*

(c) 10 bins – 30 records (ASI*)

DB IM: ASI* - IM: VSI

(d) 10 bins – 30 records (VSI)

DB IM: ASI* - IM: Sa

(e) 10 bins – 30 records (Sa)

DB IM: ASI* - IM: ASA40

(f) 10 bins – 30 records (ASA40)

IO (resample)   IO (mean)   IO (± 1 sigma)
LS (resample)   LS (mean)   LS (± 1 sigma)
CP (resample)   CP (mean)   CP (± 1 sigma)
Original curve   Regression Eqn. based curve
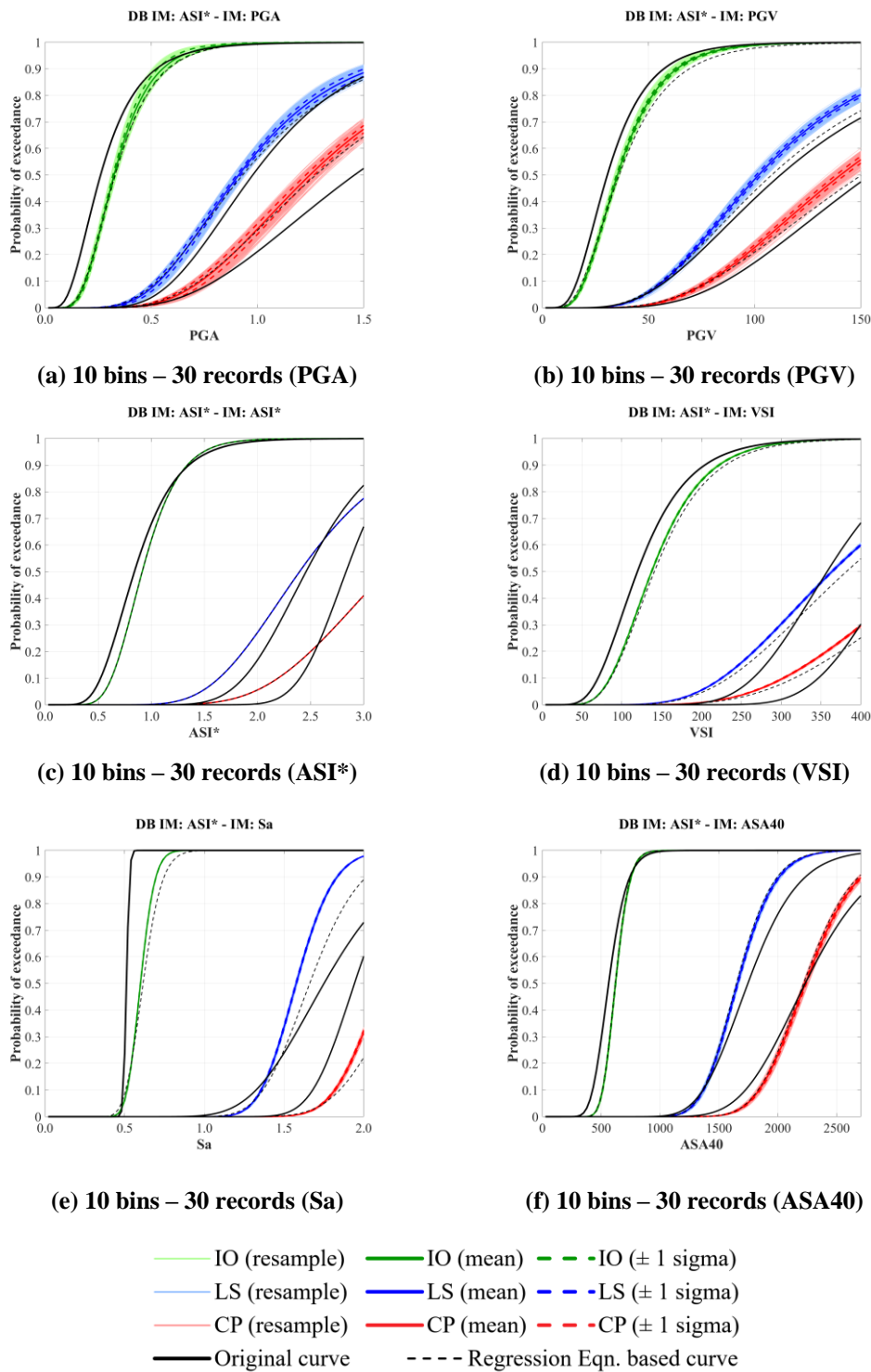
Figure A.166. Alternative IM-based fragility curves for F3S2B (MIDR) under ASI*-based set (10 bins – 30 records considered)

(a) 10 bins – 30 records (PGA)

(b) 10 bins – 30 records (PGV)

(c) 10 bins – 30 records (ASI*)

(d) 10 bins – 30 records (VSI)

(e) 10 bins – 30 records (Sa)

(f) 10 bins – 30 records (ASA40)
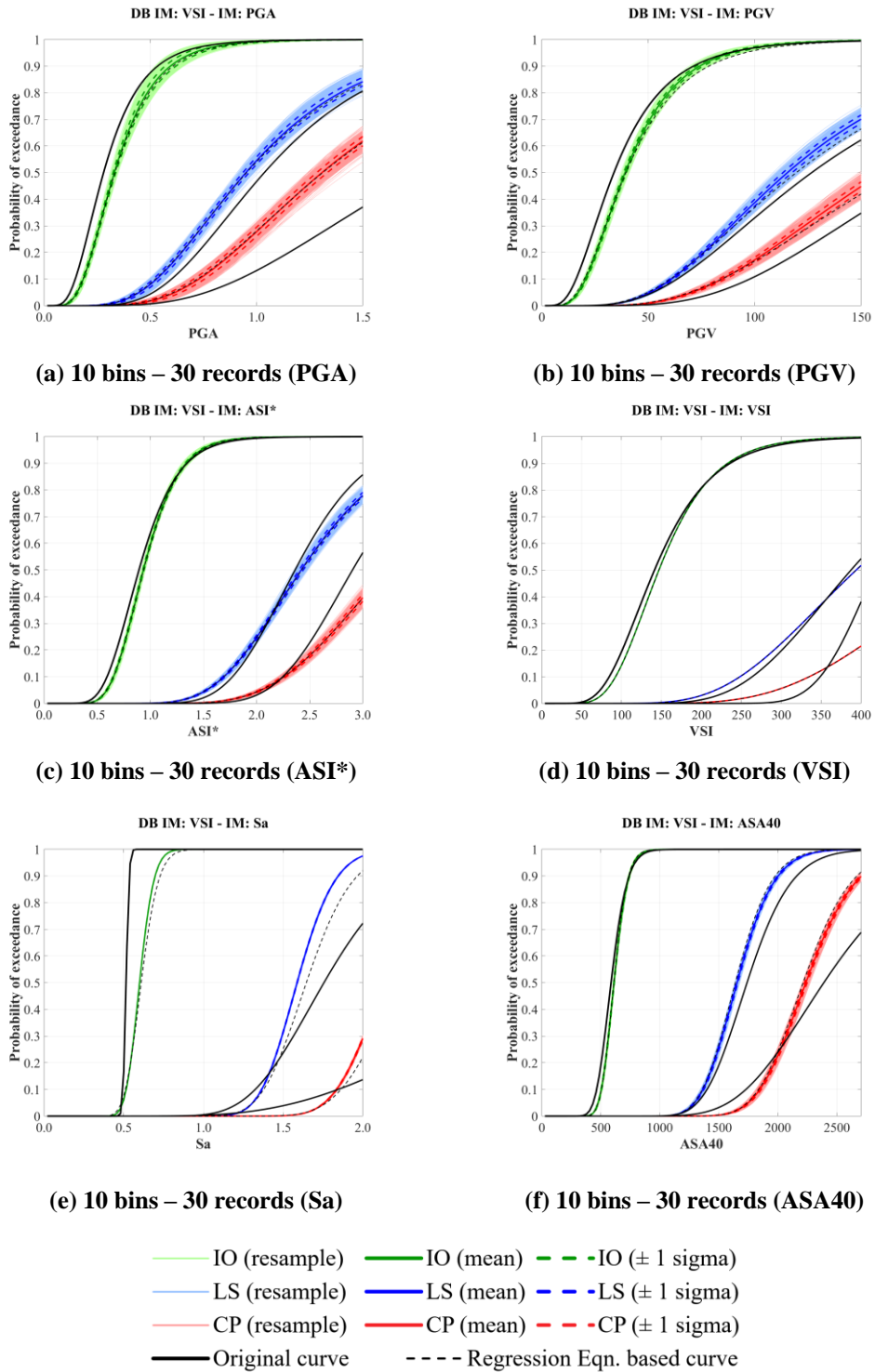
Figure A.167. Alternative IM-based fragility curves for F3S2B (MIDR) under VSI-based set (10 bins – 30 records considered)

(a) 10 bins – 30 records (PGA)

(b) 10 bins – 30 records (PGV)

(c) 10 bins – 30 records (ASI*)

(d) 10 bins – 30 records (VSI)

(e) 10 bins – 30 records (Sa)

(f) 10 bins – 30 records (ASA40)
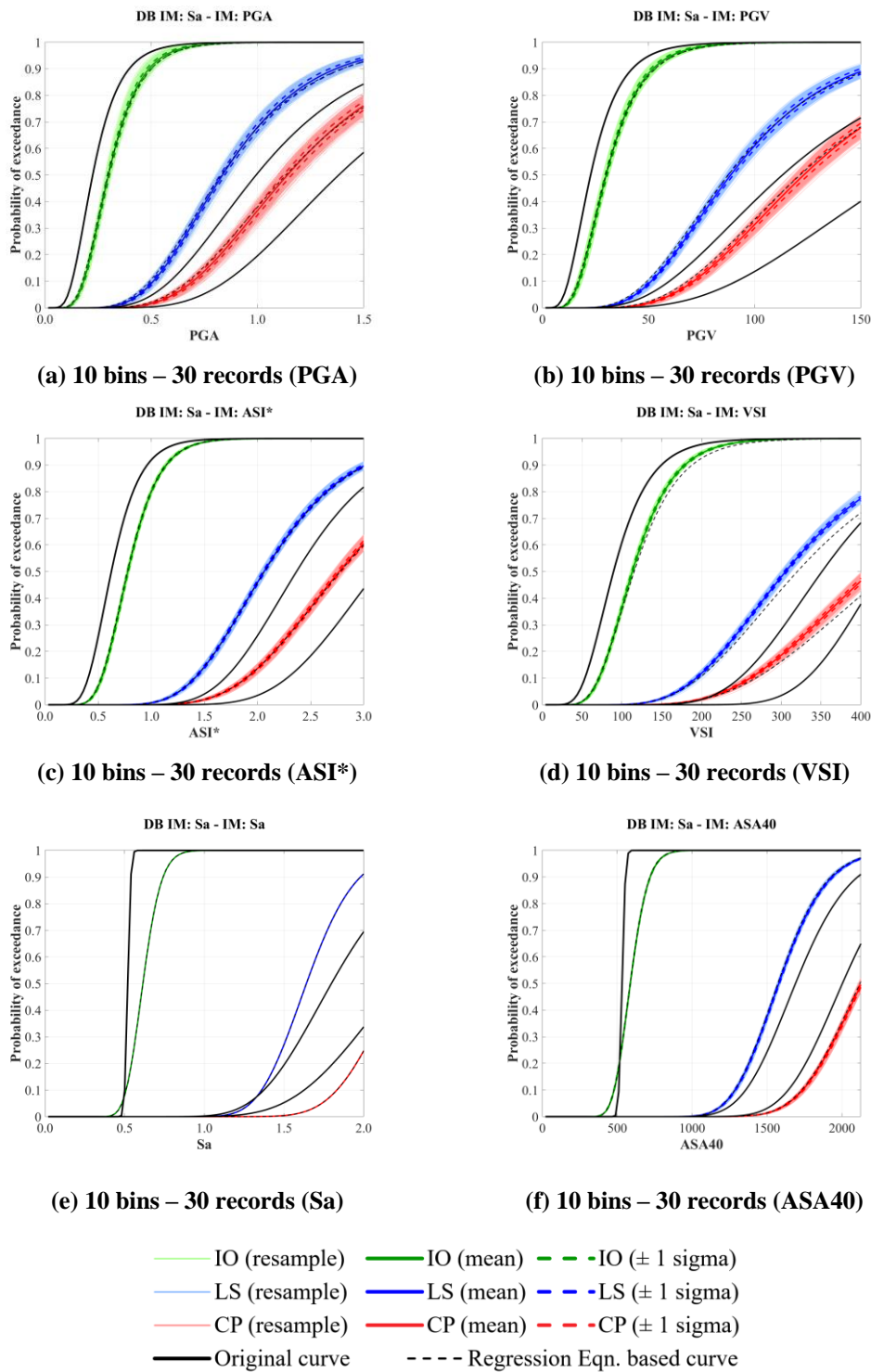
Figure A.168. Alternative IM-based fragility curves for F3S2B (MIDR) under S_a-based set (10 bins – 30 records considered)

(a) 3 bins – 7 records

(b) 3 bins – 11 records

(c) 3 bins – 20 records

(d) 3 bins – 30 records
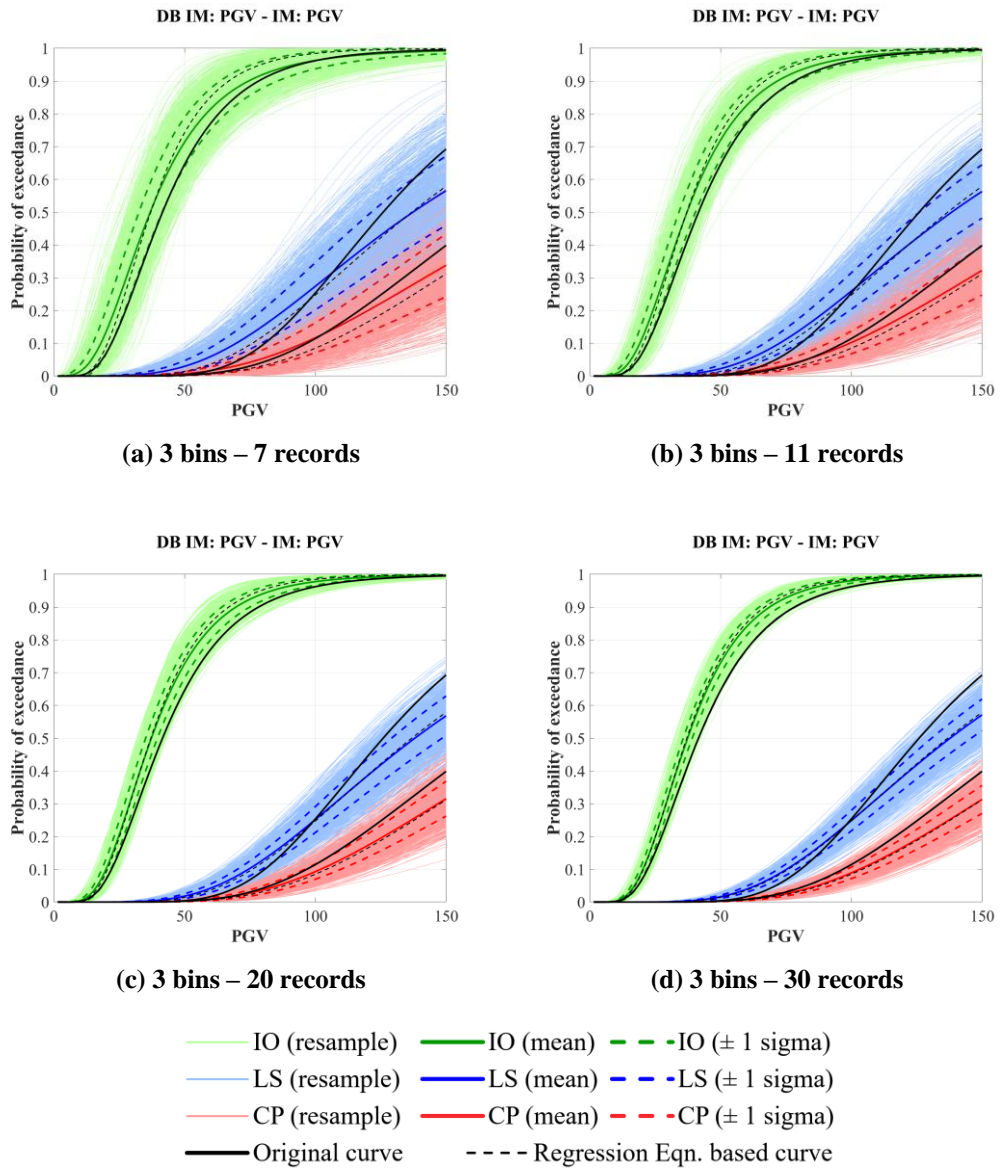
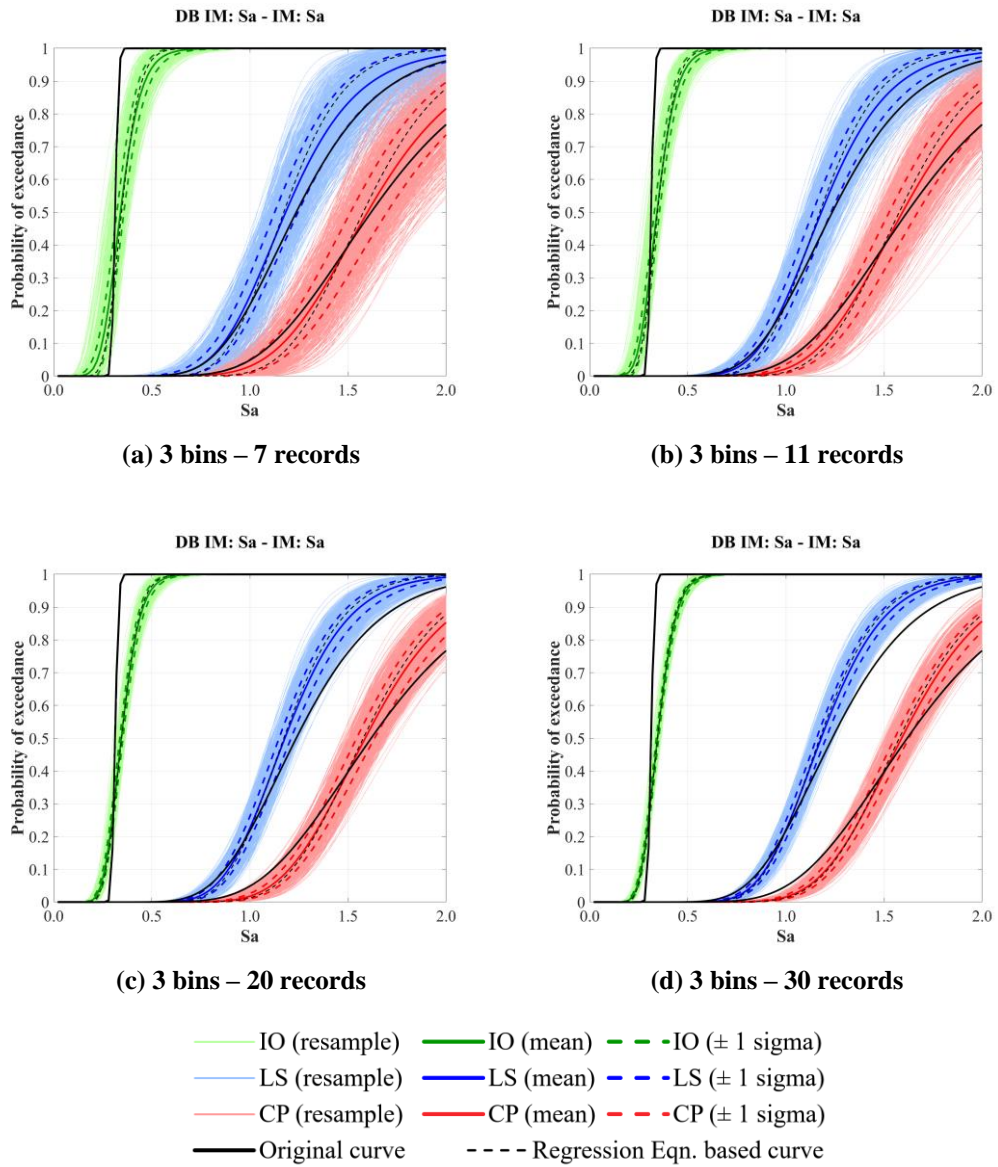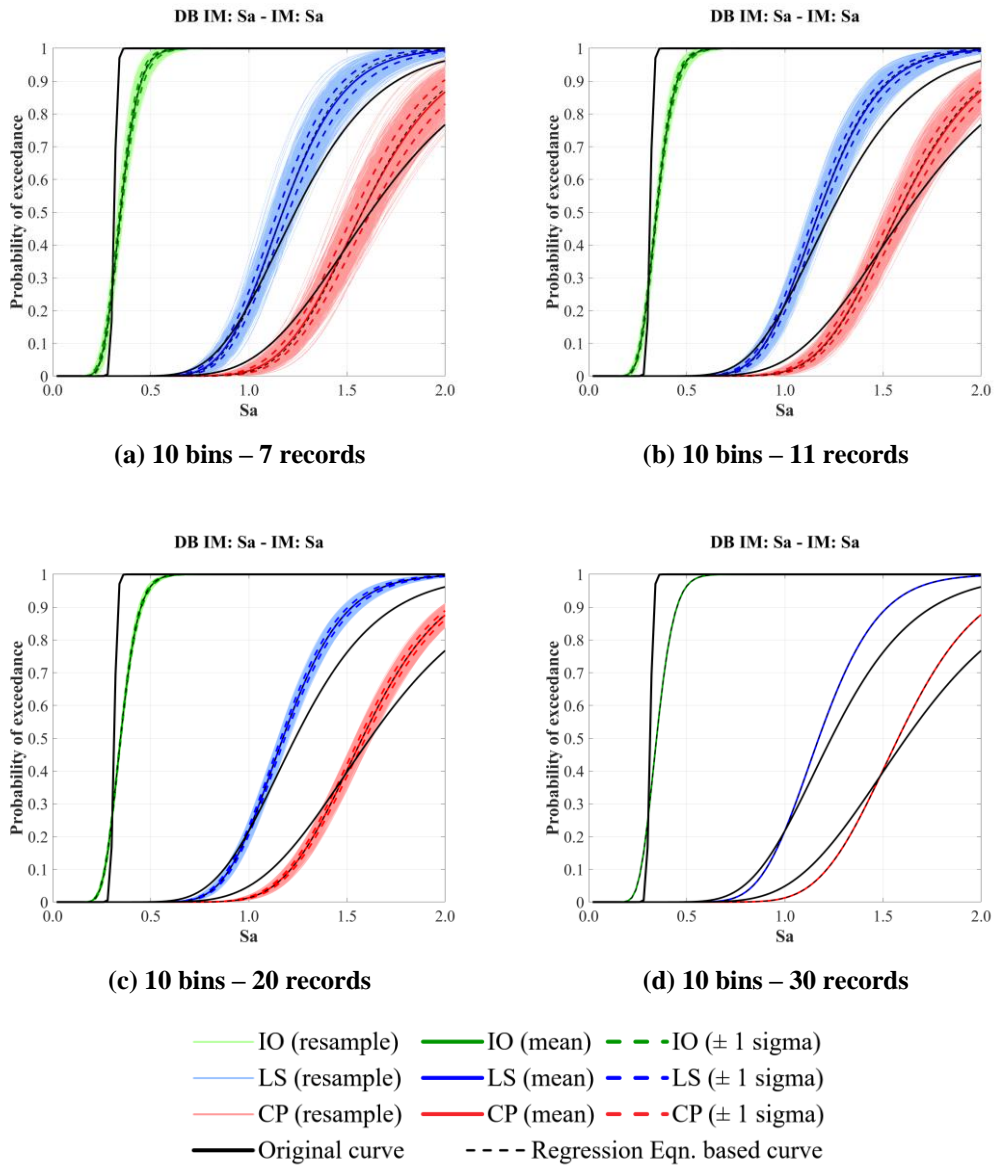Figure A.169. PGV-based fragility curves for F5S4B (MIDR) under PGV-based set (3 bins considered)

(a) 5 bins – 7 records

(b) 5 bins – 11 records

(c) 5 bins – 20 records

(d) 5 bins – 30 records
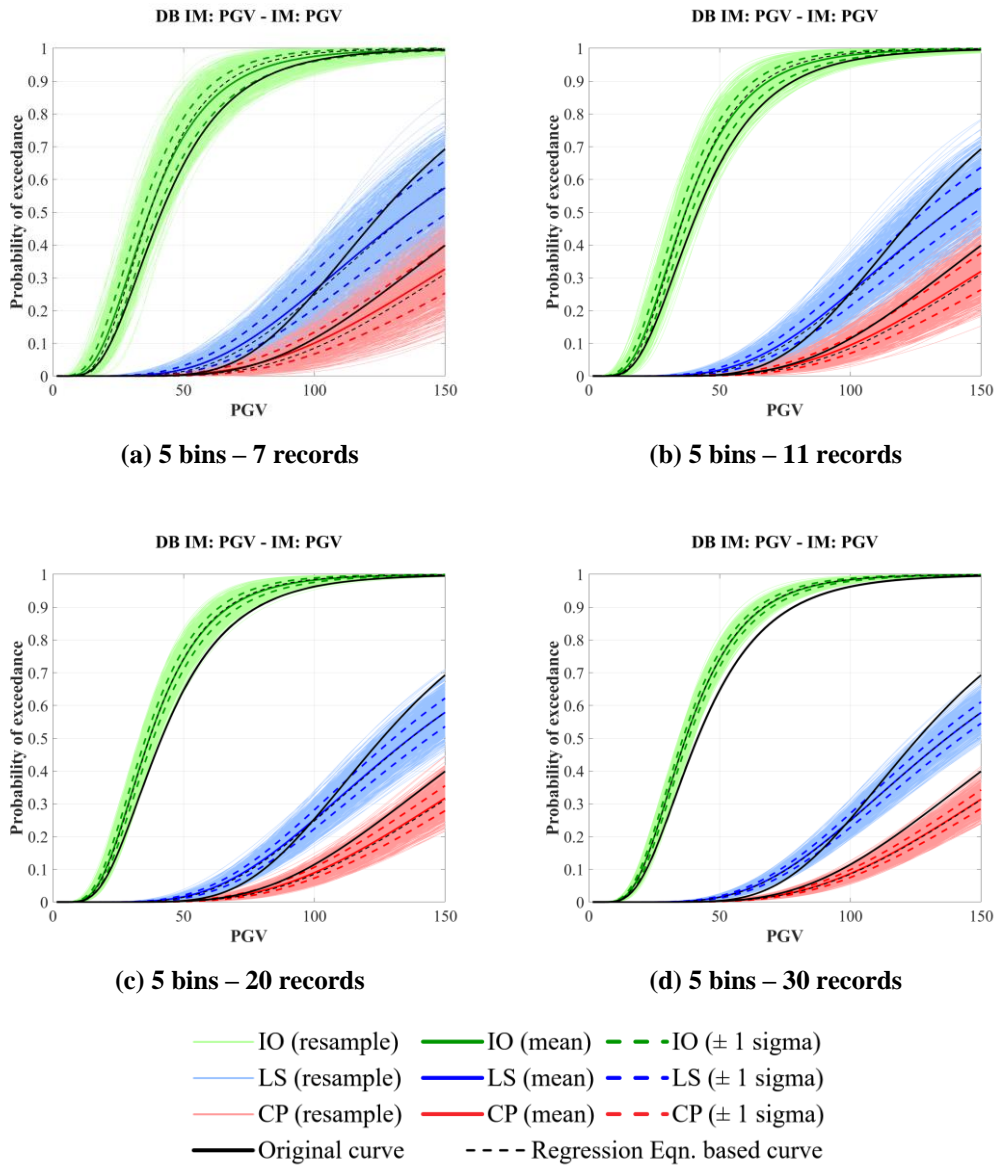
Figure A.170. PGV-based fragility curves for F5S4B (MIDR) under PGV-based set (5 bins considered)

(a) 8 bins – 7 records

(b) 8 bins – 11 records

(c) 8 bins – 20 records

(d) 8 bins – 30 records

IO (resample) —— IO (mean) – – – IO (± 1 sigma)

LS (resample) —— LS (mean) – – – LS (± 1 sigma)

CP (resample) —— CP (mean) – – – CP (± 1 sigma)

—— Original curve – – – – Regression Eqn. based curve
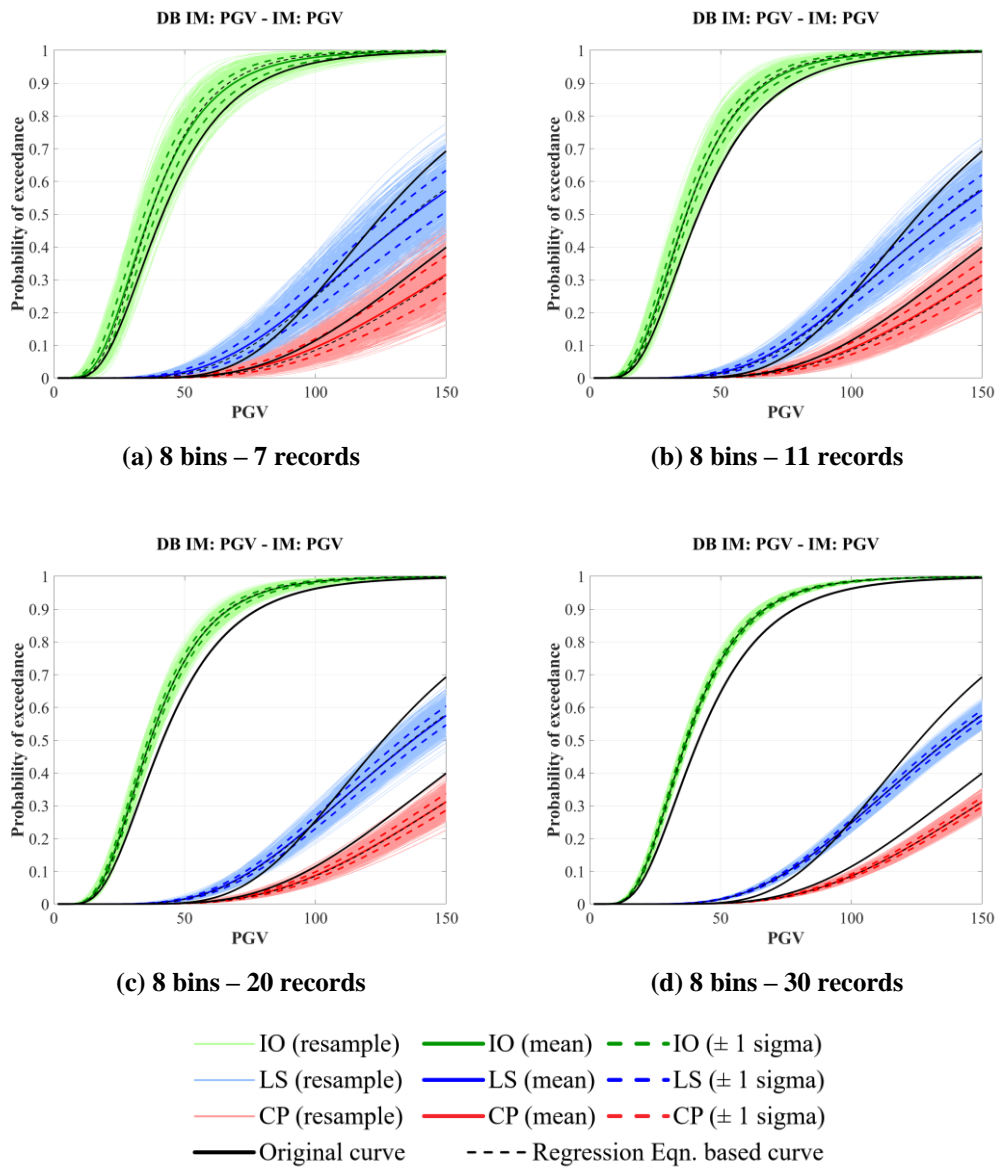
Figure A.171. PGV-based fragility curves for F5S4B (MIDR) under PGV-based set

(8 bins considered)

(a) 10 bins – 7 records

(b) 10 bins – 11 records

(c) 10 bins – 20 records

(d) 10 bins – 30 records
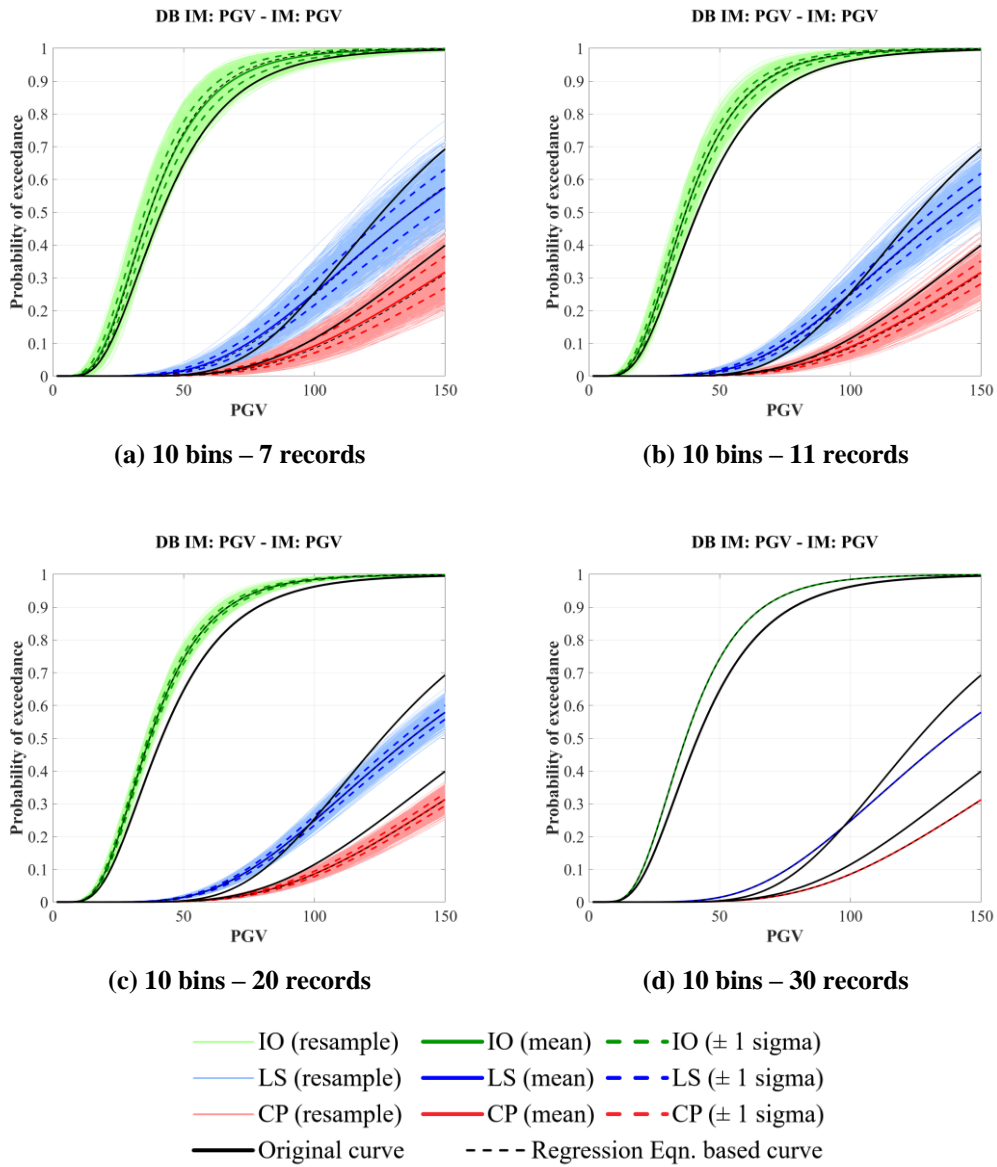
Figure A.172. PGV-based fragility curves for F5S4B (MIDR) under PGV-based set
(10 bins considered)

(a) 3 bins – 7 records

(b) 3 bins – 11 records

(c) 3 bins – 20 records

(d) 3 bins – 30 records
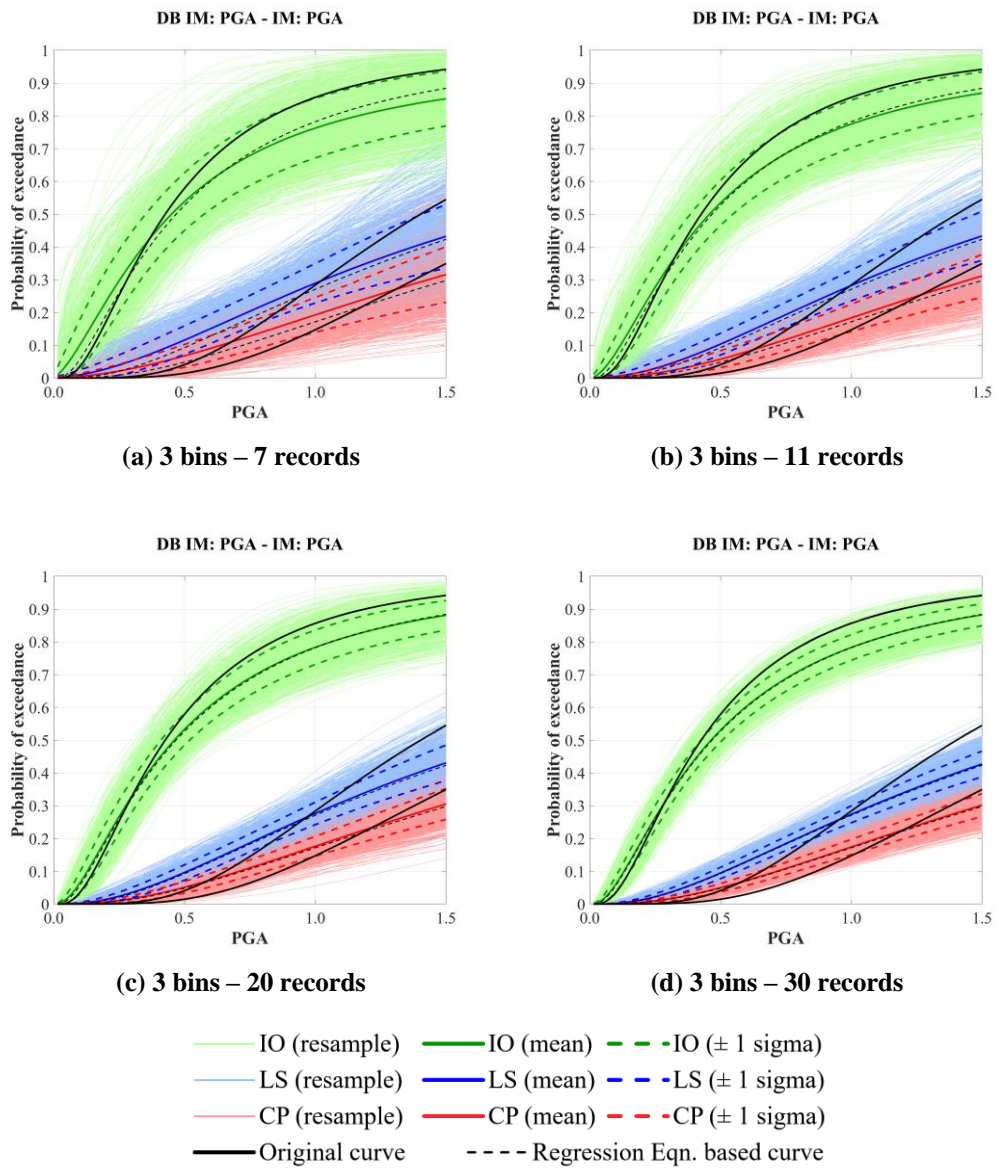
Figure A.173. PGA-based fragility curves for F5S4B (MIDR) under PGA-based set

(3 bins considered)

(a) 10 bins – 7 records

(b) 10 bins – 11 records
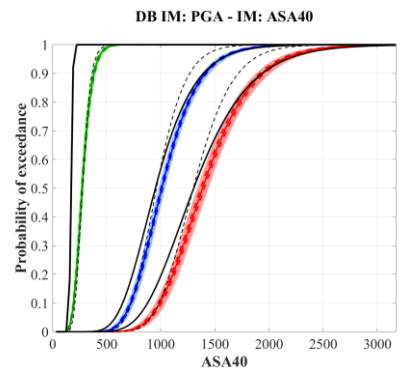
(c) 10 bins – 20 records

(d) 10 bins – 30 records

IO (resample) — IO (mean) – – IO (± 1 sigma)
LS (resample) — LS (mean) – – LS (± 1 sigma)
CP (resample) — CP (mean) – – CP (± 1 sigma)
— Original curve – – – Regression Eqn. based curve
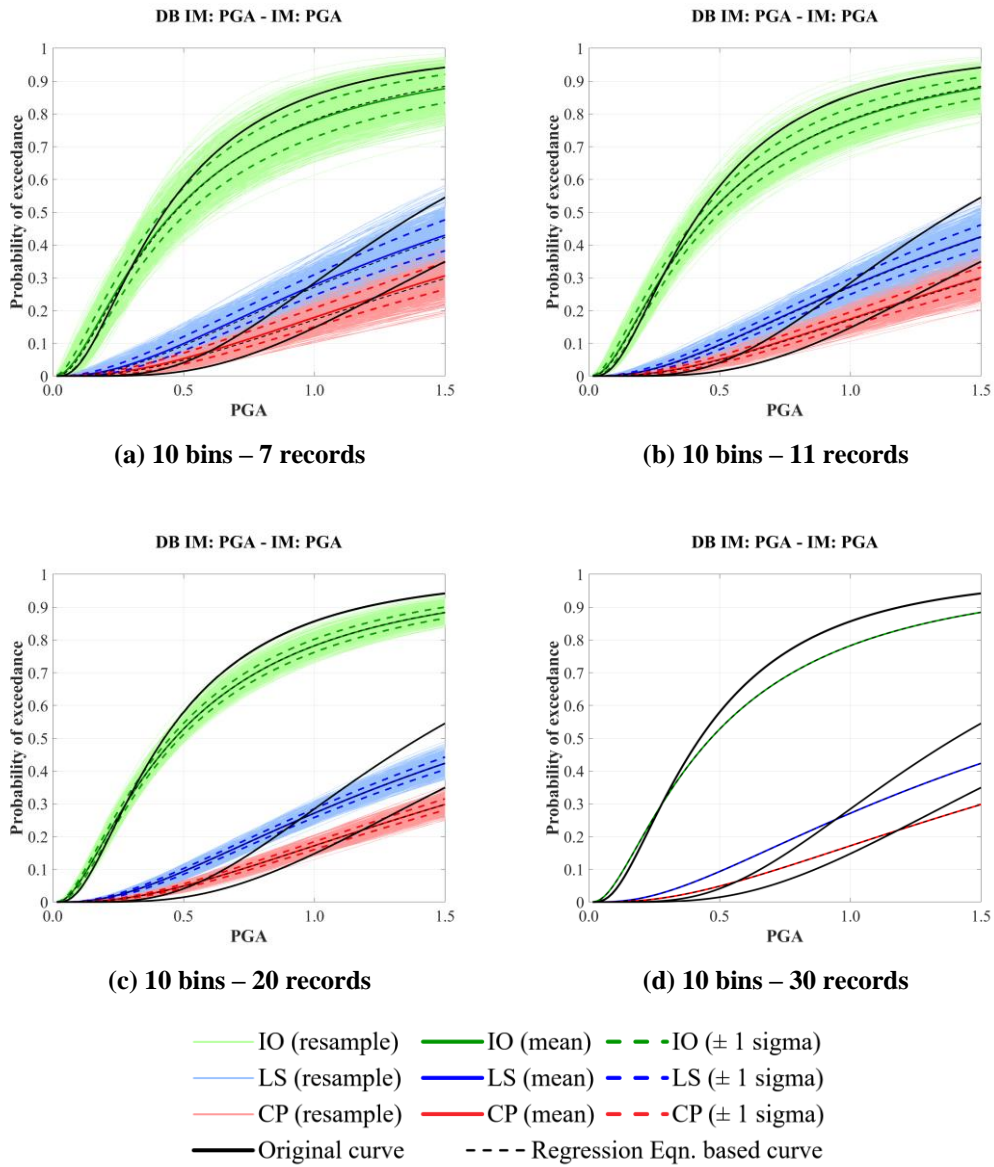
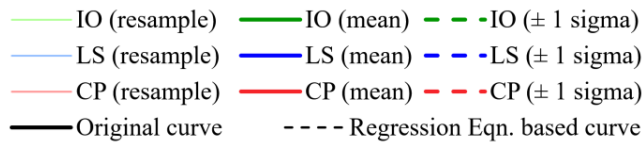Figure A.174. PGA-based fragility curves for F5S4B (MIDR) under PGA-based set
(10 bins considered)
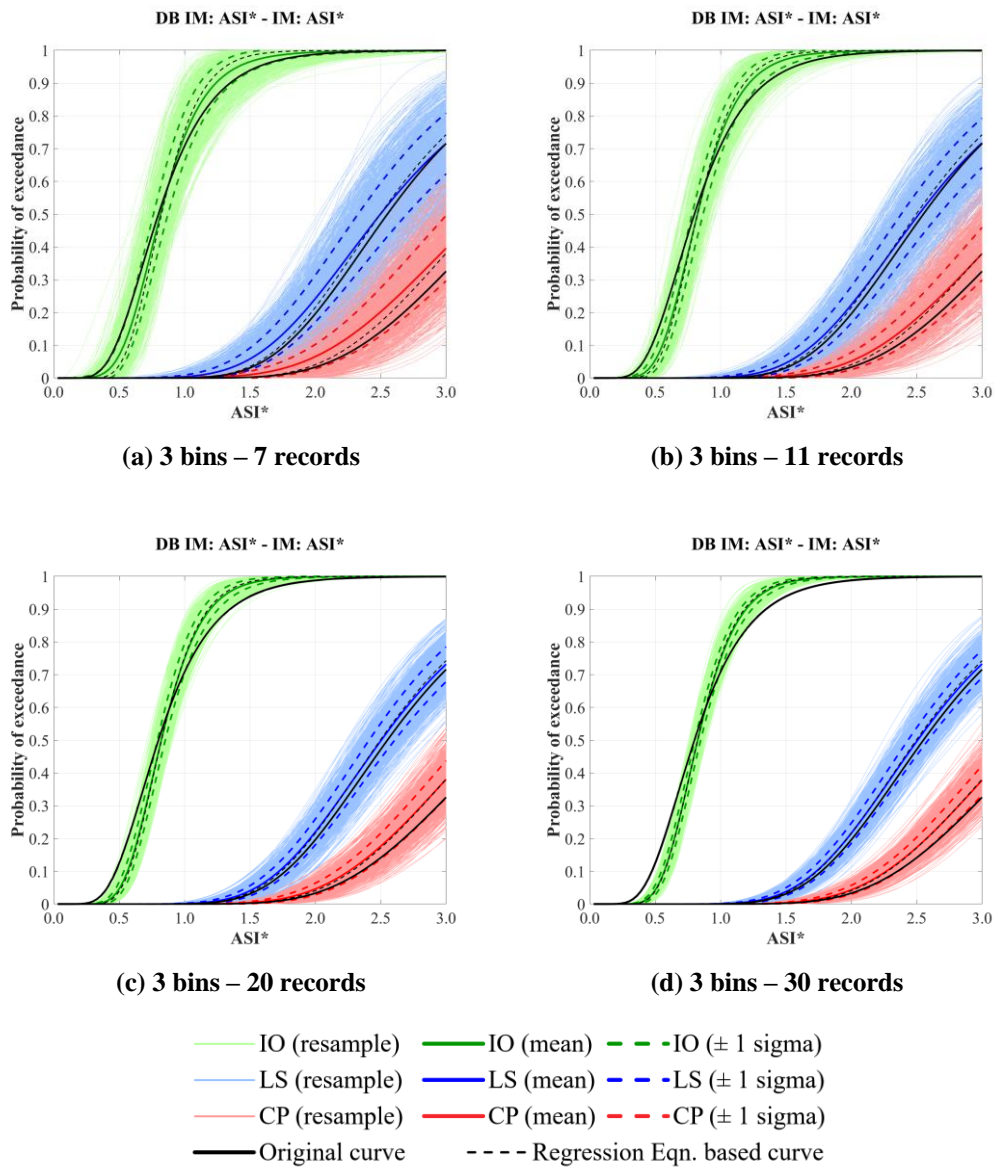
Figure A.175. ASI*-based fragility curves for F5S4B (MIDR) under ASI*-based set (3 bins considered)
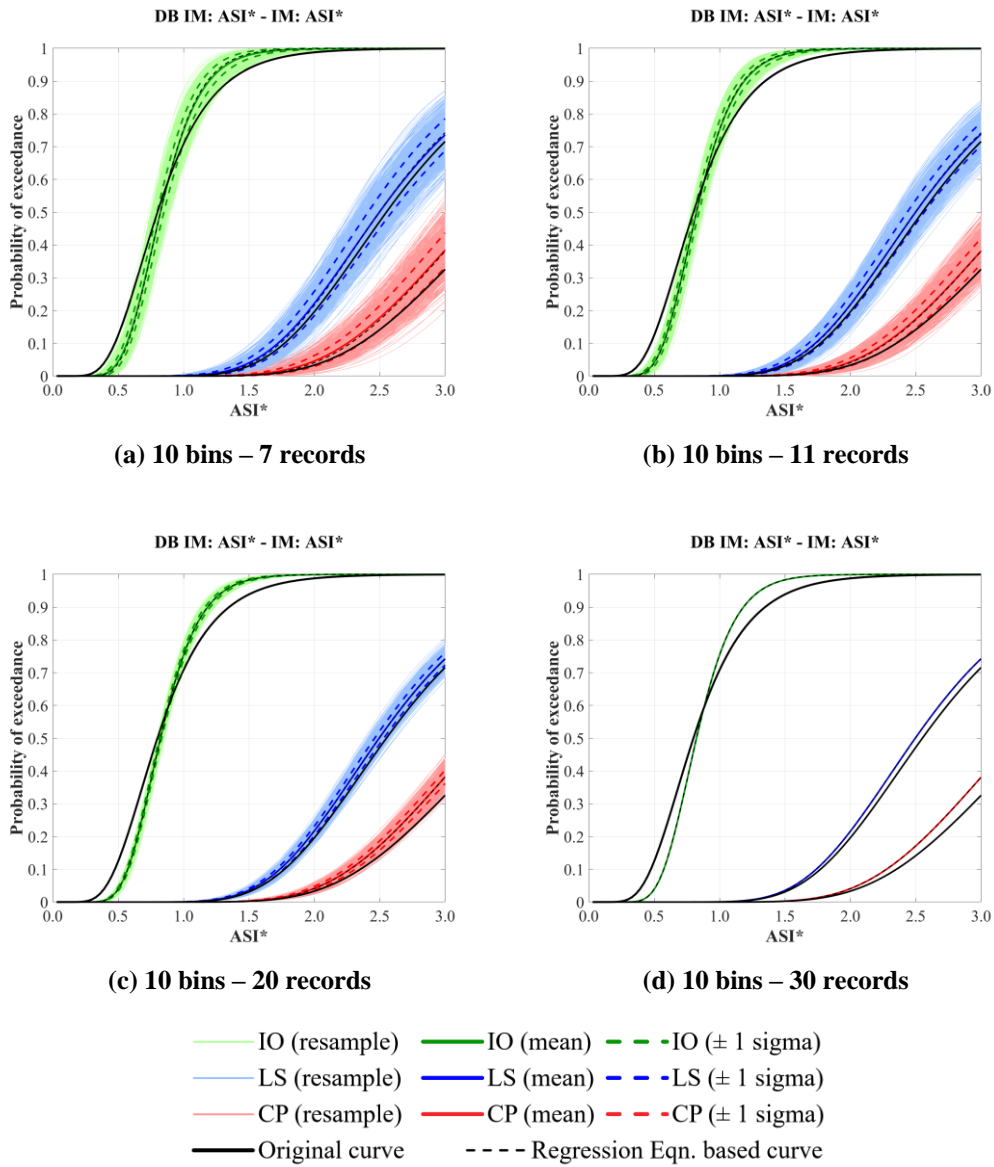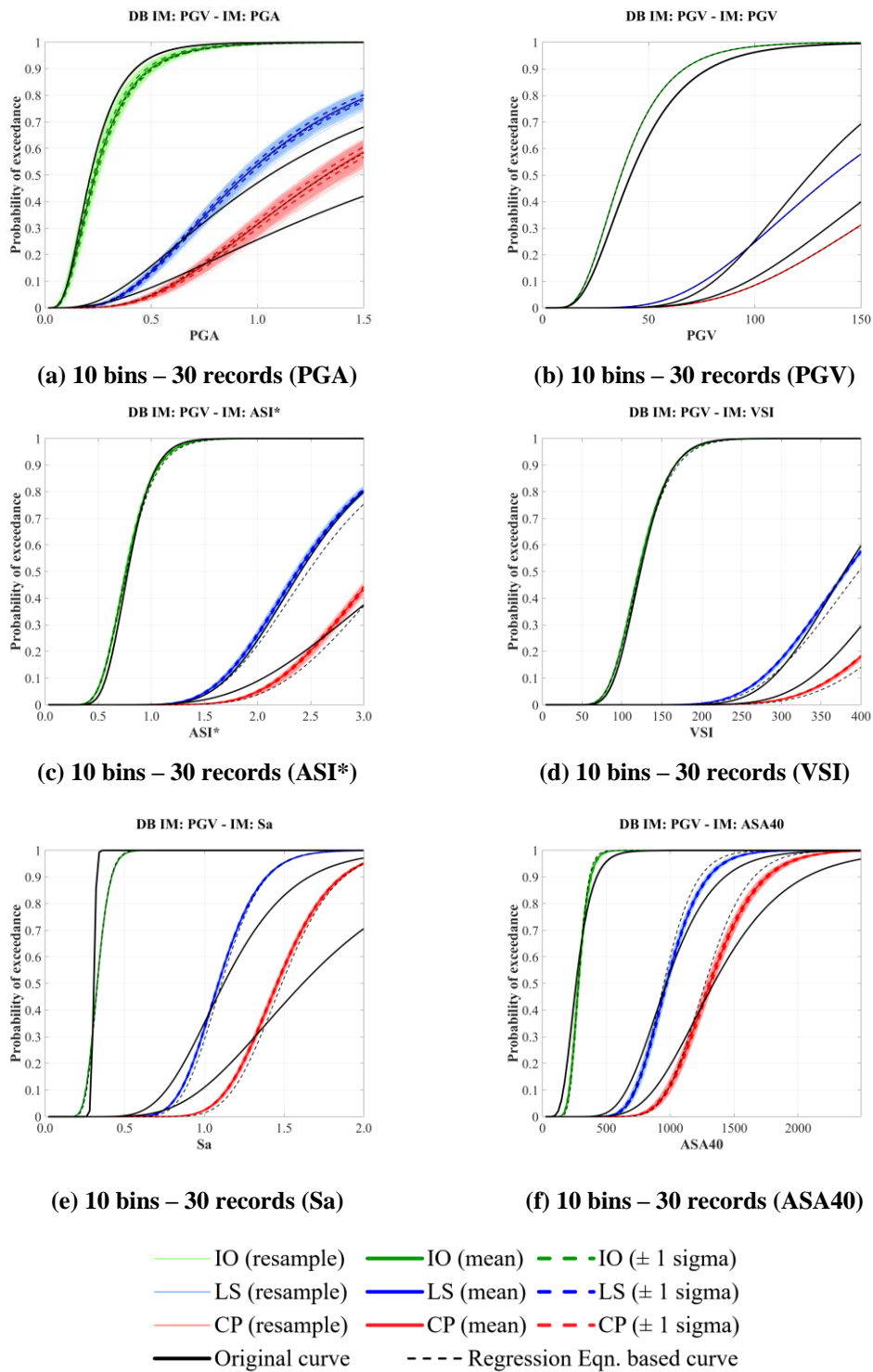
Figure A.176. ASI*-based fragility curves for F5S4B (MIDR) under ASI*-based set (10 bins considered)

(a) 3 bins – 7 records

(b) 3 bins – 11 records

(c) 3 bins – 20 records

(d) 3 bins – 30 records
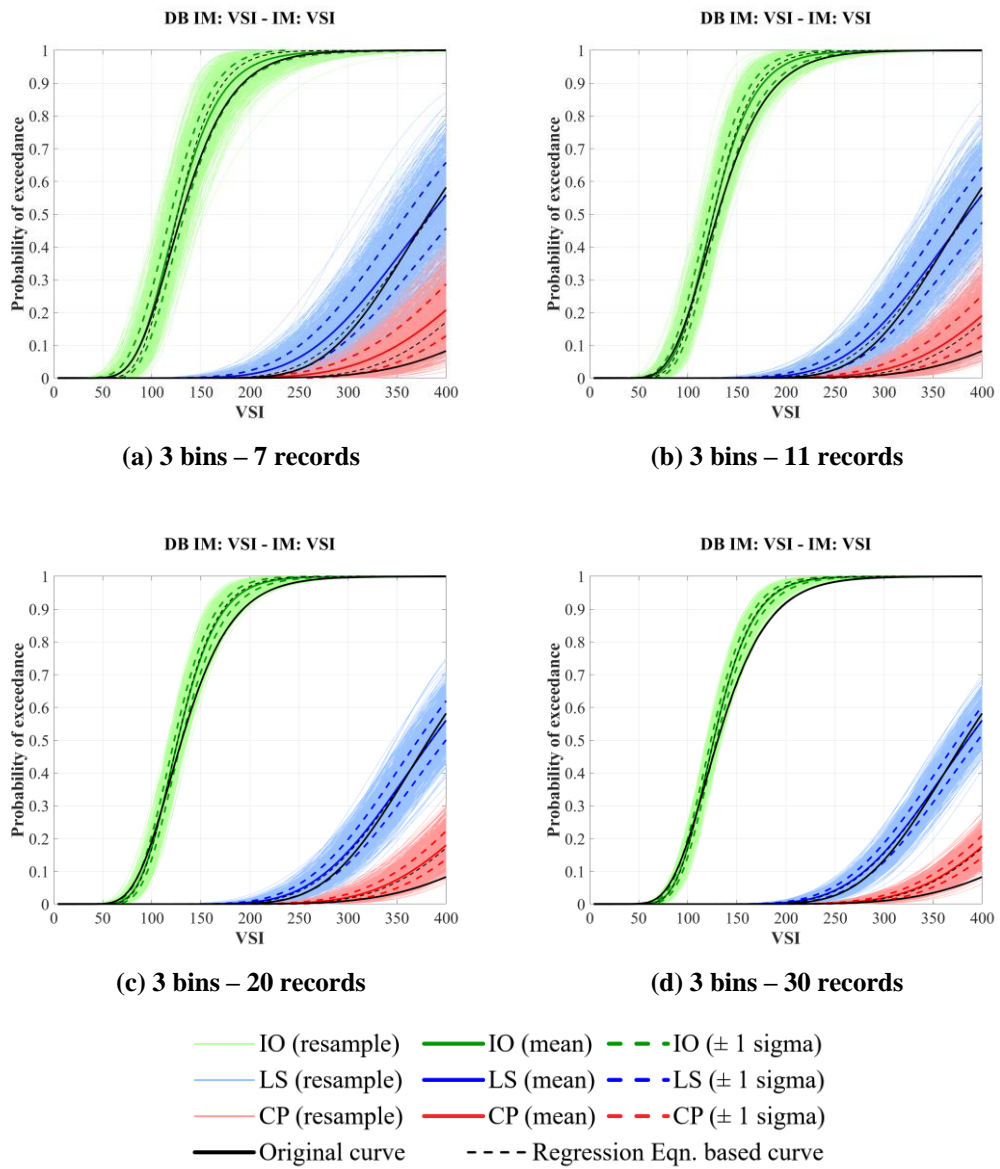
Figure A.177. VSI-based fragility curves for F5S4B (MIDR) under VSI-based set
(3 bins considered)

(a) 10 bins – 7 records
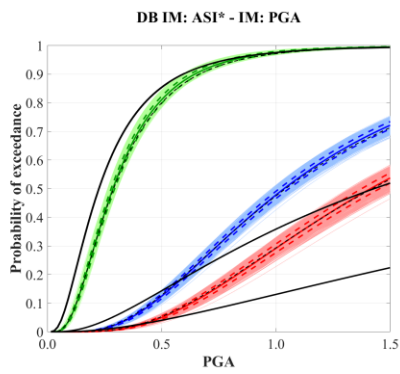
(b) 10 bins – 11 records

(c) 10 bins – 20 records

(d) 10 bins – 30 records
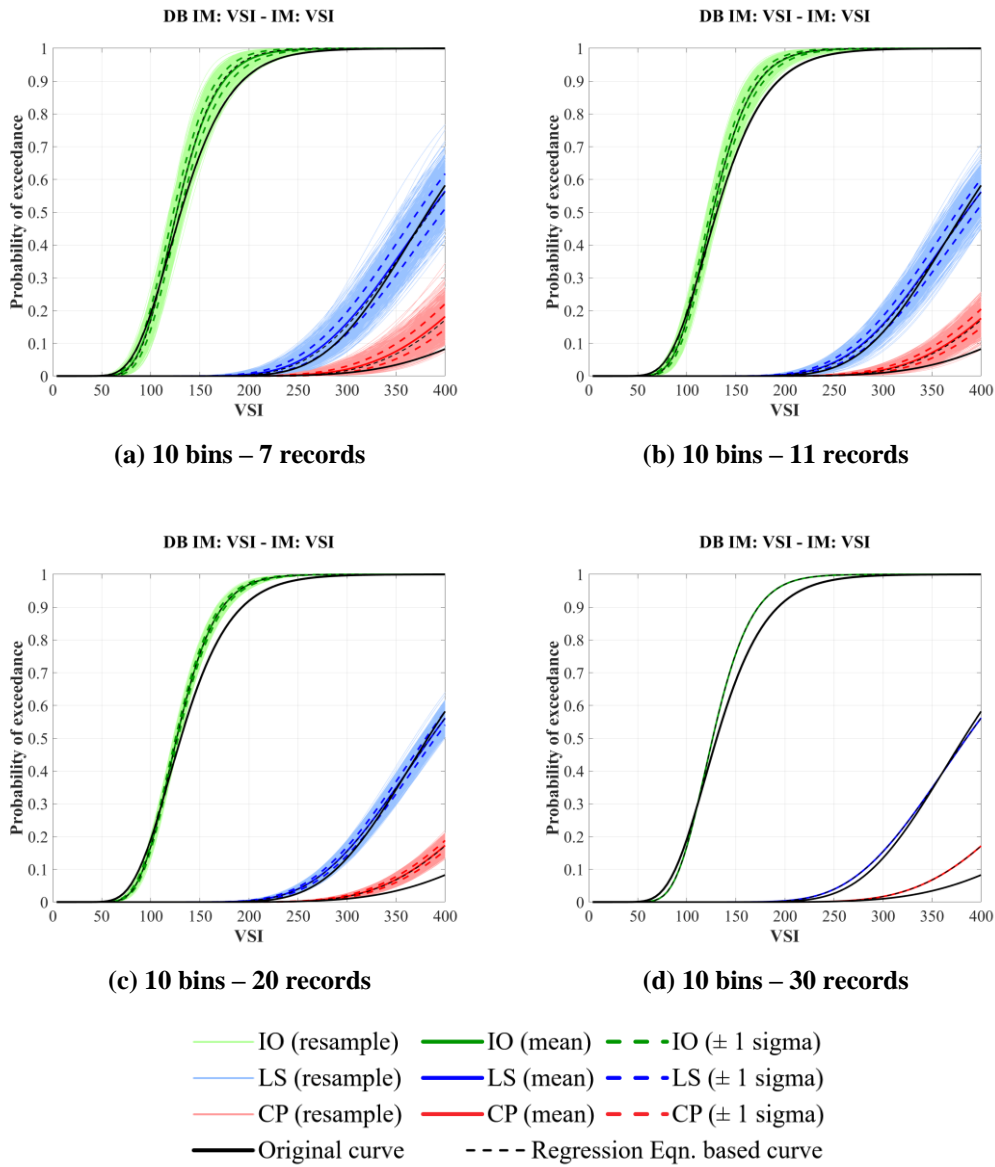
Figure A.178. VSI-based fragility curves for F5S4B (MIDR) under VSI-based set
(10 bins considered)

(a) 3 bins – 7 records

(b) 3 bins – 11 records

(c) 3 bins – 20 records

(d) 3 bins – 30 records

Figure A.179. S_a-based fragility curves for F5S4B (MIDR) under S_a-based set (3 bins considered)

(a) 10 bins – 7 records

(b) 10 bins – 11 records

(c) 10 bins – 20 records

(d) 10 bins – 30 records

IO (resample) — IO (mean) – – IO (± 1 sigma)
LS (resample) — LS (mean) – – LS (± 1 sigma)
CP (resample) — CP (mean) – – CP (± 1 sigma)
— Original curve ---- Regression Eqn. based curve

Figure A.180. S_a-based fragility curves for F5S4B (MIDR) under S_a-based set (10 bins considered)
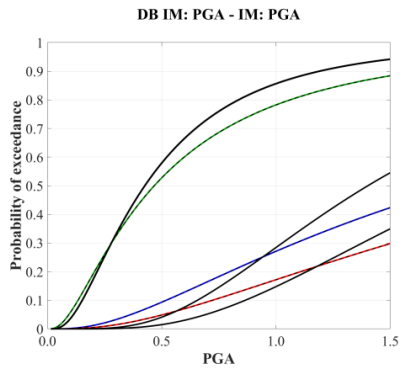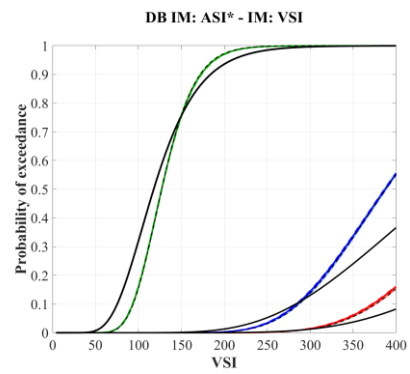
(a) 10 bins – 30 records (PGA) **(b) 10 bins – 30 records (PGV)**
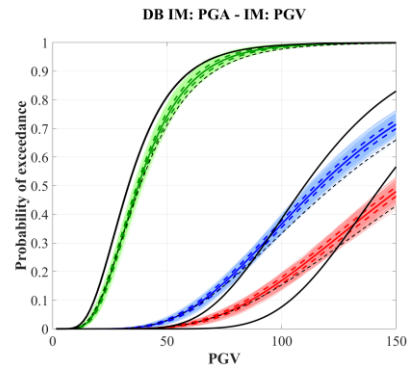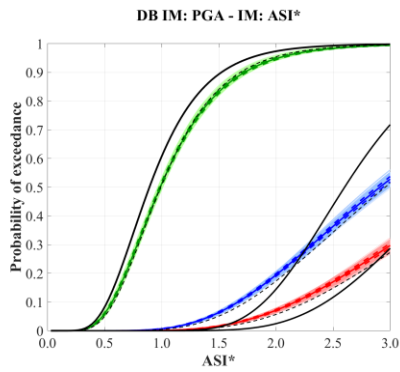
(c) 10 bins – 30 records (ASI*) **(d) 10 bins – 30 records (VSI)**
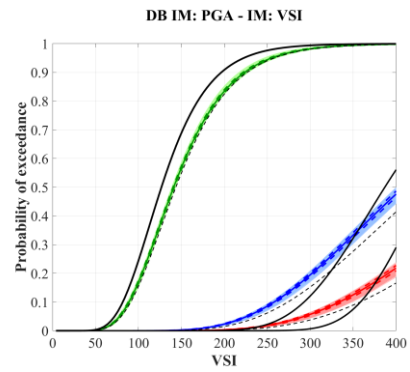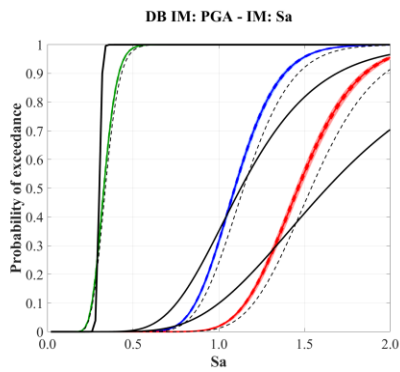
(e) 10 bins – 30 records (Sa) **(f) 10 bins – 30 records (ASA40)**

Figure A.181. Alternative IM-based fragility curves for F5S4B (MIDR) under PGA-based set (10 bins – 30 records considered)
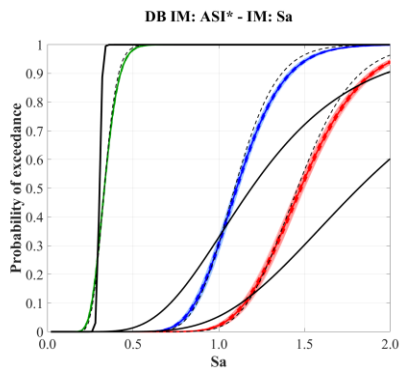
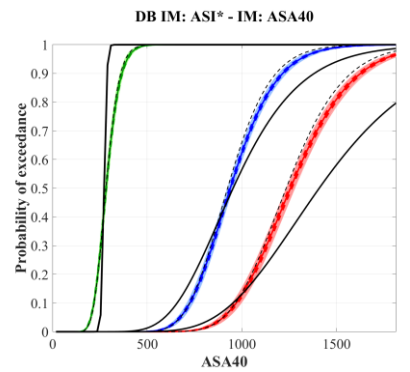**(a) 10 bins – 30 records (PGA)**

(b) 10 bins – 30 records (PGV)

(c) 10 bins – 30 records (ASI*)

(d) 10 bins – 30 records (VSI)
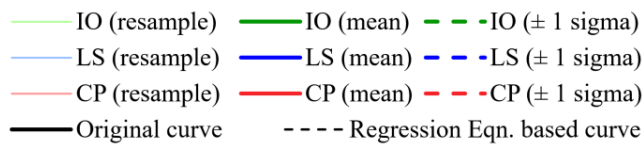
(e) 10 bins – 30 records (Sa)

(f) 10 bins – 30 records (ASA40)

IO (resample) — IO (mean) — – IO (± 1 sigma)
LS (resample) — LS (mean) — – LS (± 1 sigma)
CP (resample) — CP (mean) — – CP (± 1 sigma)
— Original curve — – – – Regression Eqn. based curve

Figure A.182. Alternative IM-based fragility curves for F5S4B (MIDR) under
PGV-based set (10 bins – 30 records considered)

(a) 10 bins – 30 records (PGA)
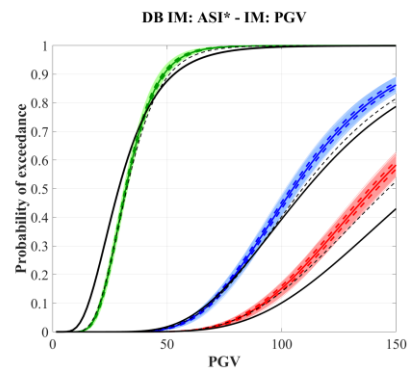
(b) 10 bins – 30 records (PGV)
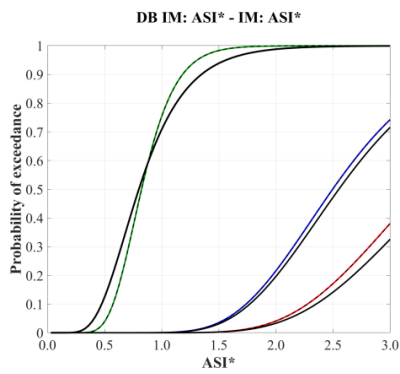
(c) 10 bins – 30 records (ASI*)

(d) 10 bins – 30 records (VSI)

(e) 10 bins – 30 records (Sa)

(f) 10 bins – 30 records (ASA40)

Figure A.183. Alternative IM-based fragility curves for F5S4B (MIDR) under ASI*-based set (10 bins – 30 records considered)
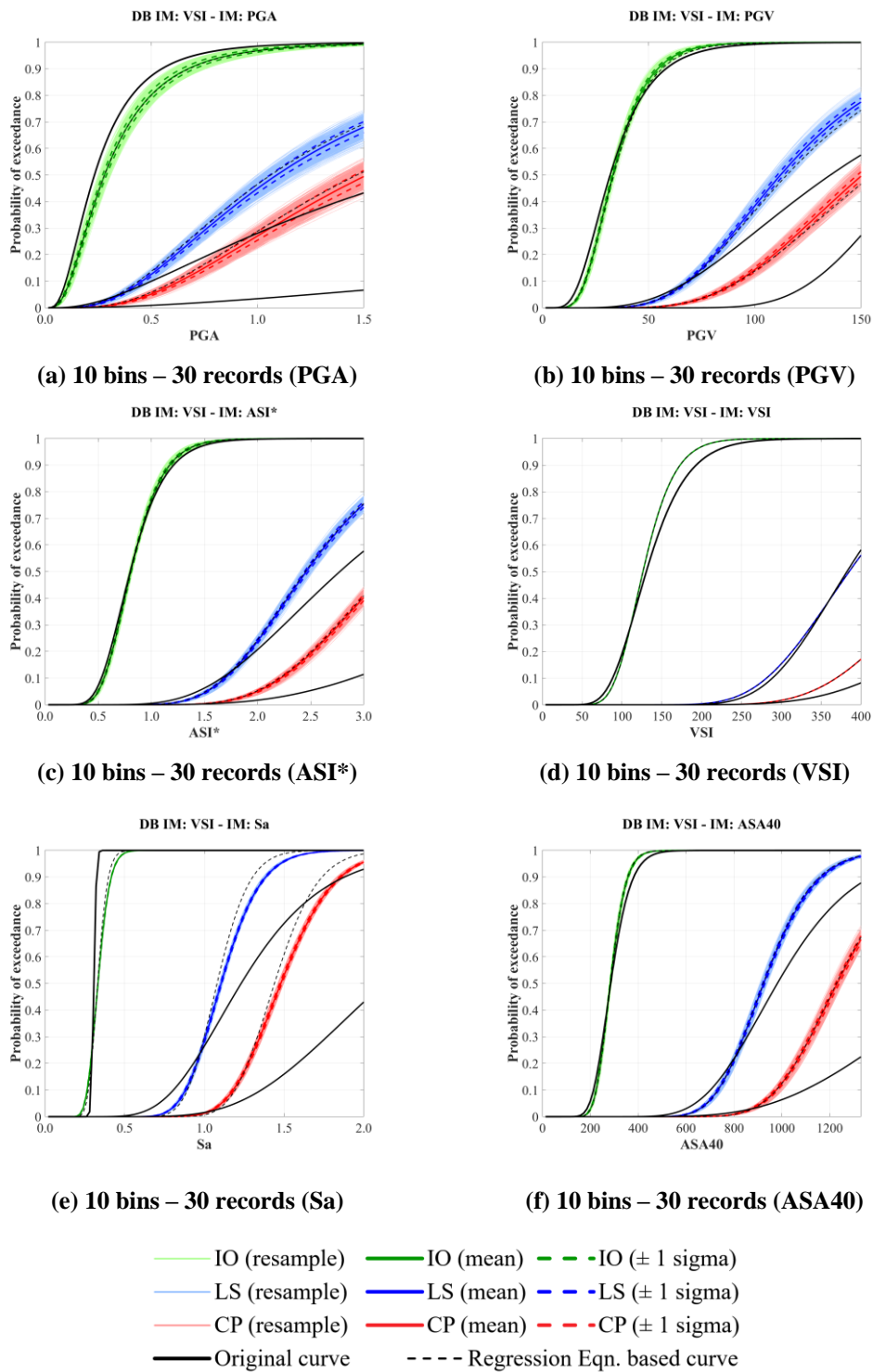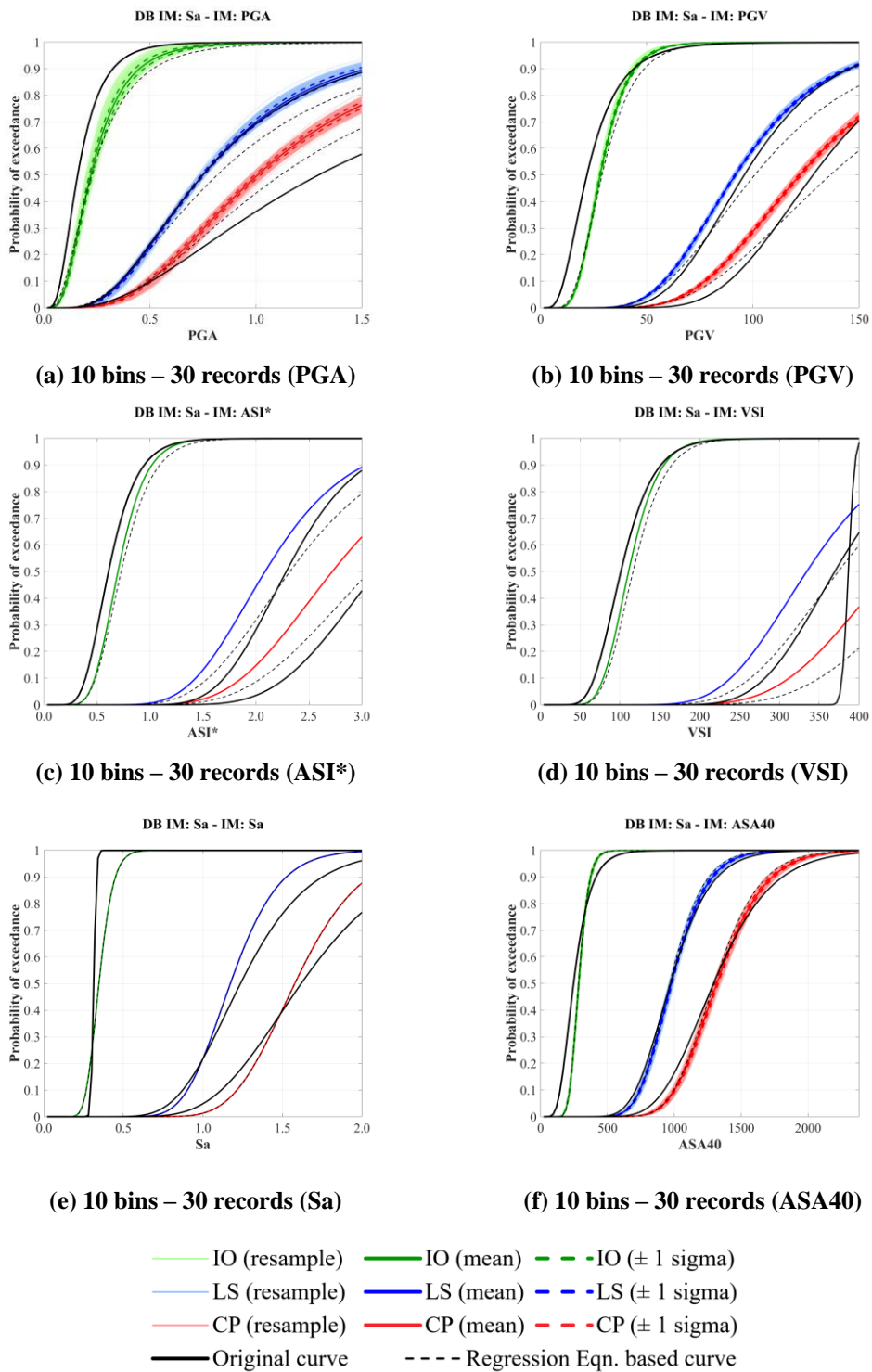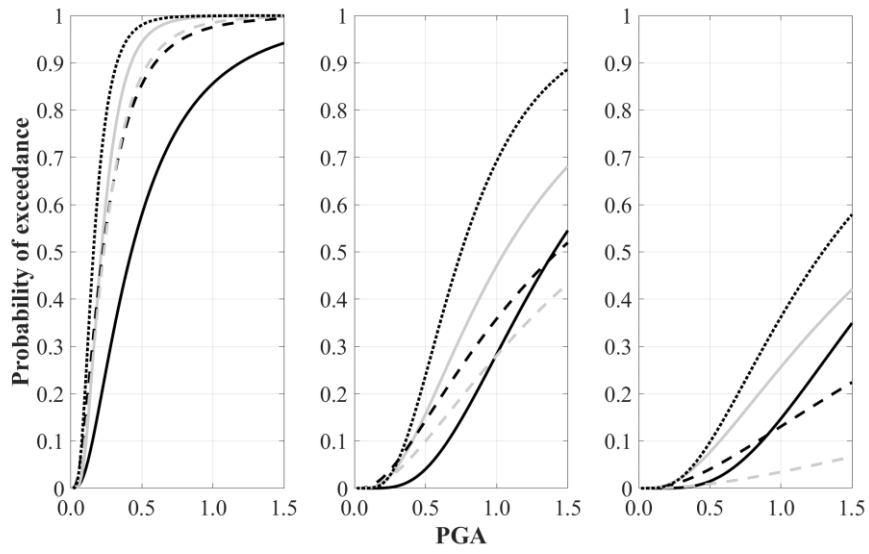
(a) 10 bins – 30 records (PGA)

(b) 10 bins – 30 records (PGV)

(c) 10 bins – 30 records (ASI*)

(d) 10 bins – 30 records (VSI)
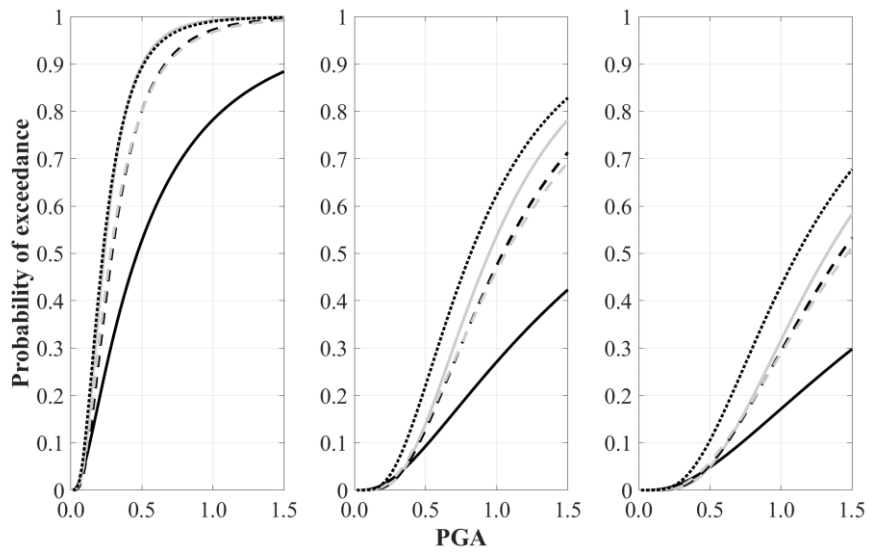
(e) 10 bins – 30 records (Sa)

(f) 10 bins – 30 records (ASA40)

Figure A.184. Alternative IM-based fragility curves for F5S4B (MIDR) under VSI-based set (10 bins – 30 records considered)
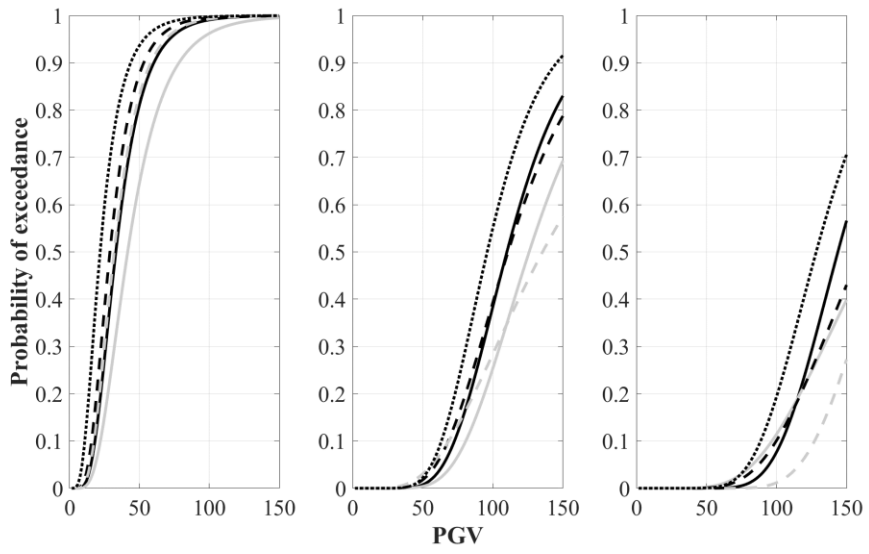
(a) 10 bins – 30 records (PGA)

(b) 10 bins – 30 records (PGV)

(c) 10 bins – 30 records (ASI*)

(d) 10 bins – 30 records (VSI)

(e) 10 bins – 30 records (Sa)

(f) 10 bins – 30 records (ASA40)

Figure A.185. Alternative IM-based fragility curves for F5S4B (MIDR) under S_a-based set (10 bins – 30 records considered)
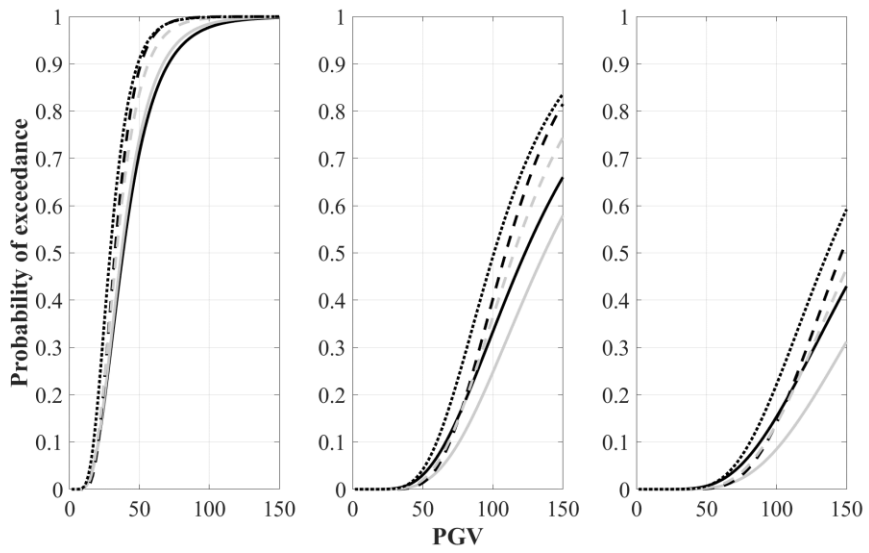
(a) Original Data Based

(b) Regression Equation Based

——— PGA ——— PGV – – –ASI* – – –VSI ·········Sa

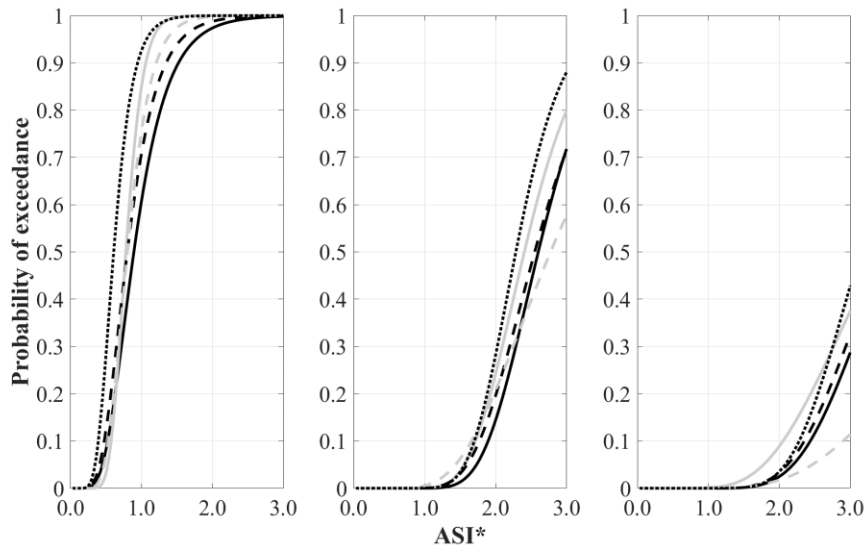Figure A.186. PGA-based fragility curves for F5S4B (MIDR) under different GM record sets (10 bins – 30 records)

(a) Original Data Based

(b) Regression Equation Based

——PGA ——PGV – – –ASI* – – –VSI ⋯⋯⋯Sa

Figure A.187. PGV-based fragility curves for F5S4B (MIDR) under different GM record sets (10 bins – 30 records)
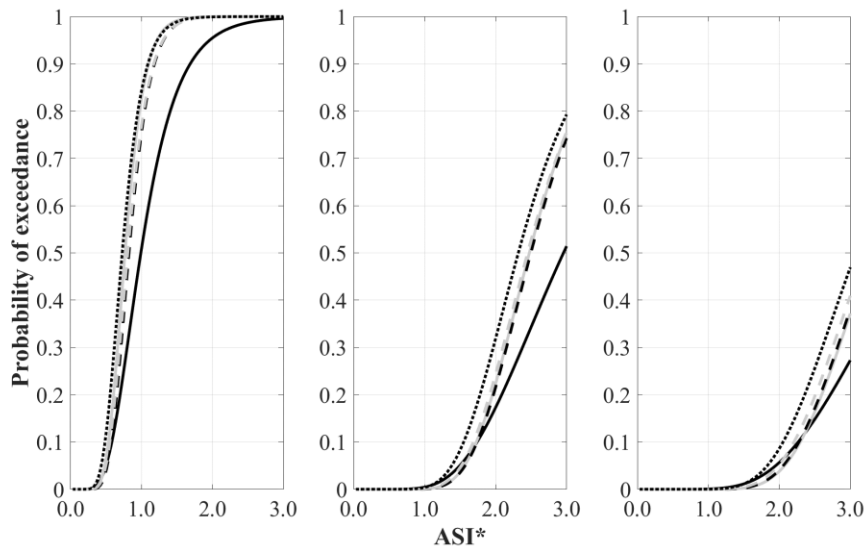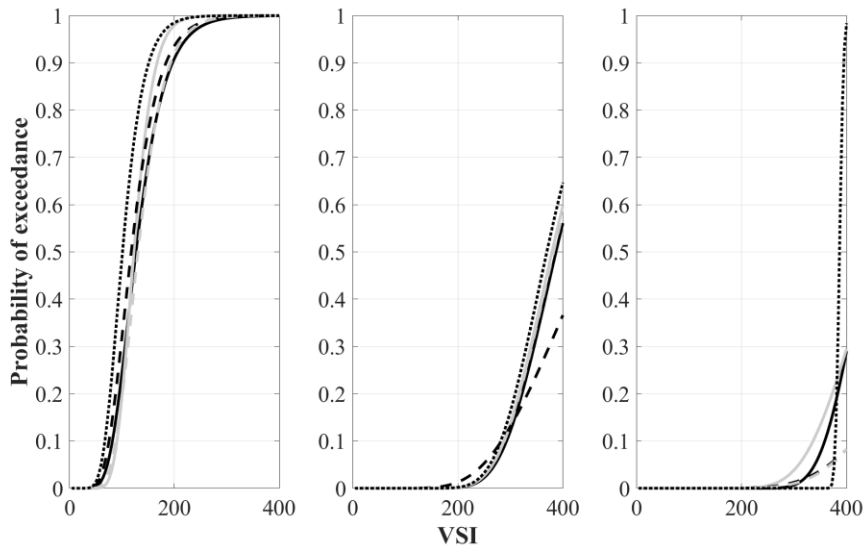
(a) Original Data Based

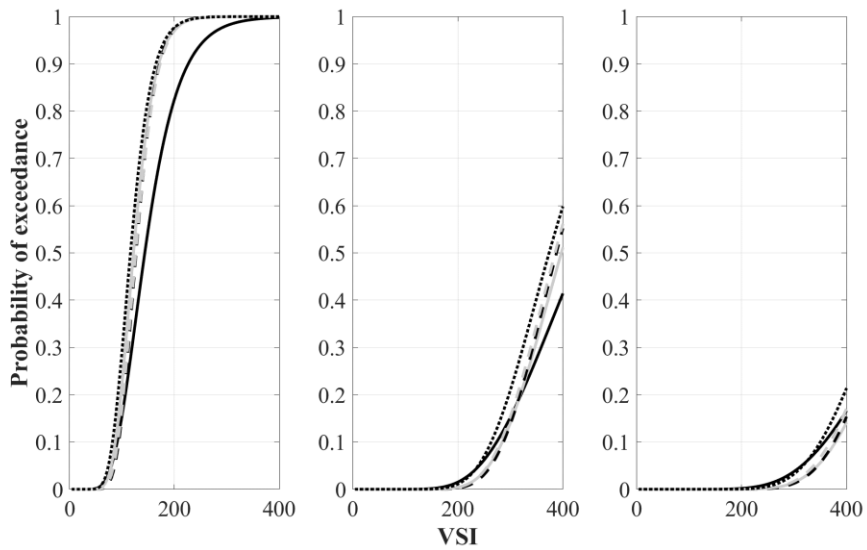**(b) Regression Equation Based**

PGA   PGV   ASI*   VSI   Sa

Figure A.188. ASI*-based fragility curves for F5S4B (MIDR) under different GM record sets (10 bins – 30 records)

(a) Original Data Based

(b) Regression Equation Based

—— PGA   —— PGV   – – –ASI*   – – –VSI   ········ Sa

Figure A.189. VSI-based fragility curves for F5S4B (MIDR) under different GM
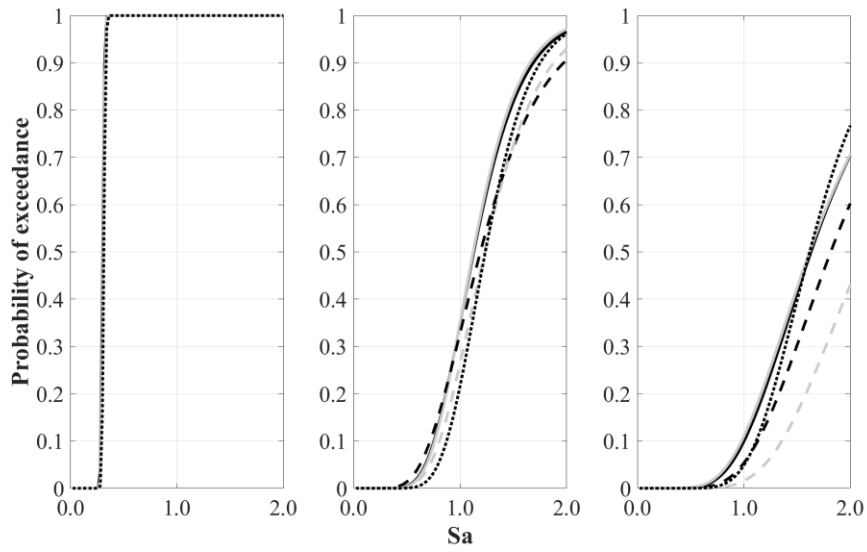record sets (10 bins – 30 records)

(a) Original Data Based

(b) Regression Equation Based

PGA ——— PGV — — ·ASI* — — ·VSI ········ Sa

Figure A.190. S_a-based fragility curves for F5S4B (MIDR) under different GM record sets (10 bins – 30 records)
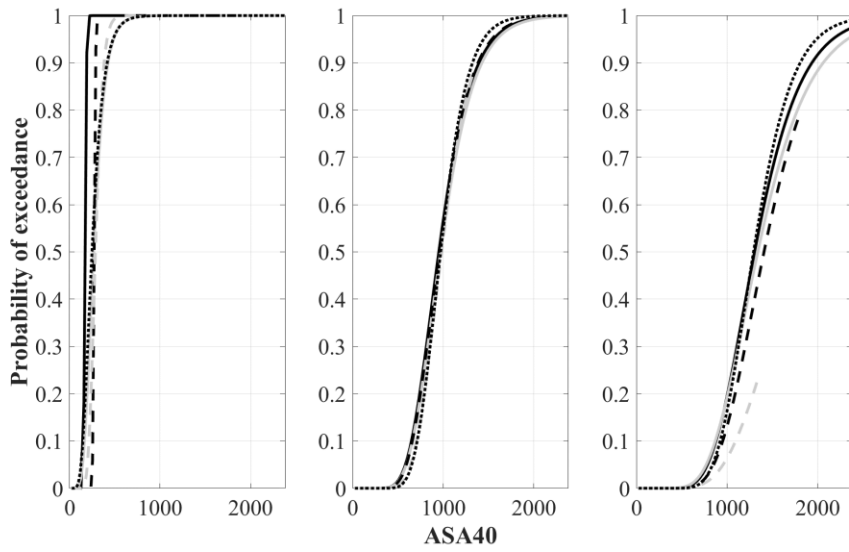
(a) Original Data Based

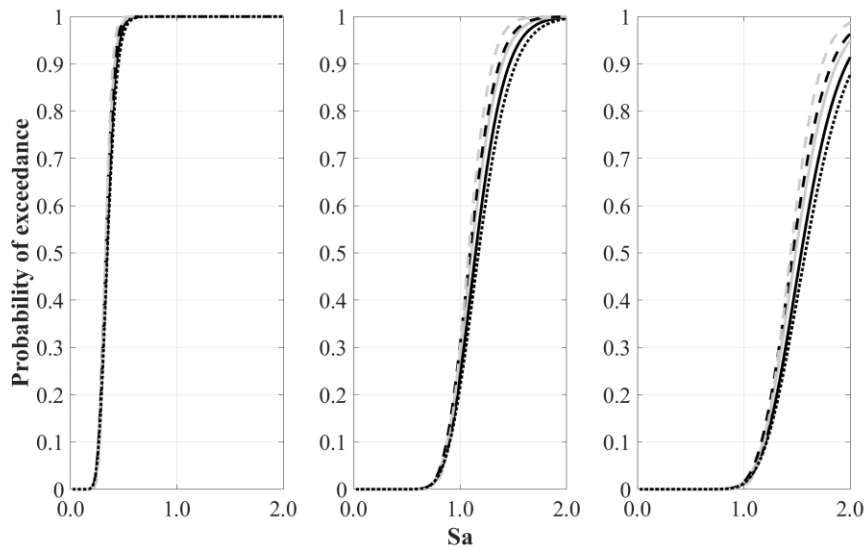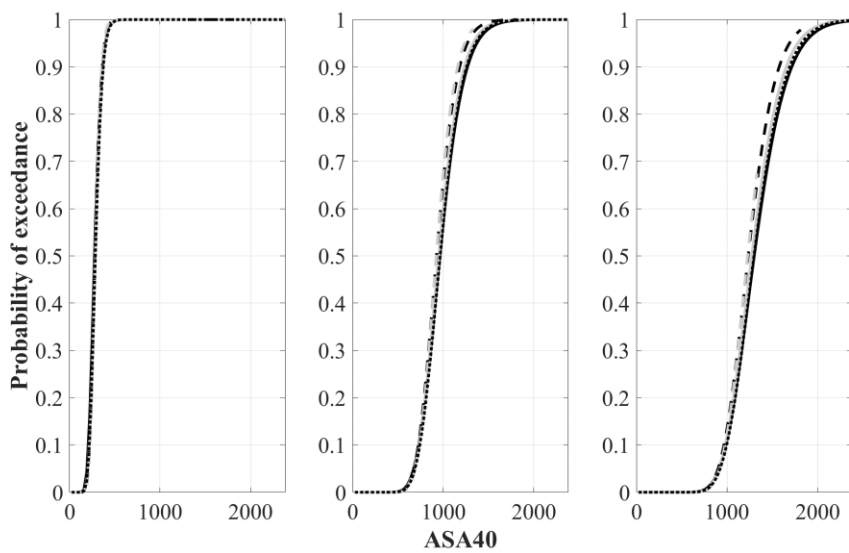
(b) Regression Equation Based

——— PGA ——— PGV – – – ASI* – – – VSI ········ Sa

Figure A.191. ASA$_{40}$-based fragility curves for F5S4B (MIDR) under different GM record sets (10 bins – 30 records)

411

DB IM: PGA - IM: PGA - 5 bins

DB IM: PGA - IM: PGA - 10 bins

30 ——— 20 – – ·11 – – ·7

(thinner lines are ± 1 sigma bands)

Figure A.192. Alternative PGA-based fragility curves for F5S4B (MIDR) under PGA-based record sets formed with different number of records in each bin

DB IM: PGV - IM: PGV - 5 bins

DB IM: PGV - IM: PGV - 10 bins

(thinner lines are ± 1 sigma bands)

Figure A.193. Alternative PGV-based fragility curves for F5S4B (MIDR) under PGV-based record sets formed with different number of records in each bin

413

DB IM: ASI* - IM: ASI* - 5 bins

DB IM: ASI* - IM: ASI* - 10 bins

30   20   11   7

(thinner lines are ± 1 sigma bands)

Figure A.194. Alternative ASI*-based fragility curves for F5S4B (MIDR) under ASI*-based record sets formed with different number of records in each bin
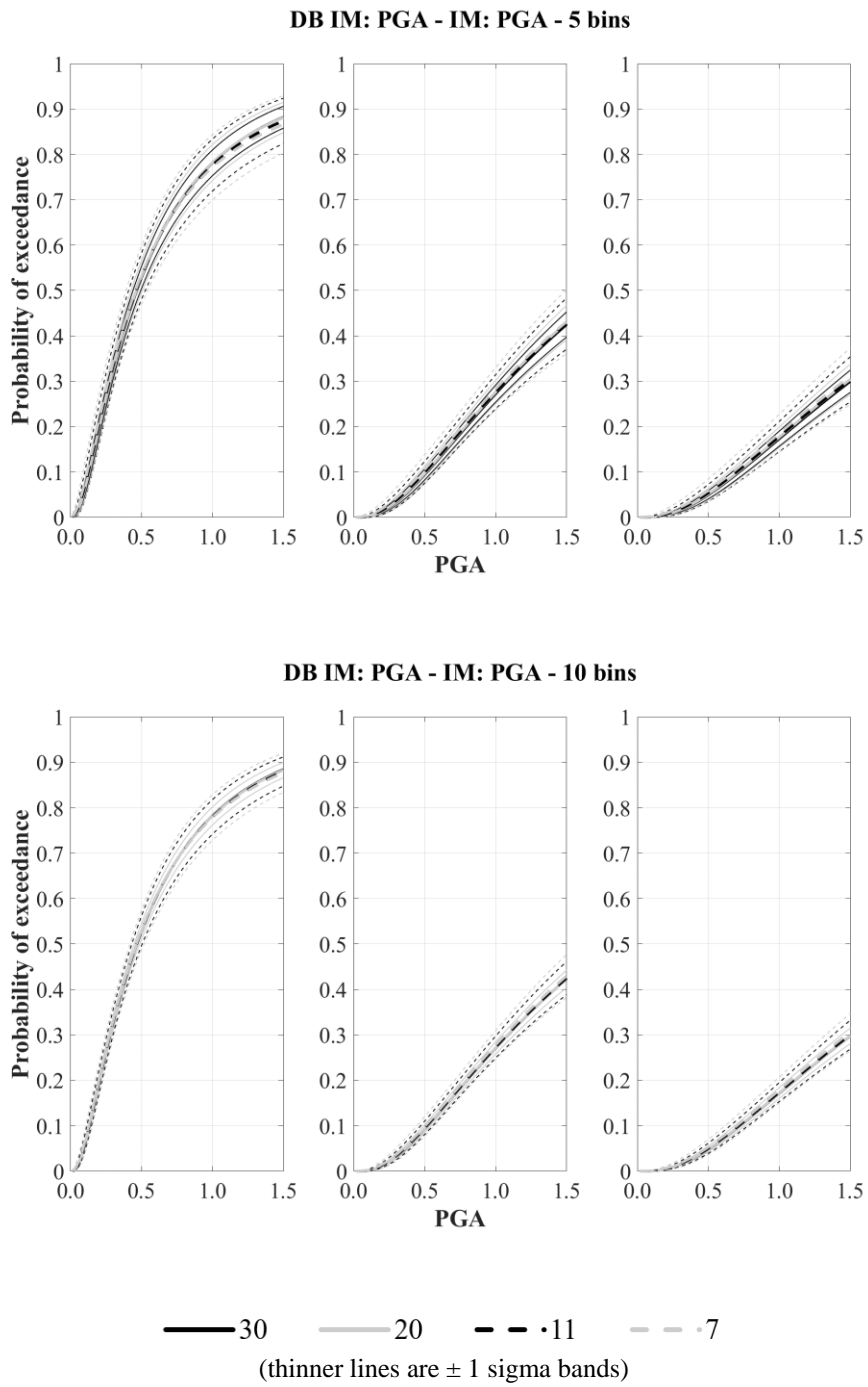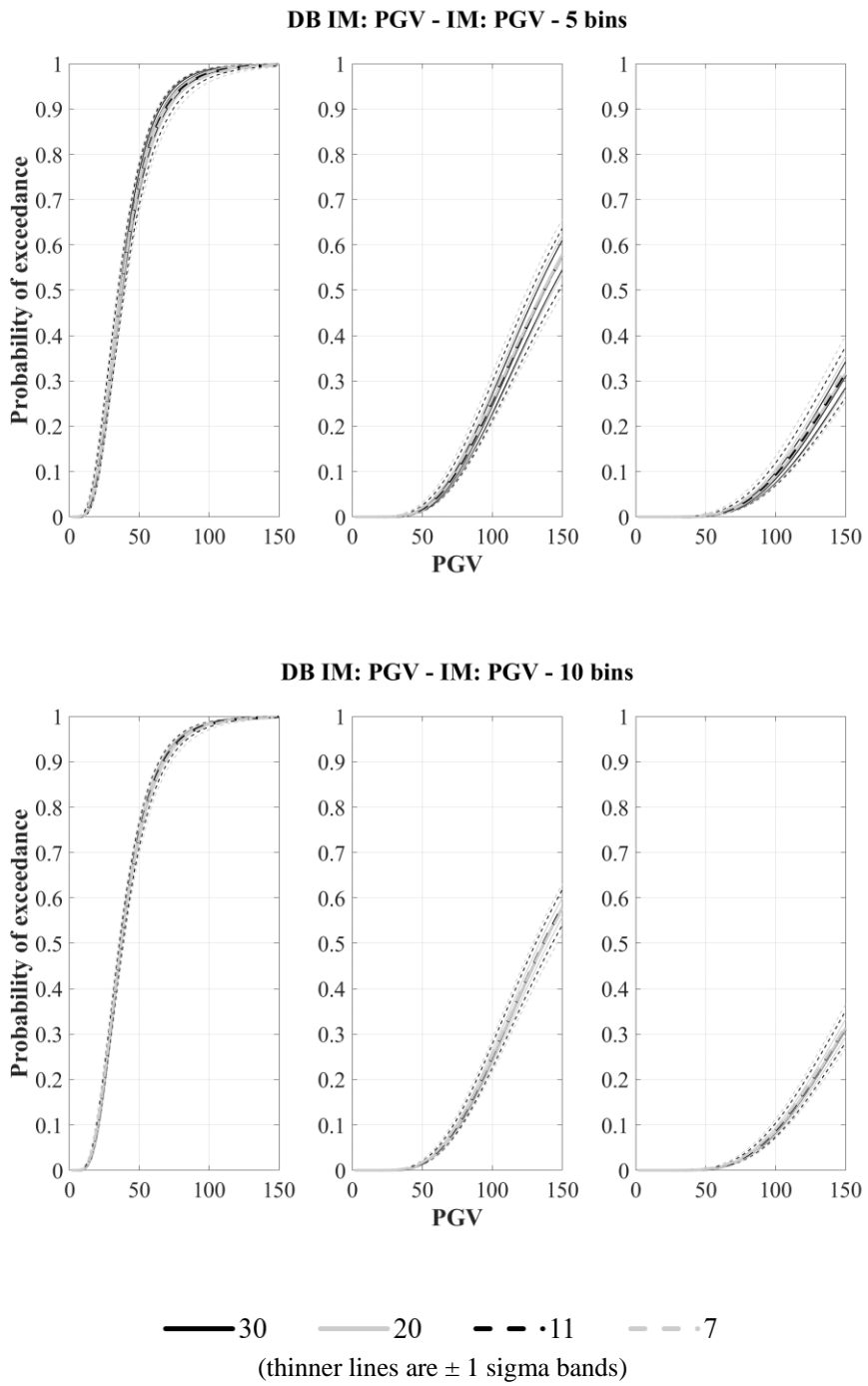
Figure A.195. Alternative VSI-based fragility curves for F5S4B (MIDR) under
VSI-based record sets formed with different number of records in each bin

———— 30   ———— 20   ‒ ‒ ·11   ‒ ‒ ·7

(thinner lines are ± 1 sigma bands)

Figure A.196. Alternative S_a-based fragility curves for F5S4B (MIDR) under S_a-based record sets formed with different number of records in each bin
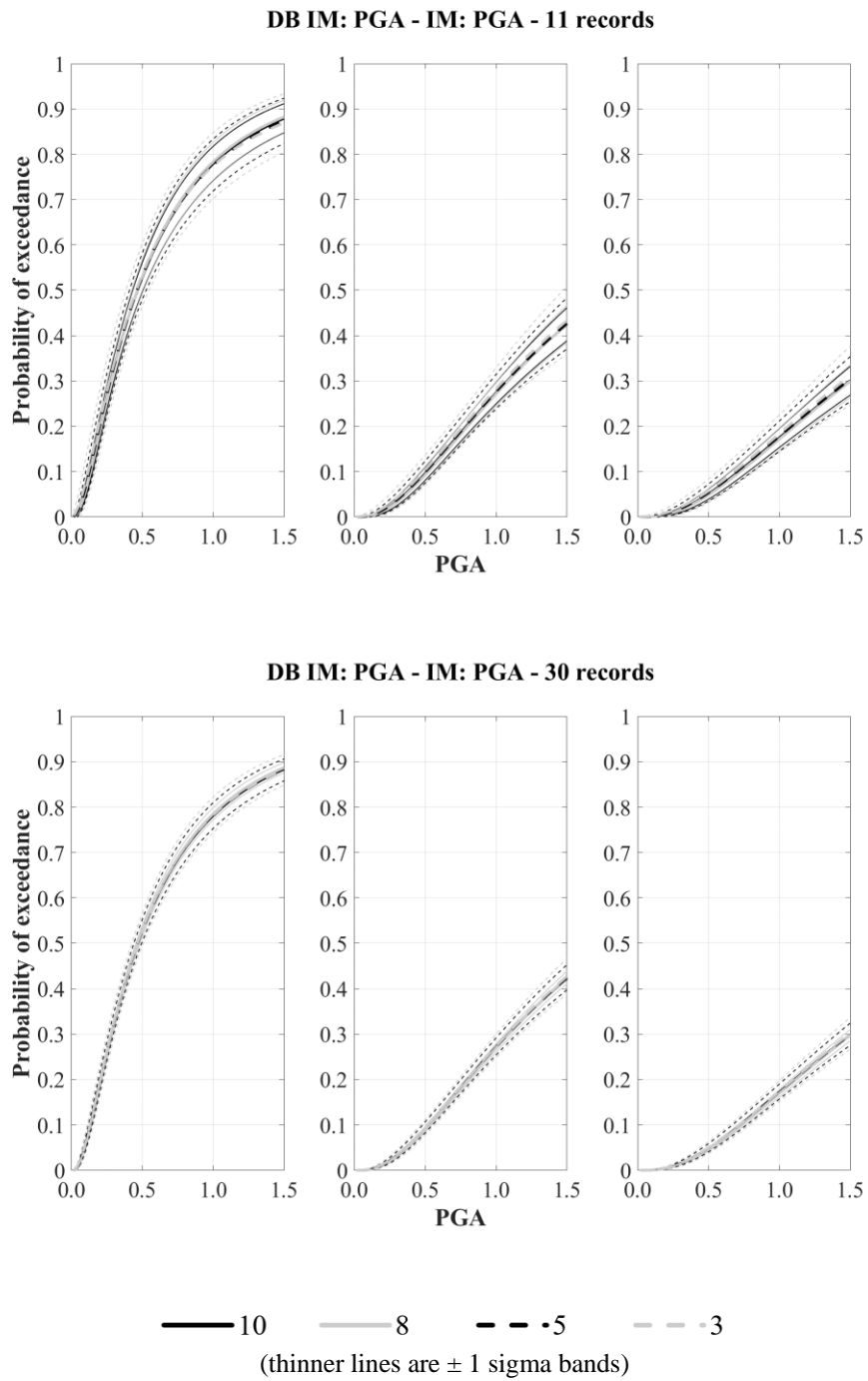
Figure A.197. Alternative PGA-based fragility curves for F5S4B (MIDR) under PGA-based record sets formed with different number of bins

10   8   ·5   ·3

(thinner lines are ± 1 sigma bands)

Figure A.198. Alternative PGV-based fragility curves for F5S4B (MIDR) under PGV-based record sets formed with different number of bins
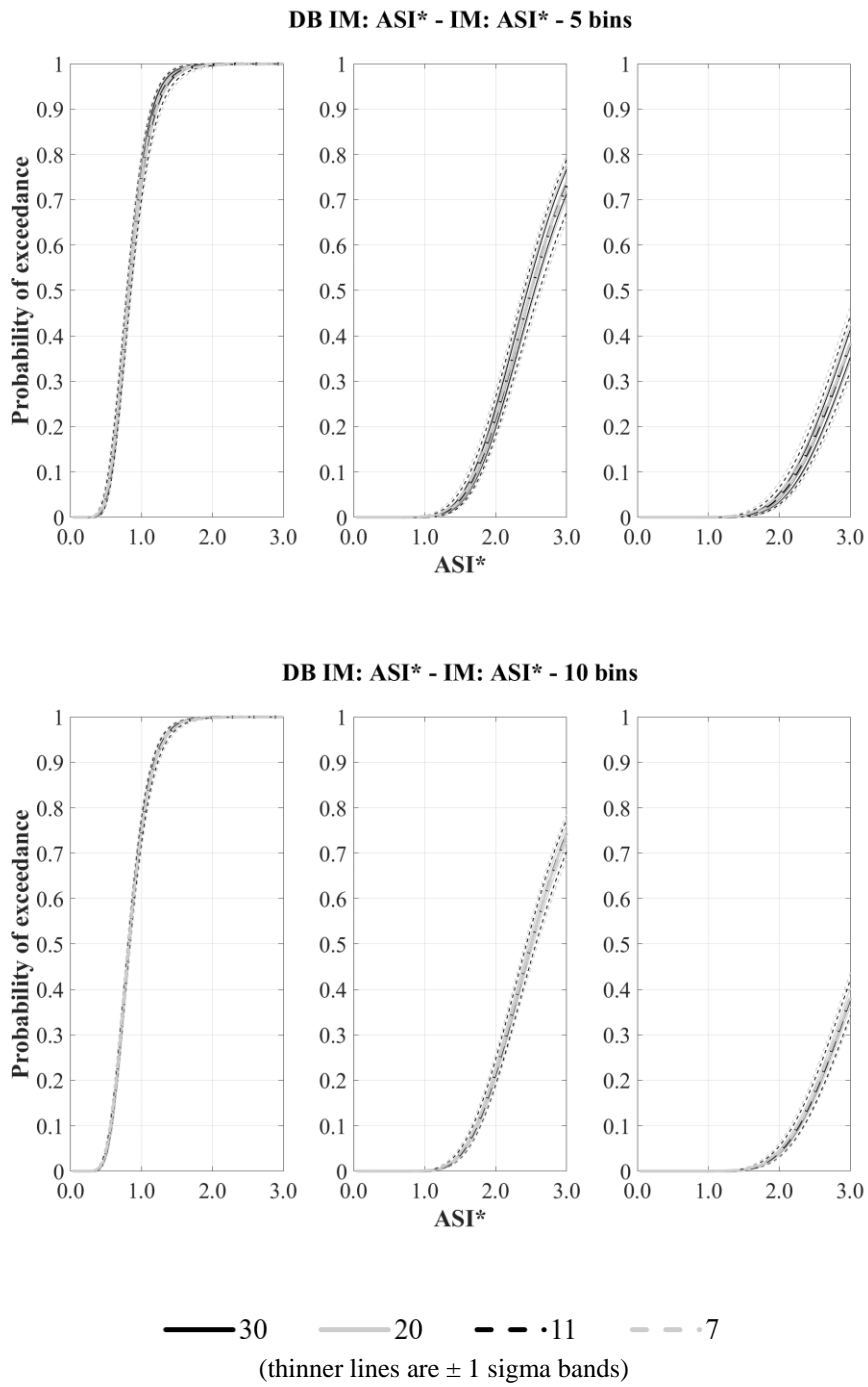
DB IM: ASI* - IM: ASI* - 11 records

DB IM: ASI* - IM: ASI* - 30 records

———— 10 ———— 8 – – ·5 – – · 3
(thinner lines are ± 1 sigma bands)

Figure A.199. Alternative ASI*-based fragility curves for F5S4B (MIDR) under ASI*-based record sets formed with different number of bins
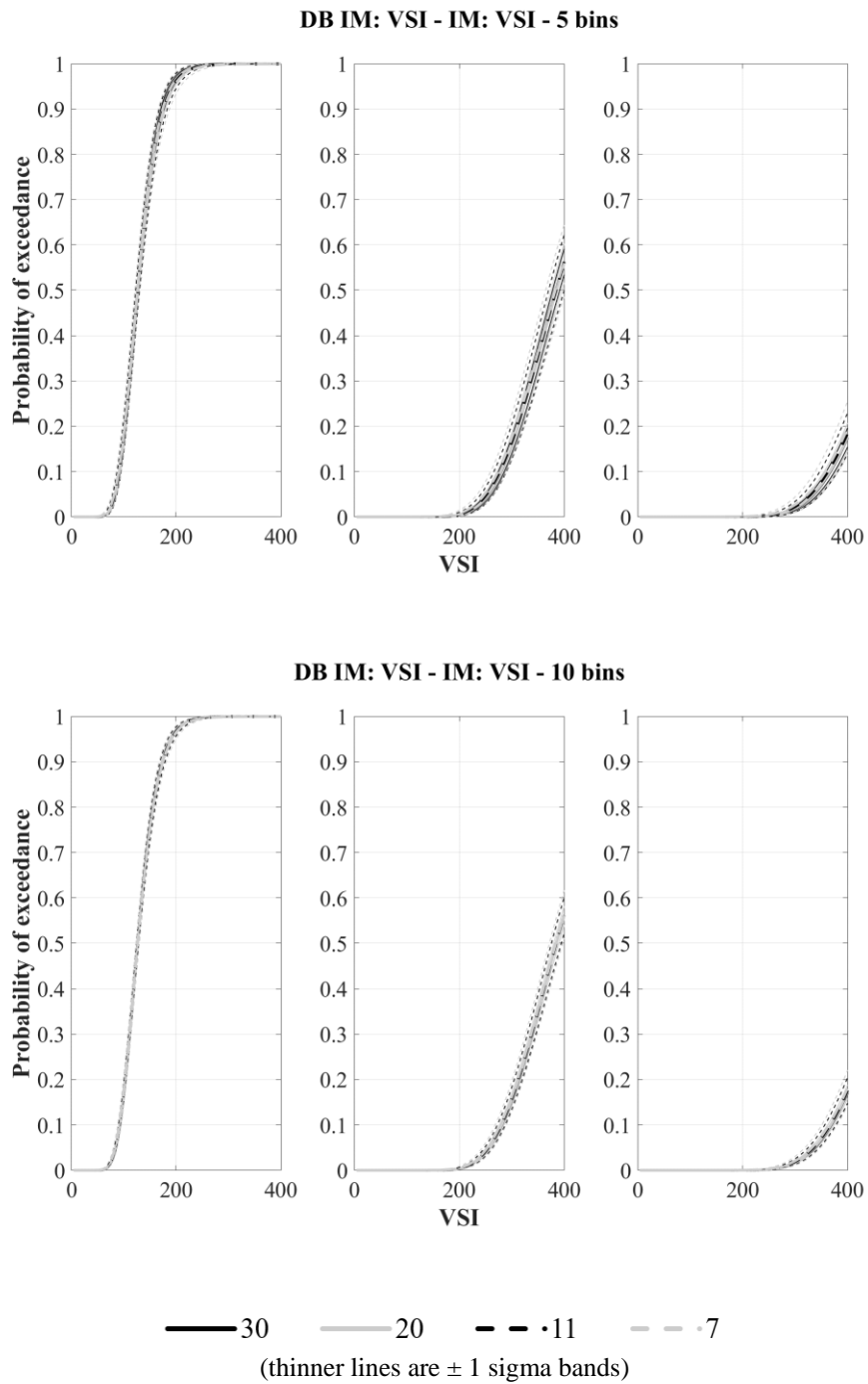
419

Figure A.200. Alternative VSI-based fragility curves for F5S4B (MIDR) under VSI-based record sets formed with different number of bins

DB IM: Sa - IM: Sa - 11 records

DB IM: Sa - IM: Sa - 30 records
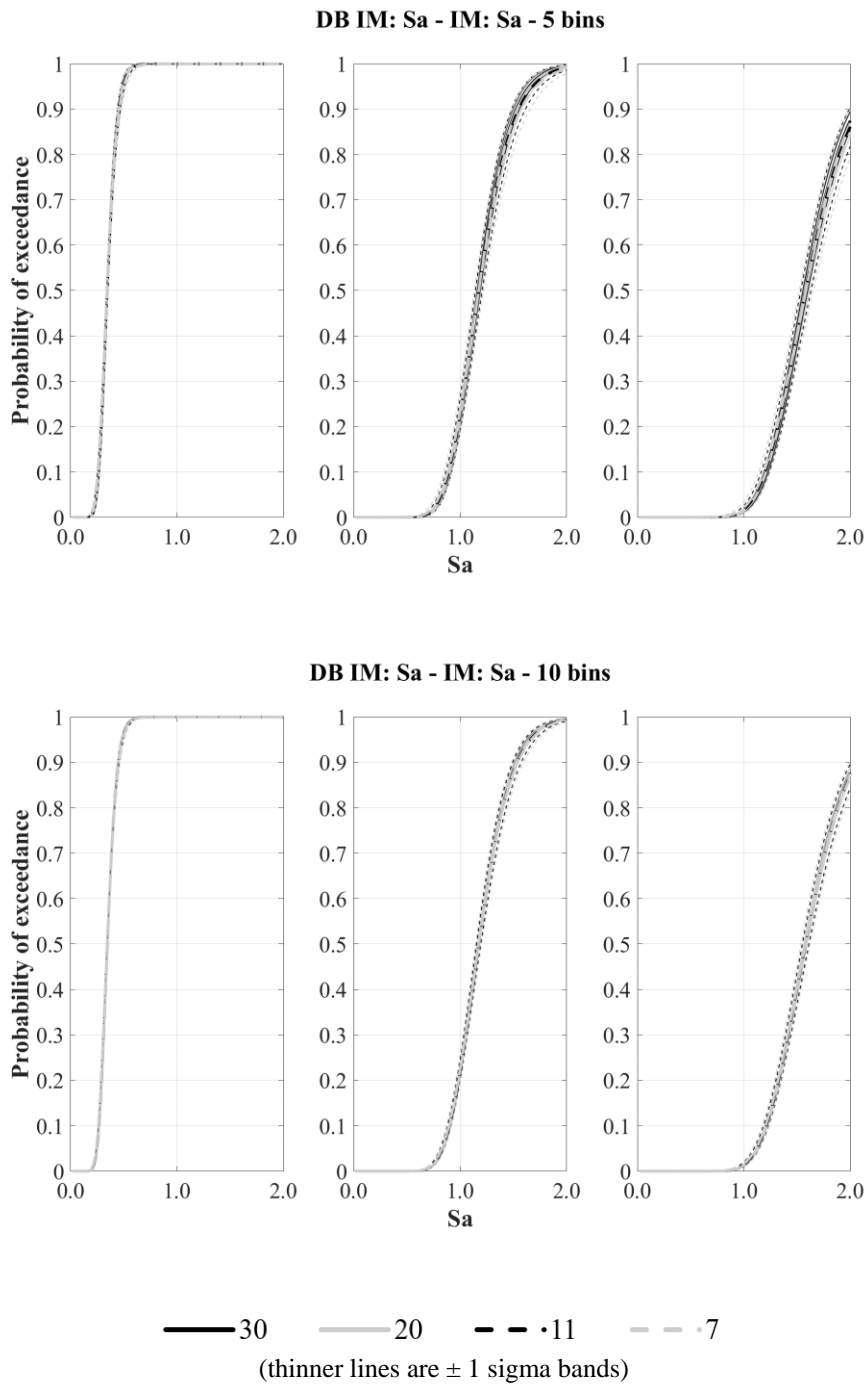
10   8   5   3

(thinner lines are ± 1 sigma bands)
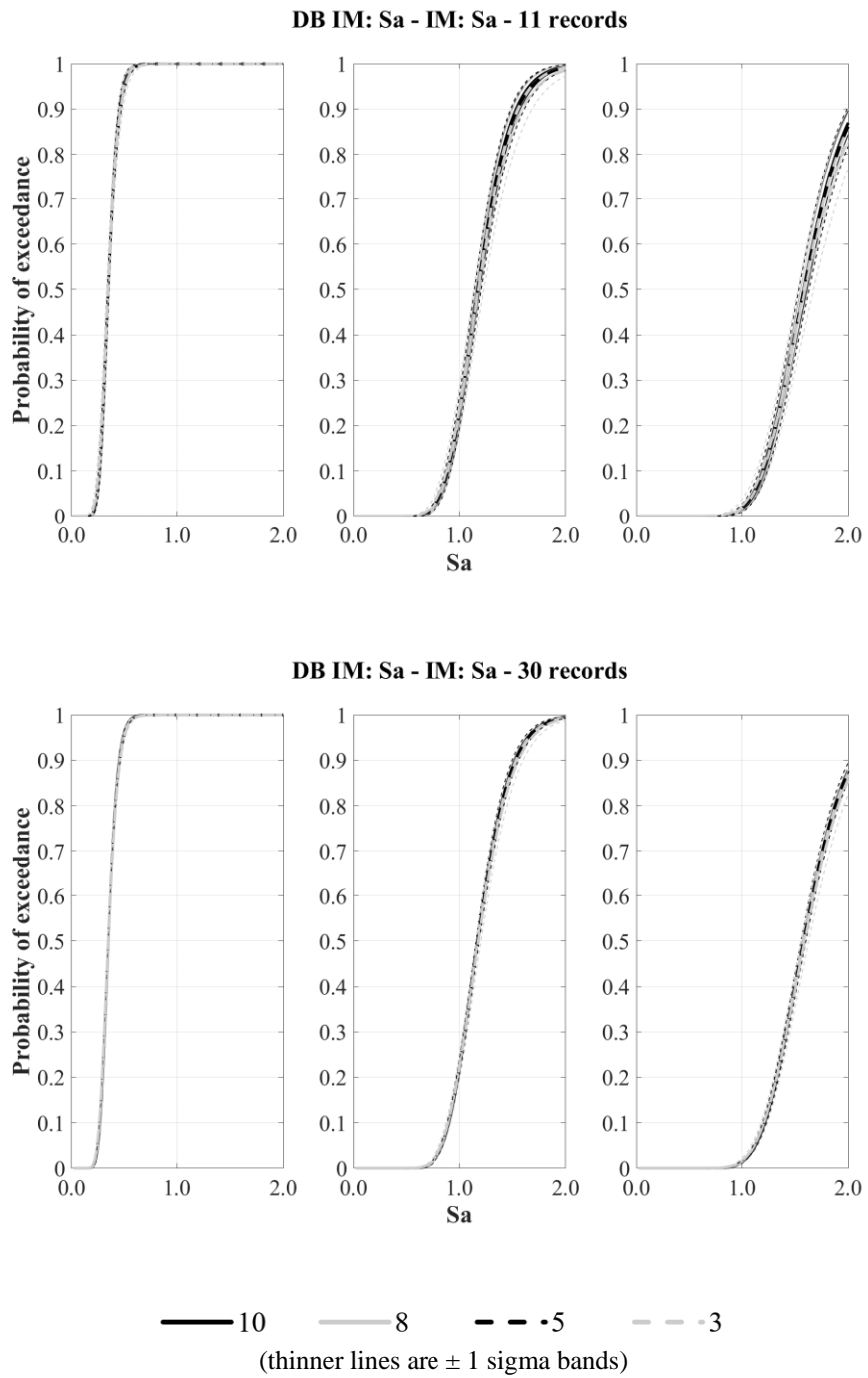
Figure A.201. Alternative S_a-based fragility curves for F5S4B (MIDR) under S_a-based record sets formed with different number of bins
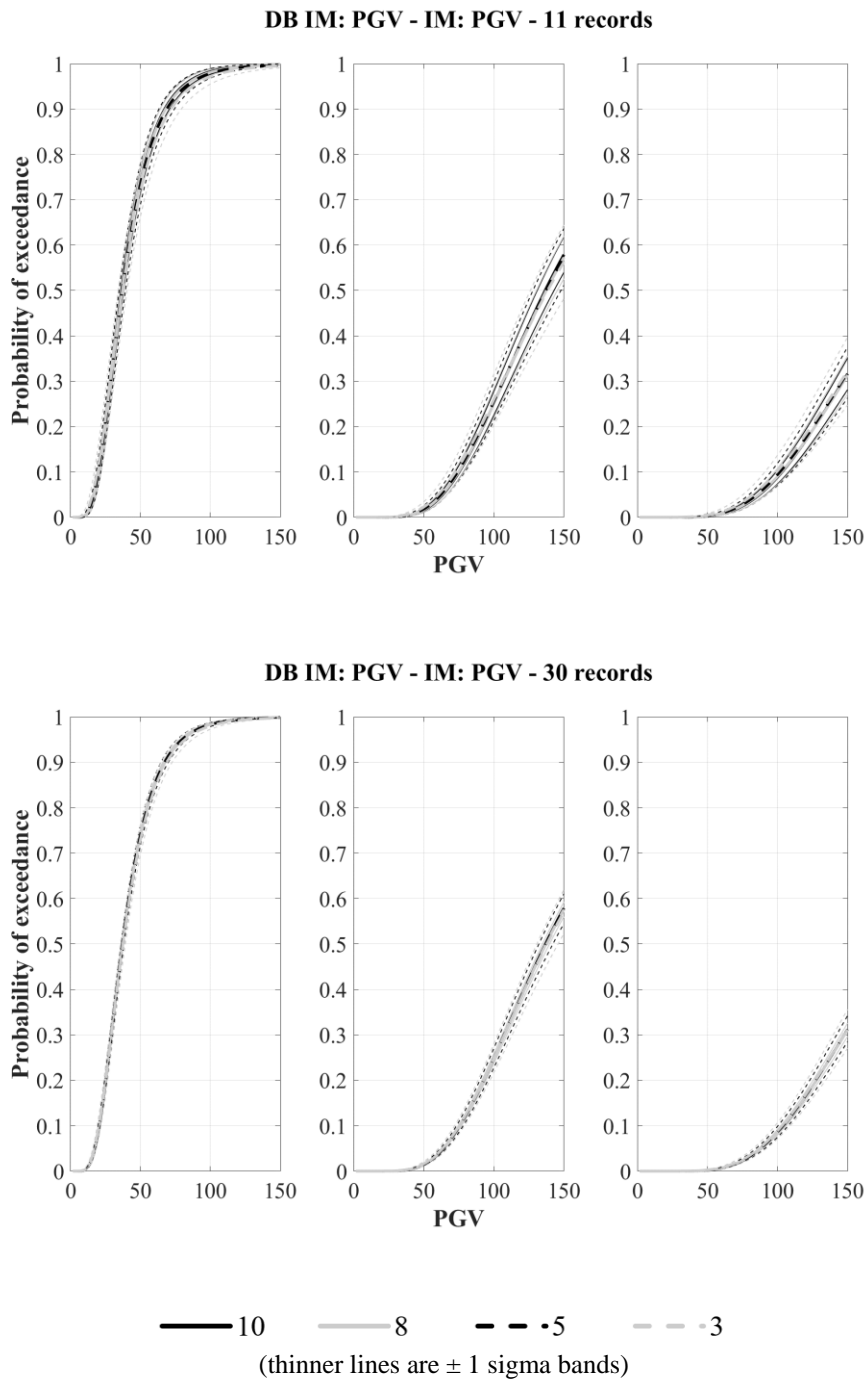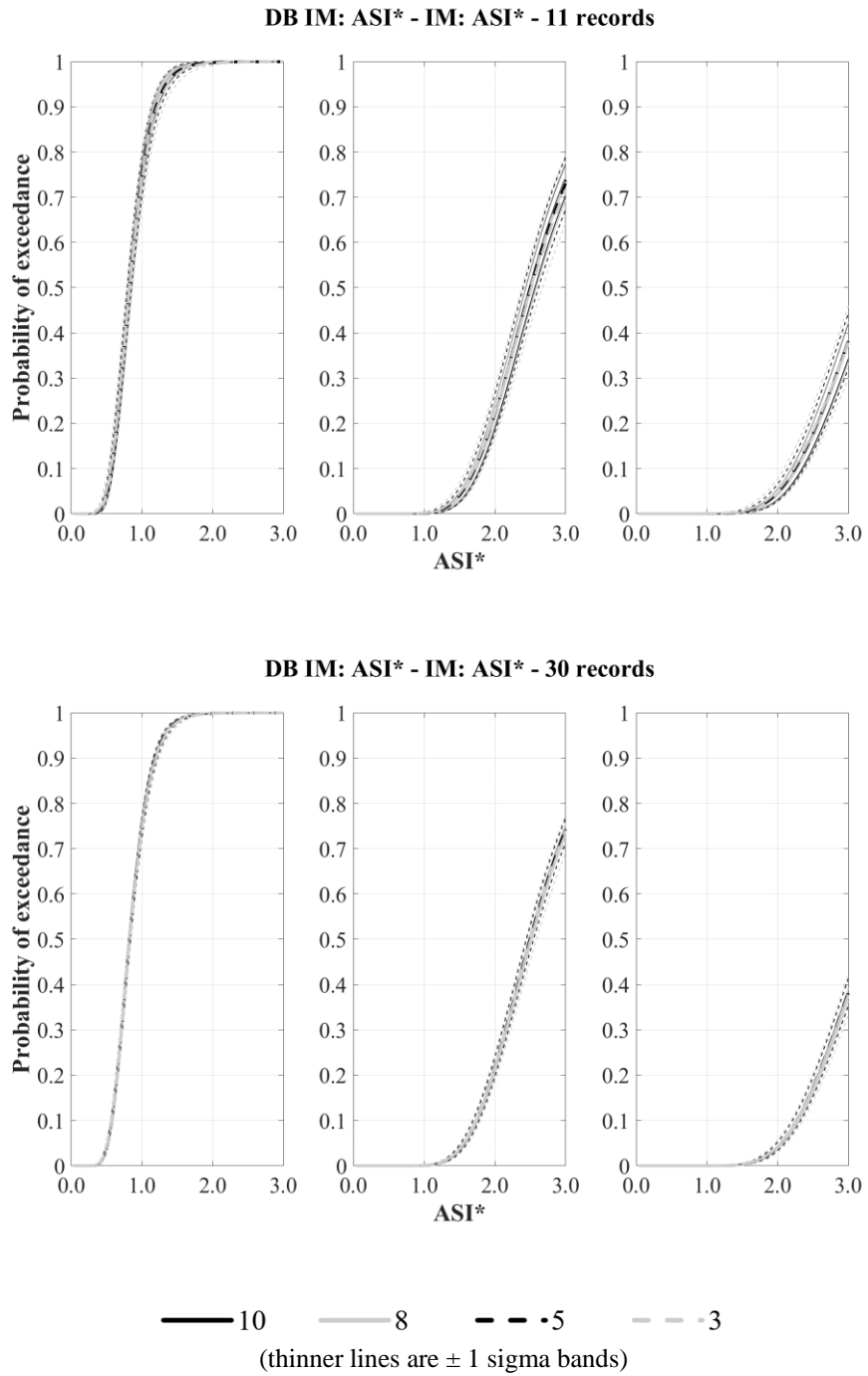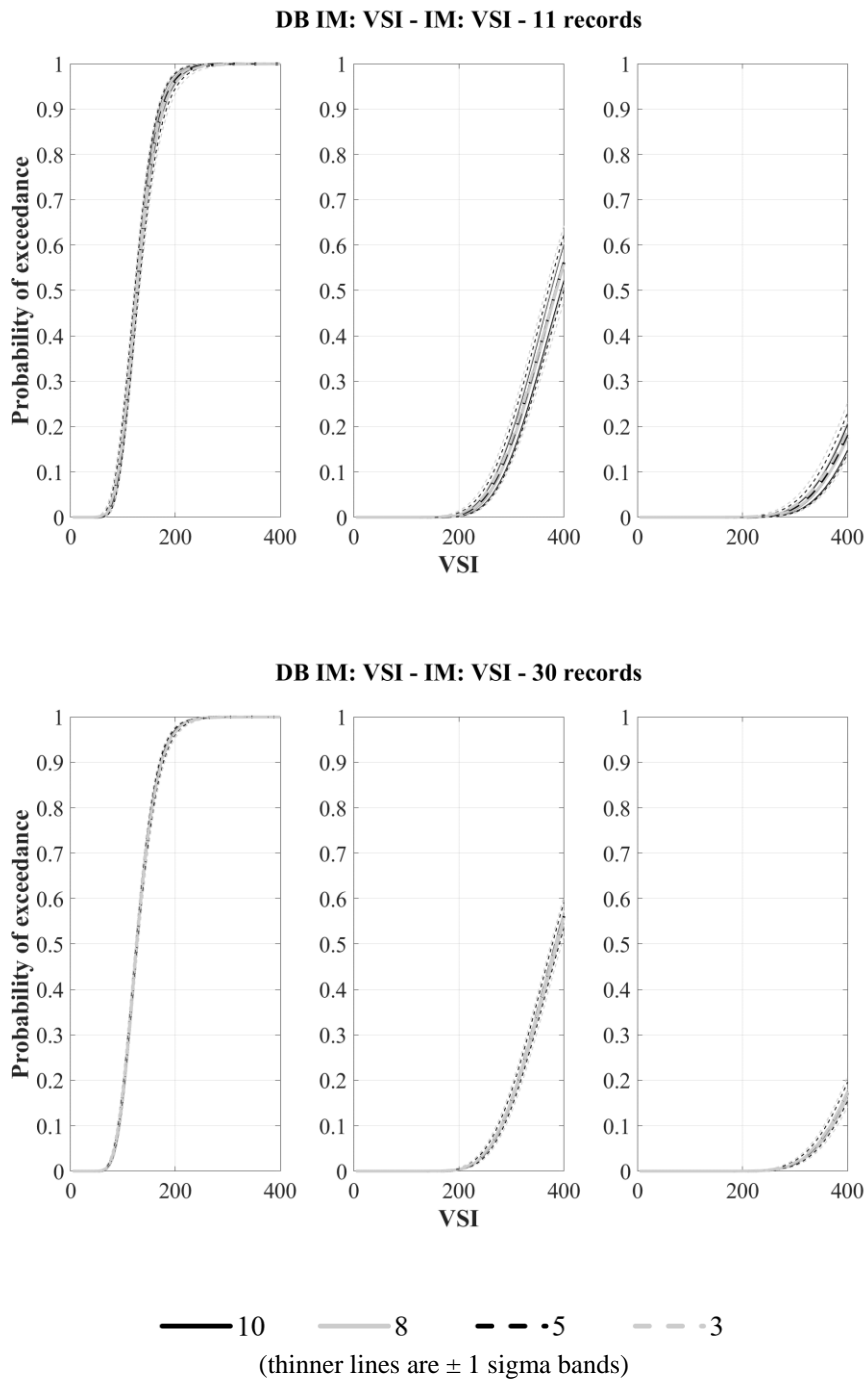
CURRICULUM VITAE

PERSONAL INFORMATION

Surname, Name: Kadaş, Koray
Nationality: Turkish (TC)

EDUCATION

Degree	Institution	Year of Graduation
MSc	METU Civil Engineering	2006
BSc	METU Civil Engineering	2004
High School	Çankaya Atatürk Anadolu High School, Ankara	1999

WORK EXPERIENCE

Year	Place	Enrollment
2018-Present	-	Freelance Civil Eng.
2014-2018	Stucky-Teknik Eng.Cons.Co.Ltd.	Civil Engineer
2008-2014	Yapı-Teknik Eng.Cons.Co.Ltd.	Civil Engineer
2008 Jan-Jul	Tenda Engineering	Civil Engineer
2007-2008	SUNY–Buffalo Dept. of Civil Eng.	Teaching Assistant
2005-2007	METU Dept. of Civil Eng.	Research Assistant

FOREIGN LANGUAGES

Advanced English

PUBLICATIONS

Thesis

1. **Kadaş, K.** (2006). Influence of idealized pushover curves on seismic response. MSc Thesis, Department of Civil Engineering, Middle East Technical University, Ankara.

Journal Papers

1. Karimzadeh, S., **Kadaş, K.**, Askan, A., Yakut, A. (2021). Comparison of Real and Simulated Records Using Ground Motion Intensity Measures, Soil Dynamics and Earthquake Engineering, 147. doi: 10.1016/j.soildyn.2021.106796

2. Akansel, V. H., Soysal, B. F., **Kadaş, K.**, Gülkan, P. (2020). Spektrum Şiddeti Perspektifinden 2018 Türkiye Deprem Tehlike Haritası Değerlendirmesi, Türk Deprem Araştırma Dergisi, 2 (2), 115-137. doi: 10.46464/tdad.737433

3. Karimzadeh, S., **Kadaş, K.**, Askan, A., Erberik, M. A., Yakut, A. (2020). Derivation of Analytical Fragility Curves using SDOF Models of Masonry Structures in Erzincan (Turkey), Earthquakes and Structures, An International Journal, 18 (2), 249-261. doi: 10.12989/eas.2020.18.2.249

4. **Kadaş, K.**, Yakut, A., Kazaz, I. (2011). Ground Motion Intensity Based on Capacity and Period Elongation, American Society of Civil Engineers (ASCE) Journal of Structural Engineering, Special Issue, 137 (3), 401-409. doi: 10.1061/(ASCE)ST.1943-541X.0000084

International Conference Proceeding Papers

1. **Kadaş, K.**, Soysal, B. F., Akansel, V. H., Mazılıgüney, L., Yakut, A. (2019). Comparison of 2007 and 2019 Seismic Hazard Maps Based on Spectrum Intensities and Corresponding Engineering Demands – A Case Study with RC School Buildings in Istanbul, Proceedings, 5th International Conference on Earthquake Engineering and Seismology, Ankara, Turkey, 8-11 October 2019.

2. Akansel, V. H., Soysal, B. F., **Kadaş, K.**, Gülkan, P. (2019). An Evaluation of the 2019 Seismic Hazard Map of Turkey on the Basis of Spectrum Intensity, Proceedings, 5th International Conference on Earthquake Engineering and Seismology, Ankara, Turkey, 8-11 October 2019.

3. Mazılıgüney, L., Akansel, V. H., Soysal, B. F., **Kadaş, K.**, Yakut, A. (2019). Seismic Risk Assessment of School Buildings on the Basis of Recent Turkish Seismic Hazard Map, Proceedings, 6th International Earthquake Symposium Kocaeli 2019, Kocaeli, Turkey, 25-27 September 2019.

4. Karimzadeh, S., **Kadaş, K.**, Askan, A.,Yakut, A. (2019). Use of Seismic Intensity Measures for Comparison of Real and Simulated Records, Proceedings, 6th International Earthquake Symposium Kocaeli 2019, Kocaeli, Turkey, 25-27 September 2019.

5. Yakut, A., Karimzadeh, S., **Kadaş, K.**, Askan, A. (2019). Correlation of Ground Motion Intensity Parameters with Structural Demand, Proceedings, 4th International Conference on Civil, Environmental, Geology and Mining Engineering (ICOCEM), Trabzon, Turkey, April 20-22, 2019.

6. **Kadaş, K.**, Karimzadeh, S., Askan, A., Erberik, M. A., Yakut, A. (2018). Fragility Curves for RC Buildings of Duzce (Turkey) Using Simulated Records, Proceedings, 11th U.S. National Conference on Earthquake Engineering, Earthquake Engineering Research Institute, Los Angeles, California, June 25-29, 2018.

7. Karimzadeh, S., **Kadaş, K.**, Askan, A., Erberik, M. A., Yakut, A. (2018). The Comparison of Different Fragility Curve Generation Techniques to Estimate Observed Damage Distributions, Proceedings, 16th European Conference on Earthquake Engineering (ECEE), Thessaloniki, Greece, 18-21 June 2018.

8. **Kadaş, K.**, Karimzadeh, S., Askan, A., Erberik, M. A., Yakut, A. (2017). An Investigation on the Use of Simulated Records in Derivation of Fragility Curves for RC Buildings in Düzce, Proceedings, 4th International Conference on Earthquake Engineering and Seismology, Eskişehir, Turkey, 11-13 October 2017.

9. Mazılıgüney, L., **Kadaş, K.**, Akansel, V. H., Yakut, A. (2017). Fragility Curves for Reinforced Concrete School Buildings in Turkey due to Repeated Earthquakes, Proceedings, 4th International Conference on Earthquake Engineering and Seismology, Eskişehir, Turkey, 11-13 October 2017.

10. Karimzadeh, S., **Kadaş, K.**, Askan, A., Erberik, M. A., Yakut, A. (2017). A Study on Fragility Analyses of Masonry Buildings in Erzincan (Turkey) Utilizing Simulated and Real Ground Motion Records, Proceedings, 10th International Conference on Structural Dynamics (EURODYN), Rome, Italy, 10-13 September 2017 (Proceeding Paper Reference: Procedia Engineering, 199, 188-193).

11. **Kadaş, K.**, Yakut, A. (2014). Correlation of Seismic Demands with Ground Motion Intensity Parameters Evaluated through Different Ground Motion Record Sets, Proceedings, 10th U.S. National Conference on Earthquake Engineering, Earthquake Engineering Research Institute, Anchorage, Alaska, 21-25 July 2014.

12. **Kadaş, K.**, Yakut, A. (2012). Re-examination of a Spectral Ground Motion Intensity Measure Based on Predicted Period Elongation, Proceedings, 10th International Congress on Advances in Civil Engineering, Middle East Technical University, Ankara, Turkey, 17-19 October 2012.

13. Mazılıgüney, L., Yakut, A., **Kadaş, K.**, Kalem, İ. (2012). Evaluation of Preliminary Assessment Procedures for Reinforced Concrete School Buildings in Turkey, Proceedings, 10th International Congress on Advances in Civil Engineering, Middle East Technical University, Ankara, Turkey, 17-19 October 2012.

14. **Kadaş, K.**, Yakut, A., Kazaz, I. (2008). Ground Motion Intensity Based on Period Elongation, Proceedings, 8th International Congress on Advances in Civil Engineering, Eastern Mediterranean University, Famagusta, North Cyprus, 15-17 September 2008.

15. **Kadaş, K.**, Binici, B., Yakut, A. (2006). Influence of Capacity Curve Approximations on Seismic Response, Proceedings, 1st European Conference on Earthquake Engineering and Seismology, Geneva, Switzerland, September 2006.

National Conferences Proceeding Papers

1. **Kadaş, K.**, Yakut, A. (2013). Utilization of Alternative Intensity Measures in the Formation of Ground Motion Record Sets for Seismic Demand Analyses, Bildiriler, 2. Türkiye Deprem Mühendisliği ve Sismoloji Konferansı, Mustafa Kemal Üniversitesi, Hatay, Türkiye, 25-27 Eylül 2013.

2. Mazılıgüney, L., Yakut, A., **Kadaş, K.**, Kalem, İ. (2013). Fragility Analysis of Reinforced Concrete School Buildings Using Alternative Intensity Measure-Based Ground Motion Sets, Bildiriler, 2. Türkiye Deprem Mühendisliği ve Sismoloji Konferansı, Mustafa Kemal Üniversitesi, Hatay, Türkiye, 25-27 Eylül 2013.

Poster Presentations

1. Karimzadeh, S., **Kadaş, K.**, Askan, A., Yakut, A. (2018). Comparisons of Alternative Seismic Intensity Parameters for Selected Sets of Real and Simulated Ground Motion Records, Poster Presentation, 36th General Assembly of the European Seismological Commission, Valletta, Malta, 2-7 September 2018.

2. Karimzadeh, S., **Kadaş, K.**, Askan, A., Yakut, A. (2017). Comparison of Real and Simulated Records Through Selected Seismic Intensity Measures, Poster Presentation (Paper no.: S41B-0747), American Geophysical Union (AGU) Fall Meeting, New Orleans, USA, 11-15 December 2017.

3. Karimzadeh, S., **Kadaş, K.**, Askan, A., Erberik, M. A., Yakut, A. (2016). A Study on Fragility Analyses of Masonry Buildings in Erzincan (Turkey) Utilizing Simulated and Real Ground Motion Records, Poster Presentation, 35th General Assembly of the European Seismological Commission, Trieste, Italy, 4-10 September 2016.

4. Yakut, A., **Kadaş, K.** (2012). Evaluation of Ground Motion Intensity Measures for Seismic Demand of Buildings, Poster Presentation, 7th Gulf Seismic Forum 2012, Seismology and Earthquake Engineering in the Arabian Gulf Region.

HOBBIES

Basketball, Hiking, Cycling, Scuba Diving, Photography, Cultural Heritage, Archeology, Ecotourism, Volunteering